NEURONAL DEVELOPMENT AND DEGENERATION

EDITED BY: Wenbo Zhang, Patrice E. Fort and Nan-Jie Xu
PUBLISHED IN: Frontiers in Neuroscience, Frontiers in Genetics and Frontiers in Neurology

frontiers Research Topics

frontiers

ISSN 1664-8714
ISBN 978-2-88963-345-6
DOI 10.3389/978-2-88963-345-6

About Frontiers

Frontiers is more than just an open-access publisher of scholarly articles: it is a pioneering approach to the world of academia, radically improving the way scholarly research is managed. The grand vision of Frontiers is a world where all people have an equal opportunity to seek, share and generate knowledge. Frontiers provides immediate and permanent online open access to all its publications, but this alone is not enough to realize our grand goals.

Frontiers Journal Series

The Frontiers Journal Series is a multi-tier and interdisciplinary set of open-access, online journals, promising a paradigm shift from the current review, selection and dissemination processes in academic publishing. All Frontiers journals are driven by researchers for researchers; therefore, they constitute a service to the scholarly community. At the same time, the Frontiers Journal Series operates on a revolutionary invention, the tiered publishing system, initially addressing specific communities of scholars, and gradually climbing up to broader public understanding, thus serving the interests of the lay society, too.

Dedication to Quality

Each Frontiers article is a landmark of the highest quality, thanks to genuinely collaborative interactions between authors and review editors, who include some of the world's best academicians. Research must be certified by peers before entering a stream of knowledge that may eventually reach the public - and shape society; therefore, Frontiers only applies the most rigorous and unbiased reviews.
Frontiers revolutionizes research publishing by freely delivering the most outstanding research, evaluated with no bias from both the academic and social point of view. By applying the most advanced information technologies, Frontiers is catapulting scholarly publishing into a new generation.

What are Frontiers Research Topics?

Frontiers Research Topics are very popular trademarks of the Frontiers Journals Series: they are collections of at least ten articles, all centered on a particular subject. With their unique mix of varied contributions from Original Research to Review Articles, Frontiers Research Topics unify the most influential researchers, the latest key findings and historical advances in a hot research area! Find out more on how to host your own Frontiers Research Topic or contribute to one as an author by contacting the Frontiers Editorial Office: researchtopics@frontiersin.org

NEURONAL DEVELOPMENT AND DEGENERATION

Topic Editors:
Wenbo Zhang, Department of Ophthalmology & Visual Sciences, University of Texas Medical Branch, United States
Patrice E. Fort, Kellogg Eye Center, University of Michigan, United States
Nan-Jie Xu, Shanghai Jiao Tong University School of Medicine, China

Citation: Zhang, W., Fort, P. E., Xu, N.-J., eds. (2020). Neuronal Development and Degeneration. Lausanne: Frontiers Media SA. doi: 10.3389/978-2-88963-345-6

Table of Contents

frontiers in Genetics

EDITORIAL
published: 22 November 2019
doi: 10.3389/fgene.2019.01213

Editorial: Neuronal Development and Degeneration

Patrice E. Fort[1], Nan-Jie Xu[2] and Wenbo Zhang[3]*

[1] Department of Ophathalmology and Visual Sciences, University of Michigan, Ann Arbor, MI, United States, [2] Department of Anatomy and Physiology, Shanghai Jiao Tong University School of Medicine, Shanghai, China, [3] Department of Ophthalmology & Visual Sciences, University of Texas Medical Branch, Galveston, TX, United States

Keywords: neuronal development, degeneration, retina, brain, neurodegenerative disease

Editorial on the Research Topic

Neuronal Development and Degeneration

This research topic combined exciting new findings in original research articles with well-rounded in-depth reviews of some of the most important mechanisms and pathways involved in two major aspects controlling the central nervous system (CNS)'s function: neurodevelopment and at the other end, neurodegeneration.

Among some of the most burning questions in the field of CNS research are the role of the immune response and the resident immune cells in the development of the central nervous system on one hand, and that of neuroinflammation and its regulation in the context of neurodegenerative conditions on the other. In their original study, Duncan et al. showed a new central role of the chemokine Ccl5 as a mediator of inner retinal circuitry during development using functional, morphometric and immunohistochemical analysis in transgenic mice deficient for this protein. In doing so, the authors nicely showed how lack of this protein led to significant perturbations of the intra-retinal wiring of retinal bipolar and ganglion cells of the retina. While the underlying mechanism and pathways involved remain to be identified, in this special topic, a study by Pozner et al. used inducible pluripotent stem cells (iPSCs)-derived cortical neurons to study the role of GSK3β/βCateninsignaling in the process of neurite growth, especially so in the context of hereditary spastic paraplegias. Using a GSK3β inhibitor and patient derived iPSCs, they showed that mutations in SPG11, the most common genetic cause of this disease, they could restore neurite growth, but also improve overall neuronal health and survival.

In addition to providing interesting tools to study mechanistic aspects of normal and diseased development, studies are being conducted to harness the potential of pluripotent stem cells as a therapeutic option. Rabesandratana et al. put together an exciting and in depth review of the current state of the field of pluripotent stem cells as a mechanistic tool but also as an avenue for the treatment of optic neuropathies. The authors are nicely summarizing the recent advancement of this field relative to the production, characterization and delivery of iPSCs-derived retinal ganglion cells, highlighting the potential of the field but also its remaining challenges.

Another group of publications in this research topic focused on different neuroprotective pathways and their role in normal neurodevelopment as well as in neurodegenerative conditions. An in depth review by Miller and Fort nicely summarizes the current knowledge relative to the role and function of heat shock proteins in neurodevelopment, to put in prospective with their better known role in neuroprotection. In this review, the authors highlight the critical roles that these chaperone proteins play in the regulation of neuronal and glial maturation by way of regulation of several developmental pathways. This research topic also includes 3 original research articles pertaining to the topic of neuroprotective molecular mechanisms. One of them is exploring more in depth the mechanisms

OPEN ACCESS

Edited and reviewed by:
Blanka Rogina,
University of Connecticut Health Center, United States

****Correspondence:***
Patrice E. Fort
patricef@umich.edu

Specialty section:
This article was submitted to Genetics of Aging, a section of the journal Frontiers in Genetics

Received: *10 October 2019*
Accepted: *04 November 2019*
Published: *22 November 2019*

Citation:
Fort PE, Xu N-J and Zhang W (2019) Editorial: Neuronal Development and Degeneration. Front. Genet. 10:1213. doi: 10.3389/fgene.2019.01213

of action of the well-recognized antioxidant and pro-survival transcription factor NRF2, and reports the discovery of its regulation by the ER stress related factor XBP-1. The authors of this manuscript nicely demonstrate this regulation using loss and gain of function approaches in primary retinal pigment epithelial (RPE) cells (Chen et al.). Focusing on the excitotoxicity-induced neurodegenerative model, another group reported the potential of polyamine oxidase as a therapeutic target. This study reports that a systemically administered polyamine oxidase inhibitor is associated with a significant improvement of ganglion cell survival, suggesting a role for this enzyme in the regulation of pro-survival signaling pathways (Pichavaram et al.). In a separate manuscript, the same group used a loss of function approach to show an important role of another enzyme, Arginase 2, in the regulation of axonal injury. In this work, the authors have gathered data suggesting that this effect is due to its role in regulating the potent growth factor BDNF concomitantly with a reduction of the injury-associated inflammation/glial activation (Xu et al.).

This paper by Xu et al. interestingly substantiate the review by Ngwenya and Danzer, which focused on the consequences of traumatic brain injury (TBI) on hippocampal change, and the relationship to adult neurogenesis. The authors further discuss how current treatments for TBI can also alter adult neurogenesis, and the dire need for less neurogenesis destabilizing new treatments for TBI. Another study looked at the impact of diffuse axonal injury in corpus callosum and brain stem, once again emphasizing the role of inflammation and glial dysfunction/activation in the progressive degeneration. The main finding of this study was the difference in pathophysiology between those brain regions, and the distinct processes of myelin disruption and axonal degeneration (Mu et al.).

When neurodegeneration could not be prevented, regeneration is the remaining option. In their review, Zhang et al. report on the complexity of this approach and the recent realization of the need for a coordination of multiple inhibitory and permissive signals involving the central phosphatase PTEN.

Finally, this research topic includes manuscript relative to developmental and aging brain disorders, including Autism Spectrum Disorder (ASD) and Alzheimer's disease (AD), and some of the new findings obtained by multiple approaches focusing on human tissue analysis: genetic, histopathologic, and primary cell culture and transcriptomic. Du et al. demonstrated that whole exome sequencing could be an effective method for early diagnose of ASD, especially those with negative findings of copy number variants. A separate manuscript of this research topic reports the results of a novel study of the relationship between brain region volume and polygenic risk factor in the brain of patients with AD, which identified a specific region of the brain to be associated with polygenic risk factor (Wang et al.). In a separate perspective article, Zhao et al. focused on the role of miRNA in the pathogenic mechanisms of AD, and how these miRNA have been studied in primary neuroglial cells isolated from AD and normal donors to assess their role in regulation of the neuroglial transcriptome and more specifically the control of synaptogenesis. These miRNA have received significantly more attention since the discovery of their increased abundance in the neocortex of patients with sporadic AD associated with the down-regulation of critical brain-specific genes.

Altogether, the papers published in this special research topic of Frontiers in Neuroscience clearly support the emerging paradigm of interconnection between neurodegeneration and neuroinflammation on one side and normal neurodevelopment and disease mechanisms on the other. It also emphasize the need for a general understanding of normal physiological mechanisms in order to define pathophysiological ones and develop the knowledge necessary for the identification and characterization of new therapies for neurodegenerative conditions.

AUTHOR CONTRIBUTIONS

PF wrote the manuscript, and PF, N-JX and WZ edited the manuscript.

FUNDING

Supported by National Institutes of Health grants EY020895 (PF), EY022694, EY026629 and Retina Research Foundation (to WZ), and National Natural and Science Foundation of China 31671062 and 81870820 (to N-JX).

Conflict of Interest: The authors declare that the research was conducted in the absence of any commercial or financial relationships that could be construed as a potential conflict of interest.

frontiers in Neuroscience

MINI REVIEW
published: 13 August 2018
doi: 10.3389/fnins.2018.00558

Coordination of Necessary and Permissive Signals by PTEN Inhibition for CNS Axon Regeneration

*Jie Zhang[1,2], Dakai Yang[1], Haoliang Huang[1], Yang Sun[1] and Yang Hu[1]**

[1] Department of Ophthalmology, Stanford University School of Medicine, Palo Alto, CA, United States, [2] Department of Ophthalmology, Union Hospital, Tongji Medical College, Huazhong University of Science and Technology, Wuhan, China

In the nearly 10 years since PTEN was identified as a prominent intrinsic inhibitor of CNS axon regeneration, the PTEN negatively regulated PI3K-AKT-mTOR pathway has been intensively explored in diverse models of axon injury and diseases and its mechanism for axon regeneration is becoming clearer. It is therefore timely to summarize current knowledge and discuss future directions of translational regenerative research for neural injury and neurodegenerative diseases. Using mouse optic nerve crush as an *in vivo* retinal ganglion cell axon injury model, we have conducted an extensive molecular dissection of the PI3K-AKT pathway to illuminate the cross-regulating mechanisms in axon regeneration. AKT is the nodal point that coordinates both positive and negative signals to regulate adult CNS axon regeneration through two parallel pathways, activating mTORC1 and inhibiting GSK3ββ. Activation of mTORC1 or its effector S6K1 alone can only slightly promote axon regeneration, whereas blocking mTORC1 significantly prevent axon regeneration, suggesting the necessary role of mTORC1 in axon regeneration. However, mTORC1/S6K1-mediated feedback inhibition prevents potent AKT activation, which suggests a key permissive signal from an unidentified AKT-independent pathway is required for stimulating the neuron-intrinsic growth machinery. Future studies into this complex neuron-intrinsic balancing mechanism involving necessary and permissive signals for axon regeneration is likely to lead eventually to safe and effective regenerative strategies for CNS repair.

Keywords: axon regeneration, PTEN/PI3K/Akt, optic nerve, mTOR, GSK3β

OPEN ACCESS

Edited by:
Wenbo Zhang,
The University of Texas Medical Branch at Galveston, United States

Reviewed by:
Bo Chen,
Icahn School of Medicine at Mount Sinai, United States
Fengquan Zhou,
Johns Hopkins University, United States

****Correspondence:***
Yang Hu
huyang@stanford.edu

Specialty section:
This article was submitted to Neurogenesis, a section of the journal Frontiers in Neuroscience

Received: *31 May 2018*
Accepted: *24 July 2018*
Published: *13 August 2018*

Citation:
Zhang J, Yang D, Huang H, Sun Y and Hu Y (2018) Coordination of Necessary and Permissive Signals by PTEN Inhibition for CNS Axon Regeneration. Front. Neurosci. 12:558. doi: 10.3389/fnins.2018.00558

INTRODUCTION

Axon injury is a frequent consequence of trauma and a common early feature of CNS degenerative diseases causing life-long neurological deficits. Injuries of CNS axons often result in loss of vital functions because CNS axons fail to regenerate in adult mammals (Schwab and Bartholdi, 1996; Goldberg et al., 2002b; Fitch and Silver, 2008). Both the diminished intrinsic regenerative capacity of mature neurons (Park et al., 2010) and the inhibitory environment of the adult CNS (Yiu and He, 2006) contribute to the growth failure. Neutralizing extracellular inhibitory molecules genetically or pharmacologically yields only limited regeneration and functional recovery (Lee et al., 2010), highlighting the critical importance of neuron-intrinsic factors (Benowitz et al., 2017). To explore the intrinsic regenerative signaling molecules, mouse retinal ganglion cell (RGC) and optic nerve (ON) provide a valuable *in vivo* neural injury system that is relatively simple but robustly replicates CNS traumatic injury and permits straightforward interpretation (**Figure 1**).

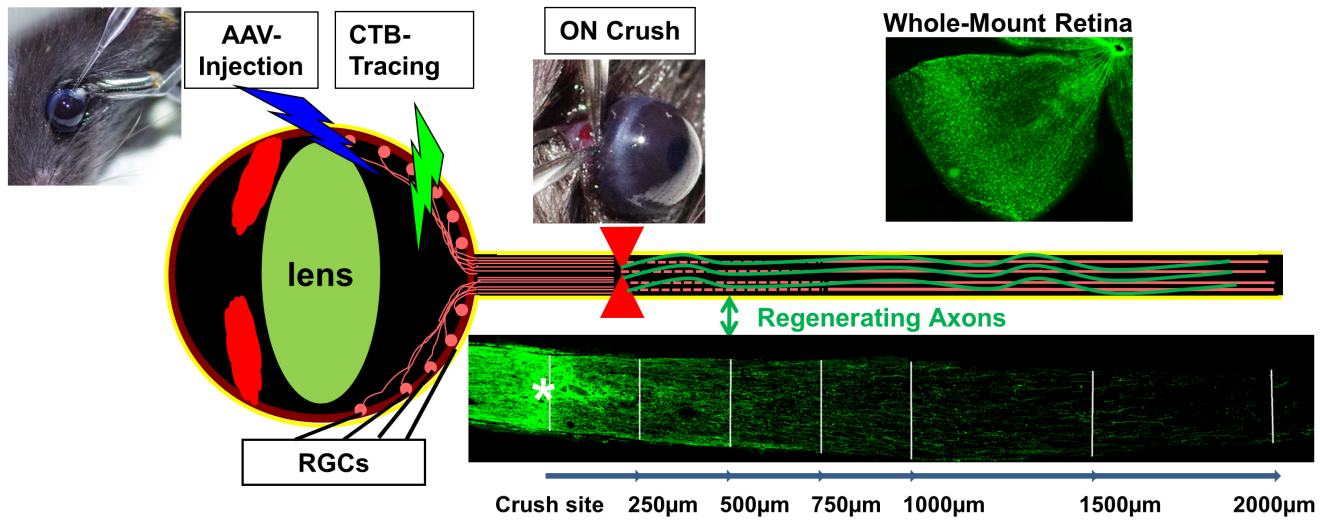

FIGURE 1 | RGC/ON crush provides a straightforward *in vivo* CNS axon injury/regeneration model with clear readout, easy access and amenable to genetic manipulation. Mouse eye can be injected with AAV for genetic manipulation of RGCs and fluorescence-labeled CTB for regenerating axon tracing. Whole-mount retina is for RGC detection and ON longitudinal cryostat section is for visualizing regenerating axons.

Retinal ganglion cells are the only projection neurons in retina to relay visual information from retina to brain. The ON is formed by the projection axons sent exclusively from RGCs; it has the simplicity of an unidirectional axon pathway, which ensures that any nerve fibers passing through the complete crush site are regenerated and do not represent spared axons that underwent collateral sprouting. Adeno-associated viruses (AAV) can be injected directly into the vitreous chamber of the eye to express transgenes specifically and efficiently in adult RGCs. This spatially and temporally controlled genetic manipulation allows us to overcome developmental issues associated with germ line manipulation and to test interventions that can potentially be translated to therapies (Hu, 2015). Exploiting the anatomical and technical advantages of the RGC/ON crush model, multiple signal transduction pathways and transcriptional factors have been linked with CNS axon regeneration (Benowitz et al., 2017; Mahar and Cavalli, 2018). Here we focused on the PTEN/mTOR pathway that we and others have conducted an extensive molecular dissection of the cross-regulating mechanisms in axon regeneration that involve the downstream effectors of PTEN and PI3K to understand the intrinsic mechanisms of CNS axon regeneration (Park et al., 2008; Yang et al., 2014; Guo et al., 2016; Miao et al., 2016; Al-Ali et al., 2017).

PTEN DELETION PROMOTES SIGNIFICANT CNS AXON REGENERATION

The initial efforts to understand the intrinsic mechanisms of regenerative failure have led us to postulate that CNS neurons tightly regulate the evolutionarily conserved molecular pathways that control cell growth (Weinberg, 2007) to prevent overgrowth when development is complete. We subsequently used the mouse ON crush model to screen multiple tumor suppressor genes and discovered that deletion of phosphatase and tensin homolog (PTEN), but not Rb (retinoblastoma), P53, Smad4, or LKB1 (liver kinase B1), promotes significant ON regeneration and RGC survival (Park et al., 2008). PTEN, a lipid phosphatase, is a major negative regulator of the phosphatidylinositol 3-kinase (PI3K)-mammalian target of rapamycin complex 1 (mTORC1) pathway (**Figure 2**). Similar axon regeneration phenotypes after PTEN deletion have been reported for mouse cortical motor neurons (Liu et al., 2010; Jin et al., 2015), drosophila sensory neurons (Song Y. et al., 2012) and *Caenorhabditis elegans* motor neurons (Byrne et al., 2014), presumably through activating PI3K-mTORC1-controlled cell growth. Direct activation of mTORC1 also promotes axon regeneration in dopaminergic neurons (Kim S.R. et al., 2011) and RGCs (Duan et al., 2015; Bei et al., 2016; Lim et al., 2016) and peripheral nerves (Abe et al., 2010), providing further support for the critical role of PI3K-mTORC1 in axon regeneration. However, deregulated PTEN/mTOR activities have been implicated in various disorders including metabolic diseases, tumor formation and even senescence (Zoncu et al., 2011). Presumably, uncontrolled or non-specific activation of mTOR and protein synthesis may result in severe negative consequences, such as tumor formation or cognitive impairment. However, not all tumor suppressor genes involved in axon regeneration in our initial screen (Park et al., 2008), indicating the unique role of PTEN/mTOR in determining the neuronal intrinsic regenerative ability. It is scientifically intriguing and clinically important to carry out a molecular dissection of the PTEN/mTOR pathway to acquire unambiguous understanding of the roles of their downstream signaling molecules in axon regeneration, in hope of differentiating to their tumorigenesis roles.

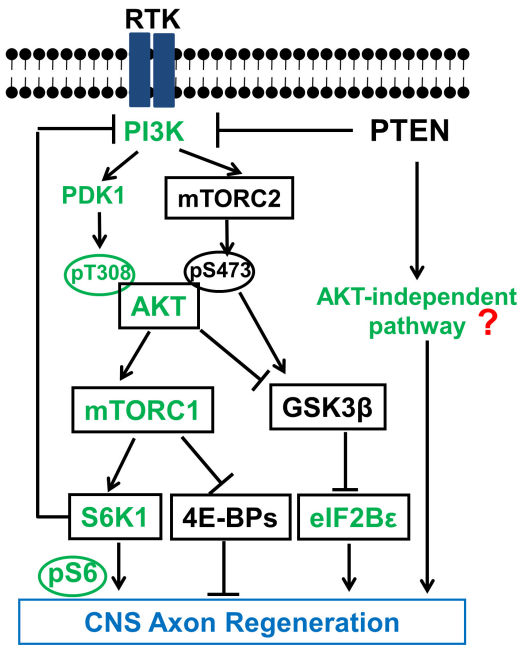

FIGURE 2 | Schematic illustration of the PTEN regulated PI3K-AKT-mTOR signaling pathways in CNS axon regeneration. AKT is positively regulated by the PI3K/PDK1 pathway through phosphorylation of T308, and negatively regulated by the PI3K/mTORC2 pathway through phosphorylation of S473, through at least partially regulation of GSK3β phosphorylation and inhibition. Both AKT downstream effectors, activation of mTORC1 and phosphorylation/inhibition of GSK3β, synergistically promote axon regeneration; inhibition of GSK3β alone is also sufficient for axon regeneration, at least partially through eIF2Bε. The activation of mTORC1 and its substrates 4E-BP and S6K is necessary but not sufficient for potent axon regeneration. The question mark represents unknown effectors downstream of PTEN that are AKT-independent and sufficient to initiate CNS axon regeneration, and which potentially interact with the translational targets of mTORC1 to promote potent axon regeneration. Green color-coated molecules are pro-axon regeneration and dark color-coated molecules are anti-axon regeneration.

THE NECESSARY ROLE OF mTORC1 IN CNS AXON REGENERATION

PI3K is a lipid kinase which can be activated by growth factors, such as insulin and insulin-like growth factor-1 (IGF1), through receptor tyrosine kinase (RTK) (**Figure 2**). PI3K phosphorylates phosphatidylinositol 4,5-bisphosphate (PIP_2) to produce phosphatidylinositol (3,4,5)-triphosphate (PIP_3) in the lipid membrane. PIP_3 in turn recruits AKT to the membrane to be phosphorylated at T308 and activated by phosphoinositide-dependent kinase-1 (PDK1) (Manning and Cantley, 2007). One of the multiple AKT downstream effectors is the complex formed by tuberous sclerosis 1 and 2 (TSC1/TSC2) heterodimer, the negative regulator of mTORC1. AKT activation removes the inhibition of TSC and activates mTORC1. PTEN converts PIP_3 to PIP2 and thus inhibits the activation of AKT and its downstream effectors. PTEN deletion therefore results in constitutive activation of the PI3K-AKT-mTORC1 pathway, suggesting an important role of mTORC1 in the intrinsic regenerative ability of injured adult CNS neurons. Consistently, rapamycin, an inhibitor of mTORC1, blocked PTEN knockout (KO)-induced ON regeneration (Park et al., 2008), indicating mTORC1 activation is required for axon regeneration.

The functional complex mTORC1 regulates cell growth, proliferation, metabolism, motility and survival (Ma and Blenis, 2009; Laplante and Sabatini, 2012) and its downstream effectors are potential targets for promoting axon regeneration and functional recovery after CNS injury. Unfortunately, the clinical usefulness of mTORC1 activation is limited by the threat of deleterious side effects such as malignancy and cognitive deficits due to uncontrolled protein synthesis and cell proliferation (Laplante and Sabatini, 2012; Song M.S. et al., 2012). We studied the two best-characterized downstream signaling molecules of mTORC1, ribosomal protein S6 kinase (S6K) and eukaryotic translation initiation factor 4E (eIF4E)-binding protein (4E-BP) (Hay and Sonenberg, 2004) in ON regeneration (Yang et al., 2014). Phosphorylation of 4E-BP by mTORC1 releases its binding and inhibition from eIF4E, thus to initiate cap-dependent translation. Through different mechanisms, S6K also promotes protein and lipid synthesis (Hannan et al., 2003; Duvel et al., 2010). Although they are both involved in protein synthesis, previous studies suggested that S6K regulates cell size but not cell division (Ohanna et al., 2005), whereas 4E-BP controls cell proliferation but not cell size (Dowling et al., 2010). In RGC neurons, we found that over-expression of the constitutively active mutant of S6K1 significantly increases RGC cell size after ON crush but only promote axon regeneration to a small degree (Yang et al., 2014). Together with the similar effect of TSC deletion, which activates mTORC1 to a greater extent than PTEN deletion but results in very little axon regeneration (Park et al., 2008), we conclude that mTORC1 activation itself is necessary for axon regeneration but has only minimal effect on initiating axon regeneration. Another evidence to support the necessary role of mTORC1 in axon regeneration comes from 4E-BP1-4A mutant, which cannot be inhibited by mTORC1 since it cannot be phosphorylated, as it largely blocks PTEN KO-induced axon regeneration (Yang et al., 2014). However, double deletion of 4E-BP1 and 4E-BP2 in RGCs does not promote axon regeneration, indicating the necessary but insufficient role of 4E-BP inhibition by mTORC1 in axon regeneration. The possibility that other substrates of mTORC1 in addition to S6K1 and 4E-BP may contribute to axon regeneration cannot be rule out, however, we do favor the idea that the mTORC1 pathway essentially plays a necessary role in axon regeneration which requires a key permissive signal from unidentified effectors downstream of PTEN to trigger the neuron-intrinsic growth machinery.

AKT1 AND AKT3 ARE THE PREDOMINANT ISOFORMS OF AKT IN RGCS AND DISPLAY DIFFERENT EFFECTS ON ON REGENERATION

AKT is downstream of PTEN/PI3K but upstream of mTORC1. AKT1 and AKT2 are widely expressed in almost any tissues,

however, AKT3 is the predominant isoform in brain (Easton et al., 2005) and retina (Miao et al., 2016). Consistently, AKT1 deletion reduces whole body size and AKT2 deletion results in diabetes-like syndrome (Cho et al., 2001a,b). Deletion only of AKT3 reduces brain size (Easton et al., 2005), indicating a specific role of AKT3 in CNS growth control. We determined quantitatively the expression levels of the three AKT isoforms in RGCs and their distinct roles in axon regeneration, which provides strong evidence of the unique properties of AKT3 in retina: AKT1 and AKT3 are the major isoforms of AKTs in RGCs and activation of AKT3 promotes significantly greater RGC survival and ON regeneration than AKT1, presumably through its unique ability to activate mTORC1 (higher pS6) in retina (Miao et al., 2016). This is consistent with the results in brain, as AKT3 but not AKT1 deletion, decreases pS6 significantly (Easton et al., 2005). AKT3 may also selectively activate neuronal-specific signaling molecules that are currently unidentified.

AKT COORDINATES POSITIVE SIGNALS FROM PI3K-PDK1 AND NEGATIVE SIGNALS FROM MTORC2 IN REGULATING MTORC1 ACTIVATION AND GSK3β PHOSPHORYLATION FOR AXON REGENERATION

In addition to T308 phosphorylation by PI3K-PDK1, AKT is also phosphorylated at S473 by mTORC2 (Hresko and Mueckler, 2005; Sarbassov et al., 2005; Guertin et al., 2006). mTORC2 is activated by PI3K in an uncharacterized way but depends on ribosome (Zinzalla et al., 2011) and its activation promotes cell survival and actin cytoskeleton dynamics (Jacinto et al., 2004). Like mTORC1, mTORC2 also plays a role in lipogenesis (Lamming and Sabatini, 2013; Yao et al., 2013). It is not clear how mTORC1 and mTORC2 interact to determine multiple downstream cellular events. AKT-pS473 enhances AKT-T308 phosphorylation (Scheid et al., 2002; Yang et al., 2002) and blocking S473 phosphorylation decreases AKT-T308 phosphorylation (Hresko and Mueckler, 2005; Sarbassov et al., 2005; Guertin et al., 2009; Yuan et al., 2012; Carson et al., 2013).

We confirmed the phosphorylation of AKT-T308 and the kinase activity of AKT are essential for axon regeneration by overexpression kinase dead mutant or T308A mutant of AKT in RGCs; whereas AKT-S473A mutant results in even more axon regeneration than wild type AKT, indicating the negative role of AKT-S473 phosphorylation in axon regeneration (Miao et al., 2016). This surprising finding implies that pT308 and pS473 of AKT may have different substrates or regulate the same substrates differentially, to allow their opposite roles in axon regeneration. Interestingly, pAKT-S473 regulates β-cell proliferation whereas pAKT-T308 controls β-cell (Hashimoto et al., 2006; Gu et al., 2011), possibly through different downstream effectors (Jacinto et al., 2004, 2006; Guertin et al., 2006; Yang et al., 2006; Gu et al., 2011). Phosphorylation of glycogen synthase kinase 3β-S9 (GSK3β-S9) by AKT inhibits GSK3β activity, which is critical for neuronal polarization, axon branching and axon growth (Kim Y.T. et al., 2011). The significantly increased pGSK3β-S9 after blocking mTORC2 or overexpression of AKT3-S472A mutant suggests that GSK3β is one of the AKT effectors that are differentially regulated by pAKT-T308 and pAKT-S473 (Miao et al., 2016). The results of our studies using GSK3β-S9A mutant and GSK3β KO mice further proved the inhibitory role of GSK3β in axon regeneration (Miao et al., 2016), thus to definitively resolve the contradictory results in the literature regarding the role of GSK3β in CNS axon regeneration (Dill et al., 2008; Abe et al., 2010; Christie et al., 2010; Saijilafu Hur et al., 2013; Gobrecht et al., 2014). More interestingly, Guo et al identified eIF2Bε as an important downstream effector of GSK3β for axon regeneration (Guo et al., 2016), indicating the critical role of translation regulatory machinery and protein synthesis in axon regeneration.

mTORC2 and pAKT-S473 are necessary for PTEN deletion-induced tissue overgrowth in prostate cancer of mice (Guertin et al., 2009) and eyes of drosophila (Hietakangas and Cohen, 2007). Thus blocking mTORC2 and pAKT-S473 in PTEN KO mice may allow us to minimize their deleterious tumorigenic effect but boost PTEN/AKT's regeneration-promoting effect. mTORC1 inhibition (deletion of *RPTOR* or *mTOR*, over-expression of dominant negative mutant S6K1-DN or 4E-BP1-4A) decreased AKT3-induced ON regeneration (Miao et al., 2016), consistent with our conclusion that mTORC1 is necessary for AKT-induced axon regeneration. In summary, mTORC1 activation and GSK3β inhibition act in parallel and synergistically downstream of AKT to promote CNS axon regeneration as we and others have shown (Guo et al., 2016; Miao et al., 2016).

FEEDBACK INHIBITION OF PI3K-AKT MEDIATED BY mTORC1-S6K1 AND AKT-INDEPENDENT PATHWAYS

Proper translational control is crucial for normal cell growth. The increased protein synthesis induced by PI3K-mTORC1 activation needs to be balanced by an antagonistic mechanism. It has previously been shown that a negative feedback loop involved with S6K1 and insulin receptor substrate 1 (IRS-1) reduces activities of PI3K and its downstream effectors (Laplante and Sabatini, 2012). Indeed we detected decreased AKT phosphorylation and axon regeneration in PTEN KO mice after overexpression of S6K1 (Yang et al., 2014). Possibly through a similar mechanism, S6K inhibits axon regeneration in *C. elegans* (Hubert et al., 2014) and inhibition of S6K1 promotes corticospinal tract regeneration in mice (Al-Ali et al., 2017). It would not be surprising if additional balancing mechanisms can fine-tune the growth control loop of PI3K-AKT-mTORC1-PI3K. This feedback inhibition keeps AKT activation at minimum even after PTEN deletion (Laplante and Sabatini, 2012; Yang et al., 2014), suggesting AKT-independent signals downstream of PTEN for axon regeneration. PTEN deletion-induced PIP3-dependent signaling includes many AKT-independent pathways (Lien et al., 2017). In addition, PTEN can dephosphorylate focal adhesion kinase (FAK) and Shc, and deletion of PTEN activates FAK, RAS, and ERK (Godena and Ning, 2017). Furthermore,

PTEN is also present in the nucleus to play a non-catalytic role in chromosomal instability and DNA repair (Shen et al., 2007; Song et al., 2011). Elucidation of these PTEN-dependent but AKT-independent pathways in axon regeneration will be an important future direction for the field.

NEURONAL SURVIVAL AND AXON REGENERATION

Neuronal survival is an obvious prerequisite for axon regeneration. But our observation is that the increased neuron survival is not invariably linked with proportionately greater axon regeneration and this is consistent with others findings (Benowitz et al., 2015). For example, ON crush injured RGC survival can be increased significantly by inhibition of apoptosis, deleting tumor suppressor genes or by manipulating ER stress, but these manipulations do not induce more ON regeneration (Goldberg et al., 2002a; Park et al., 2008; Hu et al., 2012). On the other hand, spinal cord injury does not cause significant death of corticospinal neurons (Nielson et al., 2010, 2011), but they fail to regenerate axons (Schwab and Bartholdi, 1996; Goldberg et al., 2002b; Fitch and Silver, 2008). These results indicate that the neuronal intrinsic growth signals for axon regeneration is different to the signals for neuron survival. But no convincing evidence proves a direct causative relationship between these two events cannot totally exclude the possibility that more RGC survival contributes to more potent axon regeneration. PTEN deletion or AKT activation and their signaling effectors are normally related to both intrinsic growth control and cell survival, suggesting partially overlapping functionalities of these two events. Currently we can only allow a small percentage of surviving RGCs to regenerate their axons and different subtypes of RGCs have different regeneration abilities (Duan et al., 2015). Elucidating the mechanisms caused this difference will be a hot topic in the field to maximize RGC axon regeneration.

AXONAL mRNA TRANSLATION AND AXON REGENERATION

The importance of localized protein synthesis in peripheral and central axon regeneration has been demonstrated *in vitro* and *in vivo* (Willis and Twiss, 2006; Jung et al., 2012; Baleriola et al., 2014; Perry and Fainzilber, 2014). And certain components of translation machinery including pS6 and 4E-BP1 have been detected in rat regenerating spinal cord (Kalinski et al., 2015). We also found that wildtype AKT and AKT-S473A mutant were localized in RGC axons whereas AKT mutants that cannot promote axon regeneration were excluded from RGC axons (Miao et al., 2016). Is the axonal AKT related with axonal mRNA translation? If so, does the regeneration phenotype caused by AKT activation rely on local protein synthesis in axons? These are very intriguing questions for future studies to investigate the significance of axonal protein synthesis and axonal signal transduction in axon regeneration.

CONCLUSION AND FUTURE PERSPECTIVE

In summary, genetic manipulations specifically in RGCs provide a molecular dissection of the PTEN, PI3K-AKT-mTORC1/GSK3β, and PI3K-mTORC2-AKT-mTORC1/GSK3β pathways and definitively determine the linear and parallel signals that contribute to CNS axon regeneration (**Figure 2**). The balance between mTORC1 and mTORC2's activities after PT3K activation converges on AKT phosphorylation of T308 and S473, which in turn control the activation of mTORC1 and inhibition of GSK3β that act in parallel and synergistically downstream of AKT to promote potent CNS axon regeneration. mTORC1/S6K also functions as feedback inhibition of PI3K signaling (Laplante and Sabatini, 2012) to keep AKT and mTORC1 on check (Yang et al., 2014), which suggests that another proactive signal originating from PTEN deletion may trigger the neuron-intrinsic growth capability (Hu, 2015). It is extremely intriguing scientifically and critical clinically to identify these permissive signals of axon regeneration and elucidate the mechanisms by which they are cross regulated with the necessary mTORC1 signals. The increased understanding of the complicated cross-regulation and feedback-control mechanisms involved in PTNE-PI3K-AKT-mTORC1/2 will certainly inspire more studies on these critical growth control mechanisms, which will eventually lead to safe and effective therapeutic strategies for CNS injury, and to isolate them from targets that mediate deleterious effects.

AUTHOR CONTRIBUTIONS

YH and JZ contributed to bibliographical search, writing, and figure design. HH, DY, and YS wrote the paper.

FUNDING

This work was supported by grants from NIH NEI (EY024932 and EY023295 to YH and EY022058 and EY025295 to YS) and VA merit CX001298 to YS, and partially supported by Research for Prevention of Blindness Unrestricted grant and NEI P30-EY026877.

REFERENCES

Abe, N., Borson, S. H., Gambello, M. J., Wang, F., and Cavalli, V. (2010). Mammalian target of rapamycin (mTOR) activation increases axonal growth capacity of injured peripheral nerves. *J. Biol. Chem.* 285, 28034–28043. doi: 10.1074/jbc.M110.125336

Al-Ali, H., Ding, Y., Slepak, T., Wu, W., Sun, Y., Martinez, Y., et al. (2017). The mTOR substrate S6 kinase 1 (S6K1) is a negative regulator of axon regeneration and a potential drug target for central nervous system injury. *J. Neurosci.* 37, 7079–7095. doi: 10.1523/JNEUROSCI.0931-17.2017

Baleriola, J., Walker, C. A., Jean, Y. Y., Crary, J. F., Troy, C. M., Nagy, P. L., et al. (2014). Axonally synthesized ATF4 transmits a neurodegenerative

signal across brain regions. *Cell* 158, 1159–1172. doi: 10.1016/j.cell.2014.07.001

Bei, F., Lee, H. H., Liu, X., Gunner, G., Jin, H., Ma, L., et al. (2016). Restoration of visual function by enhancing conduction in regenerated axons. *Cell* 164, 219–232. doi: 10.1016/j.cell.2015.11.036

Benowitz, L. I., He, Z., and Goldberg, J. L. (2015). Reaching the brain: advances in optic nerve regeneration. *Exp. Neurol.* 15, 30141–30142.

Benowitz, L. I., He, Z., and Goldberg, J. L. (2017). Reaching the brain: advances in optic nerve regeneration. *Exp. Neurol.* 287, 365–373. doi: 10.1016/j.expneurol.2015.12.015

Byrne, A. B., Walradt, T., Gardner, K. E., Hubbert, A., Reinke, V., and Hammarlund, M. (2014). Insulin/IGF1 signaling inhibits age-dependent axon regeneration. *Neuron* 81, 561–573. doi: 10.1016/j.neuron.2013.11.019

Carson, R. P., Fu, C., Winzenburger, P., and Ess, K. C. (2013). Deletion of Rictor in neural progenitor cells reveals contributions of mTORC2 signaling to tuberous sclerosis complex. *Hum. Mol. Genet.* 22, 140–152. doi: 10.1093/hmg/dds414

Cho, H., Mu, J., Kim, J. K., Thorvaldsen, J. L., Chu, Q., Crenshaw, E. B., et al. (2001a). Insulin resistance and a diabetes mellitus-like syndrome in mice lacking the protein kinase Akt2 (PKB beta). *Science* 292, 1728–1731. doi: 10.1126/science.292.5522.1728

Cho, H., Thorvaldsen, J. L., Chu, Q., Feng, F., and Birnbaum, M. J. (2001b). Akt1/PKBalpha is required for normal growth but dispensable for maintenance of glucose homeostasis in mice. *J. Biol. Chem.* 276, 38349–38352. doi: 10.1074/jbc.C100462200

Christie, K. J., Webber, C. A., Martinez, J. A., Singh, B., and Zochodne, D. W. (2010). PTEN inhibition to facilitate intrinsic regenerative outgrowth of adult peripheral axons. *J. Neurosci.* 30, 9306–9315. doi: 10.1523/JNEUROSCI.6271-09.2010

Dill, J., Wang, H., Zhou, F., and Li, S. (2008). Inactivation of glycogen synthase kinase 3 promotes axonal growth and recovery in the CNS. *J. Neurosci.* 28, 8914–8928. doi: 10.1523/JNEUROSCI.1178-08.2008

Dowling, R. J., Topisirovic, I., Alain, T., Bidinosti, M., Fonseca, B. D., Petroulakis, E., et al. (2010). mTORC1-mediated cell proliferation, but not cell growth, controlled by the 4E-BPs. *Science* 328, 1172–1176. doi: 10.1126/science.1187532

Duan, X., Qiao, M., Bei, F., Kim, I. J., He, Z., and Sanes, J. R. (2015). Subtype-specific regeneration of retinal ganglion cells following axotomy: effects of osteopontin and mTOR signaling. *Neuron* 85, 1244–1256. doi: 10.1016/j.neuron.2015.02.017

Duvel, K., Yecies, J. L., Menon, S., Raman, P., Lipovsky, A. I., Souza, A. L., et al. (2010). Activation of a metabolic gene regulatory network downstream of mTOR complex 1. *Mol. Cell.* 39, 171–183. doi: 10.1016/j.molcel.2010.06.022

Easton, R. M., Cho, H., Roovers, K., Shineman, D. W., Mizrahi, M., Forman, M. S., et al. (2005). Role for Akt3/protein kinase Bgamma in attainment of normal brain size. *Mol. Cell. Biol.* 25, 1869–1878. doi: 10.1128/MCB.25.5.1869-1878.2005

Fitch, M. T., and Silver, J. (2008). CNS injury, glial scars, and inflammation: inhibitory extracellular matrices and regeneration failure. *Exp. Neurol.* 209, 294–301. doi: 10.1016/j.expneurol.2007.05.014

Gobrecht, P., Leibinger, M., Andreadaki, A., and Fischer, D. (2014). Sustained GSK3 activity markedly facilitates nerve regeneration. *Nat. Commun.* 5:4561. doi: 10.1038/ncomms5561

Godena, V. K., and Ning, K. (2017). Phosphatase and tensin homologue: a therapeutic target for SMA. *Signal. Trans. Target Ther.* 2:17038. doi: 10.1038/sigtrans.2017.38

Goldberg, J. L., Espinosa, J. S., Xu, Y., Davidson, N., Kovacs, G. T., and Barres, B. A. (2002a). Retinal ganglion cells do not extend axons by default: promotion by neurotrophic signaling and electrical activity. *Neuron* 33, 689–702. doi: 10.1016/S0896-6273(02)00602-5

Goldberg, J. L., Klassen, M. P., Hua, Y., and Barres, B. A. (2002b). Amacrine-signaled loss of intrinsic axon growth ability by retinal ganglion cells. *Science* 296, 1860–1864. doi: 10.1126/science.1068428

Gu, Y., Lindner, J., Kumar, A., Yuan, W., and Magnuson, M. A. (2011). Rictor/mTORC2 is essential for maintaining a balance between beta-cell proliferation and cell size. *Diabetes Metab. Res. Rev.* 60, 827–837.

Guertin, D. A., Stevens, D. M., Saitoh, M., Kinkel, S., Crosby, K., Sheen, J. H., et al. (2009). mTOR complex 2 is required for the development of prostate cancer induced by Pten loss in mice. *Cancer Cell* 15, 148–159. doi: 10.1016/j.ccr.2008.12.017

Guertin, D. A., Stevens, D. M., Thoreen, C. C., Burds, A. A., Kalaany, N. Y., Moffat, J., et al. (2006). Ablation in mice of the mTORC components raptor, rictor, or mLST8 reveals that mTORC2 is required for signaling to Akt-FOXO and PKCalpha, but not S6K1. *Dev. Cell* 11, 859–871. doi: 10.1016/j.devcel.2006.10.007

Guo, X., Snider, W. D., and Chen, B. (2016). GSK3beta regulates AKT-induced central nervous system axon regeneration via an eIF2Bepsilon-dependent, mTORC1-independent pathway. *Elife* 5:e11903. doi: 10.7554/eLife.11903

Hannan, K. M., Brandenburger, Y., Jenkins, A., Sharkey, K., Cavanaugh, A., Rothblum, L., et al. (2003). mTOR-dependent regulation of ribosomal gene transcription requires S6K1 and is mediated by phosphorylation of the carboxy-terminal activation domain of the nucleolar transcription factor UBF. *Mol. Cell. Biol.* 23, 8862–8877. doi: 10.1128/MCB.23.23.8862-8877.2003

Hashimoto, N., Kido, Y., Uchida, T., Asahara, S., Shigeyama, Y., Matsuda, T., et al. (2006). Ablation of PDK1 in pancreatic beta cells induces diabetes as a result of loss of beta cell mass. *Nat. Genet.* 38, 589–593. doi: 10.1038/ng1774

Hay, N., and Sonenberg, N. (2004). Upstream and downstream of mTOR. *Genes Dev.* 18, 1926–1945. doi: 10.1101/gad.1212704

Hietakangas, V., and Cohen, S. M. (2007). Re-evaluating AKT regulation: role of TOR complex 2 in tissue growth. *Genes Dev.* 21, 632–637. doi: 10.1101/gad.416307

Hresko, R. C., and Mueckler, M. (2005). mTOR.RICTOR is the Ser473 kinase for Akt/protein kinase B in 3T3-L1 adipocytes. *J. Biol. Chem.* 280, 40406–40416. doi: 10.1074/jbc.M508361200

Hu, Y. (2015). The necessary role of mTORC1 in central nervous system axon regeneration. *Neural Regen Res* 10, 186–188. doi: 10.4103/1673-5374.152363

Hu, Y., Park, K. K., Yang, L., Wei, X., Yang, Q., Cho, K. S., et al. (2012). Differential effects of unfolded protein response pathways on axon injury-induced death of retinal ganglion cells. *Neuron* 73, 445–452. doi: 10.1016/j.neuron.2011.11.026

Hubert, T., Wu, Z., Chisholm, A. D., and Jin, Y. (2014). S6 kinase inhibits intrinsic axon regeneration capacity via AMP kinase in *Caenorhabditis elegans*. *J. Neurosci.* 34, 758–763. doi: 10.1523/JNEUROSCI.2886-13.2014

Jacinto, E., Facchinetti, V., Liu, D., Soto, N., Wei, S., Jung, S. Y., et al. (2006). SIN1/MIP1 maintains rictor-mTOR complex integrity and regulates Akt phosphorylation and substrate specificity. *Cell* 127, 125–137. doi: 10.1016/j.cell.2006.08.033

Jacinto, E., Loewith, R., Schmidt, A., Lin, S., Ruegg, M. A., Hall, A., et al. (2004). Mammalian TOR complex 2 controls the actin cytoskeleton and is rapamycin insensitive. *Nat. Cell Biol.* 6, 1122–1128. doi: 10.1038/ncb1183

Jin, D., Liu, Y., Sun, F., Wang, X., Liu, X., and He, Z. (2015). Restoration of skilled locomotion by sprouting corticospinal axons induced by co-deletion of PTEN and SOCS3. *Nat. Commun.* 6:8074. doi: 10.1038/ncomms9074

Jung, H., Yoon, B. C., and Holt, C. E. (2012). Axonal mRNA localization and local protein synthesis in nervous system assembly, maintenance and repair. *Nat. Rev. Neurosci.* 13, 308–324. doi: 10.1038/nrn3210

Kalinski, A. L., Sachdeva, R., Gomes, C., Lee, S. J., Shah, Z., Houle, J. D., et al. (2015). mRNAs and protein synthetic machinery localize into regenerating spinal cord axons when they are provided a substrate that supports growth. *J. Neurosci.* 35, 10357–10370. doi: 10.1523/JNEUROSCI.1249-15.2015

Kim, S. R., Chen, X., Oo, T. F., Kareva, T., Yarygina, O., Wang, C., et al. (2011). Dopaminergic pathway reconstruction by Akt/Rheb-induced axon regeneration. *Ann. Neurol.* 70, 110–120. doi: 10.1002/ana.22383

Kim, Y. T., Hur, E. M., Snider, W. D., and Zhou, F. Q. (2011). Role of GSK3 signaling in neuronal morphogenesis. *Front. Mol Neurosci.* 4:48. doi: 10.3389/fnmol.2011.00048

Lamming, D. W., and Sabatini, D. M. (2013). A central role for mTOR in lipid homeostasis. *Cell Metab.* 18, 465–469. doi: 10.1016/j.cmet.2013.08.002

Laplante, M., and Sabatini, D. M. (2012). mTOR signaling in growth control and disease. *Cell* 149, 274–293. doi: 10.1016/j.cell.2012.03.017

Lee, J. K., Geoffroy, C. G., Chan, A. F., Tolentino, K. E., Crawford, M. J., Leal, M. A., et al. (2010). Assessing spinal axon regeneration and sprouting in Nogo-, MAG-, and OMgp-deficient mice. *Neuron* 66, 663–670. doi: 10.1016/j.neuron.2010.05.002

Lien, E. C., Dibble, C. C., and Toker, A. (2017). PI3K signaling in cancer: beyond AKT. *Curr. Opin. Cell Biol.* 45, 62–71. doi: 10.1016/j.ceb.2017.02.007

Lim, J. H., Stafford, B. K., Nguyen, P. L., Lien, B. V., Wang, C., Zukor, K., et al. (2016). Neural activity promotes long-distance, target-specific regeneration of adult retinal axons. *Nat. Neurosci.* 19, 1073–1084. doi: 10.1038/nn.4340

Liu, K., Lu, Y., Lee, J. K., Samara, R., Willenberg, R., Sears-Kraxberger, I., et al. (2010). PTEN deletion enhances the regenerative ability of adult corticospinal neurons. *Nat. Neurosci.* 13, 1075–1081. doi: 10.1038/nn.2603

Ma, X. M., and Blenis, J. (2009). Molecular mechanisms of mTOR-mediated translational control. *Nat. Rev. Mol. Cell Biol.* 10, 307–318. doi: 10.1038/nrm2672

Mahar, M., and Cavalli, V. (2018). Intrinsic mechanisms of neuronal axon regeneration. *Nat. Rev. Neurosci.* 19, 323–337. doi: 10.1038/s41583-018-0001-8

Manning, B. D., and Cantley, L. C. (2007). AKT/PKB signaling: navigating downstream. *Cell* 129, 1261–1274. doi: 10.1016/j.cell.2007.06.009

Miao, L., Yang, L., Huang, H., Liang, F., Ling, C., and Hu, Y. (2016). mTORC1 is necessary but mTORC2 and GSK3beta are inhibitory for AKT3-induced axon regeneration in the central nervous system. *Elife* 5:e14908. doi: 10.7554/eLife.14908

Nielson, J. L., Sears-Kraxberger, I., Strong, M. K., Wong, J. K., Willenberg, R., and Steward, O. (2010). Unexpected survival of neurons of origin of the pyramidal tract after spinal cord injury. *J. Neurosci.* 30, 11516–11528. doi: 10.1523/JNEUROSCI.1433-10.2010

Nielson, J. L., Strong, M. K., and Steward, O. (2011). A reassessment of whether cortical motor neurons die following spinal cord injury. *J. Comp. Neurol.* 519, 2852–2869. doi: 10.1002/cne.22661

Ohanna, M., Sobering, A. K., Lapointe, T., Lorenzo, L., Praud, C., Petroulakis, E., et al. (2005). Atrophy of S6K1(-/-) skeletal muscle cells reveals distinct mTOR effectors for cell cycle and size control. *Nat. Cell Biol.* 7, 286–294. doi: 10.1038/ncb1231

Park, K. K., Liu, K., Hu, Y., Kanter, J. L., and He, Z. (2010). PTEN/mTOR and axon regeneration. *Exp. Neurol.* 223, 45–50. doi: 10.1016/j.expneurol.2009.12.032

Park, K. K., Liu, K., Hu, Y., Smith, P. D., Wang, C., Cai, B., et al. (2008). Promoting axon regeneration in the adult CNS by modulation of the PTEN/mTOR pathway. *Science* 322, 963–966. doi: 10.1126/science.1161566

Perry, R. B., and Fainzilber, M. (2014). Local translation in neuronal processes–in vivo tests of a "heretical hypothesis". *Dev. Neurobiol.* 74, 210–217. doi: 10.1002/dneu.22115

Saijilafu Hur, E. M., Liu, C. M., Jiao, Z., Xu, W. L., and Zhou, F. Q. (2013). PI3K-GSK3 signalling regulates mammalian axon regeneration by inducing the expression of Smad1. *Nat. Commun.* 4:2690. doi: 10.1038/ncomms3690

Sarbassov, D. D., Guertin, D. A., Ali, S. M., and Sabatini, D. M. (2005). Phosphorylation and regulation of Akt/PKB by the rictor-mTOR complex. *Science* 307, 1098–1101. doi: 10.1126/science.1106148

Scheid, M. P., Marignani, P. A., and Woodgett, J. R. (2002). Multiple phosphoinositide 3-kinase-dependent steps in activation of protein kinase B. *Mol. Cell. Biol.* 22, 6247–6260. doi: 10.1128/MCB.22.17.6247-6260.2002

Schwab, M. E., and Bartholdi, D. (1996). Degeneration and regeneration of axons in the lesioned spinal cord. *Physiol. Rev.* 76, 319–370. doi: 10.1152/physrev.1996.76.2.319

Shen, W. H., Balajee, A. S., Wang, J., Wu, H., Eng, C., Pandolfi, P. P., et al. (2007). Essential role for nuclear PTEN in maintaining chromosomal integrity. *Cell* 128, 157–170. doi: 10.1016/j.cell.2006.11.042

Song, M. S., Carracedo, A., Salmena, L., Song, S. J., Egia, A., Malumbres, M., et al. (2011). Nuclear PTEN regulates the APC-CDH1 tumor-suppressive complex in a phosphatase-independent manner. *Cell* 144, 187–199. doi: 10.1016/j.cell.2010.12.020

Song, M. S., Salmena, L., and Pandolfi, P. P. (2012). The functions and regulation of the PTEN tumour suppressor. *Nat. Rev. Mol. Cell Biol.* 13, 283–296. doi: 10.1038/nrm3330

Song, Y., Ori-Mckenney, K. M., Zheng, Y., Han, C., Jan, L. Y., and Jan, Y. N. (2012). Regeneration of *Drosophila* sensory neuron axons and dendrites is regulated by the Akt pathway involving Pten and microRNA bantam. *Genes Dev.* 26, 1612–1625. doi: 10.1101/gad.193243.112

Weinberg, R. A. (2007). *In the Biology of Cancer*. New York, NY: Garland Science.

Willis, D. E., and Twiss, J. L. (2006). The evolving roles of axonally synthesized proteins in regeneration. *Curr. Opin. Neurobiol.* 16, 111–118. doi: 10.1016/j.conb.2006.01.002

Yang, J., Cron, P., Thompson, V., Good, V. M., Hess, D., Hemmings, B. A., et al. (2002). Molecular mechanism for the regulation of protein kinase B/Akt by hydrophobic motif phosphorylation. *Mol. Cell.* 9, 1227–1240. doi: 10.1016/S1097-2765(02)00550-6

Yang, L., Miao, L., Liang, F., Huang, H., Teng, X., Li, S., et al. (2014). The mTORC1 effectors S6K1 and 4E-BP play different roles in CNS axon regeneration. *Nat. Commun.* 5:5416. doi: 10.1038/ncomms6416

Yang, Q., Inoki, K., Ikenoue, T., and Guan, K. L. (2006). Identification of Sin1 as an essential TORC2 component required for complex formation and kinase activity. *Genes Dev.* 20, 2820–2832. doi: 10.1101/gad.1461206

Yao, Y., Suraokar, M., Darnay, B. G., Hollier, B. G., Shaiken, T. E., Asano, T., et al. (2013). BSTA promotes mTORC2-mediated phosphorylation of Akt1 to suppress expression of FoxC2 and stimulate adipocyte differentiation. *Sci. Signal.* 6:ra2. doi: 10.1126/scisignal.2003295

Yiu, G., and He, Z. (2006). Glial inhibition of CNS axon regeneration. *Nat. Rev. Neurosci.* 7, 617–627. doi: 10.1038/nrn1956

Yuan, M., Pino, E., Wu, L., Kacergis, M., and Soukas, A. A. (2012). Identification of Akt-independent regulation of hepatic lipogenesis by mammalian target of rapamycin (mTOR) complex 2. *J. Biol. Chem.* 287, 29579–29588. doi: 10.1074/jbc.M112.386854

Zinzalla, V., Stracka, D., Oppliger, W., and Hall, M. N. (2011). Activation of mTORC2 by association with the ribosome. *Cell* 144, 757–768. doi: 10.1016/j.cell.2011.02.014

Zoncu, R., Efeyan, A., and Sabatini, D. M. (2011). mTOR: from growth signal integration to cancer, diabetes and ageing. *Nat. Rev. Mol. Cell Biol.* 12, 21–35. doi: 10.1038/nrm3025

Conflict of Interest Statement: The authors declare that the research was conducted in the absence of any commercial or financial relationships that could be construed as a potential conflict of interest.

frontiers in Neuroscience

REVIEW
published: 20 September 2018
doi: 10.3389/fnins.2018.00651

Pluripotent Stem Cell-Based Approaches to Explore and Treat Optic Neuropathies

Oriane Rabesandratana, Olivier Goureau and Gaël Orieux*

Sorbonne Université, INSERM, CNRS, Institut de la Vision, Paris, France

Sight is a major sense for human and visual impairment profoundly affects quality of life, especially retinal degenerative diseases which are the leading cause of irreversible blindness worldwide. As for other neurodegenerative disorders, almost all retinal dystrophies are characterized by the specific loss of one or two cell types, such as retinal ganglion cells, photoreceptor cells, or retinal pigmented epithelial cells. This feature is a critical point when dealing with cell replacement strategies considering that the preservation of other cell types and retinal circuitry is a prerequisite. Retinal ganglion cells are particularly vulnerable to degenerative process and glaucoma, the most common optic neuropathy, is a frequent retinal dystrophy. Cell replacement has been proposed as a potential approach to take on the challenge of visual restoration, but its application to optic neuropathies is particularly challenging. Many obstacles need to be overcome before any clinical application. Beyond their survival and differentiation, engrafted cells have to reconnect with both upstream synaptic retinal cell partners and specific targets in the brain. To date, reconnection of retinal ganglion cells with distal central targets appears unrealistic since central nervous system is refractory to regenerative processes. Significant progress on the understanding of molecular mechanisms that prevent central nervous system regeneration offer hope to overcome this obstacle in the future. At the same time, emergence of reprogramming of human somatic cells into pluripotent stem cells has facilitated both the generation of new source of cells with therapeutic potential and the development of innovative methods for the generation of transplantable cells. In this review, we discuss the feasibility of stem cell-based strategies applied to retinal ganglion cells and optic nerve impairment. We present the different strategies for the generation, characterization and the delivery of transplantable retinal ganglion cells derived from pluripotent stem cells. The relevance of pluripotent stem cell-derived retinal organoid and retinal ganglion cells for disease modeling or drug screening will be also introduced in the context of optic neuropathies.

Keywords: glaucoma, retinal ganglion cells (RGCs), human iPSCs, cell transplantation, disease modeling

OPEN ACCESS

Edited by:
Patrice E. Fort,
University of Michigan, United States

Reviewed by:
George A. Garinis,
Foundation for Research and Technology - Hellas, Greece
Argyris Papantonis,
Universität zu Köln, Germany

****Correspondence:***
Olivier Goureau
olivier.goureau@inserm.fr

Specialty section:
This article was submitted to Neurodegeneration, a section of the journal Frontiers in Neuroscience

Received: *24 May 2018*
Accepted: *30 August 2018*
Published: *20 September 2018*

Citation:
Rabesandratana O, Goureau O and Orieux G (2018) Pluripotent Stem Cell-Based Approaches to Explore and Treat Optic Neuropathies. Front. Neurosci. 12:651. doi: 10.3389/fnins.2018.00651

INTRODUCTION

Sight is defined first as the faculty to detect light (non-image forming visual functions), then enabling to form an image of the environment (image forming visual function). This sense appeared very early in the evolution (Gehring, 2002) showing that this faculty is essential for many species to apprehend their environment and survive. Vision impairment is particularly disabling,

especially irreversible and untreatable blindness that is often due to degeneration of the retina, the light-sensitive tissue located at the back of the eye. Retina consists of a stratified neural layer and the non-neural supporting retinal pigmented epithelium (RPE). Virtually all retinal dystrophies can be separated in two major groups; on one hand, those affecting photoreceptor and RPE cells including inherited retinal dystrophies (i.e., Retinitis Pigmentosa) and Age-related Macular Degeneration. On the other hand, retinal ganglion cell (RGC) disorders affecting the output neurons of the retina that project through the optic nerve to all retinal targets in the brain. Since the optic nerve consists of RGC axons, RGC disorders and optic neuropathies are usually grouped together. RGCs disorders are common, highlighting the vulnerability of these cells. Some optic neuropathies are very common with glaucoma which is the first cause of irreversible blindness while others are scarce like Leber's hereditary optic neuropathy (LHON). There is currently no treatment available for inherited optic neuropathies such as LHON or dominant optic atrophy (DOA), and for glaucoma, current treatments aim to lower the intraocular pressure (IOP). However, RGC death can progress despite lowered IOP and no current treatments promoting RGC surveillance and regeneration are available (Almasieh et al., 2012; Sluch and Zack, 2014; Greco et al., 2016; Jonas et al., 2017). Moreover, RGC degeneration is often silent with no conscious impact on vision acuity before reaching a high percent of cell loss. Since RGC disorders can be detected at an advanced stage of the disease, innovative treatments for patients showing advanced RGC degeneration is required. The retina presents some attractive features for innovative treatments dedicated to neurodegenerative diseases, including gene therapy, cell therapy or prosthetic therapy. It is a more accessible structure, compared to other structures of the central nervous system and as part of the eye, the retina is relatively isolated from the rest of the body insuring limited systemic diffusion of the therapeutic product. Finally, structural and functional benefits or adverse effects can be easily followed-up by imaging, electrophysiology and behavioral tests. Cell-based therapies have been largely explored over the past few decades, notably for retinopathies due to photoreceptor and/or RPE cell death (Goureau et al., 2014; Jayakody et al., 2015; Zarbin, 2016; Aghaizu et al., 2017; Jones et al., 2017; Llonch et al., 2018), and more recently for RGC disorders (Sluch and Zack, 2014; Chamling et al., 2016; Daliri et al., 2017).

Cell therapy can address two major issues. One objective is to deliver a trophic and neuroprotective support (Mead et al., 2015; Ding et al., 2017; Park et al., 2017) in order to limit or to stop the degenerative process and the worsening of the visual deficit. This strategy should be compared to pharmacological approaches designed to deliver neuroprotective agents. The other one is more ambitious as transplanted cells may replace lost cells and contribute to functional restoration. Regenerative medicine has experienced a huge expansion for the past two decades, since the isolation of human embryonic stem cells (ESCs) (Thomson et al., 1998). Indeed, human ESCs can be maintained virtually endlessly in undifferentiated state *in vitro* and can differentiate into all the three germ layers (endoderm, mesoderm, and ectoderm). In 2006, the group of S. Yamanaka generated another type of pluripotent stem cells (PSCs) by reprogramming mouse fibroblasts with four specific transcription factors, POU domain, class 5 transcription factor 1 (Pou5f1, also known as Oct3/4), SRY (sex determining region Y)-box 2 (Sox2), myc proto-oncogene protein (c-Myc) and Kruppel-like factor 4 (Klf4) (Takahashi and Yamanaka, 2006). Shortly after, this group validated the reprogramming of human cells with the same four human-homologous factors (Takahashi et al., 2007). At the same time, the group of J. A. Thomson obtained similar results with a slightly different combination of reprogramming factors comprising OCT4, SOX2, Nanog homeobox (NANOG) and Lin-28 homolog A (LIN28) (Yu et al., 2007). These cells, named induced pluripotent stem cells (iPSCs) display almost all the ESC features and represent an incredibly promising source of cells for transplantation approaches. Additionally, human iPSCs, overcome ethical issues inherent to the use of human embryonic material. Following its original discovery, different methods of delivery of reprogramming factors have been designed, notably to avoid integrative approaches that would represent an obstacle to clinical application (Junying et al., 2009; González et al., 2011).

One key point for cell therapy is to obtain a well-characterized cell population with the appropriate identity at a specific stage of differentiation. This requires recapitulating *in vivo* development, in a stepwise fashion of specification. The generation of retinal cells involves the generation of anterior neuroblasts, then the commitment into eye field lineage, and afterwards, the specification into neural retina or RPE identity (Graw, 2010; Jayakody et al., 2015; Stenkamp, 2015; Rathod et al., 2018). During the last decade, most efforts have been concentrated, successfully, on the generation of photoreceptors and RPE cells (Lamba et al., 2006; Osakada et al., 2008; Meyer et al., 2009; Nakano et al., 2012; Reichman et al., 2014, 2017; Zhong et al., 2014). Several human clinical trials have been approved and already started for RPE cell replacement (Schwartz et al., 2016; Zarbin, 2016; Mandai et al., 2017; da Cruz et al., 2018; Kashani et al., 2018).

The literature dedicated to the generation of PSC-derived RGCs and to cell therapy designed to RGC disorders is less abundant. One explanation may be the challenging goal of optic nerve regeneration that may look daunting to some. However, important progress has been achieved in order to generate well characterized transplantable cells (Gill et al., 2014; Tanaka et al., 2016; Teotia et al., 2016; Liu et al., 2017; Sluch et al., 2017; Langer et al., 2018) and to address the question of axonal regeneration (Park et al., 2008; Sun et al., 2011; de Lima et al., 2012; Benowitz et al., 2017; Calkins et al., 2017; Laha et al., 2017). In this review, we discuss the feasibility of regenerative strategies applied to RGC disorders such as glaucoma and inherited optic neuropathies using PSCs. For this purpose, the different strategies for the generation of PSC-derived RGCs are described. Complementary cell therapy approaches dedicated to deliver a trophic support for cell survival and optic nerve regeneration will be also evoked since all information provided by these studies may be useful for cell replacement strategies.

RGC DISORDERS AND ASSOCIATED-OPTIC NEUROPATHIES

A wide variety of mechanisms, e.g., traumatic, inflammatory, ischemic, or infectious leads to optic neuropathies (Levin and Gordon, 2002). In this chapter, we will focus on the glaucoma-associated optic neuropathy as the leading cause of irreversible blindness and some sporadic inherited optic neuropathies with no current treatment.

Glaucoma-Associated Optic Neuropathy

According to the literature, the global prevalence of glaucoma in a population aged 40–80 years is 3.54% worldwide (Tham et al., 2014) and the number of patients is estimated to be more than 60 million. Commonly, glaucoma develops initially without self-detection of visual deficit and detectable visual field defects appear at an advanced-stage of the disease. Nevertheless, earlier diagnosis is still possible, looking at the *fundus oculi*, since RGC loss manifests as optic nerve head modification even without self-detection of visual deficit.

Glaucoma can be separated into open-angle and angle-closure glaucoma depending on the morphology of the anterior chamber. Some inherited forms of primary open-angle glaucoma (Allingham et al., 2009) have been reported to be associated with expression of a specific variant or mutation in different genes such as *sine oculis-related homeobox 6* (*SIX6)* (Carnes et al., 2014) or *OPTINEURIN* (*OPTN*) (Rezaie et al., 2002). The common feature of all forms of glaucoma is the progressive degeneration of the optic nerve and loss of RGCs detectable by morphological features, i.e., the reduction of the retinal nerve fiber layer, thinning of the neuroretinal rim of the optic disk and cupping of the optic disk (Alhadeff et al., 2017; Jonas et al., 2017). Different risk factors have been reported such as aging, ethnic background, high myopia and family history (Jonas et al., 2017), but the best-characterized risk factor is an excessive IOP. The relation between high IOP and RGC death is not fully understood but many authors agree to incriminate a mechanical stress to the *lamina criblosa* in the optic nerve head, as a critical site of axonal damage (Chidlow et al., 2011). Mechanical constraints may affect both anterograde and retrograde axonal transport resulting in the degeneration of RGC axons (Pease et al., 2000; Salinas-Navarro et al., 2010; Almasieh et al., 2012). Axonal transport failure has been reported in experimental or genetic models of glaucoma such as DBA/2J mice (Anderson and Hendrickson, 1974; Chihara and Honda, 1981; Pease et al., 2000; Kim et al., 2004; Martin et al., 2006; Balaratnasingam et al., 2007; Crish et al., 2010; Dengler-Crish et al., 2014). One hypothesis points to the impairment of neurotrophic factor delivery compromising RGC survival, as a consequence of the axonal transport blockade caused by excessive IOP (Pease et al., 2000; Salinas-Navarro et al., 2010; Almasieh et al., 2012; Fahy et al., 2016; Kimura et al., 2016). However, glaucoma can take place without abnormal IOP, especially in the case of primary open-angle form and some patients display evolving RGC degeneration despite the normalization of IOP (Sluch and Zack, 2014; Demer et al., 2017). Finally, some people display high IOP without any symptoms of the disease (Friedman et al., 2004), suggesting that other mechanisms may exist and/or that the degenerative process persists despite the abolition of the initial cause of the disease.

A vast number of extrinsic and intrinsic signals have been reported to trigger RGC death by apoptosis during glaucoma (**Figure 1**). Oxidative stress, hypoxia, excitotoxicity or trophic factor deprivation have been extensively detailed (Qu et al., 2010; Almasieh et al., 2012; Munemasa and Kitaoka, 2013). Intrinsically, the role of specific neurotrophic factors for RGC development and survival is widely accepted (Cellerino et al., 1997; Ma et al., 1998; Almasieh et al., 2012; Harvey et al., 2012; Marler et al., 2014; Kimura et al., 2016). The promotion of RGC survival by Brain-Derived Neurotrophic Factor (BDNF) is well documented both *in vitro* (Johnson et al., 1986; Barres et al., 1988; Meyer-Franke et al., 1995) and *in vivo* after RGC injury (Mansour-Robaey et al., 1994; Sawai et al., 1996; Di Polo et al., 1998; Yip and So, 2000; Almasieh et al., 2012; Harvey et al., 2012). It is widely accepted that the blockage of both anterograde and retrograde axonal transports may disrupt the delivery of neuroprotective factors (Pease et al., 2000; Salinas-Navarro et al., 2010; Almasieh et al., 2012; Fahy et al., 2016). In addition to BDNF, many other neurotrophic factors such as Nerve Growth Factor (NGF), Glial cell-Derived Neurotrophic Factor, Insulin-like Growth Factor-1 (IGF-1) or Leukemia Inhibitory Factor (Yan et al., 1999; Kermer et al., 2000; Mao et al., 2008; Leibinger et al., 2009; Kimura et al., 2016), have been reported to delay or prevent RGC death. In this context, acute glial cell activation is involved in neuroprotection via the delivery of trophic support but depending on the kinetic of glial activation. Acute activation of glial cells is believe to mediate neuroprotection via the delivery of trophic support but conversely chronic gliosis may be essentially neurotoxic via inflammatory mechanisms (Almasieh et al., 2012; Munemasa and Kitaoka, 2013; Vecino et al., 2016).

LHON and DOA

Inherited optic neuropathies represent a group of genetic disorders causing visual loss characterized by the degeneration of the optic nerve, usually bilateral, associated to the death of RGCs. These pathologies are classified according to the mode of transmission and their non-syndromic (isolated) or syndromic features. Many hereditary optic neuropathies, including the most frequent non-syndromic ones, LHON and DOA, are related to the impairment of mitochondrial function (Yu-Wai-Man et al., 2011; Newman, 2012; Carelli et al., 2017) (**Figure 1**). LHON is a mitochondrial disorder affecting predominately children or young adult, characterized by a rapid and severe visual loss, with rare partial recovery. The prevalence is variable according to the geographic zone ranging from 1 in 30 000 to 1 in 100 000 (Milea and Verny, 2012; Carelli et al., 2017; Jurkute and Yu-Wai-Man, 2017). Three primary mutations, associated with a weak penetrance, have been reported in the mitochondrial genome – revealed by a maternal transmission – which account for approximately 90% of all cases, and all located in genes encoding subunits of the complex I of the respiratory chain (Wallace et al., 1988; Yu-Wai-Man et al., 2011; Carelli et al., 2017; Jurkute and Yu-Wai-Man, 2017). The pathogenic mechanism is mainly

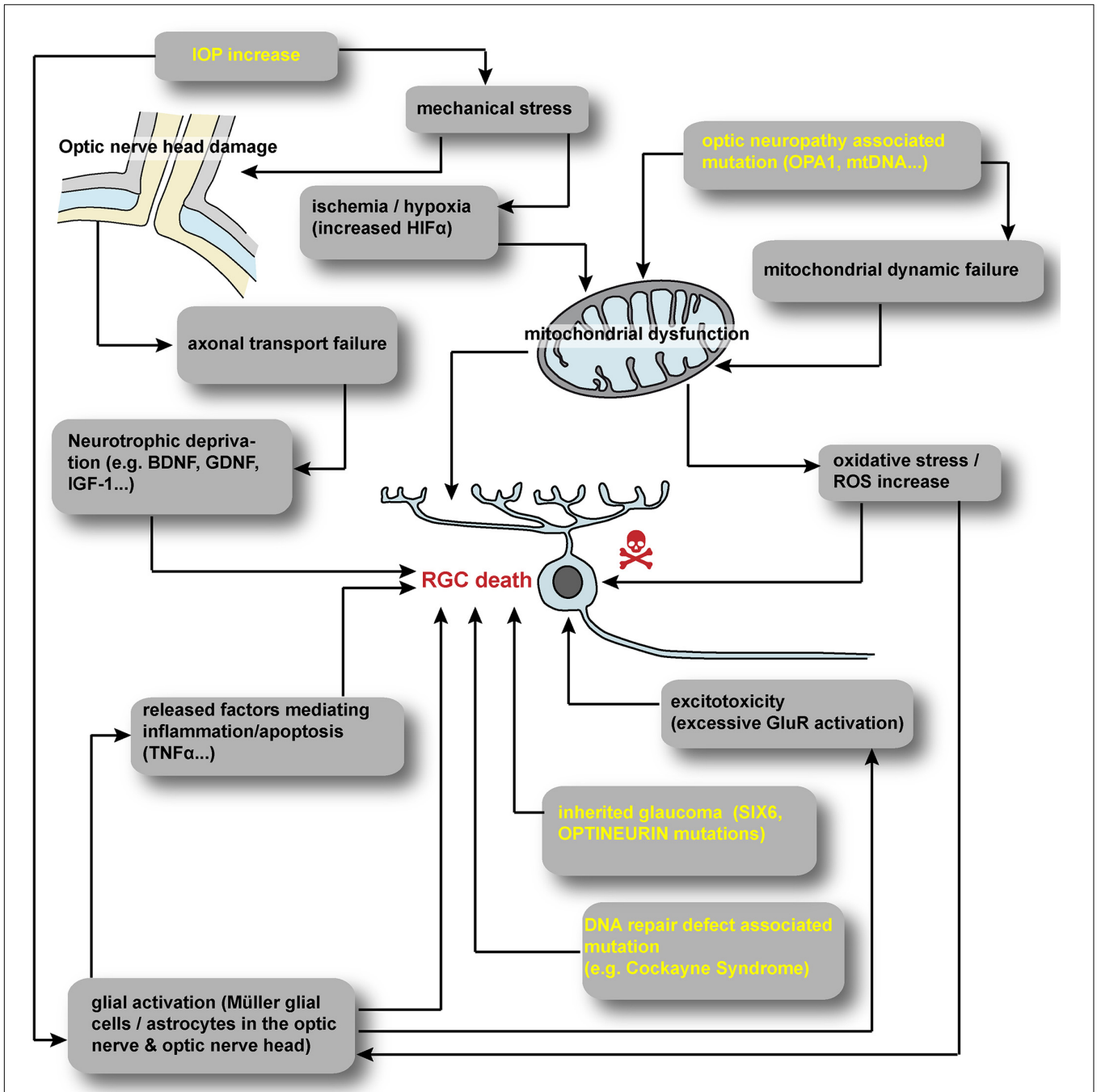

FIGURE 1 | Summary of hypothesized scenarios of RGC degeneration. A vast number of extrinsic and intrinsic cues have been reported to trigger RGC degeneration. Increased IOP in glaucoma may induce mechanical stress at the optic nerve head leading to hypoxia and axonal transport defect. Inherited optic neuropathies often involve directly or indirectly mitochondrial defect. In all RGC disorders, glial cells are suspected to contribute to RGC degeneration. IOP, intraocular pressure; HIF, hypoxia inducible factor; ROS, reactive oxygen species; mtDNA, mitochondrial DNA; GluR, glutamate receptor.

due to a reduced energetic efficiency, an increased production of reactive oxygen species, and a disruption of anti-apoptotic pathways (Carelli et al., 2017). DOA is also a mitochondrial disorder starting frequently during early childhood but usually associated with a less severe visual impairment than LHON. Its prevalence is similar to that of LHON and the most frequent mutation is located in the *OPA1* gene (Alexander et al., 2000; Delettre et al., 2000). *OPA1* gene is located in the nuclear genome and encodes for a dynamin-related GTPase addressed to the mitochondrial inner membrane. This protein has been implicated in many functions including mitochondria dynamics, oxidative phosphorylation and apoptosis (Newman, 2012; Chun and Rizzo,

2016; MacVicar and Langer, 2016). Mitochondria display an asymmetric distribution, abundant in the unmyelinated segment of RGC axons in the retinal nerve fiber layer and far less numerous in myelinated parts after crossing the *lamina criblosa*. This specific distribution is tightly linked to the mitochondrial dynamics involving OPA1 function (Yu-Wai-Man et al., 2011; Carelli et al., 2017), suggesting that a disruption of this dynamic process may account for the pathogenesis associated to *OPA1* gene mutations.

Although Cockayne syndrome related to mutations in genes involved in DNA repair cannot be considered as an optic neuropathy disease, phenotypic analysis of several cases showed a loss of RGCs and degeneration of the optic nerve in some patients (Weidenheim et al., 2009). These observations suggest that the loss of RGCs could be also related to gene mutations affecting DNA repair mechanisms but reflects a more global neuronal toxicity taking place in these patients, where a severe neuropathy affecting many regions of the central nervous system is observed. However, in progeroid mouse models, data on retinal changes are rare and when observed cell degeneration is restricted to photoreceptors and/or RPE (Harkema et al., 2016), similar to situations observed in Retinitis Pigmentosa or Age-related Macular Degeneration.

RETINAL DEVELOPMENT

Based on our knowledge of retinal development in animal models, a large number of protocols used for the generation of retinal cells have tried to recapitulate "*in the dish*" the major developmental steps required for specification, differentiation and maturation of the retina.

During gastrulation, the eye formation initiates with a series of patterning events governed by specific signals that lead to the specification of a group of neuroepithelial cells within the midline of the anterior neural plate, corresponding to the eye field territory. Delimitation of this territory depends on activation of Fibroblast Growth Factor (FGF) and IGF-1 signaling pathways and repression of both Transforming Growth Factor beta (TGFβ)/Bone Morphogenetic Protein (BMP) and Wnt pathways (Graw, 2010; Zuber, 2010). This region expresses several eye-field transcription factors (EFTFs), including different homeodomain-containing factors, such as Paired box 6 (Pax6), T-box transcription factor TBX3, LIM homeobox protein 2 (Lhx2), Orthodenticle homeobox 2 (Otx2), Retina and anterior neural fold homeobox (Rax), Six3 and Six6. These transcription factors act synergistically to form and maintain the eye field territory in a self-regulating feedback highly conserved between species (Zuber, 2010). Recent experiments in xenopus by injection of blastomeres of 2-cell staged embryos demonstrated that Tbx3 and Pax6 are the only EFTFs sufficient to determine pluripotent cells to a retinal lineage (Motahari et al., 2016).

This EFTF-expressing region expands bilaterally during midline formation to form two optic areas, where the evagination of the neuroepithelium leads to the optic vesicle formation. The lens placode invaginates into the optic vesicle resulting in the formation of the lens vesicle. Simultaneously, the optic vesicle invaginates to form the optic cup with an outer and inner layer committed, respectively, into the RPE and the neural retina lineage under the influence of exogenous signals coming from adjacent tissues, such as FGF, Sonic hedgehog (Shh) or agonists of the TGFβ/BMP pathway (Fuhrmann, 2010; Fuhrmann et al., 2014). At this time, the future neural retina consists of immature multipotent retinal progenitor cells (RPCs), that have the ability to give rise to all retinal cell types in an overlapping chronological order, generally conserved among many species. Early-born cell types include retinal ganglion, amacrine and horizontal cells and cone photoreceptors while rod photoreceptors, bipolar and Müller glial cells are generated mainly at later stages (Young, 1985; Turner and Cepko, 1987). The competence model is widely accepted and it supports the idea for the generation of neuronal diversity, where intrinsic factors control the temporal identity of RPCs, a period during which they are able to generate different cell types but only within a specific subset (Boije et al., 2014; Cepko, 2014; Goetz et al., 2014). Ikaros and Casz1 have been proposed as factors that contribute to the establishment of the temporally restricted progenitor cell fates in developing murine retina (Elliott et al., 2008; Mattar et al., 2015). Several lines of evidence demonstrate that a hierarchical gene regulatory network with basic-loop-helix (bHLH)-type and homeodomain-containing factors is at the basis of specific retinal cell fate acquisition made by RPCs (Boije et al., 2014). The expression of transcription factors influencing specific cell fate such as bHLH transcription factor atonal homolog 7 (Atoh7, also known as Math5), Forkhead box N4 (FoxN4) and Pancreas specific transcription factor 1a (Ptf1a) is inhibited by Visual system homeobox 2 (Vsx2) which is largely expressed in proliferative RPCs. When Vsx2 expression diminished during the development, each RPC is committed to a different cell lineage: RGC lineage governed by Atoh7 and amacrine and horizontal cell lineages by transitory expression of Atoh7 and the presence of FoxN4 and Ptf1a. Later, the loss of Atoh7 expression in RPCs provides a permissive environment for a photoreceptor cell fate in absence of both FoxN4 and Ptf1a (Bassett and Wallace, 2012; Boije et al., 2014).

Retinal ganglion cells are the first retinal cell type to be specified and the basic helix-loop-helix transcription factor Atoh7 is a major determinant of RGC commitment. Atoh7 expression is required for RPCs to acquire competence for an RGC precursors fate (Brown et al., 2001; Wang et al., 2001) and its overexpression promotes cell cycle exit and enhances production of RGCs (Zhang et al., 2018). Atoh7 controls the expression of both POU domain, class 4, transcription factor 2 (POU4F2, as known as Brn3b) and homeobox transcription factor insulin gene enhancer protein ISL-1 (Isl1), two transcription factors required for controlling the initiation of the whole RGC transcriptional program (Wu et al., 2015). Mutations or knockdown of these genes result in failure or disruption of RGC development in animal models (Gan et al., 1996; Brown et al., 2001; Kay et al., 2001; Wang et al., 2001; Mu et al., 2008). Downstream RGC-specific gene network is involved in RGC cell subtype specification and/or RGC maturation, as recently shown for POU domain, class 4, transcription factor 1 (POU4F1, as known as Brn3a), and 3 (POU4F3, as known as Brn3c), Ebf helix-loop-helix

transcription factors (Ebf1 and 3) and Onecut 1 and 2 (Gan et al., 1996; Badea et al., 2009; Jin et al., 2010; Sapkota et al., 2014). Conditional knock-out of Sox4 and Sox11, two members of Sox C gene family, led to a moderate to a complete loss of RGCs in double Sox4/Sox11-null retinas (Jiang et al., 2013). These SoxC genes have been reported as essential contributors to RGC development implicated in intermediate position between Atoh7 and POU4F2 (Jiang et al., 2013) and to participate to the control of axon projections (Kuwajima et al., 2017). Recent transcriptome analysis by RNA sequencing of genetically labeled RGC targeting the three POU4F transcription factors allowed the identification of combinatorial molecular codes (transcription factors and cell surface molecules) expressed in different RGC subtypes (Sajgo et al., 2017).

Main extrinsic factors known to regulate RGC neurogenesis are members of the FGF family and Shh. Elegant experiments in fish and chick using specific FGF mutants or pharmacological inactivation of FGF signaling demonstrated that secreted FGF3 and FGF8 from cells located into the organizing center, such as optic stalk, coordinate the progression of RGC development (Martinez-Morales et al., 2005). This propagation of RGC neurogenesis is also controlled by Shh signaling, since an arrest of RGC differentiation has been observed in zebrafish shh mutant (Neumann and Nuesslein-Volhard, 2000). Interestingly in mouse and chick retina, the Shh pathway has been described as a negative feedback regulator of RGC neurogenesis, where nascent RGCs secreted Shh and modulate RGC differentiation within a normal period of retinogenesis (Zhang and Yang, 2001; Wang et al., 2005).

During differentiation, RGCs extent their axons on the retinal surface, toward the optic cup, to exit the eye. Axon growth in the optic fiber layer is mainly under the control of inhibitory signals such as Slit1/2 preventing aberrant extension into the retina (Herrera and Erskine, 2017). Then, the axons fasciculate and continue to grow in order to reach the optic chiasm where a complex set of cues including both transcription factors and extrinsic signals leads the axon to cross or not the midline, forming the contralateral and ipsilateral projections (Assali et al., 2014; Herrera and Erskine, 2017). Finally, RGC axons have to reach different brain targets including lateral geniculate nuclei, superior colliculi and other accessory visual structures; topographic mapping and synaptic refinement are both strongly activity-dependent and continue with visual experience (Priebe and McGee, 2014; Arroyo and Feller, 2016).

PLURIPOTENT-STEM CELLS-DERIVED RGCs

Generation of RGC From Mouse PSCs

One of the first robust protocols for the generation of retinal cells used factors known to pattern anterior neural and retinal fate *in vivo* (Ikeda et al., 2005). In this protocol, 3D serum-free floating embryoid bodies (SFEB) were generated from mouse ESCs with the addition of specific factors, Lefty-A (a Nodal antagonist) and Dickkopf-1 (Dkk-1), a Wnt pathway antagonist. Just before plating the cells, the addition of serum and Activin-A induced a significant generation of RPCs co-expressing Rx and Pax6. Interestingly, 9% of cells in SFEBs expressed the specific RGC marker Islet1. Based on this protocol, the group of M. Takahashi, using a mouse *Rx*-reporter ESC line demonstrated that Rx-positive SFEBs displayed an RGC population co-expressing Pax6 and Islet1 (10.1%) after blockade of NOTCH pathway (Osakada et al., 2008).

A full adherent culture system (2D) relies on the direct differentiation of mouse PSCs into RPCs including RGCs, where PSCs were directly cultured into gelatin-coated plates without any preliminary 3D embryoid bodies (EB) formation. In this context, using a similar medium as previously described (Osakada et al., 2008), the overexpression of a specific RGC marker, *Atoh7,* promoted the differentiation of mouse iPSCs into retinal ganglion-like cells, displaying long synapses and specific expression patterns including Atoh7, Isl1, Brn3b, and Thy1.2 (Chen et al., 2010). Other groups have adapted this protocol to generate RGCs from mouse PSCs by overexpressing RPC markers such as NeuroD1 (Huang et al., 2018) or Pax6 (Kayama et al., 2010). The co-culture of adherent mouse ESCs with adult mouse retina tissue improved their differentiation toward the retinal lineage as well as the generation and maturation of RGCs (Aoki et al., 2007, 2008).

A pioneer paper by the group of Y. Sasai demonstrated the self-organized generation of 3D neuro-retinal structures from mouse ESCs, recapitulating the overall retinal induction (Eiraku et al., 2011). The quick re-aggregation of SFEB in presence of knockout serum (KSR) and Matrigel promoted the formation of optic cup-like structures containing invaginated neural retina of a rigid continuous stratified epithelium, directly self-organized in an apical-basal manner. This epithelium recapitulated the stepwise acquisition of domain-specific properties, including RGCs (Brn3-, Pax6- and Calretinin-positive cells) that are localized in the innermost region.

Different groups have developed 3D/2D stepwise protocols (**Table 1**) by first promoting the neural and retinal induction of 3D mouse iPSC-derived EBs before transferring the RPCs obtained in an adherent culture system (2D), which is crucial for promoting RGC axonal growth (Jagatha et al., 2009; Xie et al., 2014; Parameswaran et al., 2015; Tanaka et al., 2016; Teotia et al., 2017). The iPSC-derived EBs cultured in a classical neural induction medium (Ikeda et al., 2005) supplemented with fibronectin and Noggin generated a RPC pool. These cells were then plated on poly-D-lysine/laminin coated dishes in the same medium in presence of FGF2 to favor the enrichment in RPCs. In some of these protocols, the addition of specific factors, such as Shh, FGF8, DAPT (an inhibitor of Notch signaling pathway), follistatin and cyclopamine, followed by treatment with BDNF, Forskolin, cAMP and Ciliary neurotrophic factor (CNTF) in specific time windows promoted, respectively, the generation and the maturation of RGC. The efficiency of these protocols was assessed by the expression of different RGC markers like Brn3b, Rpf1, Isl1, and Thy1 and the functional maturation, using electrophysiological approaches. An interesting strategy to obtain adequate amounts of RGC neurites, was performed by Maekawa et al. (2015) whom directly replated the optic vesicles derived

TABLE 1 | Retinal ganglion cell (RGC) differentiation protocols from mouse pluripotent stem cells.

Culture system 3D/2D	Reference	PSC type	Neural retina induction medium	RGC differentiation conditions	RGC identification	RGC isolation
3D	Eiraku et al., 2011	ESC	GMEM + 1.5% KSR + pyruvate + mercaptoethanol + NEAA + Matrigel	N.A.	Brn3a, Pax6, Calretinin	N.A.
	DiStefano et al., 2018	ESC/iPSC	DMEM-F12 + Glutamax + N2 + B27 + mercaptoethanol + taurine + 9-*cis* retinal + 2% FBS + IGF-1	N.A.	Brn3a	N.A.
3D (EB) → 2D	Ikeda et al., 2005	ESC	GMEM + 5% KSR + pyruvate + mercaptoethanol + NEAA + Lefty-A + FCS + DKK1 + Activin-A	Medium: no modif* Coating: PDL/laminin/fibronectin	Islet1	N.A.
	Osakada et al., 2008	ESC	GMEM + 5% KSR + pyruvate + mercaptoethanol + NEAA + Lefty-A + 5% FBS + DKK1 + Activin-A	Medium: no modif* Coating: PDL/laminin/fibronectin	Pax6, Islet1	N.A.
	Jagatha et al., 2009	ESC	DMEM-F12 + N2 + 0.5% FBS + heparin + FGF2	Medium: DMEM-F12 + N2 + 0.5% FBS + FGF2 Coating: PDL/laminin	Ath5, Brn3b, RPF-1, Thy-1 and Islet-1,	N.A.
	Xie et al., 2014	iPS reporter cell line: Atoh7-Cre/ROSA YFP knock in line	DMEM-F12 + 10% FBS + N2 + B27 + NEAA + sodium pyruvate + CKI-7 + SB431542 + DAPT	Medium: DMEM-F12 + N2 + B27 + NEAA + sodium pyruvate + CKI-7 + SB431542 + DAPT Coating: Matrigel	Brn3a, NF68	N.A.
	Parameswaran et al., 2015	iPSC	DMEM-F12 + N2 + B27 + insulin + transferrin + sodium selenite + glutamine + fibronectin + Noggin + FGF2	Medium: DMEM-F12 + N2 + glutamine + SHH + FGF8 + DAPT + follistatin + cyclopamine Coating: PDL/laminin	Brn3b, Rpf1, Islet1, Thy1	THY1.2 magnetic beads purification
	Maekawa et al., 2015	ES reporter cell line: Follistatin4::Venus mice line	Neurobasal-A + B27 + L-glutamine + Retinoic acid + L-taurine	Medium: no modif* Coating: 100% Growth factor reduced - Matrigel	BRN3a, Brn3b, Fstl4, SMI312, βIII tubulin	N.A.
	Tanaka et al., 2016	ESC/iPSC	DMEM-F12 + GlutaMAX + N2	Medium: DMEM-F12 + Glutamax + N2 + BDNF + Retinoic acid + (1–10%) FBS Coating: PDL/laminin	Brn3, Math5, βIII tubulin, Sncg, Islet1, Tau, NFM, NFH, NFL	N.A.
	Teotia et al., 2016	ES modified cell line: shRNA-mediated REST loss of function	DMEM-F12 + N2 + B27 + glutamine + Noggin + DKK1 + FGF2 + IGF-1	Medium: DMEM-F12 + N2 + B27 + glutamine + fibronectin + Noggin + FGF2 + SHH + FGF8 + DAPT + follistatin + cyclopamine + BDNF + CNTF + Forskolin + cAMP + Y27632 + NT4 Coating: PDL/laminin	Atoh7, Brn3b, Islet1, βIII tubulin	N.A.

(Continued)

TABLE 1 | Continued

Culture system 3D/2D	Reference	PSC type	Neural retina induction medium	RGC differentiation conditions	RGC identification	RGC isolation
2D	Aoki et al., 2007	ESC	A-MEM + 10% FCS Co-culture with adult mouse retina ± NMDA injection	Medium: no modif* Adherent condition: PA6 stromal cells	Hu, Brn3b	N.A.
	Chen et al., 2010	iPSC	GlutaMAX + 15% FBS + FGF2 + NEAA + N2 + B27 + DKK1 + Noggin + DAPT	Medium: Neurobasal + 3% FBS + N2 + B27 + GlutaMAX + DKK1 + Noggin + DAPT + NEAA Coating: Gelatin 0.1% Overexpression: Math5	Math5, Isl1, Brn3b, Thy1	N.A.
	Kayama et al., 2010	ES reporter cell line: Pax6 reporter cell line	DMEM-F12 + N2 + 0,05% fibronectin	Medium: no modif* Coating: Gelatin	Six3, Shh, Brn3a, Brn3b, Thy1, Math5, Pax6, Islet1, melanopsin	N.A.
	Huang et al., 2018	iPSC	Neurobasal + 10% FBS + L-glutamine + NEAA + N2 + B27	Medium: no modif* Coating: Gelatin 0.1% Overexpression: NeuroD1	Brn3b, Islet1, Math5, Thy1.2	N.A.

A-MEM, Minimum Essential Medium Eagle with Alpha modification; BDNF, brain-derived Neurotrophic Factor; FGF2, beta fibroblast growth factor; cAMP, cyclic adenosine monophosphate; CNTF, Ciliary Neurotrophic Factor; DAPT, N-[N-(3,5-Difluorophenacetyl)-L-alanyl]-S-phenylglycine t-butyl ester; DKK1, Dickkopf-1; DMEM-F12, Dulbecco's Modified Eagle Medium: Nutrient Mixture F-12; EB, embryoid bodies; ESC, embryonic stem cells; FBS, fetal bovine serum; FCS, fetal calf serum; FGF2, fibroblast growth factor 2; FGF8, fibroblast growth factor 8; GMEM, Glasgow Modified Eagle Medium; IGF-1, insulin growth factor-1; iPSC, induced pluripotent stem cells; KSR, knockout serum replacement; NEAA, non-essential amino acids; NT4, neurotrophin-4; PDL, poly-D-lysin; REST, repressor element-1 silencing transcription factor; RWV, rotating-wall vessel; SHH, Sonic Hedgehog; shRNA, short hairpin RNA; N.A., not applicable; No modif, same medium as the corresponding neuro-retinal medium.*

from EBs on matrigel-coated plates, rather than dissociated the 3D structures.

In these protocols, different strategies have been used to isolate PSC-derived RGCs, such as the use of atoh7 reporter cell line (Xie et al., 2014), or by targeting the Thy1 glycoprotein (Parameswaran et al., 2015), a well-known RGC specific surface marker in the retina (Barres et al., 1988).

To go further in disease modeling and future regenerative medicine applications, a recent 3D culture system was developed to culture retinal organoids derived from mouse PSCs in rotating-wall vessels (RWV) bioreactors (DiStefano et al., 2018). This bioprocess recapitulated spatiotemporal development and maturation of retinal organoids in an accelerated manner (25 days) in comparison with static culture conditions (32 days), similar to the development of postnatal day 6 mouse retina *in vivo*. Brn3a-expressing RGCs were detected at the basal side of the neural retina organoids as earlier as 15-days.

Generation of RGCs From Human PSCs

Original protocol was described by the group of T. Reh, where neural induction was induced in EB suspension (similar to SFEB system), by a combination of the key factors Noggin (a BMP antagonist), Dkk-1 and IGF-1 (Lamba et al., 2006). After seeding the cells onto coated poly-D-lysine/Matrigel plates, this cocktail of factors supplemented with FGF2 and pro-neural supplements was used for further differentiation. Among early retinal cell types generated, RGCs were identified by several specific markers, such as PAX6, HuC/D, Neurofilament-M and βIII tubulin. Instead of making EB, plating the clumps of human ESCs directly on Matrigel with the same differentiation media led to similar retinal differentiation in complete adherent cell culture conditions (Lamba et al., 2010). This pioneer "Lamba protocol" led to other protocols (**Table 2**) improving the generation of RPCs and mature RGCs (Gill et al., 2014). Retinal structures containing RGCs identified by Brn3b and Neurofilament-200 have been obtained in similar adherent conditions in absence of Matrigel by addition of Noggin, FGF2, DKK-1, IGF-1, and FGF-9 in specific time windows (Singh et al., 2015). Another recent study, based on "Lamba protocol" (Lamba et al., 2010), validated a simple 2D-adherent differentiation protocol of human iPSC-derived neural rosettes (Teotia et al., 2017), similar to protocol developed using mouse PSCs (Parameswaran et al., 2010, 2015). One strategy combining EBs and subsequent human PSC-derived neurosphere cultures obtained from EB-derived neural rosettes has been developed to enhance RGC differentiation (Riazifar et al., 2014). Interestingly the final culture of neurospheres in laminin-coated plates in presence of serum and DAPT led to approximately 30% of the cells expressing a whole range of RGC markers (BRN3A, BRN3B, THY1, ISLET1, γ-SYNUCLEIN, and ATOH7) (Riazifar et al., 2014).

An original protocol allowing the generation of RGCs from adherent human ESCs was recently reported (Sluch et al., 2015). Retinal development recapitulation was confirmed by evaluation of the expression of some EFTFs and the development of a CRISPR-engineered RGC fluorescent reporter cell line, where mCherry was knock-in in the BRN3B locus, led to the identification and the selection of RGCs by FACS. Surprisingly, subsequent isolated RGCs, immunoreactive for different RGC

TABLE 2 | Retinal ganglion cell differentiation protocols from human PSCs.

Culture system 3D/2D	Reference	PSC type	Neuro-retinal induction medium	RGC maturation conditions	RGC identification	RGC isolation
3D	Nakano et al., 2012	ESC	Induction: GMEM + 20% KSR + NEAA + pyruvate + mercaptoethanol + 10% FBS + Matrigel-growth factor reduced + SAG + CHIR99021 Neuro-retinal culture: DMEM-F12 + N2 + GlutaMAX	Medium: no modif* Coating: N.A.	Brn3a, Rxrγ	N.A.
	Reichman et al., 2017	iPSC	Induction: DMEM-F12 + N2 Maturation: DMEM-F12 + B27 + NEAA	Medium: DMEM-F12 + B27 + NEAA (preliminary datas) Coating: PDL/laminin (preliminary datas)	Brn3a (preliminary datas: Pax6, Thy1, βIII tubulin)	N.A.
3D → 2D	Meyer et al., 2011	iPSC/ESC	DMEM-F12 + B27 + N2 + glutamine + NEAA + Noggin + DKK-1 + IGF-1 + FGF2	Medium: DMEM-F12 + B27 + N2 + glutamine + Shh + FGF8 + DAPT + follistatin + cyclopamine + BDNF + CNTF + Forskolin + cAMP + Y27632 Coating: Matrigel	Brn3, Pax6, βIII tubulin, Calretinin	N.A.
	Zhong et al., 2014	iPSC	DMEM-F12 + B27 + NEAA + 10% FBS + Taurine + GlutaMAX	Medium: no modif* Coating: Matrigel	Brn3, Hu C/D	N.A.
	Deng et al., 2016	iPSC	Neurobasal + B27 (without VitA) + N2 supp + NEAA + L-glutamine + β-mercaptoethanol	Medium: no modif* Coating: Matrigel. Overexpression: Atoh7	Brn3b, Tuj, Islet1, Calretinin	N.A.
	Gill et al., 2016	ESC	DMEM-F12 + GlutaMAX + 10% KSR + B27 + Noggin + IGF-1 + DKK1	Medium: DMEM-F12 + N2 + B27 + GlutaMAX + Noggin + IGF-1 + DKK1 + FGF2 Coating: Matrigel/PDL	NFM, βIII tubulin, Brn3a, Hu C/D	CD90-coupled magnetic microbeads (MACS)
	Langer et al., 2018	iPSC/ESC	DMEM-F12 + B27 + N2 + glutamine + NEAA + Noggin + DKK-1 + IGF-1 + FGF2	Medium: DMEM-F12 + B27 + N2 + glutamine + Shh + FGF8 + DAPT + follistatin + cyclopamine + BDNF + CNTF + Forskolin + cAMP + Y27632 Coating: Laminin	Brn3, Islet1, Rbpms, Sncg, βIII tubulin, Smi32, Map2	N.A.
	Kobayashi et al., 2018	iPSC	DMEM-F12 + 10% KSR + BMP4 + N2 + GSK3 inhibitor + VEGFR/FGFR	Medium: Neurobasal + CNTF + BDNF + forskolin + *N*-acetylcysteine + FGF2 + B27 + glutamine + insulin + sodium pyruvate + progesterone + putrescine + sodium selenite + triiodothyronine Coating: PDL/Laminin	Atoh7, Smi32, Brn3b, Islet1, Rbpms, Thy1	Anti-Thy1 antigen (immunopanning)

(Continued)

TABLE 2 | Continued

Culture system 3D/2D	Reference	PSC type	Neural retina induction medium	RGC differentiation conditions	RGC identification	RGC isolation
2D	Lamba et al., 2006	ESC	DMEM-F12 + 10% KSR + Noggin + DKK1 + IGF-1 + FGF2 + B27 + N2	Medium: no modif* Coating: Matrigel/PDL	Pax6 (RPC population), HuC/D, Tuj1	N.A.
	Sluch et al., 2015	ESC	DMEM-F12 + Neurobasal + GlutaMAX + N2 + B27 + FGF8 + FGF-A + Taurine + 10% FBS	Medium: no modif* Coating: Matrigel.	Brn3b, Tuj1, Rbpms, Map2	Specific fluorescent reporter expression (FACS)
	Singh et al., 2015	ESC	Neurobasal + N2 + B27 (without RA) + Noggin Induction medium: DKK-1 + IGF-1 Differentiation medium: L-glutamine + β-mercaptoethanol + FGF2 + FGF9 + BSA + amphotericin-B + gentamicin	Medium: no modif* Coating: Gelatin/Laminin	Brn3b, NF200	N.A.
	Teotia et al., 2016	iPSC	DMEM-F12 + Noggin + DKK-1 + IGF-1 + B27 + N2	Medium: DMEM-F12 + Shh + FGF8 + DAPT + follistatin + cyclopamine + BDNF + CNTF + Forskolin + cAMP + Y27632 Coating: Matrigel.	Atoh7, Brn3, βIII tubulin, Thy1.2	N.A.

BDNF, brain-derived Neurotrophic Factor; FGF2, beta fibroblast growth factor; BMP4, bone morphogenetic protein 4; BSA, bovine serum albumin; cAMP, cyclic adenosine monophosphate; CNTF, ciliary Neurotrophic Factor; DAPT, N-[N-(3,5-Difluorophenacetyl)-L-alanyl]-S-phenylglycine t-butyl ester; DKK1, Dickkopf-1; DMEM-F12, Dulbecco's Modified Eagle Medium: Nutrient Mixture F-12; ESC, embryonic stem cells; FACS, fluorescent-activating cell sorting; FBS, fetal bovine serum; FGF2, fibroblast growth factor 2; FGF8, fibroblast growth factor 8; FGF9, fibroblast growth factor 9; FGF-A, fibroblast growth factor-acidic; FGF-R, fibroblast growth factor receptor; GMEM, Glasgow Modified Eagle Medium; IGF-1, insulin growth factor-1; iPSC, induced pluripotent stem cells; KSR, knockout serum replacement; NEAA, non-essential amino acids; NF200, Neurofilament-200; NFM, Neurofilament-M; PDL, poly-D-lysin; RA, retinoic acid; VEGFR, vascular endothelial growth factor receptor; VitA, vitamin A; SAG, Sonic Hedgehog agonist; SHH, Sonic Hedgehog; N.A., not applicable; No modif, same medium as the corresponding neuro-retinal medium.*

markers (BRN3B/TUJ1, RBPMS) developed neurite networks and displayed physiological properties associated with mature RGCs (Sluch et al., 2015). This particular reporter cell line contributed to the identification of three cell sub-populations, after Thy1 FAC-sorting and single cell RNA sequencing analysis. These sub-populations exhibited different levels of maturity and contained upregulated genes for neuronal outgrowth, neuronal function and axon guidance, from the earliest to the latest cell clusters, respectively (Daniszewski et al., 2018).

Currently, a considerable panel of novel *in vitro* 3D/2D stepwise differentiation protocols (**Table 2**) were designed (Meyer et al., 2011; Nakano et al., 2012; Zhong et al., 2014; Gill et al., 2016). A compelling 3D/2D stepwise differentiation protocol from human PSC lines achieved the isolation of structures displaying the characteristics of optic vesicle (OV)-like structures (Meyer et al., 2011). Self-formed cell aggregates from human iPS colonies were plated to form neural clusters and then manually picked up. RGCs were identified in floating OV-like structures mostly at the periphery of the structures, and characterized by several markers, such as BRN3a/b, βIII-TUBULIN, CALRETININ, and PAX6. This protocol has been nicely improved for the generation of photoreceptors in 3D retinal optic cup (OC)-like structures, recapitulating the developmental organization of retina *in vivo* (Zhong et al., 2014). RGCs, identified as BRN3- and Hu C/D-expressing cells were observed in the innermost zone of the laminated OC-like structures.

Studies focusing on the differentiation of RGCs, adapting this 3D/2D stepwise protocol have been recently reported allowing the identification of different types of RGCs based on morphological, phenotypic, and functional characteristics (Langer et al., 2018). Different RGC subtypes were determined by morphological features and single-cell RNA sequencing analysis confirmed the expression of subtype-specific markers. Among the identified RGC subtypes, the direction-selective ON-OFF RGCs, ON RGCs, α-RGCs and intrinsically photosensitive RGCs were presumptively observed (Langer et al., 2018).

Alternatively and based on previous mouse work, Nakano et al. (2012) initiated a relevant 3D-retinal differentiation approach, with self-forming of OC-like structures derived from human ESCs, based on their similar protocol for mouse ESCs (Eiraku et al., 2011). At early stages of development (around 24 days), the RGC population constituted the first-born cell population that gradually increased to form a distinct layer at the

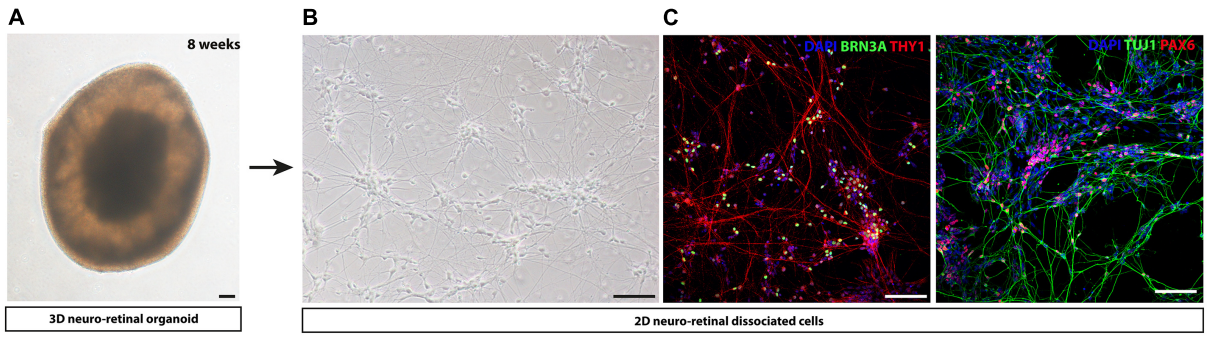

FIGURE 2 | Representative images of human iPS cell-derived RGCs by adapting protocol from Reichman et al. (2017). **(A)** Representative image of a self-organized 8-week-old 3D retinal organoid **(B)** Retinal cells dissociated from 8-week-old 3D retinal organoids observed using phase contrast microscopy. **(C)** Immunostaining on retinal cells dissociated from 8-week-old 3D retinal organoids reveal the expression of neuronal markers (THY1, TUJ1), retinal progenitor cell-associated marker (PAX6) and RGC-associated marker (BRN3A). Nuclei were counterstained by DAPI (blue). Scale bars: 100 μm.

most basal region of the human ESC-derived NR epithelium in 1 week. Many retinal differentiation strategies have been adapted from this pioneer "Nakano protocol" to study functional axonal extensions (Maekawa et al., 2015; Tanaka et al., 2015, 2016; Völkner et al., 2016; Yokoi et al., 2017; Kobayashi et al., 2018).

An innovative strategy bypassing EB formation, addition of Matrigel and other exogenous factors has been developed for different human iPSC lines (Reichman et al., 2014). Overgrowing iPSCs in absence of pluripotency factor FGF2 and in presence of proneural supplements such as N2 and/or B27, could generate self-forming neuro-retinal structures. Maintenance of the isolated retinal organoids in long-term floating culture with B27 supplement allowed the differentiation of all retinal cell types including the RGC population, identified by BRN3A immunostaining. This protocol can be adapted in a xeno-free and feeder-free culture conditions (Reichman et al., 2017), compatible to a clinical setting allowing the production of cells of therapeutic interest. One example of 8-week-old retinal organoid is illustrated in **Figure 2A**. As previously described for the different strategies, the survival and maturation of RGCs can be promoted by a subsequent adherent cell culture step, seeding cells onto poly-D-lysine/laminin-coated plates after enzymatic dissociation of 8-week-old retinal organoids (**Figures 2B,C**).

Even though retinal organoids resume the self-generation of 3D structures with specific retinal cell types, some limitations exist to study the maturation of RGCs. Indeed, it has been clearly reported that the percentage of RGC gradually decreased *in vitro* as the culture was extended (Meyer et al., 2011; Nakano et al., 2012; Reichman et al., 2014). Floating culture of retinal organoids is a strong hindrance to axon growth outside the structure and the lack of projection targets should prevent the normal development of RGC and may induce their death, probably by apoptosis. Brain organoid technologies derived from pioneer work from (Lancaster et al., 2013) allow now the generation of organoids that can model the development of different human brain regions (Di Lullo and Kriegstein, 2017). Recent work from the group of P. Arlotta analyzed gene expression in over 80,000 individual cells from human brain organoids and found the presence of different clusters of neuronal-specific genes identified at 6 months of differentiation, including a cluster of retinal population-specific genes (Quadrato et al., 2017). Subclustering of the retinal cluster revealed that RGCs were observed in 55% of organoids, but no clear fasciculation of axons was observed, asking the question of the ability of RGC to form an optic nerve-like structure. Fusing retinal and brain organoids could be a way to model the specific optic nerve circuitry. An alternative strategy could be the development of specific device for axon fascicle formation allowing the formation of a RGC nerve organoid, as recently reported for hPSC-derived motoneurons (Kawada et al., 2017).

For the translation of iPSC technology to the clinics, transplantable cells should be purified into a homogenous RGC population isolated from mitotically active cells or residual undifferentiated iPSCs that could be teratogenic. As genetic engineering or viral labeling of the cells are not suitable for clinical applications, the identification of cell surface markers characterizing human PSC-derived RGCs is important. As for mouse RGCs isolated from post-natal retina (Barres et al., 1988) or derived from mouse PSCs (Parameswaran et al., 2015), the CD90 (THY1) cell surface marker has been recently used to select human PSC-derived RGCs (Gill et al., 2016; Kobayashi et al., 2018).

Based on "Lamba protocol" (Lamba et al., 2006), Gill et al. (2016) used a magnetic-activated cell sorting (MACS) strategy, with microbeads coupled with a CD90 antibody and demonstrated that MACS enrichment yielded 77 ±9% THY1-positive cells, while less than 5% of the differentiating EB-dissociated cells (around 30–45 days of differentiation) expressed THY1 in the culture. Transcriptome analysis and electrophysiological recordings revealed similarity of enriched human ESC-derived RGCs to RGCs *in vivo* (Gill et al., 2016). Another selection strategy of RGCs derived from human iPSCs, adapted from the "Nakano protocol" (Nakano et al., 2012), was achieved with a CD90-based immunopanning of the retinal cell population (Kobayashi et al., 2018). Surprisingly, the BRN3B-positive RGCs collected at older stages of maturation (around 90–110 days) extended longer neurites compared to RGCs at earlier stages (70–90 days).

TABLE 3 | Published PSC lines carrying mutation for optic neuropathies and disease modeling studies/PSC-derived pathological models for optic neuropathies.

Clinical diagnosis	Gene	Mutation	Cell type origin	Reprogrammation	Differentiated cells	Reference
Glaucoma	OPTINEURIN	E50K	PBMCs (Blood)	Sendai Virus (OKSM)	Neurons	Minegishi et al., 2013
Glaucoma	TBK1	780 kb duplication 12q14	Fibroblasts	Sendai Virus (OKSM)	RGCs	Tucker et al., 2014
Glaucoma	OPTINEURIN	E50K	Fibroblasts	mRNA (OKSM)	RGCs	Ohlemacher et al., 2016
Glaucoma	CYP1B1	c.1403_1429dup	Fibroblasts	Sendai Virus (OKSM)	N.A.	Bolinches-Amorós et al., 2018
Glaucoma	SIX6	rs33912345; C > A; His141Asn	PBMCs (Blood)	Retrovirus (OKSM)	N.A.	Teotia et al., 2017
DOA	OPA1	intron24 c.2496+1 G > T	Fibroblasts	Retrovirus (OKSM)	RGCs	Chen et al., 2016
DOA	OPA1	c1861 C > T; p.Gln621Ter	Fibroblasts	Sendai Virus (OKSM)	N.A.	Galera-Monge et al., 2016
DOA	OPA1	c.610+364G > A, c.1311A > G het.	Fibroblasts	Episomal (OKSM)	N.A.	Hauser et al., 2016
LHON	MT-ND6	14484 T to C	Fibroblasts	Retrovirus (OKSM)	RPE	Zahabi et al., 2012
LHON	MT-ND4	m.11778G > C	Fibroblasts	Episomal (OKSM/Lin28/ shRNAp53)	RGCs	Hung et al., 2016; Wong et al., 2017
	MT-ND1/MT-ND6	m.4160T > C/m. 14484T > C	Fibroblasts			
LHON	MT-ND4	m.11778G > A	PBMCs (Blood)	Sendai Virus (OKSM)	N.A.	Lu et al., 2018
LHON	MT-ND4	m.11778G > A	PBMCs (Blood)	Sendai Virus (OKSM)	RGCs	Wu et al., 2018
Optic atrophy (Wolfram syndrome)	CISD2	c.103+1 G > A (hom; & het.)	Fibroblasts	Episomal (OKSM/Lin28)	N.A.	La Spada et al., 2018

All these data reporting, selection, maturation and/or functional assessment of human PSC-derived RGCs should allow to study patient-derived iPSC lines, for a better understanding of ocular disease related to RGC impairment. In this context, different groups have already derived iPSCs from somatic cells of patients diagnosed for different optic neuropathies (Chen et al., 2016; Ohlemacher et al., 2016; Teotia et al., 2017; Wong et al., 2017) (**Table 3**). For example, the generation of LHON-patient iPSC allowed the exploration of oxidative phosphorylation defect (Hung et al., 2016). In a more recent study, the same group demonstrated that replacing LHON mitochondrial DNA using cybrid technology in patient iPSCs can prevented the death of iPSC-derived RGCs (Wong et al., 2017). Another iPSC line carrying mutation in the *Optineurin* (*OPTN*) gene has been recently derived (Ohlemacher et al., 2016) and higher cell death of iPSC-derived RGCs carrying the mutation has been observed. iPSCs derived from a DOA-patient carrying an *OPA1* mutation was also reported and these mutated iPSCs were unable to correctly differentiate into RGCs and exhibited signs of apoptosis compared to free-mutation iPSCs (Chen et al., 2016).

OPTIC NEUROPATHIES AND CELL THERAPY: CELL REPLACEMENT STRATEGIES

Two major strategies can be developed to regenerate the optic nerve. One strategy aims to promote survival of remaining RGCs and regrowth of residual axons; the other strategy deals with the replacement of lost RGCs derived from different cell types, mainly from PSCs. The second one is probably more challenging but should have the advantage to be suitable for patients with very few remaining endogenous RGCs and both strategies are not exclusive. Co-administration of neurotrophic factors with transplantation of PSC-derived RGCs could be envisaged to favor both survival and axonal growth of both endogenous and exogenous RGCs.

With regards to glaucoma, some strategies aiming at transplanting mesenchymal stem cells (MSCs) and/or stem cell-derived trabecular meshwork cells with the questionable purpose to improve the drainage of aqueous humor and the control of IOP (Chamling et al., 2016; Yun et al., 2016; Zhu et al., 2016). This review is essentially focused on cell therapy approaches for the replacement of RGC and/or regeneration of the optic nerve. Therefore, literature covering transplantation of cell-derived trabecular meshwork cells will not be further detailed. Different cell types have been used to address the issue of RGC replacement. Even though PSCs are currently considered as the most promising source of cells for cell replacement, some proof of concept and informative studies reporting retinal transplantation feasibility have been performed with other cell types, such as RGC precursors or adult neural stem cells.

Non-pluripotent Stem Cells

Transplantation of embryonic or young postnatal RGC isolated from embryonic retina of green fluorescent protein (GFP)-mice showed the presence of GFP-positive cells in the retina of axotomized adult rats (Hertz et al., 2014; Venugopalan et al., 2016). Despite a low percentage of successful transplantation (around 10%), some engrafted GFP-positive cells harbored neurite elongation on the retinal surface with diverse dendrite architecture. Interestingly, recording engrafted cells revealed a response to light indicating a functional integration of grafted RGCs into the retinal circuitry (Venugopalan et al., 2016).

Other pioneer works have been performed with adult neural stem cells isolated from the hippocampus and expanded *in vitro*, showing that intravitreal injections of these cells can result in integration at some extend in young neonatal retina (Takahashi et al., 1998; Suzuki, 2003; Van Hoffelen et al., 2003) or dystrophic retina (Young et al., 2000; Mellough et al., 2004) but not in normal adult retina (Young et al., 2000). Interestingly, Mellough et al. (2004) reported the presence of grafted cells 4 and 8 weeks after intravitreal injection in the RGC layer of RGC-depleted mouse retina by previous intraocular administration of *N*-methyl-D-aspartate (NMDA). Even if the authors failed to detect the expression of specific RGC markers such as Brn3b, grafted cells were immunoreactive for a neuronal-specific marker β3-tubulin, suggesting that the *in vivo* neural maturation of grafted cells was possible.

Depending on the species, different endogenous neurogenic sources allow the generation of all retinal cell types in adults and Muller glial cells (MGC) have been of particular interest (Jadhav et al., 2009; Fischer and Bongini, 2010; Ramachandran et al., 2010; Goldman, 2014). Notably, mature adult MGCs have shown to maintain some characteristics of mammalian retinal progenitors (Reichenbach and Bringmann, 2013; Surzenko et al., 2013) after ectopic expression of Ascl1 (Pollak et al., 2013; Ueki et al., 2015) and have the potential to be amplified *in vitro* (Limb et al., 2002; Lawrence et al., 2007). For this reason, MGCs have been considered a good candidate for retinal transplantation and surprisingly, MGCs can efficiently differentiate into RGC-like cells *in vitro* after ectopic expression of key factors favoring RGC fate (Song et al., 2013, 2016) or in presence of FGF2 and a Notch pathway inhibitor (Singhal et al., 2012). Transplantation of these MGC-derived RGC-like cells in NMDA-injured rat retina, revealed a few cells expressing RGC markers like Isl1 in the host RGC layer, 4 weeks after transplantation. A modest functional improvement was observed while grafted cells failed to extend long processes toward the optic disk reflecting a neuroprotective effect. Similar results have been also obtained with RGC-like cells derived from feline MGCs (Becker et al., 2016).

Pluripotent Stem Cells

Different groups have explored the ability of mouse ESC-derived neural progenitors (NPs) to integrate and differentiate into the retina. Using GFP-expressing ESC-derived NPs, Meyer et al. (2006) reported the presence of GFP-positive cells with RGC-like morphology in the ganglion cell layer (GCL), 16 weeks after intravitreal injection in mouse model of Batten disease, characterized by neuronal lost in many regions of the CNS, including the retina. Similar results have been obtained after intraocular injection of mouse ESC-derived NPs into young post-natal rats without any retinal lesion (Jagatha et al., 2009). The immature state of the host retina may account for the ability for some transplanted cells to integrate into the retina as previously reported with embryonic NPs (Van Hoffelen et al., 2003).

Focusing on RGC degeneration, retinal-like structures derived from GFP-expressing mouse ESCs have been injected in RGC-depleted mouse retina (Aoki et al., 2008). In this condition, the presence of ESC-derived retinal cells expressing some RGC markers (Tuj1 or Brn3a) can be observed in the remaining GCL of NMDA-injured retina. However, the main limitation of these different studies is the weak characterization of the injected cells, as illustrated by teratoma formation in half of the animals (Aoki et al., 2008), a potential risk also reported with injection of mouse ESC-derived retinal progenitors (Cui et al., 2013). In order to address this issue, developing strategies to deplete the transplantable cell population from PSCs is required. One strategy aiming at forcing the differentiation of mouse iPSCs into RGC-like cells has been developed by overexpressing *Atoh7* before transplantation (Chen et al., 2010). In this condition, 2 weeks after transplantation into NMDA-injured adult mouse retina, RGC-like cells were found in the vitreous, close to the retinal surface, but never integrated into the retina. An excessive stage of differentiation of engrafted cells may explain integration failure, highlighting the importance of the differentiation stage for cell therapy. A more recent study using GFP-expressing ESC-derived NPs has assessed the functionality of injected cells in two different models of RGC degeneration (DBA/2J mice and NMDA-injured retina) (Divya et al., 2017). The authors showed a modest integration of grafted cells in both models and a relative improvement of visual function only in NMDA-injected mice. The phenotype of integrated cells was not precisely characterized but according to the authors, c-fos immunoreactivity of the transplanted cells could suggest functional integration in the retinal circuitry. Additionally, no projection into the optic nerve from GFP-positive transplanted cells was observed, suggesting, as also reported by Satarian et al. (2013), that grafted cells could provide a neuroprotective support limiting the cell death induced by NMDA, which could explain the functional benefit observed. The authors hypothesized that integration failure of injected cells in DBA2J mice could be due to an inherent high IOP.

Cell sorting methods based on the expression of specific cell-surface markers allow the enrichment of a cell type of interest. They represent an improvement in order to transplant an homogenous and well-characterized cell population, devoid of PSCs. Parameswaran et al. (2015) performed transplantation of mouse PSC-derived Thy1-positive RGC-like cells after isolation carried out using MACS method and anti-mouse CD90.2 (Thy1.2) magnetic particles. Immunohistochemical analysis 2–4 weeks after transplantation in a rat model of glaucomatous neuropathy with high IOP revealed the presence of few cells expressing two RGC markers, Brn3b and β3-tubulin, in the host retina (Parameswaran et al., 2015).

Altogether, these data collected using mouse ESC or iPSC-derived neural or retinal cells are promising even if their interpretation may be reconsidered to some extent in view of recent data observed after allogenic transplantation of photoreceptors. Indeed, refinement in the follow-up of injected cells has revealed that material transfer or exchange between donor and host cells can be observed rather than real donor cell integration (Pearson et al., 2016; Santos-Ferreira et al., 2016; Singh et al., 2016; Waldron et al., 2018).

Transplantation of human PSC-derived RGCs is currently poorly documented. Banin et al. (2006) have been the first to test the ability of transplanted human ESC derivatives, i.e., NPs, to survive and integrate into the rat retina after injection either in the subretinal space or in to vitreous (Banin et al., 2006).

Transplanted cells expressed some key regulator genes of retinal development such as VSX2 and PAX6 and the authors hypothesized that microenvironment would help transplanted cells to differentiate into retinal neurons. Few transplanted cells can be detected in the host GCL but their precise phenotype was not explored further. Similar observation has been reported by Lamba et al. (2009), after intravitreally injection of uncharacterized human ESC-derived retinal cells in neonatal mice (Lamba et al., 2009). Since their study was mainly dedicated to the integration of photoreceptor-like cells in a model of outer retina impairment, the phenotype of cells integrated into the inner retina was not more detailed.

An alternative approach using engineering biomaterials has been recently reported, where human iPSC-derived RGCs were seeded on a biodegradable poly lactic-co-glycolic acid (PLGA) scaffold. According to morphological and functional criteria, *in vitro* analysis revealed nice differentiation and maturation of iPSC-derived RGCs after seeding on PLGA scaffold. Implantation of the engineered human RGC-scaffold biomaterial by posterior sclerotomy in both rabbit and monkey retina did not revealed any sign of rejection; unfortunately, the phenotype of survival cells has not been explored further (Li et al., 2017). Since attachment of grafted cells precisely onto the surface of the host retina is critical, the use of an RGC-scaffold biomaterial should limit the diffusion of engrafted cells in the vitreous.

Despite the high potential of human PSCs for cell therapy application, some obstacles linked to intrinsic properties of PSCs represent some impediment to the development of cell therapy. Because these cells have the faculty to generate tumors, all efforts have to be done to eliminate any remaining PSCs from the transplantable cell population (Conesa et al., 2012; Lee et al., 2013). Methodological improvement and cell-sorting methods allowing the generation and isolation of well-characterized cells of interest will also improve the safety.

RGC DISORDERS: CELL THERAPY AND THE CHALLENGE OF OPTIC NERVE REGENERATION

Significant progress has been performed to provide cell sources suitable for transplantation approaches. However, all these efforts would be useless if in parallel any progress could be done concerning the ability of neurons, e.g., RGCs, to regenerate their axon in adult, allowing rewiring of visual pathways. Important progress has also been realized regarding this issue and extensively reported in different reviews (Fischer and Leibinger, 2012; Crair and Mason, 2016; Leibinger et al., 2016; Benowitz et al., 2017; Laha et al., 2017).

Endogenous Regeneration Capacity

Glial cells have multiple role during degenerative and regenerative process. Oligodendrocytes, the myelinated cells of the CNS express different inhibitory factors for axon regrowth (Geoffroy and Zheng, 2014) and removing myelin-associated proteins such as NOGO enhances optic nerve regeneration (Fischer et al., 2004; Schwab, 2004). Injury-induced glial scar or more generally gliosis constitute also a hindrance to axon outgrowth (Koprivica et al., 2005; Qu et al., 2010; Usher et al., 2010; Nickells et al., 2012), even though some evidence of positive effect of gliosis on neuronal survival and regenerative process have been reported (Leibinger et al., 2009; Benowitz et al., 2017; Laha et al., 2017). Different intrinsic modifications after developmental phase contribute also to axon outgrowth limitation (Goldberg et al., 2002). For example, deletion of cytokine signaling 3 (SOCS3), transcription factor KLF4 or Phosphatase and tensin homolog (PTEN), a negative regulator of the mammalian target or rapamycin (mTOR) have been shown to strongly stimulate axon regeneration after optic nerve injury (Park et al., 2008; Smith et al., 2009; Sun et al., 2011). Interestingly, axon outgrowth was virtually absent beyond the optic chiasm after optic nerve injury.

Manipulation of the environment can also promote axon regeneration, as demonstrated for example by the co-administration of Osteopontin and IGF-1 for a specific subtype of RGCs (Duan et al., 2015). Oncomodulin, a macrophage-secreted factor can also promote axon regeneration (Yin et al., 2006, 2009) and combined with a cAMP analog and PTEN deletion, de Lima et al. (2012) have been able to demonstrate a full-length axon regeneration after optic nerve injury associated with a transitory visual function recovery. Finally, we can cited exogenous electrical activity as an important process for RGC survival and regeneration (Goldberg et al., 2002; Morimoto, 2012; Lim et al., 2016). Interestingly, many of these processes are complementary, as recently demonstrated by the combination of enhancement of electric activity with PTEN/SOCS3 deletion or osteopontin, IGF-1 and CNTF delivery via Adeno-associated virus injection, that led to an important RGC regeneration and visual function enhancement (Bei et al., 2016).

Recent progress that make possible long-length axon regeneration is considerably promising but leads also to new challenges. Rewiring visual pathways will enable some restoration of visual function only if axons terminals reach their target respecting the topographical arrangement of visual projections (Lemke and Reber, 2005; Huberman et al., 2008; Assali et al., 2014; Lim et al., 2016; Kuwajima et al., 2017; Ito and Feldheim, 2018). In the same way, transplanted RGCs have to connect retinal partners, i.e., bipolar and amacrine cells with regard to precise partners (Seung and Sümbül, 2014; Demb and Singer, 2015; Mauss et al., 2017) in order to send a pertinent signal to high-order visual structures.

Cell Transplantation – Axon Regeneration Support

Because cell replacement for RGC disorders can appear unrealistic short term, some groups aim at developing cell-based therapies suitable for neuroprotective and regenerative support to endogenous RGCs (Johnson et al., 2011). Different cell sources have been tested for this purpose (Mead et al., 2015) but MSCs are probably one of the best candidates. MSCs are unable to differentiate into retinal cells and to integrate into the retina (Hill et al., 2009) but have been reported to operate paracrine activity supporting RGC neuroprotection in some models of

RGC injury (Yu et al., 2006; Johnson et al., 2010; Levkovitch-Verbin et al., 2010; Harper et al., 2011; Paul and Anisimov, 2013; Teixeira et al., 2013; Mesentier-Louro et al., 2014; Mead et al., 2015, 2016; Ding et al., 2017). This neuroprotective effect has been attributed alternatively to Platelet-derived growth factor, NGF, BDNF, or Neurotrophin-3 secretion (Johnson et al., 2011, 2014; Mead et al., 2013; Osborne et al., 2018). Interestingly, this trophic support was reported to affect both RGC survival and axon regeneration. Microvesicles released by MSCs could also mediate in part the neuroprotective effect of these cells (Yu et al., 2014; Yang T.C. et al., 2017), by the delivery of specific neutrophic factor and/or miRNAs (Mead and Tomarev, 2017; Mead et al., 2018). Finally, in agreement with the role of inflammation in optic nerve regeneration (Yin et al., 2006, 2009; Hauk et al., 2010), modulation of immune and inflammatory responses has been partially attributed to MSCs (Lee et al., 2015; Mac Nair and Nickells, 2015).

iPSC-derived NPs are also believed to deliver neuroprotective support (Satarian et al., 2013). Functional and histological analysis showed some protection due to intraocular injection of iPSC-derived NPs, few days after optic nerve crush (Satarian et al., 2013). Histological analysis revealed the presence of engrafted cells in the GCL immunoreactive for pan-neuronal markers (Neurofilament, microtubule-associated protein 2) but without long distance neurite outgrowth. This observation led the authors to attribute the functional benefit to the secretion of neurotrophic factors instead of cell integration, strengthened by *in vitro* release of CNTF, FGF2, and IGF-1 by the iPSC-derived NPs (Satarian et al., 2013).

PERSPECTIVES AND FUTURE DIRECTIONS

Much progress has been made toward differentiating human PSCs into RGCs thanks to our knowledge of *in vivo* retinal development. Even though the majority of the RGC differentiation protocols described above use animal-derived products some of these protocols have been adapted to a completely defined xeno-free system (Sridhar et al., 2013; Lee et al., 2016; Reichman et al., 2017) for the generation of GMP-compliant RGCs compatible for transplantation. Another key issue for a future stem cell-based therapy is the purification of donor cell type with elimination of contaminating cells; a strategy that has been started by targeting the cell surface antigen THY1 to isolate an homogenous population of RGCs (Gill et al., 2016). With protocols developed to generate highly enriched populations of human RGCs, further *in vivo* transplantation studies are required to understand how grafted RGCs can integrate into the GCL. RGC transplantation pose other significant challenges: (i) connecting RGC dendrites with presynaptic amacrine and bipolar cells in host retina; (ii) extending RGC axons radially to the optic nerve head and (iii) targeting the central nervous system through the optic nerve tract. Attachment of grafted cells precisely onto the surface of host retina is therefore critical. The absence of physical support for injected cells is also a possible limitation for their survival and correct axon regeneration, as recently demonstrated with the use of biomaterial or synthetic polymers to orientate RGC axon growth *in vitro* (Kador et al., 2014; Sluch et al., 2015; Li et al., 2017; Yang Y. et al., 2017). Introducing a RGC-scaffold biomaterial into the eye is technically challenging, compared to simple injection of cells into the vitreous cavity. Nevertheless, successful transplantation of engineered RGC-scaffold biomaterial has been reported recently in monkey eyes (Li et al., 2017), paving the way of the generation and transplantation of complex 3D bio-scaffolds. In this context, combining the use of specific scaffolds and 3D bioprinting has the potential to control RGC positioning. Recent papers, demonstrated that RGCs can be successfully printed without loss of viability and some phenotypic features, such as neurite outgrowth and electrophysiological responses (Lorber et al., 2014; Kador et al., 2016). Further advances in bioprinting research, particularly with the use of neurons that cannot be easily manipulated by printing, should facilitated the development of novel cell therapies aiming at promoting neural regeneration, that could be used for RGC replacement in different ocular diseases.

Lastly, the rejection of grafted cells inherent to transplantation approaches remains an important challenge for cell therapy targeting RGCs. Producing specific patient iPSCs and autologous transplantation should bypass the problem of immune rejection but this customized cell therapy is extremely expensive and time-consuming. Alternatively, the development of a bank of iPSC lines designed to match the human leukocyte antigen (HLA) cell type should limit immune cell response and reduce the financial cost.

Whilst many challenges remain, the exciting progress made in these pioneering studies offer a hope for patients with untreatable advanced-stages RGC disorders. Improvement of RGC production from PSCs and regenerative technologies offer the opportunity to consider the replacement of lost cells and visual restoration, not only stabilization of the remaining visual acuity.

AUTHOR CONTRIBUTIONS

All authors participated in the conception of the review and literature search. GO wrote the first draft of the manuscript. OR and OG wrote sections of the manuscript and prepared the tables. OR and GO prepared the figures. All authors approved the final version.

REFERENCES

Aghaizu, N. D., Kruczek, K., Gonzalez-Cordero, A., Ali, R. R., and Pearson, R. A. (2017). *Pluripotent Stem Cells and their Utility in Treating Photoreceptor Degenerations*, 1st Edn. Amsterdam: Elsevier B.V, doi: 10.1016/bs.pbr.2017.01.001

Alexander, C., Votruba, M., Pesch, U. E., Thiselton, D. L., Mayer, S., Moore, A., et al. (2000). OPA1, encoding a dynamin-related GTPase, is mutated in autosomal

dominant optic atrophy linked to chromosome 3q28. *Nat. Genet.* 26, 211–215. doi: 10.1038/79944

Alhadeff, P. A., De Moraes, C. G., Chen, M., Raza, A. S., Ritch, R., and Hood, D. C. (2017). The association between clinical features seen on fundus photographs and glaucomatous damage detected on visual fields and optical coherence tomography scans. *J. Glaucoma* 26, 498–504. doi: 10.1097/IJG.0000000000000640

Allingham, R. R., Liu, Y., and Rhee, D. J. (2009). The genetics of primary open-angle glaucoma: a review. *Exp. Eye Res.* 88, 837–844. doi: 10.1016/j.exer.2008.11.003

Almasieh, M., Wilson, A. M., Morquette, B., Cueva Vargas, J. L., and Di Polo, A. (2012). The molecular basis of retinal ganglion cell death in glaucoma. *Prog. Retin. Eye Res.* 31, 152–181. doi: 10.1016/j.preteyeres.2011.xyb11.002

Anderson, D. R., and Hendrickson, A. (1974). Effect of intraocular pressure on rapid axoplasmic transport in monkey optic nerve. *Invest. Ophthalmol.* 13, 771–783.

Aoki, H., Hara, A., Niwa, M., Motohashi, T., Suzuki, T., and Kunisada, T. (2007). An in vitro mouse model for retinal ganglion cell replacement therapy using eye-like structures differentiated from ES cells. *Exp. Eye Res.* 84, 868–875. doi: 10.1016/j.exer.2007.01.007

Aoki, H., Hara, A., Niwa, M., Motohashi, T., Suzuki, T., and Kunisada, T. (2008). Transplantation of cells from eye-like structures differentiated from embryonic stem cells in vitro and in vivo regeneration of retinal ganglion-like cells. *Graefes Arch. Clin. Exp. Ophthalmol.* 246, 255–265. doi: 10.1007/s00417-007-0710-6

Arroyo, D. A., and Feller, M. B. (2016). Spatiotemporal features of retinal waves instruct the wiring of the visual circuitry. *Front. Neural Circuits* 10:54. doi: 10.3389/fncir.2016.00054

Assali, A., Gaspar, P., and Rebsam, A. (2014). Activity dependent mechanisms of visual map formation - From retinal waves to molecular regulators. *Semin. Cell Dev. Biol.* 35, 136–146. doi: 10.1016/j.semcdb.2014.08.008

Badea, T. C., Cahill, H., Ecker, J., Hattar, S., and Nathans, J. (2009). Distinct roles of transcription factors brn3a and brn3b in controlling the development, morphology, and function of retinal ganglion cells. *Neuron* 61, 852–864. doi: 10.1016/j.neuron.2009.01.020

Balaratnasingam, C., Morgan, W. H., Bass, L., Matich, G., Cringle, S. J., and Yu, D.-Y. (2007). Axonal transport and cytoskeletal changes in the laminar regions after elevated intraocular pressure. *Invest. Ophthalmol. Vis. Sci.* 48, 3632–3644. doi: 10.1167/iovs.06-1002

Banin, E., Obolensky, A., Idelson, M., Hemo, I., Reinhardtz, E., Pikarsky, E., et al. (2006). Retinal incorporation and differentiation of neural precursors derived from human embryonic stem cells. *Stem Cells* 24, 246–257. doi: 10.1634/stemcells.2005-0009

Barres, B. A., Silverstein, B. E., Corey, D. P., and Chun, L. L. (1988). Immunological, morphological, and electrophysiological variation among retinal ganglion cells purified by panning. *Neuron* 1, 791–803. doi: 10.1016/0896-6273(88)90127-4

Bassett, E. A., and Wallace, V. A. (2012). Cell fate determination in the vertebrate retina. *Trends Neurosci.* 35, 565–573. doi: 10.1016/j.tins.2012.05.004

Becker, S., Eastlake, K., Jayaram, H., Jones, M. F., Brown, R. A., McLellan, G. J., et al. (2016). Allogeneic transplantation of Müller-derived retinal ganglion cells improves retinal function in a feline model of ganglion cell depletion. *Stem Cells Transl. Med.* 5, 192–205. doi: 10.5966/sctm.2015-0125

Bei, F., Lee, H. H. C., Liu, X., Gunner, G., Jin, H., Ma, L., et al. (2016). Restoration of visual function by enhancing conduction in regenerated axons. *Cell* 164, 219–232. doi: 10.1016/j.cell.2015.11.036

Benowitz, L. I., He, Z., and Goldberg, J. L. (2017). Reaching the brain: advances in optic nerve regeneration. *Exp. Neurol.* 287, 365–373. doi: 10.1016/j.expneurol.2015.12.015

Boije, H., MacDonald, R. B., and Harris, W. A. (2014). Reconciling competence and transcriptional hierarchies with stochasticity in retinal lineages. *Curr. Opin. Neurobiol.* 27, 68–74. doi: 10.1016/j.conb.2014.02.014

Bolinches-Amorós, A., Lukovic, D., Castro, A. A., León, M., Kamenarova, K., Kaneva, R., et al. (2018). Generation of a human iPSC line from a patient with congenital glaucoma caused by mutation in CYP1B1 gene. *Stem Cell Res.* 28, 96–99. doi: 10.1016/j.scr.2018.01.004

Brown, N. L., Patel, S., Brzezinski, J., and Glaser, T. (2001). Math5 is required for retinal ganglion cell and optic nerve formation. *Development* 128, 2497–2508.

Calkins, D. J., Pekny, M., Cooper, M. L., and Benowitz, L. (2017). The challenge of regenerative therapies for the optic nerve in glaucoma. *Exp. Eye Res.* 157, 28–33. doi: 10.1016/j.exer.2017.01.007

Carelli, V., La Morgia, C., Ross-Cisneros, F. N., and Sadun, A. A. (2017). Optic neuropathies: the tip of the neurodegeneration iceberg. *Hum. Mol. Genet.* 26, R139–R150. doi: 10.1093/hmg/ddx273

Carnes, M. U., Liu, Y. P., Allingham, R. R., Whigham, B. T., Havens, S., Garrett, M. E., et al. (2014). Discovery and functional annotation of SIX6 variants in primary open-angle glaucoma. *PLoS Genet.* 10:e1004372. doi: 10.1371/journal.pgen.1004372

Cellerino, A., Carroll, P., Thoenen, H., and Barde, Y. A. (1997). Reduced size of retinal ganglion cell axons and hypomyelination in mice lacking brain-derived neurotrophic factor. *Mol. Cell. Neurosci.* 9, 397–408. doi: 10.1006/mcne.1997.0641

Cepko, C. (2014). Intrinsically different retinal progenitor cells produce specific types of progeny. *Nat. Rev. Neurosci.* 15, 615–627. doi: 10.1038/nrn3767

Chamling, X., Sluch, V. M., and Zack, D. J. (2016). The potential of human stem cells for the study and treatment of glaucoma. *Invest. Opthalmol. Vis. Sci.* 57, ORSFi1–ORSFi6. doi: 10.1167/iovs.15-18590

Chen, J., Riazifar, H., Guan, M.-X., and Huang, T. (2016). Modeling autosomal dominant optic atrophy using induced pluripotent stem cells and identifying potential therapeutic targets. *Stem Cell Res. Ther.* 7:2. doi: 10.1186/s13287-015-0264-1

Chen, M., Chen, Q., Sun, X., Shen, W., Liu, B., Zhong, X., et al. (2010). Generation of retinal ganglion-like cells from reprogrammed mouse fibroblasts. *Invest. Ophthalmol. Vis. Sci.* 51, 5970–5978. doi: 10.1167/iovs.09-4504

Chidlow, G., Ebneter, A., Wood, J. P. M., and Casson, R. J. (2011). The optic nerve head is the site of axonal transport disruption, axonal cytoskeleton damage and putative axonal regeneration failure in a rat model of glaucoma. *Acta Neuropathol.* 121, 737–751. doi: 10.1007/s00401-011-0807-1

Chihara, E., and Honda, Y. (1981). Analysis of orthograde fast axonal transport and nonaxonal transport along the optic pathway of albino rabbits during increased and decreased intraocular pressure. *Exp. Eye Res.* 32, 229–239. doi: 10.1016/0014-4835(81)90011-7

Chun, B. Y., and Rizzo, J. F. (2016). Dominant optic atrophy: updates on the pathophysiology and clinical manifestations of the optic atrophy 1 mutation. *Curr. Opin. Ophthalmol.* 27, 475–480. doi: 10.1097/ICU.0000000000000314

Conesa, C., Doss, M. X., Antzelevitch, C., Sachinidis, A., Sancho, J., and Carrodeguas, J. A. (2012). Identification of specific pluripotent stem cell death–inducing small molecules by chemical screening. *Stem Cell Rev.* 8, 116–127. doi: 10.1007/s12015-011-9248-4

Crair, M. C., and Mason, C. A. (2016). Reconnecting eye to brain. *J. Neurosci.* 36, 10707–10722. doi: 10.1523/JNEUROSCI.1711-16.2016

Crish, S. D., Sappington, R. M., Inman, D. M., Horner, P. J., and Calkins, D. J. (2010). Distal axonopathy with structural persistence in glaucomatous neurodegeneration. *Proc. Natl. Acad. Sci. U.S.A.* 107, 5196–5201. doi: 10.1073/pnas.0913141107

Cui, L., Guan, Y., Qu, Z., Zhang, J., Liao, B., Ma, B., et al. (2013). WNT signaling determines tumorigenicity and function of ESC-derived retinal progenitors. *J. Clin. Invest.* 123, 1647–1661. doi: 10.1172/JCI65048

da Cruz, L., Fynes, K., Georgiadis, O., Kerby, J., Luo, Y. H., Ahmado, A., et al. (2018). Phase 1 clinical study of an embryonic stem cell-derived retinal pigment epithelium patch in age-related macular degeneration. *Nat. Biotechnol.* 36, 328–337. doi: 10.1038/nbt.4114

Daliri, K., Ljubimov, A. V., and Hekmatimoghaddam, S. (2017). Glaucoma, stem cells, and gene therapy: where are we now? *Int. J. Stem Cells* 10, 119–128. doi: 10.15283/ijsc17029

Daniszewski, M., Senabouth, A., Nguyen, Q. H., Crombie, D. E., Lukowski, S. W., Kulkarni, T., et al. (2018). Single cell RNA sequencing of stem cell-derived retinal ganglion cells. *Sci. Data* 5:180013. doi: 10.1038/sdata.2018.13

de Lima, S., Koriyama, Y., Kurimoto, T., Oliveira, J. T., Yin, Y., Li, Y., et al. (2012). Full-length axon regeneration in the adult mouse optic nerve and partial recovery of simple visual behaviors. *Proc. Natl. Acad. Sci. U.S.A.* 109, 9149–9154. doi: 10.1073/pnas.1119449109

Delettre, C., Lenaers, G., Griffoin, J. M., Gigarel, N., Lorenzo, C., Belenguer, P., et al. (2000). Nuclear gene OPA1, encoding a mitochondrial dynamin-related protein, is mutated in dominant optic atrophy. *Nat. Genet.* 26, 207–210. doi: 10.1038/79936

Demb, J. B., and Singer, J. H. (2015). Functional circuitry of the retina. *Annu. Rev. Vis. Sci.* 1, 263–289. doi: 10.1146/annurev-vision-082114-035334

Demer, J. L., Clark, R. A., Suh, S. Y., Giaconi, J. A., Nouri-Mahdavi, K., Law, S. K., et al. (2017). Magnetic resonance imaging of optic nerve traction during adduction in primary open-angle glaucoma with normal intraocular pressure. *Invest. Ophthalmol. Vis. Sci.* 58, 4114–4125. doi: 10.1167/iovs.17-22093

Deng, F., Chen, M., Liu, Y., Hu, H., Xiong, Y., Xu, C., et al. (2016). Stage-specific differentiation of iPSCs toward retinal ganglion cell lineage. *Mol. Vis.* 22, 536–547.

Dengler-Crish, C. M., Smith, M. A., Inman, D. M., Wilson, G. N., Young, J. W., and Crish, S. D. (2014). Anterograde transport blockade precedes deficits in retrograde transport in the visual projection of the DBA/2J mouse model of glaucoma. *Front. Neurosci.* 8:290. doi: 10.3389/fnins.2014.00290

Di Lullo, E., and Kriegstein, A. R. (2017). The use of brain organoids to investigate neural development and disease. *Nat. Rev. Neurosci.* 18, 573–584. doi: 10.1038/nrn.2017.107

Di Polo, A., Aigner, L. J., Dunn, R. J., Bray, G. M., and Aguayo, A. J. (1998). Prolonged delivery of brain-derived neurotrophic factor by adenovirus-infected Müller cells temporarily rescues injured retinal ganglion cells. *Proc. Natl. Acad. Sci. U.S.A.* 95, 3978–3983. doi: 10.1073/pnas.95.7.3978

Ding, S. L. S., Kumar, S., and Mok, P. L. (2017). Cellular reparative mechanisms of mesenchymal stem cells for retinal diseases. *Int. J. Mol. Sci.* 18:1406. doi: 10.3390/ijms18081406

DiStefano, T., Chen, H. Y., Panebianco, C., Kaya, K. D., Brooks, M. J., Gieser, L., et al. (2018). Accelerated and improved differentiation of retinal organoids from pluripotent stem cells in rotating-wall vessel bioreactors. *Stem Cell Rep.* 10, 300–313. doi: 10.1016/j.stemcr.2017.11.001

Divya, M. S., Rasheed, V. A., Schmidt, T., Lalitha, S., Hattar, S., and James, J. (2017). Intraocular injection of ES cell-derived neural progenitors improve visual function in retinal ganglion cell-depleted mouse models. *Front. Cell. Neurosci.* 11:295. doi: 10.3389/fncel.2017.00295

Duan, X., Qiao, M., Bei, F., Kim, I.-J., He, Z., and Sanes, J. R. (2015). Subtype-specific regeneration of retinal ganglion cells following axotomy: effects of osteopontin and mTOR signaling. *Neuron* 85, 1244–1256. doi: 10.1016/j.neuron.2015.02.017

Eiraku, M., Takata, N., Ishibashi, H., Kawada, M., Sakakura, E., Okuda, S., et al. (2011). Self-organizing optic-cup morphogenesis in three-dimensional culture. *Nature* 472, 51–56. doi: 10.1038/nature09941

Elliott, J., Jolicoeur, C., Ramamurthy, V., and Cayouette, M. (2008). Ikaros confers early temporal competence to mouse retinal progenitor cells. *Neuron* 60, 26–39. doi: 10.1016/j.neuron.2008.08.008

Fahy, E. T., Chrysostomou, V., and Crowston, J. G. (2016). Mini-review: impaired axonal transport and glaucoma. *Curr. Eye Res.* 41, 273–283. doi: 10.3109/02713683.2015.1037924

Fischer, A. J., and Bongini, R. (2010). Turning Müller glia into neural progenitors in the retina. *Mol. Neurobiol.* 42, 199–209. doi: 10.1007/s12035-010-8152-2

Fischer, D., He, Z., and Benowitz, L. I. (2004). Counteracting the Nogo receptor enhances optic nerve regeneration if retinal ganglion cells are in an active growth state. *J. Neurosci.* 24, 1646–1651. doi: 10.1523/JNEUROSCI.5119-03.2004

Fischer, D., and Leibinger, M. (2012). Promoting optic nerve regeneration. *Prog. Retin. Eye Res.* 31, 688–701. doi: 10.1016/j.preteyeres.2012.06.005

Friedman, D. S., Wilson, M. R., Liebmann, J. M., Fechtner, R. D., and Weinreb, R. N. (2004). An evidence-based assessment of risk factors for the progression of ocular hypertension and glaucoma. *Am. J. Ophthalmol.* 138, S19–S31. doi: 10.1016/j.ajo.2004.04.058

Fuhrmann, S. (2010). Eye morphogenesis and patterning of the optic vesicle. *Curr. Top. Dev. Biol.* 93, 61–84. doi: 10.1016/B978-0-12-385044-7.00003-5

Fuhrmann, S., Zou, C., and Levine, E. M. (2014). Retinal pigment epithelium development, plasticity, and tissue homeostasis. *Exp. Eye Res.* 123, 141–150. doi: 10.1016/j.exer.2013.09.003

Galera-Monge, T., Zurita-Díaz, F., Moreno-Izquierdo, A., Fraga, M. F., Fernández, A. F., Ayuso, C., et al. (2016). Generation of a human iPSC line from a patient with an optic atrophy 'plus' phenotype due to a mutation in the *OPA1* gene. *Stem Cell Res.* 16, 673–676. doi: 10.1016/j.scr.2016.03.011

Gan, L., Xiang, M., Zhou, L., Wagner, D. S., Klein, W. H., and Nathans, J. (1996). POU domain factor Brn-3b is required for the development of a large set of retinal ganglion cells. *Proc. Natl. Acad. Sci. U.S.A.* 93, 3920–3925. doi: 10.1073/pnas.93.9.3920

Gehring, W. J. (2002). The genetic control of eye development and its implications for the evolution of the various eye-types. *Int. J. Dev. Biol.* 46, 65–73.

Geoffroy, C. G., and Zheng, B. (2014). Myelin-associated inhibitors in axonal growth after CNS injury. *Curr. Opin. Neurobiol.* 27, 31–38. doi: 10.1016/j.conb.2014.02.012

Gill, K. P., Hewitt, A. W., Davidson, K. C., Pébay, A., and Wong, R. C. B. (2014). Methods of retinal ganglion cell differentiation from pluripotent stem cells. *Transl. Vis. Sci. Technol.* 3:7. doi: 10.1167/tvst.3.3.7

Gill, K. P., Hung, S. S. C., Sharov, A., Lo, C. Y., Needham, K., Lidgerwood, G. E., et al. (2016). Enriched retinal ganglion cells derived from human embryonic stem cells. *Sci. Rep.* 6:30552. doi: 10.1038/srep30552

Goetz, J. J., Farris, C., Chowdhury, R., and Trimarchi, J. M. (2014). Making of a retinal cell: insights into retinal cell-fate determination. *Int. Rev. Cell Mol. Biol.* 308, 273–321. doi: 10.1016/B978-0-12-800097-7.00007-5

Goldberg, J. L., Espinosa, J. S., Xu, Y., Davidson, N., Kovacs, G. T. A., and Barres, B. A. (2002). Retinal ganglion cells do not extend axons by default: promotion by neurotrophic signaling and electrical activity. *Neuron* 33, 689–702. doi: 10.1016/S0896-6273(02)00602-5

Goldman, D. (2014). Müller glial cell reprogramming and retina regeneration. *Nat. Rev. Neurosci.* 15, 431–442. doi: 10.1038/nrn3723

González, F., Boué, S., and Izpisúa Belmonte, J. C. (2011). Methods for making induced pluripotent stem cells: reprogramming à la carte. *Nat. Rev. Genet.* 12, 231–242. doi: 10.1038/nrg2937

Goureau, O., Terray, A., Matho, K. S., Reichman, R., and Orieux, G. (2014). "Stem cells in the retina: regeneration and cell therapy," in *Stem Cell Biology and Regenerative Medecine*, eds C. H. Durand and P. Charbord (Aalborg: River Publishers), 549–573.

Graw, J. (2010). Eye development. *Curr. Top. Dev. Biol.* 90, 343–386. doi: 10.1016/S0070-2153(10)90010-0

Greco, A., Rizzo, M. I., De Virgilio, A., Gallo, A., Fusconi, M., and de Vincentiis, M. (2016). Emerging concepts in glaucoma and review of the literature. *Am. J. Med* 129, 1000.e7–1000.e13. doi: 10.1016/j.amjmed.2016.03.038

Harkema, L., Youssef, S. A., and de Bruin, A. (2016). Pathology of mouse models of accelerated aging. *Vet. Pathol.* 53, 366–389. doi: 10.1177/0300985815625169

Harper, M. M., Grozdanic, S. D., Blits, B., Kuehn, M. H., Zamzow, D., Buss, J. E., et al. (2011). Transplantation of BDNF-secreting mesenchymal stem cells provides neuroprotection in chronically hypertensive rat eyes. *Invest. Ophthalmol. Vis. Sci.* 52, 4506–4515. doi: 10.1167/iovs.11-7346

Harvey, A. R., Ooi, J. W. W., and Rodger, J. (2012). Neurotrophic factors and the regeneration of adult retinal ganglion cell axons. *Int. Rev. Neurobiol.* 106, 1–33. doi: 10.1016/B978-0-12-407178-0.00002-8

Hauk, T. G., Leibinger, M., Müller, A., Andreadaki, A., Knippschild, U., and Fischer, D. (2010). Stimulation of axon regeneration in the mature optic nerve by intravitreal application of the toll-like receptor 2 agonist Pam3Cys. *Invest. Ophthalmol. Vis. Sci.* 51, 459–464. doi: 10.1167/iovs.09-4203

Hauser, S., Schuster, S., Theurer, Y., Synofzik, M., and Schöls, L. (2016). Generation of optic atrophy 1 patient-derived induced pluripotent stem cells (iPS-OPA1-BEHR) for disease modeling of complex optic atrophy syndromes (Behr syndrome). *Stem Cell Res.* 17, 426–429. doi: 10.1016/j.scr.2016.09.012

Herrera, E., and Erskine, L. (2017). Guidance of retinal axons in mammals. *Semin. Cell Dev. Biol.* doi: 10.1016/j.semcdb.2017.11.027 [Epub ahead of print].

Hertz, J., Qu, B., Hu, Y., Patel, R. D., Valenzuela, D. A., and Goldberg, J. L. (2014). Survival and integration of developing and progenitor-derived retinal ganglion cells following transplantation. *Cell Transplant.* 23, 855–872. doi: 10.3727/096368913X667024

Hill, A. J., Zwart, I., Tam, H. H., Chan, J., Navarrete, C., Jen, L.-S., et al. (2009). Human umbilical cord blood-derived mesenchymal stem cells do not differentiate into neural cell types or integrate into the retina after intravitreal grafting in neonatal rats. *Stem Cells Dev.* 18, 399–409. doi: 10.1089/scd.2008.0084

Huang, L., Chen, M., Zhang, W., Sun, X., Liu, B., and Ge, J. (2018). Retinoid acid and taurine promote NeuroD1-induced differentiation of induced pluripotent stem cells into retinal ganglion cells. *Mol. Cell. Biochem.* 438, 67–76. doi: 10.1007/s11010-017-3114-x

Huberman, A. D., Feller, M. B., and Chapman, B. (2008). Mechanisms underlying development of visual maps and receptive fields. *Annu. Rev. Neurosci.* 31, 479–509. doi: 10.1146/annurev.neuro.31.060407.125533

Hung, S. S. C., Van Bergen, N. J., Jackson, S., Liang, H., Mackey, D. A. A., Hernández, D., et al. (2016). Study of mitochondrial respiratory defects on reprogramming to human induced pluripotent stem cells. *Aging* 8, 945–956. doi: 10.18632/aging.100950

Ikeda, H., Osakada, F., Watanabe, K., Mizuseki, K., Haraguchi, T., Miyoshi, H., et al. (2005). Generation of Rx+/Pax6+ neural retinal precursors from embryonic stem cells. *Proc. Natl. Acad. Sci. U.S.A.* 102, 11331–11336. doi: 10.1073/pnas.0500010102

Ito, S., and Feldheim, D. A. (2018). The mouse superior colliculus: an emerging model for studying circuit formation and function. *Front. Neural Circuits* 12:10. doi: 10.3389/fncir.2018.00010

Jadhav, A. P., Roesch, K., and Cepko, C. L. (2009). Development and neurogenic potential of Müller glial cells in the vertebrate retina. *Prog. Retin. Eye Res.* 28, 249–262. doi: 10.1016/j.preteyeres.2009.05.002

Jagatha, B., Divya, M. S., Sanalkumar, R., Indulekha, C. L., Vidyanand, S., Divya, T. S., et al. (2009). In vitro differentiation of retinal ganglion-like cells from embryonic stem cell derived neural progenitors. *Biochem. Biophys. Res. Commun.* 380, 230–235. doi: 10.1016/j.bbrc.2009.01.038

Jayakody, S. A., Gonzalez-Cordero, A., Ali, R. R., and Pearson, R. A. (2015). Cellular strategies for retinal repair by photoreceptor replacement. *Prog. Retin. Eye Res.* 46, 31–66. doi: 10.1016/j.preteyeres.2015.01.003

Jiang, Y., Ding, Q., Xie, X., Libby, R. T., Lefebvre, V., and Gan, L. (2013). Transcription factors SOX4 and SOX11 function redundantly to regulate the development of mouse retinal ganglion cells. *J. Biol. Chem.* 288, 18429–18438. doi: 10.1074/jbc.M113.478503

Jin, K., Jiang, H., Mo, Z., and Xiang, M. (2010). Early B-cell factors are required for specifying multiple retinal cell types and subtypes from postmitotic precursors. *J. Neurosci.* 30, 11902–11916. doi: 10.1523/JNEUROSCI.2187-10.2010

Johnson, J. E., Barde, Y. A., Schwab, M., and Thoenen, H. (1986). Brain-derived neurotrophic factor supports the survival of cultured rat retinal ganglion cells. *J. Neurosci.* 6, 3031–3038. doi: 10.1523/JNEUROSCI.06-10-03031.1986

Johnson, T. V., Bull, N. D., Hunt, D. P., Marina, N., Tomarev, S. I., and Martin, K. R. (2010). Neuroprotective effects of intravitreal mesenchymal stem cell transplantation in experimental glaucoma. *Invest. Ophthalmol. Vis. Sci.* 51, 2051–2059. doi: 10.1167/iovs.09-4509

Johnson, T. V., Bull, N. D., and Martin, K. R. (2011). Neurotrophic factor delivery as a protective treatment for glaucoma. *Exp. Eye Res.* 93, 196–203. doi: 10.1016/j.exer.2010.05.016

Johnson, T. V., DeKorver, N. W., Levasseur, V. A., Osborne, A., Tassoni, A., Lorber, B., et al. (2014). Identification of retinal ganglion cell neuroprotection conferred by platelet-derived growth factor through analysis of the mesenchymal stem cell secretome. *Brain* 137, 503–519. doi: 10.1093/brain/awt292

Jonas, J. B., Aung, T., Bourne, R. R., Bron, A. M., Ritch, R., and Panda-Jonas, S. (2017). Glaucoma. *Lancet* 390, 2183–2193. doi: 10.1016/S0140-6736(17)31469-1

Jones, M. K., Lu, B., Girman, S., and Wang, S. (2017). Cell-based therapeutic strategies for replacement and preservation in retinal degenerative diseases. *Prog. Retin. Eye Res.* 58, 1–27. doi: 10.1016/j.preteyeres.2017.01.004

Junying, Y., Kejin, H., Kim, S. O., Shulan, T., Stewart, R., Slukvin, I. I., et al. (2009). Human induced pluripotent stem cells free of vector and transgene sequences. *Science* 324, 797–801. doi: 10.1126/science.1172482

Jurkute, N., and Yu-Wai-Man, P. (2017). Leber hereditary optic neuropathy: bridging the translational gap. *Curr. Opin. Ophthalmol.* 28, 403–409. doi: 10.1097/ICU.0000000000000410

Kador, K. E., Alsehli, H. S., Zindell, A. N., Lau, L. W., Andreopoulos, F. M., Watson, B. D., et al. (2014). Retinal ganglion cell polarization using immobilized guidance cues on a tissue-engineered scaffold. *Acta Biomater.* 10, 4939–4946. doi: 10.1016/j.actbio.2014.08.032

Kador, K. E., Grogan, S. P., Dorthé, E. W., Venugopalan, P., Malek, M. F., Goldberg, J. L., et al. (2016). Control of retinal ganglion cell positioning and neurite growth: combining 3D printing with radial electrospun scaffolds. *Tissue Eng. Part A* 22, 286–294. doi: 10.1089/ten.tea.2015.0373

Kashani, A. H., Lebkowski, J. S., Rahhal, F. M., Avery, R. L., Salehi-Had, H., Dang, W., et al. (2018). A bioengineered retinal pigment epithelial monolayer for advanced, dry age-related macular degeneration. *Sci. Transl. Med.* 10:eaao4097. doi: 10.1126/scitranslmed.aao4097

Kawada, J., Kaneda, S., Kirihara, T., Maroof, A., Levi, T., Eggan, K., et al. (2017). Generation of a motor nerve organoid with human stem cell-derived neurons. *Stem Cell Rep.* 9, 1441–1449. doi: 10.1016/j.stemcr.2017.09.021

Kay, J. N., Finger-Baier, K. C., Roeser, T., Staub, W., and Baier, H. (2001). Retinal ganglion cell genesis requires lakritz, a Zebrafish atonal Homolog. *Neuron* 30, 725–736. doi: 10.1016/S0896-6273(01)00312-9

Kayama, M., Kurokawa, M. S., Ueda, Y., Ueno, H., Kumagai, Y., Chiba, S., et al. (2010). Transfection with pax6 gene of mouse embryonic stem cells and subsequent cell cloning induced retinal neuron progenitors, including retinal ganglion cell-like cells, in vitro. *Ophthalmic Res.* 43, 79–91. doi: 10.1159/000247592

Kermer, P., Klöcker, N., Labes, M., and Bähr, M. (2000). Insulin-like growth factor-I protects axotomized rat retinal ganglion cells from secondary death via PI3-K-dependent Akt phosphorylation and inhibition of caspase-3 In vivo. *J. Neurosci.* 20, 2–8. doi: 10.1523/JNEUROSCI.20-02-00722.2000

Kim, D. H., Kim, H. S., Ahn, M. D., and Chun, M. H. (2004). Ganglion cell death in rat retina by persistent intraocular pressure elevation. *Korean J. Ophthalmol.* 18, 15–22. doi: 10.3341/kjo.2004.18.1.15

Kimura, A., Namekata, K., Guo, X., Harada, C., and Harada, T. (2016). Neuroprotection, growth factors and BDNF-TrkB signalling in retinal degeneration. *Int. J. Mol. Sci.* 17:E1584. doi: 10.3390/ijms17091584

Kobayashi, W., Onishi, A., Tu, H., Takihara, Y., Matsumura, M., Tsujimoto, K., et al. (2018). Culture systems of dissociated mouse and human pluripotent stem cell-derived retinal ganglion cells purified by two-step immunopanning. *Invest. Ophthalmol. Vis. Sci.* 59, 776–787. doi: 10.1167/iovs.17-22406

Koprivica, V., Cho, K.-S., Park, J. B., Yiu, G., Atwal, J., Gore, B., et al. (2005). EGFR activation mediates inhibition of axon regeneration by myelin and chondroitin sulfate proteoglycans. *Science* 310, 106–110. doi: 10.1126/science.1115462

Kuwajima, T., Soares, C. A., Sitko, A. A., Lefebvre, V., and Mason, C. (2017). SoxC transcription factors promote contralateral retinal ganglion cell differentiation and axon guidance in the mouse visual system. *Neuron* 93, 1110–1125.e5. doi: 10.1016/j.neuron.2017.01.029

La Spada, A., Ntai, A., Genovese, S., Rondinelli, M., De Blasio, P., and Biunno, I. (2018). Generation of human-induced pluripotent stem cells from Wolfram syndrome type 2 patients bearing the c.103 + 1G>A *CISD2* mutation for disease modeling. *Stem Cells Dev.* 27, 287–295. doi: 10.1089/scd.2017.0158

Laha, B., Stafford, B. K., and Huberman, A. D. (2017). Regenerating optic pathways from the eye to the brain. *Science* 356, 1031–1034. doi: 10.1126/science.aal5060

Lamba, D. A., Gust, J., and Reh, T. A. (2009). Transplantation of human embryonic stem cell-derived photoreceptors restores some visual function in Crx-deficient mice. *Cell Stem Cell* 4, 73–79. doi: 10.1016/j.stem.2008.10.015

Lamba, D. A., Karl, M. O., Ware, C. B., and Reh, T. A. (2006). Efficient generation of retinal progenitor cells from human embryonic stem cells. *Proc. Natl. Acad. Sci. U.S.A.* 103, 12769–12774. doi: 10.1073/pnas.0601990103

Lamba, D. A., McUsic, A., Hirata, R. K., Wang, P.-R., Russell, D., and Reh, T. A. (2010). Generation, purification and transplantation of photoreceptors derived from human induced pluripotent stem cells. *PLoS One* 5:e8763. doi: 10.1371/journal.pone.0008763

Lancaster, M. A., Renner, M., Martin, C.-A., Wenzel, D., Bicknell, L. S., Hurles, M. E., et al. (2013). Cerebral organoids model human brain development and microcephaly. *Nature* 501, 373–379. doi: 10.1038/nature12517

Langer, K. B., Ohlemacher, S. K., Phillips, M. J., Fligor, C. M., Jiang, P., Gamm, D. M., et al. (2018). Retinal ganglion cell diversity and subtype specification from human pluripotent stem cells. *Stem Cell Rep.* 10, 1282–1293. doi: 10.1016/j.stemcr.2018.02.010

Lawrence, J. M., Singhal, S., Bhatia, B., Keegan, D. J., Reh, T. A., Luthert, P. J., et al. (2007). MIO-M1 cells and similar muller glial cell lines derived from adult human retina exhibit neural stem cell characteristics. *Stem Cells* 25, 2033–2043. doi: 10.1634/stemcells.2006-0724

Lee, M. J., Ko, A. Y., Ko, J. H., Lee, H. J., Kim, M. K., Wee, W. R., et al. (2015). Mesenchymal stem/stromal cells protect the ocular surface by suppressing

inflammation in an experimental dry eye. *Mol. Ther.* 23, 139–146. doi: 10.1038/mt.2014.159

Lee, M.-O., Moon, S. H., Jeong, H.-C., Yi, J.-Y., Lee, T.-H., Shim, S. H., et al. (2013). Inhibition of pluripotent stem cell-derived teratoma formation by small molecules. *Proc. Natl. Acad. Sci. U.S.A.* 110, E3281–E3290. doi: 10.1073/pnas.1303669110

Lee, S. C. S., Weltzien, F., Madigan, M. C., Martin, P. R., and Grünert, U. (2016). Identification of AII amacrine, displaced amacrine, and bistratified ganglion cell types in human retina with antibodies against calretinin. *J. Comp. Neurol.* 524, 39–53. doi: 10.1002/cne.23821

Leibinger, M., Andreadaki, A., Gobrecht, P., Levin, E., Diekmann, H., and Fischer, D. (2016). Boosting central nervous system axon regeneration by circumventing limitations of natural cytokine signaling. *Mol. Ther.* 24, 1712–1725. doi: 10.1038/mt.2016.102

Leibinger, M., Muller, A., Andreadaki, A., Hauk, T. G., Kirsch, M., and Fischer, D. (2009). Neuroprotective and axon growth-promoting effects following inflammatory stimulation on mature retinal ganglion cells in mice depend on ciliary neurotrophic factor and leukemia inhibitory factor. *J. Neurosci.* 29, 14334–14341. doi: 10.1523/JNEUROSCI.2770-09.2009

Lemke, G., and Reber, M. (2005). Retinotectal mapping: new insights from molecular genetics. *Annu. Rev. Cell Dev. Biol.* 21, 551–580. doi: 10.1146/annurev.cellbio.20.022403.093702

Levin, L. A., and Gordon, L. K. (2002). Retinal ganglion cell disorders: types and treatments. *Prog. Retin. Eye Res.* 21, 465–484. doi: 10.1016/S1350-9462(02)00012-5

Levkovitch-Verbin, H., Sadan, O., Vander, S., Rosner, M., Barhum, Y., Melamed, E., et al. (2010). Intravitreal injections of neurotrophic factors secreting mesenchymal stem cells are neuroprotective in rat eyes following optic nerve transection. *Invest. Ophthalmol. Vis. Sci.* 51, 6394–6400. doi: 10.1167/iovs.09-4310

Li, K., Zhong, X., Yang, S., Luo, Z., Li, K., Liu, Y., et al. (2017). HiPSC-derived retinal ganglion cells grow dendritic arbors and functional axons on a tissue-engineered scaffold. *Acta Biomater.* 54, 117–127. doi: 10.1016/j.actbio.2017.02.032

Lim, J.-H. A., Stafford, B. K., Nguyen, P. L., Lien, B. V., Wang, C., Zukor, K., et al. (2016). Neural activity promotes long-distance, target-specific regeneration of adult retinal axons. *Nat. Neurosci.* 19, 1073–1084. doi: 10.1038/nn.4340

Limb, G. A., Salt, T. E., Munro, P. M. G., Moss, S. E., and Khaw, P. T. (2002). In vitro characterization of a spontaneously immortalized human Müller cell line (MIO-M1). *Invest. Ophthalmol. Vis. Sci.* 43, 864–869.

Liu, C., Zhang, C. W., Zhou, Y., Wong, W. Q., Lee, L. C., Ong, W. Y., et al. (2017). APP upregulation contributes to retinal ganglion cell degeneration via JNK3. *Cell Death Differ.* 25, 661–676. doi: 10.1038/s41418-017-0005-3

Llonch, S., Carido, M., and Ader, M. (2018). Organoid technology for retinal repair. *Dev. Biol.* 433, 132–143. doi: 10.1016/j.ydbio.2017.09.028

Lorber, B., Hsiao, W.-K., Hutchings, I. M., and Martin, K. R. (2014). Adult rat retinal ganglion cells and glia can be printed by piezoelectric inkjet printing. *Biofabrication* 6:015001. doi: 10.1088/1758-5082/6/1/015001

Lu, H.-E., Yang, Y.-P., Chen, Y.-T., Wu, Y.-R., Wang, C.-L., Tsai, F.-T., et al. (2018). Generation of patient-specific induced pluripotent stem cells from Leber's hereditary optic neuropathy. *Stem Cell Res.* 28, 56–60. doi: 10.1016/j.scr.2018.01.029

Ma, Y. T., Hsieh, T., Forbes, M. E., Johnson, J. E., and Frost, D. O. (1998). BDNF injected into the superior colliculus reduces developmental retinal ganglion cell death. *J. Neurosci.* 18, 2097–2107. doi: 10.1523/JNEUROSCI.18-06-02097.1998

Mac Nair, C. E., and Nickells, R. W. (2015). Neuroinflammation in glaucoma and optic nerve damage. *Prog. Mol. Biol. Transl. Sci.* 134, 343–363. doi: 10.1016/bs.pmbts.2015.06.010

MacVicar, T., and Langer, T. (2016). OPA1 processing in cell death and disease - the long and short of it. *J. Cell Sci.* 129, 2297–2306. doi: 10.1242/jcs.159186

Maekawa, Y., Onishi, A., Matsushita, K., Koide, N., Mandai, M., Suzuma, K., et al. (2015). Optimized culture system to induce neurite outgrowth from retinal ganglion cells in three-dimensional retinal aggregates differentiated from mouse and human embryonic stem cells. *Curr. Eye Res.* 41, 558–568. doi: 10.3109/02713683.2015.1038359

Mandai, M., Watanabe, A., Kurimoto, Y., Hirami, Y., Morinaga, C., Daimon, T., et al. (2017). Autologous induced stem-cell-derived retinal cells for macular degeneration. *N. Engl. J. Med.* 376, 1038–1046. doi: 10.1056/NEJMoa1608368

Mansour-Robaey, S., Clarke, D. B., Wang, Y. C., Bray, G. M., and Aguayo, A. J. (1994). Effects of ocular injury and administration of brain-derived neurotrophic factor on survival and regrowth of axotomized retinal ganglion cells. *Proc. Natl. Acad. Sci. U.S.A.* 91, 1632–1636. doi: 10.1073/pnas.91.5.1632

Mao, W., Yan, R.-T., and Wang, S.-Z. (2008). Proneural gene ash1 promotes amacrine cell production in the chick retina. *Dev. Neurobiol.* 69, 88–104. doi: 10.1002/dneu.20693

Marler, K. J., Suetterlin, P., Dopplapudi, A., Rubikaite, A., Adnan, J., Maiorano, N. A., et al. (2014). BDNF promotes axon branching of retinal ganglion cells via miRNA-132 and p250GAP. *J. Neurosci.* 34, 969–979. doi: 10.1523/JNEUROSCI.1910-13.2014

Martin, K. R. G., Quigley, H. A., Valenta, D., Kielczewski, J., and Pease, M. E. (2006). Optic nerve dynein motor protein distribution changes with intraocular pressure elevation in a rat model of glaucoma. *Exp. Eye Res.* 83, 255–262. doi: 10.1016/j.exer.2005.11.025

Martinez-Morales, J.-R., Del Bene, F., Nica, G., Hammerschmidt, M., Bovolenta, P., and Wittbrodt, J. (2005). Differentiation of the vertebrate retina is coordinated by an FGF signaling center. *Dev. Cell* 8, 565–574. doi: 10.1016/j.devcel.2005.01.022

Mattar, P., Ericson, J., Blackshaw, S., and Cayouette, M. (2015). A conserved regulatory logic controls temporal identity in mouse neural progenitors. *Neuron* 85, 497–504. doi: 10.1016/j.neuron.2014.12.052

Mauss, A. S., Vlasits, A., Borst, A., and Feller, M. (2017). Visual circuits for direction selectivity. *Annu. Rev. Neurosci.* 40, 211–230. doi: 10.1146/annurev-neuro-072116

Mead, B., Amaral, J., and Tomarev, S. (2018). Mesenchymal stem cell-derived small extracellular vesicles promote neuroprotection in rodent models of glaucoma. *Invest. Ophthalmol. Vis. Sci.* 59, 702–714. doi: 10.1167/iovs.17-22855

Mead, B., Berry, M., Logan, A., Scott, R. A. H., Leadbeater, W., and Scheven, B. A. (2015). Stem cell treatment of degenerative eye disease. *Stem Cell Res.* 14, 243–257. doi: 10.1016/j.scr.2015.02.003

Mead, B., Hill, L. J., Blanch, R. J., Ward, K., Logan, A., Berry, M., et al. (2016). Mesenchymal stromal cell-mediated neuroprotection and functional preservation of retinal ganglion cells in a rodent model of glaucoma. *Cytotherapy* 18, 487–496. doi: 10.1016/j.jcyt.2015.12.002

Mead, B., Logan, A., Berry, M., Leadbeater, W., and Scheven, B. A. (2013). Intravitreally transplanted dental pulp stem cells promote neuroprotection and axon regeneration of retinal ganglion cells after optic nerve injury. *Invest. Ophthalmol. Vis. Sci.* 54, 7544–7556. doi: 10.1167/iovs.13-13045

Mead, B., and Tomarev, S. (2017). Bone marrow-derived mesenchymal stem cells-derived exosomes promote survival of retinal ganglion cells through miRNA-dependent mechanisms. *Stem Cells Transl. Med.* 6, 1273–1285. doi: 10.1002/sctm.16-0428

Mellough, C. B., Cui, Q., Spalding, K. L., Symons, N. A., Pollett, M. A., Snyder, E. Y., et al. (2004). Fate of multipotent neural precursor cells transplanted into mouse retina selectively depleted of retinal ganglion cells. *Exp. Neurol.* 186, 6–19. doi: 10.1016/j.expneurol.2003.10.021

Mesentier-Louro, L. A., Zaverucha-do-Valle, C., da Silva-Junior, A. J., Nascimento-Dos-Santos, G., Gubert, F., de Figueirêdo, A. B. P., et al. (2014). Distribution of mesenchymal stem cells and effects on neuronal survival and axon regeneration after optic nerve crush and cell therapy. *PLoS One* 9:e110722. doi: 10.1371/journal.pone.0110722

Meyer, J. S., Howden, S. E., Wallace, K. A., Verhoeven, A. D., Wright, L. S., Capowski, E. E., et al. (2011). Optic vesicle-like structures derived from human pluripotent stem cells facilitate a customized approach to retinal disease treatment. *Stem Cells* 29, 1206–1218. doi: 10.1002/stem.674

Meyer, J. S., Katz, M. L., Maruniak, J. A., and Kirk, M. D. (2006). Embryonic stem cell-derived neural progenitors incorporate into degenerating retina and enhance survival of host photoreceptors. *Stem Cells* 24, 274–283. doi: 10.1634/stemcells.2005-0059

Meyer, J. S., Shearer, R. L., Capowski, E. E., Wright, L. S., Wallace, K. A., McMillan, E. L., et al. (2009). Modeling early retinal development with human embryonic and induced pluripotent stem cells. *Proc. Natl. Acad. Sci. U.S.A.* 106, 16698–16703. doi: 10.1073/pnas.0905245106

Meyer-Franke, A., Kaplan, M. R., Pfrieger, F. W., and Barres, B. A. (1995). Characterization of the signaling interactions that promote the survival and growth of developing retinal ganglion cells in culture. *Neuron* 15, 805–819. doi: 10.1016/0896-6273(95)90172-8

Milea, D., and Verny, C. (2012). [Hereditary optic neuropathies]. *Rev. Neurol.* 168, 706–709. doi: 10.1016/j.neurol.2012.08.005

Minegishi, Y., Iejima, D., Kobayashi, H., Chi, Z.-L., Kawase, K., Yamamoto, T., et al. (2013). Enhanced optineurin E50K–TBK1 interaction evokes protein insolubility and initiates familial primary open-angle glaucoma. *Hum. Mol. Genet.* 22, 3559–3567. doi: 10.1093/hmg/ddt210

Morimoto, T. (2012). Role of electrical activity of neurons for neuroprotection. *Int. Rev. Neurobiol.* 105, 19–38. doi: 10.1016/B978-0-12-398309-1.00003-2

Motahari, Z., Martinez-De Luna, R. I., Viczian, A. S., and Zuber, M. E. (2016). Tbx3 represses bmp4 expression and, with Pax6, is required and sufficient for retina formation. *Development* 143, 3560–3572. doi: 10.1242/dev.130955

Mu, X., Fu, X., Beremand, P. D., Thomas, T. L., and Klein, W. H. (2008). Gene-regulation logic in retinal ganglion cell development: Isl1 defines a critical branch distinct from but overlapping with Pou4f2. *Proc. Natl. Acad. Sci. U.S.A.* 105, 6942–6947. doi: 10.1073/pnas.0802627105

Munemasa, Y., and Kitaoka, Y. (2013). Molecular mechanisms of retinal ganglion cell degeneration in glaucoma and future prospects for cell body and axonal protection. *Front. Cell. Neurosci.* 6:60. doi: 10.3389/fncel.2012.00060

Nakano, T., Ando, S., Takata, N., Kawada, M., Muguruma, K., Sekiguchi, K., et al. (2012). Self-formation of optic cups and storable stratified neural retina from human ESCs. *Cell Stem Cell* 10, 771–785. doi: 10.1016/j.stem.2012.05.009

Neumann, C. J., and Nuesslein-Volhard, C. (2000). Patterning of the zebrafish retina by a wave of sonic hedgehog activity. *Science* 289, 2137–2139. doi: 10.1126/science.289.5487.2137

Newman, N. J. (2012). Treatment of hereditary optic neuropathies. *Nat. Rev. Neurol.* 8, 545–556. doi: 10.1038/nrneurol.2012.167

Nickells, R. W., Howell, G. R., Soto, I., and John, S. W. M. (2012). Under pressure: cellular and molecular responses during glaucoma, a common neurodegeneration with axonopathy. *Annu. Rev. Neurosci.* 35, 153–179. doi: 10.1146/annurev.neuro.051508.135728

Ohlemacher, S. K., Sridhar, A., Xiao, Y., Hochstetler, A. E., Sarfarazi, M., Cummins, T. R., et al. (2016). Stepwise differentiation of retinal ganglion cells from human pluripotent stem cells enables analysis of glaucomatous neurodegeneration. *Stem Cells* 34, 1553–1562. doi: 10.1002/stem.2356

Osakada, F., Ikeda, H., Mandai, M., Wataya, T., Watanabe, K., Yoshimura, N., et al. (2008). Toward the generation of rod and cone photoreceptors from mouse, monkey and human embryonic stem cells. *Nat. Biotechnol.* 26, 215–224. doi: 10.1038/nbt1384

Osborne, A., Sanderson, J., and Martin, K. R. (2018). Neuroprotective effects of human mesenchymal stem cells and platelet-derived growth factor on human retinal ganglion cells. *Stem Cells* 36, 65–78. doi: 10.1002/stem.2722

Parameswaran, S., Balasubramanian, S., Babai, N., Qiu, F., Eudy, J. D., Thoreson, W. B., et al. (2010). Induced pluripotent stem cells generate both retinal ganglion cells and photoreceptors: therapeutic implications in degenerative changes in glaucoma and age-related macular degeneration. *Stem Cells* 28, 695–703. doi: 10.1002/stem.320

Parameswaran, S., Dravid, S. M., Teotia, P., Krishnamoorthy, R. R., Qiu, F., Toris, C., et al. (2015). Continuous non-cell autonomous reprogramming to generate retinal ganglion cells for glaucomatous neuropathy. *Stem Cells* 33, 1743–1758. doi: 10.1002/stem.1987

Park, K. K., Liu, K., Hu, Y., Smith, P. D., Wang, C., Cai, B., et al. (2008). Promoting axon regeneration in the adult CNS by modulation of the PTEN/mTOR pathway. *Science* 322, 963–966. doi: 10.1126/science.1161566

Park, S. S., Moisseiev, E., Bauer, G., Anderson, J. D., Grant, M. B., Zam, A., et al. (2017). Advances in bone marrow stem cell therapy for retinal dysfunction. *Prog. Retin. Eye Res.* 56, 148–165. doi: 10.1016/j.preteyeres.2016.10.002

Paul, G., and Anisimov, S. V. (2013). The secretome of mesenchymal stem cells: potential implications for neuroregeneration. *Biochimie* 95, 2246–2256. doi: 10.1016/j.biochi.2013.07.013

Pearson, R. A., Gonzalez-Cordero, A., West, E. L., Ribeiro, J. R., Aghaizu, N., Goh, D., et al. (2016). Donor and host photoreceptors engage in material transfer following transplantation of post-mitotic photoreceptor precursors. *Nat. Commun.* 7:13029. doi: 10.1038/ncomms13029

Pease, M. E., McKinnon, S. J., Quigley, H. A., Kerrigan-Baumrind, L. A., and Zack, D. J. (2000). Obstructed axonal transport of BDNF and its receptor TrkB in experimental glaucoma. *Invest. Ophthalmol. Vis. Sci.* 41, 764–774.

Pollak, J., Wilken, M. S., Ueki, Y., Cox, K. E., Sullivan, J. M., Taylor, R. J., et al. (2013). ASCL1 reprograms mouse Muller glia into neurogenic retinal progenitors. *Development* 140, 2619–2631. doi: 10.1242/dev.091355

Priebe, N. J., and McGee, A. W. (2014). Mouse vision as a gateway for understanding how experience shapes neural circuits. *Front. Neural Circuits* 8:123. doi: 10.3389/fncir.2014.00123

Qu, J., Wang, D., and Grosskreutz, C. L. (2010). Mechanisms of retinal ganglion cell injury and defense in glaucoma. *Exp. Eye Res.* 91, 48–53. doi: 10.1016/j.exer.2010.04.002

Quadrato, G., Nguyen, T., Macosko, E. Z., Sherwood, J. L., Min Yang, S., Berger, D. R., et al. (2017). Cell diversity and network dynamics in photosensitive human brain organoids. *Nature* 545, 48–53. doi: 10.1038/nature22047

Ramachandran, R., Fausett, B. V., and Goldman, D. (2010). Ascl1a regulates Müller glia dedifferentiation and retinal regeneration through a Lin-28-dependent, let-7 microRNA signalling pathway. *Nat. Cell Biol.* 12, 1101–1107. doi: 10.1038/ncb2115

Rathod, R., Surendran, H., Battu, R., Desai, J., and Pal, R. (2018). Induced pluripotent stem cells (iPSC)- derived retinal cells in disease modeling and regenerative medicine. *J. Chem. Neuroanat.* doi: 10.1016/j.jchemneu.2018.02.002 [Epub ahead of print].

Reichenbach, A., and Bringmann, A. (2013). New functions of Müller cells. *Glia* 61, 651–678. doi: 10.1002/glia.22477

Reichman, S., Slembrouck, A., Gagliardi, G., Chaffiol, A., Terray, A., Nanteau, C., et al. (2017). Generation of storable retinal organoids and retinal pigmented epithelium from adherent human iPS cells in Xeno-Free and Feeder-Free conditions. *Stem Cells* 35, 1176–1188. doi: 10.1002/stem.2586

Reichman, S., Terray, A., Slembrouck, A., Nanteau, C., Orieux, G., Habeler, W., et al. (2014). From confluent human iPS cells to self-forming neural retina and retinal pigmented epithelium. *Proc. Natl. Acad. Sci. U.S.A.* 111, 8518–8523. doi: 10.1073/pnas.1324212111

Rezaie, T., Child, A., Hitchings, R., Brice, G., Miller, L., Coca-Prados, M., et al. (2002). Adult-onset primary open-angle glaucoma caused by mutations in optineurin. *Science* 295, 1077–1079. doi: 10.1126/science.1066901

Riazifar, H., Jia, Y., Chen, J., Lynch, G., and Huang, T. (2014). Chemically induced specification of retinal ganglion cells from human embryonic and induced pluripotent stem cells. *Stem Cells Transl.* 424–432. doi: 10.1002/stem.13

Sajgo, S., Ghinia, M. G., Brooks, M., Kretschmer, F., Chuang, K., Hiriyanna, S., et al. (2017). Molecular codes for cell type specification in Brn3 retinal ganglion cells. *Proc. Natl. Acad. Sci. U.S.A.* 114, E3974–E3983. doi: 10.1073/pnas.1618551114

Salinas-Navarro, M., Alarcón-Martínez, L., Valiente-Soriano, F. J., Jiménez-López, M., Mayor-Torroglosa, S., Avilés-Trigueros, M., et al. (2010). Ocular hypertension impairs optic nerve axonal transport leading to progressive retinal ganglion cell degeneration. *Exp. Eye Res.* 90, 168–183. doi: 10.1016/j.exer.2009.10.003

Santos-Ferreira, T., Llonch, S., Borsch, O., Postel, K., Haas, J., and Ader, M. (2016). Retinal transplantation of photoreceptors results in donor-host cytoplasmic exchange. *Nat. Commun.* 7:13028. doi: 10.1038/ncomms13028

Sapkota, D., Chintala, H., Wu, F., Fliesler, S. J., Hu, Z., and Mu, X. (2014). Onecut1 and Onecut2 redundantly regulate early retinal cell fates during development. *Proc. Natl. Acad. Sci. U.S.A.* 111, E4086–E4095. doi: 10.1073/pnas.1405354111

Satarian, L., Javan, M., Kiani, S., Hajikaram, M., Mirnajafi-Zadeh, J., and Baharvand, H. (2013). Engrafted human induced pluripotent stem cell-derived anterior specified neural progenitors protect the rat crushed optic nerve. *PLoS One* 8:e71855. doi: 10.1371/journal.pone.0071855

Sawai, H., Clarke, D. B., Kittlerova, P., Bray, G. M., and Aguayo, A. J. (1996). Brain-derived neurotrophic factor and neurotrophin-4/5 stimulate growth of axonal branches from regenerating retinal ganglion cells. *J. Neurosci.* 16, 3887–3894. doi: 10.1523/JNEUROSCI.16-12-03887.1996

Schwab, M. E. (2004). Nogo and axon regeneration. *Curr. Opin. Neurobiol.* 14, 118–124. doi: 10.1016/j.conb.2004.01.004

Schwartz, S. D., Tan, G., Hosseini, H., and Nagiel, A. (2016). Subretinal transplantation of embryonic stem cell-derived retinal pigment epithelium for the treatment of macular degeneration: an assessment at 4 years.

Invest. Ophthalmol. Vis. Sci. 57, ORSFc1–ORSFc9. doi: 10.1167/iovs.15-18681

Seung, H. S., and Sümbül, U. (2014). Neuronal cell types and connectivity: lessons from the retina. *Neuron* 83, 1262–1272. doi: 10.1016/j.neuron.2014.08.054

Singh, M. S., Balmer, J., Barnard, A. R., Aslam, S. A., Moralli, D., Green, C. M., et al. (2016). Transplanted photoreceptor precursors transfer proteins to host photoreceptors by a mechanism of cytoplasmic fusion. *Nat. Commun.* 7:13537. doi: 10.1038/ncomms13537

Singh, R. K., Mallela, R. K., Cornuet, P. K., Reifler, A. N., Chervenak, A. P., West, M. D., et al. (2015). Characterization of three-dimensional retinal tissue derived from human embryonic stem cells in adherent monolayer cultures. *Stem Cells Dev.* 24, 2778–2795. doi: 10.1089/scd.2015.0144

Singhal, S., Bhatia, B., Jayaram, H., Becker, S., Jones, M. F., Cottrill, P. B., et al. (2012). Human Müller glia with stem cell characteristics differentiate into retinal ganglion cell (RGC) precursors in vitro and partially restore RGC function in vivo following transplantation. *Stem Cells Transl. Med.* 1, 188–199. doi: 10.5966/sctm.2011-0005

Sluch, V. M., Chamling, X., Liu, M. M., Berlinicke, C. A., Cheng, J., Mitchell, K. L., et al. (2017). Enhanced stem cell differentiation and immunopurification of genome engineered human retinal ganglion cells. *Stem Cells Transl. Med.* 6, 1972–1986. doi: 10.1002/sctm.17-0059

Sluch, V. M., Davis, C.-H. O., Ranganathan, V., Kerr, J. M., Krick, K., Martin, R., et al. (2015). Differentiation of human ESCs to retinal ganglion cells using a CRISPR engineered reporter cell line. *Sci. Rep.* 5:16595. doi: 10.1038/srep16595

Sluch, V. M., and Zack, D. J. (2014). Stem cells, retinal ganglion cells and glaucoma. *Dev. Ophthalmol.* 53, 111–121. doi: 10.1159/000358409

Smith, P. D., Sun, F., Park, K. K., Cai, B., Wang, C., Kuwako, K., et al. (2009). SOCS3 deletion promotes optic nerve regeneration in vivo. *Neuron* 64, 617–623. doi: 10.1016/j.neuron.2009.11.021

Song, W., Zhang, X., and Xia, X. (2013). Atoh7 promotes the differentiation of retinal stem cells derived from Müller cells into retinal ganglion cells by inhibiting Notch signaling. *Stem Cell Res. Ther.* 4:94. doi: 10.1186/scrt305

Song, W.-T., Zeng, Q., Xia, X.-B., Xia, K., and Pan, Q. (2016). Atoh7 promotes retinal Müller cell differentiation into retinal ganglion cells. *Cytotechnology* 68, 267–277. doi: 10.1007/s10616-014-9777-1

Sridhar, A., Steward, M. M., and Meyer, J. S. (2013). Nonxenogeneic growth and retinal differentiation of human induced pluripotent stem cells. *Stem Cells Transl. Med.* 2, 255–264. doi: 10.5966/sctm.2012-0101

Stenkamp, D. L. (2015). *Development of the Vertebrate Eye and Retina*, 1st Edn. ı Atlanta, GA: Elsevier Inc, doi: 10.1016/bs.pmbts.2015.06.006

Sun, F., Park, K. K., Belin, S., Wang, D., Lu, T., Chen, G., et al. (2011). Sustained axon regeneration induced by co-deletion of PTEN and SOCS3. *Nature* 480, 372–375. doi: 10.1038/nature10594

Surzenko, N., Crowl, T., Bachleda, A., Langer, L., and Pevny, L. (2013). SOX2 maintains the quiescent progenitor cell state of postnatal retinal Muller glia. *Development* 140, 1445–1456. doi: 10.1242/dev.071878

Suzuki, T. (2003). Effects of prolonged delivery of brain-derived neurotrophic factor on the fate of neural stem cells transplanted into the developing rat retina. *Biochem. Biophys. Res. Commun.* 309, 843–847. doi: 10.1016/j.bbrc.2003.08.076

Takahashi, K., Tanabe, K., Ohnuki, M., Narita, M., Ichisaka, T., Tomoda, K., et al. (2007). Induction of pluripotent stem cells from adult human fibroblasts by defined factors. *Cell* 131, 861–872. doi: 10.1016/j.cell.2007.11.019

Takahashi, K., and Yamanaka, S. (2006). Induction of pluripotent stem cells from mouse embryonic and adult fibroblast cultures by defined factors. *Cell* 126, 663–676. doi: 10.1016/j.cell.2006.07.024

Takahashi, M., Palmer, T. D., Takahashi, J., and Gage, F. H. (1998). Widespread integration and survival of adult-derived neural progenitor cells in the developing optic retina. *Mol. Cell. Neurosci.* 12, 340–348. doi: 10.1006/mcne.1998.0721

Tanaka, T., Yokoi, T., Tamalu, F., Watanabe, S.-I., Nishina, S., and Azuma, N. (2015). Generation of retinal ganglion cells with functional axons from human induced pluripotent stem cells. *Sci. Rep.* 5:8344. doi: 10.1038/srep08344

Tanaka, T., Yokoi, T., Tamalu, F., Watanabe, S.-I., Nishina, S., and Azuma, N. (2016). Generation of retinal ganglion cells with functional axons from mouse embryonic stem cells and induced pluripotent stem cells. *Invest. Ophthalmol. Vis. Sci.* 57, 3348–3359. doi: 10.1167/iovs.16-19166

Teixeira, F. G., Carvalho, M. M., Sousa, N., and Salgado, A. J. (2013). Mesenchymal stem cells secretome: a new paradigm for central nervous system regeneration? *Cell. Mol. Life Sci.* 70, 3871–3882. doi: 10.1007/s00018-013-1290-8

Teotia, P., Chopra, D. A., Dravid, S. M., Van Hook, M. J., Qiu, F., Morrison, J., et al. (2016). Generation of functional human retinal ganglion cells with target specificity from pluripotent stem cells by chemically defined recapitulation of developmental mechanism. *Stem Cells* 35, 572–585. doi: 10.1002/stem.2513

Teotia, P., Van Hook, M. J., Wichman, C. S., Allingham, R. R., Hauser, M. A., and Ahmad, I. (2017). Modeling glaucoma: retinal ganglion cells generated from induced pluripotent stem cells of patients with SIX6 risk allele show developmental abnormalities. *Stem Cells* 35, 2239–2252. doi: 10.1002/stem.2675

Tham, Y. C., Li, X., Wong, T. Y., Quigley, H. A., Aung, T., and Cheng, C. Y. (2014). Global prevalence of glaucoma and projections of glaucoma burden through 2040: a systematic review and meta-analysis. *Ophthalmology* 121, 2081–2090. doi: 10.1016/j.ophtha.2014.05.013

Thomson, J. A., Itskovitz-Eldor, J., Shapiro, S. S., Waknitz, M. A., Swiergiel, J. J., Marshall, V. S., et al. (1998). Embryonic stem cell lines derived from human blastocysts. *Science* 282, 1145–1147. doi: 10.1126/science.282.5391.1145

Tucker, B. A., Solivan-Timpe, F., Roos, B. R., Anfinson, K. R., Robin, A. L., Wiley, L. A., et al. (2014). Duplication of TBK1 stimulates autophagy in iPSC-derived retinal cells from a patient with normal tension glaucoma. *J. Stem Cell Res. Ther.* 3:61. doi: 10.4172/2157-7633.1000161

Turner, D. L., and Cepko, C. L. (1987). A common progenitor for neurons and glia persists in rat retina late in development. *Nature* 328, 131–136. doi: 10.1038/328131a0

Ueki, Y., Wilken, M. S., Cox, K. E., Chipman, L., Jorstad, N., Sternhagen, K., et al. (2015). Transgenic expression of the proneural transcription factor Ascl1 in Müller glia stimulates retinal regeneration in young mice. *Proc. Natl. Acad. Sci. U.S.A.* 112, 13717–13722. doi: 10.1073/pnas.1510595112

Usher, L. C., Johnstone, A., Ertürk, A., Hu, Y., Strikis, D., Wanner, I. B., et al. (2010). A chemical screen identifies novel compounds that overcome glial-mediated inhibition of neuronal regeneration. *J. Neurosci.* 30, 4693–4706. doi: 10.1523/JNEUROSCI.0302-10.2010

Van Hoffelen, S. J., Young, M. J., Shatos, M. A., and Sakaguchi, D. S. (2003). Incorporation of murine brain progenitor cells into the developing mammalian retina. *Invest. Opthalmol. Vis. Sci.* 44, 426–434. doi: 10.1167/iovs.02-0269

Vecino, E., Rodriguez, F. D., Ruzafa, N., Pereiro, X., and Sharma, S. C. (2016). Glia-neuron interactions in the mammalian retina. *Prog. Retin. Eye Res.* 51, 1–40. doi: 10.1016/j.preteyeres.2015.06.003

Venugopalan, P., Wang, Y., Nguyen, T., Huang, A., Muller, K. J., and Goldberg, J. L. (2016). Transplanted neurons integrate into adult retinas and respond to light. *Nat. Commun.* 7:10472. doi: 10.1038/ncomms10472

Völkner, M., Zschätzsch, M., Rostovskaya, M., Overall, R. W., Busskamp, V., Anastassiadis, K., et al. (2016). Retinal organoids from pluripotent stem cells efficiently recapitulate retinogenesis. *Stem Cell Rep.* 6, 525–538. doi: 10.1016/j.stemcr.2016.03.001

Waldron, P. V., Di Marco, F., Kruczek, K., Ribeiro, J., Graca, A. B., Hippert, C., et al. (2018). Transplanted donor- or stem cell-derived cone photoreceptors can both integrate and undergo material transfer in an environment-dependent manner. *Stem Cell Rep.* 10, 406–421. doi: 10.1016/j.stemcr.2017.12.008

Wallace, D. C., Singh, G., Lott, M. T., Hodge, J. A., Schurr, T. G., Lezza, A. M., et al. (1988). Mitochondrial DNA mutation associated with Leber's hereditary optic neuropathy. *Science* 242, 1427–1430. doi: 10.1126/science.3201231

Wang, S. W., Kim, B. S., Ding, K., Wang, H., Sun, D., Johnson, R. L., et al. (2001). Requirement for math5 in the development of retinal ganglion cells. *Genes Dev.* 15, 24–29. doi: 10.1101/gad.855301.mined

Wang, Y., Dakubo, G. D., Thurig, S., Mazerolle, C. J., and Wallace, V. (2005). Retinal ganglion cell-derived sonic hedgehog locally controls proliferation and the timing of RGC development in the embryonic mouse retina. *Development* 132, 5103–5113. doi: 10.1242/dev.02096

Weidenheim, K. M., Dickson, D. W., and Rapin, I. (2009). Neuropathology of Cockayne syndrome: evidence for impaired development, premature aging, and neurodegeneration. *Mech. Ageing Dev.* 130, 619–636. doi: 10.1016/j.mad.2009.07.006

Wong, R. C. B., Lim, S. Y., Hung, S. S. C., Jackson, S., Khan, S., Van Bergen, N. J., et al. (2017). Mitochondrial replacement in an iPSC model of leber hereditary optic neuropathy. *Aging* 9, 1341–1350. doi: 10.1101/120659

Wu, F., Kaczynski, T. J., Sethuramanujam, S., Li, R., Jain, V., Slaughter, M., et al. (2015). Two transcription factors, Pou4f2 and Isl1, are sufficient to specify the retinal ganglion cell fate. *Proc. Natl. Acad. Sci. U.S.A.* 112, E1559–E1568. doi: 10.1073/pnas.1421535112

Wu, Y.-R., Wang, A.-G., Chen, Y.-T., Yarmishyn, A. A., Buddhakosai, W., Yang, T.-C., et al. (2018). Bioactivity and gene expression profiles of hiPSC-generated retinal ganglion cells in *MT-ND4* mutated Leber's hereditary optic neuropathy. *Exp. Cell Res.* 363, 299–309. doi: 10.1016/j.yexcr.2018.01.020

Xie, B.-B., Zhang, X.-M., Hashimoto, T., Tien, A. H., Chen, A., Ge, J., et al. (2014). Differentiation of retinal ganglion cells and photoreceptor precursors from mouse induced pluripotent stem cells carrying an Atoh7/Math5 lineage reporter. *PLoS One* 9:e112175. doi: 10.1371/journal.pone.0112175

Yan, Q., Wang, J., Matheson, C. R., and Urich, J. L. (1999). Glial cell line-derived neurotrophic factor (GDNF) promotes the survival of axotomized retinal ganglion cells in adult rats: comparison to and combination with brain-derived neurotrophic factor (BDNF). *J. Neurobiol.* 38, 382–390. doi: 10.1002/(SICI)1097-4695(19990215)38:3<382::AID-NEU7>3.0.CO;2-5

Yang, T.-C., Chuang, J.-H., Buddhakosai, W., Wu, W.-J., Lee, C.-J., Chen, W.-S., et al. (2017). Elongation of axon extension for human iPSC-derived retinal ganglion cells by a nano-imprinted scaffold. *Int. J. Mol. Sci.* 18:E2013. doi: 10.3390/ijms18092013

Yang, Y., Ye, Y., Su, X., He, J., Bai, W., and He, X. (2017). MSCs-derived exosomes and neuroinflammation, neurogenesis and therapy of traumatic brain injury. *Front. Cell. Neurosci.* 11:55. doi: 10.3389/fncel.2017.00055

Yin, Y., Cui, Q., Gilbert, H.-Y., Yang, Y., Yang, Z., Berlinicke, C., et al. (2009). Oncomodulin links inflammation to optic nerve regeneration. *Proc. Natl. Acad. Sci. U.S.A.* 106, 19587–19592. doi: 10.1073/pnas.0907085106

Yin, Y., Henzl, M. T., Lorber, B., Nakazawa, T., Thomas, T. T., Jiang, F., et al. (2006). Oncomodulin is a macrophage-derived signal for axon regeneration in retinal ganglion cells. *Nat. Neurosci.* 9, 843–852. doi: 10.1038/nn1701

Yip, H. K., and So, K. F. (2000). Axonal regeneration of retinal ganglion cells: effect of trophic factors. *Prog. Retin. Eye Res.* 19, 559–575. doi: 10.1016/S1350-9462(00)00009-4

Yokoi, T., Tanaka, T., Matsuzaka, E., Tamalu, F., Watanabe, S.-I., Nishina, S., et al. (2017). Effects of neuroactive agents on axonal growth and pathfinding of retinal ganglion cells generated from human stem cells. *Sci. Rep.* 7:16757. doi: 10.1038/s41598-017-16727-1

Young, M. J., Ray, J., Whiteley, S. J. O., Klassen, H., and Gage, F. H. (2000). Neuronal differentiation and morphological integration of hippocampal progenitor cells transplanted to the retina of immature and mature dystrophic rats. *Mol. Cell. Neurosci.* 16, 197–205. doi: 10.1006/mcne.2000.0869

Young, R. W. (1985). Cell differentiation in the retina of the mouse. *Anat. Rec.* 212, 199–205. doi: 10.1002/ar.1092120215

Yu, B., Zhang, X., and Li, X. (2014). Exosomes derived from mesenchymal stem cells. *Int. J. Mol. Sci.* 15, 4142–4157. doi: 10.3390/ijms15034142

Yu, J., Vodyanik, M. A., Smuga-Otto, K., Antosiewicz-Bourget, J., Frane, J. L., Tian, S., et al. (2007). Induced pluripotent stem cell lines derived from human somatic cells. *Science* 318, 1917–1920. doi: 10.1126/science.1151526

Yu, S., Tanabe, T., Dezawa, M., Ishikawa, H., and Yoshimura, N. (2006). Effects of bone marrow stromal cell injection in an experimental glaucoma model. *Biochem. Biophys. Res. Commun.* 344, 1071–1079. doi: 10.1016/j.bbrc.2006.03.231

Yun, H., Zhou, Y., Wills, A., and Du, Y. (2016). Stem cells in the trabecular meshwork for regulating intraocular pressure. *J. Ocul. Pharmacol. Ther.* 32, 253–260. doi: 10.1089/jop.2016.0005

Yu-Wai-Man, P., Griffiths, P. G., and Chinnery, P. F. (2011). Mitochondrial optic neuropathies - disease mechanisms and therapeutic strategies. *Prog. Retin. Eye Res.* 30, 81–114. doi: 10.1016/j.preteyeres.2010.11.002

Zahabi, A., Shahbazi, E., Ahmadieh, H., Hassani, S.-N., Totonchi, M., Taei, A., et al. (2012). A new efficient protocol for directed differentiation of retinal pigmented epithelial cells from normal and retinal disease induced pluripotent stem cells. *Stem Cells Dev.* 21, 2262–2272. doi: 10.1089/scd.2011.0599

Zarbin, M. (2016). Cell-based therapy for degenerative retinal disease. *Trends Mol. Med.* 22, 115–134. doi: 10.1016/j.molmed.2015.12.007

Zhang, X., Hashimoto, T., Tang, R., and Yang, X. (2018). Elevated expression of human bHLH factor ATOH7 accelerates cell cycle progression of progenitors and enhances production of avian retinal ganglion cells. *Sci. Rep.* 8:6823. doi: 10.1038/s41598-018-25188-z

Zhang, X. M., and Yang, X. J. (2001). Temporal and spatial effects of Sonic hedgehog signaling in chick eye morphogenesis. *Dev. Biol.* 233, 271–290. doi: 10.1006/dbio.2000.0195

Zhong, X., Gutierrez, C., Xue, T., Hampton, C., Vergara, M. N., Cao, L.-H., et al. (2014). Generation of three-dimensional retinal tissue with functional photoreceptors from human iPSCs. *Nat. Commun.* 5:4047. doi: 10.1038/ncomms5047

Zhu, W., Gramlich, O. W., Laboissonniere, L., Jain, A., Sheffield, V. C., Trimarchi, J. M., et al. (2016). Transplantation of iPSC-derived TM cells rescues glaucoma phenotypes in vivo. *Proc. Natl. Acad. Sci. U.S.A.* 113, E3492–E3500. doi: 10.1073/pnas.1604153113

Zuber, M. E. (2010). "Eye field specification in *Xenopus laevis*," in *Current Topics in Developmental Biology*, eds T. A. Cagan and R. L. Reh (Atlanta, GA: Elsevier Inc), 29–60. doi: 10.1016/B978-0-12-385044-7.00002-3

Conflict of Interest Statement: The authors declare that the research was conducted in the absence of any commercial or financial relationships that could be construed as a potential conflict of interest.

frontiers in Neuroscience

ORIGINAL RESEARCH
published: 12 October 2018
doi: 10.3389/fnins.2018.00702

Ccl5 Mediates Proper Wiring of Feedforward and Lateral Inhibition Pathways in the Inner Retina

D'Anne S. Duncan[1†], Rebecca L. Weiner[2,3†], Carl Weitlauf[1], Michael L. Risner[1], Abigail L. Roux[1], Emily R. Sanford[1], Cathryn R. Formichella[1] and Rebecca M. Sappington[1,2,3]*

[1] Vanderbilt Eye Institute, Vanderbilt University Medical Center, Nashville, TN, United States, [2] Department of Pharmacology, Vanderbilt University School of Medicine, Nashville, TN, United States, [3] Department of Ophthalmology and Visual Sciences, Vanderbilt University School of Medicine, Nashville, TN, United States

OPEN ACCESS

Edited by:
Patrice E. Fort, University of Michigan, United States

Reviewed by:
Victoria P. Connaughton, American University, United States
Ralph Francis Nelson, National Institute of Neurological Disorders and Stroke (NINDS), United States

***Correspondence:**
Rebecca M. Sappington
rebecca.m.sappington@vumc.org

[†] These authors have contributed equally to this work

Specialty section:
This article was submitted to Neurogenesis, a section of the journal Frontiers in Neuroscience

Received: *03 July 2018*
Accepted: *18 September 2018*
Published: *12 October 2018*

Citation:
Duncan DS, Weiner RL, Weitlauf C, Risner ML, Roux AL, Sanford ER, Formichella CR and Sappington RM (2018) Ccl5 Mediates Proper Wiring of Feedforward and Lateral Inhibition Pathways in the Inner Retina. Front. Neurosci. 12:702. doi: 10.3389/fnins.2018.00702

The β-chemokine Ccl5 and its receptors are constitutively expressed in neurons of the murine inner retina. Here, we examined the functional and structural significance of this constitutive Ccl5 signaling on retinal development. We compared outcomes of electrophysiology, ocular imaging and retinal morphology in wild-type mice (WT) and mice with Ccl5 deficiency (*Ccl5*$^{-/-}$). Assessment of retinal structure by ocular coherence tomography and histology revealed slight thinning of the inner plexiform layer (IPL) and inner nuclear layer (INL) in *Ccl5*$^{-/-}$ mice, compared to WT ($p < 0.01$). Assessment of postnatal timepoints important for development of the INL (P7 and P10) revealed Ccl5-dependent alterations in the pattern and timing of apoptotic pruning. Morphological analyses of major inner retinal cell types in WT, *Ccl5*$^{-/-}$, gustducin^{gfp} and gustducin^{gfp}/*Ccl5*$^{-/-}$ mice revealed Ccl5-dependent reduction in GNAT3 expression in rod bipolar cells as well as a displacement of their terminals from the IPL into the GCL. RGC dendritic organization and amacrine cell morphology in the IPL was similarly disorganized in *Ccl5*$^{-/-}$ mice. Examination of the intrinsic electrophysiological properties of RGCs revealed higher spontaneous activity in *Ccl5*$^{-/-}$ mice that was characterized by higher spiking frequency and a more depolarized resting potential. This hyperactive phenotype could be negated by current clamp and correlated with both membrane resistance and soma area. Overall, our findings identify Ccl5 signaling as a mediator of inner retinal circuitry during development of the murine retina. The apparent role of Ccl5 in retinal development further supports chemokines as trophic modulators of CNS development and function that extends far beyond the inflammatory contexts in which they were first characterized.

Keywords: Ccl5, chemokine, retinal ganglion cell, amacrine cell, bipolar cell, gustducin, PKCα

Abbreviations: Ccl5, C-C motif chemokine ligand 5; CNS, central nervous system; CTB, cholera toxin beta-subunit; GCL, ganglion cell layer; GFP, green fluorescent protein; GNAT3, guanine nucleotide binding protein, alpha transducing 3; GUS, gustducin; INL, inner nuclear layer; IPL, inner plexiform layer; NFL, nerve fiber layer; OD, optic disk; ONH, optic nerve head; ONL, outer nuclear layer; OPL, outer plexiform layer; P7, postnatal day 7; P10, postnatal day 10; PKCα, protein kinase c alpha; RANTES, regulated on activation, normal T cell expressed and secreted; RGC, retinal ganglion cell; SC, superior colliculus; SD-OCT, spectral domain optical coherence tomography.

INTRODUCTION

Developmentally, the laminar structure of the retina is formed by timed waves of retinal progenitor cell production and migration that is mediated by numerous transcription factors driving early- and late-born cell types (Ohsawa and Kageyama, 2008; Agathocleous and Harris, 2009; Mattar and Cayouette, 2015). Subsequent induction of additional transcription factors mediates differentiation into major cell type classifications, including photoreceptors, horizontal cells, bipolar cells, amacrine cells, and ganglion cells (Jeon et al., 1998; Ohsawa and Kageyama, 2008; Agathocleous and Harris, 2009). Further differentiation into subtypes of these cells is mediated by induction of additional factors (Reese and Keeley, 2016). These subtypes are defined by differences in expression of neurotransmitters, neurotransmitter receptors, and ion channel classes, i.e., metabotropic versus ionotropic channels (Brandstätter et al., 1998; Huang et al., 2003; Ghosh et al., 2004). It is the proper wiring between subtypes of these broad cell classifications that ensures proper encoding to photon stimuli in the retina from a graded glutamate potential to action potentials that can be interpreted by higher visual centers in the brain.

Retinal ganglion cells, whose axons form the optic nerve, transform the graded glutamate potential into action potentials. The excitatory center of the RGC receptive field is established by glutamatergic input to RGC dendrites from bipolar cells in the IPL of the retina (Ghosh et al., 2004). The physiological properties of the RGC receptive fields are further fine-tuned by inhibitory inputs from amacrine cells that establish the surround of the RGC receptive field (Ghosh et al., 2004). Thus, proper formation of this synaptic triad between excitatory feedforward and lateral inhibitory pathways in the IPL is critical for establishment of the RGC receptive field and subsequent neurotransmission of all visual sensory information. While intrinsic factors mediating development and maturation of bipolar cells, amacrine cells and RGCs are well-documented, extrinsic factors that direct formation of circuits at this critical synapse are largely unknown (Morgan and Wong, 2005).

Our previous work indicated that the β-chemokine Ccl5 and its high-affinity receptors are constitutively expressed by neurons of the inner retina, including RGCs and amacrine cells (Duncan et al., 2017). Like other chemokines, Ccl5, formerly known as RANTES, is classically associated with chemotaxis and immune cell migration (Rossi and Zlotnik, 2000; Appay and Rowland-Jones, 2001). However, studies elsewhere in the CNS suggest that Ccl5 and its receptors are also constitutively expressed by neurons and glia (He et al., 1997; Babcock et al., 2003; Pham et al., 2005; Subileau et al., 2009; Sorce et al., 2011; Fe Lanfranco et al., 2018) and may play a role in neuron survival, development and neurotransmission (Galasso et al., 1998; Mennicken et al., 2002; Gamo et al., 2008; Sorce et al., 2010, 2011; Tripathy et al., 2010).

Here, we report the surprising finding that the β-chemokine Ccl5 mediates critical interactions between bipolar cells, amacrine cells and RGC dendrites that are necessary for appropriate development and wiring of the bipolar cell-amacrine cell-RGC circuit. We found that Ccl5 deficiency in $Ccl5^{-/-}$ mice results in thinning of the inner retina, particularly the INL and IPL. Ccl5 deficiency altered the pattern and timing of cell migration and apoptotic pruning during late-stage development. Assessment of major cell classifications in the mature inner retina revealed Ccl5-dependent changes in: (1) rod bipolar cell phenotypes, including displacement of their terminals from the IPL into the GCL, (2) RGC dendritic organization, and (3) amacrine cell morphology in the IPL. Examination of the intrinsic electrophysiological properties of RGCs revealed higher spontaneous activity in $Ccl5^{-/-}$ mice that was characterized by higher spiking frequency and a more depolarized resting potential. This hyperactive phenotype could be negated by current clamp and correlated with both membrane resistance and soma area. Overall, our findings identify Ccl5 signaling as a mediator of inner retinal circuitry during development of the murine retina. The apparent role of Ccl5 in retinal development further supports chemokines as trophic modulators of CNS development and function that extends far beyond the inflammatory contexts in which they were first characterized.

MATERIALS AND METHODS

Animals

This study was conducted in accordance with regulations set forth in the ARVO Statement for the Use of Animals in Ophthalmic and Vision Research. Animal protocols were approved by the Institutional Animal Care and Use Committees of the Vanderbilt University Medical Center. Breeding pairs of C57BL/6 and $Ccl5^{-/-}$ mice were obtained from Charles River Laboratories (Wilmington, MA, United States) and Jackson Laboratories (Bar Harbor, ME, United States), respectively. Breeder pairs of Gusducin reporter mice (Gus^{gfp}; Huang et al., 2003) were obtained as a generous gift from Dr. Benjamin Reese (University of Southern California, Santa Barbara, CA, United States). In the Gus^{gpf} mouse, GFP is expressed under the promoter for GNAT3, which is expressed by Type 7 cone bipolar cells and rod bipolar cells (Huang et al., 2003). Mouse colonies were established and maintained in-house at Vanderbilt University Medical Center. We crossed Gus^{gfp} mice with $Ccl5^{-/-}$ mice to establish and maintain a colony of $Gus^{gfp}/Ccl5^{-/-}$. All colonies were maintained on a 12 h light, 12 h dark cycle with food and water available *ad libitum*. We conducted experiments in adult mice at 2–4 months of age. For developmental series, samples were obtained from pups at postnatal days 7 and 10.

Tissue Procurement and Preparation

For fresh tissue, mice were sacrificed by cervical dislocation followed by decapitation. For protein and gene analyses, whole eyes were enucleated, flash-frozen and stored at −80°C until use. For electrophysiological recordings, eyes were enucleated and retina dissected for immediate use. For fixed tissue, mice received an overdose of pentobarbital (200 mg/kg; Hospira, Inc., Lake Forest, IL, United States) and were sacrificed by *trans*-cardial perfusion with 1X phosphate buffered saline (PBS; Fisher Scientific; Pittsburg, PA, United States) followed by 4% paraformaldehyde (PFA; Electron Microscopy Sciences, Hatfield,

PA, United States). Whole eyes were enucleated and optic nerve and brain harvested. Whole eyes and brain were post-fixed for 1 h in PFA. Optic nerves were post-fixed at least 48 h in 2.5% glutaraldehyde. For paraffin retina sections, 6 μm serial sections of the entire globe were obtained. For cryosections, whole eyes were cryoprotected in a sucrose series, frozen and sectioned on a cryostat at 10 or 40 μm thickness. To obtain serial sections of SC, cortices were removed and brains were cryoprotected in a sucrose series, frozen, and sectioned (50 μm) on a sliding microtome. For semi-thin sections of optic nerve, distal and proximal segments of optic nerve were embedded in epon and sectioned at 700 nm thickness on an ultra-microtome.

Retinal Morphology and Layer Thickness

To visualize longitudinal, cross-sections of the retina *in vivo*, we utilized spectral domain ocular coherence tomography (SD-OCT), as previously described (Echevarria et al., 2017). Briefly, mice were anesthetized with an intraperitoneal injection of ketamine and xylazine, and pupils were dilated using 0.5% Tropicamide (Akorn, Inc., Lake Forest, IL, United States) and kept moist using Systane Ultra. B-line scans of retinas were imaged at the level of the OD (eccentricity = 0) using the Bioptigen ultra-high resolution spectral domain OCT system, Envisu class R2200 and a mouse retina bore (Bioptigen, Morrisville, NC, United States). Representative images of C57BL/6 (n = 5) and $Ccl5^{-/-}$ (n = 5) retinas were collected, and layer-specific measurements of the retinal nerve fiber layer (RNFL), IPL, INL, OPL, and ONL were analyzed using In VivoVue Diver 2.0 software (Bioptigen). Briefly, a 5 × 5 quadrant overlaid each representative image to measure approximately 25 positions of the retina. Each layer was manually identified at each position, and specific layer thickness, measured in μm, was averaged for each image by experimenters blind to genotype.

Quantification of Developmental Apoptosis

We performed TUNEL labeling in whole eye cryosections from C57Bl/6 and $Ccl5^{-/-}$ mice at postnatal days 7 and 10, using a commercially available *in situ* apoptosis detection kit (Cat No. 11684795910; Sigma). TUNEL labeling was performed as per manufacturer's instructions. Briefly, whole eye sections were permeabilized in 0.1 M Citrate buffer, pH 6.0 by microwave irradiation for 1 min. Slides were rinsed in ddH_2O followed by PBS. Sections were incubated in blocking serum (3% BSA+ 20% normal bovine serum in 0.1 M Tris-HCl, pH 7.5) for 30 min at room temperature. After PBS washes, sections were incubated for 60 min at 37°C in TUNEL reaction mixture containing terminal deoxynucleotidyl transferase and fluorophore-conjugated nucleotides. Sections were then washed in PBS, counterstained with the nuclear dye DAPI (Life Technologies) and mounted with Fluoromount-G (Southern Biotech; Birmingham, AL, United States). Fluorescent images of retina sections were taken with an inverted epifluorescent microscope (Nikon Instruments) at similar eccentricities (mid-peripheral) across samples. The number of TUNEL+ and DAPI+ cells were counted in their respective retinal layers by at least two independent experimenters blind to genotype, using ImageJ 1.47v. To accurately depict the rate of apoptosis in each layer, TUNEL reactivity is presented as a percentage of the total number of DAPI+ cells. For IPL measurements, where DAPI+ cells were sparsely observed, fields without DAPI+ or TUNEL+ cells were still considered an apoptotic rate of zero and included in the analysis.

Immunohistochemistry

Immunohistochemistry was performed on whole eye sections of paraffin-embedded or cryostat sections, as previously described (Sims et al., 2012; Echevarria et al., 2013; Duncan et al., 2017). To quench autofluorescence, tissue samples were treated with 0.1% sodium borohydride (Fisher Scientific), blocked in a solution containing 5% normal horse serum (NHS; Life Technologies) and 0.1% Triton X-100 (Fisher Scientific). Tissue was incubated overnight at 4°C in a solution containing the primary antibody (**Table 1**), 3% NHS, and 0.1% Triton X-100 in PBS, followed by a 2-h incubation with the appropriate secondary antibody solution containing 1:200 secondary antibody (donkey anti-mouse, -goat, -rabbit, and -guinea pig; Jackson Immuno, West Grove, PA, United States). Samples were counterstained with DAPI (Life Technologies) and mounted with Fluoromount-G (Southern Biotech; Birmingham, AL, United States). Fluorescent images of retina sections were taken with an inverted epifluorescent microscope (Nikon Instruments) or inverted confocal microscope (Olympus) and analyzed using FluoView Imaging program (Olympus) and ImageJ (NIH). Antibody isotype controls were used to identify non-specific labeling.

Quantification of Neuronal Density and Layer-Specific Immunolabeling

The total number of bipolar cells ($PKCa^+$, Gus^{gfp+}), amacrine ($syntaxin^+$) and RGCs ($Brna3^+$) in C57BL/6, Gus^{gfp}, $Ccl5^{-/-}$ and/or $Gus^{gfp}/Ccl5^{-/-}$ retinas was quantified in 40× or 60×

TABLE 1 | Primary antibodies utilized for immunohistochemistry.

Primary antibody	Concentration	Catalog #	Company
Mouse anti-Brn3a	20 μg/ml	MAB1585	Millipore
Rabbit anti-PKCa	1.67 μg/ml	AB32376	Abcam
Rabbit anti-β-tubulin [neuronal class III β-tubulin (Tuj1) monoclonal]	2.0 μg/ml	802001	BioLegend
Mouse anti-β-tubulin [neuronal class III β-tubulin (Tuj1) monoclonal]	1.33 μg/ml	801201	BioLegend
Mouse anti-syntaxin-1a	100 μg/ml	S0664	Sigma-Aldrich
Goat anti-GFP	1.29 μg/ml	NB100-1770	Novus

micrographs of immunohistochemically labeled paraffin or cryostat sections, using the 'freehand selections' tool in ImageJ 1.47v. The number of immunolabeling+ cells were counted in their respective retinal layers by at least two independent experimenters blind to genotype, using ImageJ 1.47v.

Anterograde Transport

Anterograde transport to SC of C57BL/6 and *Ccl5*$^{-/-}$ mice was performed, as previously described (Crish et al., 2010; Bond et al., 2016; Echevarria et al., 2017). Briefly, mice were anesthetized using 2.5% isoflurane for intravitreal injection of 1 μL of CTB conjugated to Alexa Fluor-594 (1 μL of 1% CTB in sterile PBS solution; Invitrogen). Forty-eight hours post-injection, mice were sacrificed, brain harvested and serial coronal brain sections obtained, as described above. CTB signal in serial coronal brain sections was imaged *en montage* at 10× magnification on an inverted epifluorescent microscope (Nikon Instruments). CTB fluorescent density in the SC was analyzed using ImagePro (Media Cybernetics; Silver Spring, MD, United States). Background intensity for each brain section was set independently for normalization, using pixel strength of the non-retinorecipient SC (layers IV–VII) and the periaqueductal gray. To determine CTB density, area of pixels with CTB signal above background was divided by total pixel area. To further quantify CTB density, colorimetric representation was generated that corresponded with 0% saturation (blue) to 100% saturation (red) at each mediolateral location in the SC section. Using section thickness and intersection distance, we adjoined sections to construct a colorimetric representation of CTB density across the retinotopic SC map. For each SC, we determined the percentage of intact retinotopic map, defined as the percent area with CTB signal ≥70% density.

Optic Nerve Axon Counts

Axon density and total nerve area was quantified, as previously described (Crish et al., 2010; Sappington et al., 2010; Echevarria et al., 2017). Semi-thin, cross-sections of optic nerve from C57Bl/6 and *Ccl5*$^{-/-}$ mice were counterstained with 1% p-Phenylenediamine (PPD) and 1% toluidine blue and imaged *en montage* at 100× magnification on an upright microscope (Olympus). To calculate axon density, a 50 μm × 50 μm grid mask was placed on the montaged image, using NIS elements AR software. The number of axons was manually counted by a blind-observer in 8–10 squares of the grid (Image Pro; Media Cybernetics). Each square counted was equal in area. To measure nerve area, the circumference of the entire nerve was traced in montaged images of optic nerve cross-sections. Nerve area was calculated as the area (mm^2) within this outline, using NIS elements software. Total number of axons was estimated by multiplying axon counts by total nerve area.

Whole-Cell Patch-Clamp Recordings

Whole-cell patch-clamp recordings were conducted, as previously described (Weitlauf et al., 2015). Retinas from 6- to 8-week-old C57Bl/6 (n = 13) and *Ccl5*$^{-/-}$ (n = 10) mice were harvested, as described above, hemisected, and stored in oxygenated Ames' solution (Sigma-Aldrich, St. Louis, MO, United States) at room temperature in the dark for 30 min. Retinal halves were transferred to a temperature-controlled perfusion chamber on an Olympus BX50 upright microscope equipped for fluorescent imaging with a 40× water immersion DIC objective (LUMPlanFI/IR; Olympus, Center Valley, PA, United States). Retinas were submerged with the GCL up and perfused with Ames' solution at a rate of 2 ml/min in the dark at 24–25°C. Cells in the retinal ganglion layer at mid-peripheral to peripheral eccentricities were whole-cell patch-clamped with borosilicate glass electrodes (5–10 MΩ) containing the following: 130 mM K-gluconate (Sigma), 10 mM KCl, 10 mM HEPES (Sigma), 2 mM $MgCl_2$ (Sigma), 1 mM EGTA (Santa Cruz, Dallas, TX, United States), 2 mM Na_2ATP (Sigma), and 0.3 mM NaGTP (Sigma). We included 1% Lucifer yellow dye (Life Technologies, Carlsbad, CA, United States) in the internal solution to verify that patched cells had an intact axon coursing toward the ONH and to visualize dendritic morphology. We recorded spontaneous action potentials under current-clamp using an AxoClamp 2B microelectrode amplifier outfitted with pCLAMP software (Molecular Devices, Sunnyvale, CA, United States) for a minimum of 4 min. We defined induced cells for cells that did not show a spontaneous firing rate of 0.5 Hz, a 1 s depolarizing step current ranging from 25 to 200 pA was delivered at 0.1 Hz until the firing rate exceeded 3 Hz, for a minimum of 4 min. RGCs that did not achieve a consistent firing rate for a minimum of 4 min were excluded. We used a hyperpolarizing step of 25–200 pA current to calculate membrane resistance. Recordings in which the membrane resistance changed by 20% were not included in the final analysis. For RGC subtype analysis, classifications of ON or OFF or ON/OFF were determined by dendritic stratification. Only RGCs for which stratification in specific sub-laminae of the IPL was readily apparent were included in these analyses.

Statistical Analysis

All statistical tests were performed with SigmaPlot (Systat Software Inc., San Jose, CA, United States). For RGC electrophysiology analyses, we compared C57BL/6 to *Ccl5*$^{-/-}$ mice, using one-way analysis of variance and pair-wise multiple comparisons by Bonferroni t-test following normality test validation. For comparisons between RGC electrophysiological properties within genotype, we performed Pearson Product Moment Correlation and linear regression analysis. For all other comparisons, we compared groups using Student's t-test following Shapiro–Wilk normality testing and Brown–Forsythe equal variance analysis. If equal variance testing resulted in $p < 0.05$, groups were compared by Mann–Whitney Rank Sum Test. For all analyses, $p < 0.05$ was considered statistically significant.

RESULTS

Ccl5 Deficiency Alters Inner Retina Morphology

To assess the function of constitutive Ccl5 signaling in retina, we first assessed gross retinal structure *in vivo*, using SD-OCT (Echevarria et al., 2017). In WT and *Ccl5*$^{-/-}$ mice,

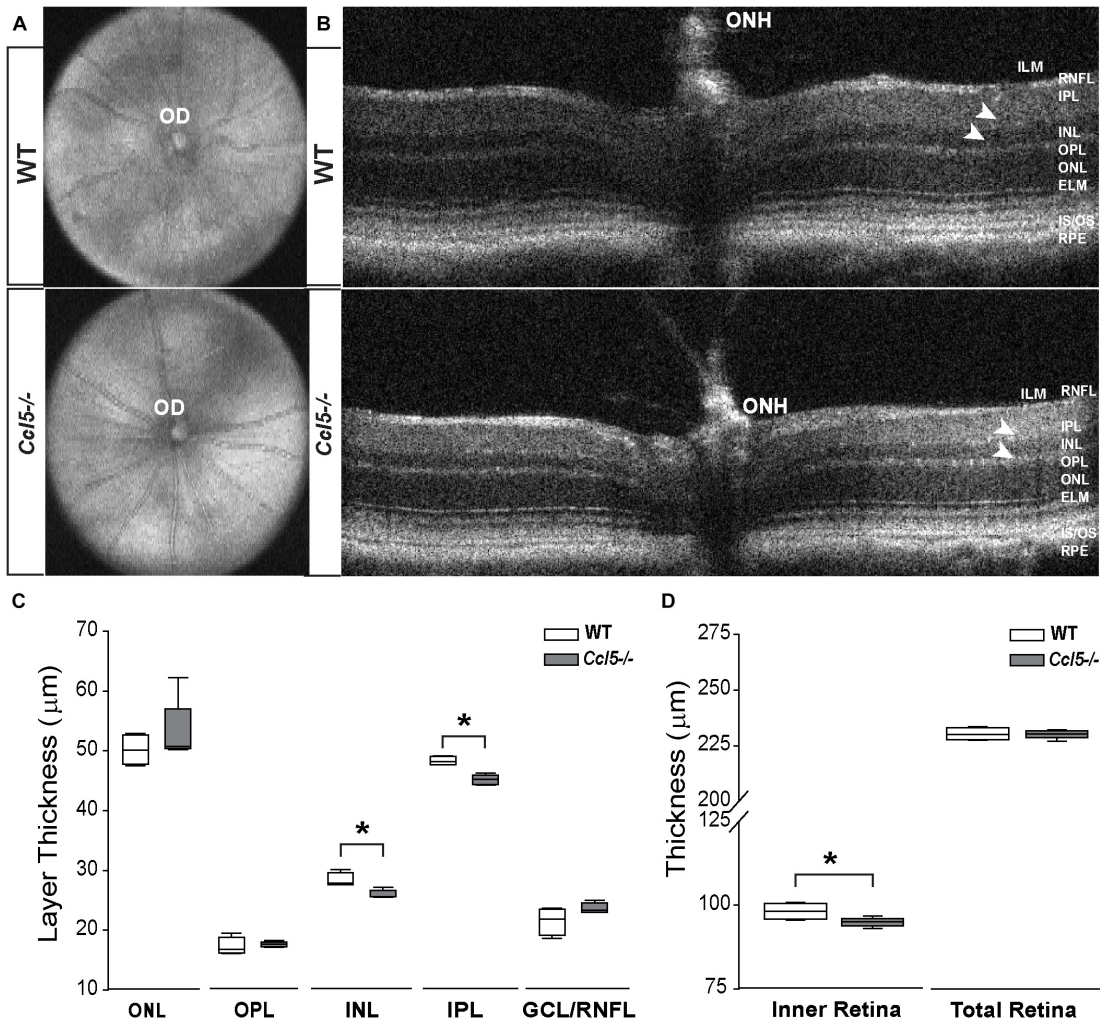

FIGURE 1 | Ccl5 deficiency results in thinning of the inner retina, particularly the INL and IPL. **(A,B)** Representative fundus scans **(A)** and longitudinal B-scans **(B)** of mature (4mo) WT (top) and *Ccl5*$^{-/-}$ (bottom) obtained by SD-OCT. **(A)** Fundus scans reveal an intact OD and patterning of vasculature in *Ccl5*$^{-/-}$ retina, as compared to WT. **(B)** B-scans reveal the presence of all retinal layers from the inner limiting membrane (ILM) to the retinal pigment epithelial (RPE) in *Ccl5*$^{-/-}$ mice. However, the INL and IPL appears thinner compared to C57BL/6 retinas (arrowheads). **(C,D)** Box plots of thickness (μm; *y*-axis) for individual layers of the retina (**C**; *x*-axis: ONL, OPL, INL, IPL, and GCL/NFL), the inner retina (**D**; *x*-axis; left) and the total retina (**D**; *x*-axis; right) in WT (white) and *Ccl5*$^{-/-}$ (gray) mice. Asterisks indicate $p < 0.05$.

fundus images were obtained to examine OD morphology and vascular patterning. B-line scans were obtained to assess gross morphology of the ONH and retinal lamination as well as to measure thickness of individual retinal layers. Fundus images from *Ccl5*$^{-/-}$ mice revealed no gross abnormalities in OD morphology or vascular patterning, as compared to WT (**Figure 1A**). Similarly, B-line scans obtained from *Ccl5*$^{-/-}$ mice demonstrated no gross abnormalities in ONH morphology or retinal lamination, with all layers of retina apparent and morphologically intact (**Figure 1B**). Quantification of B-line scans revealed slight, but statistically significant, thinning of the INL (26.00 ± 0.69 μm vs. 28.37 ± 1.18 μm) and IPL (45.19 ± 0.84 μm vs. 48.33 ± 0.71 μm) in *Ccl5*$^{-/-}$ mice, as compared to WT mice ($p < 0.05$ for both; $n = 5$/group; **Figure 1C**). This resulted in a 4% reduction in inner retina thickness in *Ccl5*$^{-/-}$ mice ($p < 0.05$; $n = 5$/group; **Figure 1D**). However, this difference in inner retina thickness did not translate to a change in total retina thickness compared to WT ($p > 0.05$; $n = 5$/group; **Figure 1D**). Together, these data suggest that, while Ccl5 deficiency does not alter the gross laminar structure of the retina, it does alter inner retinal structure, particularly the INL and IPL.

Ccl5 Deficiency Alters Cell Migration and Apoptotic Pruning During Retinal Development

In the inner retina, the primary neuronal cell types that constitute the INL, IPL, and GCL are bipolar cells, amacrine cells and RGCs, respectively. To determine whether Ccl5-dependent changes

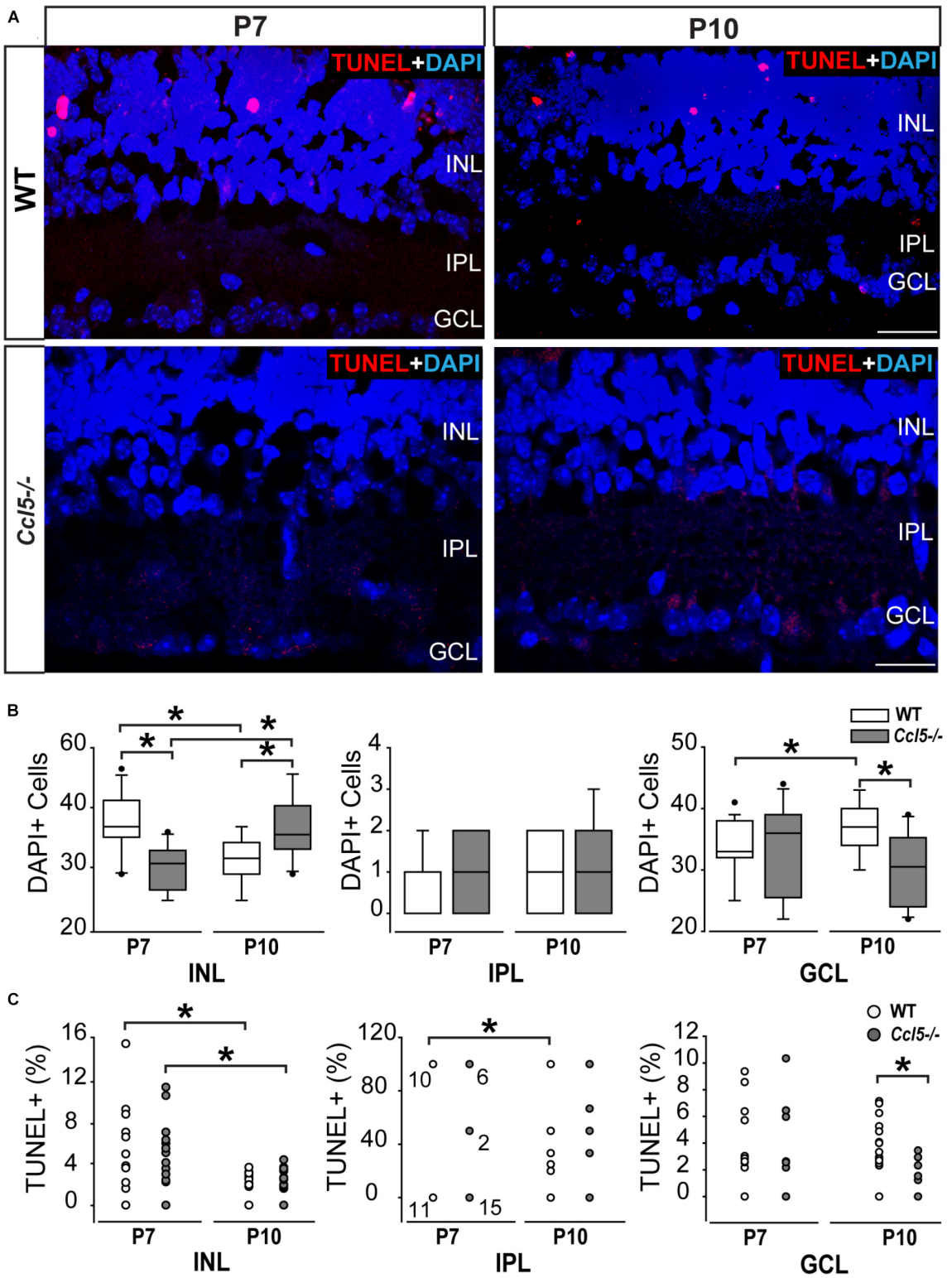

FIGURE 2 | Ccl5 deficiency alters temporal and spatial patterning of inner retinal development. **(A)** Representative micrographs (20×) of TUNEL labeling (red) with DAPI counterstain (blue) in mid-peripheral retina from postnatal day 7 (P7) and 10 (P10) WT and *Ccl5*$^{-/-}$ mice. TUNEL reactivity is greater at P7 than at P10 for both genotypes and most apparent in the INL. Scale bar = 20 μm. **(B)** Box plots of the number of DAPI+ cells (*y*-axis) in the INL (*x*-axis; left), IPL (*x*-axis; middle) and GCL (*x*-axis; right) in WT (white) and *Ccl5*$^{-/-}$ (gray) retina. Asterisks indicate $p < 0.05$. **(C)** Scatter plots of the percentage of TUNEL+ DAPI+ cells (*y*-axis) in the INL (*x*-axis; left), IPL (*x*-axis; middle) and GCL (*x*-axis; right) of WT (white) and *Ccl5*$^{-/-}$ (gray) retina. *N* values are provided for P7 measurements in IPL, which tended to be either 0, 50, or 100% TUNEL+. Asterisks indicate $p < 0.05$.

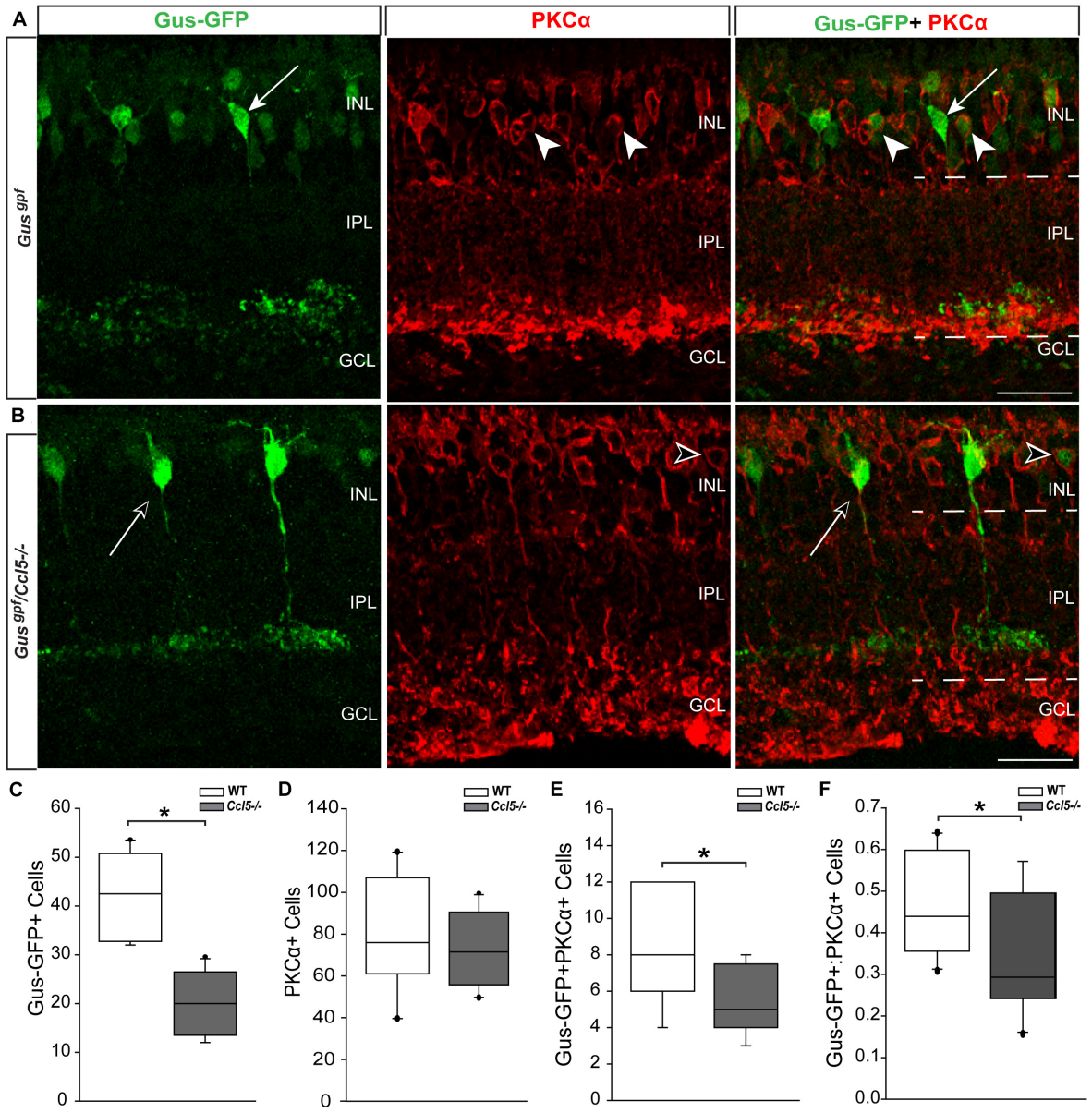

FIGURE 3 | Ccl5 deficiency alters rod bipolar cell phenotypes and morphology. **(A,B)** Representative confocal micrographs (60×) of retina from Gus^{gfp} mice **(A)** and $Gus^{gpf}/Ccl5^{-/-}$ mice **(B)** co-immunolabeled with primary antibodies against GFP (green) and the rod bipolar cell marker PKCα (red). Scale = 20 μm. **(A)** GFP labels PKCα- type 7 cone bipolar cells (filled arrows) and some PKCα+ rod bipolar cells (filled arrowheads) in WT Gus^{gfp} retina. **(B)** In $Gus^{gpf}/Ccl5^{-/-}$, GFP +/PKCα– cone bipolar cells (unfilled arrow) appear unremarkable. However, GFP+/PKCα+ rod bipolar cells (unfilled arrowhead) appear far less abundant. GFP–/PKCα+ rod bipolar cells appear to terminate in the GCL rather than in the IPL (dotted lines) just below GFP+/PKCα– cone bipolar cells, as seen in WT Gus^{gfp} retina **(A)**. **(C–E)** Box plots depicting the number of Gus-GFP+ **(C)**, PKCα+ **(D)**, and GFP+/PKCα+ **(E)** cells (*y*-axes) in the INL of Gus^{gfp} (white) and $Gus^{gpf}/Ccl5^{-/-}$ (gray) mice. Asterisks indicate $p < 0.05$. **(F)** Box plot depicting the ratio of Gus-GFP+ to PKCα+ bipolar cells (*y*-axis) in WT (white) and $Ccl5^{-/-}$ (gray) mice. Asterisks indicate $p < 0.05$.

in the thickness of inner retina layers arises from altered neurogenesis or apoptotic pruning during retinal development, we quantified the number of DAPI+ cells in inner retinal layers of P7 and P10 WT and $Ccl5^{-/-}$ pups. At P7, cell genesis and migration of RGCs and amacrine cells is already complete, while bipolar cell genesis and migration is ongoing (Young, 1985; Zhang et al., 2011). By P10, RGC, amacrine cell and bipolar cell genesis and migration are all complete and the cells exhibit adult morphology (Reese, 2011). Quantification of DAPI+ cells indicated that $Ccl5^{-/-}$ retina contained 21% fewer cells in the INL at P7 than WT retina ($p < 0.01$; n = 52–66/group; **Figures 2A,B**). There was no difference in cell number between WT and $Ccl5^{-/-}$ mice at P7 for the IPL (n = 52–66/group) or GCL ($p > 0.05$ for both; n = 52–66/group; **Figure 2B**). By P10, the number of cells in the INL decreased by 18% in WT mice, as compared to P7 ($p < 0.01$; n = 35–66/group; **Figure 2B**).

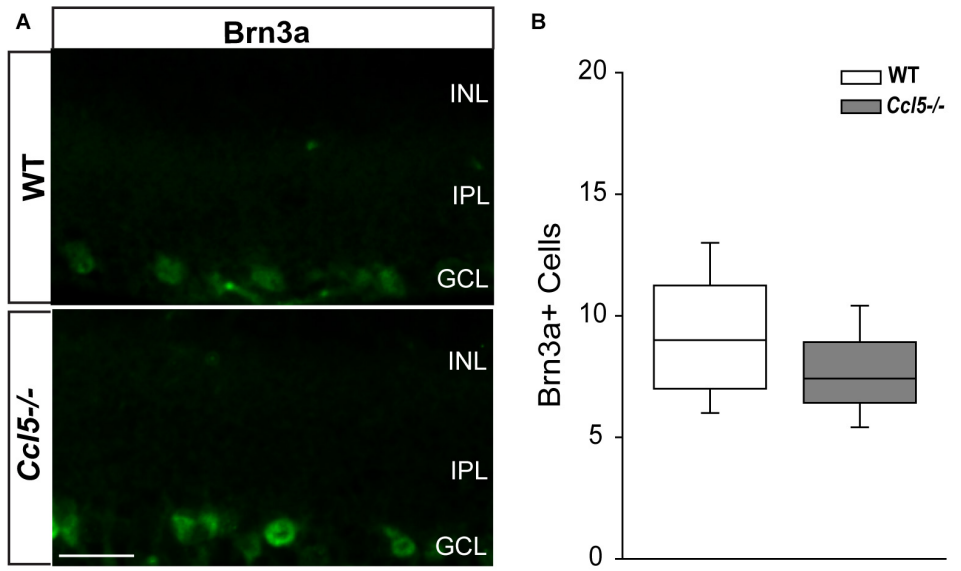

FIGURE 4 | Ccl5 deficiency does not alter RGC density. **(A)** Representative fluoromicrographs of retina from WT (top) and $Ccl5^{-/-}$ mice (bottom) immunolabeled with primary antibodies against the RGC marker Brn3a reveal similar numbers of Brn3a+ RGCs in both genotypes. Scale = 20 μm. **(B)** Box plot depicting the number of Brn3a+ cells (*y*-axis) in WT (white) and $Ccl5^{-/-}$ (gray) mice. Asterisks indicate $p < 0.05$.

In contrast, the number of cells in the INL increased by 19% in $Ccl5^{-/-}$, as compared to P7 ($p < 0.01$; n = 35–66/group; **Figure 2B**). As a result, $Ccl5^{-/-}$ retina contained 16% more cells in the INL than WT mice at P10 ($p < 0.01$; n = 35–66/group; **Figure 2B**). Between P7 and P10, the number of cells in the GCL increased by 9% in WT retina ($p = 0.01$; n = 35–66/group; **Figure 2B**). In contrast, there was no change in the number of cells in the GCL of $Ccl5^{-/-}$ mice between P7 and P10 ($p > 0.05$; n = 35–66/group; **Figure 2B**). This resulted in 17% more cells in WT GCL than $Ccl5^{-/-}$ GCL at P10 ($p < 0.05$; n = 35–44/group; **Figure 2B**). In the IPL, we detected a sparse number of DAPI+ cells, which presumably are actively migrating bipolar cells. The number of cells increased by 89% between P7 and P10 in WT retina ($p < 0.05$; n = 35–66/group; **Figure 2B**). In contrast, there was no change in the number of cells in the IPL of $Ccl5^{-/-}$ retina between P7 and P10 ($p > 0.05$; n = 35–66/group; **Figure 2B**). Despite changes in cell number in IPL noted in WT retina, there was no difference in the number of DAPI+ cells in the IPL between WT and $Ccl5^{-/-}$ at P10 ($p > 0.05$; n = 35–44/group; **Figure 2B**). These data suggest that changes in mature inner retinal structure is preceded by altered cell density in individual retinal layers, which could arise from either changes in neurogenesis or cell migration.

To determine whether Ccl5-dependent changes in cell numbers within inner retinal layers during the critical developmental period between P7 and P10 arises from altered apoptotic pruning, we performed TUNEL labeling and quantified TUNEL reactivity as % of DAPI+ cells. Qualitatively, TUNEL reactivity was most notable at the P7 timepoint in WT and $Ccl5^{-/-}$ mice (**Figure 2A**). At P7, we found no difference in the percentage of TUNEL+ cells between WT and $Ccl5^{-/-}$ across all inner retina layers ($p > 0.05$ for all; n = 52–66/group; **Figure 2C**). In the INL, the percentage of TUNEL+ cells decreased between P7 and P10 by 55% in WT mice ($p < 0.01$) and 71% in $Ccl5^{-/-}$ mice ($p < 0.01$; n = 35–66/group; **Figure 2C**). In the IPL, the percentage of TUNEL+ cells decreased between P7 and P10 by 52% in WT mice (66.67 ± 48.8% vs. 31.57 ± 44.6%; $p < 0.05$; n = 35–66/group; **Figure 2C**). In contrast, there was no change in the percentage of TUNEL+ cells in the IPL of $Ccl5^{-/-}$ retina between P7 and P10 ($p > 0.05$; n = 35–66/group; **Figure 2C**). In the GCL, there was no change in the percentage of TUNEL+ cells between P7 and P10 in either WT or $Ccl5^{-/-}$ retina ($p > 0.05$ for both; n = 35–66/group; **Figure 2C**). However, the percentage of TUNEL+ cells was 78% lower in $Ccl5^{-/-}$ retina versus WT retina at P10 ($p < 0.01$; n = 35–44/group; **Figure 2C**). Together, these data suggest that Ccl5 deficiency alters the time course and/or magnitude of apoptotic pruning during a critical period of development for inner retinal neurons.

Ccl5 Deficiency Induces Abnormal Rod Bipolar Cell Differentiation

Since cell count and TUNEL analyses suggest that Ccl5 deficiency alters development of the inner retina, we examined inner retina neuron subtypes in mature retina. For bipolar cell analyses, we crossed GUS reporter mice (Gus^{gfp}) on a C57Bl/6 background with $Ccl5^{-/-}$ mice. In GUS-gfp mice, Type 7 cone bipolar cells and a subset of rod bipolar cells express GFP under the gustaducin promoter (Huang et al., 2003). To identify remaining rod bipolar cells, we immunolabled whole eye sections from Gus^{gfp} and $Gus^{gfp}/Ccl5^{-/-}$ mice with antibodies against the rod bipolar cell marker PKCα (**Figures 3A,B**). Qualitatively, GFP+ cone bipolar cells exhibited similar morphology in Gus^{gfp} and $Gus^{gfp}/Ccl5^{-/-}$ mice (arrows; **Figure 3A**). However, GFP+ rod bipolar cells were far less numerous in $Gus^{gfp}/Ccl5^{-/-}$ mice

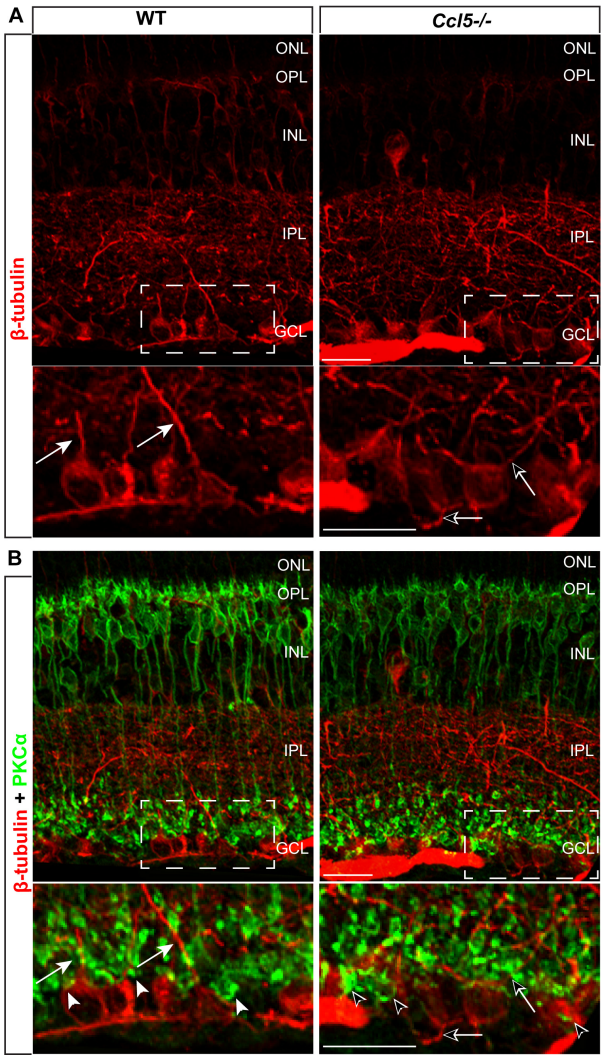

FIGURE 5 | Ccl5 deficiency alters the organizational morphology of RGC dendrites. **(A)** Representative confocal micrographs (60x) of retina from WT (left) and *Ccl5*$^{-/-}$ mice (right) immunolabeled with primary antibodies against beta-tubulin (β-tubulin; red) reveal disorganized trajectories of dendritic projections in *Ccl5*$^{-/-}$ retina (unfilled arrows), as compared to the uniform, upright trajectory observed in WT retina (filled arrows). Bottom panels are higher magnification views of the outlined area in top panels. Scale = 20 μm. **(B)** Representative confocal micrographs (60×) of retina from WT (left) and *Ccl5*$^{-/-}$ mice (right) co-immunolabeled with primary antibodies against β-tubulin (red) and PKCα (green) reveal that terminals of PKCα+ rod bipolar cells (unfilled arrowheads) encroach into the GCL and surround β-tubulin+ RGC soma. In contrast, terminals of PKCα+ rod bipolar cells in WT retina contact only the apical surface of β-tubulin+ RGC soma (filled arrowheads). Bottom panels are higher magnification views of the outlined area in top panels. Scale = 20 μm.

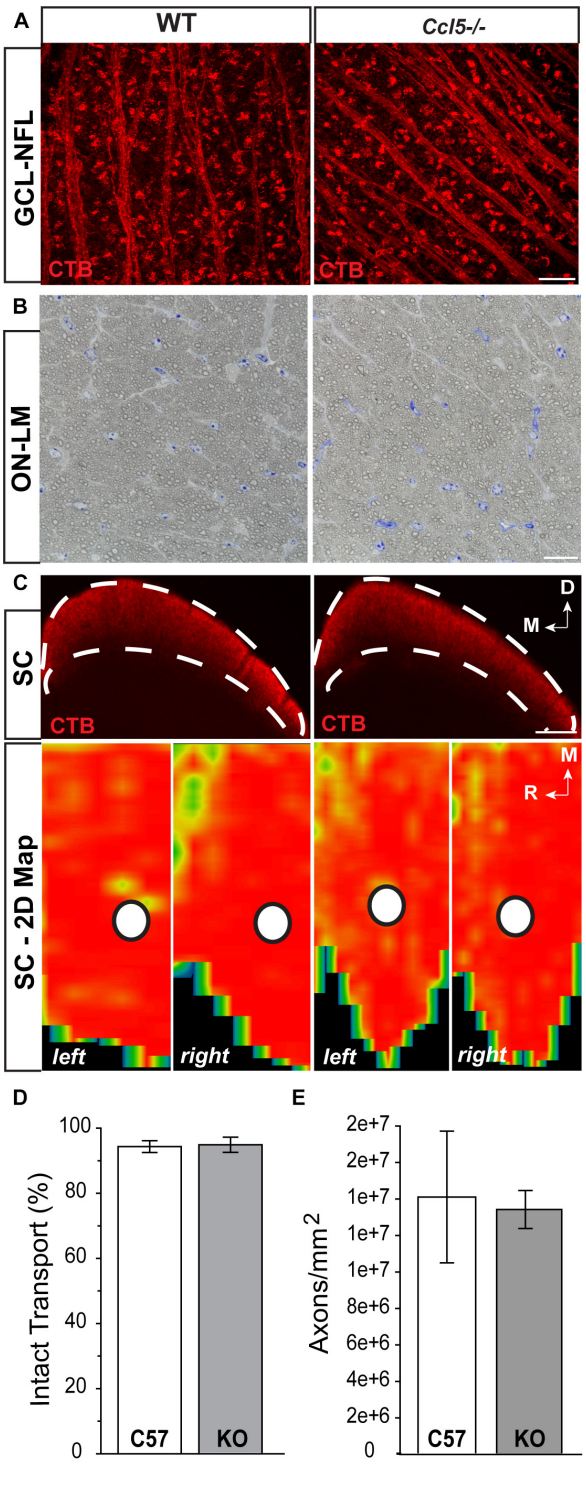

FIGURE 6 | Ccl5 deficiency does not alter the RGC projection to the superior colliculus. **(A)** Representative confocal fluoromicrographs (60×) of CTB neural tracing (red) in the GCL and NFL of whole mount retina from WT (left) and *Ccl5*$^{-/-}$ (right) mice. Both WT and *Ccl5*$^{-/-}$ retina demonstrate comprehensive uptake and transport of CTB in RGC soma and axons, respectively. Scale = 20 μm. **(B)** Representative micrographs (100×) of optic nerve cross-sections from WT (left) and *Ccl5*$^{-/-}$ (right) mice. Morphology of

(Continued)

than Gus^{gfp} mice (arrowheads; **Figures 3A,B**). Quantification of the number of Gus-GFP+ cells in the INL of Gus^{gfp} and Gus^{gfp}/*Ccl5*$^{-/-}$ mice revealed a 53% decrease in the number of Gus-GFP+ bipolar cells in Gus^{gfp}/*Ccl5*$^{-/-}$ mice, as compared to Gus^{gfp} mice ($p < 0.01$; $n = 12–19$/group; **Figure 3C**). Unlike Gus-GFP+ bipolar cells, PKCα+ rod bipolar cells in Gus^{gfp}/*Ccl5*$^{-/-}$

FIGURE 6 | Continued
RGC axons appear unremarkable in *Ccl5*$^{-/-}$ optic nerve, as compared to WT optic nerve. Scale = 100 μm. **(C)** Representative coronal sections through the superior colliculus (SC; top) and respective 2-D retinotopic heat maps of CTB labeling in the entire SC (left and right lobes; bottom) in WT (left panels) and *Ccl5*$^{-/-}$ (right panels) mice. Top: Dotted lines indicate retinorecipient layers in the superficial SC (top panels). Dorsal (D) and medial (M) orientations are indicated. Scale = 300 μm. Bottom: Density of the CTB signal for heat maps range from 0% (blue) to 50% (green) to 70% (yellow) to 100% (red). White circles indicate the OD representation in 2-D SC maps (bottom panels). Medial (M) and rostral (R) orientations are indicated. **(D)** Bar graph of average percent intact transport (>70% density of CTB signal; red/yellow areas) to the SC in WT (white) and *Ccl5*$^{-/-}$ (gray) mice reveals no difference between genotypes ($p > 0.05$). Error bars indicated standard deviation. **(E)** Bar graph of mean axon density in optic nerves from WT (white) and *Ccl5*$^{-/-}$ (gray) mice reveals no difference between genotypes ($p > 0.05$). Error bars indicate standard deviation.

mice exhibited altered morphology, where PKCα+ bipolar cells terminated well into the GCL rather than the inner sublamina of the IPL (dotted lines; **Figures 3A,B**). Quantification of the number of PKCα+ bipolar cells revealed that this alteration in bipolar cell terminations was not accompanied by a change in the number of PKCα+ bipolar cells, as compared to WT ($p > 0.05$; n = 12–20/group; **Figure 3D**). This suggests that the reduction in Gus-GFP+ rod bipolar cells represents a decrease in GUS expression in rod bipolar rather than a decrease in the actual population of rod bipolar cells. Thus, we quantified the number of Gus-GFP+/PKCα+ rod bipolar cells and the ratio of Gus-GFP+ cells to PKCα+ cells. We found that retina from Gus^{gfp}/*Ccl5*$^{-/-}$ contained 37% fewer Gus-GFP+/PKCα+ rod bipolar cells than Gus^{gfp} retina ($p < 0.01$; n = 12–20/group; **Figure 3E**). This decreased the ratio of Gus-GFP+ cells to PKCα+ cells by 26% ($p < 0.01$; n = 12–20/group; **Figure 3F**). Thus, Gus^{gfp}/*Ccl5*$^{-/-}$ retina contained fewer Gus-GFP+/PKCα+ bipolar cells and more PKCα+ only cells than wild-type Gus^{gfp} retina. Together, these data indicate that Ccl5 deficiency significantly alters the phenotype of mature rod bipolar cells, including reduced expression of GNAT3 and elongation of their terminals beyond the IPL-GCL boundary.

Ccl5 Deficiency Alters RGC Dendritic Morphology, but Not Density

To determine whether Ccl5 deficiency alters RGC maturation, we immunolabeled WT and *Ccl5*$^{-/-}$ retina with antibodies against the RGC-specific marker Brn3a and quantified the number of Brn3a+ cells. Brn3a+ RGCs were apparent in the GCL of both WT and *Ccl5*$^{-/-}$ retina (**Figure 4A**). Quantification revealed comparable numbers of Brn3a+ RGCs in the GCL in WT and *Ccl5*$^{-/-}$ mice ($p > 0.05$; **Figure 4B**). Since Ccl5 deficiency alters the position of rod bipolar cell terminals, we next examined the morphology of RGCs and their dendrites. We immunolabeled WT and *Ccl5*$^{-/-}$ retina with antibodies against beta-tubulin III (β-tubulin) and PKCα. RGCs in WT retina exhibit organized, upward trajectories of β-tubulin+ dendrites (filled arrows; **Figure 5A**). In contrast, RGCs in *Ccl5*$^{-/-}$ retina exhibit β-tubulin+ dendrites with multi-directional trajectories (unfilled arrows; **Figure 5A**). Co-immunolabeling with PKCα demonstrates clear separation between terminals of PKCα+ rod bipolar cells and β-tubulin+ RGC soma (filled arrowheads; **Figure 5B**). In *Ccl5*$^{-/-}$ retina, terminals of PKCα+ rod bipolar cells are interspersed between and around β-tubulin+ RGC soma (unfilled arrowheads; **Figure 5B**). β-Tubulin+ RGC dendrites are closely associated with these terminals, suggesting that aberrant trajectories of RGC dendrites reflect improper positioning of rod bipolar cell terminals (unfilled arrowheads vs. unfilled arrows; **Figure 5B**).

Ccl5 Deficiency Does Not Alter the RGC Projection

To determine whether Ccl5 deficiency impacts the primary RGC projection, we examined NFL and optic nerve morphology and RGC connectivity with distal brain structures. We performed neural tracing of the RGC projection with fluorophore-conjugated cholera toxin β-subunit (CTB). In rodents, approximately 90% of RGC axons terminate in the SC, with the remaining 10% terminating in the lateral geniculate nucleus, tectum and hypothalamus. Thus, we quantified anterograde transport of CTB from RGC soma to retinorecipient layers of the SC. Comparable to WT, CTB was apparent in RGC soma across the GCL and in the unmyelinated segment of RGC axons in the NFL (**Figure 6A**). Optic nerve integrity appeared intact with comparable axon myelination and glial cell content in semi-thin cross-sections of optic nerve from *Ccl5*$^{-/-}$ and WT mice (**Figure 6B**). CTB tracing revealed appropriate anterograde transport along the optic nerve to its termination in the SC in both WT and *Ccl5*$^{-/-}$ mice (**Figure 6C**). Two-dimensional reconstruction of CTB labeling in the SC and subsequent quantification of CTB labeling density revealed comparable innervation of retinorecipient layers in the SC between WT and *Ccl5*$^{-/-}$ mice ($p > 0.05$; n = 8–9/group; **Figures 6C,D**). Quantification of RGC axon density further indicated no difference between WT and *Ccl5*$^{-/-}$ mice ($p > 0.05$; n = 8–12/group; **Figure 6E**). These data demonstrate that, while Ccl5 deficiency alters the dendritic compartment of RGCs, it does not alter RGC density or their connectivity via the optic projection.

Ccl5 Deficiency Alters Amacrine Cell Morphology

Lateral inhibition in the inner retina is provided by amacrine cells, which are post-synaptic to bipolar cells and pre-synaptic partners to RGCs. To determine whether amacrine cell migration and differentiation is also affected by Ccl5 deficiency, we immunolabeled whole eye sections of WT and *Ccl5*$^{-/-}$ mice with antibodies against the amacrine cell marker syntaxin-1a. In WT mice, syntaxin immunolabeling was apparent in amacrine cell soma in the INL and GCL (arrowheads; **Figure 7A**) and, most markedly, in amacrine cell processes in the IPL (**Figure 7A**). In *Ccl5*$^{-/-}$ mice, the overall pattern of syntaxin+ labeling was similar to WT (**Figure 7A**). However, syntaxin labeling in the IPL of *Ccl5*$^{-/-}$ mice appeared more intense and concentrated, with individual processes of amacrine cells more apparent than in WT mice (**Figure 7A**). Quantification of syntaxin+ amacrine cell soma in the INL and GCL revealed no difference between

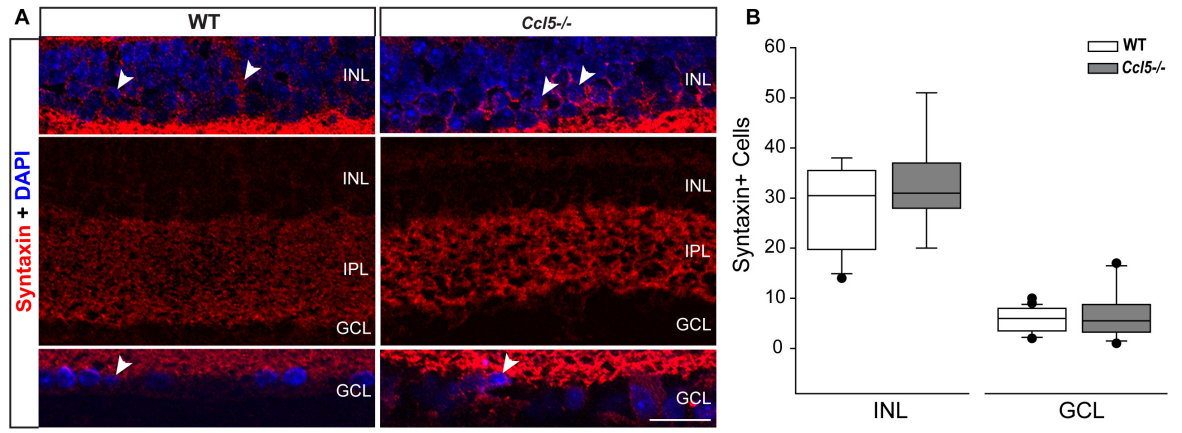

FIGURE 7 | Ccl5 deficiency alters the morphology and organization of amacrine cells. **(A)** Representative confocal micrographs (60×) of syntaxin-1A immunolabeling (red) with DAPI counterstain (blue) in INL (top), IPL (middle) and GCL (bottom) of retina from WT (left) and *Ccl5*$^{-/-}$ (right) mice. Syntaxin immunolabeling, particularly in the IPL, appears more condensed in the thinner IPL of *Ccl5*$^{-/-}$ retina, as compared to WT retina. Scale = 30 μm. **(B)** Box plot of the number of syntaxin+ cells in the INL (*y*-axis) of WT (white) and *Ccl5*$^{-/-}$ (gray) retina indicates no significant difference between genotypes. Error bars indicate standard deviation.

WT and *Ccl5*$^{-/-}$ mice ($p > 0.05$; $n = 25$–27/group; **Figure 7B**). This suggests that disorganization and altered substructure of the IPL in *Ccl5*$^{-/-}$ is not due to major alterations in amacrine cell number.

Ccl5-Deficiency Increases Spontaneous Activity of RGCs

The ultimate outcome of retinal processing is the RGC action potential. To determine the functional consequences of Ccl5-dependent changes in inner retinal structure, we characterized the physiological properties of individual RGCs in WT and *Ccl5*$^{-/-}$ retinas, using whole-cell patch clamp recordings. As suggested by our histological analyses, cell filling with Lucifer yellow during patch-clamp recording revealed the presence of an intact soma, dendritic tree (arrows) and axons (filled arrows) in both WT and *Ccl5*$^{-/-}$ retina (**Figure 8A**). RGCs in WT retina exhibited a range of spontaneous firing rates from 1 to 20 Hz (**Figure 8B**). In contrast, RGCs in *Ccl5*$^{-/-}$ mice exhibited a broader range of spontaneous spike rates ranging from 1 to 32 Hz (**Figure 8B**). RGCs in *Ccl5*$^{-/-}$ mice exhibited a more depolarized resting membrane potential (RMP) than those in WT retina (49 mV versus 53 mV; $p < 0.05$; $n = 38$–43/group; **Figure 8C**). However, there was no difference in mean membrane resistance (Rm) between the two genotypes ($p > 0.05$; $n = 37$–42/group; **Figure 8D**). As noted qualitatively (**Figure 8B**), the mean spontaneous spiking frequency was almost twofold higher in RGCs from *Ccl5*$^{-/-}$ mice than in RGCs from WT mice ($p < 0.05$; $n = 20$–33/group; **Figure 8E**). This was independent of ON/OFF or ON and OFF classification (**Supplementary Figure S1**). To determine whether this increased level of spontaneous activity is intrinsic to RGCs or arises from presynaptic circuitry, we applied depolarizing currents until the induced spike frequency exceeded 3 Hz. When the threshold firing rate of 3Hz was met or surpassed, the firing rates of RGCs from WT and *Ccl5*$^{-/-}$ retina were indistinguishable ($p > 0.05$; $n = 14$–18/group; **Figure 8E**). These data indicate that Ccl5 deficiency leads to a higher baseline activity in RGCs. However, Ccl5 deficiency does not alter RGC responses to applied current.

To better elucidate relationships between spike frequency and the physiological properties of RGCs in *Ccl5*$^{-/-}$ mice, we plotted spike frequency as function of both RMP and Rm in spontaneous and induced conditions. Based on Pearson Product Moment Correlation, there was no statistical relationship between spike frequency and RMP in either spontaneous or induced conditions ($p > 0.05$ for both; $n = 20$–33/group; **Figures 9A,B**). In contrast, spontaneous spike frequency negatively correlated with Rm in *Ccl5*$^{-/-}$ retina, such that RGCs with lower Rm exhibited higher spontaneous spiking frequencies ($p < 0.05$; $n = 32$/group; **Figure 9C**). Linear regression analysis revealed a low R-value for this relationship ($R^2 = 0.17$; $p < 0.01$; $n = 32$/group), indicating that the relationship is not direct. Unlike *Ccl5*$^{-/-}$ RGCs, spontaneous spike frequency in WT RGCs did not correlate with Rm ($p > 0.05$; $n = 19$/group; **Figure 9C**). Similarly, there was no relationship between induced spike frequency and Rm in either *Ccl5*$^{-/-}$ or WT retina ($p > 0.05$ for both; $n = 14$–18/group; **Figure 9D**). Together, these data indicate the Ccl5-deficiency leads to increased spontaneous activity that is related to membrane resistance. Furthermore, this excitability phenotype can be abolished by direct application of current, which circumvents pre-synaptic circuitry.

Since pre-synaptic circuitry may contribute to hyperexcitability of RGCs in *Ccl5*$^{-/-}$ retina and membrane resistance is dependent, in part, on cell morphology, we examined the relationship between soma area and the electrophysiological characteristics of RGCs from *Ccl5*$^{-/-}$ retina. We found that soma area negatively correlated with Rm, such that RGCs with larger soma had lower Rm ($p < 0.05$; $n = 27$–28/group; **Figure 9E**). Like the relationship between Rm and spontaneous spiking frequency (**Figure 9C**), linear regression analysis revealed a rather low, but statistically significant, R^2 value of 0.196 ($p < 0.05$; $n = 27$–28/group; **Figure 9E**). In contrast, soma

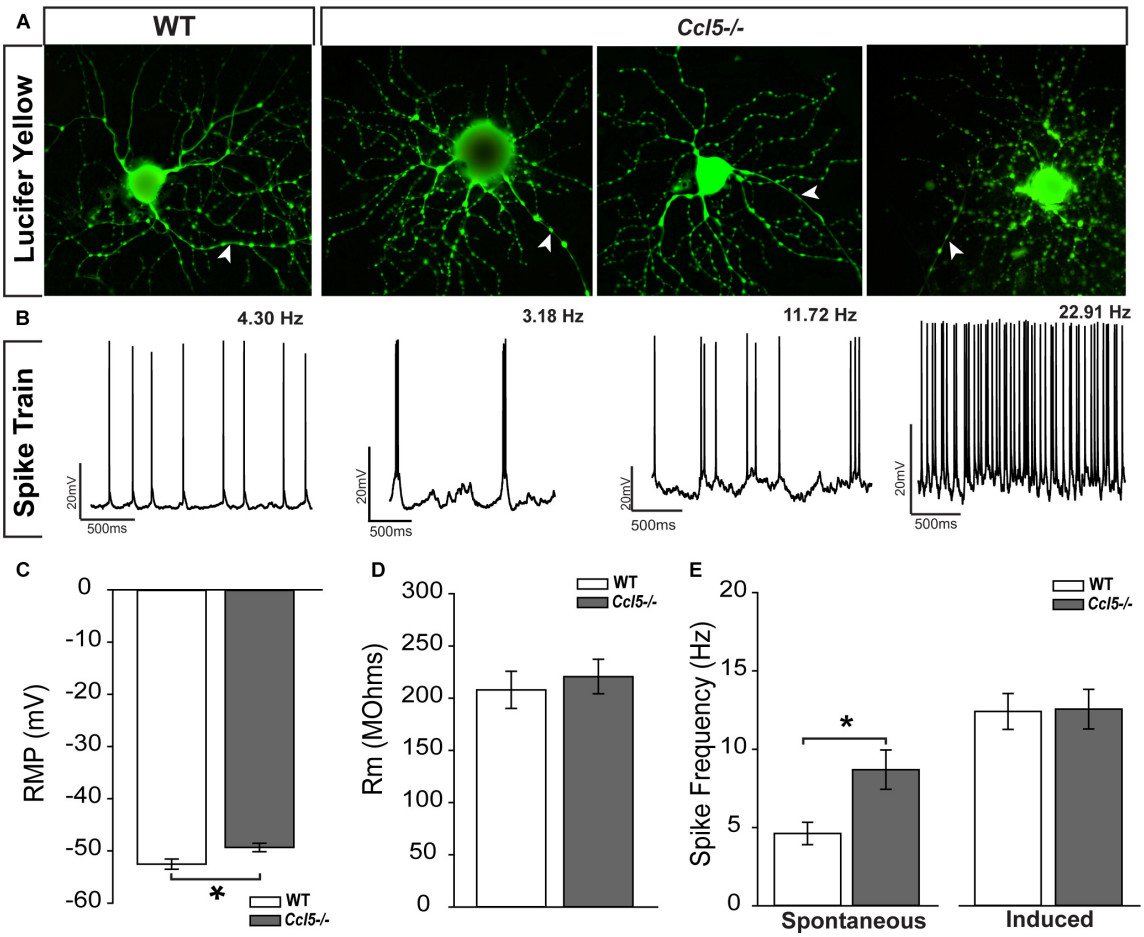

FIGURE 8 | $Ccl5^{-/-}$ deficiency increases spontaneous activity in RGCs. **(A)** Representative micrographs of RGCs from WT (right) and $Ccl5^{-/-}$ (left) filled with 1% Lucifer yellow during whole-cell patch-clamp recording reveal the presence of ramified dendritic trees and intact axons (arrowheads) in both genotypes. **(B)** Representative action potential traces from the cells depicted in **(A)** reveal a broad range of spiking frequencies in RGCs from $Ccl5^{-/-}$ mice that tend toward higher frequencies. **(C)** Graphical representation of mean intrinsic resting membrane potential (RMP; mV; *y*-axis) in RGCs from WT (white) and $Ccl5^{-/-}$ (gray) retina RGCs. Error bars indicate standard error. Asterisks indicate $p < 0.05$. **(D)** Graphical representation of intrinsic membrane resistance (Rm; MΩ; *y*-axis) in RGCs from WT (white) and $Ccl5^{-/-}$ (gray) retina reveals no difference between genotypes. Error bars indicate standard error. **(E)** Graphical representation of mean spiking frequency (Hz; *y*-axis) in spontaneous (left; *x*-axis) and current-induced (right; *x*-axis) conditions for RGCs in WT (white) and $Ccl5^{-/-}$ (gray) retina. Error bars indicate standard error. Asterisks indicate $p < 0.05$.

area positively correlated with spontaneous spiking frequency, such that RGCs with larger soma tended to have a higher level of baseline activity ($p < 0.05$; $n = 27$–28/group; **Figure 9F**). Linear regression analysis revealed a higher, but still modest, R^2 value of 0.260 ($p < 0.05$; $n = 27$–28/group; **Figure 9F**). There was no correlation between soma area and RMP ($p > 0.05$; $n = 27$–28/group). Together, these data suggest that Ccl5-dependent changes in Rm and spontaneous spiking frequency are both related to morphological changes in RGCs.

DISCUSSION

Here, we identified a role for Ccl5 signaling in development of the murine retina. We found that Ccl5 deficiency in $Ccl5^{-/-}$ mice results in thinning of the inner retina, particularly the INL and IPL (**Figure 1**). Assessment of postnatal timepoints important for development of the INL (P7 and P10) revealed Ccl5-dependent alterations in the cell density pattern and timing of apoptotic pruning (**Figure 2**). Assessment of major cell classifications in the mature inner retina revealed Ccl5-dependent changes in: (1) rod bipolar cell phenotypes, including displacement of their terminals from the IPL into the GCL (**Figure 3**), (2) RGC dendritic organization (**Figure 5**), and (3) amacrine cell morphology in the IPL (**Figure 7**). Examination of the intrinsic electrophysiological properties of RGCs revealed higher spontaneous activity in $Ccl5^{-/-}$ mice that was characterized by higher spiking frequency and a more depolarized resting potential (**Figure 8**). This hyperactive phenotype could be negated by current clamp, suggesting dependence on pre-synaptic circuitry (**Figure 8**). The putative relationship between Ccl5-dependent changes in pre-synaptic circuitry and RGC hyperactivity was further

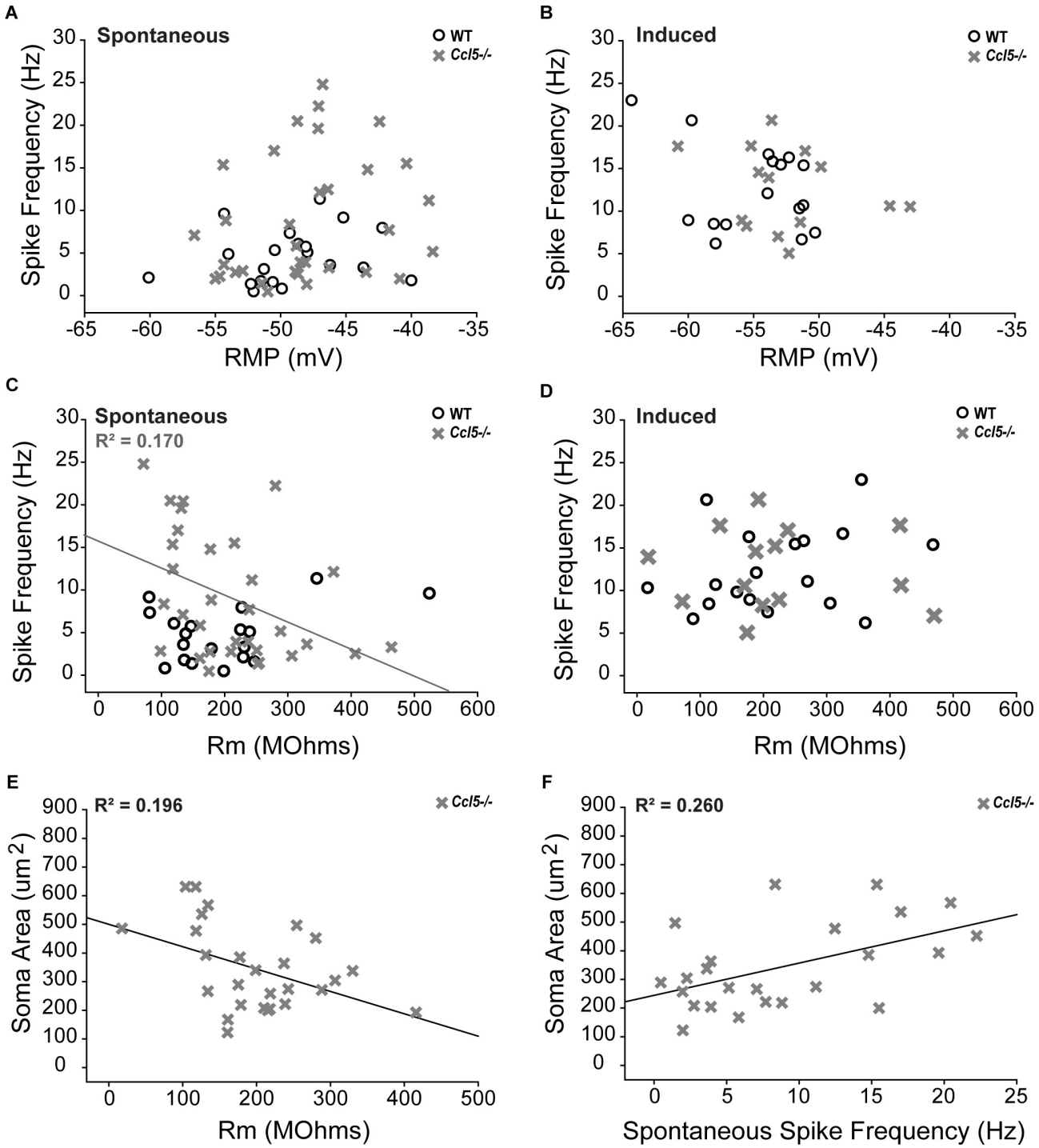

FIGURE 9 | Increased spontaneous activity in *Ccl5*$^{-/-}$ RGCs is related to Rm and soma size. **(A,B)** Graphical representation of spontaneous **(A)** and induced **(B)** spiking frequency (Hz; *y*-axis) as a function of RMP (mV; *x*-axis) in RGCs from WT (white circles) and *Ccl5*$^{-/-}$ (gray crosses) mice reveals no relationship between these intrinsic properties in either condition for both genotypes ($p > 0.05$). **(C,D)** Graphical representation of spontaneous **(C)** and induced **(D)** spiking frequency (Hz; *y*-axis) as a function of Rm (MΩ; *x*-axis) in RGCs from WT (white circles) and *Ccl5*$^{-/-}$ (gray crosses) mice reveals no relationship between these intrinsic properties in either condition for WT RGCs ($p > 0.05$). Similarly, there is no relationship between Rm and induced spiking frequency in *Ccl5*$^{-/-}$ RGCs ($p < 0.05$). However, spontaneous spiking frequency is inversely proportional to Rm in *Ccl5*$^{-/-}$ RGCs (gray line; $R^2 = 0.170$, $p < 0.05$). **(E)** Graphical representation of soma area (μm^2; *y*-axis) as a function of Rm (MΩ; *x*-axis) in RGCs from *Ccl5*$^{-/-}$ (gray crosses) mice reveals that Rm is inversely proportional to soma area in *Ccl5*$^{-/-}$ RGCs (gray line; $R^2 = 0.196$, $p < 0.05$). **(F)** Graphical representation of soma area (μm^2; *y*-axis) as a function of spontaneous spiking frequency (Hz; *x*-axis) in RGCs from *Ccl5*$^{-/-}$ (gray crosses) mice reveals that spontaneous spiking frequency proportional to soma area in *Ccl5*$^{-/-}$ RGCs (gray line; $R^2 = 0.260$, $p < 0.05$).

supported by statistical correlations between Rm, soma area and spontaneous spiking frequency (**Figure 9**). Together, our findings have implications for not only the functional role of Ccl5 in the developing retina, but also for the development of specific visual circuits within the retina more generally.

Despite CCL5-dependent changes in inner retinal development (**Figure 2**), our analyses in mature retina suggest that phenotypic changes in *Ccl5*$^{-/-}$ retina arise primarily from disorganized or aberrant wiring within the inner retina rather than loss of neurons. This is consistent with the magnitude of INL and IPL thinning, which was significant and highly consistent, but in the range of only 4–7% (**Figure 1**). We found evidence of aberrant organization of processes for all three of the major neuronal subtypes in the inner retina, including: bipolar cells, amacrine cells and RGCs (**Figures 3**, **5**, **7**). As a chemotactic cytokine, CCL5 induces migration of cells by influencing cell polarization, cytoskeleton dynamics and extracellular matrix adhesion (Weiss-Haljiti et al., 2004). In multiple contexts, CCL5-dependent modulation of these activities is linked to downstream activation and expression of a variety of cytoskeletal mediators, including the Rho family of GTPases, cyclin D1 and matrix metalloproteinases (Turner et al., 1995; Xia et al., 1996; Weiss-Haljiti et al., 2004; Murooka et al., 2008). Thus, it is conceivable that activation of Ccl5 signaling plays a role in physically attracting dendrites and terminals of synaptic partners together during wiring of inner retinal circuitry.

Our previous work indicates that Ccr5 and Ccr3, two high-affinity receptors for Ccl5, are expressed liberally in the inner retina (Duncan et al., 2017). The pattern of localization for Ccr5 and Ccr3 is similar to that of Ccl5 (Duncan et al., 2017), suggesting that Ccl5 could serve as a signaling factor between multiple cell types in the inner retina. Our current study is unable to determine the directional nature of Ccl5 signaling and thus, the cell type-specific dependency of Ccl5-mediated wiring. However, there is evidence that other chemokine signaling, i.e., Cxcl12, mediates tangential migration of interneurons during cortical development (Stumm et al., 2003, 2007; Daniel et al., 2005; Tiveron et al., 2006; Li et al., 2008; López-Bendito et al., 2008; Saìnchez-Alcañiz et al., 2011). Additionally, amacrine cells are early-born neurons, while bipolar cells are late-born neurons (Young, 1985; Ohsawa and Kageyama, 2008; Agathocleous and Harris, 2009; Mattar and Cayouette, 2015). Thus, bipolar cell orientation is dependent, in part, on proper positioning of the amacrine cell population (Reese and Keeley, 2016). Finally, our electrophysiological findings suggest that RGCs are hyperactive in *Ccl5*$^{-/-}$ mice (**Figure 8**), suggesting disruption of inhibitory neurotransmission. This is further supported by our findings that: (1) activity of *Ccl5*$^{-/-}$ and WT RGCs is indistinguishable when pre-synaptic circuitry is circumvented with current clamp (**Figure 8**) and (2) spontaneous spiking frequency correlates with both Rm and soma area (**Figure 9**). As such, amacrine cells may be preferentially impacted by Ccl5 signaling during inner retina development. Further studies are needed to determine the relevance of Ccl5 signaling for amacrine cell populations, which are the most diverse cell population in the retina in terms of both synaptic wiring and neurotransmission capabilities (Balasubramanian and Gan, 2014).

While the inner retina broadly exhibited changes in cytoarchitecture, the rod bipolar cell population was markedly affected with respect to both morphology and phenotype. This is significant from both CCL5 and retinal circuitry perspectives. Ccl5-mediated activity, including cell migration and angiogenic outcomes, in non-neuronal cell types is PKCα dependent (Maillard et al., 2014; Ya et al., 2018). We found that Ccl5 deficiency markedly reduces GFP expression under the GNAT3 promoter, which encodes expression of GUS. GUS localizes to rod bipolar cell terminals in mammalian retina (Son et al., 2011). This is interesting in light of our finding that rod bipolar cells in *Ccl5*$^{-/-}$ retina terminate improperly beyond the boundaries of the IPL (**Figure 3**). It is possible that GNAT3 expression in rod bipolar cells is either dependent upon or mediates establishment of rod bipolar cell terminals. Although we did not observe Ccl5-dependent alterations in the morphology of Type 7 cone bipolar cells in Gus^{gfp} and Gus^{gfp}/*Ccl5*$^{-/-}$ mice, the potential remains that Ccl5 signaling could play a role in the development, differentiation or synaptic partnering of other cone bipolar cells. This should be systematically examined in future studies.

Here, we focused on developmental outcomes of Ccl5 signaling. However, Ccl5 machinery is expressed constitutively in mature mouse retina (Duncan et al., 2017). This suggests that Ccl5 signaling is likely important for inner retinal neurons during both development and maturity. In the mature CNS, Ccl5 signaling linked to both inhibitory and glutamatergic neurotransmission. Ccl5 and Ccr expression is present within the ventral tegmental area, nucleus accumbens, striatum, prefrontal cortex, hippocampus, striatum and frontal cortex (Szabo et al., 2002; Campbell et al., 2013; Mocchetti et al., 2013; Fe Lanfranco et al., 2018). Given expression of Ccl5 and Ccrs are associated with known brain circuits, i.e., dopaminergic mesolimbic pathway, and can modulate neurotransmission, it has been proposed that chemokines may serve as a third neurotransmitter system in the CNS (Adler and Rogers, 2005). Thus, it is possible that Ccl5 signaling is preserved in mature retina as a modulator of neurotransmission between bipolar cells, amacrine cells and RGCs. This would have additional implications for our findings regarding RGC hyperactivity in *Ccl5*$^{-/-}$ mice (**Figure 8**).

Overall, our findings identify Ccl5 signaling as a mediator of inner retinal circuitry during development of the murine retina. Additional studies are needed to determine the specific cell-cell interactions that mediate this signaling as well as the temporal characteristics during development and in maturity. The apparent role of Ccl5 in retinal development further supports chemokines as trophic modulators of CNS development and function that extends far beyond the inflammatory contexts in which they were first characterized.

AUTHOR CONTRIBUTIONS

DD and RW equally designed the study, performed the experiments, analyzed the data, and contributed to writing of the

manuscript. AR, ES, CW, MR and CF performed the experiments and analyzed the data. All authors have read and approved the final manuscript.

FUNDING

These studies were supported by the National Eye Institute awards RO1EY020496 (RMS), RO1EY027729 (YX, DL, RMS) and P30EY08126 (Vanderbilt Vision Research Center) and Career Development (RMS) and Unrestricted (Vanderbilt Eye Institute) awards from Research to Prevent Blindness, Inc.

ACKNOWLEDGMENTS

The authors would like to thank Dr. Benjamin Reese (University of California, Santa Barbara, Santa Barbara, CA, United States) for the generous gift of Gus^{gfp} reporter mice. The authors would also like to thank the Vanderbilt University Medical Center Cell Imaging Shared Resource Core for assistance in confocal imaging.

SUPPLEMENTARY MATERIAL

The Supplementary Material for this article can be found online at: https://www.frontiersin.org/articles/10.3389/fnins.2018.00702/full#supplementary-material

FIGURE S1 | Ccl5-dependent increases in mean spontaneous spiking frequency is consistent across RGC sub-types. Graphical representation of mean spontaneous spiking frequency (Hz; *y*-axis) in ON or OFF RGCs (left; *x*-axis) and ON/OFF RGCs (right; *x*-axis) in WT (white) and $Ccl5^{-/-}$ (gray) retina. Spontaneous spiking frequency is 39% higher in ON or OFF RGCs ($n = 7$) and 45% higher in ON/OFF RGCs ($n = 11$) in $Ccl5^{-/-}$ mice, as compared to WT retina ($n = 8$ for both; $p < 0.05$). Error bars indicate standard deviation. Asterisks indicate $p < 0.05$.

REFERENCES

Adler, M. W., and Rogers, T. J. (2005). Are chemokines the third major system in the brain? *J. Leukoc. Biol.* 78, 1204–1209. doi: 10.1189/jlb.0405222

Agathocleous, M., and Harris, W. A. (2009). From progenitors to differentiated cells in the vertebrate retina. *Ann. Rev. Cell Dev. Biol.* 25, 45–69. doi: 10.1146/annurev.cellbio.042308.113259

Appay, V., and Rowland-Jones, S. L. (2001). RANTES: a versatile and controversial chemokine. *Trends Immunol.* 22, 83–87. doi: 10.1016/S1471-4906(00)01812-3

Babcock, A. A., Kuziel, W. A., Rivest, S., and Owens, T. (2003). Chemokine expression by glial cells directs leukocytes to sites of axonal injury in the CNS. *J. Neurosci.* 23, 7922–7930. doi: 10.1523/JNEUROSCI.23-21-07922.2003

Balasubramanian, R., and Gan, L. (2014). Development of retinal amacrine cells and their dendritic stratification. *Curr. Ophthalmol. Rep.* 2, 100–106. doi: 10.1007/s40135-014-0048-2

Bond, W. S., Hines-Beard, J. B., GoldenMerry, Y. P. L., Davis, M., Farooque, A., Sappington, R. M., et al. (2016). Virus-mediated EpoR76E therapy slows optic nerve axonopathy in experimental glaucoma. *Mol. Ther.* 2, 230–239. doi: 10.1038/mt.2015.198

Brandstätter, J. H., Koulen, P., and Wässle, H. (1998). Diversity of glutamate receptors in the mammalian retina. *Vision Res.* 38, 1385–1397. doi: 10.1016/S0042-6989(97)00176-4

Campbell, L. A., Avdoshina, V., Rozzi, S., and Mocchetti, I. (2013). CCL5 and cytokine expression in the rat brain: differential modulation by chronic morphine and morphine withdrawal. *Brain Behav. Immun.* 34, 130–140. doi: 10.1016/j.bbi.2013.08.006

Crish, S. D., Sappington, R. M., Inman, D. M., Horner, P. J., and Calkins, D. J. (2010). Distal axonopathy with structural persistence in glaucomatous neurodegeneration. *Proc. Nat. Acad. Sci. U.S.A.* 107, 5196–5201. doi: 10.1073/pnas.0913141107

Daniel, D., Rossel, M., Seki, T., and König, N. (2005). Stromal cell-derived factor-1 (SDF-1) expression in embryonic mouse cerebral cortex starts in the intermediate zone close to the pallial-subpallial boundary and extends progressively towards the cortical hem. *Gene Expr. Patterns* 5, 317–322. doi: 10.1016/j.modgep.2004.10.007

Duncan, D. S., McLaughlin, W. M., Vasilakes, N., Echevarria, F. D., Formichella, C. R., and Sappington, R. M. (2017). Characterization of constitutive and stress-induced Ccl5 signaling in rodent retina. *J. Clin. Cell. Immunol.* 8:506. doi: 10.4172/2155-9899.1000506

Echevarria, F. D., Formichella, C. R., and Sappington, R. M. (2017). Interleukin-6 deficiency attenuates retinal ganglion cell axonopathy and glaucoma-related vision loss. *Front. Neurosci.* 11:318. doi: 10.3389/fnins.2017.00318

Echevarria, F. D., Walker, C. C., Abella, S. K., Won, M., and Sappington, R. M. (2013). Stressor-dependent alterations in glycoprotein 130: implications for glial cell reactivity, cytokine signaling and ganglion cell health in glaucoma. *J. Clin. Exp. Ophthalmol.* 4:1000286.

Fe Lanfranco, M., Mocchetti, I., Burns, M. P., and Villapol, S. (2018). Glial- and neuronal-specific expression of CCL5 mRNA in the rat brain. *Front. Neuroanat.* 11:137. doi: 10.3389/fnana.2017.00137

Galasso, J. M., Harrison, J. K., and Silverstein, F. S. (1998). Excitotoxic brain injury stimulates expression of the chemokine receptor CCR5 in neonatal rats. *Am. J. Pathol.* 153, 1631–1640. doi: 10.1016/S0002-9440(10)65752-5

Gamo, K., Kiryu-Seo, S., Konishi, H., Aoki, S., Matsushima, K., Wada, K., et al. (2008). G-protein-coupled receptor screen reveals a role for chemokine receptor CCR5 in suppressing microglial neurotoxicity. *J. Neurosci.* 28, 11980–11988. doi: 10.1523/JNEUROSCI.2920-08.2008

Ghosh, K. K., Bujan, S., Haverkamp, S., Feigenspan, A., and Wässle, H. (2004). Types of bipolar cells in the mouse retina. *J. Comp. Neurol.* 469, 70–82. doi: 10.1002/cne.10985

He, J., Chen, Y., Farzan, M., Choe, H., Ohagen, A., Gartner, S., et al. (1997). CCR3 and CCR5 are co-receptors for HIV-1 infection of microglia. *Nature* 385, 645–649. doi: 10.1038/385645a0

Huang, L., Max, M., Margolskee, R. F., Su, H., Masland, R. H., and Euler, T. (2003). Gprotein subunit G gamma 13 is coexpressed with G alpha o, G beta 3, and G beta 4 in retinal ON bipolar cells. *J. Comp. Neurol.* 455, 1–10. doi: 10.1002/cne.10396

Jeon, C.-J., Strettoi, E., and Masland, R. H. (1998). The major cell populations of the mouse retina. *J. Neurosci.* 18, 8936–8946. doi: 10.1523/JNEUROSCI.18-21-08936.1998

Li, G., Adesnik, H., Li, J., Long, J., Nicoll, R. A., Rubenstein, J. L. R., et al. (2008). Regional distribution of cortical interneurons and development of inhibitory tone are regulated by Cxcl12/Cxcr4 signaling. *J. Neurosci.* 28, 1085–1098. doi: 10.1523/JNEUROSCI.4602-07.2008

López-Bendito, G., Saìnchez-Alcanþiz, J. A., Pla, R., Borrell, V., Picoì, E., Valdeolmillos, M., et al. (2008). Chemokine signaling controls intracortical migration and final distribution of GABAergic interneurons. *J. Neurosci.* 28, 1613–1624. doi: 10.1523/JNEUROSCI.4651-07.2008

Maillard, L., Saito, N., Hlawaty, H., Friand, V., Suffee, N., Chmilewsky, F., et al. (2014). RANTES/CCL5 mediated-biological effects depend on the syndecan-4/PKCa signaling pathway. *Biol. Open* 3, 995–1004. doi: 10.1242/bio.20148227

Mattar, P., and Cayouette, M. (2015). Mechanisms of temporal identity regulation in mouse retinal progenitor cells. *Neurogenesis* 2:e1125409. doi: 10.1080/23262133.2015.1125409

Mennicken, F., Chabot, J. G., and Quirion, R. (2002). Systemic administration of kainic acid in adult rat stimulates expression of the chemokine receptor CCR5 in the forebrain. *Glia* 37, 124–138. doi: 10.1002/glia.10021

Mocchetti, I., Campbell, L. A., Harry, G. J., and Avdoshina, V. (2013). When human immunodeficiency virus meets chemokines and microglia: neuroprotection

or neurodegeneration? *J. Neuroimmune Pharmacol.* 8, 118–131. doi: 10.1007/s11481-012-9353-4

Morgan, J., and Wong, R. (2005). "Development of cell types and synaptic connections in the retina," in *Webvision: The Organization of the Retina and Visual System*, eds H. Kolb, E. Fernandez, and R. Nelson (Salt Lake City: UT: University of Utah Health Sciences Center).

Murooka, T. T., Rahbar, R., Platanias, L. C., and Fish, E. N. (2008). CCL5-mediated T-cell chemotaxis involves the initiation of mRNA translation through mTOR/4E-BP1. *Blood* 111, 4892–4901. doi: 10.1182/blood-2007-11-125039

Ohsawa, R., and Kageyama, R. (2008). Regulation of retinal cell fate specification by multiple transcription factors. *Brain Res.* 1192, 90–98. doi: 10.1016/j.brainres.2007.04.014

Pham, V. T., Wen, L., McCluskey, P., Madigan, M. C., and Penfold, P. L. (2005). Human retinal microglia express candidate receptors for HIV-1 infection. *Br. J. Ophthalmol.* 89, 753–757. doi: 10.1136/bjo.2004.057828

Reese, B. E. (2011). Development of the retina and optic pathway. *Vision Res.* 51, 613–632. doi: 10.1016/j.visres.2010.07.010

Reese, B. E., and Keeley, P. W. (2016). Genomic control of neuronal demographics in the retina. *Prog. Retin. Eye Res.* 55, 246–259. doi: 10.1016/j.preteyeres.2016.07.003

Rossi, D., and Zlotnik, A. (2000). The biology of chemokines, and their receptors. *Annu. Rev. Immunol.* 18, 217–242. doi: 10.1146/annurev.immunol.18.1.217

Sappington, R. M., Carlson, B. J., Crish, S., and Calkins, D. J. (2010). The microbead occlusion model: a paradigm for induced ocular hypertension in rats, and mice. *Invest. Ophthalmol. Vis. Sci.* 51, 207–216. doi: 10.1167/iovs.09-3947

Saìnchez-Alcañiz, J. A., Haege, S., Mueller, W., Pla, R., Mackay, F., Schulz, S., et al. (2011). Cxcr7 controls neuronal migration by regulating chemokine responsiveness. *Neuron* 69, 77–90. doi: 10.1016/j.neuron.2010.12.006

Sims, S. M., Holmgren, L., and Cathcart, H. M. (2012). Sappington RM. Spatial regulation of interleukin-6 signaling in response to neurodegenerative stressors in the retina. *Am. J. Neurodegen. Dis.* 1, 168–179.

Son, M. J., Hu, Y. J., Kim, S. A., Chun, M. H., Kim, I. B., and Kim, M. S. (2011). Expression of α-gustducin in mammalian retinas. *Neuroreport* 22, 146–150. doi: 10.1097/WNR.0b013e328343701f

Sorce, S., Bonnefont, J., Julien, S., Marq-Lin, N., Rodriguez, I., Dubois-Dauphin, M., et al. (2010). Increased brain damage after ischaemic stroke in mice lacking the chemokine receptor CCR5. *Br. J. Pharmacol.* 160, 311–321. doi: 10.1111/j.1476-5381.2010.00697.x

Sorce, S., Myburgh, R., and Krause, K. H. (2011). The chemokine receptor CCR5 in the central nervous system. *Prog. Neurobiol.* 93, 297–311. doi: 10.1016/j.pneurobio.2010.12.003

Stumm, R., Kolodziej, A., Schulz, S., Kohtz, J. D., and Höllt, V. (2007). Patterns of SDF-1alpha and SDF-1gamma mRNAs, migration pathways, and phenotypes of CXCR4-expressing neurons in the developing rat telencephalon. *J. Comp. Neurol.* 502, 382–399. doi: 10.1002/cne.21336

Stumm, R. K., Zhou, C., Ara, T., Lazarini, F., Dubois-Dalcq, M., Nagasawa, T., et al. (2003). CXCR4 regulates interneuron migration in the developing neocortex. *J. Neurosci.* 23, 5123–5130. doi: 10.1523/JNEUROSCI.23-12-05123.2003

Subileau, E. A., Rezaie, P., Davies, H. A., Colyer, F. M., Greenwood, J., Male, D. K., et al. (2009). Expression of chemokines and their receptors by human brain endothelium: implications for multiple sclerosis. *J. Neuropathol. Exp. Neurol.* 68, 227–240. doi: 10.1097/NEN.0b013e318197eca7

Szabo, I., Chen, X. H., Xin, L., Adler, M. W., Howard, O. M., Oppenheim, J. J., et al. (2002). Heterologous desensitization of opioid receptors by chemokines inhibits chemotaxis and enhances the perception of pain. *Proc. Natl. Acad. Sci. U.S.A.* 2002, 10276–10281. doi: 10.1073/pnas.102327699

Tiveron, M.-C., Rossel, M., Moepps, B., Zhang, Y. L., Seidenfaden, R., Favor, J., et al. (2006). Molecular interaction between projection neuron precursors and invading interneurons via stromal-derived factor 1 (CXCL12)/CXCR4 signaling in the cortical subventricular zone/intermediate zone. *J. Neurosci.* 26, 13273–13278. doi: 10.1523/JNEUROSCI.4162-06.2006

Tripathy, D., Thirumangalakudi, L., and Grammas, P. (2010). RANTES upregulation in the Alzheimer's disease brain: a possible neuroprotective role. *Neurobiol. Aging* 31, 8–16. doi: 10.1016/j.neurobiolaging.2008.03.009

Turner, L., Ward, S. G., and Westwick, J. (1995). RANTES-activated human T lymphocytes. A role for phosphoinositide 3-kinase. *J. Immunol.* 155, 2437–2444.

Weiss-Haljiti, C., Pasquali, C., Ji, H., Gillieron, C., Chabert, C., Curchod, M. L., et al. (2004). Involvement of phosphoinositide 3-kinase gamma, rac, and PAK signaling in chemokine-induced macrophage migration. *J. Biol. Chem.* 279, 43273–43284. doi: 10.1074/jbc.M402924200

Weitlauf, C., Ward, N., Lambert, W., Sidorova, T., Ho, K., Sappington, R. M., et al. (2015). Transiently increased TRPV1 mediates stress-induced enhancement of neuronal excitation. *J. Neurosci.* 34, 15369–15381. doi: 10.1523/JNEUROSCI.3424-14.2014

Xia, M., Gaufo, G. O., Wang, Q., Sreedharan, S. P., and Goetzl, E. J. (1996). Transduction of specific inhibition of HuT 78 human T cell chemotaxis by type I vasoactive intestinal peptide receptors. *J. Immunol.* 157, 1132–1138.

Ya, F., Zhang, P., Zeshong, T., Li, Q., Ling, W., and Yang, Y. (2018). Coenzyme Q10 reduces platelet hyperreactivity and attenuates atherosclerosis via inhibiting platelet αIIbβ3-mediated signaling pathway. *Atherosclerosis* 32, 126–127. doi: 10.1016/j.atherosclerosissup.2018.04.389

Young, R. W. (1985). Cell differentiation in the retina of the mouse. *Anat. Rec.* 212, 199–205. doi: 10.1002/ar.1092120215

Zhang, X., Serb, J. M., and Greenlee, M. H. W. (2011). Mouse retinal development: a dark horse model for systems biology research. *Bioinform. Biol. Insights* 5, 99–113. doi: 10.4137/BBI.S6930

Conflict of Interest Statement: The authors declare that the research was conducted in the absence of any commercial or financial relationships that could be construed as a potential conflict of interest.

frontiers in Neuroscience

REVIEW
published: 12 November 2018
doi: 10.3389/fnins.2018.00821

Heat Shock Proteins Regulatory Role in Neurodevelopment

David J. Miller[1,2] *and Patrice E. Fort*[1,2]*

[1] Department of Ophthalmology and Visual Sciences, University of Michigan, Ann Arbor, MI, United States, [2] Department of Molecular and Integrative Physiology, University of Michigan, Ann Arbor, MI, United States

Heat shock proteins (Hsps) are a large family of molecular chaperones that are well-known for their roles in protein maturation, re-folding and degradation. While some Hsps are constitutively expressed in certain regions, others are rapidly upregulated in the presence of stressful stimuli. Numerous stressors, including hyperthermia and hypoxia, can induce the expression of Hsps, which, in turn, interact with client proteins and co-chaperones to regulate cell growth and survival. Such interactions must be tightly regulated, especially at critical points during embryonic and postnatal development. Hsps exhibit specific patterns of expression consistent with a spatio-temporally regulated role in neurodevelopment. There is also growing evidence that Hsps may promote or inhibit neurodevelopment through specific pathways regulating cell differentiation, neurite outgrowth, cell migration, or angiogenesis. This review will examine the regulatory role that these individual chaperones may play in neurodevelopment, and will focus specifically on the signaling pathways involved in the maturation of neuronal and glial cells as well as the underlying vascular network.

Keywords: heat shock proteins, neurodevelopment, neurite extension, cell migration, axon guidance, neurovascular unit

OPEN ACCESS

Edited by:
Alfonso Represa, INSERM U901 Institut de Neurobiologie de la Méditerranée, France

Reviewed by:
Carlos Vicario-Abejón, Consejo Superior de Investigaciones Científicas (CSIC), Spain
Hari S. Sharma, Uppsala University, Sweden

***Correspondence:**
Patrice E. Fort
patricef@med.umich.edu;
patricef@umich.edu

Specialty section:
This article was submitted to Neurogenesis, a section of the journal Frontiers in Neuroscience

Received: *06 July 2018*
Accepted: *22 October 2018*
Published: *12 November 2018*

Citation:
Miller DJ and Fort PE (2018) Heat Shock Proteins Regulatory Role in Neurodevelopment. Front. Neurosci. 12:821. doi: 10.3389/fnins.2018.00821

INTRODUCTION

Heat shock proteins (Hsps) are a large family of evolutionarily conserved molecular chaperones with pivotal roles in cell survival and development. Hsps can be broadly classified into two families based on comparable molecular mass. First, the small, ATP-independent Hsps are chaperones of a molecular mass between 8 and 28 kDa. These chaperones include ubiquitin, the α-crystallins, HspB1 (also known as Hsp25 in mice or Hsp27 in rats and humans), and many others (for review, see Bakthisaran et al., 2015). These small Hsps have received increasing attention in recent years, mostly due to their potential in protective approaches. Second, the large, ATP-dependent Hsps are chaperones of a molecular mass between 40 and 105 kDA. These include the well-known chaperones of the 70 and 90 kDa families. The 70 kDa group consists of the stress-inducible Hsp70 and the constitutively expressed

heat shock cognate 70 (Hsc70). Similarly, the 90-kDa group consists of two major isoforms, namely the inducible Hsp90α and the constitutively expressed Hsp90β. However, because these isoforms are often difficult to isolate, many studies have resorted to studying co-purified aggregates containing both Hsp90α and Hsp90β, simply referring to the whole as Hsp90 (Sreedhar et al., 2004). Other large Hsps include the Hsp40s or J-proteins, which interact with Hsp70 through their J domain and serve as regulatory co-chaperones (Walsh et al., 2004).

Hsps confer thermotolerance in all organisms in which they have been studied (Lindquist and Craig, 1988), but also provide protection from insults such as hypoxia and cytotoxic exposure. Initially discovered as a group of proteins upregulated in heat-stressed *Drosophila melanogaster* (Ritossa, 1962; Tissières et al., 1974), Hsps are now understood to perform critical functions both in stressed and "unstressed" conditions (i.e., in the absence of supraphysiologic stress). The protective effects of Hsps are mediated at least in part through their chaperone functions. Molecular chaperones are proteins that facilitate native protein stabilization, translocation, re-folding, and degradation. These functions are often performed with the assistance of co-chaperones, which regulate chaperone affinity for a given substrate. Together, Hsps and their respective co-chaperones not only ensure protein quality control, but also prevent protein aggregation that would otherwise overwhelm the cell and lead to programmed cell death or necrosis. Despite these functional similarities, individual Hsps vary considerably in their expression, protein structure, localization, and ability to be induced (**Table 1**).

One of the essential roles of Hsps under "normal" conditions is to promote proper embryonic and postnatal development of multiple organ systems, particularly the nervous system (Gershon et al., 1990; Walsh et al., 1997; Luo et al., 2006; Mimura et al., 2007; Patterson and Zhang, 2010). During embryonic development, neuronal and glial progenitors must survive a relatively hypoxic microenvironment, and simultaneously take on energetically expensive endeavors such as neurite outgrowth and cell migration. These events must occur in concert so that neurons can form the appropriate connections and receive support from the nearby glia and microvasculature. Independent of development, such challenging environments are strongly associated with the stress-inducible Hsps, suggestive of a potential role for these proteins also during neurodevelopment. Indeed, recent studies have uncovered that individual Hsps directly regulate neurodevelopment itself through modulation of pathways involved in cell growth and migration, such as the PI3K/Akt and RhoA signaling cascades (Konishi et al., 1997; Sato et al., 2000; Hennessy et al., 2005; Dou et al., 2007; Banz et al., 2009; Wang et al., 2012; Sun et al., 2013; Benitez et al., 2014).

Here, we review the regulatory role of Hsps in embryonic and postnatal neurodevelopment. After an overview of the spatio-temporal expression of Hsps during embryogenesis, the specific signaling pathways by which these chaperones regulate neuronal and glial differentiation and migration are examined. Finally, this review concludes with the contribution of these chaperones to the development of the neurovascular unit. The studies presented herein demonstrate that Hsps are not simply pro-survival factors expressed during cellular stress. Rather, Hsps are also critical mediators of cell growth and migration, axon guidance, and angiogenesis (Frebel et al., 2007; Kase et al., 2010; Colvin et al., 2014; DeGeer et al., 2015; Li et al., 2015; Shimizu et al., 2016).

HEAT SHOCK PROTEIN EXPRESSION AND REGULATION DURING NEURODEVELOPMENT

Heat Shock Protein Expression During Embryonic Neurodevelopment

Numerous studies have shown that individual Hsps have specific patterns of expression during embryonic neurodevelopment. Walsh et al. (1997) performed extensive work on cultured rat embryos and showed that the expression of inducible and constitutive Hsps is tightly regulated at critical steps in early embryogenesis, particularly during neural plate induction at E9.5. Specifically, they showed that expression of Hsp90 and Hsp70 is correlated with the cell cycle, with Hsp90 being highly expressed between G_0-G_1, whereas Hsp70 is most highly expressed between G_2-M. More expectedly, they showed that these patterns are altered with heat shock treatment. Differential expression of these proteins in untreated and heat-stressed neuroectodermal cells suggests distinct roles of these proteins in neurodevelopment. Subsequent research has extended this work by examining regulation of Hsps in later stages of embryogenesis. In the mouse brain, the small Hsp, HspB1, is closely associated with cortical neurons and radial glia undergoing differentiation at E12.5 (Loones et al., 2000). In addition, HspB1 is strongly associated with the first endothelial cells originating from the neural crest cells. Constitutively expressed Hsps, namely Hsc70 and Hsp90β are present at high levels during this developmental stage, whereas their inducible counterparts, Hsp70 and Hsp90α, are not seen until E15.5. These findings are consistent with a previous study conducted by Tanaka et al. (1995), and suggest that the ATP-dependent inducible Hsps may have greater importance in the later stages of embryonic development. Late embryonic development is also characterized by a decline in constitutive expression of Hsc70 in the hippocampus (Hatayama et al., 1997), further supporting the hypothesis that inducible Hsps may have a relatively greater contribution during the final stages of embryonic neurodevelopment, when oxidative stress is also increased.

The retina, an extension of the central nervous system (CNS), is an excellent tissue to study neurodevelopment. Using *in situ* hybridization, Tanaka et al. (1995) characterized the mRNA expression of large Hsps during embryonic and postnatal development of the retina and other ocular tissues. While certain Hsps, such as Hsp70, were not detectable, others exhibited a specific pattern of expression. The authors showed that Hsc70 is expressed in the cornea, lens, choroid, sclera, and neuroectoderm during early embryogenesis. Toward mid to late gestation (i.e., E15.5-E16.5), Hsc70 expression is downregulated

in most ocular tissues, but not the retina. In the retina, Hsc70 expression persists into adulthood. Similarly, Hsp86 (murine homolog of Hsp90α) expression persists exclusively in the retina. Subsequent studies showed that Hsc70 has a specific pattern of expression in chick retinal neurogenesis (Morales et al., 1998). While Hsc70 is initially expressed in most neuroepithelial cells, this expression becomes restricted to a subset of these cells in the peripheral retina as development proceeds. Those cells identified as retinal ganglion cells (RGCs), the first neurons to differentiate in the retina, continue to exhibit Hsc70-positivity throughout development. In these cases, continued Hsc70 expression may be necessary due to the absence of Hsp70.

Heat Shock Proteins Continued Role in Postnatal Neurodevelopment

Differential expression of Hsps continues into the postnatal period, during which neurons and glia continue to differentiate and migrate to their final destinations. As mentioned previously, Hsp70 and Hsp90α are first detectable in the mouse brain toward mid to late gestation (i.e., E15.5) (Tanaka et al., 1995; Loones et al., 2000). In contrast, Hsc70 expression begins to decline in the chick retina and mouse hippocampus at this time (Hatayama et al., 1997; Morales et al., 1998). In the postnatal period, however, Hsc70 expression does not simply continue to decline but remains relatively constant

TABLE 1 | Nomenclature, function, and distribution of heat shock proteins.

Gene symbol	Description	Stress-inducible	Localization*	Reference
HSPB1	HspB1; Hsp25 (mice); Hsp27 (rats, humans)	+	Brain, retina, spinal cord, sciatic nerve	Dean and Tytell, 2001; Kirbach and Golenhofen, 2011
HSPB2	HspB2; MKBP	-	Brain, sciatic nerve	Kirbach and Golenhofen, 2011
HSPB3	HspB3	-	Brain, spinal cord, sciatic nerve	Kirbach and Golenhofen, 2011
HSPB4	HspB4; αA-crystallin	+	Retina, sciatic nerve	Xi et al., 2003; Kirbach and Golenhofen, 2011; Ruebsam et al., 2018
HSPB5	HspB5; αB-crystallin	+	Brain, retina, spinal cord, sciatic nerve	Bhat and Nagineni, 1989; Xi et al., 2003; Kida et al., 2010; Kirbach and Golenhofen, 2011
HSPB6	HspB6; αC-crystallin	-	Brain, spinal cord, sciatic nerve	Kirbach and Golenhofen, 2011
HSPB7	HspB7	-	Sciatic nerve	Kirbach and Golenhofen, 2011
HSPB8	HspB8; Hsp22; H11 kinase	+	Brain, spinal cord, sciatic nerve	Kirbach and Golenhofen, 2011; Ramirez-Rodriguez et al., 2013
HSPB9	HspB9	Unknown	Testis	Kappé et al., 2001
HSPB10	HspB10	Unknown	Testis	Fontaine et al., 2003
HSPB11	HspB11	-	Brain, spinal cord, sciatic nerve	Kirbach and Golenhofen, 2011
HSPA1A, B	Hsp70 family A, members 1A and 1B	+	Brain, retina, spinal cord	Manzerra and Brown, 1992; Tytell et al., 1994; D'Souza and Brown, 1998; Dean et al., 1999; Loones et al., 2000
HSPA8	Hsc70	-	Brain, retina, spinal cord	D'Souza and Brown, 1998; Dean et al., 1999; Loones et al., 2000; Chen and Brown, 2007
HSP90AA1	Hsp90α family class A, member 1	+	Brain, retina, spinal cord	Ishimoto et al., 1998; Loones et al., 2000; Bernstein et al., 2001; Zuehlke et al., 2015
HSP90B1	Hsp90β family member 1; Gp96; Grp94	-	Brain, retina, spinal cord	Ishimoto et al., 1998; Loones et al., 2000; Bernstein et al., 2001
HSPH1	Hsp105	+	Brain, dorsal root ganglion	Hatayama et al., 1997; Saito et al., 2007

**Not an exhaustive list. Special attention was given to the distribution of heat shock proteins in the nervous system.*

throughout all regions of the rat brain, from the cerebrum to the brainstem and cerebellum (D'Souza and Brown, 1998; **Table 1**). On a subcellular level, Hsc70 is specifically localized in the perikarya and apical dendrites of Purkinje cells and deep cerebellar neurons from P1 into adulthood. Similarly, Hsp90 expression remains relatively constant, and shares a common subcellular localization in Purkinje cells throughout the postnatal period and into adulthood. The continued spatio-temporal regulation of Hsps suggests that these chaperones remain important in the later stages of CNS development. Given their subcellular localization, Hsc70 and Hsp90 may also contribute to processes such as neurite outgrowth, which will be discussed in a subsequent section of this review.

Small Heat Shock Proteins in Embryonic and Postnatal Neurodevelopment

By mid- to late-stage gestation, many of the small Hsps are detectable in one or more structures of the mammalian brain, each with their own individual pattern of expression (**Table 1**). In the rat hippocampus, several small Hsps, including HspB1 and HspB8, are expressed at low basal levels at E17-E19 (Kirbach and Golenhofen, 2011). Expression of these chaperones remains low in the early postnatal period, but is significantly increased by 9–10 weeks, suggesting a temporally regulated role, at least in the hippocampus. While HspB1 has been implicated in processes such as neuronal differentiation and neurite extension, less is known about the specific function of HspB8. Recent studies have indicated that this chaperone may play a key role both in neurogenesis and neurodegenerative diseases. Ramirez-Rodriguez et al. (2013) showed that overexpression of HspB8 promotes differentiation and survival of dentate gyrus precursor cells *in vitro*. The same authors also showed that removal of the highly conserved α-crystallin domain abrogates HspB8-mediated differentiation and survival. In addition, HspB8 mutations are associated with Charcot-Marie-Tooth disease, a neurodegenerative disease characterized by demyelination or impaired axon transport (Gentil and Cooper, 2012). Similar to HspB8, relatively little is known about the role of other small Hsps such as the α-crystallins. However, it has been postulated that the α-crystallins could play an important role in neurodevelopment since their expression is regulated by the transcription factor Pax6, the "master regulator" of brain and eye development (Piri et al., 2016). A role of α-crystallins in neurodevelopment is supported by the finding that Pax6 regulates the survival of adult dopaminergic olfactory bulb neurons via αA-crystallin (Ninkovic et al., 2010). Given that Pax6 is even more abundantly expressed during embryonic CNS development (Duan et al., 2013), this finding strongly suggests that Pax6 and αA-crystallin may also regulate the survival of neuronal progenitors. Further evidence for a role of α-crystallins in neurodevelopment can be seen in the work of Shao et al. (2013) who showed that the anti-inflammatory properties of αB-crystallin are regulated at least in part by the astrocytic dopamine D2 receptor. Importantly, the astrocytic D2 receptor is expressed in the corpus striatum during embryonic development (Lin et al., 2001), raising the possibility that this receptor and its downstream target, αB-crystallin, could suppress neuroinflammation and promote cell survival in the early stages of neurodevelopment. However, the astrocytic dopamine D2 receptor also regulates GSK3β, which is known to regulate neuronal cell growth, polarity, proliferation, and survival (Cui et al., 1998; Gärtner et al., 2006). Because of these overlapping functions, the exact role of astrocytic dopamine D2 receptor remains unclear; however, it is likely to involve αB-crystallin. In addition to regulation by Pax6 and membrane-bound receptors, embryonic and postnatal expression of the α-crystallins may also be regulated by one or more heat shock factors (HSFs), which will be discussed next.

Essential Regulatory Role of Heat Shock Factors During Neurodevelopment

Gene knockout studies have highlighted a requirement of certain Hsps during neurodevelopment. During early embryogenesis, the developing CNS is particularly sensitive to heat shock, and prolonged heat exposure is associated with neural tube defects as well as microphthalmia (Walsh et al., 1997). In the postnatal period, Hsps continue to protect the developing CNS from unfavorable conditions. Hsps are also important in unstressed conditions, during which the stress-inducible Hsps are transcribed at low basal levels. Expression of Hsps is regulated at the transcriptional level by factors known as HSFs. These factors promote transcription by interacting with adjacent or intronic heat shock elements (HSEs). HSF1 and HSF2 promote transcription of numerous genes, including HspB1, Hsp40, Hsp70, Hsp90α, Hsp90β, and other non-Hsp genes such as p35 (Trinklein et al., 2004; Åkerfelt et al., 2007; Östling et al., 2007; Metchat et al., 2009). HSF1, in particular, is critical to proper neurodevelopment, which is demonstrated in $HSF1^{-/-}$ mice that have impaired olfactory neurogenesis (Takaki et al., 2006), as well as impaired hippocampal spinogenesis and neurogenesis (Uchida et al., 2011). Consistent with the spatio-temporal expression of Hsps described above, there is a narrow time-window in the neonatal period during which restoration of HSF1 can rescue hippocampal development. Restoration of $HSF1^{-/-}$ in neonates with a vector overexpressing constitutively active HSF1 Rephrased for clarity; see previous comment rescues the phenotype, whereas the same treatment in adults confers no such benefit. These findings strengthen the argument that Hsps have a critical, time-dependent role during normal neurodevelopment. However, because HSF1 regulates transcription of many proteins, it has been difficult so far to narrow down which of its targets are most essential.

HSF2 is highly homologous to HSF1 and shares overlapping DNA-binding activity at certain HSEs (Trinklein et al., 2004; Åkerfelt et al., 2007; Östling et al., 2007); however, HSF2 is not clearly involved in the temporally-regulated expression of Hsps (Loones et al., 1997). This is supported by the fact that HSF2 cannot compensate for the loss of HSF1 function in heat-stressed $HSF1^{-/-}$ mouse embryonic fibroblasts *in vitro* (McMillan et al., 1998). Nevertheless, HSF2 appears to play complex regulatory roles in neurodevelopment. Although one study reported that $HSF2^{-/-}$ mice have normal brain architecture and cognitive

development (Mcmillan et al., 2002), several others have since made opposite observations. Those subsequent studies indeed reported that HSF2$^{-/-}$ mice have neurodevelopmental or reproductive abnormalities, namely ventricle enlargement and reduced viability of pachytene spermatocytes (Kallio et al., 2002; Wang et al., 2003, 2004; Chang et al., 2006). Such opposing results were suggested to be due to differences in the knockout model or genetic background, the latter of which could alter penetrance of the phenotype (Mcmillan et al., 2002). Subsequently, Chang et al. (2006) showed that neither the reduced number of radial glia and radial glia-derived astrocytes nor the impaired neuronal migration in HSF2$^{-/-}$ mice were directly associated with Hsps. Rather, these changes were associated with reduced p35-Cyclin-dependent kinase 5 signal transduction. While a role of HSF2 cannot be totally ruled out, these data suggest that Hsps rely primarily on HSF1 during embryogenesis.

HEAT SHOCK PROTEINS POTENTIAL ROLE IN NEURONAL AND GLIAL DIFFERENTIATION

HspB1 Expression Is Correlated With Neuronal Differentiation

During neurodevelopment, HspB1 exhibits a specific spatio-temporal pattern of expression that coincides with neuronal differentiation. In the CNS, neural tube closure and the appearance of the first neurons occurs at E8.5, whereas HspB1 expression is first detectable shortly thereafter (Easter et al., 1993; Walsh et al., 1997; Loones et al., 2000). In mice, HspB1 is relatively abundant in specific brain regions, including the zona limitans interthalamica as well as the axons that comprise the peripheral and longitudinal tracts. Between E12.5 and E15.5, HspB1 synthesis is further enriched in regions such as the olfactory bulbs and corpus striatum. This specific pattern of expression suggests that HspB1 is associated with neuronal differentiation. A key role of HspB1 in neuronal differentiation is further supported by the finding that this chaperone is upregulated in human embryonic stem cell-derived differentiating motor neurons, but subsequently downregulated following maturation, all of which in the absence of additional stressful stimuli (Chaerkady et al., 2009). Similarly, in the developing mouse brain, HspB1 is globally downregulated after the first round of neuronal differentiation (i.e., E12-E16) (Cheng et al., 2016). This reduced expression of Hsps during maturation is consistent with *in vitro* studies suggesting that differentiation reduces neuronal cells' resistance to stress. Indeed, Hsp60 and Hsp70 are not as readily induced in differentiated neuronal phaeochromocytoma (PC12) cells in the setting of hyperthermia or cytotoxic exposure (Dwyer et al., 1996). Similarly, several Hsps, including HspB1, are less readily induced in differentiated neuroblastoma-glioma hybrid cells (Oza et al., 2008). Together, these studies are consistent with the notion that that neuronal differentiation regulates basal and inducible Hsp expression. Interestingly, there is growing evidence that the reverse is also true; Hsps influence neuronal differentiation.

Heat Shock Proteins Complex Regulatory Role in Neuronal Differentiation

The requirement of HSF1 for embryogenesis, coupled with the diverse chaperone functions of Hsps, suggests that Hsps could mediate cell differentiation. Recent research has shown that prolonged heat exposure promotes differentiation and proliferation of hippocampus-derived neuronal, and, to some extent, glial progenitor cells (Matsuzaki et al., 2009). The same group also showed that even mild heat exposure promotes differentiation of hippocampal neuronal progenitor cells, and that this increase in differentiation is accompanied by changes in Hsp mRNA expression (Hossain et al., 2017). In particular, HspB1 expression increases in neuronal progenitors undergoing differentiation, whereas Hsp70 and Hsp90 expression declines. As the authors noted, HspB1 may promote differentiation through its chaperone interactions with the client protein Akt (protein kinase B; **Figure 1A**), which is central to cell growth and survival (Konishi et al., 1997; Hennessy et al., 2005). However, Akt also interacts with Hsp90, suggesting a complex regulation of its function through dynamic interaction with Hsps during differentiation.

Consistent with this complex dynamic of protein–protein interaction of Hsps with specific client proteins, recent studies have also suggested that a non-specific reduction in Hsp expression may promote differentiation. Hsps are regulated at the transcriptional level by the transcription factor HSF1, which, in turn, is regulated at the protein level by various stressors and negative feedback (for review, see Anckar and Sistonen, 2011). HSF1 is also regulated by nicotinamide adenine dinucleotide (NAD)-dependent deacetylase sirtuin-1 (SIRT-1) (Westerheide et al., 2009). Knockdown of SIRT-1 was recently reported to promote neuronal differentiation in rat embryonic and N2a progenitor cells *in vitro* (Liu et al., 2014). Of note, the authors reported that increased neuronal differentiation is associated with a reduction in Hsp70. While this finding is consistent with a role of Hsps in neuronal differentiation, it is important to note that HSF1 regulates transcription of numerous Hsp and non-Hsp genes (Trinklein et al., 2004; Metchat et al., 2009). Knockdown of SIRT-1, therefore, likely results in a non-specific, widespread reduction of chaperone activity and an accumulation of denatured proteins. Hsps not only manage compromised proteins, but also regulate protein maturation and stability. Thus, reduced Hsp expression associated with SIRT-1 knockdown could affect the stability of specific targets critical for neuronal differentiation. Because this study focused exclusively on Hsp70, subsequent studies are necessary to examine other Hsps, including HspB1, to help elucidate the exact role of stress-inducible Hsps in neuronal differentiation.

Hsp90 Is Necessary for Neuronal Polarization and Axon Specification

Hsp90 is known to be critical for spermatogenesis and embryonic development (Voss et al., 2000; Grad et al., 2010), and due to its ubiquitous expression in the CNS, is likely to play an important role in neurodevelopment as well. Over the past two decades,

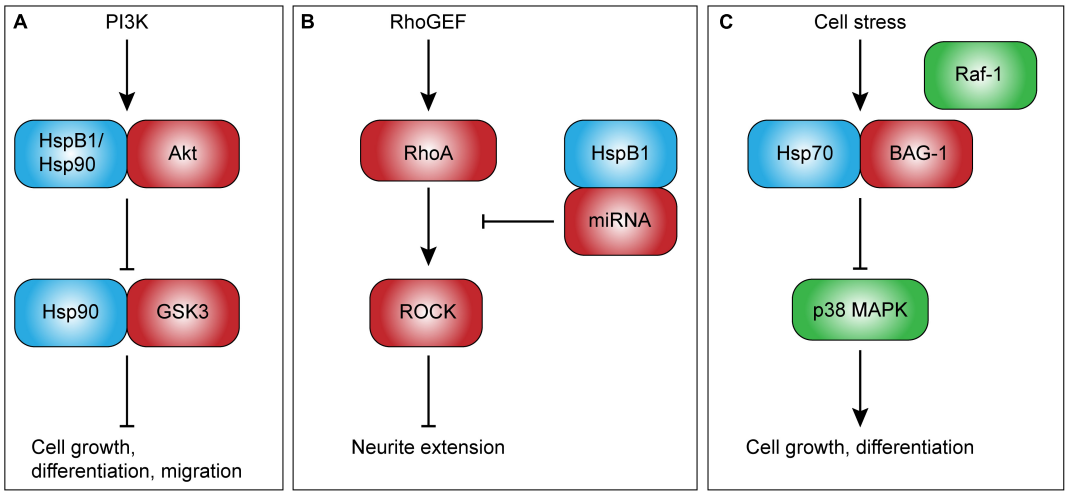

FIGURE 1 | Potential intracellular roles of heat shock proteins in development. Intracellular Hsps, such as HspB1 and Hsp90, directly regulate client proteins involved in cell growth and migration **(A)**, and may play an important role in neurodevelopment. HspB1, in particular, may also regulate neurite extension through the upregulation of non-coding RNAs that inhibit RhoA-ROCK signaling **(B)**. Other Hsps, such as Hsp70, have been shown to competitively inhibit Raf-1-BAG-1-mediated cell growth and differentiation **(C).** This novel role of Hsp70 may be especially important given its ability to be rapidly induced. Abbreviations: PI3K, phosphoinositide 3-kinase; GSK3, glycogen synthase kinase 3; BAG-1, Bcl2-associated anthogene-1; RhoGEF, Ras homolog guanine exchange factor; RhoA, Ras homolog gene family, member A; ROCK, Rho-associated protein kinase.

several studies have shown that Hsp90 is correlated with neuronal differentiation. Loones et al. (2000) reported that the inducible isoform of Hsp90, Hsp90α, is first detectable in the developing mouse brain at E15.5, several days after the first neuronal and glial progenitors begin to differentiate. Several others have confirmed that Hsp90 expression is correlated with neuronal differentiation *in vitro*. Specifically, Hsp90 is markedly increased in neuronal P19 cells and embryonic hippocampal neurons undergoing differentiation (Quintá et al., 2010; Afzal et al., 2011). Subsequent experiments showed that Hsp90 becomes associated with the cytoskeleton of differentiating hippocampal neurons, particularly in branch points and terminal ends (Quintá and Galigniana, 2012). These findings suggest that intracellular Hsp90 could modulate cytoskeleton dynamics and key developmental events such as neuronal polarization.

Neuronal polarization is the process by which a neuron establishes an axon and dendrites, and is a critical step in neuronal differentiation. Interestingly, one recent study has shown that Hsp90 is required for key events in neuronal polarization. Using neurons isolated from moues embryos at E17, Benitez et al. (2014) showed that pharmacologic inhibition of Hsp90 with the Hsp90 inhibitor, 17-demethoxygeldanamycin (17-AAG), both disturbs neuronal polarization and slows axon elongation. In addition, these perturbations were accompanied with a reduction in PI3K/Atk/GSK3 signal transduction. The PI3K/Akt/GSK3 signaling cascade is well-known to mediate cell growth, differentiation, proliferation, migration, and even apoptosis (Gregory et al., 2003; Hennessy et al., 2005). Of note, both Akt and GSK3 are client proteins for Hsp90 (Sato et al., 2000; Dou et al., 2007; Banz et al., 2009), immediately suggesting a possible mechanism by which Hsp90 could regulate functions such as cell differentiation in the context of normal neurodevelopment (**Figure 1A**). An interesting finding in aforementioned work is that inhibition of Hsp90 was associated with an increase in Hsp70 and Hsc70, which the authors noted may reflect a compensatory response in an attempt to maintain signal transduction. Besides the regulation of signal transduction cascades, Hsp90 has been implicated as a paracrine factor promoting dendrite-like outgrowth and differentiation *in vitro* (Park et al., 2015). A role for extracellular Hsps, including Hsp90, has also been suggested, and will be discussed in a subsequent section of this review.

Heat Shock Proteins in Differentiating Glia

Although there is limited research on the role of Hsps in differentiating glia, Hsps are expressed and induced in mature glia (Krueger et al., 1999; Dean and Tytell, 2001; Kalesnykas et al., 2008), and our group and others have recently suggested that Hsps play an important role in these cells (Ruebsam et al., 2018). In addition to their critical house-keeping functions and pro-survival role in mature cells under stress, Hsps also exhibit specific patterns of expression during glial development. For instance, in human fetal telencephalon, αB-crystallin is expressed in numerous radial glia, a subset of oligodendrocyte progenitors, and a small number of astrocytes (Kida et al., 2010). Similar to what has been reported in neurons, the ability to induce Hsps synthesis in mature glia is reduced compared to progenitor cells (Zhang et al., 2001). These data strongly suggest tightly regulated roles for Hsps in glial development. Because neurons and glia are intimately connected, it is possible that synthesis of Hsps in glia may regulate adjacent neuronal cells' growth. Some researchers have already demonstrated this phenomenon *in vitro*, and their findings will be reviewed here in subsequent sections.

HEAT SHOCK PROTEINS REGULATE NEURONAL AND GLIAL CELL GROWTH

Small Heat Shock Proteins Promote Neurite Outgrowth and Extension

HspB1 is primarily known for its role in thermotolerance and cytoprotection (Arrigo and Welch, 1987; Lavoie et al., 1993a; Bartelt-Kirbach et al., 2017), but recently it has been implicated as a potential contributor to neurodevelopment. The first evidence that this chaperone not only promotes cell survival, but also axonal growth, came from a study showing that HspB1 is rapidly upregulated in response to peripheral nerve injury and promotes its regeneration (Costigan et al., 1998). The role of HspB1 in the regulation of neurite outgrowth has since been further characterized. In the early stages of neurite growth initiation, HspB1 is mainly localized in lamellipodia and focal adhesions, whereas in the later stages of neurite extension, HspB1 is found in branch points, processes, and growth cones (Williams et al., 2005), suggesting a role in the promotion of growth by modulation of cytoskeletal dynamics. This role in neurite outgrowth has been subsequently confirmed by studies showing that overexpression of HspB1 enhances neurite extension and branching, whereas inhibition with short interfering ribonucleic acid (siRNA) reduces neurite length and complexity (Williams et al., 2006; Ma et al., 2011).

Despite strong evidence for a role of HspB1 in neurite outgrowth and extension, the exact mechanisms remain unclear. HspB1 is well-known to interact with the cytoskeleton in a phosphorylation state-dependent manner (Lavoie et al., 1993b; Guay et al., 1997; Pichon, 2004), leading some to hypothesize that this chaperone could mediate cell growth through direct modulation of cytoskeleton dynamics (Lavoie et al., 1993a; Costigan et al., 1998). This hypothesis is supported by the observation that HspB1 co-localizes with actin in the early stages of neurite initiation (Williams et al., 2005). However, the significance of this interaction in terms of neuronal cell growth, has not been demonstrated. Another possible mechanism is that HspB1 regulates cytoskeletal dynamics through signal transduction cascades. One study supporting this hypothesis showed that HspB1 indirectly inhibits RhoA signal transduction by upregulating non-coding RNAs that inhibit Rho guanine exchange factor 11 (**Figure 1B**; Sun et al., 2013). RhoA is a small GTPase known to inhibit neurite extension through Rho-associated protein kinase (ROCK)-mediated inhibition of the actin cytoskeleton (Bito et al., 2000). Thus, HspB1 may promote neurite extension through inhibition of this negative feedback loop.

αA- and αB-crystallin are two other members of the small Hsps initially thought to be present exclusively in the crystalline lens, but now understood to be expressed in numerous tissue types, including the brain, retina, heart, and skeletal muscle (Taylor and Benjamin, 2005; Bakthisaran et al., 2015). While their roles in retinal neuroinflammation and neuroprotection have been clearly demonstrated (for review, see Dulle and Fort, 2016; Rübsam et al., 2018), their contribution to neuronal cell growth is still under investigation. Wang et al. (2011) showed that α-crystallins can promote neurite initiation and extension of retinal ganglion cells (RGCs) grown on inhibitory myelin substrate in a dose-dependent manner. The same group subsequently demonstrated that intravitreal injection of α-crystallins significantly enhances axonal regeneration following optic nerve crush in newborn rats (P0-P2) (Wang et al., 2012). Furthermore, this enhanced axonal regeneration was associated with a reduction in the protein activity of RhoA/ROCK, consistent with the above suggested mechanism of increased neurite extension. An important limitation of these studies is that the researchers studied co-purified aggregates containing αA- and αB-crystallins, precluding at this point a clear understanding of the relative contribution of each individual chaperone. Starting to clarify the individual roles of αA- and αB-crystallin, a recent study reported an association between αA-crystallin, inhibition of astrocyte activation, and axon elongation following optic nerve crush (Shao et al., 2016). On the other hand, cell culture experiments using hippocampal neurons have shown that αB-crystallin regulates dendritic complexity, and does so in a phosphorylation-dependent manner (Bartelt-Kirbach et al., 2016). In addition, recent reports suggest that the small Hsps could mediate neurite extension not only through modulation of microtubule assembly (Ghosh et al., 2007), but also as a guidance cue. Before further examining these mechanisms and a possible extracellular role of Hsps, this review will focus on the potential role of other Hsps in cell growth.

Hsp70 and Hsp90α Regulate Cell Growth Through Their Chaperone Activity

Hsp70 is most well-known for its role in cytoprotection (Park et al., 2001; Ishii et al., 2003; Sabirzhanov et al., 2012; Kwong et al., 2015), but has also been suggested to regulate cell growth by regulating specific signaling pathways. Hsp70 is an ATP-dependent chaperone with two distinct binding domains: a functional substrate-binding domain and a regulatory nucleotide-binding domain (Blatch and Edkins, 1997). In an ATP-bound state, Hsp70 exists in a relatively open conformation, and has a low affinity for client proteins at the substrate binding domain. Upon ATP hydrolysis, however, Hsp70 undergoes a conformational change that increases its affinity for a given substrate. This cycle is called the chaperone cycle, and is regulated by co-chaperones that promote ATP hydrolysis or nucleotide exchange factors that catalyze the addition of phosphate. One such factor is the B-cell lymphoma 2-associated anthogene-1 (BAG-1), which has been reported to alter the conformation of Hsp70 and reduces its affinity for client proteins at the substrate-binding domain (Bimston et al., 1998). In addition, BAG-1 is known to activate the Raf-1/MAPK/ERK signal transduction cascade, thereby promoting differentiation and proliferation, including in the CNS. Interestingly, Hsp70 has been shown to compete with Raf-1 for binding to BAG-1 *in vitro* (Song et al., 2001), suggesting that Hsp70 could indirectly inhibit cell growth *in vivo*, particularly during stress (**Figure 1C**). Subsequent studies have confirmed that overexpression of the cytoplasmic isoform of BAG-1, BAG-1s, reduces neurite outgrowth in an Hsp70-dependent manner (Frebel et al., 2007). In the context

of neurodevelopment, this negative regulation is consistent with the proposed hypothesis that it may be necessary to temporarily halt energetically expensive processes to ensure cell survival in suboptimal conditions. Although Hsp70's interactions with BAG-1 seem to inhibit cell growth, interactions with BAG-3 have been reported to promote growth. Consistent with a role in cell survival and growth, several studies have shown that the Hsp70-BAG-3 interaction promotes tumorigenesis through the modulation of specific signal transduction cascades, including those that involve Src and FoxM1 (Colvin et al., 2014; Li et al., 2015). These studies illustrate a co-chaperone-driven role of Hsp70 in cell growth. Like tumorigenesis, neurodevelopment is characterized by high metabolic demands and rapid proliferation. Hsp70, as one of the stress-inducible chaperones, could play a key role in modulating cell growth signaling in such highly demanding conditions.

Hsp90, like Hsp70, is an ATP-dependent chaperone that interacts with numerous client proteins, including transcription factors, tyrosine receptor kinases, and matrix metalloproteinases (Bernstein et al., 2001; Eustace et al., 2004; Wang et al., 2017). Because many of these client proteins are critical to cell growth, proliferation, and migration, numerous researchers are investigating the therapeutic potential of Hsp90 inhibitors as anti-cancer agents. There is growing evidence that the inducible isoform of Hsp90, Hsp90α, also promotes neurite outgrowth. Hsp90 has been long known to be responsible for neurite extension observed in chick embryonic telencephalic and spinal neurons (Ishimoto et al., 1998). However, this observation has received relatively little attention until recent years. Increased Hsp90α synthesis was only recently associated with NGF-mediated neurite outgrowth in the setting of aripiprazole treatment *in vitro* (Ishima et al., 2012). The same authors also showed that silencing of Hsp90α results in attenuated neurite outgrowth, supporting a potential role of Hsp90α in normal neuronal cell growth, particularly through its chaperone activity. This hypothesis is further supported by the observation that inhibition of Hsp90 results in reduced membrane translocation of the growth factor tyrosine receptor kinase A (TrkA) in human acute myeloid leukemia cells (Rao et al., 2010). Interestingly, in this study, inhibition of Hsp90 was associated with an increase in Hsp70, which could reflect a compensatory response similar to what was described by Benitez et al. (2014). Although additional studies are necessary to further understand the specific functions of Hsps in cell growth, collectively, these studies clearly support an important role for Hsps in tumorigenesis, as well as normal development.

HEAT SHOCK PROTEINS PARTICIPATE IN MIGRATION AND PROMOTE AXON GUIDANCE

Heat Shock Proteins Participate in Neuronal and Glial Migration

Neuronal migration requires the cell to establish polarity, extend a leading process, survey the extracellular environment, translocate nuclear content, and, finally, advance toward its final destination (Craig and Banker, 1994; Kater and Rehder, 1995). All of these processes rely on remarkably coordinated cytoskeletal dynamics (Mitchison and Kirschner, 1984; Tanaka et al., 2004; Schaar and McConnell, 2005). As mentioned previously, Hsps are well-known to interact with and stabilize cytoskeletal elements (Lavoie et al., 1993b; Sánchez et al., 1994; Weis et al., 2010; Almeida-Souza et al., 2011; Kayser et al., 2013), and, thus, may play a key role in regulating neuronal and glial migration in the developing nervous system. In support of this concept, αB-crystallin was recently reported to promote the formation of mature focal adhesions and slow migration of unstressed C6 glial cells (Shimizu et al., 2016). These new data suggest that αB-crystallin, in addition to its normal chaperone activity, could also regulate cell migration and the proper formation of a neuroglial network. Although αB-crystallin expression in the embryonic brain is mainly limited to glial progenitors (Kida et al., 2010), recent evidence for secretion of αB-crystallin support a separate role on neuronal migration.

Stress-inducible Hsps, including Hsp70 and α-crystallins, were recently shown to be secreted into the extracellular milieu, suggestive of novel paracrine and autocrine functions in addition to their classical, intracellular chaperone activity. The first observation of the sort was the fact that Hsp70 can be transferred from heat-stressed squid glia to adjacent neuronal axons (Tytell et al., 1986), suggesting that glia-derived Hsp70 could confer thermotolerance in nearby neurons – a hypothesis that has since been validated *in vitro* (Guzhova et al., 2001). Several Hsps, including HspB1, αA- and αB-crystallin, and Hsp90α, have since been shown to be secreted in exosomes or plasma membrane-derived vesicles (Graner et al., 2007; Wang et al., 2009; Sreekumar et al., 2010; Nafar et al., 2015; Barreca et al., 2017; Ruebsam et al., 2018). On a mechanistic level, HspB1 and Hsp90α, were also shown to be secreted in a phosphorylation-dependent manner, suggesting that secretion of other Hsps may be similarly regulated through phosphorylation of specific residues (Wang et al., 2009; Lee et al., 2012). In the extracellular environment, Hsps have the potential to be taken up by endocytosis or bind to extracellular receptors (**Figure 2**). Indeed, recent research has confirmed that Hsps can act as a ligand and mediate cell migration in several cell lines (Asea et al., 2002; Barreca et al., 2017).

Hsps are secreted by numerous cell-types, from neurons to glia and endothelial cells (Guzhova et al., 2001; Zhan et al., 2009; Sreekumar et al., 2010; Lee et al., 2012; Ruebsam et al., 2018), and have been implicated as potential contributors to cell migration. Using specific antibodies and inhibitors, Miyakoshi et al. (2017) showed that Hsp70, Hsp90, and co-chaperone Hsp70-Hsp90-organizing protein (HOP) all regulate neuroblast migration from the subventricular zone. Interestingly, Hsp70 and HOP were also found in membrane-associated complexes, suggesting a potential, extracellular role of these chaperones in migration. Although this mechanism has not yet been investigated, one possible explanation is that extracellular Hsps regulate migration through binding to a receptor such as TLR4 (**Figure 2**), which has been reported to regulate migration of cortical neurons (Moraga et al., 2014). This hypothesis is supported by the finding that extracellular Hsp70 and Hsp90α promote TLR4-dependent

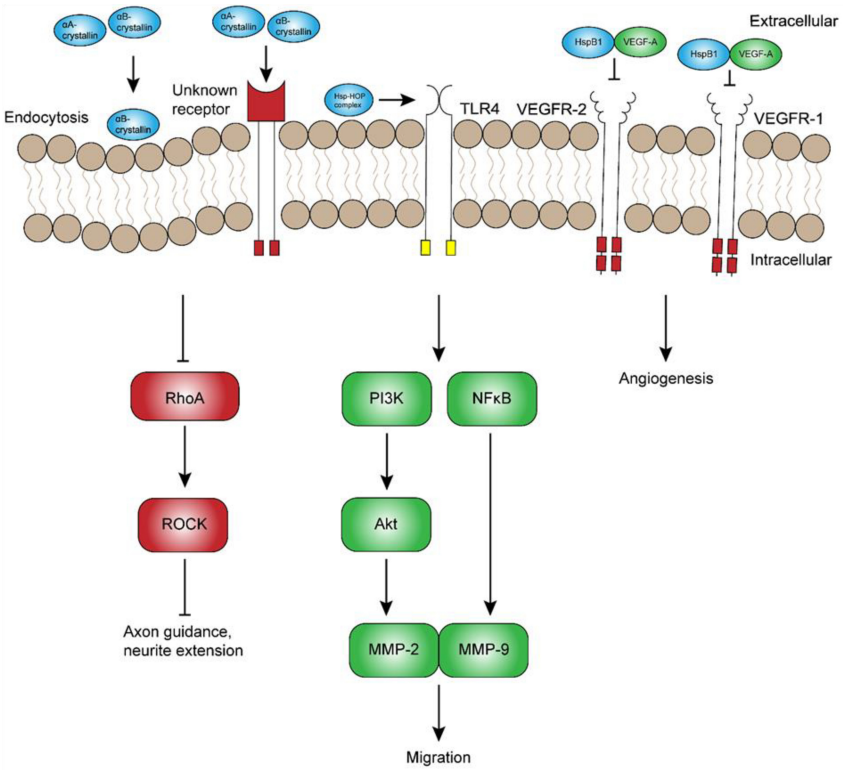

FIGURE 2 | Potential extracellular roles of heat shock proteins in development. Although the exact mechanisms remain unclear, extracellular α-crystallins have been shown to promote axon guidance and neurite extension through inhibition of RhoA-ROCK signaling. Other extracellular Hsps, namely Hsp70 and Hsp90, have been suggested to interact with the Hsp70-Hsp90-organizing protein (HOP) and promote neuronal and glial migration through receptors such as toll-like receptor 4 (TLR4). In contrast, extracellular HspB1 has been shown to inhibit vascular endothelial growth factor (VEGF)-A signaling and angiogenesis by direct inhibition of VEGF-A. Abbreviations: RhoA, Ras homolog gene family, member A; ROCK, Rho-associated protein kinase; PI3K, phosphoinositide 3-kinase; MMP, matrix metalloproteinase; NFκB, nuclear factor κ light chain enhancer of activated B cells.

migration in mesoangioblasts and glioblastoma cells, respectively (Thuringer et al., 2011; Barreca et al., 2017). While TLR4 is a good candidate, extracellular Hsps could mediate cell migration through several other receptors that remain to be characterized. In any case, significant research is still required to elucidate the role and regulation of extracellular Hsps *in vivo*. In addition to the indirect regulation of cell migration signaling, Hsps may also promote migration by directly serving as guidance cues that promote axon growth and guidance.

Heat Shock Proteins May Contribute to Axon Guidance

During neurodevelopment, migratory neurons rely on the glial scaffold and extracellular guidance cues to reach their final destination (Marín et al., 2010; Hatten, 1999). As might be expected, Hsps exert numerous chaperone functions within the cell that are critical to transduction of extracellular cues, some of which are necessary for axon guidance (DeGeer et al., 2015). In addition, Hsps have been shown to perform non-classical, extracellular roles that may also promote axon guidance. One of the first studies suggesting this role showed that lens injury-derived factors promote axonal regeneration and pathfinding in a subset of RGCs (Leon et al., 2000). The axons of these RGCs were highly immunopositive for growth associated protein 43, which is known to play a critical role in axon pathfinding during normal neurodevelopment (Strittmatter et al., 1995). Subsequent studies by Fischer et al. (2001, 2008) showed that lens injury-induced axonal regeneration and pathfinding is due mainly to the β-crystallins, a group of non-Hsp crystallins that are similarly found in the vertebrate lens. However, the α-crystallins also appeared to exert some effect, although this effect was not as strong as that of β-crystallins. As discussed in a previous section of this review, other studies have since shown that the co-purified aggregates containing αA- and αB-crystallins can promote neurite extension *in vitro*. Furthermore, both αA- and αB-crystallin are secreted in vesicles (Sreekumar et al., 2010; Ruebsam et al., 2018), raising the possibility that these chaperones could mediate numerous, novel functions, such as axon guidance, through endocytic or receptor-mediated pathways that remain to be discovered. Given that αB-crystallin is not highly expressed in developing telencephalic neurons (Kida et al., 2010), it most likely promotes axon outgrowth and guidance through a paracrine mechanism, similar to the β-crystallins (Fischer et al., 2001, 2008).

HEAT SHOCK PROTEINS CONTRIBUTION TO THE FORMATION OF THE RETINAL NEUROVASCULAR UNIT

Heat Shock Proteins Regulate Angiogenesis

Successful neurodevelopment depends on the anatomic and physiologic integration of neurons, glia, and the underlying vascular network. This functional unit has been termed the neurovascular unit, and its importance is reflected in congenital conditions such as persistent hyperplastic primary vitreous (Kurihara, 2016), as well as neurodegenerative diseases such as Alzheimer's disease and diabetic retinopathy (Iadecola, 2004; Gardner and Davila, 2017). HspB1 is strongly associated with the first endothelial cells in the developing CNS (Loones et al., 2000), suggestive of a potential role of Hsps in endothelial cell proliferation. In the past decade, several studies have implicated Hsps as novel regulators of specific angiogenic factors, and, therefore, these chaperones may also regulate formation of the neurovascular unit. One such factor is vascular endothelial growth factor A (VEGF-A), an endothelial cell-specific mitogen and potent agonist of angiogenesis (Kim et al., 1993; Ferrara et al., 2003). Kase et al. (2010) clearly demonstrated the necessity of αB-crystallin in two murine models of angiogenesis, namely oxygen-induced retinopathy (OIR) and laser-induced choroidal neovascularization (CNV). In the OIR model, αB-crystallin$^{-/-}$ mice exhibited significantly reduced VEGF-A protein levels and angiogenesis compared to wild-type mice, particularly in the highly vascular inner plexiform layer of the retina. Using a laser-induced CNV model, the same authors showed that pharmacologic inhibition of the proteasome restores VEGF-A protein levels in αB-crystallin$^{-/-}$ mice, suggesting that αB-crystallin protects VEGF-A from proteasomal degradation. Because αB-crystallin is induced in response to stress, this chaperone could contribute to hypoxia-mediated angiogenesis during neurodevelopment, particularly through the stabilization of VEGF.

The pro-angiogenic effect of αB-crystallin appears to be balanced at least in part by HspB1 and αA-crystallin, both of which have been reported to attenuate angiogenesis. HspB1 expression during CNS development is not only associated with endothelial cell migration and differentiation, but also secreted from endothelial cells into the extracellular environment, where it participates in a negative feedback loop and directly inhibits VEGF-mediated angiogenesis and tumorigenesis (**Figure 2**; Lee et al., 2012). Subsequent experiments indicated that HspB1 secretion from endothelial cells is inhibited by a feedback mechanism involving VEGF-mediated phosphorylation. Similarly, others have shown that the exogenous application of αA-crystallin inhibits corneal neovascularization (Zhu et al., 2012). In the context of neurodevelopment, one group has shown that αA-, as well as αB-crystallin, undergoes a marked increase in mRNA expression between P17 and P21 in the OIR model (Shi et al., 2015). Unlike αB-crystallin, however, increased expression of αA-crystallin is not associated with an obvious change in Hsp synthesis detectable by immunofluorescence, suggesting that chaperone-mediated regulation of angiogenesis may occur mainly through αB-crystallin.

Recent research has also uncovered a critical role of βA3/A1-crystallin, a member of the β-crystallin family, in the formation of the neurovascular unit. Although the β-crystallins are not Hsps, these proteins were similarly first identified in the vertebrate lens, and are now understood to be equally necessary in non-lenticular tissues, especially in the retina (Zhang et al., 2005). One group has performed extensive research on the role of βA3/A1-crystallin in retinal vasculature development, and has shown that βA3/A1-crystallin mutations are associated with abnormal structure and function of retinal astrocytes, leading to persistent hyperplastic primary vitreous (Sinha et al., 2008, 2012; Valapala et al., 2015; Zigler et al., 2016). While the α- and β-crystallins are generally considered to be evolutionarily distinct, it is possible these proteins share some functional similarities that remain to be discovered.

In contrast to the small Hsps, relatively little research has been performed on the large Hsps in the context of angiogenesis. Although Hsp90 has not been demonstrated to interact directly with VEGF, Hsp90 is known to interact with hypoxia-inducible factor-1α as well as VEGF receptors 1 and 2 (Minet et al., 1999; Park et al., 2008), potentially modulating VEGF activity and angiogenesis. Using the OIR model, a study showed that Hsp90 inhibitors reduce hypoxia-inducible factor 1α-mediated angiogenesis in the hypoxic mouse retina (Jo et al., 2014). These conditions enhance the hypoxia-driven formation of new blood vessels during normal embryogenesis, suggesting that Hsps could contribute to the formation of the neurovascular network during normal development. While the relative contribution of each Hsp remains to be determined, Hsps likely play a key role in the complex balance of pro- and anti-angiogenic processes that result in the normal vascular network.

RECENT CONTROVERSIES AND DEVELOPMENTS

Heat Shock Proteins Are an Important Determinant of Cell Survival

This review has focused on the neuroprotective role of Hsps in the setting of developmental or physiologic stress and in the absence of stress, but some have suggested that overexpression of Hsps could be detrimental to cell survival (Narayanan et al., 2006; Richter-Landsberg et al., 2010). At least one study has suggested that αB-crystallin is associated with amyloid-β accumulation and may contribute to neurodegenerative diseases (Narayanan et al., 2006). However, many more studies have shown that αA- and αB-crystallin, as well as Hsp27, inhibit the formation of amyloid-β and neurofibrillary tangles (Waudby et al., 2010; Shammas et al., 2011; Hochberg et al., 2014; Cox et al., 2018). This apparent controversy is nicely summarized by Kannan et al. (2012), who recently reviewed the role of α-crystallins in neurodegenerative disease and discuss the potential therapeutic

benefit of αB-crystallin, in particular. Additional evidence for the neuroprotective role of Hsps can be seen in different models of retinal neurodegeneration, in which αA- and αB-crystallin knockouts have shown markedly enhanced pathologic findings compared to wild-type controls (for review, see Fort and Lampi, 2011). Pharmacologic studies, too, support a neuroprotective role of Hsps. One of the most well-known examples is the pharmacologic agent arimoclomol, which upregulates the heat shock response and protects against neurodegenerative diseases such as amyotrophic lateral sclerosis and retinitis pigmentosa (Kieran et al., 2004; Parfitt et al., 2014). Although this drug recently completed phase II clinical trials (Benatar et al., 2018), further research will be required to determine whether a therapeutic benefit exists. In all likelihood, Hsps are one of the key factors that can tip the balance between survival and apoptosis.

CONCLUDING REMARKS

There is an accumulation of evidence to suggest that Hsps play a critical role in neurodevelopment; however, the exact role of these chaperones remains largely unexplored. Hsps are expressed early in neurodevelopment and exhibit a specific spatio-temporal pattern that coincides with neuronal differentiation. Furthermore, recent research has highlighted the potential regulatory role of these chaperones in key events, including neurite extension, migration, and axon guidance. Whether these chaperones perform similar functions *in vivo* remains to be seen and will require additional studies, but represents an exciting possibility not only in neurodevelopment, but also in anti-cancer therapy and the treatment of neurodegenerative diseases.

AUTHOR CONTRIBUTIONS

DM wrote the manuscript, produced the supporting table and figures, and obtained funding. PF obtained funding, directed the writing, and edited the manuscript.

FUNDING

This work was supported by an NIH R01 EY020895 (PF), and in part by a Rackham Graduate Student Research Grant (DM). This work utilized the Core Center for Vision Research funded by P30 EY007003 from the National Eye Institute.

REFERENCES

Afzal, E., Ebrahimi, M., Najafi, S. M. A., Daryadel, A., and Baharvand, H. (2011). Potential role of heat shock proteins in neural differentiation of murine embryonal carcinoma stem cells (P19). *Cell Biol. Int.* 35, 713–720. doi: 10.1042/CBI20100457

Åkerfelt, M., Trouillet, D., Mezger, V., and Sistonen, L. (2007). Heat shock factors at a crossroad between stress and development. *Ann. N. Y. Acad. Sci.* 1113, 15–27. doi: 10.1196/annals.1391.005

Almeida-Souza, L., Asselbergh, B., D'Ydewalle, C., Moonens, K., Goethals, S., de Winter, V., et al. (2011). Small heat-shock protein HSPB1 mutants stabilize microtubules in charcot-marie-tooth neuropathy. *J. Neurosci.* 31, 15320–15328. doi: 10.1523/JNEUROSCI.3266-11.2011

Anckar, J., and Sistonen, L. (2011). Regulation of HSF1 function in the heat stress response: implications in aging and disease. *Annu. Rev. Biochem.* 80, 1089–1115. doi: 10.1146/annurev-biochem-060809-095203

Arrigo, A. P., and Welch, W. J. (1987). Characterization and purification of the small 28,000-dalton mammalian heat shock protein. *J. Biol. Chem.* 262, 15359–15369.

Asea, A., Rehli, M., Kabingu, E., Boch, J. A., Baré, O., Auron, P. E., et al. (2002). Novel signal transduction pathway utilized by extracellular HSP70. Role of toll-like receptor (TLR) 2 and TLR4. *J. Biol. Chem.* 277, 15028–15034. doi: 10.1074/jbc.M200497200

Bakthisaran, R., Tangirala, R., and Rao, C. M. (2015). Small heat shock proteins: role in cellular functions and pathology. *Biochim. Biophys. Acta* 1854, 291–319. doi: 10.1016/j.bbapap.2014.12.019

Banz, V. M., Medová, M., Keogh, A., Furer, C., Zimmer, Y., Candinas, D., et al. (2009). Hsp90 transcriptionally and post-translationally regulates the expression of NDRG1 and maintains the stability of its modifying kinase GSK3β. *Biochim. Biophys. Acta* 1793, 1597–1603. doi: 10.1016/j.bbamcr.2009.08.002

Barreca, M. M., Spinello, W., Cavalieri, V., Turturici, G., Sconzo, G., Kaur, P., et al. (2017). Extracellular Hsp70 enhances mesoangioblast migration via an autocrine signaling pathway. *J. Cell. Physiol.* 232, 1845–1861. doi: 10.1002/jcp.25722

Bartelt-Kirbach, B., Moron, M., Glomb, M., Beck, C. M., Weller, M. P., and Golenhofen, N. (2016). HspB5/αB-crystallin increases dendritic complexity and protects the dendritic arbor during heat shock in cultured rat hippocampal neurons. *Cell. Mol. Life Sci.* 73, 3761–3775. doi: 10.1007/s00018-016-2219-9

Bartelt-Kirbach, B., Slowik, A., Beyer, C., and Golenhofen, N. (2017). Upregulation and phosphorylation of HspB1/Hsp25 and HspB5/αB-crystallin after transient middle cerebral artery occlusion in rats. *Cell Stress Chaperones* 22, 653–663. doi: 10.1007/s12192-017-0794-9

Benatar, M., Wuu, J., Andersen, P. M., Atassi, N., David, W., Cudkowicz, M., et al. (2018). Randomized, double-blind, placebo-controlled trial of arimoclomol in rapidly progressive SOD1 ALS. *Neurology* 90, e565–e574. doi: 10.1212/WNL.0000000000004960

Benitez, M. J., Sanchez-Ponce, D., Garrido, J. J., and Wandosell, F. (2014). Hsp90 activity is necessary to acquire a proper neuronal polarization. *Biochim. Biophys. Acta* 1843, 245–252. doi: 10.1016/j.bbamcr.2013.11.013

Bernstein, S. L., Russell, P., Wong, P., Fishelevich, R., and Smith, L. E. (2001). Heat shock protein 90 in retinal ganglion cells: association with axonally transported proteins. *Vis. Neurosci.* 18, 429–436. doi: 10.1017/S0952523801183094

Bhat, S. P., and Nagineni, C. N. (1989). αB subunit of lens-specific protein α-crystallin is present in other ocular and non-ocular tissues. *Biochem. Biophys. Res. Commun.* 158, 319–325. doi: 10.1016/S0006-291X(89)80215-3

Bimston, D., Song, J., Winchester, D., Takayama, S., Reed, J. C., and Morimoto, R. I. (1998). BAG-1, a negative regulator of Hsp70 chaperone activity, uncouples nucleotide hydrolysis from substrate release. *EMBO J.* 17, 6871–6878. doi: 10.1093/emboj/17.23.6871

Bito, H., Furuyashiki, T., Ishihara, H., Shibasaki, Y., Ohashi, K., Mizuno, K., et al. (2000). A critical role for a Rho-associated kinase, p160ROCK, in determining axon outgrowth in mammalian CNS neurons. *Neuron* 26, 431–441. doi: 10.1016/S0896-6273(00)81175-7

Blatch, G. L., and Edkins, A. L. (1997). The networking of chaperones by co-chaperones. Control of cellular protein homeostasis. *J. Med. Genet.* 78, 1–33. doi: 10.1007/978-3-319-11731-7

Chaerkady, R., Kerr, C. L., Marimuthu, A., Kelkar, D. S., Kashyap, M. K., Gucek, M., et al. (2009). Temporal analysis of neural differentiation using quantitative proteomics. *J. Proteome Res.* 8, 1315–1326. doi: 10.1021/pr8006667

Chang, Y., Östling, P., Åkerfelt, M., Trouillet, D., Rallu, M., Gitton, Y., et al. (2006). Role of heat-shock factor 2 in cerebral cortex formation and as a regulator of p35 expression. *Genes Dev.* 20, 836–847. doi: 10.1101/gad.366906

Chen, S., and Brown, I. R. (2007). Neuronal expression of constitutive heat shock proteins: implications for neurodegenerative diseases. *Cell Stress Chaperones* 12, 51–58. doi: 10.1379/CSC-236R.1

Cheng, Y. C., Huang, C. J., Lee, Y. J., Tien, L. T., Ku, W. C., Chien, R., et al. (2016). Knocking down of heat-shock protein 27 directs differentiation of functional glutamatergic neurons from placenta-derived multipotent cells. *Sci. Rep.* 6:30314. doi: 10.1038/srep30314

Colvin, T. A., Gabai, V. L., Gong, J., Calderwood, S. K., Li, H., Gummuluru, S., et al. (2014). Hsp70-Bag3 interactions regulate cancer-related signaling networks. *Cancer Res.* 74, 4731–4741. doi: 10.1158/0008-5472.CAN-14-0747

Costigan, M., Mannion, R. J., Kendall, G., Lewis, S. E., Campagna, J. A., Coggeshall, R. E., et al. (1998). Heat shock protein 27: developmental regulation and expression after peripheral nerve injury. *J. Neurosci.* 18, 5891–5900. doi: 10.1155/2014/307106

Cox, D., Whiten, D. R., Brown, J. W. P., Horrocks, M. H., Gil, R. S., Dobson, C. M., et al. (2018). The small heat shock protein Hsp27 binds α-synuclein fibrils, preventing elongation and cytotoxicity. *J. Biol. Chem.* 293, 4486–4497. doi: 10.1074/jbc.M117.813865

Craig, A., and Banker, G. (1994). Neuronal polarity. *Annu. Rev. Neurosci.* 17, 267–310. doi: 10.1146/annurev.ne.17.030194.001411

Cui, H., Meng, Y., and Bulleit, R. F. (1998). Inhibition of glycogen synthase kinase 3β activity regulates proliferation of cultured cerebellar granule cells. *Brain Res. Dev. Brain Res.* 111, 177–188. doi: 10.1016/S0165-3806(98)00136-9

Dean, D. O., Kent, C. R., and Tytell, M. (1999). Constitutive and inducible heat shock protein 70 immunoreactivity in the normal rat eye. *Invest. Ophthalmol. Vis. Sci.* 40, 2952–2962.

Dean, D. O., and Tytell, M. (2001). Hsp25 and -90 immunoreactivity in the normal rat eye. *Investig. Ophthalmol. Vis. Sci.* 42, 3031–3040.

DeGeer, J., Kaplan, A., Mattar, P., Morabito, M., Stochaj, U., Kennedy, T. E., et al. (2015). Hsc70 chaperone activity underlies Trio GEF function in axon growth and guidance induced by netrin-1. *J. Cell Biol.* 210, 817–832. doi: 10.1083/jcb.201505084

Dou, F., Chang, X., and Ma, D. (2007). Hsp90 maintains the stability and function of the tau phosphorylating kinase GSK3β. *Int. J. Mol. Sci.* 8, 51–60. doi: 10.3390/i8010060

D'Souza, S. M., and Brown, I. R. (1998). Constitutive expression of heat shock proteins Hsp90, Hsc70, Hsp70 and Hsp60 in neural and non-neural tissues of the rat during postnatal development. *Cell Stress Chaperones* 3, 188–199. doi: 10.1379/1466-1268(1998)003<0188:CEOHSP>2.3.CO;2

Dulle, J. E., and Fort, P. E. (2016). Crystallins and neuroinflammation: the glial side of the story. *Biochim. Biophys. Acta* 1860, 278–286. doi: 10.1016/j.bbagen.2015.05.023

Duan, D., Fu, Y., Paxinos, G., and Watson, C. (2013). Spatiotemporal expression patterns of Pax6 in the brain of embryonic, newborn, and adult mice. *Brain Struct. Funct.* 218, 353–372. doi: 10.1007/s00429-012-0397-2

Dwyer, D. S., Liu, Y., Miao, S., and Bradley, R. J. (1996). Neuronal differentiation in PC12 cells is accompanied by diminished inducibility of Hsp70 and Hsp60 in response to heat and ethanol. *Neurochem. Res.* 21, 659–666. doi: 10.1007/BF02527722

Easter, S. S., Ross, L. S., and Frankfurter, A. (1993). Initial track formation in the mouse brain. *J. Neurosci.* 13, 285–299. doi: 10.1523/JNEUROSCI.13-01-00285.1993

Eustace, B. K., Sakurai, T., Stewart, J. K., Yimlamai, D., Unger, C., Zehetmeier, C., et al. (2004). Functional proteomic screens reveal an essential extracellular role for Hsp90α in cancer cell invasiveness. *Nat. Cell Biol.* 6, 507–514. doi: 10.1038/ncb1131

Ferrara, N., Gerber, H. P., and LeCouter, J. (2003). The biology of VEGF and its receptors. *Nat. Med.* 9, 669–676. doi: 10.1038/nm0603-669

Fischer, D., Hauk, T. G., Müller, A., and Thanos, S. (2008). Crystallins of the β/γ-superfamily mimic the effects of lens injury and promote axon regeneration. *Mol. Cell. Neurosci.* 37, 471–479. doi: 10.1016/j.mcn.2007.11.002

Fischer, D., Heiduschka, P., and Thanos, S. (2001). Lens-injury-stimulated axonal regeneration throughout the optic pathway of adult rats. *Exp. Neurol.* 172, 257–272. doi: 10.1006/exnr.2001.7822

Fontaine, J. M., Rest, J. S., Welsh, M. J., and Benndorf, R. (2003). The sperm outer dense fiber protein is the 10th member of the superfamily of mammalian small stress proteins. *Cell Stress Chaperones* 8, 62–69. doi: 10.1379/1466-1268(2003)8<62:TSODFP>2.0.CO;2

Fort, P. E., and Lampi, K. J. (2011). New focus on alpha-crystallins in retinal neurodegenerative diseases. *Exp. Eye Res.* 92, 98–103. doi: 10.1016/j.exer.2010.11.008

Frebel, K., Wiese, S., Funk, N., Pühringer, D., and Sendtner, M. (2007). Differential modulation of neurite growth by the S- and the L-forms of bag1, a co-chaperone of Hsp70. *Neurodegener. Dis.* 4, 261–269. doi: 10.1159/000101850

Gardner, T. W., and Davila, J. R. (2017). The neurovascular unit and the pathophysiologic basis of diabetic retinopathy. *Graefes Arch. Clin. Exp. Ophthalmol.* 255, 1–6. doi: 10.1007/s00417-016-3548-y

Gärtner, A., Huang, X., and Hall, A. (2006). Neuronal polarity is regulated by glycogen synthase kinase-3 (GSK-3β) independently of Akt/PKB serine phosphorylation. *J. Cell Sci.* 119, 3927–3934. doi: 10.1242/jcs.03159

Gentil, B. J., and Cooper, L. (2012). Molecular basis of axonal dysfunction and traffic impairments in CMT. *Brain Res. Bull.* 88, 444–453. doi: 10.1016/j.brainresbull.2012.05.003

Gershon, D., Blake, M., Holbrook, N., and Fargnoli, J. (1990). Discordant expression of heat shock protein mRNAs in tissues of heat-stressed rats. *J. Biol. Chem.* 265, 15275–15279.

Ghosh, J. G., Houck, S. A., and Clark, J. I. (2007). Interactive domains in the molecular chaperone human αB crystallin modulate microtubule assembly and disassembly. *PLoS One* 2:e498. doi: 10.1371/journal.pone.0000498

Grad, I., Cederroth, C. R., Walicki, J., Grey, C., Barluenga, S., Winssinger, N., et al. (2010). The molecular chaperone HSP90A is required for meiotic progression of spermatocytes beyond pachytene in the mouse. *PLoS One* 5:e15770. doi: 10.1371/journal.pone.0015770

Graner, M. W., Cumming, R. I., and Bigner, D. D. (2007). The heat shock response and chaperones/heat shock proteins in brain tumors: surface expression, release, and possible immune consequences. *J. Neurosci.* 27, 11214–11227. doi: 10.1523/JNEUROSCI.3588-07.2007

Gregory, M. A., Qi, Y., and Hann, S. R. (2003). Phosphorylation by glycogen synthase kinase-3 controls c-Myc proteolysis and subnuclear localization. *J. Biol. Chem.* 278, 51606–51612. doi: 10.1074/jbc.M310722200

Guay, J., Lambert, H., Gingras-Breton, G., Lavoie, J. N., Huot, J., and Landry, J. (1997). Regulation of actin filament dynamics by p38 map kinase-mediated phosphorylation of heat shock protein 27. *J. Cell Sci.* 110(Pt 3), 357–368.

Guzhova, I., Kislyakova, K., Moskaliova, O., Fridlanskaya, I., Tytell, M., Cheetham, M., et al. (2001). In vitro studies show that Hsp70 can be released by glia and that exogenous Hsp70 can enhance neuronal stress tolerance. *Brain Res.* 914, 66–73. doi: 10.1016/S0006-8993(01)02774-3

Hatayama, T., Takigawa, T., Takeuchi, S., and Shiota, K. (1997). Characteristic expression of high molecular mass heat shock protein HSP105 during mouse embryo development. *Cell Struct. Funct.* 22, 517–525. doi: 10.1247/csf.22.517

Hatten, M. E. (1999). Central nervous system neuronal migration. *Nucl. Med.* 22, 511–539. doi: 10.1146/annurev.neuro.22.1.511

Hennessy, B. T., Smith, D. L., Ram, P. T., Lu, Y., and Mills, G. B. (2005). Exploiting the PI3K/AKT pathway for cancer drug discovery. *Nat. Rev. Drug Discov.* 4, 988–1004. doi: 10.1038/nrd1902

Hochberg, G. K. A., Ecroyd, H., Liu, C., Cox, D., Cascio, D., Sawaya, M. R., et al. (2014). The structured core domain of B-crystallin can prevent amyloid fibrillation and associated toxicity. *Proc. Natl. Acad. Sci. U.S.A.* 111, E1562–E1570. doi: 10.1073/pnas.1322673111

Hossain, M. E., Matsuzaki, K., Katakura, M., Sugimoto, N., Mamun, A. A., Islam, R., et al. (2017). Direct exposure to mild heat promotes proliferation and neuronal differentiation of neural stem/progenitor cells in vitro. *PLoS One* 12:e0190356. doi: 10.1371/journal.pone.0190356

Iadecola, C. (2004). Neurovascular regulation in the normal brain and in Alzheimer's disease. *Nat. Rev. Neurosci.* 5, 347–360. doi: 10.1038/nrn1387

Ishii, Y., Kwong, J. M. K., and Caprioli, J. (2003). Retinal ganglion cell protection with geranylgeranylacetone, a heat shock protein inducer, in a rat glaucoma model. *Investig. Ophthalmol. Vis. Sci.* 44, 1982–1992. doi: 10.1167/iovs.02-0912

Ishima, T., Iyo, M., and Hashimoto, K. (2012). Neurite outgrowth mediated by the heat shock protein Hsp90α: a novel target for the antipsychotic drug aripiprazole. *Transl. Psychiatry* 2:e170. doi: 10.1038/tp.2012.97

Ishimoto, T., Kamei, A., Koyanagi, S., Nishide, N., Uyeda, A., Kasai, M., et al. (1998). HSP90 has neurite-promoting activity in vitro for telencephalic and spinal neurons of chick embryos. *Biochem. Biophys. Res. Commun.* 253, 283–287. doi: 10.1006/bbrc.1998.9701

Jo, D. H., An, H., Chang, D. J., Baek, Y. Y., Cho, C. S., Jun, H. O., et al. (2014). Hypoxia-mediated retinal neovascularization and vascular leakage in diabetic retina is suppressed by HIF-1α destabilization by SH-1242 and SH-1280, novel Hsp90 inhibitors. *J. Mol. Med.* 92, 1083–1092. doi: 10.1007/s00109-014-1168-8

Kalesnykas, G., Tuulos, T., Uusitalo, H., and Jolkkonen, J. (2008). Neurodegeneration and cellular stress in the retina and optic nerve in rat cerebral ischemia and hypoperfusion models. *Neuroscience* 155, 937–947. doi: 10.1016/j.neuroscience.2008.06.038

Kallio, M., Chang, Y., Manuel, M., Alastalo, T. P., Rallu, M., Gitton, Y., et al. (2002). Brain abnormalities, defective meiotic chromosome synapsis and female subfertility in HSF2 null mice. *EMBO J.* 21, 2591–2601. doi: 10.1093/emboj/21.11.2591

Kannan, R., Sreekumar, P. G., and Hinton, D. R. (2012). Novel roles for α-crystallins in retinal function and disease. *Prog. Retin. Eye Res.* 31, 576–604. doi: 10.1016/j.preteyeres.2012.06.001

Kappé, G., Verschuure, P., Philipsen, R. L., Staalduinen, A. A., Van de Boogaart, P., Boelens, W. C., et al. (2001). Characterization of two novel human small heat shock proteins: protein kinase-related HspB8 and testis-specific HspB9. *Biochim. Biophys. Acta* 1520, 1–6. doi: 10.1016/S0167-4781(01)00237-8

Kase, S., He, S., Sonoda, S., Kitamura, M., Spee, C., Wawrousek, E., et al. (2010). αB-crystallin regulation of angiogenesis by modulation of VEGF. *Blood* 115, 3398–3406. doi: 10.1182/blood-2009-01-197095

Kater, S. B., and Rehder, V. (1995). The sensory-motor role of growth cone filopodia. *Curr. Opin. Neurobiol.* 5, 68–74. doi: 10.1016/0959-4388(95)80089-1

Kayser, J., Haslbeck, M., Dempfle, L., Krause, M., Grashoff, C., Buchner, J., et al. (2013). The small heat shock protein Hsp27 affects assembly dynamics and structure of keratin intermediate filament networks. *Biophys. J.* 105, 1778–1785. doi: 10.1016/j.bpj.2013.09.007

Kida, E., Wierzba-Bobrowicz, T., Palminiello, S., Kaur, K., Jarzabek, K., Walus, M., et al. (2010). Molecular chaperone alphaB-crystallin is expressed in the human fetal telencephalon at midgestation by a subset of progenitor cells. *J. Neuropathol. Exp. Neurol.* 69, 745–759. doi: 10.1097/NEN.0b013e3181e5f515

Kieran, D., Kalmar, B., Dick, J. R. T., Riddoch-Contreras, J., Burnstock, G., and Greensmith, L. (2004). Treatment with arimoclomol, a coinducer of heat shock proteins, delays disease progression in ALS mice. *Nat. Med.* 10, 402–405. doi: 10.1038/nm1021

Kim, K. J., Li, B., Winer, J., Armanini, M., Gillett, N., and Phillips, H. S. (1993). Inhibition of vascular endothelial growth factor-induced angiogenesis suppresses tumour growth in vivo. *Nature* 362, 841–844. doi: 10.1038/362841a0

Kirbach, B. B., and Golenhofen, N. (2011). Differential expression and induction of small heat shock proteins in rat brain and cultured hippocampal neurons. *J. Neurosci. Res.* 89, 162–175. doi: 10.1002/jnr.22536

Konishi, H., Matsuzaki, H., Tanaka, M., Takemura, Y., Kuroda, S., Ono, Y., et al. (1997). Activation of protein kinase B (Akt/RAC-protein kinase) by cellular stress and its association with heat shock protein Hsp27. *FEBS Lett.* 410, 493–498. doi: 10.1016/S0014-5793(97)00541-3

Krueger, A. M. R., Armstrong, J. N., Plumier, J. C., Robertson, H. A., and Currie, R. W. (1999). Cell specific expression of Hsp70 in neurons and glia of the rat hippocampus after hyperthermia and kainic acid-induced seizure activity. *Mol. Brain Res.* 71, 265–278. doi: 10.1016/S0169-328X(99)00198-9

Kurihara, T. (2016). Development and pathological changes of neurovascular unit regulated by hypoxia response in the retina. *Prog. Brain Res.* 225, 201–211. doi: 10.1016/bs.pbr.2016.03.006

Kwong, J. M. K., Gu, L., Nassiri, N., Bekerman, V., Kumar-Singh, R., Rhee, K. D., et al. (2015). AAV-mediated and pharmacological induction of Hsp70 expression stimulates survival of retinal ganglion cells following axonal injury. *Gene Ther.* 22, 138–145. doi: 10.1038/gt.2014.105

Lavoie, J. N., Gingras-Breton, G., Tanguay, R. M., and Landry, J. (1993a). Induction of Chinese hamster HSP27 gene expression in mouse cells confers resistance to heat shock. HSP27 stabilization of the microfilament organization. *J. Biol. Chem.* 268, 3420–3429.

Lavoie, J. N., Hickey, E., Weber, L. A., and Landry, J. (1993b). Modulation of actin microfilament dynamics and fluid phase pinocytosis by phosphorylation of heat shock protein 27. *J. Biol. Chem.* 268, 24210–24214.

Lee, Y. J., Lee, H. J., Choi, S. H., Jin, Y. B., An, H. J., Kang, J. H., et al. (2012). Soluble HSPB1 regulates VEGF-mediated angiogenesis through their direct interaction. *Angiogenesis* 15, 229–242. doi: 10.1007/s10456-012-9255-3

Leon, S., Yin, Y., Nguyen, J., Irwin, N., and Benowitz, L. I. (2000). Lens injury stimulates axon regeneration in the mature rat optic nerve. *J. Neurosci.* 20, 4615–4626. doi: 10.1523/JNEUROSCI.20-12-04615.2000

Li, X., Colvin, T., Rauch, J. N., Acosta-Alvear, D., Kampmann, M., Dunyak, B., et al. (2015). Validation of the Hsp70-Bag3 protein-protein interaction as a potential therapeutic target in cancer. *Mol. Cancer Ther.* 14, 642–648. doi: 10.1158/1535-7163.MCT-14-0650

Lin, R., Karpa, K., Kabbani, N., Goldman-Rakic, P., and Levenson, R. (2001). Dopamine D2 and D3 receptors are linked to the actin cytoskeleton via interaction with filamin A. *Proc. Natl. Acad. Sci. U.S.A.* 98, 5258–5263. doi: 10.1073/pnas.011538198

Lindquist, S., and Craig, E. A. (1988). The heat-shock proteins. *Annu. Rev. Genet.* 22, 631–677. doi: 10.1146/annurev.ge.22.120188.003215

Liu, D. J., Hammer, D., Komlos, D., Chen, K. Y., Firestein, B. L., and Liu, A. Y. C. (2014). SIRT1 knockdown promotes neural differentiation and attenuates the heat shock response. *J. Cell. Physiol.* 229, 1224–1235. doi: 10.1002/jcp.24556

Loones, M. T., Chang, Y., and Morange, M. (2000). The distribution of heat shock proteins in the nervous system of the unstressed mouse embryo suggests a role in neuronal and non-neuronal differentiation. *Cell Stress Chaperones* 5, 291–305. doi: 10.1379/1466-1268(2000)005<0291:TDOHSP>2.0.CO;2

Loones, M. T., Rallu, M., Mezger, V., and Morange, M. (1997). HSP gene expression and HSF2 in mouse development. *Cell. Mol. Life Sci.* 53, 179–190. doi: 10.1007/PL00000590

Luo, S., Mao, C., Lee, B., and Lee, A. S. (2006). GRP78/BiP is required for cell proliferation and protecting the inner cell mass from apoptosis during early mouse embryonic development. *Mol. Cell. Biol.* 26, 5688–5697. doi: 10.1128/MCB.00779-06

Ma, C. H. E., Omura, T., Cobos, E. J., Latremoliere, A., Ghasemlou, N., Brenner, G. J., et al. (2011). Accelerating axonal growth promotes motor recovery after peripheral nerve injury in mice. *J. Clin. Invest.* 121, 4332–4347. doi: 10.1172/JCI58675DS1

Manzerra, P., and Brown, I. R. (1992). Expression of heat-shock genes (Hsp70) in the rabbit spinal cord: localization of constitutive and hyperthermia-inducible mRNA species. *J. Neurosci. Res.* 31, 606–615. doi: 10.1002/jnr.490310404

Marín, O., Valiente, M., Ge, X., and Tsai, L. H. (2010). Guiding neuronal cell migrations. *Cold Spring Harb. Perspect. Biol.* 2:a001834. doi: 10.1101/cshperspect.a001834

Matsuzaki, K., Katakura, M., Hara, T., Li, G., Hashimoto, M., and Shido, O. (2009). Proliferation of neuronal progenitor cells and neuronal differentiation in the hypothalamus are enhanced in heat-acclimated rats. *Pflugers Arch. Eur. J. Physiol.* 458, 661–673. doi: 10.1007/s00424-009-0654-2

McMillan, D., Xiao, X., Shao, L., Graves, K., and Benjamin, I. J. (1998). Targeted disruption of heat shock transcription factor 1 abolishes thermotolerance and protection against heat-inducible apoptosis. *J. Biol. Chem.* 273, 7523–7528. doi: 10.1074/jbc.273.13.7523

Mcmillan, D. R., Christians, E., Forster, M., Xiao, X., Connell, P., Plumier, J., et al. (2002). Heat shock transcription factor 2 is not essential for embryonic development, fertility, or adult cognitive and psychomotor function in mice. *Society* 22, 8005–8014. doi: 10.1128/MCB.22.22.8005

Metchat, A., Akerfelt, M., Bierkamp, C., Delsinne, V., Sistonen, L., Alexandre, H., et al. (2009). Mammalian heat shock factor 1 is essential for oocyte meiosis and directly regulates Hsp90α expression. *J. Biol. Chem.* 284, 9521–9528. doi: 10.1074/jbc.M808819200

Mimura, N., Hamada, H., Kashio, M., Jin, H., Toyama, Y., Kimura, K., et al. (2007). Aberrant quality control in the endoplasmic reticulum impairs the biosynthesis of pulmonary surfactant in mice expressing mutant BiP. *Cell Death Differ.* 14, 1475–1485. doi: 10.1038/sj.cdd.4402151

Minet, E. Y., Mottet, D., Michel, G., Roland, I., Raes, M., Remacle, J., et al. (1999). Hypoxia-induced activation of HIF-1: role of HIF-1α-Hsp90 interaction. *FEBS Lett.* 460, 251–256. doi: 10.1016/S0014-5793(99)01359-9

Mitchison, T., and Kirschner, M. (1984). Dynamic instability of microtubule growth. *Nature* 312, 237–242. doi: 10.1038/312237a0

Miyakoshi, L. M., Marques-Coelho, D., De Souza, L. E. R., Lima, F. R. S., Martins, V. R., Zanata, S. M., et al. (2017). Evidence of a cell surface role for Hsp90 complex proteins mediating neuroblast migration in the subventricular zone. *Front. Cell. Neurosci.* 11:138. doi: 10.3389/fncel.2017.00138

Moraga, A., Pradillo, J. M., Cuartero, M. I., Hernández-Jiménez, M., Oses, M., Moro, M. A., et al. (2014). Toll-like receptor 4 modulates cell migration and cortical neurogenesis after focal cerebral ischemia. *FASEB J.* 28, 4710–4718. doi: 10.1096/fj.14-252452

Morales, A. V., Hadjiargyrou, M., Díaz, B., Hernández-Sánchez, C., de Pablo, F., and de la Rosa, E. J. (1998). Heat shock proteins in retinal neurogenesis: identification of the PM1 antigen as the chick Hsc70 and its expression in comparison to that of other chaperones. *Eur. J. Neurosci.* 10, 3237–3245. doi: 10.1046/j.1460-9568.1998.00332.x

Nafar, F., Williams, J. B., and Mearow, K. M. (2015). Astrocytes release HspB1 in response to amyloid-β exposure in vitro. *J. Alzheimers Dis.* 49, 251–263. doi: 10.3233/JAD-150317

Narayanan, S., Kamps, B., Boelens, W. C., and Reif, B. (2006). αB-crystallin competes with Alzheimer's disease β-amyloid peptide for peptide-peptide interactions and induces oxidation of Abeta-Met35. *FEBS Lett.* 580, 5941–5946. doi: 10.1016/j.febslet.2006.09.063

Ninkovic, J., Pinto, L., Petricca, S., Lepier, A., Sun, J., and Rieger, M. A. (2010). The transcription factor Pax6 regulates survival of dopaminergic olfactory bulb neurons via crystallin αA. *Neuron* 68, 682–694. doi: 10.1016/j.neuron.2010.09.030

Östling, P., Björk, J. K., Roos-Mattjus, P., Mezger, V., and Sistonen, L. (2007). Heat Shock Factor 2 (HSF2) contributes to inducible expression of Hsp genes through interplay with HSF1. *J. Biol. Chem.* 282, 7077–7086. doi: 10.1074/jbc.M607556200

Oza, J., Yang, J., Chen, K. Y., and Liu, A. Y. C. (2008). Changes in the regulation of heat shock gene expression in neuronal cell differentiation. *Cell Stress Chaperones* 13, 73–84. doi: 10.1007/s12192-008-0013-9

Parfitt, D. A., Aguila, M., McCulley, C. H., Bevilacqua, D., Mendes, H. F., Athanasiou, D., et al. (2014). The heat-shock response co-inducer arimoclomol protects against retinal degeneration in rhodopsin retinitis pigmentosa. *Cell Death Dis.* 5:e1236. doi: 10.1038/cddis.2014.214

Park, J. H., Kim, S. H., Choi, M. C., Lee, J., Oh, D. Y., Im, S. A., et al. (2008). Class II histone deacetylases play pivotal roles in heat shock protein 90-mediated proteasomal degradation of vascular endothelial growth factor receptors. *Biochem. Biophys. Res. Commun.* 368, 318–322. doi: 10.1016/j.bbrc.2008.01.056

Park, K. H., Cozier, F., Ong, O. C., and Caprioli, J. (2001). Induction of heat shock protein 72 protects retinal ganglion cells in a rat glaucoma model. *Invest. Ophthalmol. Vis. Sci.* 42, 1522–1530.

Park, S., Ahn, E. S., and Kim, Y. (2015). Neuroblastoma SH-SY5Y cell-derived exosomes stimulate dendrite- like outgrowths and modify the differentiation of A375 melanoma cells. *Cell Biol. Int.* 39, 379–387. doi: 10.1002/cbin.10401

Patterson, A. J., and Zhang, L. (2010). Hypoxia and fetal heart development. *Curr. Mol. Med.* 10, 653–666. doi: 10.2174/156652410792630643

Pichon, S. (2004). Control of actin dynamics by p38 MAP kinase-Hsp27 distribution in the lamellipodium of smooth muscle cells. *J. Cell Sci.* 117, 2569–2577. doi: 10.1242/jcs.01110

Piri, N., Kwong, J. M. K., Gu, L., and Caprioli, J. (2016). Heat shock proteins in the retina: focus on HSP70 and alpha crystallins in ganglion cell survival. *Prog. Retin. Eye Res.* 52, 22–46. doi: 10.1016/j.preteyeres.2016.03.001

Quintá, H., and Galigniana, M. (2012). The neuroregenerative mechanism mediated by the Hsp90-binding immunophilin FKBP52 resembles the early steps of neuronal differentiation. *Br. J. Pharmacol.* 166, 637–649. doi: 10.1111/j.1476-5381.2011.01783.x

Quintá, H. R., Maschi, D., Gomez-Sanchez, C., Piwien-Pilipuk, G., and Galigniana, M. D. (2010). Subcellular rearrangement of Hsp90-binding immunophilins accompanies neuronal differentiation and neurite outgrowth. *J. Neurochem.* 115, 716–734. doi: 10.1111/j.1471-4159.2010.06970.x

Ramirez-Rodriguez, G., Babu, H., Klempin, F., Krylyshkina, O., Baekelandt, V., Gijsbers, R., et al. (2013). The crystallin domain of small heat shock protein b8 (Hspb8) acts as survival and differentiation factor in adult hippocampal neurogenesis. *J. Neurosci.* 33, 5785–5796. doi: 10.1523/JNEUROSCI.6452-11.2013

Rao, R., Nalluri, S., Fiskus, W., Balusu, R., Joshi, A., Mudunuru, U., et al. (2010). Heat shock protein 90 inhibition depletes TrkA levels and signaling in human acute leukemia cells. *Mol. Cancer Ther.* 9, 2232–2242. doi: 10.1158/1535-7163.MCT-10-0336

Richter-Landsberg, C., Schwarz, L., and Vollmer, G. (2010). The small heat shock protein HSP25/27 (HspB1) is abundant in cultured astrocytes and associated with astrocytic pathology in progressive supranuclear palsy and corticobasal degeneration. *Int. J. Cell Biol.* 2010:717520. doi: 10.1155/2010/717520

Ritossa, F. (1962). A new puffing pattern induced by temperature shock and DNP in drosophila. *Experientia* 18, 571–573. doi: 10.1007/BF02172188

Rübsam, A., Parikh, S., and Fort, P. (2018). Role of inflammation in diabetic retinopathy. *Int. J. Mol. Sci.* 19:E942. doi: 10.3390/ijms19040942

Ruebsam, A., Schey, K., Fort, P. E., Ruebsam, A., Dulle, J. E., Myers, A. M., et al. (2018). A specific phosphorylation regulates the protective role of αA-crystallin in diabetes. *JCI Insight* doi: 10.1172/jci.insight.97919.Research [Epub ahead of print].

Sabirzhanov, B., Stoica, B. A., Hanscom, M., Piao, C. S., and Faden, A. I. (2012). Over-expression of HSP70 attenuates caspase-dependent and caspase-independent pathways and inhibits neuronal apoptosis. *J. Neurochem.* 123, 542–554. doi: 10.1111/j.1471-4159.2012.07927.x

Saito, Y., Yamagishi, N., and Hatayama, T. (2007). Different localization of Hsp105 family proteins in mammalian cells. *Exp. Cell Res.* 313, 3707–3717. doi: 10.1016/j.yexcr.2007.06.009

Sánchez, C., Padilla, R., Paciucci, R., Zabala, J. C., and Avila, J. (1994). Binding of heat-shock protein 70 (Hsp70) to Tubulin. *Arch. Biochem. Biophys.* 310, 428–432. doi: 10.1006/abbi.1994.1188

Sato, S., Fujita, N., and Tsuruo, T. (2000). Modulation of Akt kinase activity by binding to Hsp90. *Proc. Natl. Acad. Sci. U.S.A.* 97, 10832–10837. doi: 10.1073/pnas.170276797

Schaar, B. T., and McConnell, S. K. (2005). Cytoskeletal coordination during neuronal migration. *Proc. Natl. Acad. Sci. U.S.A.* 102, 13652–13657. doi: 10.1073/pnas.0506008102

Shammas, S. L., Waudby, C. A., Wang, S., Buell, A. K., Knowles, T. P. J., Ecroyd, H., et al. (2011). Binding of the molecular chaperone αB-crystallin to Aβ amyloid fibrils inhibits fibril elongation. *Biophys. J.* 101, 1681–1689. doi: 10.1016/j.bpj.2011.07.056

Shao, W., Zhang, S. Z., Tang, M., Zhang, X. H., Zhou, Z., Yin, Y. Q., et al. (2013). Suppression of neuroinflammation by astrocytic dopamine D2 receptors via αb-crystallin. *Nature* 494, 90–94. doi: 10.1038/nature11748

Shao, W.-Y., Liu, X., Gu, X.-L., Ying, X., Wu, N., Xu, H.-W., et al. (2016). Promotion of axon regeneration and inhibition of astrocyte activation by alpha A-crystallin on crushed optic nerve. *Int. J. Ophthalmol.* 9, 955–966. doi: 10.18240/ijo.2016.07.04

Shi, Y., Su, C., Wang, J., Du, B., Dong, L., Liu, A., et al. (2015). Temporal and spatial changes in VEGF, αA- and αB-crystallin expression in a mouse model of oxygen-induced retinopathy. *Int. J. Clin. Exp. Med.* 8, 3349–3359.

Shimizu, M., Tanaka, M., and Atomi, Y. (2016). Small heat shock protein αB-Crystallin controls shape and adhesion of glioma and myoblast cells in the absence of stress. *PLoS One* 11:e0168136. doi: 10.1371/journal.pone.0168136

Sinha, D., Klise, A., Sergeev, Y., Hose, S., Bhutto, I. A., Hackler, L., et al. (2008). βA3/A1-crystallin in astroglial cells regulates retinal vascular remodeling during development. *Mol. Cell. Neurosci.* 37, 85–95. doi: 10.1016/j.mcn.2007.08.016

Sinha, D., Valapala, M., Bhutto, I., and Patek, B. (2012). βA3/A1-crystallin is required for proper astrocyte template formation and vascular remodeling in the retina. *Transgenic Res.* 21, 1033–1042. doi: 10.1007/s11248-012-9608-0

Song, J., Takeda, M., and Morimoto, R. I. (2001). Bag1–Hsp70 mediates a physiological stress signalling pathway that regulates Raf-1/ERK and cell growth. *Nat. Cell. Biol.* 3, 277–282. doi: 10.1038/35060068

Sreedhar, A. S., Kalmár, É., Csermely, P., and Shen, Y. F. (2004). Hsp90 isoforms: functions, expression and clinical importance. *FEBS Lett.* 562, 11–15. doi: 10.1016/S0014-5793(04)00229-7

Sreekumar, P. G., Kannan, R., Kitamura, M., Spee, C., Barron, E., Ryan, S. J., et al. (2010). αB crystallin is apically secreted within exosomes by polarized human retinal pigment epithelium and provides neuroprotection to adjacent cells. *PLoS One* 5:e12578. doi: 10.1371/journal.pone.0012578

Strittmatter, S. M., Fankhauser, C., Huang, P. L., Mashimo, H., and Fishman, M. C. (1995). Neuronal pathfinding is abnormal in mice lacking the neuronal growth cone protein GAP-43. *Cell* 80, 445–452. doi: 10.1016/0092-8674(95)90495-6

Sun, X., Zhou, Z., Fink, D. J., and Mata, M. (2013). HspB1 silences translation of PDZ-RhoGEF by enhancing miR-20a and miR-128 expression to promote

neurite extension. *Mol. Cell. Neurosci.* 57, 111–119. doi: 10.1016/j.mcn.2013.10.006

Takaki, E., Fujimoto, M., Sugahara, K., Nakahari, T., Yonemura, S., Tanaka, Y., et al. (2006). Maintenance of olfactory neurogenesis requires HSF1, a major heat shock transcription factor in mice. *J. Biol. Chem.* 281, 4931–4937. doi: 10.1074/jbc.M506911200

Tanaka, T., Serneo, F. F., Higgins, C., Gambello, M. J., Wynshaw-Boris, A., and Gleeson, J. G. (2004). Lis1 and doublecortin function with dynein to mediate coupling of the nucleus to the centrosome in neuronal migration. *J. Cell Biol.* 165, 709–721. doi: 10.1083/jcb.200309025

Tanaka, Y., Kobayashi, K., Kita, M., Kinoshita, S., and Imanishi, J. (1995). Messenger RNA expression of heat shock proteins (HSPs) during ocular development. *Curr. Eye Res.* 14, 1125–1133. doi: 10.3109/02713689508995819

Taylor, R. P., and Benjamin, I. J. (2005). Small heat shock proteins: a new classification scheme in mammals. *J. Mol. Cell. Cardiol.* 38, 433–444. doi: 10.1016/j.yjmcc.2004.12.014

Thuringer, D., Hammann, A., Benikhlef, N., Fourmaux, E., Bouchot, A., Wettstein, G., et al. (2011). Transactivation of the epidermal growth factor receptor by heat shock protein 90 via toll-like receptor 4 contributes to the migration of glioblastoma cells. *J. Biol. Chem.* 286, 3418–3428. doi: 10.1074/jbc.M110.154823

Tissières, A., Mitchell, H. K., and Tracy, U. M. (1974). Protein synthesis in salivary glands of *Drosophila melanogaster*: relation to chromosome puffs. *J. Mol. Biol.* 84, 389–398. doi: 10.1016/0022-2836(74)90447-1

Trinklein, N. D., Chen, W. C., Kingston, R. E., and Myers, R. M. (2004). Transcriptional regulation and binding of heat shock factor 1 and heat shock factor 2 to 32 human heat shock genes during thermal stress and differentiation. *Cell Stress Chaperones* 9, 21–28. doi: 10.1379/481.1

Tytell, M., Barbe, M. F., and Brown, I. R. (1994). Induction of stress (heat shock) protein 70 and its mRNA in rat corneal epithelium hyperthermia. *Curr. Eye Res.* 9, 913–918.

Tytell, M., Greenberg, S. G., and Lasek, R. J. (1986). Heat shock-like protein is transferred from glia to axon. *Brain Res.* 363, 161–164. doi: 10.1016/0006-8993(86)90671-2

Uchida, S., Hara, K., Kobayashi, A., Fujimoto, M., Otsuki, K., Yamagata, H., et al. (2011). Impaired hippocampal spinogenesis and neurogenesis and altered affective behavior in mice lacking heat shock factor 1. *Proc. Natl. Acad. Sci. U.S.A.* 108, 1681–1686. doi: 10.1073/pnas.1016424108

Valapala, M., Edwards, M., Hose, S., Hu, J., Wawrousek, E., Lutty, G. A., et al. (2015). βa3/A1-crystallin is a critical mediator of STAT3 signaling in optic nerve astrocytes. *Sci. Rep.* 5:8755. doi: 10.1038/srep08755

Voss, A. K., Thomas, T., and Gruss, P. (2000). Mice lacking HSP90β fail to develop a placental labyrinth. *Development* 127, 1–11.

Walsh, D., Li, Z., Wu, Y., and Nagata, K. (1997). Heat shock and the role of the HSPs during neural plate induction in early mammalian CNS and brain development. *Cell. Mol. Life Sci.* 53, 198–211. doi: 10.1007/PL00000592

Walsh, P., Bursać, D., Law, Y. C., Cyr, D., and Lithgow, T. (2004). The J-protein family: modulating protein assembly, disassembly and translocation. *EMBO Rep.* 5, 567–571. doi: 10.1038/sj.embor.7400172

Wang, G., Ying, Z., Jin, X., Tu, N., Zhang, Y., Phillips, M., et al. (2004). Essential requirement for both Hsf1 and Hsf2 transcriptional activity in spermatogenesis and male fertility. *Genesis* 38, 66–80. doi: 10.1002/gene.20005

Wang, G., Zhang, J., Moskophidis, D., and Mivechi, N. F. (2003). Targeted disruption of the heat shock transcription factor (Hsf)-2 gene results in increased embryonic lethality, neuronal defects, and reduced spermatogenesis. *Genesis* 36, 48–61. doi: 10.1002/gene.10200

Wang, X., Song, X., Zhuo, W., Fu, Y., Shi, H., Liang, Y., et al. (2009). The regulatory mechanism of Hsp90alpha secretion and its function in tumor malignancy. *Proc. Natl. Acad. Sci. U.S.A.* 106, 21288–21293. doi: 10.1073/pnas.0908151106

Wang, Y. H., Wang, D. W., Wu, N., Wang, Y., and Yin, Z. Q. (2011). Alpha-crystallin promotes rat retinal neurite growth on myelin substrates in vitro. *Ophthalmic Res.* 45, 164–168. doi: 10.1159/000319944

Wang, Y. H., Wang, D. W., Wu, N., Wang, Y., and Yin, Z. Q. (2012). Alpha-crystallin promotes rat axonal regeneration through regulation of RhoA/rock/cofilin/MLC signaling pathways. *J. Mol. Neurosci.* 46, 138–144. doi: 10.1007/s12031-011-9537-z

Wang, Z., Hu, Y., Xiao, D., Wang, J., Liu, C., Xu, Y., et al. (2017). Stabilization of Notch1 by the Hsp90 chaperone is crucial for T-cell leukemogenesis. *Clin. Cancer Res.* 23, 3834–3846. doi: 10.1158/1078-0432.CCR-16-2880

Waudby, C. A., Knowles, T. P. J., Devlin, G. L., Skepper, J. N., Ecroyd, H., Carver, J. A., et al. (2010). The interaction of αB-crystallin with mature α-synuclein amyloid fibrils inhibits their elongation. *Biophys. J.* 98, 843–851. doi: 10.1016/j.bpj.2009.10.056

Weis, F., Moullintraffort, L., Heichette, C., Chrétien, D., and Garnier, C. (2010). The 90-kDa heat shock protein Hsp90 protects tubulin against thermal denaturation. *J. Biol. Chem.* 285, 9525–9534. doi: 10.1074/jbc.M109.096586

Westerheide, S., Anckar, J., Stevens, S. M. Jr., Sistonen, L., and Morimoto, R. (2009). Stress-inducible regulation of heat shock factor 1 by the deacetylase SIRT1. *Science* 323, 1063–1066. doi: 10.1126/science.1165946

Williams, K. L., Rahimtula, M., and Mearow, K. M. (2005). Hsp27 and axonal growth in adult sensory neurons in vitro. *BMC Neurosci.* 6:24. doi: 10.1186/1471-2202-6-24

Williams, K. L., Rahimtula, M., and Mearow, K. M. (2006). Heat shock protein 27 is involved in neurite extension and branching of dorsal root ganglion neurons in vitro. *J. Neurosci. Res.* 85, 2352–2359. doi: 10.1002/jnr.20983

Xi, J., Farjo, R., Yoshida, S., Kern, T. S. S., Swaroop, A., and Andley, U. P. P. (2003). A comprehensive analysis of the expression of crystallins in mouse retina. *Mol. Vis.* 9, 410–419.

Zhan, R., Leng, X., Liu, X., Wang, X., Gong, J., Yan, L., et al. (2009). Heat shock protein 70 is secreted from endothelial cells by a non-classical pathway involving exosomes. *Biochem. Biophys. Res. Commun.* 387, 229–233. doi: 10.1016/j.bbrc.2009.06.095

Zhang, C., Gehlbach, P., Gongora, C., Cano, M., Fariss, R., Hose, S., et al. (2005). A potential role for β- and γ-crystallins in the vascular remodeling of the eye. *Dev. Dyn.* 234, 36–47. doi: 10.1002/dvdy.20494

Zhang, W., Tsuneishi, S., and Nakamura, H. (2001). Induction of heat shock proteins and its effects on glial. *Differentiation* 47, 77–95.

Zhu, W., Qi, X., Ren, S., Jia, C., Song, Z., and Wang, Y. (2012). αA-crystallin in the pathogenesis and intervention of experimental murine corneal neovascularization. *Exp. Eye Res.* 98, 44–51. doi: 10.1016/j.exer.2012.03.005

Zigler, J. S., Valapala, M., Shang, P., Hose, S., Goldberg, M. F., and Sinha, D. (2016). βA3/A1-crystallin and persistent fetal vasculature (PFV) disease of the eye. *Biochim. Biophys. Acta* 1860(1 Pt B), 287–298. doi: 10.1016/j.bbagen.2015.05.017

Zuehlke, A. D., Beebe, K., Neckers, L., and Prince, T. (2015). Regulation and function of the human HSP90AA1 gene. *Gene* 570, 8–16. doi: 10.1016/j.gene.2015.06.018

Conflict of Interest Statement: The authors declare that the research was conducted in the absence of any commercial or financial relationships that could be construed as a potential conflict of interest.

frontiers in Genetics

ORIGINAL RESEARCH
published: 30 November 2018
doi: 10.3389/fgene.2018.00594

Genetic Diagnostic Evaluation of Trio-Based Whole Exome Sequencing Among Children With Diagnosed or Suspected Autism Spectrum Disorder

Xiujuan Du[1†], Xueren Gao[2†], Xin Liu[3], Lixiao Shen[3], Kai Wang[4], Yanjie Fan[2], Yu Sun[2], Xiaomei Luo[2], Huili Liu[2], Lili Wang[2], Yu Wang[2], Zhuwen Gong[2], Jianguo Wang[2], Yongguo Yu[2] and Fei Li[1]**

[1] Developmental and Behavioral Pediatric Department – Child Primary Care Department, Brain and Behavioral Research Unit of Shanghai Institute for Pediatric Research and MOE Shanghai Key Laboratory for Children's Environmental Health, Xinhua Hospital, Shanghai Jiao Tong University School of Medicine, Shanghai, China, [2] Department of Pediatric Endocrinology and Genetics, Shanghai Institute for Pediatric Research, Xinhua Hospital, Shanghai Jiao Tong University School of Medicine, Shanghai, China, [3] Developmental and Behavioral Pediatric Department – Child Primary Care Department, Xinhua Hospital, Shanghai Jiao Tong University School of Medicine, Shanghai, China, [4] Shanghai Children's Medical Center, Shanghai Jiao Tong University School of Medicine, Shanghai, China

Autism spectrum disorder (ASD) is a group of clinically and genetically heterogeneous neurodevelopmental disorders. Recent tremendous advances in the whole exome sequencing (WES) enable rapid identification of variants associated with ASD including single nucleotide variations (SNVs) and indels. To further explore genetic etiology of ASD in Chinese children with negative findings of copy number variants (CNVs), we applied WES in 80 simplex families with a single affected offspring with ASD or suspected ASD, and validated variations predicted to be damaging by Sanger sequencing. The results showed that an overall diagnostic yield of 8.8% (9.2% in the group of ASD and 6.7% in the group of suspected ASD) was observed in our cohort. Among patients with diagnosed ASD, developmental delay or intellectual disability (DD/ID) was the most common comorbidity with a diagnostic yield of 13.3%, followed by seizures (50.0%) and craniofacial anomalies (40.0%). All of identified *de novo* SNVs and indels among patients with ASD were loss of function (LOF) variations and were slightly more frequent among female (male vs. female: 7.3% vs. 8.5%). A total of seven presumed causative genes (*CHD8*, *AFF2*, *ADNP*, *POGZ*, *SHANK3*, *IL1RAPL1,* and *PTEN*) were identified in this study. In conclusion, WES is an efficient diagnostic tool for diagnosed ASD especially those with negative findings of CNVs and other neurological disorders in clinical practice, enabling early identification of disease related genes and contributing to precision and personalized medicine.

Keywords: autism spectrum disorder, whole exome sequencing, diagnostic yield, comorbidity, genetic etiology

OPEN ACCESS

Edited by:
Wenbo Zhang,
The University of Texas Medical Branch at Galveston, United States

Reviewed by:
Jing Dong,
Baylor College of Medicine, United States
Srinivas Ayyadevara,
Central Arkansas Veterans Healthcare System Eugene J. Towbin Healthcare Center, United States

***Correspondence:**
Yongguo Yu
yuyongguo@shsmu.edu.cn
Fei Li
feili@shsmu.edu.cn

[†] These authors have contributed equally to this work

Specialty section:
This article was submitted to Genetics of Aging, a section of the journal Frontiers in Genetics

Received: *01 July 2018*
Accepted: *15 November 2018*
Published: *30 November 2018*

Citation:
Du X, Gao X, Liu X, Shen L, Wang K, Fan Y, Sun Y, Luo X, Liu H, Wang L, Wang Y, Gong Z, Wang J, Yu Y and Li F (2018) Genetic Diagnostic Evaluation of Trio-Based Whole Exome Sequencing Among Children With Diagnosed or Suspected Autism Spectrum Disorder. Front. Genet. 9:594. doi: 10.3389/fgene.2018.00594

INTRODUCTION

Autism spectrum disorder (ASD) is a group of highly heterogeneous neurodevelopmental disorders affecting 1 in 59 children aged 8 years, with boys four times more likely to be affected than girls (Baio et al., 2018). It's characterized by impaired reciprocal social interaction and communication, as well as restricted repetitive interests and behaviors (The Lancet, 2010). The symptoms could develop gradually from early childhood, affecting daily functioning and persisting throughout one's life (Stefanatos, 2008). Given the variety of phenotypes and severity, it's believed that genetic factors play a key role in the pathogenesis of ASD, in combination with developmental environmental factors (Hofvander et al., 2009; Mattila et al., 2010; Anagnostou et al., 2014).

The clinical and genetic heterogeneity of ASD has proved to be challenging to the diagnostic workup of affected patients. Routine testing for Fragile X syndrome, karyotyping and chromosomal microarray (CMA) have been established as the first-tier tests for patients with ASD for several years, accounting only for about 1–2%, 5%, and 5–10% cases, respectively (Shen et al., 2010; Betancur, 2011; State and Levitt, 2011; Devlin and Scherer, 2012). Certain loci were identified to confer risk for ASD, and 16p11.2, 15q11-q13, and 22q11.2 were the most frequent (Marshall et al., 2008; Weiss et al., 2008; Fernandez et al., 2010; Hogart et al., 2010; Hiroi et al., 2013). In addition, several genes identified by copy number variants (CNVs) screening and target sequencing for candidate genes were related to ASD susceptibility, such as *PTCHD1*, *NRXN1*, *NLGN3*, *SHANK3*, *SHANK1* and so on (Jamain et al., 2003; Moessner et al., 2007; Kim et al., 2008; Noor et al., 2010; Sato et al., 2012; Dabell et al., 2013). Recent rapidly improved accuracy and decreased cost of whole-exome sequencing (WES) enabled the application among proband-parent trios of ASD in clinical practice, opening the way to the discovery of single nucleotide variations (SNVs) and indels (Sanders et al., 2012; O'Roak et al., 2014). By using WES, ∼ 20.0% patients with sporadic ASD could be identified and this rate even reached to ∼90% because of the highly inbred nature of the Saudi population, making it useful in complementing CMA designed to detect CNVs, and better characterizing the genetic architecture for ASD in simplex families (O'Roak et al., 2011; Yu et al., 2013; Tammimies et al., 2015; Al-Mubarak et al., 2017). However, thus far, there remains a gap in our knowledge of the diagnostic yield of trio-WES among Chinese children with autistic features when CMA is unable to detect risk-related variations, and its impacts on clinical practice.

It is estimated that more than 70% of individuals with ASD have comorbidities including developmental and psychiatric disorders (Hofvander et al., 2009; Kohane et al., 2012). Based on the suspicion that genetic mechanism of children suffered an abnormality of morphogenesis differed from those who did not, Miles et al. (2005) collected data of dysmorphisms among children with ASD. The patients were further divided into two subsets of patients with documented dysmorphology (complex group) and without evident disrupted morphogenesis (essential group). The findings demonstrated that an abnormal karyotype (2.3%) or a clinically recognized syndrome (1.9%) were identified and restricted to complex group. Triggered by this incentive, we classified patients into different subgroups according to clinical manifestations, to explore the utility of WES and better characterize the underlining genetic differences.

In an attempt to expand the genetic spectrum of ASD by identifying novel SNV and indels, and evaluate how well WES could make up the deficiency of CMA in China, trio-based WES was further implemented among 80 children diagnosed as ASD and suspected of having ASD with negative findings of CMA.

MATERIALS AND METHODS

Patients

Data were collected from children visiting the outpatient clinic of Department of Developmental Behavioral Pediatric and Children Healthcare at Xinhua Hospital, Shanghai, China during March to December 2017. Without detection of CNVs related to ASD, a total of 80 unrelated children (aged 4 months to 13 years) with autistic features were enrolled to further complete trio-based whole exome sequencing (WES). All probands did not have neurological disorders (such as cerebral palsy and schizophrenia) or have the known chromosome/genetic disorders (such as trisomy 21 syndrome, trisomy 18 syndrome, trisomy 13 syndrome, Rett syndrome, Fragile X syndrome). Chromosome microarray analysis were applied by using Cyto Scan HD array (Affymetrix, Santa Clara, CA, United States).

Of these children, 65 (55 males and 10 females) were diagnosed as ASD using standard evaluation including Diagnostic and Statistical Manual of Mental Disorders, Fifth Edition (DMS-5), the Autism Diagnostic Observation Schedule (ADOS), Childhood Autism Rating Scale (CARS) and the intellectual assessment by clinicians. By intellectual assessment, the patients with developmental quotient (DQ) < 75 assessed using Gesell development scales, and intelligence quotient (IQ) < 70 assessed using WISC-R or WPPSI (Wechsler Intelligence Scale for children) were diagnosed as developmental delay or intellectual disability (DD/ID). With related evaluation not available, the rest of children exhibiting clinician-reported autistic features were suspected of having ASD. The study was approved by the ethical committee at Xinhua hospital and conducted in accordance with the relevant guidelines and regulations. Written informed consent in accordance with the Declaration of Helsinki was obtained from the patients and parents. And we have been adhered to standard biosecurity and institutional safety procedures in this study.

DNA Samples, WES, and Bioinformatics Analysis

Peripheral blood leukocytes from 80 children and parents were obtained. Genomic DNA (gDNA) was extracted using Lab-Aid Nucleic Acid (DNA) Isolation Kit (Zeesan, China), according to the manufacturer's instructions. The preparation of library of WES was completed using xGen Exome research panel v1.0 (Integrated DNA Technologies, Coralville, IA, United States). Sequencing was performed using paired 150-end, 150-cycle chemistry on the Illumina HiSeq 4000 (Illumina, San Diego,

CA, United States), according to the manufacturer's instructions. Burrows-Wheeler Aligner (BWA, version 0.7.10) was used for FASTQ files to mapping reads to the human reference genome (GRCh37/hg19). Base calling, QC analysis and coverage analysis was performed with Picard tools-1.124 and GATK software. Variants were then annotated using SnpEff version 4.2. Stepwise variant filtering are as follows: variants that demonstrated >1% frequency in the population variant databases including 1000 Genomes Project, Exome Variant Server (EVS) and Exome Aggregation Consortium (ExAC) or >5% frequency in our in-house database (based on 150 exome datasets), and intergenic and 3′/5′ untranslated region variants, none splice-related intronic and synonymous variants were filtered, with those located at canonical splice sites excluded.

Combined with clinical manifestation and modes of inheritance, Sanger sequencing and DNA-based paternity testing were performed to validate the putative pathogenic mutation for all family members. Sequencing products were analyzed using an ABI 3730xl DNA Analyzer (Applied Biosystems, Foster City, CA, United States). For DNA-based paternity testing, the Identifiler^{TM} system and the ABI 3730xL DNA Analyzer (Applied Biosystems) were used to perform multiplex polymerase chain reaction (PCR) amplification and genotyping of PCR products with capillary electrophoresis, respectively. Primer sequences used for validation have been showed in **Supplementary Table S1**.

MutationTaster[1], SIFT[2], and PolyPhen-2[3] were used to assess the effect of variants on protein function. Validated variants were classified as pathogenic, likely pathogenic, variants of uncertain clinical significance (VUS), likely benign and benign, based on standards and guidelines of the American College of Medical Genetics and Genomics (ACMG). Potential causative genetic variants have been deposited in database of LOVD[4], with associated accession numbers ranging from #0000379121 to #0000379127.

RESULTS

Clinical Characteristics of Patients

The clinical characteristics of children with diagnosed ASD and suspected ASD were summarized in **Table 1**. Among the patients with ASD, there were 23 children younger than 3 years, 30 children from 3 to 6 year of age (diagnostic rate = 16.7%) and 12 children older than 6 years (diagnostic rate = 8.3%) and the male/female ratio was 53/12. 41 out of 60 patients diagnosed as ASD with available behavioral assessments had CARS scores ≧37 (diagnostic rate = 7.3%), suggesting a severe autistic behavior.

In terms of other clinical phenotypes, DD/ID was the most common comorbidity in both groups of patients with ASD and suspected ASD. A variety of neurological and non-neurological deficits were exhibit among patients with ASD, including DD/ID (n = 45, diagnostic rate = 13.3%), seizures (n = 2, diagnostic rate = 50.0%), craniofacial anomalies (n = 5, diagnostic rate = 40.0%), etc. (**Table 1**).

Molecular Genetic Findings of WES

WES was performed among 80 trios with diagnosed or suspected ASD. Quality control of sequencing showed that 97.8% of the reads were mapped to the reference genome, and 97.7% of the targeted regions were covered by ≧10X reads with enough average depth (138X) (**Supplementary Table S2**). And details of QC (the depth, the coverage and the target regions covered by ≧10X reads) were shown in **Figure 1**. Potential causative variants were subsequently confirmed by Sanger sequencing.

A conclusive genetic diagnosis were obtained in seven of 80 children identified by WES, corresponding to an overall diagnostic yield of 8.8% (9.2% in the group of ASD and 6.7% in the group of suspected ASD). We detected and validated a total of seven variants and each was identified in a different gene (**Table 2**). Based on the distribution of the confirmed variants, frameshift were the most common (3/7), followed by the missense (2/7), stop gained (1/7) and start lost variants (1/7). Among the causative variants, the presumed mode of inheritance was autosomal dominant in 71.4% (71.4% *de novo*), and X-linked in 28.6% (14.3% *de novo* and 14.3% inherited).

De novo mutations accounted for 85.7% (six of seven) of the overall molecular diagnoses. Among patients with diagnosed ASD, all of identified *de novo* SNVs and indels were loss of function (LOF) variations and were slightly more frequent among female (male vs. female: 7.3% vs. 8.5%). In addition, all of patients with diagnosed ASD revealed to carry *de novo* LOF variations were co-occurring with DD/ID. A *de novo* missense variation was identified in one patient with suspected ASD. In total, seven genes (*CHD8*, *AFF2*, *ADNP*, *POGZ*, *SHANK3*, *IL1RAPL1*, and *PTEN*) with presumed pathogenic variations were identified in this study.

Impact of WES on Clinical Management

The discovery of WES makes both early clinical detection and genetic counseling possible in various ways among four of seven probands with a conclusive molecular diagnosis. In addition to the following up for ASD based on the risk genes, these patients received further workup of systemic involvement in this cohort. For example, developmental and behavioral evaluation were conducted in the patients with variants of *AFF2* and *IL1RAPL1*, respectively; seizures, short stature, abnormalities of skeleton system, eye, ear, brain and gastrointestinal tract screening, and developmental and behavioral evaluation were implemented in the patient with a *de novo* SNV of *POGZ*; hormone deficiency, short stature, obesity, hypotonia, seizures and feeding problems screening were evaluated in the patient with a *de novo* SNV of *ADNP*. And correspondingly, medication was changed. Growth hormone was applied in patients with *ADNP* and *POGZ* based on the diagnosis of short stature. Brain protein hydrolysate was discontinued in patients with seizures. Two couples with future pregnancy were informed the importance of prenatal testing and preimplantation genetic diagnosis.

[1]http://www.mutationtaster.org

[2]http://sift.jcvi.org

[3]http://genetics.bwh.harvard.edu/pph2/

[4]https://databases.lovd.nl/shared/variants?search_owned_by_=%3D%22Fei%20Li%22

TABLE 1 | Clinical characteristics of children with ASD and suspected ASD in the current study.

Characteristic	Children with ASD		Children with suspected ASD	
	No.	Diagnostic rate	No.	Diagnostic rate
Age at testing, y				
<3	23	0/23 (0)	7	1/7 (14.3%)
3–6	30	5/30 (16.7%)	5	0/5 (0)
≧6	12	1/12 (8.3%)	3	0/3 (0)
Sex				
Male	53	5/53 (9.4%)	10	1/10 (10.0%)
Female	12	1/12 (8.3%)	5	0/5 (0)
CARS				
30.0–36.5	19	3/19 (15.8 %)	–	–
37.0–60.0	41	3/41 (7.3%)	–	–
Principal phenotypic feature				
DD/ID	45	6/45 (13.3%)	7	1/7 (14.3%)
Gastrointestinal disorders	25	3/25 (12.0%)	1	0/1 (0)
ADHD	8	0/8 (0)	1	0/1 (0)
Sleep disturbances	6	0/6 (0)	–	–
Craniofacial anomalies	5	2/5 (40.0%)	4	0/4 (0)
Short stature	5	2/5 (40.0%)	1	0/1 (0)
Seizures	2	1/2 (50.0%)	2	0/2 (0)
Congenital heart disease	2	0/2 (0)	1	0/1 (0)
Obesity	3	0/3 (0)	–	–
Microcephaly/Macrocephaly	2	0/2 (0)	2	1/2 (50.0%)

ASD, autism spectrum disorder; CARS, Childhood Autism Rating Scale; DD/ID, developmental delay or intellectual disability; ADHD, attention deficit hyperactivity disorder; –, absent.

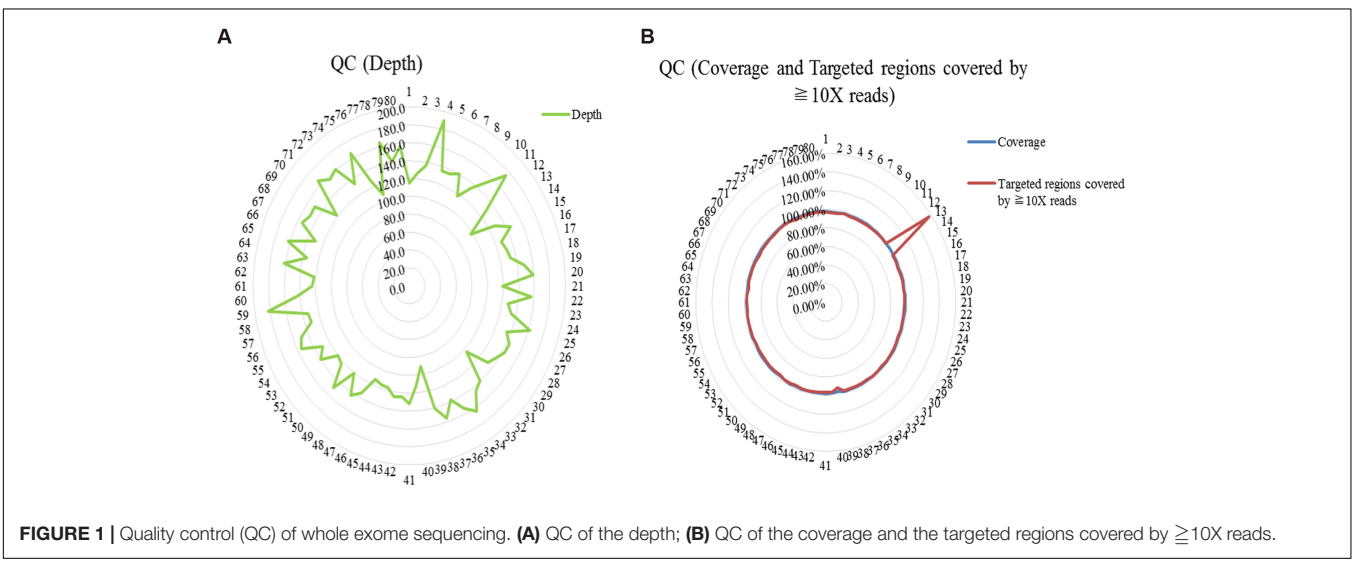

FIGURE 1 | Quality control (QC) of whole exome sequencing. **(A)** QC of the depth; **(B)** QC of the coverage and the targeted regions covered by ≧10X reads.

DISCUSSION

With the advent of decreasing cost combined with superior efficiency of WES, studies focusing on the contribution of *de novo* and/or inherited mutations become affordable as well as avoid the potential 'diagnostic odyssey' (Bamshad et al., 2011; O'Roak et al., 2011; Tan et al., 2017). In this study, with negative findings of ASD-related CNVs by using CMA, we further confirmed utility of trio-WES for diagnosis among children with ASD or suspected ASD in clinical practice. All *de novo* and inherited variants with predicted damaging effect were validated by Sanger sequencing in both patients and parents. Genetic etiology was identified in seven of 80 trios with an overall detection rate of 8.8%. Within the diagnosed ASD group, six of 65 (9.2%) patients received molecular diagnoses, which was similar to the results observed among sporadic ASD (8.4%), as well as those focusing on either *de novo* or inherited variations, ranging from 6.3% to 13.8% (Neale et al., 2012; Sanders et al., 2012; De Rubeis et al., 2014;

TABLE 2 | Clinical and molecular findings in children with positive results of WES.

ID	Sex	Age at testing, y	Clinical presentation	Molecular diagnosis	Gene	Sequence variant	Zygosity	Interpretation	ACMG classification
Diagnosed ASD									
ASD-685	M	4 years 7 months	DD/ID	Phelan-McDermid syndrome (OMIM:606232)	*SHANK3*	NM_033517.1: c.3630dupG; p.L1210fs	*De novo* het	Frameshift	P
ASD-667	M	4 years 8 months	DD/ID, gastrointestinal disorders	Mental retardation X-linked FRAXE type (OMIM:309548)	*AFF2*	NM_002025.3: c.2509C>T; p.Arg837Cys	Maternal hemi	Missense	P
ASD-706	M	4 years 11 months	DD/ID, seizures, craniofacial anomalies	Mental retardation X-linked 21/34 (OMIM:300143)	*IL1RAPL1*	NM_014271.3: c.1489C>T; p.Arg497*	*De novo* hemi	Stop gained	P
ASD-817	M	7 years 11 months	DD/ID, short stature	White-Sutton syndrome (OMIM:616364)	*POGZ*	NM_015100.3: c.1178_1181 delinsCC; p.H393Pfs*10	*De novo* het	Frameshift	P
ASD-867	F	3 years 2 months	DD/ID	{Autism, susceptibility to, 18} (OMIM:615032)	*CHD8*	NM_001170629 .1:c.4611dupA; p.Val1538fs	*De novo* het	Frameshift	P
ASD-821	M	4 years 11 months	DD/ID, craniofacial anomalies, short stature micropenis, anal stenosis,	Helsmoortel-van der Aa syndrome (OMIM:615873)	*ADNP*	NM_015339.3: c.2T>C; p. Met1Thr	*De novo* het	Start lost	P
Suspected ASD									
1	M	2 years	DD/ID, Macrocephaly	Macrocephaly/ autism syndrome (OMIM:605309)	*PTEN*	NM_000314.6: c.737C>T; p.Pro246Leu	*De novo* het	Missense	P

ASD, autism spectrum disorder; WES, whole exome sequencing; DD/ID, developmental delay or intellectual disability; P, pathogenic; -, absent.

Dong et al., 2014; Iossifov et al., 2014; Tammimies et al., 2015). An interesting finding emerging from this study implied the importance of completed ASD-related assessments in enabling a higher diagnostic yield among patients with suspected ASD. Our data showed that compared with children with suspected ASD (6.7%), the diagnostic yield was higher among patients with diagnosed ASD (9.2%). Moreover, diagnostic rate seemed high among ASD patients suffering from other neurodevelopmental disorders including DD/ID, suggesting that patients with these comorbidities may benefit more from WES. These findings were supported by the work of Tammimies et al. who recommended WES as a first-tier test for ASD, especially when comorbid with physical and congenital anomalies (Tammimies et al., 2015). To some extent, the relatively higher yield might result from the patients diagnosed and managed in the outpatient. Those who were diagnosed as ASD especially co-occurring with other neurodevelopmental disorders, are more likely undergone etiological testing including WES, given a high suspicion of genetic etiology.

The past few years have witnessed increasing studies of ASD trios published, highlighting the role of *de novo* variants and improving the identification of candidate risk genes for ASD (O'Roak et al., 2011; Iossifov et al., 2014). Given that *de novo* variation is less frequent and potentially more deleterious, we evaluated its diagnostic rates and effects to determine risk genes. Among children with diagnosed ASD, *de novo* variations were observed in 83.3% of the patients. Moreover, *de novo* LOF mutations contribute to 87.5% cases with ASD. Our findings that *de novo* variations of LOF predominant is contrary to previous population-based studies is intriguing (Iossifov et al., 2012; O'Roak et al., 2012; Sanders et al., 2012). One possible explanation is that ASD patients with other neurodevelopment disorders are prior to be tested by WES in outpatient, and may limit generalizability to the broader ASD population. Another key finding demonstrated here, was that in spite of a predominant male to female ratio (about 4:1), *de novo* LOF mutations were slightly more enriched in females with ASD. And this finding was consistent with the previous results (Levy et al., 2011; Iossifov et al., 2012). Genetic studies suggest that the strong male bias in liability might be attributed to a female protective effect, in which a higher load of mutations were tolerated by female (Gilman et al., 2011; Levy et al., 2011). An increasing body of evidence indicates that affected female with ASD are more susceptible to *de novo* SNVs and indels of LOF (Neale et al., 2012; Sanders et al., 2012; De Rubeis et al., 2014; Dong et al., 2014; Iossifov et al., 2014; Jacquemont et al., 2014). In addition to variations mentioned before, large CNVs encompassing more genes and probably more damaging, are especially abundant in affected females (Levy et al., 2011; Sanders et al., 2011; Jacquemont et al., 2014). These findings suggest to us that other underlying factors that have not yet been identified may contributes much more in males than in females.

All of genes with presumed causative mutations identified here were previously reported in ASD (Herman et al., 2007; Piton et al., 2008; Nishiyama et al., 2009; Bernier et al., 2014; Colak et al., 2014; Helsmoortel et al., 2014; Stessman et al., 2016; Yi et al., 2016). Six genes (*CHD8*, *AFF2*, *ADNP*, *POGZ*, *SHANK3*, and *IL1RAPL1*) were identified among patients with diagnosed ASD with DD/ID (Piton et al., 2008; Nishiyama et al., 2009; Bernier et al., 2014; Colak et al., 2014; Helsmoortel et al., 2014; Stessman et al., 2016; Yi et al., 2016). In spite of *de novo* LOF variations detected in *SHANK3* and *CHD8*, patient ASD-685 and ASD-867 presented ASD and DD/ID without other disorders at the age of testing. *SHANK3* was a gene encoding a scaffolding protein that is enriched in postsynaptic densities of excitatory synapses (Yi et al., 2016). And *CHD8*, allelic variants of which are associated with ASD, encoding the protein chromodomain helicase DNA binding protein 8 (Nishiyama et al., 2009), which is a chromatin regulator enzyme that is essential during fetal development (Ronan et al., 2013). At present, the mechanism of the higher incidence in males remains inconclusive, and hormones, sex-specific brain differences or variation on the sex chromosomes were speculated to play a role in. We identified two variants (one missense and one *de novo* LOF) in two X-chromosome genes (*AFF2* and *IL1RAPL1*). *AFF2* whose function is to encode a putative transcriptional activator that is a member of the AF4\FMR2 gene family, was previously associated with ASD and mental retardation, X-linked, FRAXE type (Colak et al., 2014). And in patient ASD-667 with a missense mutation in *AFF2* displayed gastrointestinal disorders in addition to DD/ID. Patient ASD-706 with a *de novo* LOF variation in *IL1RAPL1* showed ASD co-occurring with DD/ID, seizures and craniofacial anomalies. This gene is highly expressed in post-natal brain structures, which functions in the hippocampal memory system, thus suggesting a key role in the physiological processes underlying memory and learning abilities (Gambino et al., 2007). A *de novo* LOF variation in *POGZ* was identified in patient ASD-817 with DD/ID and short stature. Interestingly, previous reports showed patients with variation in *ADNP* often displayed Helsmoortel-van der Aa syndrome (Helsmoortel et al., 2014). However, without obesity and short stature at age of diagnosis, patients ASD-821 harboring a *de novo* LOF mutation (start lost) in *ADNP* presented novel phenotype of micropenis and anal stenosis. After genetic counseling, this patient were screened by biochemical tests related to hormone deficiency, short stature and suggested to be followed up in Department of Pediatric Endocrinology/Genetics. There remains one gene (*PTEN*) with a *de novo* missense variation was detected in a child with suspected ASD. This child presented typically macrocephaly and DD/ID. *PTEN* identified as a tumor suppressor is mutated in a large number of cancers at high frequency (Bonneau and Longy, 2000). These results implied that a continuum of neurological and non-neurological disorders that present in varied patterns might result from candidate risk genes by interacting with other factors.

To our knowledge, this work represents the first comprehensive analysis in Chinese children with diagnosed and suspected ASD by trio-based WES. Similar to other studies by WES, one of potential limitations is that true causative variants may be omitted as a result of stringent criteria to filter false-positives. Besides, WES has limited ability to detect genomic imbalances and could not evaluate variations located on non-coding sequences. Notwithstanding the small sample size, our study in part contributes to dataset of phenotype and genetic etiology of ASD in Chinese children. Moreover, we confirmed the utility of WES in patients without positive results of CNVs, improving the detection rate in a way. Accordingly, many challenges remain, it's hopeful for a brighter future of individuals with ASD and their families benefiting from the advantages of WES.

CONCLUSION

In conclusion, WES offers the advantage of early screening of the underlying ASD-related genes when related CNVs were not identified by CMA, providing genetic diagnoses across diverse clinical subgroups and contributing to precision and personalized medicine.

DATA AVAILABILITY STATEMENT

The potential causative variants in this study can be found in the LOVD database (https://databases.lovd.nl/shared/variants?search_owned_by_=%3D%22Fei%20Li%22), with associated accession numbers ranging from #0000379121 to #0000379127.

AUTHOR CONTRIBUTIONS

FL and YY conceived and designed the study. XG performed the experiments. XD and XG drafted the manuscript. XL and XD collected the samples from ASD families. FL and LS made diagnoses, and interpreted the clinical data. XG, YF, YS, XL, HL, LW, YW, ZG, and JW analyzed the exome sequencing data. XL and KW were responsible for obtaining study ethics and collected clinical data. The authors jointly discussed the experimental results throughout the duration of the study. All authors reviewed and approved the final manuscript.

FUNDING

The work was financially supported by funding from Shanghai Municipal Commission of Health and Family Planning (Grant Nos. 2017ZZ02026, 2018BR33, 2017EKHWYX-02, GDEK201709, and 201740192), Shanghai Shenkang Hospital Development Center (Grant No. 16CR2025B), Shanghai Municipal Education Commission (Grant No. 20152234), National Natural Science Foundation of China (Grant Nos. 81571031, 81761128035, and 81670812), Shanghai Committee of Science and Technology (Grant Nos. 17XD1403200 and 18DZ2313505), Xinhua Hospital of Shanghai Jiao Tong University School of Medicine (2018YJRC03, Talent introduction-014, Top talent-201603), Jiao Tong University Cross Biomedical Engineering (Grant No. YG2017MS72),

Shanghai Shen Kang Hospital Development Center new frontier technology joint project (Grant No. SHDC12017109), Youth Research Project of the Shanghai Municipal Health and Family Planning Commission (Grant No. 20184Y0348).

ACKNOWLEDGMENTS

The authors gratefully thank all the patients and their families.

SUPPLEMENTARY MATERIAL

The Supplementary Material for this article can be found online at: https://www.frontiersin.org/articles/10.3389/fgene.2018.00594/full#supplementary-material

TABLE S1 | Primer sequences used for validation.

TABLE S2 | Quality control of sequencing depth, coverage and the targeted regions covered by ≧10X reads (138X).

REFERENCES

Al-Mubarak, B., Abouelhoda, M., Omar, A., AlDhalaan, H., Aldosari, M., Nester, M., et al. (2017). Whole exome sequencing reveals inherited and de novo variants in autism spectrum disorder: a trio study from Saudi families. *Sci. Rep.* 7:5679. doi: 10.1038/s41598-017-06033-1

Anagnostou, E., Zwaigenbaum, L., Szatmari, P., Fombonne, E., Fernandez, B. A., Woodbury-Smith, M., et al. (2014). Autism spectrum disorder: advances in evidence-based practice. *CMAJ* 186, 509–519. doi: 10.1503/cmaj.121756

Baio, J., Wiggins, L., Christensen, D. L., Maenner, M. J., Daniels, J., Warren, Z., et al. (2018). Prevalence of autism spectrum disorder among children aged 8 years - autism and developmental disabilities monitoring network, 11 sites, United States, 2014. *MMWR Surveill. Summ.* 67, 1–23. doi: 10.15585/mmwr.ss6706a1

Bamshad, M. J., Ng, S. B., Bigham, A. W., Tabor, H. K., Emond, M. J., Nickerson, D. A., et al. (2011). Exome sequencing as a tool for mendelian disease gene discovery. *Nat. Rev. Genet.* 12, 745–755. doi: 10.1038/nrg3031

Bernier, R., Golzio, C., Xiong, B., Stessman, H. A., Coe, B. P., Penn, O., et al. (2014). Disruptive CHD8 mutations define a subtype of autism early in development. *Cell* 158, 263–276. doi: 10.1016/j.cell.2014.06.017

Betancur, C. (2011). Etiological heterogeneity in autism spectrum disorders: more than 100 genetic and genomic disorders and still counting. *Brain Res.* 1380, 42–77. doi: 10.1016/j.brainres.2010.11.078

Bonneau, D., and Longy, M. (2000). Mutations of the human PTEN gene. *Hum. Mutat.* 16, 109–122. doi: 10.1002/1098-1004(200008)16:2<109::AID-HUMU3>3.0.CO;2-0

Colak, D., Zaninovic, N., Cohen, M. S., Rosenwaks, Z., Yang, W. Y., Gerhardt, J., et al. (2014). Promoter-bound trinucleotide repeat mRNA drives epigenetic silencing in fragile X syndrome. *Science* 343, 1002–1005. doi: 10.1126/science.1245831

Dabell, M. P., Rosenfeld, J. A., Bader, P., Escobar, L. F., El-Khechen, D., Vallee, S. E., et al. (2013). Investigation of NRXN1 deletions: clinical and molecular characterization. *Am. J. Med. Genet. A* 161A, 717–731. doi: 10.1002/ajmg.a.35780

De Rubeis, S., He, X., Goldberg, A. P., Poultney, C. S., Samocha, K., Cicek, A. E., et al. (2014). Synaptic, transcriptional and chromatin genes disrupted in autism. *Nature* 515, 209–215. doi: 10.1038/nature13772

Devlin, B., and Scherer, S. W. (2012). Genetic architecture in autism spectrum disorder. *Curr. Opin. Genet. Dev.* 22, 229–237. doi: 10.1016/j.gde.2012.03.002

Dong, S., Walker, M. F., Carriero, N. J., DiCola, M., Willsey, A. J., Ye, A. Y., et al. (2014). De novo insertions and deletions of predominantly paternal origin are associated with autism spectrum disorder. *Cell Rep.* 9, 16–23. doi: 10.1016/j.celrep.2014.08.068

Fernandez, B. A., Roberts, W., Chung, B., Weksberg, R., Meyn, S., Szatmari, P., et al. (2010). Phenotypic spectrum associated with de novo and inherited deletions and duplications at 16p11.2 in individuals ascertained for diagnosis of autism spectrum disorder. *J. Med. Genet.* 47, 195–203. doi: 10.1136/jmg.2009.069369

Gambino, F., Pavlowsky, A., Begle, A., Dupont, J. L., Bahi, N., Courjaret, R., et al. (2007). IL1-receptor accessory protein-like 1 (IL1RAPL1), a protein involved in cognitive functions, regulates N-type Ca2+-channel and neurite elongation. *Proc. Natl. Acad. Sci. U.S.A.* 104, 9063–9068. doi: 10.1073/pnas.0701133104

Gilman, S. R., Iossifov, I., Levy, D., Ronemus, M., Wigler, M., and Vitkup, D. (2011). Rare de novo variants associated with autism implicate a large functional network of genes involved in formation and function of synapses. *Neuron* 70, 898–907. doi: 10.1016/j.neuron.2011.05.021

Helsmoortel, C., Vulto-van Silfhout, A. T., Coe, B. P., Vandeweyer, G., Rooms, L., van den Ende, J., et al. (2014). A SWI/SNF-related autism syndrome caused by de novo mutations in ADNP. *Nat. Genet.* 46, 380–384. doi: 10.1038/ng.2899

Herman, G. E., Butter, E., Enrile, B., Pastore, M., Prior, T. W., and Sommer, A. (2007). Increasing knowledge of PTEN germline mutations: two additional patients with autism and macrocephaly. *Am. J. Med. Genet. A* 143A, 589–593. doi: 10.1002/ajmg.a.31619

Hiroi, N., Takahashi, T., Hishimoto, A., Izumi, T., Boku, S., and Hiramoto, T. (2013). Copy number variation at 22q11.2: from rare variants to common mechanisms of developmental neuropsychiatric disorders. *Mol. Psychiatry* 18, 1153–1165. doi: 10.1038/mp.2013.92

Hofvander, B., Delorme, R., Chaste, P., Nyden, A., Wentz, E., Stahlberg, O., et al. (2009). Psychiatric and psychosocial problems in adults with normal-intelligence autism spectrum disorders. *BMC Psychiatry* 9:35. doi: 10.1186/1471-244X-9-35

Hogart, A., Wu, D., LaSalle, J. M., and Schanen, N. C. (2010). The comorbidity of autism with the genomic disorders of chromosome 15q11.2-q13. *Neurobiol. Dis.* 38, 181–191. doi: 10.1016/j.nbd.2008.08.011

Iossifov, I., O'Roak, B. J., Sanders, S. J., Ronemus, M., Krumm, N., Levy, D., et al. (2014). The contribution of de novo coding mutations to autism spectrum disorder. *Nature* 515, 216–221. doi: 10.1038/nature13908

Iossifov, I., Ronemus, M., Levy, D., Wang, Z., Hakker, I., Rosenbaum, J., et al. (2012). De novo gene disruptions in children on the autistic spectrum. *Neuron* 74, 285–299. doi: 10.1016/j.neuron.2012.04.009

Jacquemont, S., Coe, B. P., Hersch, M., Duyzend, M. H., Krumm, N., Bergmann, S., et al. (2014). A higher mutational burden in females supports a "female protective model" in neurodevelopmental disorders. *Am. J. Hum. Genet.* 94, 415–425. doi: 10.1016/j.ajhg.2014.02.001

Jamain, S., Quach, H., Betancur, C., Rastam, M., Colineaux, C., Gillberg, I. C., et al. (2003). Mutations of the X-linked genes encoding neuroligins NLGN3 and NLGN4 are associated with autism. *Nat. Genet.* 34, 27–29. doi: 10.1038/ng1136

Kim, H. G., Kishikawa, S., Higgins, A. W., Seong, I. S., Donovan, D. J., Shen, Y., et al. (2008). Disruption of neurexin 1 associated with autism spectrum disorder. *Am. J. Hum. Genet.* 82, 199–207. doi: 10.1016/j.ajhg.2007.09.011

Kohane, I. S., McMurry, A., Weber, G., MacFadden, D., Rappaport, L., Kunkel, L., et al. (2012). The co-morbidity burden of children and young adults with autism spectrum disorders. *PLoS One* 7:e33224. doi: 10.1371/journal.pone.0033224

Levy, D., Ronemus, M., Yamrom, B., Lee, Y. H., Leotta, A., Kendall, J., et al. (2011). Rare de novo and transmitted copy-number variation in autistic spectrum disorders. *Neuron* 70, 886–897. doi: 10.1016/j.neuron.2011.05.015

Marshall, C. R., Noor, A., Vincent, J. B., Lionel, A. C., Feuk, L., Skaug, J., et al. (2008). Structural variation of chromosomes in autism spectrum disorder. *Am. J. Hum. Genet.* 82, 477–488. doi: 10.1016/j.ajhg.2007.12.009

Mattila, M. L., Hurtig, T., Haapsamo, H., Jussila, K., Kuusikko-Gauffin, S., Kielinen, M., et al. (2010). Comorbid psychiatric disorders associated with Asperger syndrome/high-functioning autism: a community- and clinic-based study. *J. Autism Dev. Disord.* 40, 1080–1093. doi: 10.1007/s10803-010-0958-2

Miles, J. H., Takahashi, T. N., Bagby, S., Sahota, P. K., Vaslow, D. F., Wang, C. H., et al. (2005). Essential versus complex autism: definition of fundamental prognostic subtypes. *Am. J. Med. Genet. A* 135, 171–180. doi: 10.1002/ajmg.a.30590

Moessner, R., Marshall, C. R., Sutcliffe, J. S., Skaug, J., Pinto, D., Vincent, J., et al. (2007). Contribution of SHANK3 mutations to autism spectrum disorder. *Am. J. Hum. Genet.* 81, 1289–1297. doi: 10.1086/522590

Neale, B. M., Kou, Y., Liu, L., Ma'ayan, A., Samocha, K. E., Sabo, A., et al. (2012). Patterns and rates of exonic de novo mutations in autism spectrum disorders. *Nature* 485, 242–245. doi: 10.1038/nature11011

Nishiyama, M., Oshikawa, K., Tsukada, Y., Nakagawa, T., Iemura, S., Natsume, T., et al. (2009). CHD8 suppresses p53-mediated apoptosis through histone H1 recruitment during early embryogenesis. *Nat. Cell Biol.* 11, 172–182. doi: 10.1038/ncb1831

Noor, A., Whibley, A., Marshall, C. R., Gianakopoulos, P. J., Piton, A., Carson, A. R., et al. (2010). Disruption at the PTCHD1 Locus on Xp22.11 in Autism spectrum disorder and intellectual disability. *Sci. Transl. Med.* 2:49ra68. doi: 10.1126/scitranslmed.3001267

O'Roak, B. J., Deriziotis, P., Lee, C., Vives, L., Schwartz, J. J., Girirajan, S., et al. (2011). Exome sequencing in sporadic autism spectrum disorders identifies severe de novo mutations. *Nat. Genet.* 43, 585–589. doi: 10.1038/ng.835

O'Roak, B. J., Stessman, H. A., Boyle, E. A., Witherspoon, K. T., Martin, B., Lee, C., et al. (2014). Recurrent de novo mutations implicate novel genes underlying simplex autism risk. *Nat. Commun.* 5:5595. doi: 10.1038/ncomms6595

O'Roak, B. J., Vives, L., Girirajan, S., Karakoc, E., Krumm, N., Coe, B. P., et al. (2012). Sporadic autism exomes reveal a highly interconnected protein network of de novo mutations. *Nature* 485, 246–250. doi: 10.1038/nature10989

Piton, A., Michaud, J. L., Peng, H., Aradhya, S., Gauthier, J., Mottron, L., et al. (2008). Mutations in the calcium-related gene IL1RAPL1 are associated with autism. *Hum. Mol. Genet.* 17, 3965–3974. doi: 10.1093/hmg/ddn300

Ronan, J. L., Wu, W., and Crabtree, G. R. (2013). From neural development to cognition: unexpected roles for chromatin. *Nat. Rev. Genet.* 14, 347–359. doi: 10.1038/nrg3413

Sanders, S. J., Ercan-Sencicek, A. G., Hus, V., Luo, R., Murtha, M. T., Moreno-De-Luca, D., et al. (2011). Multiple recurrent de novo CNVs, including duplications of the 7q11.23 Williams syndrome region, are strongly associated with autism. *Neuron* 70, 863–885. doi: 10.1016/j.neuron.2011.05.002

Sanders, S. J., Murtha, M. T., Gupta, A. R., Murdoch, J. D., Raubeson, M. J., Willsey, A. J., et al. (2012). De novo mutations revealed by whole-exome sequencing are strongly associated with autism. *Nature* 485, 237–241. doi: 10.1038/nature10945

Sato, D., Lionel, A. C., Leblond, C. S., Prasad, A., Pinto, D., Walker, S., et al. (2012). SHANK1 deletions in males with autism spectrum disorder. *Am. J. Hum. Genet.* 90, 879–887. doi: 10.1016/j.ajhg.2012.03.017

Shen, Y., Dies, K. A., Holm, I. A., Bridgemohan, C., Sobeih, M. M., Caronna, E. B., et al. (2010). Clinical genetic testing for patients with autism spectrum disorders. *Pediatrics* 125, e727–e735. doi: 10.1542/peds.2009-1684

State, M. W., and Levitt, P. (2011). The conundrums of understanding genetic risks for autism spectrum disorders. *Nat. Neurosci.* 14, 1499–1506. doi: 10.1038/nn.2924

Stefanatos, G. A. (2008). Regression in autistic spectrum disorders. *Neuropsychol. Rev.* 18, 305–319. doi: 10.1007/s11065-008-9073-y

Stessman, H. A. F., Willemsen, M. H., Fenckova, M., Penn, O., Hoischen, A., Xiong, B., et al. (2016). Disruption of POGZ is associated with intellectual disability and autism spectrum disorders. *Am. J. Hum. Genet.* 98, 541–552. doi: 10.1016/j.ajhg.2016.02.004

Tammimies, K., Marshall, C. R., Walker, S., Kaur, G., Thiruvahindrapuram, B., Lionel, A. C., et al. (2015). Molecular diagnostic yield of chromosomal microarray analysis and whole-exome sequencing in children with autism spectrum disorder. *JAMA* 314, 895–903. doi: 10.1001/jama.2015.10078

Tan, T. Y., Dillon, O. J., Stark, Z., Schofield, D., Alam, K., Shrestha, R., et al. (2017). Diagnostic impact and cost-effectiveness of whole-exome sequencing for ambulant children with suspected monogenic conditions. *JAMA Pediatr.* 171, 855–862. doi: 10.1001/jamapediatrics.2017.1755

The Lancet (2010). DSM-5: diagnosis of mental disorders. *Lancet* 376:390.

Weiss, L. A., Shen, Y., Korn, J. M., Arking, D. E., Miller, D. T., Fossdal, R., et al. (2008). Association between microdeletion and microduplication at 16p11.2 and autism. *N. Engl. J. Med.* 358, 667–675. doi: 10.1056/NEJMoa075974

Yi, F., Danko, T., Botelho, S. C., Patzke, C., Pak, C., Wernig, M., et al. (2016). Autism-associated SHANK3 haploinsufficiency causes Ih channelopathy in human neurons. *Science* 352:aaf2669. doi: 10.1126/science.aaf2669

Yu, T. W., Chahrour, M. H., Coulter, M. E., Jiralerspong, S., Okamura-Ikeda, K., Ataman, B., et al. (2013). Using whole-exome sequencing to identify inherited causes of autism. *Neuron* 77, 259–273. doi: 10.1016/j.neuron.2012.11.002

Conflict of Interest Statement: The authors declare that the research was conducted in the absence of any commercial or financial relationships that could be construed as a potential conflict of interest.

frontiers in Neuroscience

ORIGINAL RESEARCH
published: 06 December 2018
doi: 10.3389/fnins.2018.00914

Tideglusib Rescues Neurite Pathology of SPG11 iPSC Derived Cortical Neurons

*Tatyana Pozner[1†], Annika Schray[1†], Martin Regensburger[1,2,3], Dieter Chichung Lie[4], Ursula Schlötzer-Schrehardt[5], Jürgen Winkler[3,6], Soeren Turan[1,4] and Beate Winner[1,6]**

[1] Department of Stem Cell Biology, Friedrich–Alexander University Erlangen–Nürnberg, Erlangen, Germany, [2] Department of Neurology, Friedrich–Alexander University Erlangen–Nürnberg, Erlangen, Germany, [3] Department of Molecular Neurology, Friedrich–Alexander University Erlangen–Nürnberg, Erlangen, Germany, [4] Institute of Biochemistry, Friedrich–Alexander University Erlangen–Nürnberg, Erlangen, Germany, [5] Department of Ophthalmology, Friedrich–Alexander University Erlangen–Nürnberg, Erlangen, Germany, [6] Center of Rare Diseases Erlangen, Friedrich–Alexander University Erlangen–Nürnberg, Erlangen, Germany

Mutations in SPG11 cause a complicated autosomal recessive form of hereditary spastic paraplegia (HSP). Mechanistically, there are indications for the dysregulation of the GSK3β/βCat signaling pathway in SPG11. In this study, we tested the therapeutic potential of the GSK3β inhibitor, tideglusib, to rescue neurodegeneration associated characteristics in an induced pluripotent stem cells (iPSCs) derived neuronal model from SPG11 patients and matched healthy controls as well as a CRISPR-Cas9 mediated SPG11 knock-out line and respective control. SPG11-iPSC derived cortical neurons, as well as the genome edited neurons exhibited shorter and less complex neurites than controls. Administration of tideglusib to these lines led to the rescue of neuritic impairments. Moreover, the treatment restored increased cell death and ameliorated the membranous inclusions in iPSC derived SPG11 neurons. Our results provide a first evidence for the rescue of neurite pathology in SPG11-HSP by tideglusib. The current lack of disease-modifying treatments for SPG11 and related types of complicated HSP renders tideglusib a candidate compound for future clinical application.

Keywords: induced pluripotent stem cell, neuronal culture, SPG11, tideglusib, GSK3β inhibitor, hereditary spastic paraplegia, CRISPR knock-out

OPEN ACCESS

Edited by:
Nan-Jie Xu,
Shanghai Jiao Tong University, China

Reviewed by:
Makoto Sato,
Osaka University, Japan
In-Hyun Park,
Yale University, United States

****Correspondence:***
Beate Winner
beate.winner@med.uni-erlangen.de

† These authors have contributed equally to this work

Specialty section:
This article was submitted to Neurogenesis, a section of the journal Frontiers in Neuroscience

Received: *21 July 2018*
Accepted: *21 November 2018*
Published: *06 December 2018*

Citation:
Pozner T, Schray A, Regensburger M, Lie DC, Schlötzer-Schrehardt U, Winkler J, Turan S and Winner B (2018) Tideglusib Rescues Neurite Pathology of SPG11 iPSC Derived Cortical Neurons. Front. Neurosci. 12:914. doi: 10.3389/fnins.2018.00914

INTRODUCTION

Hereditary spastic paraplegias (HSPs) are a heterogeneous group of motor neuron disorders. Clinically, HSP manifests with progressive lower limb spasticity and weakness due to axonopathy of corticospinal motor neurons and ascending dorsal columns. Up to date, more than 70 distinct genetic loci (Spastic Paraplegia Gene SPG1-SPG79) and mutations in more than 50 genes have been identified in HSP patients (Lo Giudice et al., 2014; Novarino et al., 2014). HSPs can be inherited in an autosomal dominant, autosomal recessive (AR), and, rarely, in an X-linked manner. Mutations in SPG11 are the most common genetic cause of AR complicated HSP. Apart from spastic paraparesis, SPG11 patients present with additional phenotypes that in the majority of cases include cognitive impairment, thin corpus callosum (TCC), neuropathy, and amyotrophy (Lo Giudice et al., 2014). Interestingly, mutations in *SPG11* encoding spatacsin, were also found in other motor neuron diseases such as AR juvenile-onset amyotrophic lateral sclerosis (ALS5) and

AR Charcot-Marie-Tooth disease (Montecchiani et al., 2016; Orlacchio et al., 2016). This indicates an important function of *SPG11* in a variety of neuronal subtypes and shows that spatacsin causes multi system neurodegeneration.

Until now, more than 100 mutations in the 40-exon long SPG11 have been described. The majority of mutations result in premature stop codons, causing nonsense mediated RNA decay and/or truncated proteins. This implies a loss of function mechanism (Stevanin et al., 2013). SPG11 encodes spatacsin (a 2443 aa protein; ∼280 kDa), a potential transmembrane protein (Paisan-Ruiz et al., 2008) that has been implicated in axonal maintenance (Pérez-Brangulí et al., 2014). A number of studies have shown that the protein is linked to the autophagic-lysosomal machinery (Chang et al., 2014; Renvoise et al., 2014; Varga et al., 2015; Branchu et al., 2017). In addition, siRNA mediated knock-down of SPG11, led to reduced neurite complexity of mouse dissociated cortical neurons (Pérez-Brangulí et al., 2014). Moreover, membrane-bound structures were observed within the processes of SPG11 patient, induced pluripotent stem cells (iPSC) derived cortical neurons (Pérez-Brangulí et al., 2014). This observation has been related to alterations in the transport of organelles, specifically anterograde transport and a lack of synaptic vesicle movement in SPG11 neurons (Pérez-Brangulí et al., 2014). Additionally iPSC-derived neural progenitor cells (NPCs) described a prominent neurodevelopmental defect. Reduced NPC proliferation was mediated by increased GSK3β activity followed by impairment of β-catenin signaling pathway (Mishra et al., 2016). Interestingly, administration of the specific GSK3β inhibitor tideglusib rescued the observed NPC proliferation defect (Mishra et al., 2016).

In the present study, we asked, whether tideglusib might not only improve proliferation, but might also have a positive effect on neurite pathology. We evaluated the effect of tideglusib on SPG11 patients' neurons. After confirming the presence of neurite pathology in iPSC derived cortical neurons from SPG11 patients and genome edited lines, we here established a treatment regimen for differentiated cortical neurons. By analyzing neuronal morphology and survival, we demonstrate that tideglusib is capable to reduce these neuronal impairments.

MATERIALS AND METHODS

Patients

The patients included in this study (n = 3; **Table 1**) were female Caucasians with genetically confirmed compound heterozygous mutations in SPG11 (Hehr et al., 2007; Bauer et al., 2009; Pérez-Brangulí et al., 2014). SPG11-1 and SPG11-2 are sisters with a heterozygous nonsense mutation at c.3036C>A/p.Tyr1012X in exon 16 and a c.5798delC/p.Ala1933ValfsX18 mutation in exon 30. SPG11-3 has a heterozygous nonsense mutation at c.267G>A/p.Trp89X in exon 2 and a splice site mutation 1457-2A>G in intron 6. All patients were severely affected, also indicated by high scores on the Spastic Paraplegia Rate Scale (33–39 out of max. of 52; Schüle et al., 2006). All patients have a TCC accompanied by cognitive impairment, white matter lesions, cortical atrophy, as well as muscle wasting and motor-sensory neuropathy (Hehr et al., 2007). The controls (CTRL1; CTRL2) were age matched healthy Caucasian females with no previous history of movement or neurological disorders.

iPSC Derivation

Fibroblasts from SPG11 patients and controls were reprogrammed with retroviral transduction using the four Yamanaka factors (Klf4, c-Myc, Oct4, and Sox2) as previously described (Pérez-Brangulí et al., 2014). The Institutional Review Board approval (Nr. 4120: Generierung von humanen neuronalen Modellen bei neurodegenerativen Erkrankungen) and informed and written consent forms are on file at the Movement Disorder Clinic of the Department of Molecular Neurology, Universitätsklinikum Erlangen (Erlangen, Germany). All iPSC lines were screened for pluripotency and had a stable karyotype using the G-banding chromosomal analysis (data not shown). The SPG11 mutations were confirmed in the patient-derived lines. Two iPSC lines were used for each patient and control.

Targeted SPG11 Knock-Out With the CRISPR/Cas9 System

To generate the SPG11 knock-out line (cSPG11) we targeted exon 1 of SPG11 (**Figure 4A**). The single gRNAs (sgRNA) (Sigma-Aldrich) were chosen with the CRISPOR web-tool[1] and cloned into the pX330 plasmid expressing SpCas9 (Addgene plasmid #42230) and the sgRNA according to the guidelines of the Zhang lab[2]. The cutting efficiency of the sgRNAs was evaluated in transfected 293T cells, by T7 endonuclease-mediated detection of insertions/deletions (indels) as previously described (Turan et al., 2016). The highly efficient sgRNA with an off-target score of 92 (sequence at **Supplementary Figure S3**) was chosen for nucleofection of a human embryonic stem cell line (hESC; HUES6). All the experiments with HUES6 were conducted according to the German Stem Cell Act (RKI, 63. Genehmigung to BW). Forty-eight hours after nucleofection, cells were single cell sorted by flow cytometry, expanded and validated for homozygous knock-out by T7-endonuclease assay (**Supplementary Figure S2A**), sequencing (LGC genomics) and TIDE genotyping analysis[3]. The positive clones and isogenic control (clone that underwent the genome editing process but had no mutations) were evaluated for exonic off-target mutagenesis by PCR-mediated sequencing of potential off-target sites of 5 candidate genes (selected with CRISPOR) (**Supplementary Figure S3A**). The genome edited lines were cultured on Matrigel (BD Biosciences) in mTeSR1 medium (Stem Cell Technologies). Detailed experimental scheme appears in **Figure 4B**.

Neuronal Differentiation and Tideglusib Treatment

The generation of NPCs and subsequent differentiation from pluripotent stem cells into neuronal cells was conducted

[1]http://crispor.tefor.net/

[2]https://www.addgene.org/crispr/zhang/

[3]https://tide.nki.nl/

TABLE 1 | Clinical characterization of SPG11 patients and controls.

	SPG11-1	SPG11-2	SPG11-3	CTRL-1	CTRL-2
SPG11 mutations	Exon 16: c.3036C>A Exon 30: c.5798delC	Exon 16: c.3036C>A Exon 30: c.5798delC	Exon 2: c.267G>A Intron 6: c.1457-2A > G	–	–
Sex	Female	Female	Female	Female	Female
Age at onset/age at examination (years)	24/46	20/40	31/50	–/45	–/28
SPRS (0–52)	44	37	36	0	0
Cognitive impairment	+	+	+	–	–
Wheelchair dependency	+	+	+	–	–
MRI abnormalities	Cortical atrophy, WML, TCC	Cortical atrophy, WML, TCC	Cortical atrophy, WML, TCC	–	–
iPSC clones (n = 2 per line)	SPG11-1a, SPG11-1b	SPG11-2a, SPG11-2b	SPG11-3a, SPG11-3b	CTRL-1a, CTRL-1b	CTRL-2a, CTRL-2b

Patients, SPG11-1, SPG11-2, SPG11-3; controls, CTR-1, CTRl-2; SPRS, spastic paraplegia rating scale; TCC, thin corpus callosum; WML, white matter lesion; iPSC, induced pluripotent stem cells.

as described previously (Havlicek et al., 2014; **Figure 1A**). Briefly, pluripotent stem cells were cultured with mTeSR1 medium (Stemcell Technologies) and passaged using Gentle Cell Dissociation Reagent (Stemcell Technologies). For the generation of free floating embryoid bodies (EBs), they were incubated for 45 min at 37°C with Collagenase IV and transferred to ultra-low attachment plates (Corning) for 1 week. Afterwards, the EBs were transferred to polyornithine-laminin coated plates, followed by manual collection of neural rosettes. Rosettes were dissociated using TrypLE^{TM} Express and transferred to proliferation media containing FGF_2. For the induction of neuronal differentiation, the cells were cultured in N2/B27 media supplemented with the neurotrophins BDNF and GDNF, cAMP, and ascorbic acid. Tideglusib (Selleckchem; diluted in DMSO) was administered at the concentration of 1 μM to 1 week differentiated neurons and was applied twice a week, during media changes, for a period of 3 weeks (for details see paradigm **Supplementary Figure S1**).

Immunofluorescence and Image Analysis

For stainings, 100,000 NPCs were plated on 24-well plates with polyornithine-laminin coated glass cover slips and treated according to the paradigm in **Figure 1A**. To quantify neuronal cell death, PFA-fixed cells were pretreated with acetic acid and ethanol at a 1:2 ratio at −20°C for 5 min. Afterward, the cells were stained with anti βIII-tubulin (Tuj-1; 1:500; BioLegend) and anti-cleaved-caspase3 (cCasp3; 1:500; Cell Signaling Technology) antibodies and mounted on microscope slides. Triplicate coverslips were used for each cell line and three random images per coverslip with comparable cell densities (40×) were acquired using Observer.Z1 fluorescence microscope (Zeiss). Representative images were obtained with LSM-780 confocal microscope setups (Carl Zeiss). For additional stainings, anti-glial fibrillary acidic protein (1:500; DAKO), and anti-Ctip2 (1:300; Abcam) antibodies were used. The quantifications were conducted with the cell counter plugin of Fiji software (Schindelin et al., 2012).

Gene Expression Analysis

The RNA was extracted using RNeasy kit (Qiagen) according to the manufacturer's instructions. A total of 500 ng RNA was reverse-transcribed into cDNA in 20 μl reaction solution by QuantiTect Reverse Transcription Kit (Qiagen). Subsequently, 1 μl of cDNA was used for real-time polymerase chain reaction (qPCR). The qPCR program definitions were as follows: 95°C for 10 min, followed by 40 cycles at 95°C for 15 s and 60°C for 1 min and 1 cycle at 95°C for 15 s, 60°C for 30 s and 95°C for 15 s. The primers are listed in **Supplementary Table S1**.

Neurite Length and Complexity Analysis

Neurons derived from pluripotent stem cells were cultured in 24-well plates, on top of polyornithine-laminin coated glass coverslips. In order to allow visualization of single neurons, on day 26 the cells were transfected with pEF1-dTomato using Lipofectamine, 2000 (Invitrogen, reagent:DNA ratio 2:1). The cells were fixed 48 h after transfection with 4% paraformaldehyde (PFA) in phosphate-buffered saline (PBS). The cells were stained for neuronal marker expression using the anti-βIII-tubulin antibody on coverslips (Tuj-1; 1:500; BioLegend), and the coverslips were mounted on slides. Images were captured with a 10× objective lens using the TILE function of the Zen Pro Software (Zeiss) on the Observer.Z1 fluorescence microscope (Zeiss). Semi-automated tracing of individual transfected βIII-tubulin positive cells was performed using the NeuronJ plugin of Fiji (Schindelin et al., 2012). A minimum of 36 cells per patient/control and 18 cells for genome edited lines were analyzed for the number of neurites and total neurite length. Furthermore, semi-automated Sholl analysis was carried out at predefined 50 μm intervals from the soma using the Fiji software.

Electron Microscopy

Transmission electron microscopy was performed as described previously (Schlotzer-Schrehardt et al., 2012; Havlicek et al., 2014). Briefly, the neurons were fixed in 2.5% glutaraldehyde in 0.1 M phosphate buffer. Subsequently, cells were post-fixed

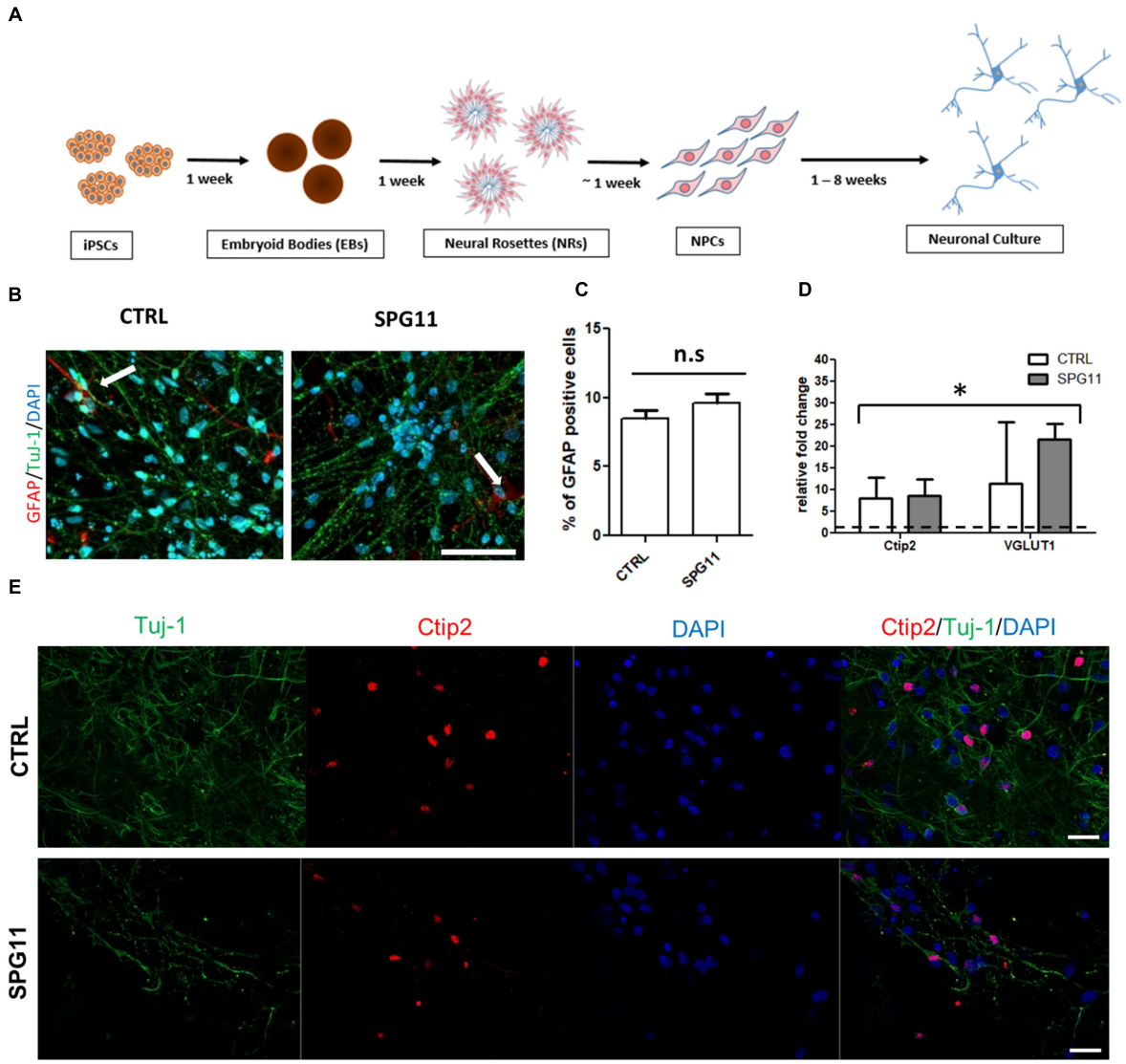

FIGURE 1 | Neuronal differentiation and characterization **(A)** Schematic representation of the differentiation of iPSCs into neuronal cultures. **(B)** Representative images of CTRL (left; CTRL-1a) and SPG11 (right; SPG11-1b) 4 weeks differentiated neurons stained for GFAP and Tuj-1. **(C)** Quantification of percentage of $GFAP^{+}/DAPI^{+}$ cells in CTRLs and SPG11. **(D)** qPCR data of 4 weeks differentiated neurons. RNA from four different iPSCs clones was used as negative control and it is indicated as a dashed line at onefold change. **(E)** Representative images Ctip2 (red) and Tuj-1 (green) of CTRL and SPG11. Quantifications represent pooled data of CTRLs (CTRL-1, CTRL-2) and SPG11 (SPG11-1, SPG11-2, SPG11-3) neurons. iPSCs, induced pluripotent stem cells; NPCs, neural progenitor cells. Scale bar = 50 μm in **(B)** and 20 μm in **(E)**. $^{*}P < 0.05$.

in 2% buffered osmium tetroxide and dehydrated in graded alcohol concentrations. Afterward, the cells were embedded in epoxy resin. Horizontal sections were stained with uranyl acetate and lead citrate. Finally, the sections were examined using a transmission electron microscope (LEO 906E; Carl Zeiss Microscopy).

Statistical Analysis

All statistical analyses were performed using IBM SPSS statistics software (version 23). The Student two tailed *t*-test for unpaired variables was applied when comparing the means between two groups. For comparison of more than three groups, one-way ANOVA followed by Bonferroni *post hoc* test was applied. *P*-values ≤ 0.05 were considered statistically significant. Unless indicated otherwise, all data are shown as mean ± SEM.

RESULTS

Characterization of iPSC Derived Neurons

The neuronal differentiation (described in **Figure 1A**) yields in cortical neurons expressing a majority of Tuj-1 positive cells with astrocytes comprising less than 10% of the cellular population

(**Figures 1B,C**). There was no significant difference in the amount of astrocytes between SPG11 lines and controls (**Figure 1C**).

Immunofluorescence stainings as well as qPCR analysis confirm the neuronal cortical identity of the iPSC derived cells (**Figures 1D,E**). Thus, both controls and SPG11 cell lines exhibited a significantly higher transcript level of the deep layer marker Ctip2 and the vesicular glutamate transporter 1 (VGLUT1) compared to iPSC lines (**Figure 1D**). The gene expression levels did not differ between patients and controls (**Figure 1D**).

Rescue of SPG11 Neurite Outgrowth Abnormalities by Tideglusib Treatment

We first evaluated the neurite morphology of SPG11 iPSC derived neuronal cultures and measured neuritic length and the number of neurites per cell, indicative of neuritic complexity (**Figure 2A**). Compared to CTRLs, neurite length was significantly decreased by 78% in SPG11 (669.44 ± 50.34 μm in SPG11, compared to 3103.48 ± 328.04 μm in CTRL; $P \leq 0.05$; **Figure 2B**). Moreover, neurite number was significantly reduced (2.87 ± 0.16 in SPG11, compared to 6.76 ± 1.0 in CTRL; $P \leq 0.05$; **Figure 2C**). These results are in agreement with the previously described neuritic impairment in SPG11 iPSC derived neuronal cultures (Pérez-Brangulí et al., 2014). We next tested the effect of the chronic administration of 1 μM tideglusib. The rationale for this dose was obtained from previous experiments, which revealed severe toxicity at a higher dose (5 μM; data not shown). We applied the compound twice a week for a period of 3 weeks until neurons reach maturity (see paradigm **Supplementary Figure S1**). Interestingly, chronic administration of tideglusib was able to significantly rescue neurite length (2856.86 ± 151.65 μm in SPG11 treated with tideglusib, compared to 3103.48 ± 328.04 μm in CTRL; $P \leq 0.05$; **Figure 2B**). Moreover, neurite number was restored to a level which was virtually comparable to CTRL (6.48 ± 0.64 in SPG11 treated with tideglusib, compared to 6.76 ± 1.04 in CTRL; $P \leq 0.05$; **Figure 2C**).

In order to further elaborate the effect of the chronic administration of tideglusib on neurite complexity, Sholl analysis was performed. The number of intersections of neurites at various radial distances from the cell soma was measured and revealed a significant increase in neuritic arborization of SPG11 patient derived neurons upon tideglusib treatment (**Figure 2D**). This effect was significant for all distances' measures (distances from soma from 10 μm to 1660 μm, $P \leq 0.05$).

Rescue of Neurodegeneration Associated Characteristics in SPG11 iPSC-Derived Neurons by Tideglusib Treatment

We next asked, whether treatment with tideglusib also has an impact on neural cell death. We quantified the number of cCasp3/Tuj1 double positive cells within the different groups (**Figure 3A**). A significantly higher amount of neuronal cell death was present in non-treated SPG11 neurons (23.34% ± 04.22% $cCas3^+$ cells in SPG11, compared to 14.17% ± 2.80% $cCas3^+$ cells in CTRL; $P \leq 0.05$; **Figure 3C**). In addition, the relative survival rate was lower in SPG11 neurons compared to control (0.87 ± 0.09 $Tuj\text{-}1^+/ cCas3^-$ cells in SPG11 treated with tideglusib, compared to 1.0 ± 0.09 $Tuj\text{-}1^+/cCas3^-$ cells in CTRL; $P \leq 0.05$; **Figures 3B,C**). The treatment decreased the number of $cCas3^+$ cells to CTRL levels (15.68 ± 2.26% $cCas3^+$ cells in SPG11 treated with tideglusib, compared to 14.17 ± 2.80% $cCas3^+$ cells in CTRL; $P \leq 0.05$; **Figures 3A,C**). Similarly, the compound was also able to increase the survival rate of SPG11 neurons (0.96 ± 0.09 $Tuj\text{-}1^+/cCas3^-$ cells in SPG11 treated with tideglusib, compared to 1.0 ± 0.09 $Tuj\text{-}1^+/cCas3-$ cells in CTRL; $P \leq 0.05$; **Figures 3B,C**) to a level which did not significantly differ from CTRL ($P \geq 0.05$ according to Bonferroni test; **Figure 3D**). We next sought to analyze the impact of tideglusib on neurite ultrastructure.

The ultrastructural analysis of SPG11 iPSC derived 4-weeks differentiated neurons revealed that the neurites accumulate membrane-bound inclusion bodies measuring 0.3–1.5 μm in diameter with electron-dense contents. Interestingly, tideglusib treatment reverted this phenotype and led to an elimination of these abnormal structures (**Figure 3E**).

CRISPR/Cas9 Mediated Generation and Characterization of SPG11 Knock-Out Line

Sequencing analysis of HUES6 line transfected with a plasmid containing Cas9 and gRNA targeting exon 1 of SPG11 revealed one clone with out-of-frame mutation (cSPG11, **Figures 4C,D**). According to TIDE analysis, the clone was positive for out-of-frame mutation in both alleles (**Figures 4C,D**). An additional clone, that underwent the genome editing process, but had no mutations (cCTRL; **Figure 4D**), was chosen as isogenic control. Both cSPG11 and cCTRL were negative for off-target activity (**Supplementary Figures S3A,B**). The reduction of spatacsin in cSPG11 confirms the efficiency of the genome editing strategy (**Supplementary Figure S2B**). The residual amount of the protein can be attributed to the lack of specific and reliable antibodies for spatacsin detection. Genome edited pluripotent stem cells were differentiated according to the paradigm in **Figure 1A** and were positive for Tuj1 (**Figure 4E**) with astrocytes levels that, similarly to iPSC-derived neuronal cultures, were lower than 10% and did not differ between cSPG11 and cCTRL (**Supplementary Figure S2C**).

Rescue of Neurite Impairments in the Genome Edited Line

Interestingly, the SPG11 genome edited line (cSPG11) recapitulates the observations from the patients' iPSC derived neurons (**Figures 4F,G**). Thus, the neurites of cSPG11 hES derived neuronal cultures are significantly shorter (1115.99 ± 490.04 μm in cSPG11, compared to 2816.25 ± 948.44 μm in cCTRL; $P \leq 0.05$; **Figure 4F**) and fewer (3.22 ± 1.09 in cSPG11, compared to 5.66 ± 1.50 in cCTRL; $P \leq 0.05$; **Figure 4G**) compared to isogenic control (cCTRL). Similarly to the rescue of the patients' lines, tideglusib administration rescued the neurite length (3211.18 ± 1080.52 μm in cSPG11 treated with tideglusib,

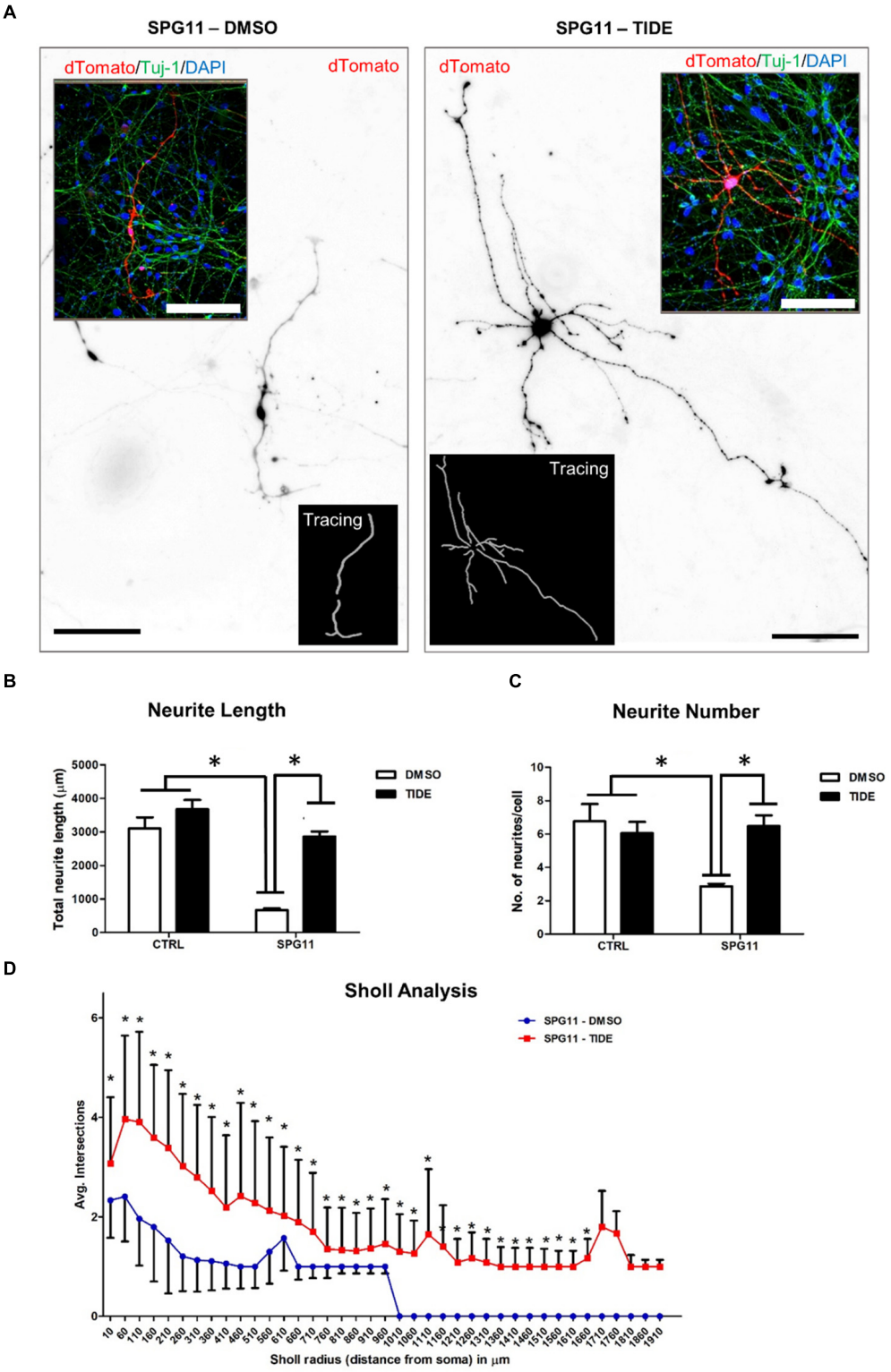

FIGURE 2 | Rescue of neurite outgrowth abnormalities of SPG11 patients by tideglusib treatment. **(A)** Representative image of non-treated (left) and tideglusib treated (right) SPG11 neurons transfected with pEF1-dTomato. Neurite tracings are shown in the inserts. **(B)** The total neuritic length is significantly decreased in SPG11 neurons and it is recovered following tideglusib treatment. **(C)** The average number of SPG11 neurites is significantly decreased and it is recovered following tideglusib treatment. **(D)** Sholl analysis confirms a significant increase in neurite number following tideglusib treatment. Quantifications in C, D represent pooled data of CTRLs (CTRL-1, CTRL-2) and SPG11 (SPG11-1, SPG11-2, SPG11-3) iPSC-derived-neurons. Scale bar = 100 μm. Data shown as means ± SEM. $^*P \leq 0.05$.

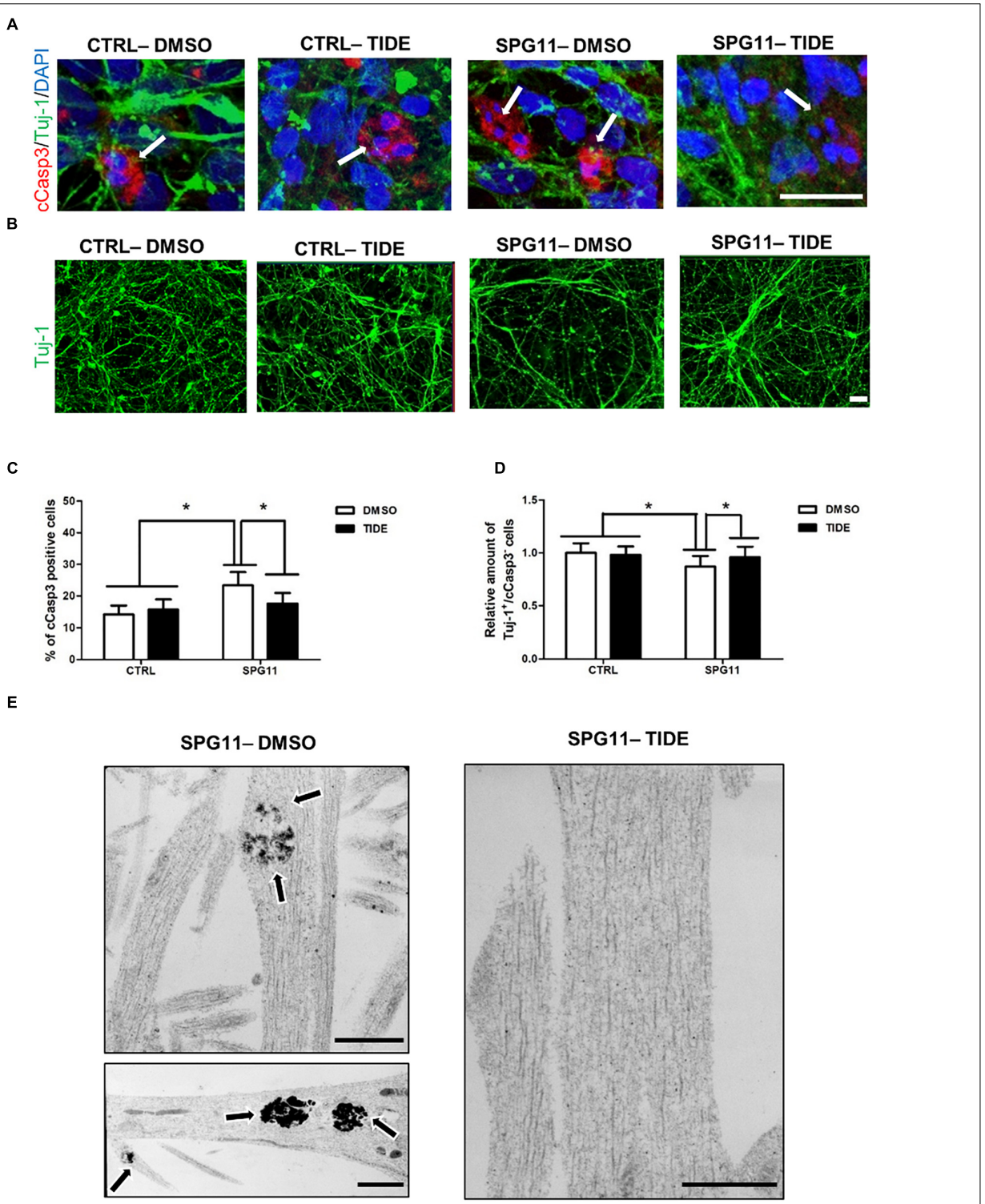

FIGURE 3 | Neurodegeneration associated impairments in SPG11 neurons are rescued by tideglusib treatment. **(A)** Merged confocal images of SPG11 and CTRL neurons generated from iPSCs and co-immunostained for βIII-tubulin (Tuj-1) and cleaved-caspase3 (cCasp3). Scale bar = 20 μm. **(B)** Representative images of TUJ-1 stained SPG11 and control neurons. **(C)** Elevated cCasp3 levels in SPG11 neurons is rescued by tideglusib treatment. **(D)** Reduced level of Tuj-1 is rescued by tideglusib treatment. **(E)** Ultrastructural analysis of the neurites of non-treated (left) and tideglusib treated (right) SPG11 4-week-differentiated-neurons reveals that the membranous inclusion bodies (indicated by arrows) in SPG11 neurons are reduced in number and size following the treatment. Quantifications in **(C,D)** represent pooled data of CTRLs (CTRL-1, CTRL-2) and SPG11 (SPG11-1, SPG11-2, SPG11-3) iPSC-derived-neurons. Scale bar = 20 μm in **(A,B)** and 1 μM in **(E)**.
$^*P < 0.05$.

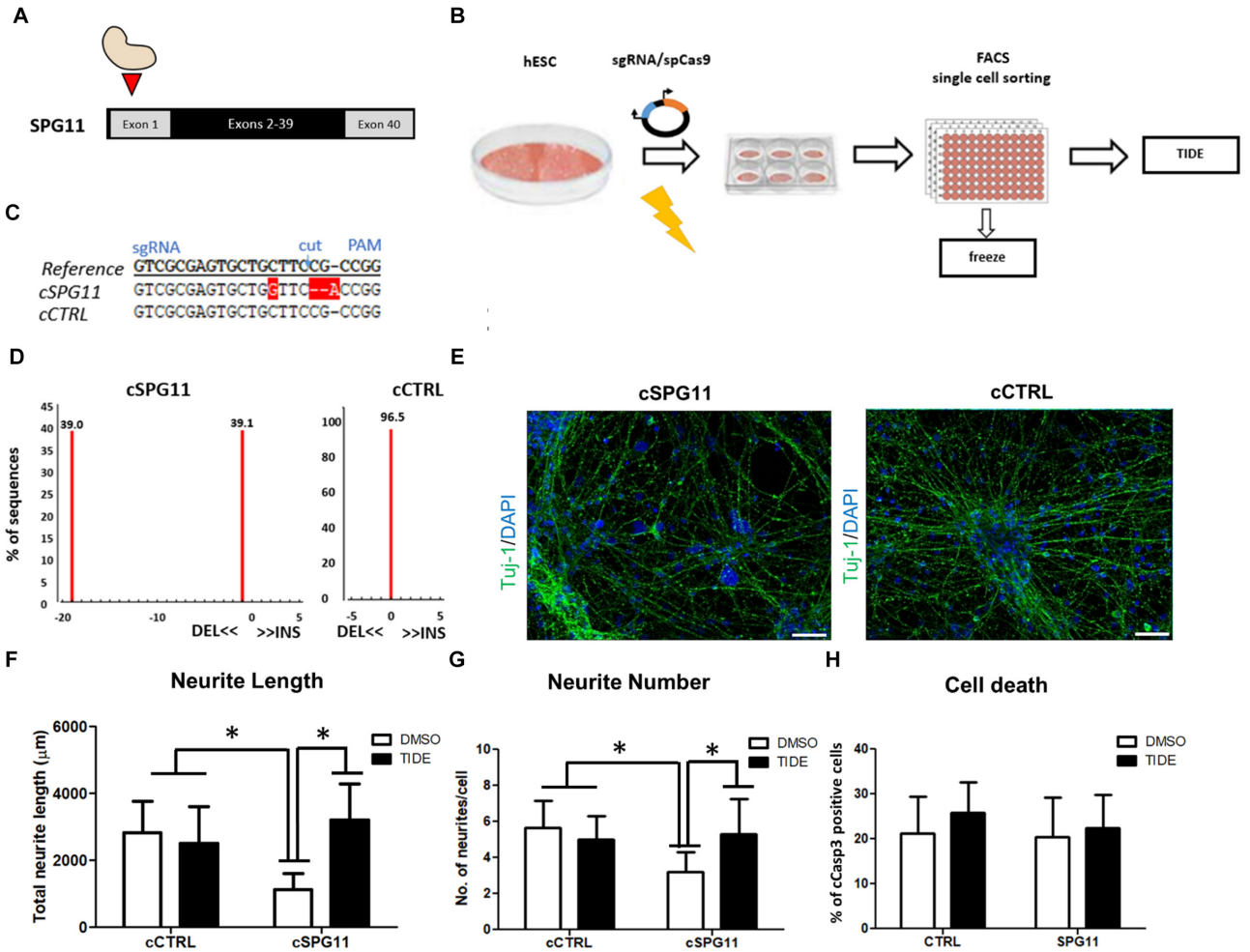

FIGURE 4 | CRISPR/Cas9 genome edited hESC-derived-neurons recapitulate the neuritic phenotypes of patient iPSC-derived-neurons. **(A)** Strategy for SPG11 knock-out by targeting exon 1 of *SPG11*. **(B)** Experimental scheme for CRISPR/Cas9 mediated genome editing of hESCs. hESCs were nucleofected with 5 μg of pX330 plasmid expressing SpCas9 and the sgRNA. After 48-h, the cells were single cell-sorted into 96-well plate. Subsequently, emerging colonies were split in 1:2 ratio. Half of the split was used for genomic DNA generation. The rest was transferred into a new 96-well plate for cryopreservation in –80°C. For identification of positive clones, PCR products were sequenced, further expanded and genotyped by Tracking Indels by Decomposition (TIDE; https://tide.nki.nl/) web-tool. **(C)** Sequence comparison between reference non-nucleofected HUES6 cell line, a positive, genome edited clone (cSPG11) and a control that underwent the genome editing process, but had no mutations (cCTRL). **(D)** TIDE analysis of cSPG11 and cCTRL. **(E)** Representative images of the genome edited lines stained for Tuj-1 (green). **(F)** The total neuritic length is significantly decreased in cSPG11 neurons and it is recovered following tideglusib treatment. **(G)** The average number of SPG11 neurites is significantly decreased and is recovered following tideglusib treatment. **(H)** Quantification of cCasp3^{+} cells reveals no significant difference between cSPG11 and cCTRL. Data shown as means ± SD. Scale bar = 50 μm. *$P < 0.05$. FACS = Fluorescence-activated cell sorting.

compared to 2816.25 ± 948.44 μm in cCTRL; $P \leq 0.05$; **Figure 4F**) and complexity (5.33 ± 1.93 in cSPG11 treated with tideglusib, compared to 5.66 ± 1.50 in cCTRL; $P \leq 0.05$; **Figure 4G**).

There was no evident change in the levels of cell death between the genome edited control (cCTRL) and SPG11 knock-out (cSPG11) lines (**Figure 4H**).

DISCUSSION

Our findings indicate a beneficial effect of tideglusib on both cellular morphology and survival of SPG11-iPSCs-derived neurons. This is the first indication of an effective therapeutic approach applied to human SPG11 differentiated neurons.

First, our data confirm the findings from a previous study (Pérez-Brangulí et al., 2014) that SPG11 neurons present with impaired neuritic length and decreased number of neurites, indicative of reduced neuronal complexity. Our study was able to rescue these impairments by administration of the irreversible GSK3 inhibitor, tideglusib, to neuronal cells. In addition, we were able to recapitulate virtually similar neuritic impairments, followed by tideglusib rescue in CRISPR/Cas9 mediated SPG11 knock-out line. Previous findings revealed that SPG11 NPCs exhibit dysregulation of GSK3β/βCat

signaling pathway (Mishra et al., 2016). The data of our current study indicate that this pathway has a prominent role not only during neural development, but also in mature neurons. We are able to show, that in SPG11 tideglusib has a significant role in rescuing the neuritic morphology.

Increased activity of GSK3β has been implicated in neurodegeneration, particularly in Alzheimer's Disease (AD). Animal models overexpressing GSK3β exhibit one of the main AD hallmarks – increased tau phosphorylation (Brownlees et al., 1997; Lucas et al., 2001), whereas overexpression of GSK3β in the dentate gyrus leads to neurodegeneration of this area (de Barreda et al., 2010). Tau hyper-phosphorylation, elevated amyloid levels and activation of GSK3β are also present in AD-iPSC derived neurons (Ochalek et al., 2017). Conversely, inhibition of GSK3β leads to reduction of β-amyloid production (Rockenstein et al., 2007) and its toxicity (Koh et al., 2008), reduction of phosphorylated tau in cultured neurons (Zhang et al., 2011) and improves learning and memory in AD mouse models (Farr et al., 2016). Although the onset and patterns of cognitive symptoms and cortical atrophy present in SPG11 patients are markedly different from those observed in AD patients, our data suggest that GSK3β over-activation may be a common molecular denominator of both diseases.

We next found that tideglusib treatment was able to rescue the increased cell death of SPG11 neurons. The potential of tideglusib to diminish apoptosis in SPG11 was first revealed in a study where tideglusib administration to SPG11-NPCs improved their survival and proliferation (Mishra et al., 2016). Here, we extended the therapeutic value of tideglusib to neurons by showing for the first time, that differentiating neurons are also responsive to its effects. Our results are compatible with the data indicating the important role of GSK3β in the regulation of apoptosis (Jacobs et al., 2012). In addition, it has been shown that GSK3β inhibition leads to neuroprotective effects (Culbert et al., 2001).

Moreover, in rat cerebellar granule neurons cultures GSK3β inhibition lead to increase of neuronal survival (Song et al., 2010), whereas in a mouse model of CNS injury it promoted axonal regeneration (Song et al., 2010; Guo et al., 2016). Overall, these studies conclude that GSK3β inhibition has a beneficial effect on mature neurons which also provides an explanation to the observed rescue of SPG11 neurodegenerative phenotypes by tideglusib.

Interestingly, SPG11 knock-out line showed no difference in cell death, and the number of cCas3 positive cells was not changed following tideglusib treatment. This result may arise from the vast heterogeneity and lack of correlation between genotype and phenotype in *SPG11*. Thus, in addition to HSP type 11, mutations in *SPG11* can lead to autosomal recessive juvenile amyotrophic lateral sclerosis and Charcot-Marie-Tooth disease (Montecchiani et al., 2016). This observation indicates the importance of the use of patient specific lines for disorders with complex genotypes.

An additional important observation is that tideglusib treatment leads to reduction of membranous inclusion bodies in SPG11 neurites. The possibility to reduce this impairment emphasizes the potency of tideglusib as a putative therapeutic compound.

Overall, our results increase the clinical relevance of the compound tideglusib and its potential to serve as a therapeutic agent for SPG11. Furthermore, they contribute to the establishment of iPSCs as a potent tool for disease modeling and drug testing. The fact that tideglusib has been approved by FDA and has been tested in clinical trials of Alzheimer's Disease, Autism Spectrum Disorder and Myotonic Dystrophy renders a potential availability also for SPG11 patients. Future studies that will utilize the advanced cerebral organoid models and delve into the mechanistic changes occurring after compound administration are essential for providing a robust basis for clinical implementation.

AUTHOR CONTRIBUTIONS

BW and JW participated in the conceptualization. ST conceived the methodology. DCL interpreted the findings and approved the final manuscript. TP, AS, and US-S performed the experiments and data analysis. BW, TP, and MR wrote and edited the manuscript and figures.

FUNDING

This study was supported by the Tom Wahlig Foundation (TP and MR) and the German Federal Ministry of Education and Research (BMBF, 01GQ113, 01GM1520A, 01EK1609B to BW). Additional funding came from the Interdisciplinary Center for Clinical Research (University Hospital Erlangen E25, MD fellowship to AS, J52 to MR) and DFG grant 410/45-1 FUGG (JW). TP, MR, ST, DCL, JW, and BW are members of the DFG funded research training group GRK2162.

ACKNOWLEDGMENTS

This work is dedicated to our patients and, in particular, to the memory of Anne Wahlig. The present work was performed in fulfillment of the requirements for obtaining the degree "Dr. med." (AS). We would like to thank Himanshu Mishra and Francesc Perez-Branguli for their valuable contributions and to Holger Wend for excellent technical support.

SUPPLEMENTARY MATERIAL

The Supplementary Material for this article can be found online at: https://www.frontiersin.org/articles/10.3389/fnins.2018.00914/full#supplementary-material

REFERENCES

Bauer, P., Winner, B., Schüle, R., Bauer, C., Häfele, V., Hehr, U., et al. (2009). Identification of a heterozygous genomic deletion in the spatacsin gene in SPG11 patients using high-resolution comparative genomic hybridization. *Neurogenetics* 10, 43–48. doi: 10.1007/s10048-008-0144-2

Branchu, J., Boutry, M., Sourd, L., Depp, M., Leone, C., Corriger, A., et al. (2017). Loss of spatacsin function alters lysosomal lipid clearance leading to upper and lower motor neuron degeneration. *Neurobiol. Dis.* 102, 21–37. doi: 10.1016/j.nbd.2017.02.007

Brownlees, J., Irving, N. G., Brion, J. P., Gibb, B. J., Wagner, U., Woodgett, J., et al. (1997). Tau phosphorylation in transgenic mice expressing glycogen synthase kinase-3β transgenes. *NeuroReport* 8, 3251–3255. doi: 10.1097/00001756-199710200-00013

Chang, J., Lee, S., and Blackstone, C. (2014). Spastic paraplegia proteins spastizin and spatacsin mediate autophagic lysosome reformation. *J. Clin. Invest.* 124, 5249–5262. doi: 10.1172/JCI77598

Culbert, A. A., Brown, M. J., Frame, S., Hagen, T., Cross, D. A., Bax, B., et al. (2001). GSK-3 inhibition by adenoviral FRAT1 overexpression is neuroprotective and induces Tau dephosphorylation and beta-catenin stabilisation without elevation of glycogen synthase activity. *FEBS Lett.* 507, 288–294. doi: 10.1016/S0014-5793(01)02990-8

de Barreda, E. G., Pérez, M., Gómez-Ramos, P., de Cristobal, J., Martín-Maestro, P., Morán, A., et al. (2010). Tau-knockout mice show reduced GSK3-induced hippocampal degeneration and learning deficits. *Neurobiol. Dis.* 37, 622–629. doi: 10.1016/j.nbd.2009.11.017

Farr, S. A., Sandoval, K. E., Niehoff, M. L., Witt, K. A., Kumar, V. B., and Morley, J. E. (2016). Peripheral administration of GSK-3β antisense oligonucleotide improves learning and memory in SAMP8 and Tg2576 mouse models of Alzheimer's disease. *J. Alzheimers Dis.* 54, 1339–1348. doi: 10.3233/JAD-160416

Guo, X., Snider, W. D., and Chen, B. (2016). GSK3β regulates AKT-induced central nervous system axon regeneration via an eIF2Bε-dependent, mTORC1-independent pathway. *eLife* 14:e11903. doi: 10.7554/eLife.11903

Havlicek, S., Kohl, Z., Mishra, H. K., Prots, I., Eberhardt, E., Denguir, N., et al. (2014). Gene dosage-dependent rescue of HSP neurite defects in SPG4 patients' neurons. *Hum. Mol. Genet.* 23, 2527–2541. doi: 10.1093/hmg/ddt644

Hehr, U., Bauer, P., Winner, B., Schule, R., Olmez, A., Koehler, W., et al. (2007). Long-term course and mutational spectrum of spatacsin-linked spastic paraplegia. *Ann. Neurol.* 62, 656–665. doi: 10.1002/ana.21310

Jacobs, K. M., Bhave, S. R., Ferraro, D. J., Jaboin, J. J., Hallahan, D. E., and Thotala, D. (2012). GSK-3β: a bifunctional role in cell death pathways. *Int. J. Cell. Biol.* 2012:930710. doi: 10.1155/2012/930710

Koh, S. H., Noh, M. Y., and Kim, S. H. (2008). Amyloid-beta-induced neurotoxicity is reduced by inhibition of glycogen synthase kinase-3. *Brain Res.* 1188, 254–262. doi: 10.1016/j.brainres.2007.10.064

Lo Giudice, T., Lombardi, F., Santorelli, F. M., Kawarai, T., and Orlacchio, A. (2014). Hereditary spastic paraplegia: clinical-genetic characteristics and evolving molecular mechanisms. *Exp. Neurol.* 261, 518–539. doi: 10.1016/j.expneurol.2014.06.011

Lucas, J. J., Hernández, F., Gómez-Ramos, P., Morán, M. A., Hen, R., and Avila, J. (2001). Decreased nuclear β-catenin, tau hyperphosphorylation and neurodegeneration in GSK-3β conditional transgenic mice. *EMBO J.* 20, 27–39. doi: 10.1093/emboj/20.1.27

Mishra, H. K., Prots, I., Havlicek, S., Kohl, Z., Perez-Branguli, F., Boerstler, T., et al. (2016). GSK3ß-dependent dysregulation of neurodevelopment in SPG11-patient iPSC model. *Ann. Neurol.* 79, 826–840. doi: 10.1002/ana.24633

Montecchiani, C., Pedace, L., Lo Giudice, T., Casella, A., Mearini, M., Gaudiello, F., et al. (2016). ALS5/SPG11/KIAA1840 mutations cause autosomal recessive axonal charcot-marie-tooth disease. *Brain* 139, 73–85. doi: 10.1093/brain/awv320

Novarino, G., Fenstermaker, A. G., Zaki, M. S., Hofree, M., Silhavy, J. L., Heiberg, A. D., et al. (2014). Exome sequencing links corticospinal motor neuron disease to common neurodegenerative disorders. *Science* 343, 506–511. doi: 10.1126/science.1247363

Ochalek, A., Mihalik, B., Avci, H. X., Chandrasekaran, A., Téglási, A., Bock, I., et al. (2017). Neurons derived from sporadic Alzheimer's disease iPSCs reveal elevated TAU hyperphosphorylation, increased amyloid levels, and GSK3B activation. *Alzheimers Res. Ther.* 29:90. doi: 10.1186/s13195-017-0317-z

Orlacchio, A., Babalini, C., Borreca, A., Patrono, C., Massa, R., Basaran, S., et al. (2016). SPATACSIN mutations cause autosomal recessive juvenile amyotrophic lateral sclerosis. *Brain* 33, 591–598. doi: 10.1093/brain/awp325

Paisan-Ruiz, C., Nath, P., Wood, N. W., Singleton, A., and Houlden, H. (2008). Clinical heterogeneity and genotype-phenotype correlations in hereditary spastic paraplegia because of Spatacsin mutations (SPG11). *Eur. J. Neurol.* 15, 1065–1070. doi: 10.1111/j.1468-1331.2008.02247.x

Pérez-Brangulí, F., Mishra, H. K., Prots, I., Havlicek, S., Kohl, Z., Saul, D., et al. (2014). Dysfunction of spatacsin leads to axonal pathology in SPG11-linked hereditary spastic paraplegia. *Hum. Mol. Genet.* 23, 4859–4874. doi: 10.1093/hmg/ddu200

Renvoise, B., Chang, J., Singh, R., Yonekawa, S., FitzGibbon, E. J., Mankodi, A., et al. (2014). Lysosomal abnormalities in hereditary spastic paraplegia types SPG15 and SPG11. *Ann. Clin. Trans. Neurol.* 1, 379–389. doi: 10.1002/acn3.64

Rockenstein, E., Torrance, M., Adame, A., Mante, M., Bar-On, P., Rose, J. B., et al. (2007). Neuroprotective effects of regulators of the glycogen synthase kinase-3beta signaling pathway in a transgenic model of Alzheimer's disease are associated with reduced amyloid precursor protein phosphorylation. *J. Neurosci.* 27, 1981–1991. doi: 10.1523/JNEUROSCI.4321-06.2007

Schindelin, J., Arganda-Carreras, I., Frise, E., Kaynig, V., Longair, M., Pietzsch, T., et al. (2012). Fiji: an open-source platform for biological-image analysis. *Nat. Methods* 9, 676–682. doi: 10.1038/nmeth.2019

Schlotzer-Schrehardt, U., Hammer, C. M., Krysta, A. W., Hofmann-Rummelt, C., Pasutto, F., Sasaki, T., et al. (2012). LOXL1 deficiency in the lamina cribrosa as candidate susceptibility factor for a pseudoexfoliation-specific risk of glaucoma. *Ophthalmology* 119, 1832–1843. doi: 10.1016/j.ophtha.2012.03.015

Schüle, R., Holland-Letz, T., Klimpe, S., Kassubek, J., Klopstock, T., Mall, V., et al. (2006). The Spastic Paraplegia Rating Scale (SPRS): a reliable and valid measure of disease severity. *Neurology* 67, 430–434. doi: 10.1212/01.wnl.0000228242.53336.90

Song, B., Lai, B., Zheng, Z., Zhang, Y., Luo, J., Wang, C., et al. (2010). Inhibitory phosphorylation of GSK-3 by CaMKII couples depolarization to neuronal survival. *J. Biol. Chem.* 285, 41122–41134. doi: 10.1074/jbc.M110.130351

Stevanin, G., Durr, A., and Brice, A. (2013). "Spastic paraplegia11," in *GeneReviews*, eds R. A. Pagon, M. P. Adam, T. D. Bird, C. R. Dolan, C. T. Fong, S. RJH, et al. (Seattle, WA: University of Washington, Seattle).

Turan, S., Farruggio, A. P., Srifa, W., Day, J. W., and Calos, M. P. (2016). Precise correction of disease mutations in induced pluripotent stem cells derived from patients with limb girdle muscular dystrophy. *Mol. Ther.* 24, 685–696. doi: 10.1038/mt.2016.40

Varga, R. E., Khundadze, M., Damme, M., Nietzsche, S., Hoffmann, B., Stauber, T., et al. (2015). In vivo evidence for lysosome depletion and impaired autophagic clearance in hereditary spastic paraplegia type SPG11. *PLoS Genet.* 11:e1005454. doi: 10.1371/journal.pgen.1005454

Zhang, Z., Zhao, R., Qi, J., Wen, S., Tang, Y., and Wang, D. (2011). Inhibition of glycogen synthase kinase-3β by Angelica sinensis extract decreases β-amyloid-induced neurotoxicity and tau phosphorylation in cultured cortical neurons. *J. Neurosci. Res.* 89, 437–447. doi: 10.1002/jnr.22563

Conflict of Interest Statement: The authors declare that the research was conducted in the absence of any commercial or financial relationships that could be construed as a potential conflict of interest.

frontiers in Neuroscience

ORIGINAL RESEARCH
published: 20 December 2018
doi: 10.3389/fnins.2018.00970

Retinal Neuroprotection From Optic Nerve Trauma by Deletion of Arginase 2

*Zhimin Xu[1,2,3†], Abdelrahman Y. Fouda[1,2,3†], Tahira Lemtalsi[1,2,3], Esraa Shosha[1,2,3], Modesto Rojas[1,2,3,4], Fang Liu[1,2,3,5], Chintan Patel[2], R. William Caldwell[3,4], Subhadra Priya Narayanan[1,2,3,5] and Ruth B. Caldwell[1,2,3,6,7]**

[1] Charlie Norwood VA Medical Center, Augusta, GA, United States, [2] Vascular Biology Center, Augusta University, Augusta, GA, United States, [3] James and Jean Culver Vision Discovery Institute, Augusta University, Augusta, GA, United States, [4] Department of Pharmacology and Toxicology, Augusta University, Augusta, GA, United States, [5] Program in Clinical and Experimental Therapeutics, University of Georgia, College of Pharmacy, Augusta, GA, United States, [6] Department of Cell Biology and Anatomy, Augusta University, Augusta, GA, United States, [7] Department of Ophthalmology, Augusta University, Augusta, GA, United States

OPEN ACCESS

Edited by:
Wenbo Zhang,
The University of Texas Medical Branch at Galveston, United States

Reviewed by:
Knut Stieger,
University of Giessen, Germany
Yang Hu,
Stanford University, United States

***Correspondence:**
Ruth B. Caldwell
rcaldwel@augusta.edu

† These authors have contributed equally to this work

Specialty section:
This article was submitted to Neurodegeneration, a section of the journal Frontiers in Neuroscience

Received: *06 August 2018*
Accepted: *04 December 2018*
Published: *20 December 2018*

Citation:
Xu Z, Fouda AY, Lemtalsi T, Shosha E, Rojas M, Liu F, Patel C, Caldwell RW, Narayanan SP and Caldwell RB (2018) Retinal Neuroprotection From Optic Nerve Trauma by Deletion of Arginase 2. Front. Neurosci. 12:970. doi: 10.3389/fnins.2018.00970

Our previous studies have implicated expression of the mitochondrial isoform of the arginase enzyme arginase 2 (A2) in neurovascular injury during ischemic retinopathies. The aim of this study was to characterize the specific involvement of A2 in retinal injury following optic nerve crush (ONC). To accomplish this, wild-type (WT) or A2 knockout ($A2^{-/-}$) mice were subjected to ONC injury. The contralateral eye served as sham control. Quantitative RT-PCR and western blot were used to evaluate mRNA and protein expression. Retinal ganglion cell (RGC) survival was assessed in retinal whole mounts. Axonal sprouting was determined by anterograde transport of Cholera Toxin B (CTB). These analyses showed increased A2 expression following ONC. Numbers of NeuN-positive neurons as well as Brn3a- and RBPMS-positive RGC were decreased in the WT retinas at 14 days after ONC as compared to the sham controls. This ONC-induced neuronal loss was diminished in the $A2^{-/-}$ retinas. Similarly, axonal degeneration was ameliorated by A2 deletion whereas axon sprouting was enhanced. Significant retinal thinning was also seen in WT retinas at 21 days after ONC, and this was blocked in $A2^{-/-}$ mice. Cell death studies showed an increase in TUNEL positive cells in the RGC layer at 5 days after ONC in the WT retinas, and this was attenuated by A2 deletion. ONC increased glial cell activation in WT retinas, and this was significantly reduced by A2 deletion. Western blotting showed a marked increase in the neurotrophin, brain derived neurotrophic factor (BDNF) and its downstream signaling in $A2^{-/-}$ retinas vs. WT after ONC. This was associated with increases in the axonal regeneration marker GAP-43 in $A2^{-/-}$ retinas. Furthermore, $A2^{-/-}$ retinas showed decreased NLRP3 inflammasome activation and lower interleukin (IL-) 1β/IL-18 levels as compared to WT retinas subjected to ONC. Collectively, our results show that deletion of A2 limits ONC-induced neurodegeneration and glial activation, and enhances axonal sprouting by a

mechanism involving increases in BDNF and decreases in retinal inflammation. These data demonstrate that A2 plays an important role in ONC-induced retinal damage. Blockade of A2 activity may offer a therapeutic strategy for preventing vision loss induced by traumatic retinal injury.

Keywords: arginase 2, retina, neuroprotection, optic nerve crush, brain derived neurotrophic factor, retinal ganglion cells

INTRODUCTION

Impaired vision secondary to optic nerve damage is a common and often unrecognized complication of numerous ophthalmologic and neurologic conditions. Traumatic ocular injury is frequently associated with degeneration of retinal ganglion cells (RGC) due to primary trauma to their axons that travel through the optic nerve to the brain. This may also involve degeneration of other retinal neurons secondary to oxidative stress, vascular dysfunction, ischemia and edema, which can eventually cause permanent vision loss (Weber et al., 2008). So far, there is no effective treatment for optic nerve trauma, because of the lack of understanding of the detailed molecular mechanisms by which the retinal neurons are damaged. The mouse model of optic nerve crush (ONC) injury has been widely used to study axonal degeneration and the subsequent RGC and neuronal losses characteristic of traumatic optic neuropathy (TON) and glaucoma induced optic nerve degeneration (Tang et al., 2011). Several pathways have been studied as molecular targets to limit neurodegeneration and enhance repair after ONC. One of the most extensively studied molecules in this context is the neurotrophin brain derived neurotrophic factor (BDNF). BDNF has been shown to protect RGC and their axons against injury via its downstream survival signaling pathways (Mysona et al., 2017) Therefore, there is a great interest in developing therapies that enhance BDNF either directly by increasing its mRNA/protein levels (e.g., via gene therapy) or indirectly by activating pathways that lead to BDNF upregulation (Ratican et al., 2018).

Our group has been investigating the role of the arginase pathway in neurovascular injury during retinopathy. Arginase is a ureohydrolase enzyme that converts L-arginine to urea and ornithine. There are two isoforms of the arginase enzyme, arginase 1 (A1) and arginase 2 (A2). Both isoforms are known to be involved in the pathophysiology of different central nervous system disorders including retinal disease (Caldwell et al., 2018). We have shown that the mitochondrial isoform, A2, is critically involved in the neurovascular injury associated with retinal ischemia-reperfusion injury (Shosha et al., 2016). In this model, A2 deletion protected against RGC and microvascular degeneration via decreased glial activation, oxidative stress and cell death by necroptosis (Shosha et al., 2016). On the other hand, we have recently shown that A1 is neurovascular protective in the same model via ameliorating macrophage inflammatory response (Fouda et al., 2018). In the current study, we examined the role of A2 in TON-induced retinal neuronal injury using $A2^{-/-}$ mice subjected to ONC. We also examined the possible cross talk between A2 and BDNF which has been extensively studied in the ONC model. We also assessed potential involvement of BDNF down-stream targets including extracellular regulated and mitogen- and stress-activated protein kinases (ERK/MSK) and growth associated protein (GAP)-43 (Gupta et al., 2009), which is induced after ONC injury (Doster et al., 1991) and is thought to be involved in axonal regeneration (Holahan, 2017).

Abbreviations: A2, arginase 2; $A2^{-/-}$ or A2 KO, A2 knockout; GCL, ganglion cell layer; H&E, hematoxylin and eosin; INL, inner nuclear layer; IPL, inner plexiform layer; OCT, optimal cutting temperature; ONC, optic nerve crush; ONL, outer nuclear layer; OPL, outer plexiform layer; PFA, paraformaldehyde; RGC, retinal ganglion cells; TON, traumatic optic neuropathy; WT, wild type.

MATERIALS AND METHODS

Animals and Optic Nerve Crush Induction

Male Wild-type C57BL/6J (WT) and Arginase-2 knockout ($A2^{-/-}$) mice on C57BL/6J background were maintained in our animal facility and used to study ONC injury. All animal procedures performed in this study complied with the ARVO statement for the use of Animals in Ophthalmic and Vision Research. All surgeries were performed under anesthesia and analgesia was provided to minimize suffering. For induction of ONC, mice (10–12 weeks old) were anesthetized by injection of Ketamine and Xylazine cocktail intraperitoneal and one drop of topical anesthesia (0.5% proparacaine hydrochloride) was applied to the eyeball and the surrounding intraocular muscles before the surgery. Briefly, the conjunctiva on the left eye was incised, the orbital muscles were deflected and the optic nerve 1–2 mm from the eyeball was clamped for 3 s using self-closing N7 forceps (Fine Science Tools, Foster City, CA, United States). The right eye was used as sham control. Mice were injected subcutaneously with buprenorphine for analgesia, returned to their home cage, and monitored until recovery (Tang et al., 2011). Eyes and retinas were harvested for analysis at various times from 3 h to 28 days after ONC. The design for these analyses is shown in **Figure 1A**.

Neurodegeneration and Ganglion Cell Survival Evaluation

NeuN (neuronal nuclei) was used as a neuronal cell marker to label surviving neurons in retinal flat mounts. Brn3a (brain-specific homeobox/POU domain protein 3A) and RBPMS (RNA binding protein, mRNA processing factor) were used as RGC markers (Nadal-Nicolas et al., 2009; Rodriguez et al., 2014). Eyeballs were collected 7, 10, or 14 days after ONC and fixed in 4% paraformaldehyde (PFA) at 4°C overnight. Isolated retinas from these eyeballs were incubated with anti-NeuN,

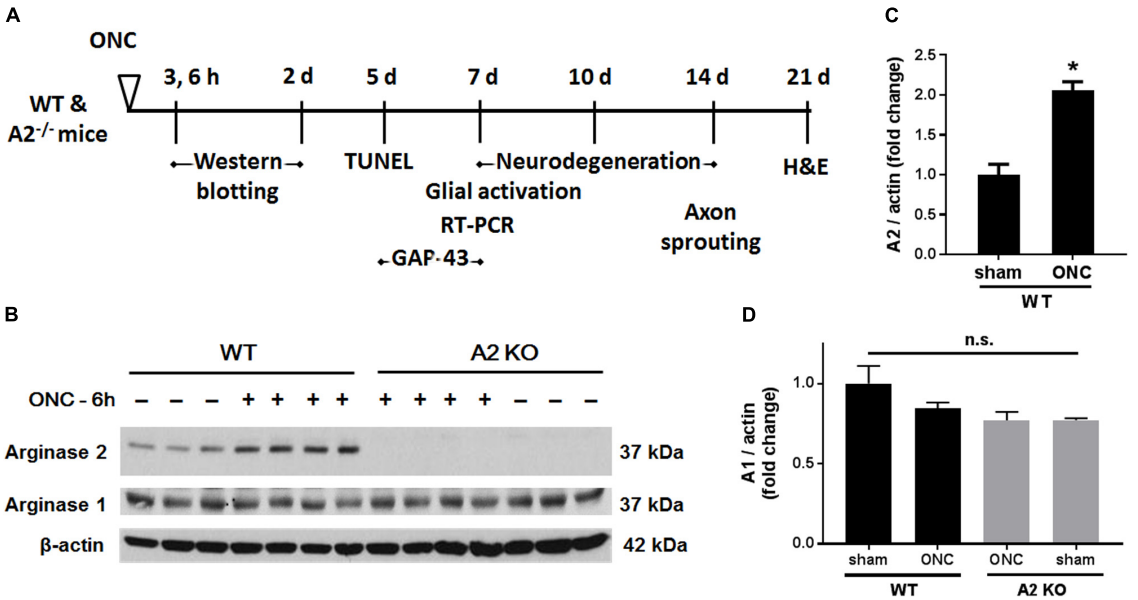

FIGURE 1 | A2 is increased in retinas subjected to ONC injury. Schematic diagram **(A)** of the different time points examined after subjecting WT and A2$^{-/-}$ mice to ONC. Western blotting **(B)** of retinal lysates for A1 and A2 protein expression and quantification **(C,D)** showed increases in A2 in response to ONC at 6 h after injury. A2$^{-/-}$ retinas lacked the A2 protein band. A1 expression was similar in all groups. N = 3–4, *p < 0.01 vs. WT sham, n.s. means no statistically significant difference.

anti-Brn3a, or anti-RBPMS (**Table 1**) in 37°C for 2 h and then incubated overnight with fluorescein-conjugated secondary antibodies (Invitrogen, Carlsbad, CA; 1:400). Retinal flat mounts were imaged using a confocal microscope (LSM 780; Carl Zeiss, Thornwood, NY, United States). Four images were taken in the mid-periphery of the ganglion cell layer (GCL) of each retina and the NeuN, Brn3a, or RBPMS positive cells were counted using ImageJ. Data are presented as percent of NeuN, Brn3a, or RBPMS positive cell numbers in the GCL of WT sham retinas.

Nerve Fiber Degeneration and Sprouting

TUJ1 (Neuron-specific class III beta-tubulin) was used as a nerve fiber marker and GAP-43 (growth associated protein 43) was used as an axonal regeneration marker in retinal flat mounts. Eyeballs were collected 7 days (for TUJ1 and GAP-43) or 14 days (for TUJ1) after ONC and fixed in 4% PFA at 4°C overnight. Isolated retinas from these eyeballs were labeled with anti-TUJ1 or anti-GAP-43 (**Table 1**) at 37°C for 2 h and then incubated overnight with Alexa Fluor 488 conjugated goat

TABLE 1 | Antibodies.

Antibody	Catalog number	Company	Dilution	Experiment
NeuN	MAB377	Millipore, Billerica, MA	1:200	Immunostaining
Brn3a	SC-31984	Santa Cruz, Dallas, TX	1:200	Immunostaining
RBPMS	ABN1362	Millipore, Billerica, MA	1:200	Immunostaining
TUJ1	801202	BioLegend, San Diego, CA	1:200	Immunostaining
GAP-43	GTX30199	GeneTex, Irvine, CA	1:200	Immunostaining
GFAP	Z0334	Dako, Carpinteria, CA	1:200	Immunostaining
Iba1	019-19741	Wako, Richmond, VA	1:200	Immunostaining
ICAM-1	SC-1511	Santa Cruz, Dallas, TX	1:500	Western blotting
Arginase 1	SC-20150	Santa Cruz, Dallas, TX	1:500	Western blotting
Arginase 2	SC-20151	Santa Cruz, Dallas, TX	1:500	Western blotting
BDNF	SC-546	Santa Cruz, Dallas, TX	1:1000	Western blotting
p-ERK1/2	4370	Cell Signaling, Danvers, MA	1:500	Western blotting
total ERK1/2	4695	Cell Signaling, Danvers, MA	1:500	Western blotting
p-MSK1	9595	Cell Signaling, Danvers, MA	1:500	Western blotting
total MSK1	3489	Cell Signaling, Danvers, MA	1:500	Western blotting
NLRP3	15101	Cell Signaling, Danvers, MA	1:500	Western blotting
IL-1β	AF-401-NA	R&D Systems, Minneapolis, MN	1:1000	Western blotting
β-actin	4511	Sigma-Aldrich, St. Louis, MO	1:5000	Western blotting

anti–mouse IgG2a or Alexa Fluor 594 conjugated goat anti–rabbit antibodies (Invitrogen, Carlsbad, CA, United States; 1:400) at 4°C for overnight. Retinal flat mounts were imaged using fluorescence microscopy (Axioplan2; Carl Zeiss, Thornwood, NY, United States) or confocal microscope (LSM 780; Carl Zeiss, Thornwood, NY, United States). For quantifying total numbers of surviving nerve fibers, retinal whole-mount images were taken and the TUJ1 positive fibers were counted at a distance 1/3 of the retina radius starting from optic nerve head using ImageJ. The results are presented as a percent of TUJ1 positive nerve fibers in the GCL of the ONC eyes compared to the sham eyes.

For analysis of axonal sprouting, mice were subjected to 1 s-ONC and sprouting axons were identified by anterograde labeling with Alexa Fluor® 647-conjugated Cholera Toxin B (CTB; ThermoFisher, cat. # C34778, Waltham, MA, United States) as described previously (Wang et al., 2018). Duration of 1 s crush was selected for this experiment vs. 3 s for others based on preliminary studies that showed more sprouting after 1 s crush. Briefly, the mice were anesthetized at 12 days after ONC and injected intravitreally with CTB (0.2%, 2 μg/eye). After 2 days, the mice were anesthetized and perfused transcardially with phosphate buffered saline (PBS) followed by 4% PFA in phosphate buffer (pH 7.3). Optic nerves were dissected, post-fixed in 4% PFA in PBS overnight, and cleared with FocusClear™ (CelExplorer, cat. # FC-101, Hsinchu, Taiwan) until transparent. Chambers were constructed on glass slides to allow space for the entire nerve thickness and prevent flattening of the nerve. The nerves were mounted using MountClear™ (CelExplorer, cat. # MC-301, Hsinchu, Taiwan), the slides were coverslipped, and sprouting axons were imaged using confocal microscopy (LSM 780; Carl Zeiss, Thornwood, NY, United States). Optical slices scanned by confocal microscope were used for counting the numbers of axons at 100 μm intervals beginning at 200 μm and extending to 1 mm away from the crush site of the optic nerves. Images were presented with pseudocolor green for better observation.

Retinal Thickness Measurement

Retinal thickness was measured on retinal sections collected 21 days after ONC injury as previously described (Shosha et al., 2016). Cross sections (10 μm thick) stained using hematoxylin and eosin (H&E) were analyzed to assess alterations in retinal morphology. Retinal images were taken at 162 μm away from the optic nerve head and two sections 20 μm apart were used for each sample. Thicknesses of whole retina at three different points per image were measured using ImageJ. Average values of thickness are presented as percentage of the values for the sham control eyes.

Detection of Glial Activation

Seven days after ONC injury, eyeballs were collected and snap frozen in optimal cutting temperature (OCT) compound or fixed in 4% PFA for later use. The snap-frozen eyeballs were processed to prepare cryostat sections (10 μm) and labeled with anti-glial fibrillary acidic protein (GFAP) antibody to detect glial activation. The PFA fixed eyeballs were prepared for either retinal flat mounts or frozen sections as described previously (Shosha et al., 2016). Retinal flat mounts or sections were incubated with anti-ionized calcium-binding adapter molecule 1 (Iba1) antibody to label microglia/macrophages. Sections or flat mounts were then incubated with fluorescein-conjugated secondary antibodies (Invitrogen, Carlsbad, CA; 1:400) as previously described (Shosha et al., 2016). After washing with PBS, sections or flat mounts were preserved with mounting medium (Vector Laboratories Cat. # H-1000, Burlingame, CA, United States) and images were taken using a fluorescent or confocal microscope. For quantification, fluorescence intensities of GFAP or Iba1 flat mount staining images were analyzed using ImageJ software.

TUNEL Assay

Apoptotic cells were studied in retinal samples collected 5 days after ONC using TUNEL (Terminal deoxynucleotidyl transferase dUTP nick end labeling) assay on cryosections from snap-frozen eyeballs. Fluorescein *In Situ* Cell Death Detection kit (Millipore cat. #S7110, Billerica, MA, United States) was used according to the manufacturer's protocol. Two sections per animal were used to collect the images and the quantification of TUNEL positive cells was performed manually on the whole retinal section.

Quantitative RT-PCR

Total RNA was extracted from retinal samples and reverse-transcribed as previously described (Shosha et al., 2016). ABI StepOne Plus Thermocycler (Applied Biosystems, Foster City, CA, United States) was used to perform quantitative PCR with master mix (Power SYBR Green, Invitrogen). Primer sequences for mouse transcripts are shown in **Table 2**. Data were normalized to hypoxanthine phosphoribosyltransferase (HPRT) and the fold change between levels of different transcripts was calculated by the $\Delta\Delta C_T$ method.

Western Blotting

Retinal proteins were extracted using RIPA buffer (Millipore) containing protease and phosphatase inhibitors (Complete Mini and phosSTOP Roche Applied Science, Indianapolis, IN, United States). Protein lysates were then separated on SDS-PAGE and transferred to nitrocellulose membranes (Millipore), blocked in 5% milk (Bio-Rad, Hercules, CA, United States) or 2% BSA (Gemini Bio-products) in Tris-buffered saline with 0.05% Tween-20 (TBS-T). The membranes were incubated overnight (4°C) with primary antibodies against: arginase 1 and 2, p-MSK1, total

TABLE 2 | RT-PCR primers.

Gene name	Forward primer	Reverse primer
ICAM1	CAGTCCGCTGTGCTTTGAGA	CGGAAACGAATACACGGTGAT
IL1β	TGCCACCTTTTGACAGTGATG	ATGTGCTGCTGCGAGATTTG
IL18	TCAAAGTGCCAGTGAACCCC	GGTCACAGCCAGTCCTCTTAC
HPRT	GAAAGACTTGCTCGAGATGTCATG	CACACAGAGGGCCACAATGT

MSK1, p-ERK1/2, total ERK1/2, BDNF, ICAM-1, NLRP3, IL-1β, and β-actin as listed in **Table 1**. The following day, horseradish peroxidase-conjugated secondary antibodies (GE Healthcare Bio-Science Corp., Piscataway, NJ, United States; 1:2000) were applied to the membranes and the protein expression levels were detected using the enhanced chemiluminescence system (GE Healthcare Bio-Science Corp., Piscataway, NJ, United States). Data were quantified by densitometry using ImageJ and normalized to β-actin as loading control.

Statistical Analysis

GraphPad Prism 7 (GraphPad Softwar Inc., La Jolla, CA, United States) was used for statistical analysis. Two-way ANOVA followed by Tukey test was used for multiple comparisons. The student's *t*-test (Two-tailed) was used for single comparisons. A value of $p < 0.05$ was considered statistically significant. Results are presented as mean ± SEM.

RESULTS

A2 Deletion Improves Neuronal Survival in the Retinal Ganglion Cell Layer After ONC

To examine the change in A2 expression in response to ONC injury, we subjected WT and A2$^{-/-}$ mice to ONC and

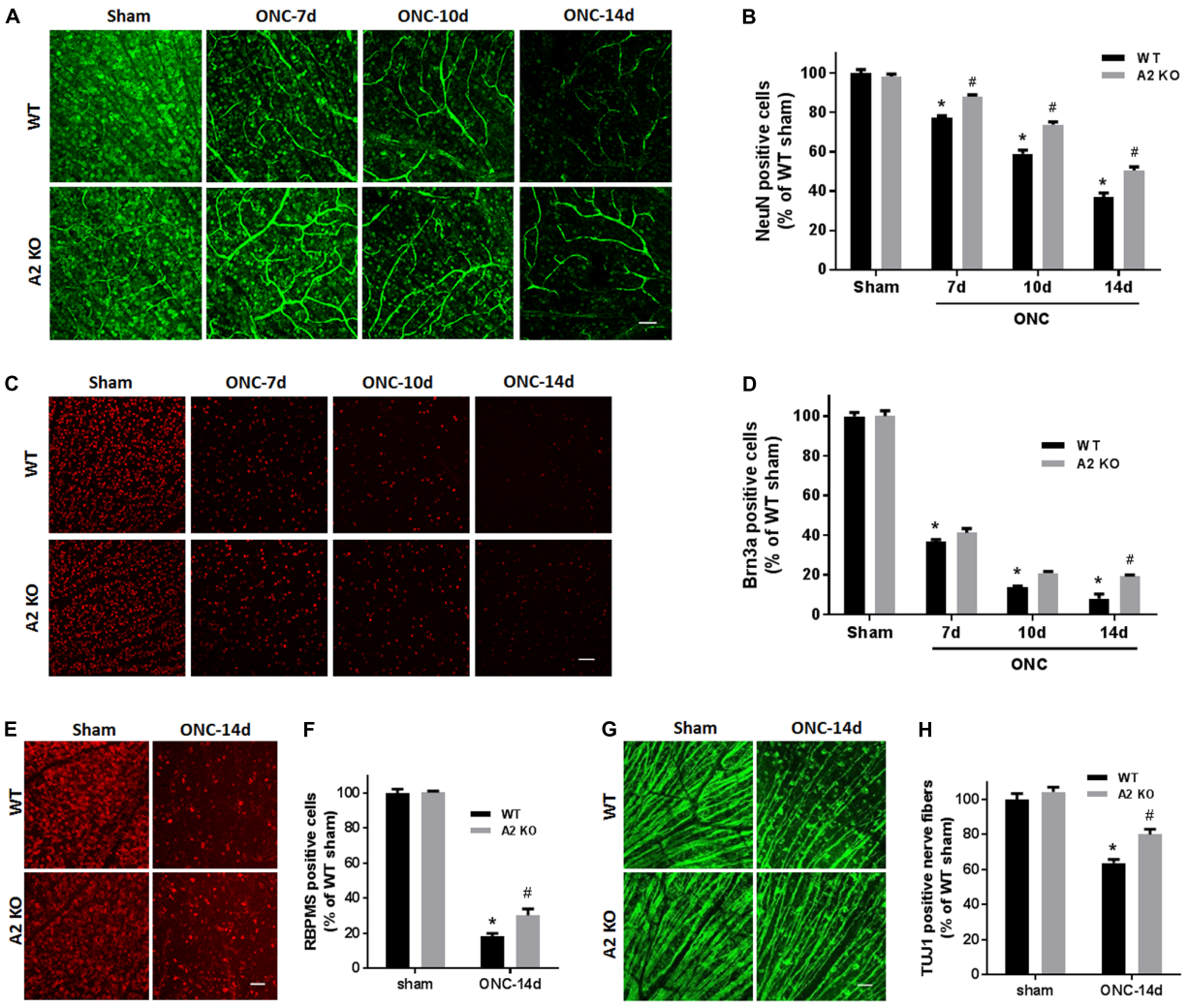

FIGURE 2 | A2 deletion ameliorates ONC-induced neuronal cell loss. Representative NeuN labeling **(A)** and quantification **(B)** of retinal neurons in the GCL of retinal flat mounts show a progressive decline in NeuN^{+} cells over 14 days after ONC. A2 deletion ameliorates the ONC-induced neuronal cell loss. Immunolabeling **(C)** and quantification **(D)** for the RGC marker, Brna3a, showed a similar trend with reduced neurodegeneration in the A2$^{-/-}$ retinas. N = 4–6 per group, $^{*}p < 0.01$ vs. WT sham, $^{\#}p < 0.01$ vs. A2$^{-/-}$ sham and respective WT ONC time point. Flat mount labeling for another RGC marker, RBPMS, at 14 days **(E)** and quantification **(F)** showed similar results with significant neuroprotection in A2$^{-/-}$ retinas. Flat-mount labeling of the retinal neurons nerve fibers using TUJ1 **(G)** and quantification **(H)** showed nerve fiber loss at 14 days after ONC. A2 deletion was associated with relative preservation of nerve fibers as compared to WT after ONC. N = 5–6, $^{*}p < 0.01$ vs. WT sham, $^{\#}p < 0.01$ vs. A2$^{-/-}$ sham and WT ONC, scale bar = 50 μm.

collected the retinas after 6 h. Western blotting on retina lysates showed upregulation of A2 expression as compared to shams, thus suggesting the involvement of A2 in ONC pathology (**Figures 1B,C**). At the same time point, A1 expression was not changed by the injury or A2 deletion (**Figure 1D**). ONC injury has been shown to induce progressive neuronal cell loss starting at day 7 (Liu et al., 2014). To assess the potential involvement of A2 in this neuronal cell loss, we collected retinas from WT and $A2^{-/-}$ mice at 7, 10, and 14 days after injury. Confocal imaging of the ganglion cell layer (GCL) in retina flat mounts labeled for the general neuronal marker NeuN, showed a progressive decrease in NeuN-positive neurons over time in both WT and $A2^{-/-}$ retinas. However, $A2^{-/-}$ retinas exhibited better preservation of neuronal cell density compared to WT retinas at the three time points examined (**Figures 2A,B**). Furthermore, we labeled the retina flat mounts for Brn3a, a marker for RGC. Similar to NeuN, Brn3a staining showed a progressive decline in Brn3a-positive cells over time. $A2^{-/-}$ retinas showed significantly higher numbers of Brn3a-positive cells at 14 days compared to WT retinas (**Figures 2C,D**) and this was further confirmed using another RGC marker, RBPMS (**Figures 2E,F**). Since RGC loss after ONC happens due to damage and degeneration of the nerve fibers, we also quantified the nerve fibers in the nerve fiber layer (NFL) in flat mounts labeled with the RGC cell body and axon marker TUJ1 as previously described (Mesentier-Louro et al., 2017). WT ONC retina flat mounts showed reduced RGC nerve fibers at 14 days. A2 deletion significantly protected against the ONC-induced loss of the RGC fibers as compared with the WT retinas (**Figures 2G,H**).

A2 Deletion Increases BDNF and GAP-43 Expression After ONC

Brain derived neurotrophic factor (BDNF) is a neurotrophin that has been shown to enhance the survival of RGC and their axons (Mysona et al., 2017). In order to examine BNDF involvement in the neuroprotective effect observed with A2 deletion, we measured BDNF levels using western blotting. $A2^{-/-}$ retinas showed increased expression of BDNF (homodimer: 28 kDa) at 3 h after ONC as compared to WT retinas. This was associated with activation of BDNF downstream signaling in

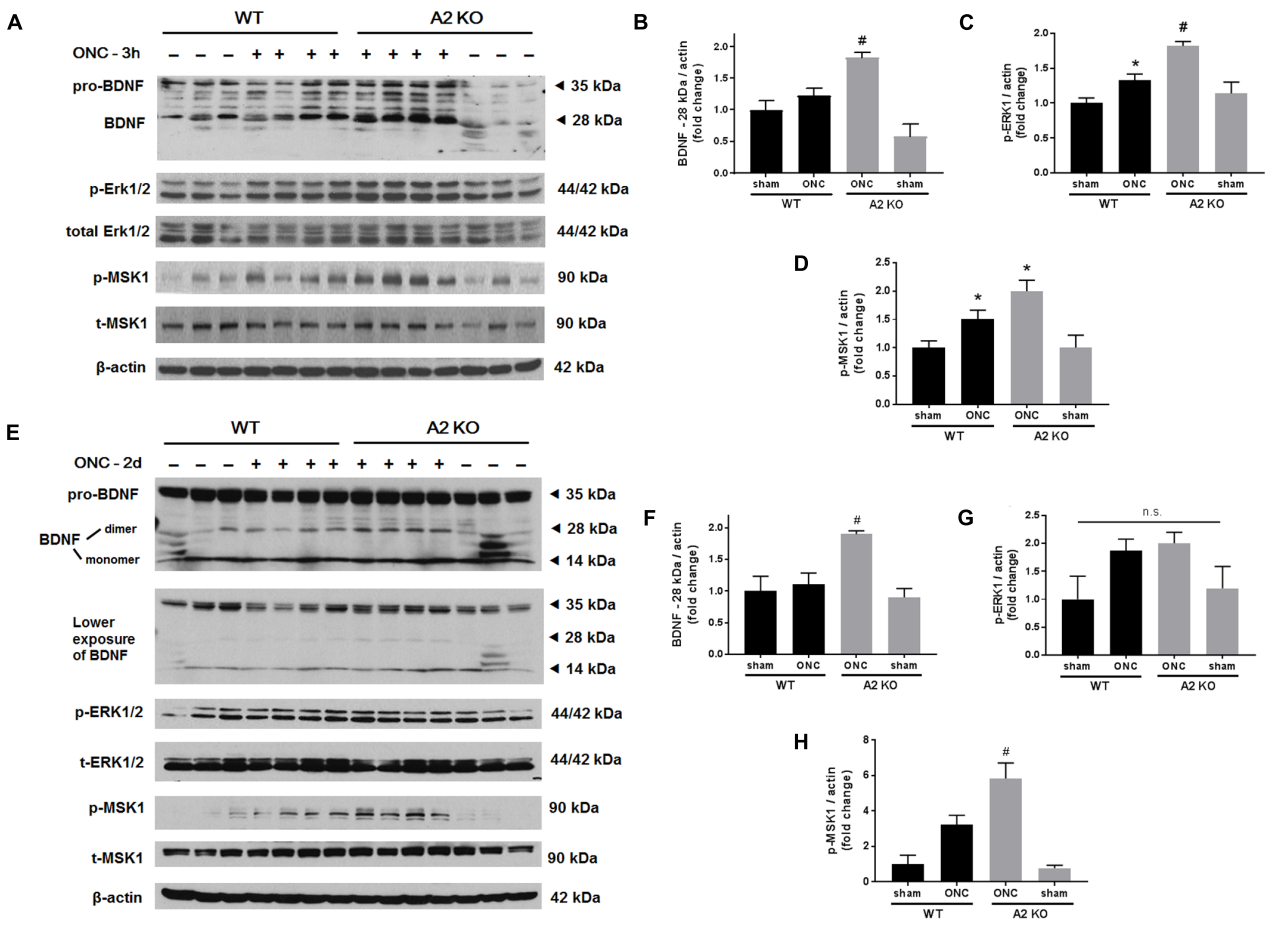

FIGURE 3 | A2 deletion increases mature BDNF and its downstream signaling targets after ONC. Western blotting on retinal lysates and quantification at 3 h **(A–D)** and 2 days **(E–H)** after injury showed increased expression of mature BDNF (28 kD) and activation of its downstream signaling pathway (ERK/MSK) in the $A2^{-/-}$ ONC retinas as compared to WT. $N = 3–4$, $^{*}p < 0.05$ vs. WT sham, $^{\#}p < 0.05$ vs. the other three groups, n.s. means no statistically significant difference.

the A2$^{-/-}$ retinas as shown by increased phosphorylation of extracellular signal–regulated kinase 1 (ERK1) and mitogen- and stress-activated protein kinase-1 (MSK1) (**Figures 3A–D**). Levels of BDNF and p-MSK1 but not p-ERK1 remained significantly elevated in the A2$^{-/-}$ retinas at 2 days after ONC (**Figures 3E–H**). We also examined the expression of the axonal regeneration marker, growth associated protein (GAP)-43, using immunolabeling and western blotting. In line with increased BDNF expression, A2$^{-/-}$ retina flat mounts showed increased GAP-43 labeling in nerve fibers as compared to WT at 7 days after ONC (**Figure 4A**). Western blotting on retina lysates confirmed an increase in GAP-43 in A2$^{-/-}$ vs. WT retinas at 5 days after ONC with a similar trend at 7 days but the latter increase did not reach statistical significance. (**Figures 4B,C**).

A2 Deletion Increases Axon Sprouting After ONC

At 14 days following ONC, RGC axons were labeled by anterograde transport of Cholera Toxin B (CTB) to examine the axonal sprouting and regrowth beyond the crush site and toward the brain. A2$^{-/-}$ mice showed a statistically significant regenerative response manifested by increases in number of CTB-positive axons at 200 and 300 μm distance from the ONC site as compared with the WT controls (**Figure 5**).

A2 Deletion Reduces Glial Activation and Retinal Inflammation After ONC

Müller cells and microglia/macrophages are activated following ONC (Mac Nair et al., 2016). To assess glial activation following ONC we labeled WT and A2$^{-/-}$ retinas for Iba1 (microglia/macrophage marker) and GFAP (marker for Müller cell activation). WT retinas showed significant increases in immunoreactivity for both Iba1 and GFAP, suggesting an increase in activation of retinal microglia/macrophages and macroglial cells (**Figure 6**). In the Iba1 labeled retinal flat mounts from the ONC retinas the microglia had an ameboid morphology with rounded cell bodies and enlarged processes suggesting an activated phenotype (**Figure 6B**) and GFAP immunoreactivity extended from the GCL through the ONL in some areas, indicating activation of the Müller cells (**Figure 6D**). A2 deletion abated this increased activation as demonstrated by the smaller cell bodies and more ramified processes of the Iba1 labeled micrgoglia and decreases in fluorescence intensity for both Iba1 (**Figure 6C**) and GFAP (**Figure 6E**).

We next examined the effects of A2 deletion on markers of retinal inflammation after ONC injury. RT-PCR analysis showed significant increases in mRNA levels for interleukin (IL-) 1β, IL-18, and the intracellular adhesion molecule (ICAM-1) at 7 days after ONC injury. Each of these changes was significantly inhibited in the A2$^{-/-}$ retinas (**Figures 7A–C**). We used western blotting to confirm these suggested protective effects

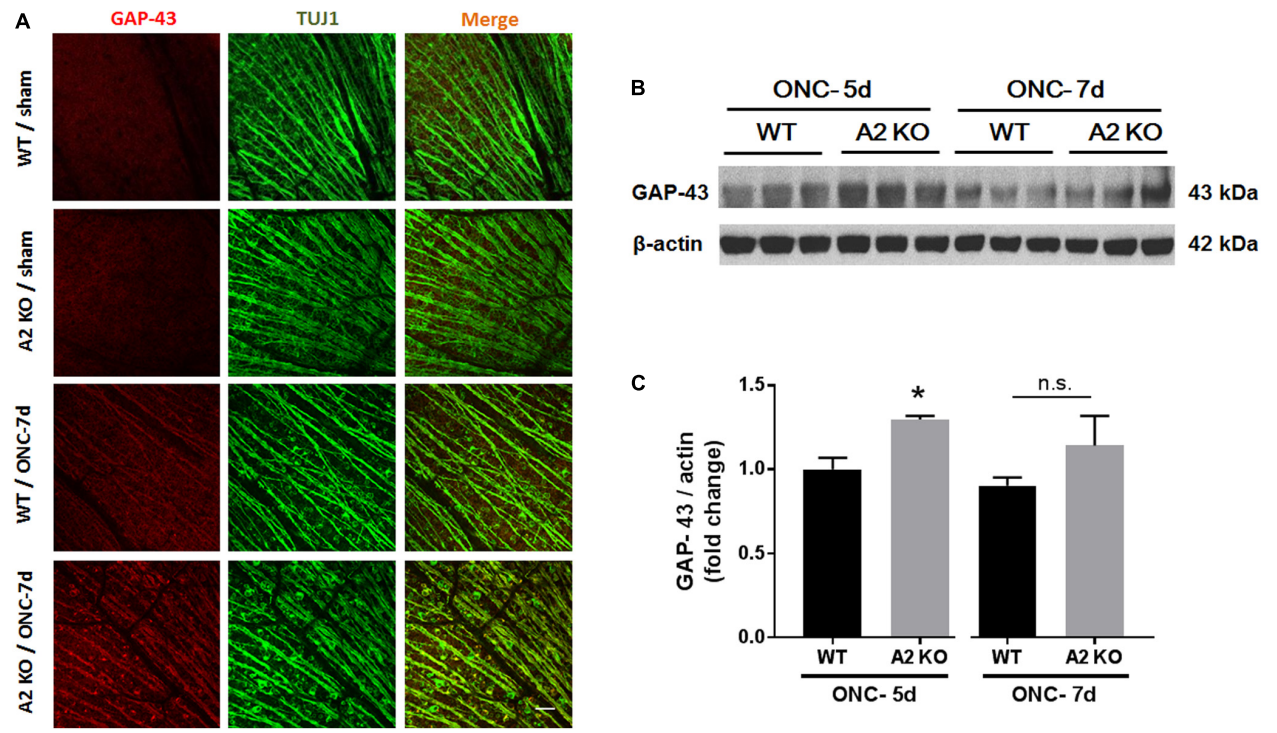

FIGURE 4 | A2 deletion increases GAP-43 expression in nerve fibers after ONC. Flat mount immunolabeling **(A)** showed higher GAP-43 expression in nerve fibers of WT ONC vs. sham retinas at 7 days and A2 deletion further increased GAP-43 immunoreactivity. *N* = 4–5, scale bar = 50 μm. Western blotting on retina lysates **(B)** and quantification **(C)** showed increased GAP-43 expression in A2$^{-/-}$ retinas as compared to WT that was significant at 5 days but did not reach statistical significance at 7 days after ONC. *N* = 3, $^{*}p < 0.05$ vs. WT ONC, n.s. means no statistically significant difference.

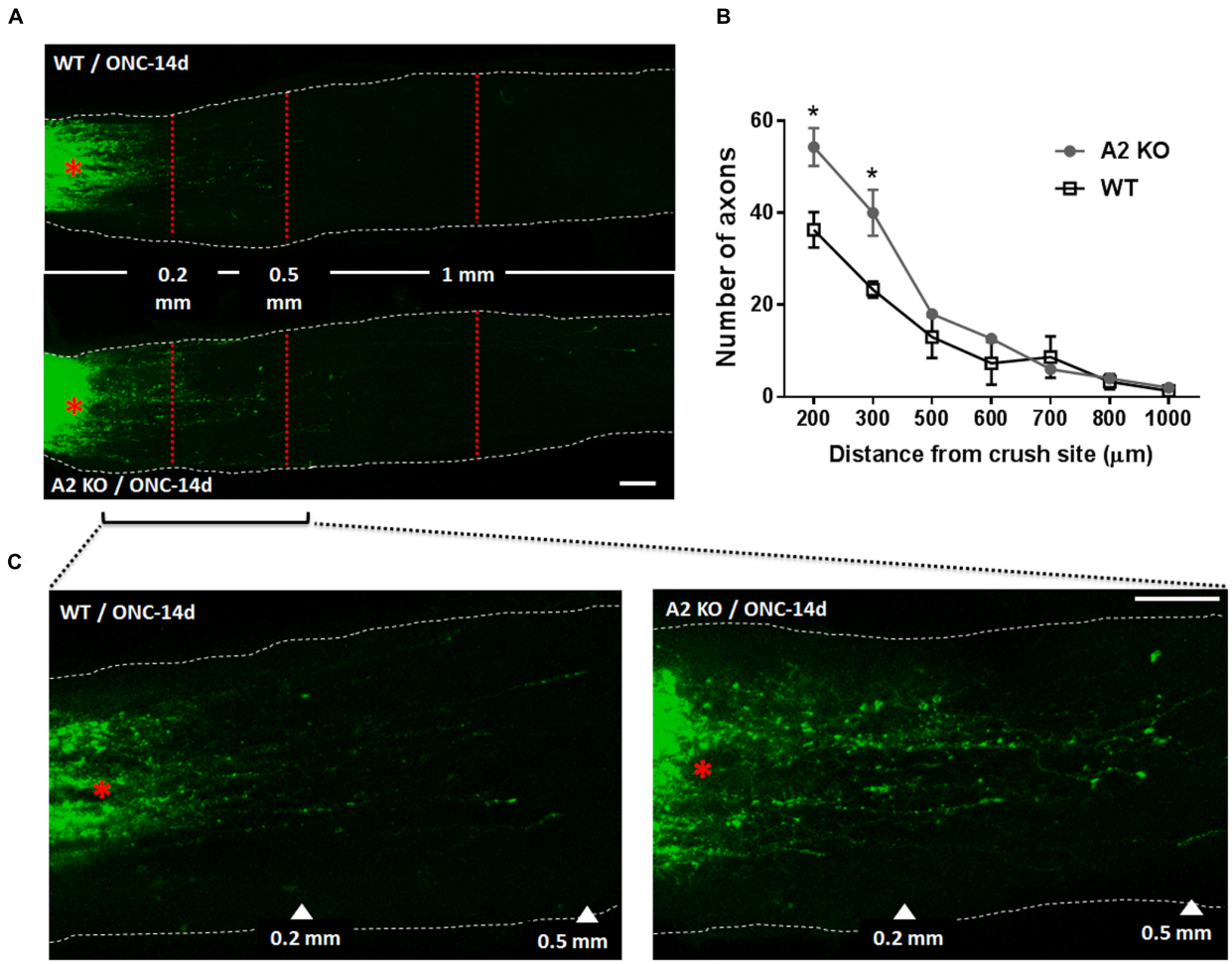

FIGURE 5 | A2 deletion enhances axonal sprouting after ONC. Anterograde labeling of RGC axons using CTB **(A)** showed a significant increase in the number of axons that traveled beyond the crush site toward the brain at 200 and 300 μm distance from crush site denoted by asterisk **(B)**, $N = 3$ per group, $^*p < 0.05$. **(C)** Shows higher magnification images of WT and $A2^{-/-}$ optic nerves from crush site to 500 μm distance toward the brain. Scale bar = 100 μm.

of the A2 deletion at the level of protein expression at 7 days after the injury. This analysis verified the effect of the A2 deletion in decreasing the nucleotide-binding domain (NOD)-like receptor protein 3 (NLRP3), pro-IL-1β and ICAM-1 protein levels (**Figures 7D–H**). Western blot analysis of samples collected at 6 h after ONC also showed a significant protective effect of A2 deletion in reducing levels of NLRP3 and pro-IL-1β (**Figures 7I–L**).

A2 Deletion Suppresses Apoptosis and Preserves Retinal Thickness After ONC

ONC induces apoptotic cell death of RGC that peaks within the first week as measured by TUNEL staining (Li et al., 1999). To examine the potential role of A2 expression in ONC-induced apoptosis we implemented TUNEL staining on WT and $A2^{-/-}$ retina sections at 5 days after ONC. A2 deletion markedly suppressed ONC-induced apoptosis as shown by a marked decrease in numbers of TUNEL positive cells in the GCL as compared with the WT retinas (**Figures 8A,B**). Furthermore, ONC injury induces thinning in the inner retina layers starting at 7 days and reaching a steady level at 14–28 days (Liu et al., 2014; Yukita et al., 2015). Our analysis of retina thickness showed improved preservation of retinal layer morphology in the $A2^{-/-}$ mice as compared with the WT mice at 21 days after ONC. $A2^{-/-}$ retinas showed reduced thinning of the whole retina as compared to WT retinas subjected to ONC (**Figures 8C,D**).

DISCUSSION

In this study, we have investigated the role of A2 in TON by studies using a mouse model of ONC. Our results show that A2 is upregulated within hours of ONC-injury. Deletion of A2 results in a delay in RGC loss and axonal degeneration together with increased expression of the regeneration marker GAP-43 and increased axonal sprouting. Furthermore, A2 deletion was associated a reduction in inflammatory mediators, a decrease in

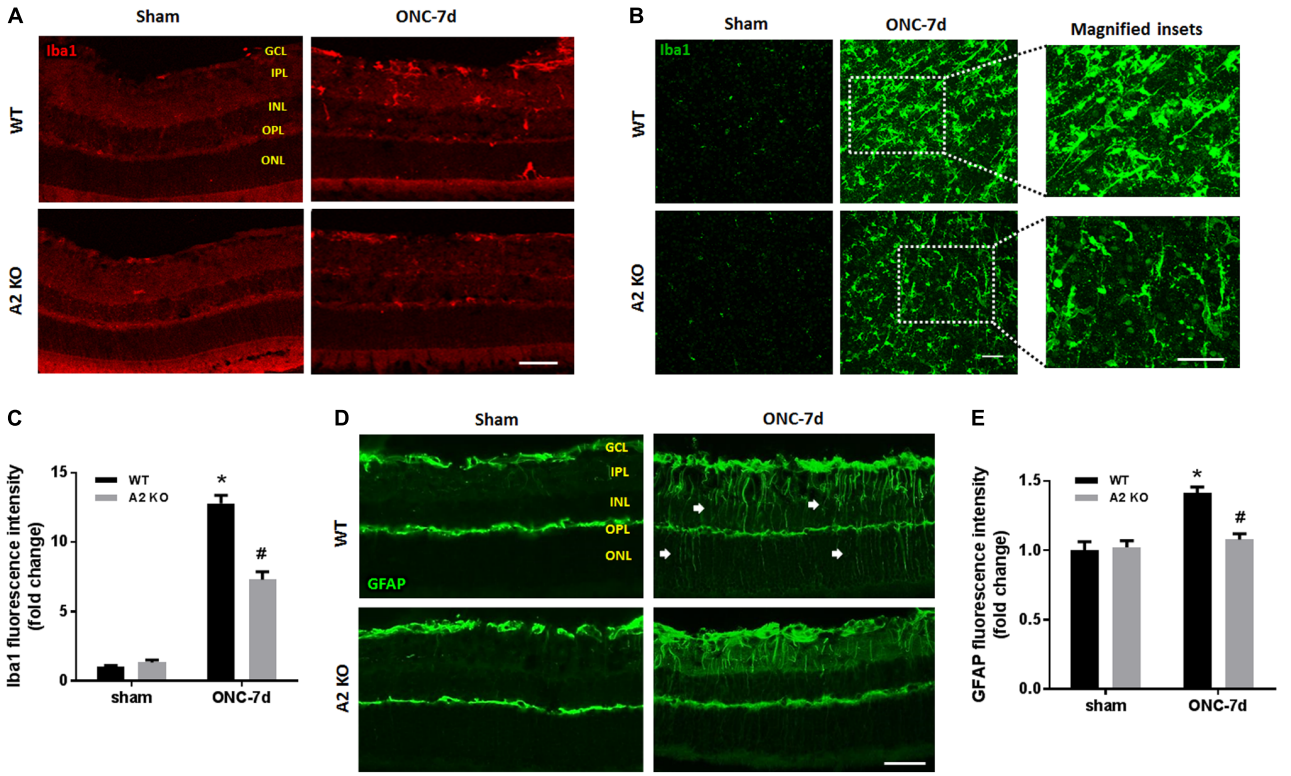

FIGURE 6 | A2 deletion reduces glial activation after ONC. Immunolabeling for Iba1 in retina cross sections **(A)** and flat-mounts **(B)** together with quantification **(C)** showed prominent activation of microglia/macrophage (numerous Iba1$^+$ cells with ameboid morphology) in WT retinas at 7 days after ONC. This was ameliorated in the A2$^{-/-}$ retinas and the Iba1$^+$ cells had a ramified morphology. $N = 4$. Labeling for GFAP on cross sections **(D)** and quantification **(E)** showed increased glial activation at 7 days after ONC which was reduced with A2 deletion. $N = 5$. $^*p < 0.01$ vs. WT sham, $^{\#}p < 0.01$ vs. WT ONC. Arrows denote upregulation of GFAP in the radial processes of activated Müller cells. Scale bar = 50 μm.

numbers of TUNEL positive cells and diminished activation of Müller cells and microglia.

ONC-injury induces progressive RGC death, which starts as early as 7 days and increases with time (Liu et al., 2014). We examined RGC loss using NeuN (general marker for neurons), Brn3a and RBPMS (specific markers for RGC). Some reports suggest that expression of Brn3a can be downregulated in RGC after injury (Nuschke et al., 2015). Therefore, we used the other markers to confirm our results. The relative percentage of lost RBPMS-positive cells at 14 days was slightly less than that of the Brn3a-positive cells, which is consistent with possible downregulation of Brn3a after RGC injury. Moreover, since NeuN labels displaced amacrine cells as well as RCGs, the relative percentage of lost NeuN-positive cells was less as compared to Brn3a at all the time points examined. While the neurodegeneration progressed with time in both WT and A2$^{-/-}$ retinas, A2 deletion resulted in significant neuronal preservation as compared to WT when evaluated using either marker.

In addition to the neuronal loss, WT retinas showed axonal degeneration after ONC as measured by immunolabeling of GCL axons with TUJ1 at 7 and 14 days. A2$^{-/-}$ retinas showed axonal preservation. This protective effect was associated with increases in axonal sprouting as shown by anterograde transport of CBT at 14 days after ONC injury and increased expression of the regeneration marker, GAP-43 at 5 and 7 days. GAP-43 is a developmental growth protein that also plays an important role in axonal regeneration and plasticity in the adult nervous system (Holahan, 2017). It is induced after ONC injury (Doster et al., 1991), and is further upregulated by BDNF administration (Fournier et al., 1997; Klocker et al., 2001). GAP-43 is an important mediator of the neuroprotective effects of BDNF (Gupta et al., 2009). In line with this, our molecular analysis showed an early increase in BDNF protein together with activation of its downstream signaling pathway (ERK/MSK) in the A2$^{-/-}$ retinas after ONC as compared to WT. BDNF (monomer: 14 kDa, homodimer: 28 kDa) is a neurotrophin that results from cleavage of its precursor protein, pro-BDNF (35 kDa). BDNF has been shown to be expressed in RGC and glia in adult rodent retinas. Several reports have shown that BDNF is an important mediator of RGC survival and axonal preservation (Mysona et al., 2017). To our knowledge, our results are the first to show a link between A2 and BDNF. Further studies are needed to address the mechanism by which A2 deletion increases BDNF levels after ONC and the cellular sources involved in the process.

Our previous studies in mouse models of OIR and retinal IR injury have shown decreased glial activation with A2 deletion (Narayanan et al., 2011; Shosha et al., 2016). Glial activation is a hallmark of ONC injury and has been implicated in its

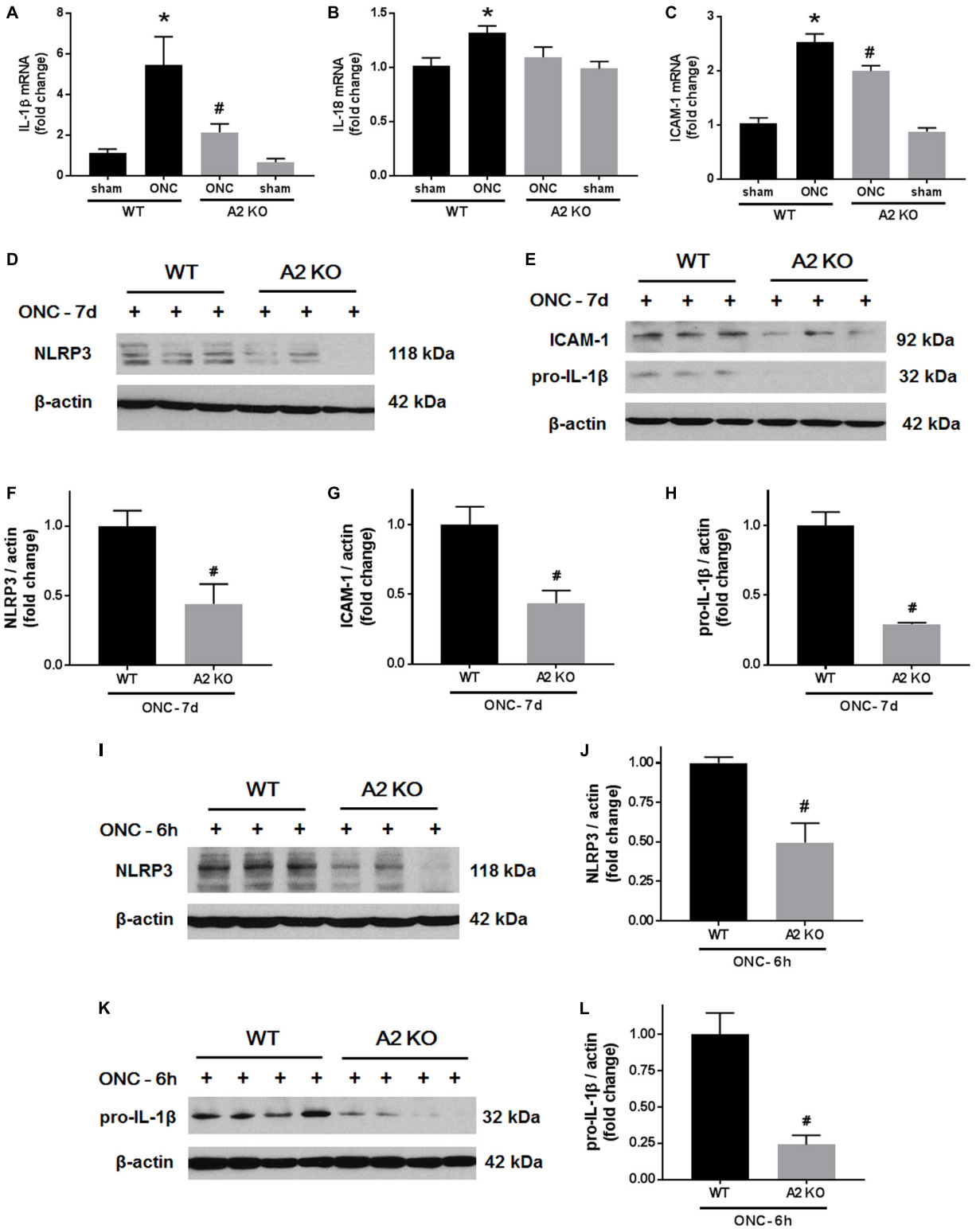

FIGURE 7 | A2 deletion ameliorates ONC-induced retinal inflammation. Quantitative RT-PCR **(A–C)** showed upregulation of pro-inflammatory mediators (IL-1β, IL-18, and ICAM-1) at 7 days after ONC in the WT retinas. A2 deletion significantly blunted these increases. $N = 4–6$, $^{*}p < 0.05$ vs. WT sham, $^{\#}p < 0.05$ vs. WT ONC. Western blotting at 7 days after ONC **(D,E)** and quantification **(F–H)** showed a significant reduction in NLRP3, ICAM-1, and pro-IL-1β protein levels in $A2^{-/-}$ retinas as compared to WT. Western blotting on retina lysates **(I,K)** and quantification **(J,L)** showed downregulation of NLRP3 and pro-IL-1β in $A2^{-/-}$ retinas as compared to WT at 6 h after ONC as well. $N = 3–4$, $^{\#}p < 0.05$ vs. WT ONC.

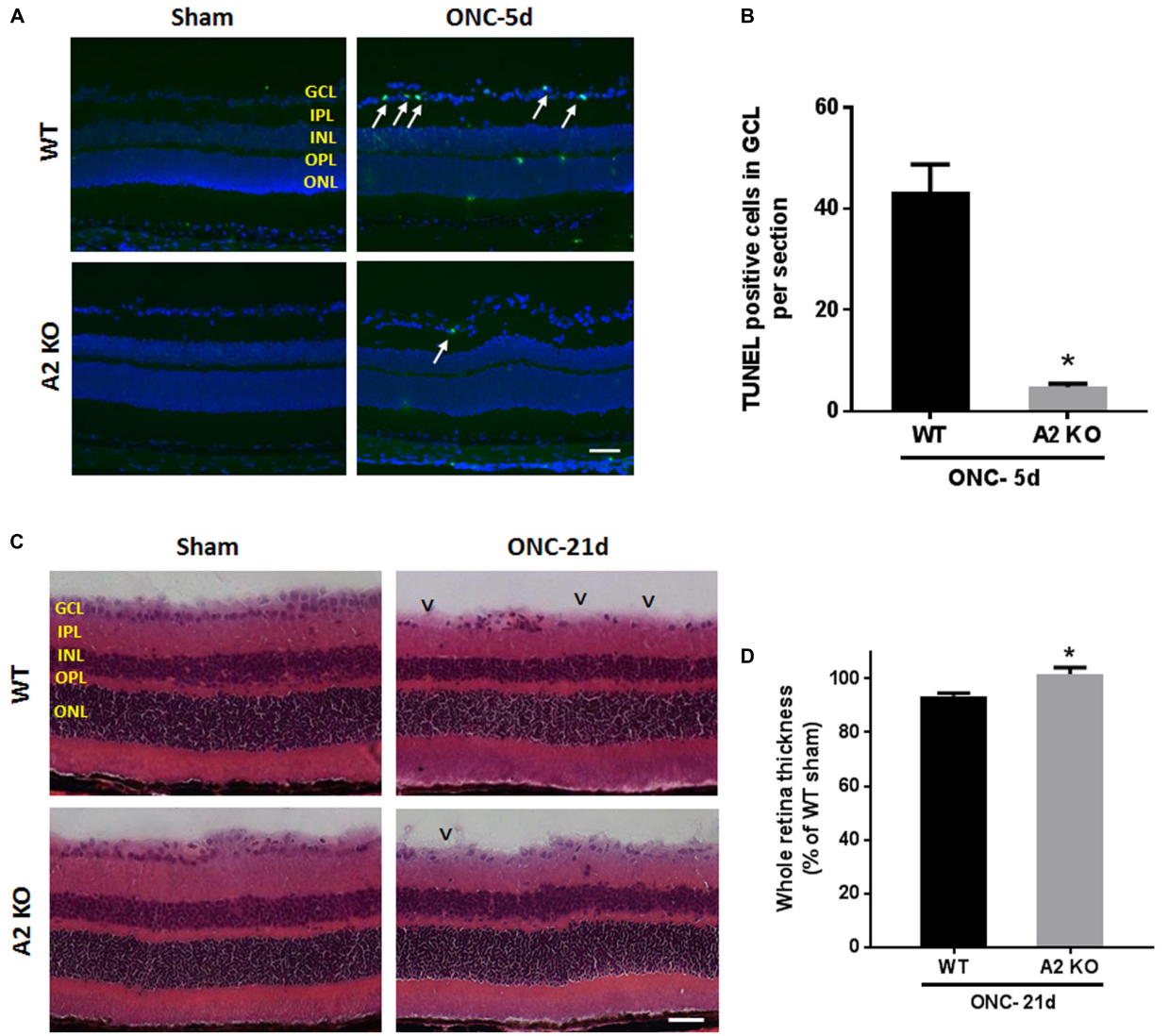

FIGURE 8 | A2 deletion ameliorates ONC-induced apoptosis and limits retinal thinning. TUNEL labeling **(A)** of retina cross sections and quantification **(B)** showed increased TUNEL positive cells in the GCL (arrows) at 5 days after ONC. $A2^{-/-}$ retinas showed a significant reduction in TUNEL positive cells. $N = 4–6$ per group, $^*p < 0.01$, scale bar = 50 μm. Hematoxylin and eosin (H&E) staining of retina cross sections **(C)** and quantification **(D)** at 21 days showed that A2 deletion preserved the total retina thickness to near sham levels. $N = 6$ per group, $^*p < 0.01$, scale bar = 50 μm. Arrowheads denote area of RGC loss.

pathogenesis. ONC stimulates both macroglia and microglia with peak activation at 7 days (Mac Nair et al., 2016). Our results show that A2 deletion ameliorates glial activation as indicated by reductions in GFAP and Iba1 labeling. Furthermore, A2 deletion dampened the ONC-induced retinal inflammation as measured by decreases in the NLRP3 inflammasome, ICAM-1 and inflammatory cytokines IL-1β/IL-18. The NLRP3 inflammasome has been shown to be upregulated in retinal microglia after ONC. This upregulation in NLRP3 was suggested to mediate the RGC and axonal loss after ONC (Puyang et al., 2016). It is suggested that the inflammatory response and glial activation elicit secondary neurodegeneration after ONC, whereby RGC with intact axons undergo apoptosis due to the ongoing inflammation (Li et al., 2014; Mac Nair et al., 2016). Therefore, A2 deletion-mediated dampening of retinal inflammation and glial activation is likely to play a role in RGC preservation and axonal sprouting.

Apoptosis, demonstrated by DNA fragmentation, has been described as the mechanism of RGC death after ONC-injury. TUNEL positive cells peaked at 7 days after ONC (Li et al., 1999). Our data showed that $A2^{-/-}$ retinas exhibited less TUNEL positive cells at 5 days as compared to WT. The decrease in apoptotic cells in $A2^{-/-}$ retinas can be attributed to the upregulation in BDNF levels and decreased retinal inflammation leading to increased RGC resistance to ONC damage. Similar to the RGC preservation, $A2^{-/-}$ retinas showed a reduction in retinal thinning as compared with the WT retinas at 21 days after ONC.

CONCLUSION

In conclusion, our study shows an important role of A2 expression in mediating ONC pathology. A2 deletion ameliorates RGC apoptotic cell death and increases regeneration markers, BDNF and GAP-43. Targeting A2 could provide a new therapy for traumatic injury to the optic nerve.

AUTHOR CONTRIBUTIONS

RBC managed and funded the project. RBC, RWC, and SPN conceptualized and designed the study, crticially revised, and edited the manuscript. ZX, TL, ES, MR, FL, and CP performed the experiments. ZX and AF analyzed and interpreted the resutts, prepared the figures, and drafted the manuscript.

FUNDING

This work was supported by grants from The National Institute of Health (NIH grant R0I-EY11766, the Department of Veterans Affairs, Veterans Health Administration, Office of Research and Development, Biomedical Laboratory Research and Development (BX001233) to RBC, American Heart Association (AHA) postdoctoral fellowship (18POST34060036) to AYF, and the Culver Vision Discovery Institute at Augusta University. RBC was the recipient of a Research Career Scientist Award from the Department of Veterans Affairs. The contents do not represent the views of the Department of Veterans Affairs or the United States Government. The funders had no role in study design, data collection and analysis, decision to publish, or preparation of the manuscript.

REFERENCES

Caldwell, R. W., Rodriguez, P. C., Toque, H. A., Narayanan, S. P., and Caldwell, R. B. (2018). Arginase: a multifaceted enzyme important in health and disease. *Physiol. Rev.* 98, 641–665. doi: 10.1152/physrev.00037.2016

Doster, S. K., Lozano, A. M., Aguayo, A. J., and Willard, M. B. (1991). Expression of the growth-associated protein GAP-43 in adult rat retinal ganglion cells following axon injury. *Neuron* 6, 635–647. doi: 10.1016/0896-6273(91)90066-9

Fouda, A. Y., Xu, Z., Shosha, E., Lemtalsi, T., Chen, J., Toque, H. A., et al. (2018). Arginase 1 promotes retinal neurovascular protection from ischemia through suppression of macrophage inflammatory responses. *Cell Death Dis.* 9:1001. doi: 10.1038/s41419-018-1051-6

Fournier, A. E., Beer, J., Arregui, C. O., Essagian, C., Aguayo, A. J., and Mckerracher, L. (1997). Brain-derived neurotrophic factor modulates GAP-43 but not T alpha1 expression in injured retinal ganglion cells of adult rats. *J. Neurosci. Res.* 47, 561–572. doi: 10.1002/(SICI)1097-4547(19970315)47:6<561::AID-JNR1>3.0.CO;2-B

Gupta, S. K., Mishra, R., Kusum, S., Spedding, M., Meiri, K. F., Gressens, P., et al. (2009). GAP-43 is essential for the neurotrophic effects of BDNF and positive AMPA receptor modulator S18986. *Cell Death. Differ.* 16, 624–637. doi: 10.1038/cdd.2008.188

Holahan, M. R. (2017). A Shift from a pivotal to supporting role for the growth-associated protein (GAP-43) in the coordination of axonal structural and functional plasticity. *Front. Cell Neurosci.* 11:266. doi: 10.3389/fncel.2017.00266

Klocker, N., Jung, M., Stuermer, C. A., and Bahr, M. (2001). BDNF increases the number of axotomized rat retinal ganglion cells expressing GAP-43, L1, and TAG-1 mRNA–a supportive role for nitric oxide? *Neurobiol. Dis.* 8, 103–113. doi: 10.1006/nbdi.2000.0329

Li, H. Y., Ruan, Y. W., Ren, C. R., Cui, Q., and So, K. F. (2014). Mechanisms of secondary degeneration after partial optic nerve transection. *Neural Regen. Res.* 9, 565–574. doi: 10.4103/1673-5374.130093

Li, Y., Schlamp, C. L., and Nickells, R. W. (1999). Experimental induction of retinal ganglion cell death in adult mice. *Invest. Ophthalmol. Vis. Sci.* 40, 1004–1008.

Liu, Y., Mcdowell, C. M., Zhang, Z., Tebow, H. E., Wordinger, R. J., and Clark, A. F. (2014). Monitoring retinal morphologic and functional changes in mice following optic nerve crush. *Invest. Ophthalmol. Vis. Sci.* 55, 3766–3774. doi: 10.1167/iovs.14-13895

Mac Nair, C. E., Schlamp, C. L., Montgomery, A. D., Shestopalov, V. I., and Nickells, R. W. (2016). Retinal glial responses to optic nerve crush are attenuated in bax-deficient mice and modulated by purinergic signaling pathways. *J. Neuroinflammation* 13:93. doi: 10.1186/s12974-016-0558-y

Mesentier-Louro, L. A., De Nicolo, S., Rosso, P., De Vitis, L. A., Castoldi, V., Leocani, L., et al. (2017). Time-dependent nerve growth factor signaling changes in the rat retina during optic nerve crush-induced degeneration of retinal ganglion cells. *Int. J. Mol. Sci.* 18:E98. doi: 10.3390/ijms18010098

Mysona, B. A., Zhao, J., and Bollinger, K. E. (2017). Role of BDNF/TrkB pathway in the visual system: therapeutic implications for glaucoma. *Exp. Rev. Ophthalmol.* 12, 69–81. doi: 10.1080/17469899.2017.1259566

Nadal-Nicolas, F. M., Jimenez-Lopez, M., Sobrado-Calvo, P., Nieto-Lopez, L., Canovas-Martinez, I., Salinas-Navarro, M., et al. (2009). Brn3a as a marker of retinal ganglion cells: qualitative and quantitative time course studies in naive and optic nerve-injured retinas. *Invest. Ophthalmol. Vis. Sci.* 50, 3860–3868. doi: 10.1167/iovs.08-3267

Narayanan, S. P., Suwanpradid, J., Saul, A., Xu, Z., Still, A., Caldwell, R. W., et al. (2011). Arginase 2 deletion reduces neuro-glial injury and improves retinal function in a model of retinopathy of prematurity. *PLoS One* 6:e22460. doi: 10.1371/journal.pone.0022460

Nuschke, A. C., Farrell, S. R., Levesque, J. M., and Chauhan, B. C. (2015). Assessment of retinal ganglion cell damage in glaucomatous optic neuropathy: axon transport, injury and soma loss. *Exp. Eye Res.* 141, 111–124. doi: 10.1016/j.exer.2015.06.006

Puyang, Z., Feng, L., Chen, H., Liang, P., Troy, J. B., and Liu, X. (2016). Retinal ganglion cell loss is delayed following optic nerve crush in NLRP3 knockout mice. *Sci. Rep.* 6:20998. doi: 10.1038/srep20998

Ratican, S. E., Osborne, A., and Martin, K. R. (2018). Progress in gene therapy to prevent retinal ganglion cell loss in glaucoma and leber's hereditary optic neuropathy. *Neural Plast.* 2018:7108948. doi: 10.1155/2018/7108948

Rodriguez, A. R., De Sevilla Muller, L. P., and Brecha, N. C. (2014). The RNA binding protein RBPMS is a selective marker of ganglion cells in the *mammalian* retina. *J. Comp. Neurol.* 522, 1411–1443. doi: 10.1002/cne.23521

Shosha, E., Xu, Z., Yokota, H., Saul, A., Rojas, M., Caldwell, R. W., et al. (2016). Arginase 2 promotes neurovascular degeneration during ischemia/reperfusion injury. *Cell Death Dis.* 7:e2483. doi: 10.1038/cddis.2016.295

Tang, Z., Zhang, S., Lee, C., Kumar, A., Arjunan, P., Li, Y., et al. (2011). An optic nerve crush injury murine model to study retinal ganglion cell survival. *J. Vis. Exp.* 50:2685. doi: 10.3791/2685

Wang, J., Li, Y., King, R., Struebing, F. L., and Geisert, E. E. (2018). Optic nerve regeneration in the mouse is a complex trait modulated by genetic background. *Mol. Vis.* 24, 174–186.

Weber, A. J., Harman, C. D., and Viswanathan, S. (2008). Effects of optic nerve injury, glaucoma, and neuroprotection on the survival, structure, and function of ganglion cells in the mammalian retina. *J. Physiol.* 586, 4393–4400. doi: 10.1113/jphysiol.2008.156729

Yukita, M., Machida, S., Nishiguchi, K. M., Tsuda, S., Yokoyama, Y., Yasuda, M., et al. (2015). Molecular, anatomical and functional changes in the retinal ganglion cells after optic nerve crush in mice. *Doc. Ophthalmol.* 130, 149–156. doi: 10.1007/s10633-014-9478-2

Conflict of Interest Statement: The authors declare that the research was conducted in the absence of any commercial or financial relationships that could be construed as a potential conflict of interest.

frontiers in Genetics

ORIGINAL RESEARCH
published: 20 December 2018
doi: 10.3389/fgene.2018.00658

Regulation of Nrf2 by X Box-Binding Protein 1 in Retinal Pigment Epithelium

Chen Chen[1,2,3], Yimin Zhong[3,4], Joshua J. Wang[3,5], Qiang Yu[4], Kendra Plafker[6], Scott Plafker[6] and Sarah X. Zhang[3,5]**

[1] Department of Ophthalmology, The Second People's Hospital of Yunnan Province, Kunming, China, [2] Key Laboratory of Yunnan Province for the Prevention and Treatment of Ophthalmic Diseases, Yunnan Eye Institute, Kunming, China, [3] Department of Medicine, The University of Oklahoma, Oklahoma City, OK, United States, [4] State Key Laboratory of Ophthalmology, Zhongshan Ophthalmic Center, Sun Yat-sen University, Guangzhou, China, [5] Department of Ophthalmology, University at Buffalo, The State University of New York, Buffalo, NY, United States, [6] Aging and Metabolism Research Program, Oklahoma Medical Research Foundation, Oklahoma City, OK, United States

Normal function of the retinal pigment epithelium (RPE) is essential for maintaining the structural integrity of retinal photoreceptors and the visual process. Sustained oxidative damage of the RPE due to aging and other risk factors contributes to the development of age-related macular degeneration (AMD). The transcription factor NF-E2-related factor 2 (Nrf2) is a central regulator of cellular antioxidant and detoxification responses. Enhancing Nrf2 function protects RPE cells from oxidation-related apoptosis and cell death. Previously, we demonstrated that Nrf2 activation can be induced by endoplasmic reticulum (ER) stress; however, the mechanisms are not fully understood. In the present study, we examined the role of X box-binding protein 1 (XBP1), an ER stress-inducible transcription factor, in regulation of Nrf2 in the RPE. We found that RPE-specific *XBP1* conditional knockout (cKO) mice exhibit a significant reduction in Nrf2 mRNA and protein levels, along with decreased expression of major Nrf2 target genes, in the RPE/choroid complex. Using primary RPE cells isolated from *XBP1* cKO mice and human ARPE-19 cell line, we confirmed that loss of *XBP1* gene or pharmacological inhibition of *XBP1* splicing drastically reduces Nrf2 levels in the RPE. Conversely, overexpression of spliced *XBP1* results in a modest but significant increase in cytosolic and nuclear Nrf2 protein levels without affecting the transcription of Nrf2 gene. Moreover, induction of ER stress by tunicamycin and thapsigargin markedly increases Nrf2 expression, which is abolished in cells pretreated with *XBP1* splicing inhibitors 4μ8C and quinotrierixin. Mechanistic studies indicate that quinotrierixin reduces Nrf2 expression likely through inhibition of protein translation. Finally, we demonstrate that overexpression of Nrf2 protected RPE cells against oxidative injury but appeared to be insufficient to rescue from XBP1 deficiency-induced cell death. Taken together, our results indicate that XBP1 modulates Nrf2 activity in RPE cells and that XBP1 deficiency contributes to oxidative injury of the RPE.

Keywords: retinal pigment epithelium, NF-E2-related factor 2, X-box binding protein 1, endoplasmic reticulum stress, oxidative stress, cell death

OPEN ACCESS

Edited by:
Nan-Jie Xu,
Shanghai Jiao Tong University, China

Reviewed by:
Nirmalya Chatterjee,
Harvard Medical School,
United States
Shusheng Wang,
Tulane University, United States

****Correspondence:***
Chen Chen
chenchenmd@aliyun.com
Sarah X. Zhang
xzhang38@buffalo.edu

Specialty section:
This article was submitted to Genetics of Aging, a section of the journal Frontiers in Genetics

Received: *15 August 2018*
Accepted: *03 December 2018*
Published: *20 December 2018*

Citation:
Chen C, Zhong Y, Wang JJ, Yu Q, Plafker K, Plafker S and Zhang SX (2018) Regulation of Nrf2 by X Box-Binding Protein 1 in Retinal Pigment Epithelium. Front. Genet. 9:658. doi: 10.3389/fgene.2018.00658

INTRODUCTION

The retinal pigment epithelium (RPE), a monolayer of pigmented epithelial cells in the eye, plays a crucial role in the nourishment and detoxification of photoreceptors (Strauss, 2005). Dysfunction of the RPE is associated with a variety of posterior segment ocular diseases including age-related macular degeneration (AMD), the leading cause of blindness in the elderly (Bressler, 2004; Augood et al., 2006). Due to its high consumption of oxygen and continuous exposure to light, the RPE is constantly subjected to oxidative stress and its unique phagocytic function further imposes an additional oxidative burden (Cai et al., 2000). Cumulative oxidative stress also increases complement activation (Thurman et al., 2009) and upregulates pathogenic genes including VEGFA and Annexin 2 promoting drusen formation and choroidal neovascularization (Rabin et al., 2013). Anti-oxidants such as melatonin and N-Acetylcysteine (NAC) successfully alleviate RPE apoptosis (Seko et al., 2001; Fu et al., 2012) and dietary supplement of anti-oxidants including vitamin A, C, and E, β-carotene and lutein modestly reduce the progression of AMD (Tan et al., 2008; Ho et al., 2011), suggesting a critical role of oxidative stress in RPE injury and AMD.

To cope with the oxidative environment, the RPE has evolved effective defenses against oxidative stress. It is rich in antioxidants such as vitamin E, as well as enzymes and proteins that neutralize free radicals, including superoxide dismutase (SOD), catalase, and glutathione (Shamsi and Boulton, 2001). In addition, RPE cells have robust anti-oxidant and anti-stress response systems to maintain redox and proteome homeostasis in the face of high oxygen tension and photo-oxidative stress, and this system is primarily regulated by NF-E2-related factor 2 (Nrf2), a bZIP transcription factor (Kaspar et al., 2009; Niture et al., 2010). By binding to antioxidant response elements (AREs) and electrophile-responsive element (EpRE), Nrf2 activates a group of ARE-containing antioxidant genes including GSTA1, GSTA2, NQO-1, and HO-1 (Kang et al., 2005), and a host of phase II detoxification enzymes (Na and Surh, 2008). In the RPE, Nrf2 signaling regulates glutathione synthesis and protects against photooxidative damage (Gao and Talalay, 2004). Mice lacking Nrf2 develop drusen-like deposits, accumulation of lipofuscin, spontaneous choroidal neovascularization (CNV) and sub-RPE deposition of inflammatory proteins, which resemble human AMD (Zhao et al., 2011). These findings, along with compelling evidence from other published studies, support the importance of Nrf2 signaling in the anti-oxidant defense system of the RPE.

It is well established that the stability and activity of Nrf2 are directly coupled to cellular redox and proteome status (Itoh et al., 1999; Nguyen et al., 2003, 2004, 2005; Hohn and Grune, 2014). During homeostasis, the majority of Nrf2 is degraded, and this turnover is mediated by the ubiquitin proteolytic system. Specifically, Nrf2 is degraded by the multi-subunit E3 ligase, CUL3KEAP1, in cooperation with the 26S proteasome (Kobayashi et al., 2004, 2006; Li and Kong, 2009). Oxidative or proteotoxic stresses, however, dissociate CUL3KEAP1, resulting in the stabilization of Nrf2 and its translocation into the nucleus to induce the transcription of anti-oxidant and chaperone genes, estimates of which number in the hundreds (Kang et al., 2005; Na and Surh, 2008).

XBP1 is a member of the CREB/ATF basic region-leucine zipper family of transcription factors. It's a central regulator in unfolded protein response (UPR) and endoplasmic reticulum stress (ER stress). Under ER stress, activated ER membrane sensor IRE1 splices a 26 bp fragment from XBP1 mRNA, resulting in the conversion of a 267 amino acid unspliced XBP1 protein to a 371 amino acid spliced XBP1 protein (Glimcher, 2010). The spliced XBP1 then translocates into the nucleus and regulates the expression of its downstream genes. In previous studies, we found that induction of ER stress by cigarette smoking, a major environmental risk factor for AMD, activates the UPR and increases Nrf2 expression in the RPE (Chen et al., 2014; Huang et al., 2015a,b). Deletion of C/EBP homolog protein 10 (CHOP) suppresses Nrf2 upregulation resulting in exacerbated cell death, suggesting a role of UPR in Nrf2 regulation (Huang et al., 2015b). In addition, ablation of XBP1 in the mouse RPE results in increased reactive oxygen species (ROS) and RPE apoptosis (Zhong et al., 2012; Chen et al., 2014); conversely, overexpression of *XBP1* protects RPE cells from cigarette smoke exact or hydroquinone induced cell death (Chen et al., 2014; Huang et al., 2015b). These results suggest a role of XBP1 in regulation of oxidative stress in RPE cells. In the present study, we investigate whether XBP1 regulates Nrf2 expression in the RPE and explore the underlying mechanism.

MATERIALS AND METHODS

Animals

Generation of RPE-specific *XBP1* conditional knockout (cKO) mice was described elsewhere (Zhong et al., 2012; Chen et al., 2014). Littermate mice (*XBP1* floxed, Cre-) were used as control in all experiments. Mice were maintained on a 12 h light/12 h dark cycle with *ad libitum* access to food and water. All animal procedures were approved by the Institutional Animal Care and Use Committees at the University of Oklahoma Health Sciences Center and the University at Buffalo, State University of New York, and in accordance with the ARVO statements for the Use of Animals in Ophthalmic and Vision Research.

Ex vivo Eyecup Incubation

Eyecups containing RPE, choroid, and sclera were incubated with 10 mg/ml tunicamycin for 6 h. Proteins were extract from the RPE by incubation of lysis buffer with the inner surface of the eyecups for 30 min and then subjected to Western blot analysis.

Immunohistochemistry of Mouse Retina

For frozen sections, the cornea and lens were removed and the eyecups were fixed with 4% paraformaldehyde for 30 min. Eyecups were then cryoprotected with a series of sucrose solution (10–30%) and cross-sections of the retina were obtained using a cryostat. Retinal sections were immunostained using anti-Nrf2 antibody (1:100; Santa Cruz Biotechnology) overnight at 4°C, followed by biotinylated secondary antibody and fluorescein

isothiocyanate avidin. The fluorescence was visualized under an Olympus AX70 microscope.

Primary Mouse RPE Cell Culture

Primary RPE cells were isolated from *XBP1*$^{flox/flox}$ and *XBP1* RPE specific knock-out mouse pups as previously described (Gibbs et al., 2003) with modifications. Briefly, 14 days pups were sacrificed by cervical dislocation, eyeballs enucleated immediately. Eyes were washed with Dulbecco's Modification of Eagle's Medium (DMEM)/Ham's F-12 50/50 mix medium (Cellgro, Manassas, VA, United States), and digested with 2% (wt/vol) dispase (GIBCO, #17105-041) in serum-free DMEM/F12 at 37°C for 45 min. Digested eyeballs were transferred to a 60 mm culture dish containing growth medium [DMEM/F12 with 10% fetal bovine serum (FBS), 1% penicillin/streptomycin] and dissected under a surgical microscope. Anterior segments and neural retinas were removed and the single sheets of RPE cells were peeled off the eyecup and collected. RPE layer was digested with 0.05% trypsin and the resulting singe cells of RPE were seeded in 12-well plate in growth medium, and allowed 7–10 days to grow until confluence before used for experiments.

ARPE-19 Cell Culture

Human RPE (ARPE-19) cells were purchased from American Type Culture Collection (ATCC, Manassas, VA, United States) and maintained in DMEM/F12 medium containing 10% FBS and 1% antibiotic/antimycotic. Cells were allowed to grow to 100% confluence and quiescent overnight with serum free DMEM/F12 medium before adding all chemicals.

Chemicals

Tunicamycin (TM) and thapsigargin (TG) were purchased from EMD Millipore Corporation (Billerica, MA, United States); Hydroquinone (HQ), tert-Butylhydroquinone (tBHQ), and cycloheximide (CHX) were purchased from Sigma-Aldrich (St. Louis, MO, United States); MG132 was purchased from Cayman Chemical (Ann Arbor, MI, United States). 4μ8C was provided by Dr. David Ron (University of Cambridge Metabolic Research Laboratories and National Institute for Health Research Cambridge Biomedical Research Centre, United Kingdom); Quinotrierixin (QT) was a kind gift from Dr. Etsu Tashiro (Keio University, Japan).

Adenoviral Transduction and siRNA Transfection

Construction of adenovirus expressing Nrf2 and adenoviral transduction were described previously (Huang et al., 2015b). Briefly, ARPE-19 cells were transduced with adenoviruses overexpressing either spliced *XBP1*, *Nrf2*, or *LacZ* (transfection control) at a multiplicity of infection (MOI) of 10 and 20 for Ad-*XBP1s* and a MOI of 50 and 100 for Ad-*Nrf2*. To knock down *XBP1* (both unspliced and spliced forms), ARPE-19 cells were transfected with *XBP1* siRNA or control siRNA (Santa Cruz Biotechnology, Santa Cruz, CA, United States) using Lipofectamine 2000 (Invitrogen, Carlsbad, CA, United States) per manufacturer's instruction. 24 h after transduction/transfection, cells were quiescent overnight with serum free DMEM/F12 medium followed by desired treatments.

Western Blot Analysis

Mouse eyecups or ARPE-19 Cells were lysed in RIPA buffer with protease inhibitor cocktail, PMSF and sodium orthovanadate (Santa Cruz Biotechnology) and sonicated by ultrasound (on ice). Protein concentration was quantified using BCA kit (Pierce Biotechnology, Inc., Rockford, IL, United States). Twenty-five micrograms of protein were resolved by SDS-PAGE gel and electro-transferred to nitrocellular membranes. After blocking with 5% non-fat milk, membranes were blotted overnight at 4°C with following primary antibodies: anti-Nrf2 (1:1000; Santa Cruz Biotechnology), anti-XBP1 (1:500; Santa Cruz Biotechnology), anti-Catalase (1:2000; Sigma-Aldrich), anti-SOD1 (1:2000; Abcam), anti-SOD2 (1:1000; Assay Designs, MI, United States) and anti-β-actin (1:5,000; Abcam). After incubation with HRP-conjugated secondary antibodies, membranes were developed with chemiluminescence substrate (Thermo Fisher Scientific, Rockford, IL, United States: #34076) using Vision Works LS image acquisition and analysis software (UVP, Upland, CA, United States), and bands were semi-quantified by densitometry.

RT-PCR and Real-Time RT-PCR

For ARPE-19 cells, total RNA were extracted using an E.Z.N.A. total RNA kit I (Omega Bio-tek, Georgia, GA, United States) and 1 μg RNA was used to synthesize cDNA. For mouse eyecups, total RNA were extracted using Trizol reagent (Invitrogen, Grand Island, NY, United States) and 200 ng RNA was used to synthesize cDNA. The Maxima First Strand cDNA synthesis kit containing oligo (dT) and random hexamer primers (Fermentas, Glen Burnie, MD, United States) was used for cDNA synthesis. To investigate *XBP1* splicing, RT-PCR was performed using the cDNA template and PCR Master Mix (Fermentas, #K1081), and PCR products were resolved on a 2.5% agarose/1 × TAE gel. The RT-PCR primers for *human XBP1* were: 5′-TTACGAGAGAAAACTCATGGC-3′, 5′-GGGTCCAAGTTGTCCAGAATGC-3′ (Lin et al., 2007). Real-time quantitative RT-PCR was performed using SYBR® Green PCR Master Mix (Bio-Rad Laboratories, Hercules, CA, United States) and primers were listed in **Table 1**. The mRNA levels of target genes were normalized by 18s ribosomal RNA.

Nrf2 Half-Life Experiments

2×10^5 ARPE19 cells were plated/well in 3 cm dishes. Two days after plating, cells were treated with QT (0.5 μM) or vehicle (DMSO) for 7 h. Cells were then starved of methionine and cysteine with or without 10 μM MG132 for 30 min before the addition of 35S-translabel for an additional 40 min. The radiolabeled media was removed, cells were washed with ice-cold PBS, and then warm media was added (+/− QT) for 0, 15, 30, or 60 min before endogenous Nrf2 was immunoprecipitated from the cell lysates, resolved by SDS-PAGE and the dried down gels were processed for fluorography, all as described previously (Plafker et al., 2010).

TABLE 1 | Primers used for quantitative real-time PCR.

Gene name	Primer sequence
Mouse XBP1 (exon2)	5′-CCTGAGCCCGGAGGAGAA-3′
	5′-CTCGAGCAGTCTGCGCTG-3′
Mouse Nrf2	5′-AGGACATGGAGCAAGTTTGG-3′
	5′-TCCTCAAAACCATGAAGGAA-3′
Mouse NQO-1	5′-AGGGTTCGGTATTACGATCC-3′
	5′-AGTACAATCAGGGCTCTTCTCG-3′
Mouse HO-1	5′-TCTATCGTGCTCGCATGAAC-3′
	5′-CTGTCTGTGAGGGACTCTGG-3′
Mouse GST	5′-TCTGCCTATATGAAGACC-3′
	5′-AGAGAAGTTACTGGAAGC-3′
Human total XBP1	5′-CCATGGATTCTGGCGGTATTGACT-3′
	5′-CCACATTAGCTTGGCTCTCTGTCT-3′
Human spliced XBP1	5′-CCGCAGCAGGTGCAGG-3′
	5′-GAGTCAATACCGCCAGAATCCA-3′
Human Nrf2	5′-AAAGAGCGCCGAGGATTTCAG-3′
	5′-CCAAGAAATGCAGTCTCGAG-3′
Human Erdj4	5′-CTGTATGCTGATTGGTAGAGTCAA-3′
	5′-AGTAGACAAAGGCATCATTTCCAA-3′
Human p58^{IPK}	5′-GAGGTTTGTGTTGGGATGCAG-3′
	5′-GCTCTTCAGCTGACTCAATCAG-3′
Human HO-1	5′-CAGTGCCACCAAGTTCAAGC-3′
	5′-GTTGAGCAGGAACGCAGTCTT-3′

Nrf2 Stabilization by MG132

ARPE19 cells were treated with QT or vehicle for 7 h and subsequently pulsed for 40 min with 35S-translabel in the presence or absence of MG132. Cells were then immediately lysed under denaturing conditions and processed for immunoprecipitation of endogenous Nrf2 as described for the half-life experiments.

TUNEL Assay

ARPE19 cell DNA fragmentation was detected using the *In Situ* Cell Death Detection TMR red kit (TUNEL Assay, Roche Diagnostics Corp., Indianapolis, IN, United States) according to manufacturer's protocol. Briefly, cells on coverslips were fixed with 4% PFA for 1 h, followed by permeabilization for 2 min on ice in 0.1% citrate buffer containing 0.1% Triton X-100. Then coverslips were incubated at 37°C in TUNEL reaction mix containing nucleotides and terminal deoxynucleotidyl transferase (TdT). Incubation without TdT enzyme was conducted as a negative control. After three washes with PBS, coverslips were mounted to a slide with a mounting medium for fluorescence with DAPI (Vector Laboratories, Burlingame, CA, United States. #H-1200), and observed under a fluorescence microscope.

Statistical Analysis

The quantitative data were expressed as mean ± SD. Statistical analyses were performed using Student's *t*-test for two-group comparisons and one-way ANOVA with Bonferroni's multiple comparison tests for three groups or more. Statistical differences were considered significant at a *P*-value of less than 0.05. When quantifying Western Blots for ARPE-19 cells, the ratio of the target protein to β-actin in control group was set as 1.0 in all experiments, and the ratios of the target protein to β-actin in other groups were expressed as folds of control.

RESULTS

Ablation of *XBP1* Reduces Nrf2 Expression in the RPE

To determine if XBP1 regulates Nrf2 expression in the RPE, we examine the mRNA and protein levels of Nrf2 in the RPE/choroid complex from RPE-specific *XBP1* cKO mice. Successful downregulation of XBP1 in the RPE was confirmed by the significant reduction of total XBP1 mRNA level in the RPE/choroid complex of the cKO mice (**Figure 1A**). Immunohistochemical analysis showed that Nrf2 was expressed in the RPE of control mice, which was reduced in the cKO mice (**Figure 1B**). To quantify the change in Nrf2, RPE/choroid complex from the cKO mice or controls were subjected to Western blot analysis, which revealed a nearly 50% decrease in Nrf2 in the cKO (**Figure 1C**). We next examined whether the induction of Nrf2 by ER stress is affected in *XBP1*-deficient RPE. Eyecups (containing the RPE and choroid) from the cKO or control mice were exposed to 10 μg/ml of tunicamycin, a potent ER stress inducer, for 6 h. Induction of Nrf2 was evaluated by Western blot analysis. We found that Nrf2 expression was drastically decreased by 70% in *XBP1* cKO RPE/choroid complex compared to the controls after tunicamycin treatment (**Figure 1D**). The Nrf2 mRNA expression was also reduced by nearly 50% in *XBP1* cKO RPE/choroid complex (**Figure 1E**). To explore the consequence of *XBP1* knockout on downstream target genes of Nrf2, we measured the mRNA levels of NQO-1, HO-1, and GST. As expected, all three genes were suppressed after *XBP1* knockout (**Figure 1E**). These results suggest that XBP1 is required for both basal and ER stress-induced Nrf2 expression in the RPE.

Nrf2 Expression Was Decreased in Primary RPE Cells Isolated From *XBP1* KO Mice

To further confirm the changes in Nrf2 expression in *XBP1*-deficient RPE, we isolated primary RPE cells from *XBP1* KO mice and WT mice. A representative image of mouse RPE cells is shown in **Figure 2A**. Given that the basal level of Nrf2 is low in normal cells due to a constant proteasomal degradation mediated by Keap1, we pretreated RPE cells with the proteasome inhibitor MG132 prior to harvesting cells for Western blot analysis. We found that in cKO RPE cells, Nrf2 protein level was about 50% of that in the WT cells (**Figure 2B**). We next examined whether induction of Nrf2 by stress is affected by exposing RPE cells to hydroquinone, a potent pro-oxidant identified in cigarette smoking that also induces ER stress (Chen et al., 2014). We found that hydroquinone-induced Nrf2 expression was significantly reduced in XBP1-null RPE cells (**Figure 2C**). These results further confirmed a role of XBP1 in Nrf2 regulation in the RPE.

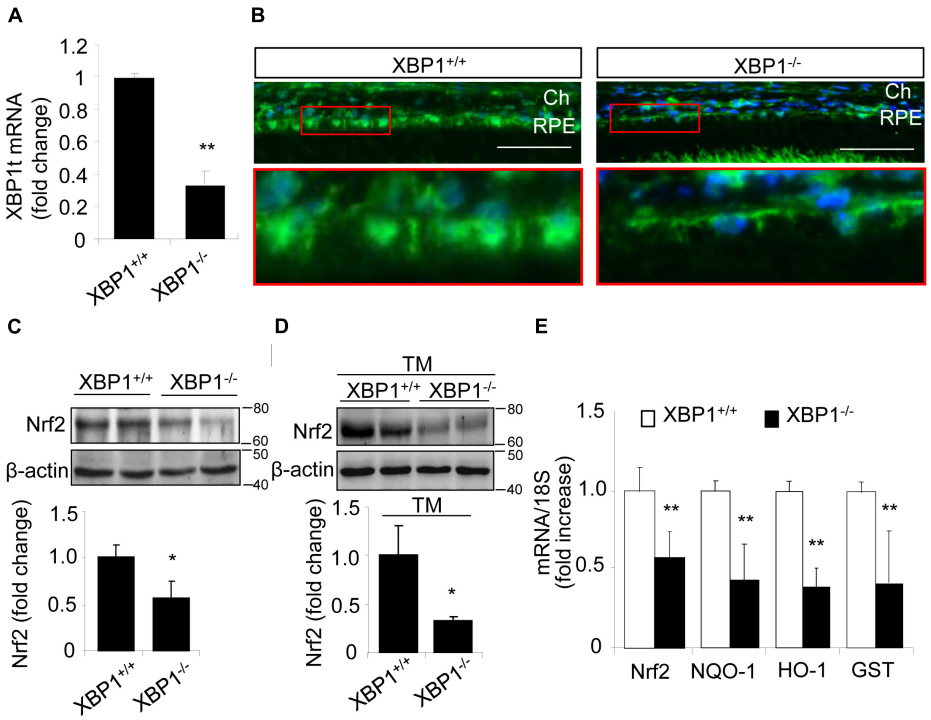

FIGURE 1 | Decreased Nrf2 expression in the RPE of XBP1 KO mice. **(A)** Total XBP1 mRNA level in the WT and KO mice eyecups (including choroid and the RPE) was detected by real-time PCR (mean ± SD, $n = 7$ for WT, $n = 5$ for KO, $^{**}p < 0.01$). **(B)** Retina sections were stained with anti-Nrf2 antibody (green) and DAPI (blue) was used to stain all nuclei. (Scale bar: 50 μm; Ch, choroid; RPE, retinal pigment epithelium). **(C)** Expression of Nrf2 in the WT and KO eyecups was determined by Western blot analysis and semi-quantified by densitometry (mean ± SD, $n = 4$, $^{*}p < 0.05$). **(D)** Freshly isolated eyecups were incubated with 10 μg/ml tunicamycin for 6 h, and the protein level of Nrf2 was detected by Western blot and semi-quantified by densitometry (mean ± SD, $n = 3$, $^{*}p < 0.05$). **(E)** mRNA levels of Nrf2, NQO-1, HO-1, and GST in the WT and KO eyecups was detected by real-time RT-PCR (mean ± SD, $n = 5$, $^{**}p < 0.01$).

Overexpression of Spliced *XBP1* Increases Nrf2 Protein in ARPE-19 Cells

Next, we determined whether overexpression of *XBP1* is sufficient to increase Nrf2 expression using a human RPE cell line, ARPE-19 cells transduced with adenovirus overexpressing spliced *XBP1* or *LacZ* as a transfection control. We found that Nrf2 protein levels in both cytoplasmic and nuclear fractions were significantly higher in Ad-*XBP1s* transduced cells compared to Ad-*LacZ* controls (**Figure 3A**). The transcription of Nrf2 was, however, not changed by overexpression of *XBP1s* (**Figure 3B**). Furthermore, we found that there is no change in the expression of other anti-oxidant genes including catalase, SOD2, and SOD1 (**Figure 3C**), indicating that overexpression of *XBP1s* did not simply increase oxidative stress. These results imply a potential role of spliced XBP1 in Nrf2 regulation.

Inhibition of *XBP1* Splicing Reduces Nrf2 Expression in ARPE-19 Cells

Spliced XBP1 is the active form of XBP1, generated by splicing off a 26 bp fragment from XBP1 mRNA by inositol-requiring enzyme 1 (IRE1) during ER stress (Glimcher, 2010). To verify a role of spliced XBP1 in Nrf2 regulation, we pretreated ARPE-19 cells with 4μ8C, a specific inhibitor that binds to the RNase domain of IRE1α to suppress *XBP1* splicing (Cross et al., 2012; Ma et al., 2016), prior to incubation with ER stress inducer thapsigargin (TG). Upon 4μ8C treatment, Nrf2 protein level was reduced in ARPE-19 cells but this reduction only reached significance in the presence of MG132 (**Figure 4A**). Furthermore, induction of ER stress by TG increased Nrf2 levels and this increase was partially suppressed in cells pretreated with 4μ8C (**Figure 4B**).

To exclude potential off-target effects of 4μ8C, we pretreated ARPE-19 cells with quinotrierixin (QT), which specifically and selectively inhibits ER stress-induced XBP1 mRNA splicing (Kawamura et al., 2008a). Like 4μ8C, QT significantly and dose-dependently reduced the increase of Nrf2 levels induced by the ER stress inducers TG and TM (**Figures 4C,D**, respectively). Using RT-PCR and qPCR, we confirmed the significant downregulation of spliced XBP1 gene and two of its target genes, ERdj4 and P58ipk in QT treated cells (**Figure 4E**). Interestingly, neither TM nor QT altered the mRNA levels of Nrf2 (**Figure 4E**), suggesting that the regulation of Nrf2 by TM and spliced XBP1 may occur at the translational or post-translational levels.

To test this hypothesis, we treated ARPE-19 cells with tBHQ, which has been shown to induce Nrf2 activity by stabilizing ubiquitinated Nrf2 protein (Li et al., 2005), in the presence or absence of QT. We found that QT dose-dependently decreased tBHQ-induced Nrf2 stabilization (**Figure 5A**), but had no effect

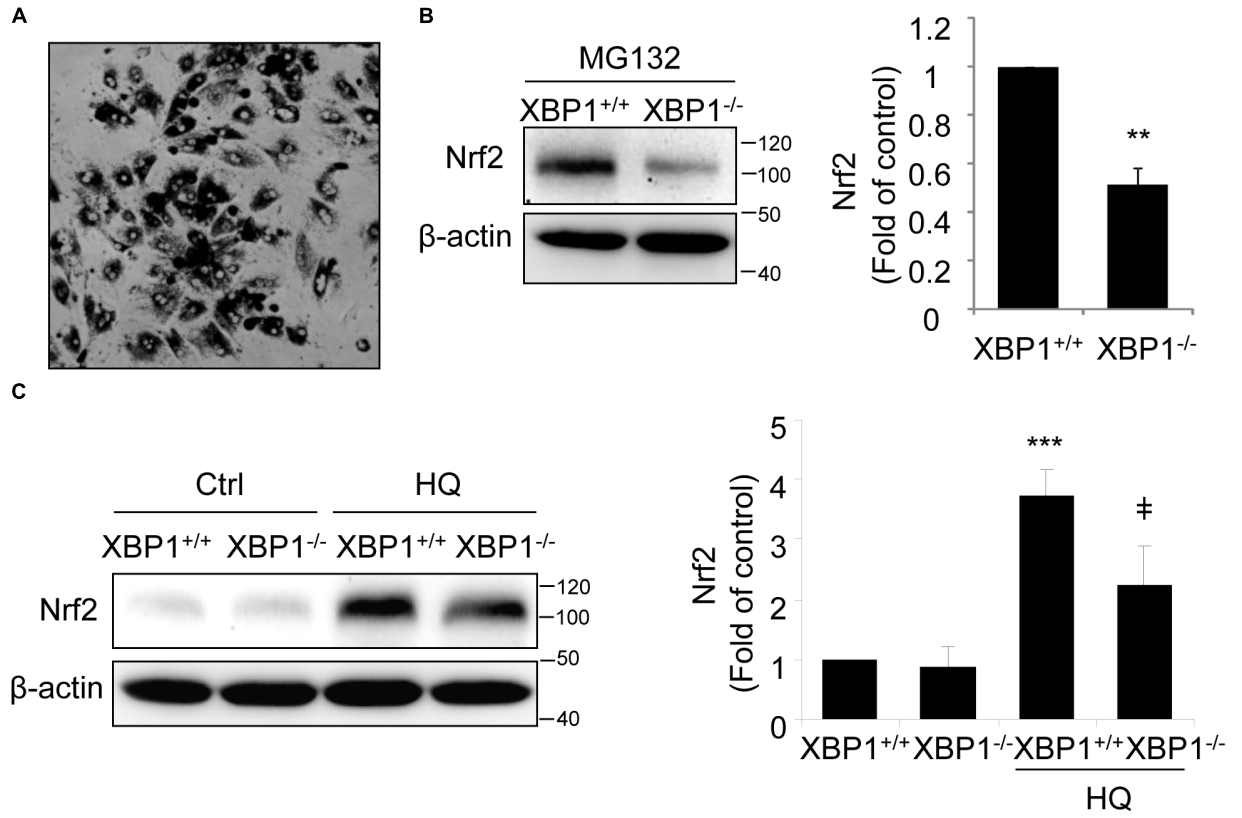

FIGURE 2 | Impaired Nrf2 activation in primary RPE cells isolated from XBP1 KO mice. Primary RPE cells were isolated from WT and KO mice and cultured in a 12-well plate until confluence. **(A)** Phase contrast image of isolated RPE cells. **(B)** After proteasome inhibitor MG132 treatment (10 μM, 30 min), Nrf2 expression in primary RPE cells was detected by Western blot and semi-quantified by densitometry ($n = 3$ independent isolations, $^{**}p < 0.01$). **(C)** Primary RPE cells were treated with a potent pro-oxidant, hydroquinone (HQ) (100 μM, 6 h), and Nrf2 expression was detected by Western blot ($n = 3$ independent isolations; $^{***}p < 0.001$ vs. XBP1$^{+/+}$ untreated control, $^{‡}p < 0.05$ vs. XBP1 $^{+/+}$ cells treated with HQ).

on SOD1 expression levels (**Figure 5B**). Furthermore, neither tBHQ nor QT altered Nrf2 mRNA levels (**Figure 5C**). These results support a post-transcriptional regulation of Nrf2 by XBP1.

Quinotrierixin Suppresses the Basal Expression Levels of Nrf2 but Not the Half-Life

To explore whether QT suppresses Nrf2 expression by accelerating protein degradation, we performed 35S-translabel, pulse-chase experiments in ARPE19 cells to measure the effect of QT on Nrf2 half-life. These studies revealed that the basal levels of Nrf2 were reduced by QT (**Figure 6A**; compare DMSO/DMSO vs. QT/DMSO) whereas the half-life was unchanged (**Figure 6A**; compare DMSO/MG132 vs. QT/MG132). Consistent with these half-life data, we found that the amount of newly synthesized Nrf2 protein (i.e., the amount synthesized in 40 min) was significantly reduced in QT-treated ARPE-19 cells versus control (**Figure 6B**). This reduction in Nrf2 synthesis was observed in both vehicle-treated cells as well as in the presence of MG132, to block proteasome-mediated degradation of the transcription factor (**Figure 6B**). These results indicate that QT reduces the *de novo* synthesis of Nrf2.

Overexpression of *Nrf2* Had No Effect on XBP1 Expression in ARPE-19 Cells

To determine whether Nrf2 reciprocally regulates XBP1 expression, we transduced ARPE-19 cells with an adenovirus to overexpress *Nrf2*. Successful transduction was evidenced by increased expression of the Nrf2 target gene *HO-1* (**Figure 7A**) and enhanced Nrf2 protein level (**Figure 7B**). However, we found that neither total XBP1 nor spliced XBP1 mRNA levels were upregulated in Nrf2 overexpressed cells (**Figure 7A**). The protein levels of unspliced and spliced XBP1 were also unchanged with or without MG132 treatment (**Figures 7B,C**). These data suggest that Nrf2 does not induce XBP1 expression in RPE cells.

Overexpression of *Nrf2* Protects Against Hydroquinone Induced DNA Damage in RPE Cells, but Is Insufficient to Reduce Cell Injury Caused by XBP1-Deficiency

Finally, we tested whether Nrf2 is sufficient to protect RPE cells from oxidative injury and to improve cell survival in *XBP1*-deficient cells. TUNEL staining was employed in this experiment. TUNEL assay detects not only fragmentation of

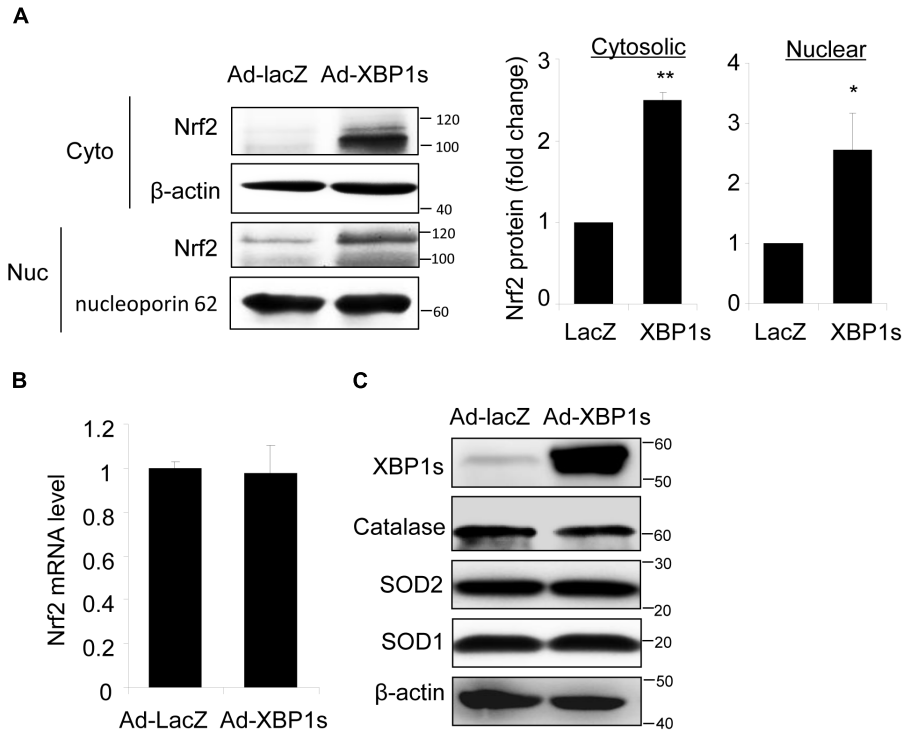

FIGURE 3 | Overexpression of Spliced *XBP1* increased Nrf2 protein level in ARPE-19 cells. ARPE-19 cells were transfected with adenovirus overexpressing spliced *XBP1*. **(A)** Nrf2 expression in the cytosol and nucleus was measured separately by Western blot and semi-quantified by densitometry (mean ± SD, $n = 3$, $^{*}p < 0.05$, $^{**}p < 0.01$). **(B)** Nrf2 mRNA level was detected by real-time PCR (mean ± SD, $n = 3$). **(C)** Protein levels of XBP1, Catalase, SOD2, and SOD1 in whole cell lysate were detected by Western blot analysis.

genomic DNA associated with apoptosis, but also DNA damage associated with non-apoptotic events such as necrotic cell death (Loo, 2002). ARPE-19 cells were transduced with Ad-*Nrf2* or Ad-*LacZ*, and then exposed to HQ. In line with previous findings (Chen et al., 2014), we demonstrated that HQ induced a significant increase in cell DNA fragmentation (**Figure 8A**). Overexpression of *Nrf2* alleviated HQ-induced cell injury (**Figure 8A**). In order to determine whether overexpression of *Nrf2* protects XBP1-deficient cells from oxidant-induced injury, we co-transfected ARPE-19 cells with *XBP1* siRNA and Ad-*Nrf2*. Knockdown efficiency of *XBP1* was shown in **Figure 8B**. Expression of Nrf2 was detected by Western Blot (**Supplementary Figure 1C**). Phase contrast pictures demonstrated that XBP1 deficiency reduced cell viability and increased DNA damage indicated by TUNEL-positive cells (**Supplementary Figure 1A**). Interestingly, overexpression of *Nrf2* did not provide a protective effect in *XBP1* siRNA transfected cells (**Supplementary Figure 1B**). In contrast, pre-treatment of N-Acetylcysteine (NAC), a potent ROS scavenger, effectively reduced HQ-induced DNA fragmentation in *XBP1*-deficient cells (**Figure 8C**). These data indicated that overexpression of Nrf2 is insufficient to compensate the loss of XBP1 in RPE protection against strong pro-oxidants like HQ. The schema of the regulation of Nrf2 by XBP1 in RPE cells was shown in **Figure 8D**.

DISCUSSION

Increasing evidence suggest that the ER play an important role in regulation of cellular response to oxidative stress-induced damage in a variety of tissues and cell types (Cao and Kaufman, 2014). Previous studies from our group and several other laboratories demonstrate that oxidative stress and other genetic and environmental risk factors in AMD pathogenesis increase ER stress and activate the UPR in RPE cells (Cano et al., 2014; Chen et al., 2014; Kunchithapautham et al., 2014; Huang et al., 2015a,b). In cultured RPE cells, inhibition of ER stress or manipulating the UPR decreases ROS generation, reduces apoptosis, and improves cell survival, suggesting that ER stress activates an integrated signaling network governing redox homeostasis and cell survival (Huang et al., 2015b). Nrf2 is a central regulator of cytoprotective genes ubiquitously expressed in a variety of cell types (Tonelli et al., 2017). Expression of Nrf2 was found reduced in degenerating RPE cells in AMD, which leads to intensified oxidative stress and complement activation resulting in RPE injury, while overexpression of *Nrf2* protects against oxidative RPE damage (Cano et al., 2014; Huang et al., 2015b). Thus, understanding the regulation of Nrf2 is critical for developing new treatment to protect the RPE in disease conditions. In the present study, we demonstrate that XBP1, a major effector of the UPR, is required for ER stress- and oxidative stress-induced Nrf2

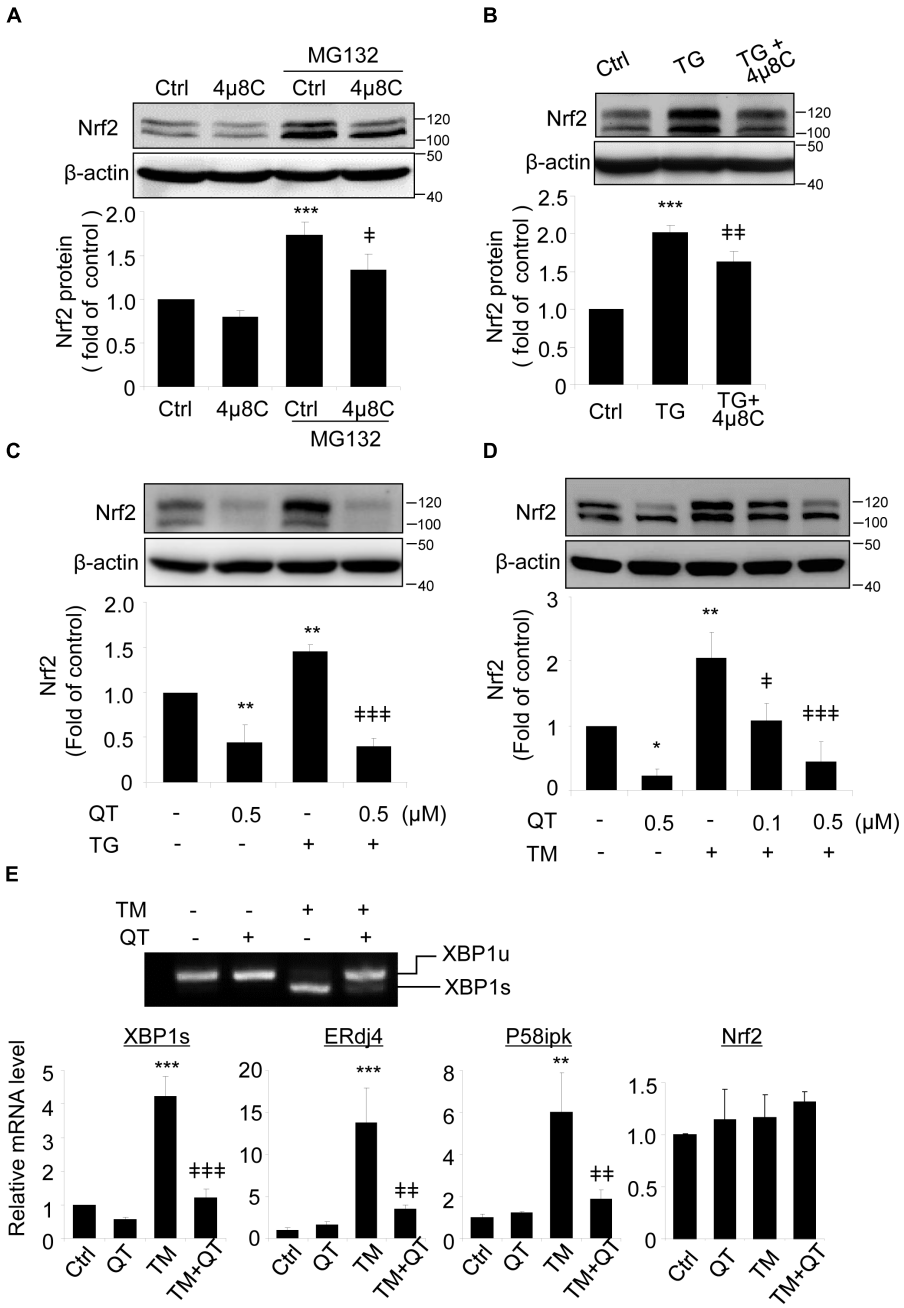

FIGURE 4 | *XBP1* splicing inhibitors reduce Nrf2 expression in ARPE-19 cells. **(A)** ARPE-19 cells were treated with proteasome inhibitor MG132 (10 μM, 20 min) with or without pre-treatment of 4μ8C, an *XBP1* splicing inhibitor (25 μM, 8 h). **(B)** ARPE-19 cells were treated with ER stress inducer thapsigargin (TG) (10 μM) with or without 4μ8C (25 μM) for 8 h. Nrf2 expression was detected by Western blot and semi-quantified by densitometry (mean ± SD, $n = 3$, $^{***}p < 0.001$ vs. control, $^{‡}p < 0.05$, $^{‡‡}p < 0.01$ vs. MG132 or TG treated cells). **(C,D)** ARPE-19 cells were treated with ER stress inducer thapsigargin (TG) (10 μM) or tunicamycin (TM) (50 ng/ml) with or without quinotrierixin (QT) for 8 h, Nrf2 expression was detected by Western blot and semi-quantified by densitometry. **(E)** ARPE-19 cells were treated with TM (50 ng/ml) with or without QT (0.5 μM) for 8 h, *XBP1* splicing was detected by RT-PCR. The levels of spliced XBP1, ERdj4, P58ipk and Nrf2 mRNA were determined by real-time PCR. (mean ± SD, $n = 3$, $^{*}p < 0.05$, $^{**}p < 0.01$, $^{***}p < 0.001$ vs. control, $^{‡}p < 0.05$, $^{‡‡}p < 0.01$, $^{‡‡‡}p < 0.001$ vs. TM or TG treated cells).

upregulation in RPE cells. This finding sheds new light on Nrf2 regulation in the RPE.

In recent years, the transcriptional factor XBP1 has been studied extensively. Various studies have demonstrated that XBP1 has an anti-apoptotic function (Romero-Ramirez et al., 2004; Kaser et al., 2008; Casas-Tinto et al., 2011). In MCF7 cells, XBP1 up-regulates the anti-apoptotic gene Bcl-2 and prevents antiestrogen therapy-induced cell death through inhibition of

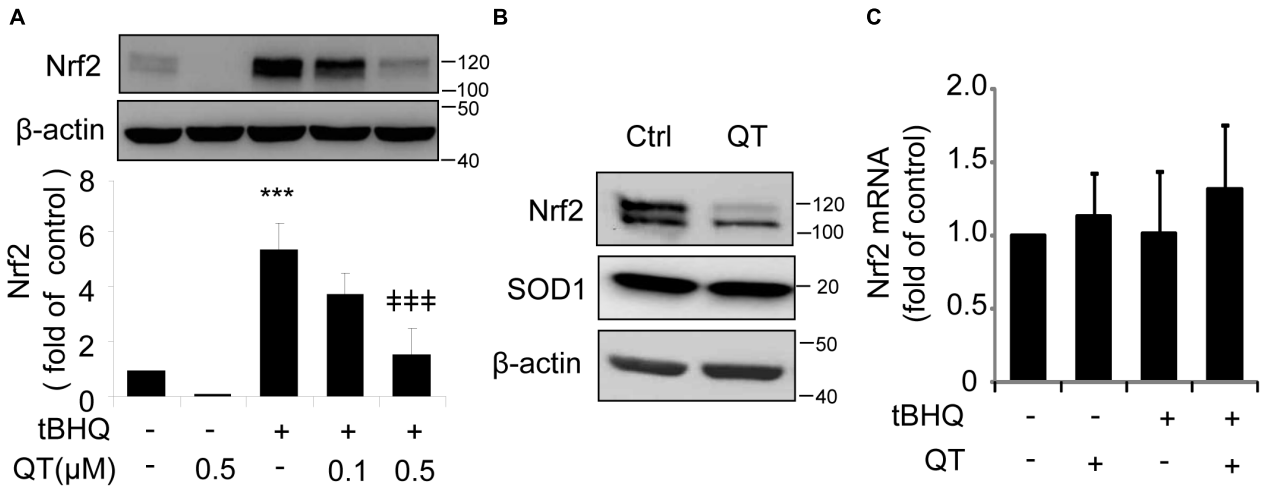

FIGURE 5 | Quinotrierixin abolishes tert-Butylhydroquinone induced Nrf2 upregulation. **(A–C)** ARPE-19 cells were treated with tert-Butylhydroquinone (tBHQ) (10 μM) in the presence or absence of QT for 8 h. Nrf2 and SOD1 protein levels were detected by Western blot analysis **(A,B)** (mean ± SD, $n = 3$, $^{***}p < 0.001$ vs. control, $^{‡‡‡}p < 0.001$ vs. tBHQ treated cells); Nrf2 mRNA level was detected by real-time PCR **(C)**.

the mitochondrial apoptotic pathway (Gomez et al., 2007). In a previous study, we have shown that ablation of XBP1 in the RPE results in decreased expression of Catalase, SOD1, and SOD2, and increased ROS production in RPE-specific *XBP1* KO mice (Zhong et al., 2012). Using this mouse line and primary RPE cells derived from *XBP1* KO mice, we confirmed that loss of XBP1 downregulated expression of Nrf2 and its downstream genes including NQO-1, HO-1, and GST in the RPE. Furthermore, *XBP1*-deficient RPE cells show an impaired response to ER stress and oxidative stress inducers in stimulating Nrf2 protein production, suggesting that XBP1 could function as a critical regulator of cellular stress response in harnessing cytoprotective genes including Nrf2 to maintain the RPE function and survival under stress conditions.

In line with the central role of Nrf2 in anti-oxidant defense, expression of the transcription factor is regulated by sophisticated mechanisms at both transcriptional and post-transcriptional levels (Tonelli et al., 2017). In resting cells, Nrf2 is sequestered by Keap1 forming an inactive complex or targeted for proteasomal degradation (Surh et al., 2008). When challenged by oxidative stress, Nrf2 is stabilized and rapidly translocates into the nucleus to elicit a coordinated antioxidant response (Surh et al., 2008; Li and Kong, 2009). In addition to interacting with Keap1, Nrf2 is a substrate for the ER stress sensor, PKR-like ER kinase (PERK) (Schroder, 2008). Phosphorylation of Nrf2 by PERK disrupts its association with Keap1 resulting in Nrf2 nuclear accumulation and upregulation of antioxidant response genes (Verfaillie et al., 2010). Moreover, CHOP, the pro-apoptotic gene downstream of the PERK/eIF2α UPR pathway, has been reported by us to be essential for Nrf2 upregulation in cigarette smoking extract stimulated RPE cells (Huang et al., 2015b). Regulation of Nrf2 by UPR related genes demonstrate a crosstalk between ER stress and oxidative stress. In the present study, we found that the IRE/XBP1 branch of UPR also regulates Nrf2 expression. The data from our current study suggest that XBP1 activation may increase Nrf2 production via a post-transcriptional mechanism, because neither induction of ER stress nor an oxidative stress that activates XBP1, nor overexpression of spliced *XBP1* (the active form of XBP1), increase Nrf2 mRNA. Interestingly, in contrast to the drastically reduced Nrf2 expression in *XBP1*-null cells, overexpression of spliced *XBP1* only induced a modest but significant increase of Nrf2 protein in the nuclear and cytosolic fractions of RPE cells. Although this effect seems to be specific for Nrf2, i.e., without affecting other anti-oxidant proteins including SOD1, SOD2 and catalase, the discrepancy in the changes indicates the possible involvement of unspliced XBP1 in Nrf2 regulation. Unspliced XBP1 has been reported to be a negative feedback regulator of spliced XBP1 in Hela cells. Unspliced XBP1 forms a complex with spliced XBP1 and mediates rapid dissociation/degradation of the complex, thus shuting off the transcription of target genes during the recovery phase of ER stress (Yoshida et al., 2006). Moreover, unspliced XBP1 itself is a regulator of anti-oxidant genes. In HUVEC cells, overexpression of unspliced XBP1 promotes Nrf2 protein stabilization and nuclear translocation, and subsequent HO-1 induction (Martin et al., 2014). In mouse embryonic fibroblasts (MEFs), overexpression of unspliced XBP1 strongly increased catalase expression. The enhancing effect depends on CCAAT boxes and NF-Y-binding sites, while IRE activation is not necessary (Liu et al., 2009). Whether unspliced XBP1 is in part responsible for maintaining Nrf2 level in stressed RPE remains to be elucidated in future studies.

It is worth noting that although the predicted molecular weight of Nrf2 protein is 55–65 kDa according to its open reading frame size of *2.2-kb, the Nrf2 banding pattern in Western blots varies significantly as reported in the literature (Lau et al., 2013). This variation is thought largely attributable

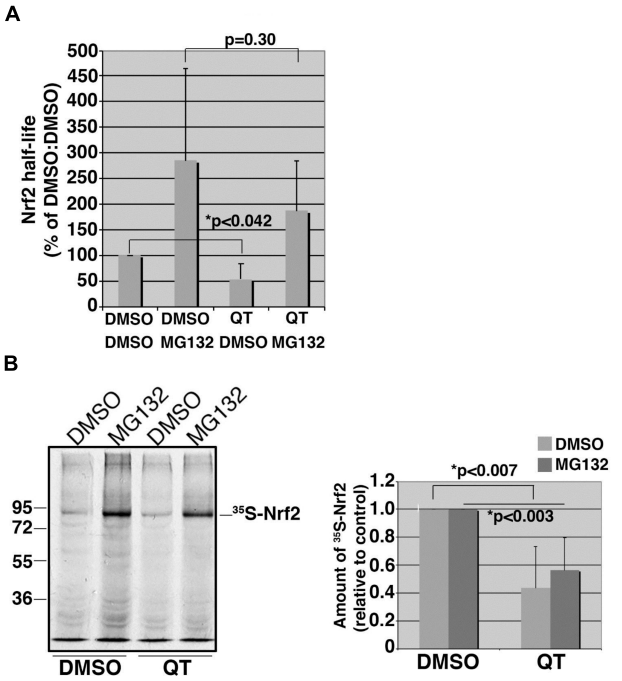

FIGURE 6 | Quinotrierixin suppresses the basal expression levels of Nrf2 but not the half-life. **(A)** Graph of pooled data from three independent 35S-translabel, pulse-chase half-life experiments for endogenous Nrf2, comparing DMSO-treated cells to those treated with QT. Additional treatment with vehicle (DMSO) or MG132 was done to compare stabilized Nrf2. Half-life measurements were calculated using the formula, T1/2 = (t*ln2)/(ln R0–ln Rt), where t = chase time, R0 = band intensity at t0, and Rt = band intensity at t. Two-tailed Student's *t*-test indicates statistically significant difference in the starting amounts of Nrf2 (DMSO/DMSO vs. QT/DMSO) but no difference in half-life (DMSO/MG132 vs. QT/MG132). Asterisks denote statistical significance. **(B)** Representative fluorography showing the amount of endogenous, 35S-labeled Nrf2 stabilized and recovered by immunoprecipitation following an acute treatment with MG132 in cells pretreated with DMSO or QT. The migration of molecular weight markers is shown to the left of the fluorograph. Graph on the right shows data pooled from three independent experiments. Statistical significance was calculated by two-tailed Student's *t*-test using the averages of three independent measurements for each treatment condition. Asterisks denote statistical significance.

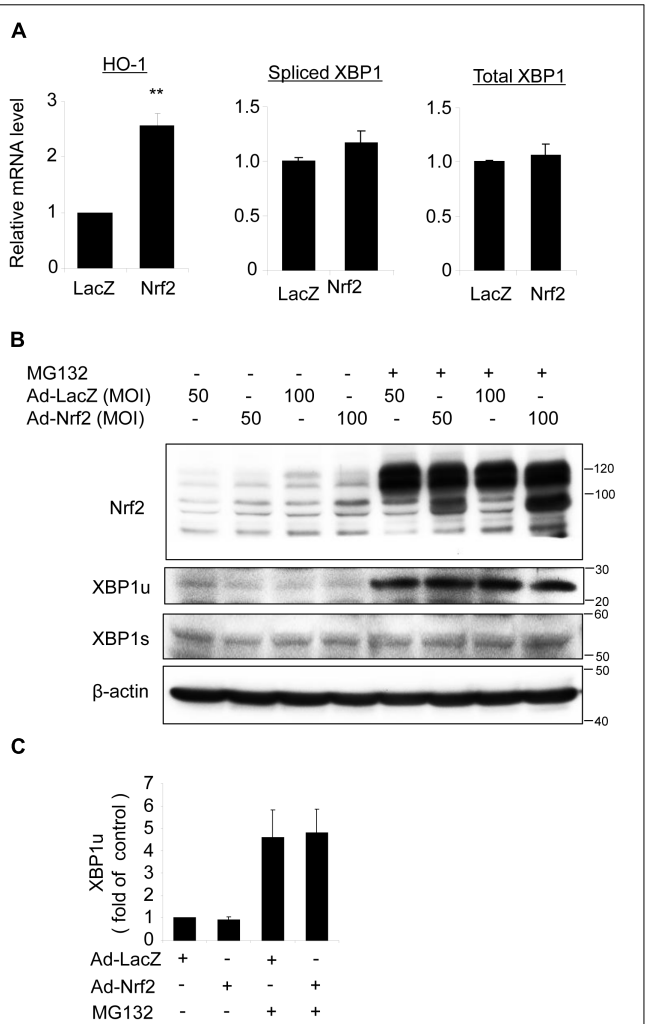

FIGURE 7 | Overexpression of *Nrf2* does not alter XBP1 expression in ARPE-19 cells. **(A)** ARPE-19 cells were transfected with adenovirus overexpressing *Nrf2* or *LacZ* as control for 24 h, mRNA level of HO-1, spliced XBP1 and total XBP1 was determined by real-time RT PCR (mean ± SD, $n = 3$, $^{**}p < 0.01$ vs. ad-LacZ transfected cells). **(B)** ARPE-19 cells were transfected with adenovirus overexpressing *Nrf2* or *LacZ* for 48 h, Nrf2, unspliced XBP1 (XBP1u) and spliced XBP1 (XBP1s) level was detected by Western blot analysis (representative of 3 independent experiments). **(C)** XBP1u expression was semi-quantified by densitometry (mean ± SD, $n = 3$).

to the different degrees of ubiquitination of Nrf2 protein. In our Western Blots with mouse eyecups, tunicamycin-induced Nrf2 band was between 60 and 80 kDa, and this band was used for quantification. However, in cultured primary mouse RPE cells and ARPE-19 cells with chemical activation and adenoviral transduction, Nrf2 bands appeared to migrate to the position of 90–120 kDa. As discussed in detail by Lau et al. (2013), Nrf2 bands at 95–110 kDa should be considered as biologically relevant Nrf2. Therefore, we included the bands within this molecular weight range for Nrf2 quantification.

One of the XBP1 inhibitors used in this study, QT, is a member of the triene-ansamycin group antibiotics. It was first identified by the Tashiro group in 2007, as a specific inhibitor of ER stress-induced XBP1 mRNA splicing (Kawamura et al., 2008a). QT dose-dependently inhibits TG-induced *XBP1* splicing in Hela cells with an IC50 of 0.067 μM (Kawamura et al., 2008b). However, a later study from the same group demonstrated that QT inhibits the protein production of UPR genes, including the 78-kDa glucose-regulated protein (GRP78), C/EBP homologous protein (CHOP), ERdj4 and P58ipk (Yamamoto et al., 2011). In our current study, we found that QT significantly reduced Nrf2 protein levels in non-stimulated RPE cells and blunted the increase of Nrf2 protein induced by ER stress or oxidative stress. Interestingly, QT showed no effect on SOD1 expression in the RPE. Further mechanistic experiments revealed that QT treatment does not seem to alter the transcription or increase

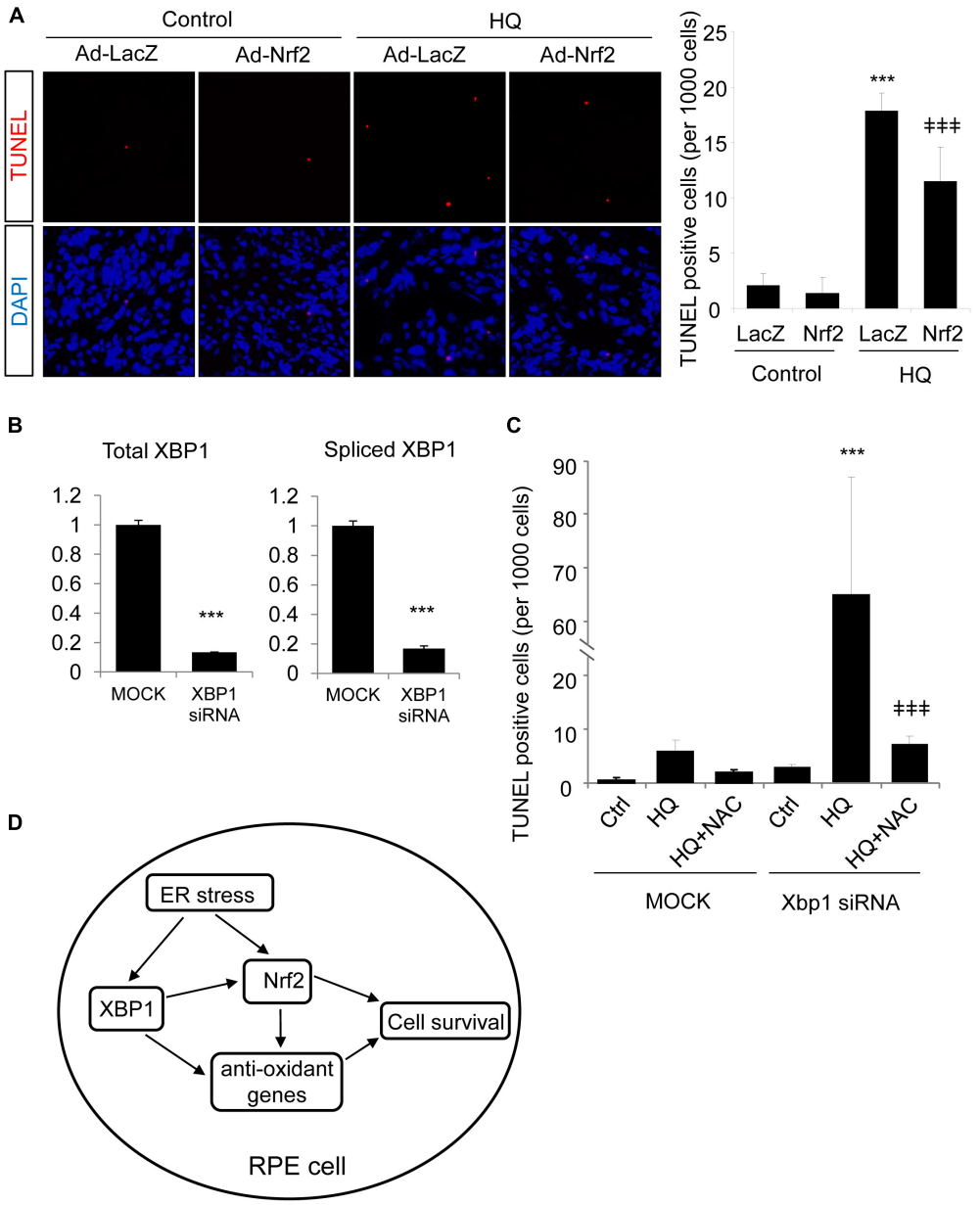

FIGURE 8 | Overexpression of *Nrf2* protects ARPE-19 cells from hydroquinone induced injury. **(A)** ARPE-19 cells were transfected with adenovirus overexpressing *Nrf2* or *LacZ* as control for 24 h, then treated with a potent pro-oxidant, hydroquinone (100 μM, 24 h), for another 24 h. Cell DNA fragmentation was detected by TUNEL assay and quantified by cell counting (mean ± SD, $n = 5$ random 10× microscope field, $^{***}p < 0.001$ vs. control, $^{‡‡‡}p < 0.001$ vs. Ad-*LacZ* transfected cells with HQ treatment). **(B)** ARPE-19 cells were transfected with *XBP1* siRNA or lipofectamine only (Mock) as control for 24 h, XBP1 knockdown efficiency was detected by real-time RT PCR ($^{***}p < 0.001$). **(C)** ARPE-19 cells were transfected with *XBP1* siRNA or lipofectamine only (Mock) as control for 24 h, then treated with hydroquinone (100 μM, 24 h) with or without N-Acetylcysteine (NAC) pre-treatment (1 mM, 2 h). Cell DNA fragmentation was detected by TUNEL assay and quantified by cell counting (mean ± SD, $n = 5$ random 10× microscope field, $^{***}p < 0.001$ vs. untreated *XBP1* siRNA transfected cells, $^{‡‡‡}p < 0.001$ vs. *XBP1* siRNA transfected and HQ treated cells). **(D)** Schema of the regulation of Nrf2 by XBP1 in RPE cells. In the RPE, XBP1 upregulates the expression of Nrf2, promotes cell survival against oxidative stress. Loss of XBP1 leads to compromised Nrf2 synthesis, which promotes cell injury induced by oxidants. Meanwhile, XBP1 also regulates other anti-oxidative genes including Catalase, SOD1 and SOD2, which also contributes to anti-oxidative response of the RPE. Overexpression of *Nrf2* protects RPE cells from oxidants-induced injury, but could not compensate the loss of XBP1 on cell survival during oxidative stress.

protein degradation of Nrf2. Thus, it indicates that likely QT reduces Nrf2 through inhibition of protein synthesis. This finding appears to be consistent with the observations by the Tashiro group. However, whether QT reduces Nrf2 protein translation and how QT selectively inhibits Nrf2 but not other antioxidative proteins are yet to be determined.

Another interesting finding of this study is that overexpression of Nrf2 was not able to rescue *XBP1*-deficient RPE cells

challenged with HQ. One possible explanation is that deprivation of XBP1 negatively influences the expression/function of multiple anti-oxidant genes such as catalase, SOD1, and SOD2 and the consequent reduction in the anti-oxidant capacity leads to increased cell injury when challenged by HQ. Supplementing with additional Nrf2 was also not sufficient to reverse cellular redox disturbance, thus cell injury in *XBP1*-deficient cells was not attenuated. In contrast, pre-treatment of N-Acetylcysteine (NAC) effectively protected cells from HQ-induced injury, suggesting that scavenging ROS can compensate for the loss of XBP1 in the RPE cells, furthering supporting the role of XBP1 in regulating the anti-oxidative response in the RPE.

Taken together, our results demonstrate that in the RPE, XBP1 is required for Nrf2 expression. Deficiency of XBP1 results in a decreased anti-oxidant response that contributes to oxidative injury of the RPE, which is highly relevant to the pathogenesis of AMD.

DATA AVAILABILITY STATEMENT

The raw data supporting the conclusions of this manuscript will be made available by the authors, without undue reservation, to any qualified researcher.

AUTHOR CONTRIBUTIONS

SZ and JW conceived and supervised the experiments, interpreted the data, and wrote the manuscript. QY designed the experiments, participated in experiments, and interpreted the data. CC, YZ, KP, and SP performed the experiments, analyzed the data, and wrote the manuscript. All authors have read and approved the final version of the manuscript.

FUNDING

This work was supported by NIH/NEI grants EY019949 and EY025061, Research Grant M2010088 from American Health Assistance Foundation (Currently Bright Focus Foundation), and an Unrestricted Grant to the Department of Ophthalmology, SUNY-Buffalo, from Research to Prevent Blindness. This work was also supported by National Natural Science Foundation of China (NSFC, Grant No. 81660167).

ACKNOWLEDGMENTS

We thank Dr. David Ron (University of Cambridge Metabolic Research Laboratories and National Institute for Health Research Cambridge Biomedical Research Centre, United Kingdom) for 4μ8C and Dr. Etsu Tashiro (Keio University, Japan) for quinotrierixin.

SUPPLEMENTARY MATERIAL

The Supplementary Material for this article can be found online at: https://www.frontiersin.org/articles/10.3389/fgene.2018.00658/full#supplementary-material

REFERENCES

Augood, C. A., Vingerling, J. R., De Jong, P. T., Chakravarthy, U., Seland, J., Soubrane, G., et al. (2006). Prevalence of age-related maculopathy in older Europeans: the European Eye Study (EUREYE). *Arch. Ophthalmol.* 124, 529–535. doi: 10.1001/archopht.124.4.529

Bressler, N. M. (2004). Age-related macular degeneration is the leading cause of blindness. *JAMA* 291, 1900–1901. doi: 10.1001/jama.291.15.1900

Cai, J., Nelson, K. C., Wu, M., Sternberg, P. Jr., and Jones, D. P. (2000). Oxidative damage and protection of the RPE. *Prog. Retin. Eye Res.* 19, 205–221. doi: 10.1016/S1350-9462(99)00009-9

Cano, M., Wang, L., Wan, J., Barnett, B. P., Ebrahimi, K., Qian, J., et al. (2014). Oxidative stress induces mitochondrial dysfunction and a protective unfolded protein response in RPE cells. *Free Radic. Biol. Med.* 69, 1–14. doi: 10.1016/j.freeradbiomed.2014.01.004

Cao, S. S., and Kaufman, R. J. (2014). Endoplasmic reticulum stress and oxidative stress in cell fate decision and human disease. *Antioxid. Redox Signal.* 21, 396–413. doi: 10.1089/ars.2014.5851

Casas-Tinto, S., Zhang, Y., Sanchez-Garcia, J., Gomez-Velazquez, M., Rincon-Limas, D. E., and Fernandez-Funez, P. (2011). The ER stress factor XBP1s prevents amyloid-beta neurotoxicity. *Hum. Mol. Genet.* 20, 2144–2160. doi: 10.1093/hmg/ddr100

Chen, C., Cano, M., Wang, J. J., Li, J., Huang, C., Yu, Q., et al. (2014). Role of unfolded protein response dysregulation in oxidative injury of retinal pigment epithelial cells. *Antioxid. Redox Signal.* 20, 2091–2106. doi: 10.1089/ars.2013.5240

Cross, B. C., Bond, P. J., Sadowski, P. G., Jha, B. K., Zak, J., Goodman, J. M., et al. (2012). The molecular basis for selective inhibition of unconventional mRNA splicing by an IRE1-binding small molecule. *Proc. Natl. Acad. Sci. U.S.A.* 109, E869–E878. doi: 10.1073/pnas.1115623109

Fu, Y., Tang, M., Fan, Y., Zou, H., Sun, X., and Xu, X. (2012). Anti-apoptotic effects of melatonin in retinal pigment epithelial cells. *Front. Biosci.* 17, 1461–1468. doi: 10.2741/3997

Gao, X., and Talalay, P. (2004). Induction of phase 2 genes by sulforaphane protects retinal pigment epithelial cells against photooxidative damage. *Proc. Natl. Acad. Sci. U.S.A.* 101, 10446–10451. doi: 10.1073/pnas.0403886101

Gibbs, D., Kitamoto, J., and Williams, D. S. (2003). Abnormal phagocytosis by retinal pigmented epithelium that lacks myosin VIIa, the Usher syndrome 1B protein. *Proc. Natl. Acad. Sci. U.S.A.* 100, 6481–6486. doi: 10.1073/pnas.1130432100

Glimcher, L. H. (2010). XBP1: the last two decades. *Ann. Rheum. Dis.* 69(Suppl. 1), i67–i71. doi: 10.1136/ard.2009.119388

Gomez, B. P., Riggins, R. B., Shajahan, A. N., Klimach, U., Wang, A., Crawford, A. C., et al. (2007). Human X-box binding protein-1 confers both estrogen independence and antiestrogen resistance in breast cancer cell lines. *FASEB J.* 21, 4013–4027. doi: 10.1096/fj.06-7990com

Ho, L., Van Leeuwen, R., Witteman, J. C., Van Duijn, C. M., Uitterlinden, A. G., Hofman, A., et al. (2011). Reducing the genetic risk of age-related macular degeneration with dietary antioxidants, zinc, and omega-3 fatty acids: the Rotterdam study. *Arch. Ophthalmol.* 129, 758–766. doi: 10.1001/archophthalmol.2011.141

Hohn, T. J., and Grune, T. (2014). The proteasome and the degradation of oxidized proteins: part III-Redox regulation of the proteasomal system. *Redox Biol.* 2, 388–394. doi: 10.1016/j.redox.2013.12.029

Huang, C., Wang, J. J., Jing, G., Li, J., Jin, C., Yu, Q., et al. (2015a). Erp29 attenuates cigarette smoke extract–induced endoplasmic reticulum stress and mitigates tight junction damage in retinal pigment epithelial cells protective role of ERp29 in RPE cells. *Invest. Ophthalmol. Visual Sci.* 56, 6196–6207. doi: 10.1167/iovs.15-16795

Huang, C., Wang, J. J., Ma, J. H., Jin, C., Yu, Q., and Zhang, S. X. (2015b). Activation of the UPR protects against cigarette smoke-induced RPE apoptosis through up-regulation of Nrf2. *J. Biol. Chem.* 290, 5367–5380. doi: 10.1074/jbc.M114.603738

Itoh, K., Ishii, T., Wakabayashi, N., and Yamamoto, M. (1999). Regulatory mechanisms of cellular response to oxidative stress. *Free Radic. Res.* 31, 319–324. doi: 10.1080/10715769900300881

Kang, K. W., Lee, S. J., and Kim, S. G. (2005). Molecular mechanism of nrf2 activation by oxidative stress. *Antioxid. Redox Signal.* 7, 1664–1673. doi: 10.1089/ars.2005.7.1664

Kaser, A., Lee, A. H., Franke, A., Glickman, J. N., Zeissig, S., Tilg, H., et al. (2008). XBP1 links ER stress to intestinal inflammation and confers genetic risk for human inflammatory bowel disease. *Cell* 134, 743–756. doi: 10.1016/j.cell.2008.07.021

Kaspar, J. W., Niture, S. K., and Jaiswal, A. K. (2009). Nrf2:INrf2 (Keap1) signaling in oxidative stress. *Free Radic. Biol. Med.* 47, 1304–1309. doi: 10.1016/j.freeradbiomed.2009.07.035

Kawamura, T., Tashiro, E., Shindo, K., and Imoto, M. (2008a). SAR study of a novel triene-ansamycin group compound, quinotrierixin, and related compounds, as inhibitors of ER stress-induced XBP1 activation. *J. Antibiot.* 61, 312–317. doi: 10.1038/ja.2008.44

Kawamura, T., Tashiro, E., Yamamoto, K., Shindo, K., and Imoto, M. (2008b). SAR study of a novel triene-ansamycin group compound, quinotrierixin, and related compounds, as inhibitors of ER stress-induced XBP1 activation. *J. Antibiot.* 61, 303–311. doi: 10.1038/ja.2008.43

Kobayashi, A., Kang, M. I., Okawa, H., Ohtsuji, M., Zenke, Y., Chiba, T., et al. (2004). Oxidative stress sensor Keap1 functions as an adaptor for Cul3-based E3 ligase to regulate proteasomal degradation of Nrf2. *Mol. Cell. Biol.* 24, 7130–7139. doi: 10.1128/MCB.24.16.7130-7139.2004

Kobayashi, A., Kang, M. I., Watai, Y., Tong, K. I., Shibata, T., Uchida, K., et al. (2006). Oxidative and electrophilic stresses activate Nrf2 through inhibition of ubiquitination activity of Keap1. *Mol. Cell. Biol.* 26, 221–229. doi: 10.1128/MCB.26.1.221-229.2006

Kunchithapautham, K., Atkinson, C., and Rohrer, B. (2014). Smoke exposure causes endoplasmic reticulum stress and lipid accumulation in retinal pigment epithelium through oxidative stress and complement activation. *J. Biol. Chem.* 289, 14534–14546. doi: 10.1074/jbc.M114.564674

Lau, A., Tian, W., Whitman, S. A., and Zhang, D. D. (2013). The predicted molecular weight of Nrf2: it is what it is not. *Antioxid. Redox Signal.* 18, 91–93. doi: 10.1089/ars.2012.4754

Li, J., Johnson, D., Calkins, M., Wright, L., Svendsen, C., and Johnson, J. (2005). Stabilization of Nrf2 by tBHQ confers protection against oxidative stress-induced cell death in human neural stem cells. *Toxicol. Sci.* 83, 313–328. doi: 10.1093/toxsci/kfi027

Li, W., and Kong, A. N. (2009). Molecular mechanisms of Nrf2-mediated antioxidant response. *Mol. Carcinog.* 48, 91–104. doi: 10.1002/mc.20465

Lin, J. H., Li, H., Yasumura, D., Cohen, H. R., Zhang, C., Panning, B., et al. (2007). IRE1 signaling affects cell fate during the unfolded protein response. *Science* 318, 944–949. doi: 10.1126/science.1146361

Liu, Y., Adachi, M., Zhao, S., Hareyama, M., Koong, A. C., Luo, D., et al. (2009). Preventing oxidative stress: a new role for XBP1. *Cell Death Differ.* 16, 847–857. doi: 10.1038/cdd.2009.14

Loo, D. T. (2002). TUNEL assay. An overview of techniques. *Methods Mol. Biol.* 203, 21–30. doi: 10.1385/1-59259-179-5:21

Ma, J. H., Wang, J. J., Li, J., Pfeffer, B. A., Zhong, Y., and Zhang, S. X. (2016). The role of IRE-XBP1 pathway in regulation of retinal pigment epithelium tight junctions XBP1 regulates the RPE tight junctions. *Invest. Ophthalmol. Vis. Sci.* 57, 5244–5252. doi: 10.1167/iovs.16-19232

Martin, D., Li, Y., Yang, J., Wang, G., Margariti, A., Jiang, Z., et al. (2014). Unspliced X-box-binding protein 1 (XBP1) protects endothelial cells from oxidative stress through interaction with histone deacetylase 3. *J. Biol. Chem.* 289, 30625–30634. doi: 10.1074/jbc.M114.571984

Na, H. K., and Surh, Y. J. (2008). Modulation of Nrf2-mediated antioxidant and detoxifying enzyme induction by the green tea polyphenol EGCG. *Food Chem. Toxicol.* 46, 1271–1278. doi: 10.1016/j.fct.2007.10.006

Nguyen, T., Sherratt, P. J., Nioi, P., Yang, C. S., and Pickett, C. B. (2005). Nrf2 controls constitutive and inducible expression of ARE-driven genes through a dynamic pathway involving nucleocytoplasmic shuttling by Keap1. *J. Biol. Chem.* 280, 32485–32492. doi: 10.1074/jbc.M503074200

Nguyen, T., Sherratt, P. J., and Pickett, C. B. (2003). Regulatory mechanisms controlling gene expression mediated by the antioxidant response element. *Annu. Rev. Pharmacol. Toxicol.* 43, 233–260. doi: 10.1146/annurev.pharmtox.43.100901.140229

Nguyen, T., Yang, C. S., and Pickett, C. B. (2004). The pathways and molecular mechanisms regulating Nrf2 activation in response to chemical stress. *Free Radic. Biol. Med.* 37, 433–441. doi: 10.1016/j.freeradbiomed.2004.04.033

Niture, S. K., Kaspar, J. W., Shen, J., and Jaiswal, A. K. (2010). Nrf2 signaling and cell survival. *Toxicol. Appl. Pharmacol.* 244, 37–42. doi: 10.1016/j.taap.2009.06.009

Plafker, K. S., Nguyen, L., Barneche, M., Mirza, S., Crawford, D., and Plafker, S. M. (2010). The ubiquitin-conjugating enzyme UbcM2 can regulate the stability and activity of the antioxidant transcription factor Nrf2. *J. Biol. Chem.* 285, 23064–23074. doi: 10.1074/jbc.M110.121913

Rabin, D. M., Rabin, R. L., Blenkinsop, T. A., Temple, S., and Stern, J. H. (2013). Chronic oxidative stress upregulates Drusen-related protein expression in adult human RPE stem cell-derived RPE cells: a novel culture model for dry AMD. *Aging* 5, 51–66. doi: 10.18632/aging.100516

Romero-Ramirez, L., Cao, H., Nelson, D., Hammond, E., Lee, A. H., Yoshida, H., et al. (2004). XBP1 is essential for survival under hypoxic conditions and is required for tumor growth. *Cancer Res.* 64, 5943–5947. doi: 10.1158/0008-5472.CAN-04-1606

Schroder, M. (2008). Endoplasmic reticulum stress responses. *Cell Mol. Life. Sci.* 65, 862–894. doi: 10.1007/s00018-007-7383-5

Seko, Y., Pang, J., Tokoro, T., Ichinose, S., and Mochizuki, M. (2001). Blue light-induced apoptosis in cultured retinal pigment epithelium cells of the rat. *Graefes Arch. Clin. Exp. Ophthalmol.* 239, 47–52. doi: 10.1007/s004170000220

Shamsi, F. A., and Boulton, M. (2001). Inhibition of RPE lysosomal and antioxidant activity by the age pigment lipofuscin. *Invest. Ophthalmol. Vis. Sci.* 42, 3041–3046.

Strauss, O. (2005). The retinal pigment epithelium in visual function. *Physiol. Rev.* 85, 845–881. doi: 10.1152/physrev.00021.2004

Surh, Y. J., Kundu, J. K., and Na, H. K. (2008). Nrf2 as a master redox switch in turning on the cellular signaling involved in the induction of cytoprotective genes by some chemopreventive phytochemicals. *Planta Med.* 74, 1526–1539. doi: 10.1055/s-0028-1088302

Tan, J. S., Wang, J. J., Flood, V., Rochtchina, E., Smith, W., and Mitchell, P. (2008). Dietary antioxidants and the long-term incidence of age-related macular degeneration: the Blue Mountains Eye Study. *Ophthalmology* 115, 334–341. doi: 10.1016/j.ophtha.2007.03.083

Thurman, J. M., Renner, B., Kunchithapautham, K., Ferreira, V. P., Pangburn, M. K., Ablonczy, Z., et al. (2009). Oxidative stress renders retinal pigment epithelial cells susceptible to complement-mediated injury. *J. Biol. Chem.* 284, 16939–16947. doi: 10.1074/jbc.M808166200

Tonelli, C., Chio, I. I. C., and Tuveson, D. A. (2017). Transcriptional Regulation by Nrf2. *Antioxid. Redox Signal.* 29, 1727–1745. doi: 10.1089/ars.2017.7342

Verfaillie, T., Salazar, M., Velasco, G., and Agostinis, P. (2010). Linking ER stress to autophagy: potential implications for cancer therapy. *Int. J. Cell Biol.* 2010:930509. doi: 10.1155/2010/930509

Yamamoto, K., Tashiro, E., and Imoto, M. (2011). Quinotrierixin inhibited ER stress-induced XBP1 mRNA splicing through inhibition of protein synthesis. *Biosci. Biotechnol. Biochem.* 75, 284–288. doi: 10.1271/bbb.100622

Yoshida, H., Oku, M., Suzuki, M., and Mori, K. (2006). pXBP1(U) encoded in XBP1 pre-mRNA negatively regulates unfolded protein response activator pXBP1(S) in mammalian ER stress response. *J. Cell Biol.* 172, 565–575. doi: 10.1083/jcb.200508145

Zhao, Z., Chen, Y., Wang, J., Sternberg, P., Freeman, M. L., Grossniklaus, H. E., et al. (2011). Age-related retinopathy in NRF2-deficient mice. *PLoS One* 6:e19456. doi: 10.1371/journal.pone.0019456

Zhong, Y., Li, J., Wang, J. J., Chen, C., Tran, J. T., Saadi, A., et al. (2012). X-box binding protein 1 is essential for the anti-oxidant defense and cell survival in the retinal pigment epithelium. *PLoS One* 7:e38616. doi: 10.1371/journal.pone.0038616

Conflict of Interest Statement: The authors declare that the research was conducted in the absence of any commercial or financial relationships that could be construed as a potential conflict of interest.

frontiers in Neuroscience

MINI REVIEW
published: 09 January 2019
doi: 10.3389/fnins.2018.01014

Impact of Traumatic Brain Injury on Neurogenesis

Laura B. Ngwenya[1,2,3] *and Steve C. Danzer*[4,5,6,7]*

[1] Department of Neurosurgery, University of Cincinnati, Cincinnati, OH, United States, [2] Department of Neurology and Rehabilitation Medicine, University of Cincinnati, Cincinnati, OH, United States, [3] Neurotrauma Center, University of Cincinnati Gardner Neuroscience Institute, Cincinnati, OH, United States, [4] Department of Anesthesia, Cincinnati Children's Hospital Medical Center, Cincinnati, OH, United States, [5] Department of Anesthesia, University of Cincinnati, Cincinnati, OH, United States, [6] Center for Pediatric Neuroscience, Cincinnati Children's Hospital Medical Center, Cincinnati, OH, United States, [7] Department of Pediatrics, University of Cincinnati, Cincinnati, OH, United States

New neurons are generated in the hippocampal dentate gyrus from early development through adulthood. Progenitor cells and immature granule cells in the subgranular zone are responsive to changes in their environment; and indeed, a large body of research indicates that neuronal interactions and the dentate gyrus milieu regulates granule cell proliferation, maturation, and integration. Following traumatic brain injury (TBI), these interactions are dramatically altered. In addition to cell losses from injury and neurotransmitter dysfunction, patients often show electroencephalographic evidence of cortical spreading depolarizations and seizure activity after TBI. Furthermore, treatment for TBI often involves interventions that alter hippocampal function such as sedative medications, neuromodulating agents, and anti-epileptic drugs. Here, we review hippocampal changes after TBI and how they impact the coordinated process of granule cell adult neurogenesis. We also discuss clinical TBI treatments that have the potential to alter neurogenesis. A thorough understanding of the impact that TBI has on neurogenesis will ultimately be needed to begin to design novel therapeutics to promote recovery.

Keywords: epilepsy, traumatic brain injury, anesthetic neurotoxicity, spreading depolarization (SD), dentate gyrus, adult neurogeneses, granule cell

OPEN ACCESS

Edited by:
Nan-Jie Xu,
Shanghai Jiao Tong University, China

Reviewed by:
Diane Lagace,
University of Ottawa, Canada
Kinichi Nakashima,
Kyushu University, Japan
Vijayalakshmi Santhakumar,
Rutgers New Jersey Medical School, United States

***Correspondence:**
Steve C. Danzer
steve.danzer@cchmc.org

Specialty section:
This article was submitted to Neurogenesis, a section of the journal Frontiers in Neuroscience

Received: *14 August 2018*
Accepted: *17 December 2018*
Published: *09 January 2019*

Citation:
Ngwenya LB and Danzer SC (2019) Impact of Traumatic Brain Injury on Neurogenesis. Front. Neurosci. 12:1014. doi: 10.3389/fnins.2018.01014

INTRODUCTION

Adult neurogenesis in the hippocampal dentate gyrus is widespread in mammals. Generation of dentate granule cells occurs late in embryonic development, continues after birth, and persists into old age in most mammals examined (Amrein et al., 2011; Amrein, 2015; Ngwenya et al., 2015). Studies in rodents indicate that adult generated granule cells play a role in hippocampal dependent learning (Nakashiba et al., 2012; Danielson et al., 2016; Johnston et al., 2016). Whether neurogenesis continues into old age in humans remains controversial (Danzer, 2018a), with studies finding evidence for (Eriksson et al., 1998; Spalding et al., 2013; Boldrini et al., 2018) and against ongoing neurogenesis (Sorrells et al., 2018). Yet there is general agreement that dentate neurogenesis occurs in childhood and continues throughout young adulthood in humans, and that newly-generated neurons are poised to contribute to hippocampal function. At a minimum, therefore, traumatic brain injuries (TBIs) occurring during adolescence have the potential to disrupt this important process.

The generation, maturation, and integration of new neurons is critical for hippocampal function. This tightly regulated process, however, is easily disrupted by pathological events, such as TBI. In this review, we discuss the coordinated process of adult neurogenesis in the hippocampal subgranular zone (SGZ) and the impact that TBI and TBI treatments have on this process. An understanding of the regulation and dysregulation of neurogenesis is important for determining whether and how therapeutic interventions targeted at adult neurogenesis are useful for TBI treatment.

NEUROGENESIS IS A COMPLEX, TIGHTLY-REGULATED PROCESS

Adult neurogenesis is characterized by multiple "control" points. The number of daughter cells produced by neural stem cells (NSC) located in the SGZ of the dentate gyrus can be modulated by the rate of cell proliferation and survival, while factors regulating fate specification control whether and how the new cells become neurons and integrate into the hippocampal circuitry (see recent review by Song et al., 2016). These control points can be regulated by signals released into the extracellular milieu by both neuronal and non-neuronal cells (Alenina and Klempin, 2015; Egeland et al., 2015), neurotrophic and transcription factors (Faigle and Song, 2013; Goncalves et al., 2016), neuroinflammatory mediators (Belarbi and Rosi, 2013), metabolic and hormonal changes (Cavallucci et al., 2016; Larson, 2018), and direct synaptic input from both glutamatergic and GABAergic neurons (Chancey et al., 2014; Alvarez et al., 2016; Song et al., 2016; Yeh et al., 2018). For additional information, the readers are referred to the excellent reviews cited for each mechanism, and the schematic in **Figure 1**. Critically, all of these factors can be disrupted by TBI, creating an environment in which immature granule cells and granule cell progenitors no longer receive the proper cues to guide their development.

NEUROGENESIS IS DISRUPTED AFTER TRAUMATIC BRAIN INJURY

Traumatic brain injury is particularly disruptive to the hippocampus due to its disparate pathomechanisms. Clinically, TBIs are classified as mild, moderate, or severe, however, the impact of TBI can include a variety of pathologies that are not sufficiently explained by clinical severity (Saatman et al., 2008). TBI can result from direct impacts or inertial forces. Pathologies include focal hemorrhage and contusions, diffuse pathology such as shear injury, and the myriad of pathoanatomic components seen in blast injury (Rosenfeld et al., 2013). Most human TBI involves a combination of forces and pathologies, and a variety of experimental TBI models exist to mimic these pathologies (Xiong et al., 2013). While not all TBIs directly involve the hippocampus, the structure nonetheless often exhibits signs of injury. For example, in the controlled cortical impact (CCI) model, which produces a focal cortical injury, cell death is apparent in the hippocampal dentate gyrus (Anderson et al., 2005). The contralateral hippocampus, remote from the injury site, can also show hippocampal injury and increased excitability after lateral fluid percussion injury (LFPI) (Tran et al., 2006). Involvement of the hippocampus raises the possibility that adult neurogenesis will be impacted.

Granule cell proliferation, survival, differentiation and maturation are impacted by TBI. Cells in the SGZ and inner granule cell layer undergo acute cell death after experimental CCI (Gao et al., 2008). In addition, however, TBI can also increase cell proliferation and neurogenesis (Dash et al., 2001; Chirumamilla et al., 2002; Urrea et al., 2007; Gao et al., 2009). Variable impacts on neurogenesis may reflect differences in injury severity (Wang et al., 2016). Notably, while there is speculation that increased neurogenesis may be beneficial (Rolfe and Sun, 2015), studies indicate that dentate gyrus neural progenitor cells are only capable of undergoing a finite number of replicative cycles before they terminally differentiate and become post-mitotic, ultimately depleting the regenerative pool (Encinas and Sierra, 2012; Neuberger et al., 2017).

Beneficial and pathological effects are also evident among the newly-integrated granule cells themselves. Inhibiting neurogenesis after CCI in mice (Blaiss et al., 2011) or after LFPI in rats (Sun et al., 2015) impairs spatial learning and cognitive recovery, suggesting that the new cells have positive effects. Consistent with this interpretation, treatment with growth differentiation factor 5 after CCI in mice was associated with increased neurogenesis and improved recovery (Wu et al., 2018). Similarly, optogenetic depolarization of immature granule cells and granule cell progenitors after LFPI in mice enhanced cell survival and maturation, while simultaneously improving cognitive measures (Zhao et al., 2018). However, while the axons of granule cells generated after LFPI follow the normal trajectory into the CA3 pyramidal cell layer (Emery et al., 2005; Sun et al., 2007), the cells can also exhibit morphological and physiological abnormalities. Following CCI, for example, newborn cells in mice exhibit abnormal dendritic branching (Villasana et al., 2015). Similarly, newborn granule cells in the LFPI model developed aberrant, hilar-projecting basal dendrites (Robinson et al., 2016). These newborn neurons also become ectopically localized to the dentate hilus (Robinson et al., 2016; Shapiro, 2017) or migrate too far into the granule cell layer (Ibrahim et al., 2016; Ngwenya et al., 2018). In line with the interpretation that neurogenesis can be pathological, treatment with a VEGFR2 antagonist after LFPI in rats suppressed injury-induced neurogenesis and prevented increases in seizure susceptibility (Neuberger et al., 2017), while treatment with the mTOR antagonist rapamycin after CCI in mice reduced neurogenesis, attenuated morphological abnormalities, and reduced seizure incidence (Butler et al., 2015). Hence, neurogenesis after TBI may produce a complex set of beneficial and pathological changes.

INFLUENCE OF ABNORMAL ELECTRICAL ACTIVITY AFTER TBI

It has recently been shown that part of the pathophysiology after TBI is the occurrence of spreading depolarizations (SD).

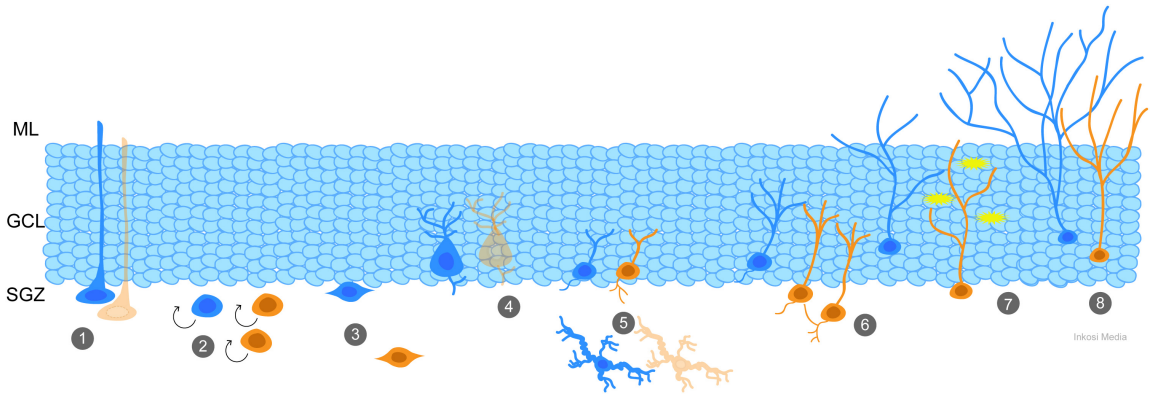

FIGURE 1 | Generation and integration of adult-born granule cells is a coordinated process that is impacted by TBI. At each stage of adult neurogenesis, the normal process (blue) has potential to be altered by TBI (orange). (1) Quiescent radial neural stem cells (NSCs) in the subgranular zone (SGZ) can be depleted by frequent activation early in life, such as by TBI-induced seizures, leading to deficiencies with age. (2) TBI and its effects, including spreading depolarizations and seizures, cause an increase in proliferation of progenitor cells. (3) Newly-generated neurons migrate from the SGZ to the granule cell layer (GCL), and after TBI abnormal hilar migration is apparent. (4) Parvalbumin interneurons and (5) mossy hilar neurons are susceptible to cell death after TBI. Reduction in their numbers results in decreased GABAergic and glutamatergic (respectively) input to the newly-generated neurons. Newly-generated neurons show additional signs of aberrant neurogenesis such as abnormal connectivity (6), hyperexcitability (7) and inappropriate integration and dendritic maturity (8) which can be caused by changes in the environmental milieu.

SDs are characterized by a massive wave of neuronal and glial depolarization that travels at 2–5 mm/min and is followed by electrical silence as neurons become temporarily refractory (Hartings et al., 2017). In patients with TBI, SDs are a predictor of mortality (Hartings et al., 2011) and are often the last electrical signal present in the brain just prior to death (Dreier et al., 2018). Their occurrence in migraine, however, suggests that the waves themselves can be relatively benign (Dreier et al., 2015). Studies have shown that this abnormal electrical activity causes an increase in neurogenesis (Urbach et al., 2008, 2016), the effects of which are currently unknown.

Acute seizures often occur immediately after TBI as a direct result of the traumatic force, and seizures are known to disrupt neurogenesis. Indeed, even a single, isolated seizure in a healthy animal is sufficient to increase granule cell neurogenesis (Bengzon et al., 1997). Seizures also disrupt granule cell integration, causing synaptic alterations (Jackson et al., 2012), abnormalities in dendritic structure (Murphy et al., 2012), migration defects and aberrant circuit formation (Scharfman et al., 2003; Parent et al., 2006; Jessberger et al., 2007b; Danzer, 2018b). In epileptic animals, seizure frequency is positively correlated with the frequency of abnormal, newborn granule cells (Hester and Danzer, 2013), suggesting that the number of seizures that occur following TBI is likely an important predictor of the degree of granule cell disruption.

TBI INDUCED CHANGES TO DENTATE GYRUS CIRCUITRY

In addition to seizure-induced cell death, direct effects of TBI and its immediate sequela can also cause death of key cellular components (Kharatishvili et al., 2006). Massive extracellular increases in glutamate follow TBI (McGuire et al., 2018), for example, and can cause excitotoxic injury. A wide variety of neurons are vulnerable. Dentate hilar neuron loss has been demonstrated after LFPI (Lowenstein et al., 1992; Grady et al., 2003) and includes parvalbumin positive, cholecystokinin positive, and GluR2/3 positive cells (Toth et al., 1997). Decreased parvalbumin immunoreactivity, for example, has been observed in the dentate following LFPI in rats (Huusko et al., 2015; Zhang et al., 2018) while time-dependent, interneuron-subtype specific changes have been described following diffuse TBI in rats (Carron et al., 2018). An observed reduction in spontaneous inhibitory post-synaptic current (sIPSC) frequency among mature granule cells months after LFPI suggests these changes have functional consequences (Pavlov et al., 2011), although impacts are temporally complex, as increases in sIPSC frequency have also been observed in granule cells after acute LFPI (Toth et al., 1997; Santhakumar et al., 2001; Gupta et al., 2012). Importantly, parvalbumin positive interneurons play key roles in regulating neurogenesis (Song et al., 2012, 2013) and their loss is likely to disrupt the process.

Glutamatergic mossy cells located in the dentate hilus are also extremely vulnerable to injury, including following TBI and seizures (Toth et al., 1997; Kienzler et al., 2009; Scharfman, 2016). Moreover, in the LFPI model, mossy cells that survive the insult are hyperexcitable (Santhakumar et al., 2000). Mossy cells directly excite granule cells, and are the first glutamatergic input to adult-generated granule cells (Chancey et al., 2014). The role of mossy cells is complex, however, as the neurons also indirectly inhibit granule cells by activating inhibitory interneurons which innervate granule cells (Scharfman, 2016). Both the direct glutamatergic and indirect GABAergic pathways have been shown to play a critical role in regulating granule cell neurogenesis (Yeh et al., 2018), so mossy cell loss and hyperexcitability following TBI will impact neurogenesis.

In addition to changes in local circuit neurons, TBI-induced changes in granule cell neurogenesis itself may exert effects on subsequent rounds of neurogenesis. Adult-generated granule cells transition through a distinct critical period during which they provide robust excitatory input to CA3 pyramidal cells, but only modest input to local circuit neurons mediating feedback inhibition (Temprana et al., 2015). As the cells mature, they integrate into and robustly activate inhibitory circuits within the dentate (Drew et al., 2016). The size of the newborn granule cell population at a distinct time point, therefore, may alter the development and integration of both more mature and less mature cohorts of granule cells. Taken together, therefore, newborn granule cell integration following TBI may reflect a complex interplay among disrupted circuits caused by interneuron loss, mossy cell loss and the size of previously-generated granule cell populations.

THE EFFECT OF TBI INTERVENTIONS

Clinical TBI interventions include a range of medically necessary and lifesaving measures, including surgery, anesthesia and treatment with neuroactive drugs to enhance care and recovery. Given the exquisite sensitivity of granule cell progenitors and immature granule cells to changes in the surrounding environment, these medications have the potential to exert both positive and negative effects on neurogenesis.

Anesthetic agents are a necessary part of clinical TBI treatment, yet they can have deleterious effects on NSCs and immature neurons. Studies in animal models demonstrate that clinically relevant doses of isoflurane induce neuronal apoptosis among newly-generated granule cells, with vulnerability peaking when the cells are about 2 weeks old (Hofacer et al., 2013; Jiang et al., 2016). This roughly corresponds to the period during which many newborn cells undergo natural apoptosis, suggesting that the anesthetic may artificially enhance the process (Deng et al., 2014; Lin et al., 2017).

Propofol, one of the most commonly used intravenous anesthetics in adult patients in both the operating room and the intensive care unit, has deleterious effects on adult neurogenesis. In the early postnatal period in rodents, propofol decreases the total number of granule cells and promotes dendritic spine loss (Huang J. et al., 2016). In adult animals, propofol impairs the maturation and differentiation of adult-born granule cells (Krzisch et al., 2013). After CCI, propofol attenuates the post-traumatic increase in adult neurogenesis and may contribute to cognitive impairment (Thal et al., 2014), although whether reduced neurogenesis and impaired cognition are mechanistically related in this model is not known.

Ketamine is a dissociative anesthetic whose impact on neuronal function is unresolved, yet has seen a recent resurgence in clinical use after TBI (Chang et al., 2013; Oddo et al., 2016). As an NMDA receptor antagonist, ketamine has been associated with both neurotoxic (Slikker et al., 2007; Yan and Jiang, 2014; Wang et al., 2017) and neuroprotective (Yan and Jiang, 2014; Bell, 2017) effects. The effect of ketamine on hippocampal neurogenesis is similarly mixed with evidence that ketamine interferes with proliferation of NSCs, but enhances neuronal differentiation (Huang H. et al., 2016; Soumier et al., 2016). The disparate effects appear dependent on timing and length of drug administration. After CCI, ketamine increased cell proliferation in the SGZ, decreased the number of newborn neurons, and ameliorated post-CCI cognitive deficits (Peters et al., 2018) suggesting that despite neurotoxic concerns, there may be beneficial effects. Indeed, ketamine is being evaluated as a promising therapy to halt SDs after TBI (Carlson et al., 2018; Hartings et al., 2018). As with propofol, the causal relationship between reduced neurogenesis and altered recovery has not been established. Moreover, the observation that propofol reduces neurogenesis and impairs cognition – while ketamine reduces neurogenesis and improves cognition – indicates that these associations should be interpreted cautiously.

Due to the occurrence of seizures following TBI, a variety of anti-epileptic drugs have been tried as potential therapies. Anti-epileptic drugs, however, often act by similar mechanisms as anesthetics, and can also induce apoptosis (Forcelli et al., 2011, 2012) and behavioral deficits (Gutherz et al., 2014) in young rodents. However, not all anti-epileptics have deleterious effects. Typical anti-epileptics phenobarbital and phenytoin have high side-effect profiles and are known to be pro-apoptotic (Bittigau et al., 2002), yet levetiracetam, a newer anti-epileptic medication that is being used with increased frequency in TBI patients (Jones et al., 2008; Szaflarski et al., 2010), may exert its effects by suppressing aberrant neurogenesis. For example, Sugaya et al. (2010) demonstrate in an animal model of status epilepticus that levetiracetam decreases the percentage of abnormally migrated hilar neurons. Levetiracetam has been shown to exert its effects on cell proliferation and neuronal differentiation by activation of the PI3/Akt pathway (Yan et al., 2018). Valproic acid, another commonly used anti-epileptic, also inhibits aberrant neurogenesis and induces neuronal differentiation. However, the mechanism of valproic acid may be through a PI3/Akt mediated epigenetic modification (Jessberger et al., 2007a; Zhang et al., 2017). This suggests that beyond suppression of seizures there may be a beneficial effect of certain anti-epileptic medications for patients with TBI.

Depression is a common post-TBI disturbance that is often treated with neuroactive medication. Post-TBI depression is generally managed with selective serotonin reuptake inhibitors (SSRIs), despite only minimal evidence of their efficacy in TBI (Yue et al., 2017; Kreitzer et al., 2018). It is suggested that there may be a causative relationship between depression and dysfunctional adult neurogenesis, with antidepressant medications exhibiting their effects via increases in neurogenesis (Santarelli et al., 2003; Eisch and Petrik, 2012; Yun et al., 2016). Chronic administration of the antidepressant medication fluoxetine increases NSC proliferation in the hippocampus (Malberg et al., 2000), however sertraline, another commonly used SSRI, appears to affect neuronal differentiation rather than proliferation (Peng et al., 2012). Antidepressant medications have also been shown to influence hippocampal neuronal plasticity by modulating dendritic spines (McAvoy et al., 2015), neurotrophic receptors (Rantamaki et al., 2007), and signaling cascades (Pilar-Cuellar et al., 2013) – all of which could impact

neurogenesis. Finally, experimental TBI studies have shown increases in neurogenesis after administration of antidepressants, with varying effects on cognitive recovery (Han et al., 2011; Wang et al., 2011). These results suggest that the effects of antidepressants may extend beyond the treatment of depression. However, the timing of administration relative to the injury, the maturational state of adult-born granule cells potentially affected by the treatment, and whether the new cells are exerting net beneficial or pathological effects may all be important variables. Currently, there is insufficient data to determine when during the temporal sequence of events an intervention such as an SSRI might be most beneficial.

CONCLUSION

Adult granule cell neurogenesis is exquisitely regulated by synaptic and extrasynaptic factors that can be directly impacted by TBI and TBI treatments. The process of neurogenesis includes proliferation, survival, maturation and functional integration. Just as each step of the process is regulated by ongoing activity in the neurogenic niche, changes in neurotransmission, electrical activity, and death of supporting cells can disrupt this process (**Figure 1**). The initial injury disrupts transmitter levels, and produces drastic changes in neuronal activity, including spreading depolarizations and seizures. The injury can also impair the function or induce the outright death of critical neuron populations providing input to new granule cells. Furthermore, exposure to anesthetic agents and other medically essential drugs alters the signals received by immature granule cells, and may have untoward effects on their survival or development. As it is becoming increasingly recognized that adult neurogenesis is an important component of TBI and cognitive recovery, disruption of this process has significant implications. Nonetheless, there does not appear to be a simple relationship between increased or decreased neurogenesis and improved or impaired recovery. Critical factors likely include the nature of the injury, the agent that alters neurogenesis, the timing of intervention, the sequence of the neurogenic process that is altered (e.g., proliferation vs. survival) and whether the new cells integrate into the hippocampal circuit in ways that are beneficial (improved cognition) or pathological (pro-epileptogenic). Despite these challenges, studies strongly suggest that neurogenesis is playing an important role in TBI, and therefore an understanding of how TBI and its interventions disrupt neurogenesis will be critical to guide the development of novel therapeutic approaches.

AUTHOR CONTRIBUTIONS

LN contributed to writing the manuscript and preparing the figures. SD contributed to writing the manuscript and preparing the figures.

FUNDING

This work was supported by grants from the National Institute of Neurological Disorders and Stroke (SD, Awards R01NS065020 and R01NS062806), the University of Cincinnati Gardner Neuroscience Institute Neurobiology Research Center (LN), and the Local Initiative for Excellence Foundation, Cincinnati, OH (LN).

ACKNOWLEDGMENTS

We would like to thank Keri Kaeding for useful comments on this manuscript, and Inkosi Media, LLC for assistance with figure design and creation.

REFERENCES

Alenina, N., and Klempin, F. (2015). The role of serotonin in adult hippocampal neurogenesis. *Behav. Brain Res.* 277, 49–57. doi: 10.1016/j.bbr.2014.07.038

Alvarez, D. D., Giacomini, D., Yang, S. M., Trinchero, M. F., Temprana, S. G., Buttner, K. A., et al. (2016). A disynaptic feedback network activated by experience promotes the integration of new granule cells. *Science* 354, 459–465. doi: 10.1126/science.aaf2156

Amrein, I. (2015). Adult hippocampal neurogenesis in natural populations of mammals. *Cold Spring Harb. Perspect. Biol.* 7:a021295. doi: 10.1101/cshperspect.a021295

Amrein, I., Isler, K., and Lipp, H. P. (2011). Comparing adult hippocampal neurogenesis in mammalian species and orders: influence of chronological age and life history stage. *Eur. J. Neurosci.* 34, 978–987. doi: 10.1111/j.1460-9568.2011.07804.x

Anderson, K. J., Miller, K. M., Fugaccia, I., and Scheff, S. W. (2005). Regional distribution of fluoro-jade b staining in the hippocampus following traumatic brain injury. *Exp. Neurol.* 193, 125–130. doi: 10.1016/j.expneurol.2004.11.025

Belarbi, K., and Rosi, S. (2013). Modulation of adult-born neurons in the inflamed hippocampus. *Front. Cell. Neurosci.* 7:145. doi: 10.3389/fncel.2013.00145

Bell, J. D. (2017). In vogue: ketamine for neuroprotection in acute neurologic injury. *Anesth. Analg.* 124, 1237–1243. doi: 10.1213/ANE.0000000000001856

Bengzon, J., Kokaia, Z., Elmer, E., Nanobashvili, A., Kokaia, M., and Lindvall, O. (1997). Apoptosis and proliferation of dentate gyrus neurons after single and intermittent limbic seizures. *Proc. Natl. Acad. Sci. U.S.A.* 94, 10432–10437. doi: 10.1073/pnas.94.19.10432

Bittigau, P., Sifringer, M., Genz, K., Reith, E., Pospischil, D., Govindarajalu, S., et al. (2002). Antiepileptic drugs and apoptotic neurodegeneration in the developing brain. *Proc. Natl. Acad. Sci. U.S.A.* 99, 15089–15094. doi: 10.1073/pnas.222550499

Blaiss, C. A., Yu, T. S., Zhang, G., Chen, J., Dimchev, G., Parada, L. F., et al. (2011). Temporally specified genetic ablation of neurogenesis impairs cognitive recovery after traumatic brain injury. *J. Neurosci.* 31, 4906–4916. doi: 10.1523/JNEUROSCI.5265-10.2011

Boldrini, M., Fulmore, C. A., Tartt, A. N., Simeon, L. R., Pavlova, I., Poposka, V., et al. (2018). Human hippocampal neurogenesis persists throughout aging. *Cell Stem Cell* 22, 589–599e585. doi: 10.1016/j.stem.2018.03.015

Butler, C. R., Boychuk, J. A., and Smith, B. N. (2015). Effects of rapamycin treatment on neurogenesis and synaptic reorganization in the dentate gyrus after controlled cortical impact injury in mice. *Front. Syst. Neurosci.* 9:163. doi: 10.3389/fnsys.2015.00163

Carlson, A. P., Abbas, M., Alunday, R. L., Qeadan, F., and Shuttleworth, C. W. (2018). Spreading depolarization in acute brain injury inhibited by ketamine: a prospective, randomized, multiple crossover trial. *J. Neurosurg.* doi: 10.3171/2017.12.JNS171665 [Epub ahead of print].

Carron, S. F., Yan, E. B., Allitt, B. J., and Rajan, R. (2018). Immediate and medium-term changes in cortical and hippocampal inhibitory neuronal populations after diffuse tbi. *Neuroscience* 388, 152–170. doi: 10.1016/j.neuroscience.2018.07.020

Cavallucci, V., Fidaleo, M., and Pani, G. (2016). Neural stem cells and nutrients: poised between quiescence and exhaustion. *Trends Endocrinol. Metab.* 27, 756–769. doi: 10.1016/j.tem.2016.06.007

Chancey, J. H., Poulsen, D. J., Wadiche, J. I., and Overstreet-Wadiche, L. (2014). Hilar mossy cells provide the first glutamatergic synapses to adult-born dentate granule cells. *J. Neurosci.* 34, 2349–2354. doi: 10.1523/JNEUROSCI.3620-13.2014

Chang, L. C., Raty, S. R., Ortiz, J., Bailard, N. S., and Mathew, S. J. (2013). The emerging use of ketamine for anesthesia and sedation in traumatic brain injuries. *CNS Neurosci. Ther.* 19, 390–395. doi: 10.1111/cns.12077

Chirumamilla, S., Sun, D., Bullock, M. R., and Colello, R. J. (2002). Traumatic brain injury induced cell proliferation in mammalian central nervous system. *J. Neurotrauma* 19, 693–703. doi: 10.1089/08977150260139084

Danielson, N. B., Kaifosh, P., Zaremba, J. D., Lovett-Barron, M., Tsai, J., Denny, C. A., et al. (2016). Distinct contribution of adult-born hippocampal granule cells to context encoding. *Neuron* 90, 101–112. doi: 10.1016/j.neuron.2016.02.019

Danzer, S. C. (2018a). Adult neurogenesis in the human brain: paradise lost? *Epilepsy Curr.* 18, 329–331. doi: 10.5698/1535-7597.18.5.329

Danzer, S. C. (2018b). Contributions of adult-generated granule cells to hippocampal pathology in temporal lobe epilepsy: a neuronal bestiary. *Brain Plast.* 3, 169–181. doi: 10.3233/bpl-170056

Dash, P. K., Mach, S. A., and Moore, A. N. (2001). Enhanced neurogenesis in rodent hippocampus following traumatic brain injury. *J. Neurosci. Res.* 63, 313–319. doi: 10.1002/1097-4547(20010215)63:4<313::AID-JNR1025>3.0.CO;2-4

Deng, M., Hofacer, R. D., Jiang, C., Joseph, B., Hughes, E. A., Jia, B., et al. (2014). Brain regional vulnerability to anaesthesia-induced neuroapoptosis shifts with age at exposure and extends into adulthood for some regions. *Br. J. Anaesth.* 113, 443–451. doi: 10.1093/bja/aet469

Dreier, J. P., Major, S., Foreman, B., Winkler, M. K. L., Kang, E. J., Milakara, D., et al. (2018). Terminal spreading depolarization and electrical silence in death of human cerebral cortex. *Ann. Neurol.* 83, 295–310. doi: 10.1002/ana.25147

Dreier, J. P., Reiffurth, C., Woitzik, J., Hartings, J. A., Drenckhahn, C., Windler, C., et al. (2015). How spreading depolarization can be the pathophysiological correlate of both migraine aura and stroke. *Acta Neurochir. Suppl.* 120, 137–140. doi: 10.1007/978-3-319-04981-6_23

Drew, L. J., Kheirbek, M. A., Luna, V. M., Denny, C. A., Cloidt, M. A., Wu, M. V., et al. (2016). Activation of local inhibitory circuits in the dentate gyrus by adult-born neurons. *Hippocampus* 26, 763–778. doi: 10.1002/hipo.22557

Egeland, M., Zunszain, P. A., and Pariante, C. M. (2015). Molecular mechanisms in the regulation of adult neurogenesis during stress. *Nat. Rev. Neurosci.* 16, 189–200. doi: 10.1038/nrn3855

Eisch, A. J., and Petrik, D. (2012). Depression and hippocampal neurogenesis: a road to remission? *Science* 338, 72–75. doi: 10.1126/science.1222941

Emery, D. L., Fulp, C. T., Saatman, K. E., Schutz, C., Neugebauer, E., and Mcintosh, T. K. (2005). Newly born granule cells in the dentate gyrus rapidly extend axons into the hippocampal ca3 region following experimental brain injury. *J. Neurotrauma* 22, 978–988. doi: 10.1089/neu.2005.22.978

Encinas, J. M., and Sierra, A. (2012). Neural stem cell deforestation as the main force driving the age-related decline in adult hippocampal neurogenesis. *Behav. Brain Res.* 227, 433–439. doi: 10.1016/j.bbr.2011.10.010

Eriksson, P. S., Perfilieva, E., Bjork-Eriksson, T., Alborn, A. M., Nordborg, C., Peterson, D. A., et al. (1998). Neurogenesis in the adult human hippocampus. *Nat. Med.* 4, 1313–1317. doi: 10.1038/3305

Faigle, R., and Song, H. (2013). Signaling mechanisms regulating adult neural stem cells and neurogenesis. *Biochim. Biophys. Acta* 1830, 2435–2448. doi: 10.1016/j.bbagen.2012.09.002

Forcelli, P. A., Janssen, M. J., Vicini, S., and Gale, K. (2012). Neonatal exposure to antiepileptic drugs disrupts striatal synaptic development. *Ann. Neurol.* 72, 363–372. doi: 10.1002/ana.23600

Forcelli, P. A., Kim, J., Kondratyev, A., and Gale, K. (2011). Pattern of antiepileptic drug-induced cell death in limbic regions of the neonatal rat brain. *Epilepsia* 52, e207–e211. doi: 10.1111/j.1528-1167.2011.03297.x

Gao, X., Deng-Bryant, Y., Cho, W., Carrico, K. M., Hall, E. D., and Chen, J. (2008). Selective death of newborn neurons in hippocampal dentate gyrus following moderate experimental traumatic brain injury. *J. Neurosci. Res.* 86, 2258–2270. doi: 10.1002/jnr.21677

Gao, X., Enikolopov, G., and Chen, J. (2009). Moderate traumatic brain injury promotes proliferation of quiescent neural progenitors in the adult hippocampus. *Exp. Neurol.* 219, 516–523. doi: 10.1016/j.expneurol.2009.07.007

Goncalves, J. T., Schafer, S. T., and Gage, F. H. (2016). Adult neurogenesis in the hippocampus: from stem cells to behavior. *Cell* 167, 897–914. doi: 10.1016/j.cell.2016.10.021

Grady, M. S., Charleston, J. S., Maris, D., Witgen, B. M., and Lifshitz, J. (2003). Neuronal and glial cell number in the hippocampus after experimental traumatic brain injury: analysis by stereological estimation. *J. Neurotrauma* 20, 929–941. doi: 10.1089/089771503770195786

Gupta, A., Elgammal, F. S., Proddutur, A., Shah, S., and Santhakumar, V. (2012). Decrease in tonic inhibition contributes to increase in dentate semilunar granule cell excitability after brain injury. *J. Neurosci.* 32, 2523–2537. doi: 10.1523/JNEUROSCI.4141-11.2012

Gutherz, S. B., Kulick, C. V., Soper, C., Kondratyev, A., Gale, K., and Forcelli, P. A. (2014). Brief postnatal exposure to phenobarbital impairs passive avoidance learning and sensorimotor gating in rats. *Epilepsy Behav.* 37, 265–269. doi: 10.1016/j.yebeh.2014.07.010

Han, X., Tong, J., Zhang, J., Farahvar, A., Wang, E., Yang, J., et al. (2011). Imipramine treatment improves cognitive outcome associated with enhanced hippocampal neurogenesis after traumatic brain injury in mice. *J. Neurotrauma* 28, 995–1007. doi: 10.1089/neu.2010.1563

Hartings, J. A., Bullock, M. R., Okonkwo, D. O., Murray, L. S., Murray, G. D., Fabricius, M., et al. (2011). Spreading depolarisations and outcome after traumatic brain injury: a prospective observational study. *Lancet Neurol.* 10, 1058–1064. doi: 10.1016/s1474-4422(11)70243-5

Hartings, J. A., Ngwenya, L. B., Carroll, C. P., and Foreman, B. (2018). Letter to the editor: ketamine sedation for the suppression of spreading depolarizations. *J. Neurosurg.* doi: 10.3171/2018.6.JNS18235 [Epub ahead of print].

Hartings, J. A., Shuttleworth, C. W., Kirov, S. A., Ayata, C., Hinzman, J. M., Foreman, B., et al. (2017). The continuum of spreading depolarizations in acute cortical lesion development: examining leao's legacy. *J. Cereb. Blood Flow Metab.* 37, 1571–1594. doi: 10.1177/0271678X16654495

Hester, M. S., and Danzer, S. C. (2013). Accumulation of abnormal adult-generated hippocampal granule cells predicts seizure frequency and severity. *J. Neurosci.* 33, 8926–8936. doi: 10.1523/JNEUROSCI.5161-12.2013

Hofacer, R. D., Deng, M., Ward, C. G., Joseph, B., Hughes, E. A., Jiang, C., et al. (2013). Cell age-specific vulnerability of neurons to anesthetic toxicity. *Ann. Neurol.* 73, 695–704. doi: 10.1002/ana.23892

Huang, H., Liu, C. M., Sun, J., Hao, T., Xu, C. M., Wang, D., et al. (2016). Ketamine affects the neurogenesis of the hippocampal dentate gyrus in 7-day-old rats. *Neurotox. Res.* 30, 185–198. doi: 10.1007/s12640-016-9615-7

Huang, J., Jing, S., Chen, X., Bao, X., Du, Z., Li, H., et al. (2016). Propofol administration during early postnatal life suppresses hippocampal neurogenesis. *Mol. Neurobiol.* 53, 1031–1044. doi: 10.1007/s12035-014-9052-7

Huusko, N., Romer, C., Ndode-Ekane, X. E., Lukasiuk, K., and Pitkanen, A. (2015). Loss of hippocampal interneurons and epileptogenesis: a comparison of two animal models of acquired epilepsy. *Brain Struct. Funct.* 220, 153–191. doi: 10.1007/s00429-013-0644-1

Ibrahim, S., Hu, W., Wang, X., Gao, X., He, C., and Chen, J. (2016). Traumatic brain injury causes aberrant migration of adult-born neurons in the hippocampus. *Sci. Rep.* 6:21793. doi: 10.1038/srep21793

Jackson, J., Chugh, D., Nilsson, P., Wood, J., Carlstrom, K., Lindvall, O., et al. (2012). Altered synaptic properties during integration of adult-born hippocampal neurons following a seizure insult. *PLoS One* 7:e35557. doi: 10.1371/journal.pone.0035557

Jessberger, S., Nakashima, K., Clemenson, G. D. Jr., Mejia, E., Mathews, E., Ure, K., et al. (2007a). Epigenetic modulation of seizure-induced neurogenesis and cognitive decline. *J. Neurosci.* 27, 5967–5975. doi: 10.1523/JNEUROSCI.0110-07.2007

Jessberger, S., Zhao, C., Toni, N., Clemenson, G. D. Jr., Li, Y., and Gage, F. H. (2007b). Seizure-associated, aberrant neurogenesis in adult rats characterized with retrovirus-mediated cell labeling. *J. Neurosci.* 27, 9400–9407. doi: 10.1523/JNEUROSCI.2002-07.2007

Jiang, Y., Tong, D., Hofacer, R. D., Loepke, A. W., Lian, Q., and Danzer, S. C. (2016). Long-term fate mapping to assess the impact of postnatal isoflurane exposure

on hippocampal progenitor cell productivity. *Anesthesiology* 125, 1159–1170. doi: 10.1097/ALN.0000000000001358

Johnston, S. T., Shtrahman, M., Parylak, S., Goncalves, J. T., and Gage, F. H. (2016). Paradox of pattern separation and adult neurogenesis: a dual role for new neurons balancing memory resolution and robustness. *Neurobiol. Learn. Mem.* 129, 60–68. doi: 10.1016/j.nlm.2015.10.013

Jones, K. E., Puccio, A. M., Harshman, K. J., Falcione, B., Benedict, N., Jankowitz, B. T., et al. (2008). Levetiracetam versus phenytoin for seizure prophylaxis in severe traumatic brain injury. *Neurosurg. Focus* 25:E3. doi: 10.3171/FOC.2008.25.10.E3

Kharatishvili, I., Nissinen, J. P., Mcintosh, T. K., and Pitkanen, A. (2006). A model of posttraumatic epilepsy induced by lateral fluid-percussion brain injury in rats. *Neuroscience* 140, 685–697. doi: 10.1016/j.neuroscience.2006.03.012

Kienzler, F., Norwood, B. A., and Sloviter, R. S. (2009). Hippocampal injury, atrophy, synaptic reorganization, and epileptogenesis after perforant pathway stimulation-induced status epilepticus in the mouse. *J. Comp. Neurol.* 515, 181–196. doi: 10.1002/cne.22059

Kreitzer, N., Ancona, R., Mccullumsmith, C., Bg, K., Foreman, B., Ngwenya, L. B., et al. (2018). The effect of anti-depressants on depression after traumatic brain injury: a meta-analysis. *J. Head Trauma Rehabil.* doi: 10.1097/HTR.0000000000000439 [Epub ahead of print].

Krzisch, M., Sultan, S., Sandell, J., Demeter, K., Vutskits, L., and Toni, N. (2013). Propofol anesthesia impairs the maturation and survival of adult-born hippocampal neurons. *Anesthesiology* 118, 602–610. doi: 10.1097/ALN.0b013e3182815948

Larson, T. A. (2018). Sex steroids, adult neurogenesis, and inflammation in cns homeostasis, degeneration, and repair. *Front. Endocrinol.* 9:205. doi: 10.3389/fendo.2018.00205

Lin, E. P., Lee, J. R., Lee, C. S., Deng, M., and Loepke, A. W. (2017). Do anesthetics harm the developing human brain? An integrative analysis of animal and human studies. *Neurotoxicol. Teratol.* 60, 117–128. doi: 10.1016/j.ntt.2016.10.008

Lowenstein, D. H., Thomas, M. J., Smith, D. H., and Mcintosh, T. K. (1992). Selective vulnerability of dentate hilar neurons following traumatic brain injury: a potential mechanistic link between head trauma and disorders of the hippocampus. *J. Neurosci.* 12, 4846–4853.

Malberg, J. E., Eisch, A. J., Nestler, E. J., and Duman, R. S. (2000). Chronic antidepressant treatment increases neurogenesis in adult rat hippocampus. *J. Neurosci.* 20, 9104–9110.

McAvoy, K., Russo, C., Kim, S., Rankin, G., and Sahay, A. (2015). Fluoxetine induces input-specific hippocampal dendritic spine remodeling along the septotemporal axis in adulthood and middle age. *Hippocampus* 25, 1429–1446. doi: 10.1002/hipo.22464

McGuire, J. L., Ngwenya, L. B., and Mccullumsmith, R. E. (2018). Neurotransmitter changes after traumatic brain injury: an update for new treatment strategies. *Mol. Psychiatry* doi: 10.1038/s41380-018-0239-6 [Epub ahead of print].

Murphy, B. L., Hofacer, R. D., Faulkner, C. N., Loepke, A. W., and Danzer, S. C. (2012). Abnormalities of granule cell dendritic structure are a prominent feature of the intrahippocampal kainic acid model of epilepsy despite reduced postinjury neurogenesis. *Epilepsia* 53, 908–921. doi: 10.1111/j.1528-1167.2012.03463.x

Nakashiba, T., Cushman, J. D., Pelkey, K. A., Renaudineau, S., Buhl, D. L., Mchugh, T. J., et al. (2012). Young dentate granule cells mediate pattern separation, whereas old granule cells facilitate pattern completion. *Cell* 149, 188–201. doi: 10.1016/j.cell.2012.01.046

Neuberger, E. J., Swietek, B., Corrubia, L., Prasanna, A., and Santhakumar, V. (2017). Enhanced dentate neurogenesis after brain injury undermines long-term neurogenic potential and promotes seizure susceptibility. *Stem Cell Rep.* 9, 972–984. doi: 10.1016/j.stemcr.2017.07.015

Ngwenya, L. B., Heyworth, N. C., Shwe, Y., Moore, T. L., and Rosene, D. L. (2015). Age-related changes in dentate gyrus cell numbers, neurogenesis, and associations with cognitive impairments in the rhesus monkey. *Front. Syst. Neurosci.* 9:102. doi: 10.3389/fnsys.2015.00102

Ngwenya, L. B., Mazumder, S., Porter, Z. R., Minnema, A., Oswald, D. J., and Farhadi, H. F. (2018). Implantation of neuronal stem cells enhances object recognition without increasing neurogenesis after lateral fluid percussion injury in mice. *Stem Cells Int.* 2018, 1–11. doi: 10.1155/2018/4209821

Oddo, M., Crippa, I. A., Mehta, S., Menon, D., Payen, J. F., Taccone, F. S., et al. (2016). Optimizing sedation in patients with acute brain injury. *Crit. Care* 20:128. doi: 10.1186/s13054-016-1294-5

Parent, J. M., Elliott, R. C., Pleasure, S. J., Barbaro, N. M., and Lowenstein, D. H. (2006). Aberrant seizure-induced neurogenesis in experimental temporal lobe epilepsy. *Ann. Neurol.* 59, 81–91. doi: 10.1002/ana.20699

Pavlov, I., Huusko, N., Drexel, M., Kirchmair, E., Sperk, G., Pitkanen, A., et al. (2011). Progressive loss of phasic, but not tonic, gabaa receptor-mediated inhibition in dentate granule cells in a model of post-traumatic epilepsy in rats. *Neuroscience* 194, 208–219. doi: 10.1016/j.neuroscience.2011.07.074

Peng, Z. W., Xue, Y. Y., Wang, H. N., Wang, H. H., Xue, F., Kuang, F., et al. (2012). Sertraline promotes hippocampus-derived neural stem cells differentiating into neurons but not glia and attenuates lps-induced cellular damage. *Prog. Neuropsychopharmacol. Biol. Psychiatry* 36, 183–188. doi: 10.1016/j.pnpbp.2011.08.014

Peters, A. J., Villasana, L. E., and Schnell, E. (2018). Ketamine alters hippocampal cell proliferation and improves learning in mice after traumatic brain injury. *Anesthesiology* 129, 278–295. doi: 10.1097/ALN.0000000000002197

Pilar-Cuellar, F., Vidal, R., Diaz, A., Castro, E., Dos Anjos, S., Pascual-Brazo, J., et al. (2013). Neural plasticity and proliferation in the generation of antidepressant effects: hippocampal implication. *Neural Plast.* 2013:537265. doi: 10.1155/2013/537265

Rantamaki, T., Hendolin, P., Kankaanpaa, A., Mijatovic, J., Piepponen, P., Domenici, E., et al. (2007). Pharmacologically diverse antidepressants rapidly activate brain-derived neurotrophic factor receptor trkb and induce phospholipase-cgamma signaling pathways in mouse brain. *Neuropsychopharmacology* 32, 2152–2162. doi: 10.1038/sj.npp.1301345

Robinson, C., Apgar, C., and Shapiro, L. A. (2016). Astrocyte hypertrophy contributes to aberrant neurogenesis after traumatic brain injury. *Neural Plast.* 2016:1347987. doi: 10.1155/2016/1347987

Rolfe, A., and Sun, D. (2015). "Stem cell therapy in brain trauma: Implications for repair and regeneration of injured brain in experimental tbi models," in *Brain Neurotrauma: Molecular, Neuropsychological, and Rehabilitation Aspects*, ed. F. H. Kobeissy (Boca Raton, FL: CRC Press/Taylor & Francis).

Rosenfeld, J. V., Mcfarlane, A. C., Bragge, P., Armonda, R. A., Grimes, J. B., and Ling, G. S. (2013). Blast-related traumatic brain injury. *Lancet Neurol.* 12, 882–893. doi: 10.1016/s1474-4422(13)70161-3

Saatman, K. E., Duhaime, A. C., Bullock, R., Maas, A. I., Valadka, A., Manley, G. T., et al. (2008). Classification of traumatic brain injury for targeted therapies. *J. Neurotrauma* 25, 719–738. doi: 10.1089/neu.2008.0586

Santarelli, L., Saxe, M., Gross, C., Surget, A., Battaglia, F., Dulawa, S., et al. (2003). Requirement of hippocampal neurogenesis for the behavioral effects of antidepressants. *Science* 301, 805–809. doi: 10.1126/science.1083328

Santhakumar, V., Bender, R., Frotscher, M., Ross, S. T., Hollrigel, G. S., Toth, Z., et al. (2000). Granule cell hyperexcitability in the early post-traumatic rat dentate gyrus: the 'irritable mossy cell' hypothesis. *J. Physiol.* 524(Pt 1), 117–134.

Santhakumar, V., Ratzliff, A. D. H., Jeng, J., Toth, Z., and Soltesz, I. (2001). Long-term hyperexcitability in the hippocampus after experimental head trauma. *Ann. Neurol.* 50, 708–717. doi: 10.1002/ana.1230

Scharfman, H. E. (2016). The enigmatic mossy cell of the dentate gyrus. *Nat. Rev. Neurosci.* 17, 562–575. doi: 10.1038/nrn.2016.87

Scharfman, H. E., Sollas, A. E., Berger, R. E., Goodman, J. H., and Pierce, J. P. (2003). Perforant path activation of ectopic granule cells that are born after pilocarpine-induced seizures. *Neuroscience* 121, 1017–1029. doi: 10.1016/s0306-4522(03)00481-0

Shapiro, L. A. (2017). Altered hippocampal neurogenesis during the first 7 days after a fluid percussion traumatic brain injury. *Cell Transplant.* 26, 1314–1318. doi: 10.1177/0963689717714099

Slikker, W. Jr., Zou, X., Hotchkiss, C. E., Divine, R. L., Sadovova, N., Twaddle, N. C., et al. (2007). Ketamine-induced neuronal cell death in the perinatal rhesus monkey. *Toxicol. Sci.* 98, 145–158. doi: 10.1093/toxsci/kfm084

Song, J., Olsen, R. H., Sun, J., Ming, G. L., and Song, H. (2016). Neuronal circuitry mechanisms regulating adult mammalian neurogenesis. *Cold Spring Harb. Perspect. Biol.* 8:a018937. doi: 10.1101/cshperspect.a018937

Song, J., Sun, J., Moss, J., Wen, Z., Sun, G. J., Hsu, D., et al. (2013). Parvalbumin interneurons mediate neuronal circuitry-neurogenesis coupling in the adult hippocampus. *Nat. Neurosci.* 16, 1728–1730. doi: 10.1038/nn.3572

Song, J., Zhong, C., Bonaguidi, M. A., Sun, G. J., Hsu, D., Gu, Y., et al. (2012). Neuronal circuitry mechanism regulating adult quiescent neural stem-cell fate decision. *Nature* 489, 150–154. doi: 10.1038/nature11306

Sorrells, S. F., Paredes, M. F., Cebrian-Silla, A., Sandoval, K., Qi, D., Kelley, K. W., et al. (2018). Human hippocampal neurogenesis drops sharply in children to undetectable levels in adults. *Nature* 555, 377–381. doi: 10.1038/nature25975

Soumier, A., Carter, R. M., Schoenfeld, T. J., and Cameron, H. A. (2016). New hippocampal neurons mature rapidly in response to ketamine but are not required for its acute antidepressant effects on neophagia in rats. *eNeuro* 3:ENEURO.0116-15.2016. doi: 10.1523/ENEURO.0116-15.2016

Spalding, K. L., Bergmann, O., Alkass, K., Bernard, S., Salehpour, M., Huttner, H. B., et al. (2013). Dynamics of hippocampal neurogenesis in adult humans. *Cell* 153, 1219–1227. doi: 10.1016/j.cell.2013.05.002

Sugaya, Y., Maru, E., Kudo, K., Shibasaki, T., and Kato, N. (2010). Levetiracetam suppresses development of spontaneous eeg seizures and aberrant neurogenesis following kainate-induced status epilepticus. *Brain Res.* 1352, 187–199. doi: 10.1016/j.brainres.2010.06.061

Sun, D., Daniels, T. E., Rolfe, A., Waters, M., and Hamm, R. (2015). Inhibition of injury-induced cell proliferation in the dentate gyrus of the hippocampus impairs spontaneous cognitive recovery after traumatic brain injury. *J. Neurotrauma* 32, 495–505. doi: 10.1089/neu.2014.3545

Sun, D., Mcginn, M. J., Zhou, Z., Harvey, H. B., Bullock, M. R., and Colello, R. J. (2007). Anatomical integration of newly generated dentate granule neurons following traumatic brain injury in adult rats and its association to cognitive recovery. *Exp. Neurol.* 204, 264–272. doi: 10.1016/j.expneurol.2006.11.005

Szaflarski, J. P., Sangha, K. S., Lindsell, C. J., and Shutter, L. A. (2010). Prospective, randomized, single-blinded comparative trial of intravenous levetiracetam versus phenytoin for seizure prophylaxis. *Neurocrit. Care* 12, 165–172. doi: 10.1007/s12028-009-9304-y

Temprana, S. G., Mongiat, L. A., Yang, S. M., Trinchero, M. F., Alvarez, D. D., Kropff, E., et al. (2015). Delayed coupling to feedback inhibition during a critical period for the integration of adult-born granule cells. *Neuron* 85, 116–130. doi: 10.1016/j.neuron.2014.11.023

Thal, S. C., Timaru-Kast, R., Wilde, F., Merk, P., Johnson, F., Frauenknecht, K., et al. (2014). Propofol impairs neurogenesis and neurologic recovery and increases mortality rate in adult rats after traumatic brain injury. *Crit. Care Med.* 42, 129–141. doi: 10.1097/CCM.0b013e3182a639fd

Toth, Z., Hollrigel, G. S., Gorcs, T., and Soltesz, I. (1997). Instantaneous perturbation of dentate interneuronal networks by a pressure wave-transient delivered to the neocortex. *J. Neurosci.* 17, 8106–8117.

Tran, L. D., Lifshitz, J., Witgen, B. M., Schwarzbach, E., Cohen, A. S., and Grady, M. S. (2006). Response of the contralateral hippocampus to lateral fluid percussion brain injury. *J. Neurotrauma* 23, 1330–1342. doi: 10.1089/neu.2006.23.1330

Urbach, A., Baum, E., Braun, F., and Witte, O. W. (2016). Cortical spreading depolarization increases adult neurogenesis, and alters behavior and hippocampus-dependent memory in mice. *J. Cereb. Blood Flow Metab.* 37, 1776–1790. doi: 10.1177/0271678X16643736

Urbach, A., Redecker, C., and Witte, O. W. (2008). Induction of neurogenesis in the adult dentate gyrus by cortical spreading depression. *Stroke* 39, 3064–3072. doi: 10.1161/STROKEAHA.108.518076

Urrea, C., Castellanos, D. A., Sagen, J., Tsoulfas, P., Bramlett, H. M., and Dietrich, W. D. (2007). Widespread cellular proliferation and focal neurogenesis after traumatic brain injury in the rat. *Restor. Neurol. Neurosci.* 25, 65–76.

Villasana, L. E., Kim, K. N., Westbrook, G. L., and Schnell, E. (2015). Functional integration of adult-born hippocampal neurons after traumatic brain injury(1,2,3). *eNeuro* 2:ENEURO.0056-15.2015. doi: 10.1523/ENEURO.0056-15.2015

Wang, C., Liu, F., Patterson, T. A., Paule, M. G., and Slikker, W. Jr. (2017). Relationship between ketamine-induced developmental neurotoxicity and nmda receptor-mediated calcium influx in neural stem cell-derived neurons. *Neurotoxicology* 60, 254–259. doi: 10.1016/j.neuro.2016.04.015

Wang, X., Gao, X., Michalski, S., Zhao, S., and Chen, J. (2016). Traumatic brain injury severity affects neurogenesis in adult mouse hippocampus. *J. Neurotrauma* 33, 721–733. doi: 10.1089/neu.2015.4097

Wang, Y., Neumann, M., Hansen, K., Hong, S. M., Kim, S., Noble-Haeusslein, L. J., et al. (2011). Fluoxetine increases hippocampal neurogenesis and induces epigenetic factors but does not improve functional recovery after traumatic brain injury. *J. Neurotrauma* 28, 259–268. doi: 10.1089/neu.2010.1648

Wu, H., Li, J., Xu, D., Zhang, Q., and Cui, T. (2018). Growth differentiation factor 5 improves neurogenesis and functional recovery in adult mouse hippocampus following traumatic brain injury. *Front. Neurol.* 9:592. doi: 10.3389/fneur.2018.00592

Xiong, Y., Mahmood, A., and Chopp, M. (2013). Animal models of traumatic brain injury. *Nat. Rev. Neurosci.* 14, 128–142. doi: 10.1038/nrn3407

Yan, B. C., Shen, H., Zhang, Y., Zhu, X., Wang, J., Xu, P., et al. (2018). The antiepileptic drug levetiracetam promotes neuroblast differentiation and expression of superoxide dismutase in the mouse hippocampal dentate gyrus via pi3k/akt signalling. *Neurosci. Lett.* 662, 84–90. doi: 10.1016/j.neulet.2017.10.010

Yan, J., and Jiang, H. (2014). Dual effects of ketamine: neurotoxicity versus neuroprotection in anesthesia for the developing brain. *J. Neurosurg. Anesthesiol.* 26, 155–160. doi: 10.1097/ANA.0000000000000027

Yeh, C. Y., Asrican, B., Moss, J., Quintanilla, L. J., He, T., Mao, X., et al. (2018). Mossy cells control adult neural stem cell quiescence and maintenance through a dynamic balance between direct and indirect pathways. *Neuron* 99, 493.e4–510.e4. doi: 10.1016/j.neuron.2018.07.010

Yue, J. K., Burke, J. F., Upadhyayula, P. S., Winkler, E. A., Deng, H., Robinson, C. K., et al. (2017). Selective serotonin reuptake inhibitors for treating neurocognitive and neuropsychiatric disorders following traumatic brain injury: an evaluation of current evidence. *Brain Sci.* 7:E93. doi: 10.3390/brainsci7080093

Yun, S., Reynolds, R. P., Masiulis, I., and Eisch, A. J. (2016). Re-evaluating the link between neuropsychiatric disorders and dysregulated adult neurogenesis. *Nat. Med.* 22, 1239–1247. doi: 10.1038/nm.4218

Zhang, B. L., Fan, Y. S., Wang, J. W., Zhou, Z. W., Wu, Y. G., Yang, M. C., et al. (2018). Cognitive impairment after traumatic brain injury is associated with reduced long-term depression of excitatory postsynaptic potential in the rat hippocampal dentate gyrus. *Neural Regen. Res.* 13, 1753–1758. doi: 10.4103/1673-5374.238618

Zhang, X., He, X., Li, Q., Kong, X., Ou, Z., Zhang, L., et al. (2017). Pi3k/akt/mtor signaling mediates valproic acid-induced neuronal differentiation of neural stem cells through epigenetic modifications. *Stem Cell Rep.* 8, 1256–1269. doi: 10.1016/j.stemcr.2017.04.006

Zhao, M. L., Chen, S. J., Li, X. H., Wang, L. N., Chen, F., Zhong, S. J., et al. (2018). Optical depolarization of dcx-expressing cells promoted cognitive recovery and maturation of newborn neurons via the wnt/beta-catenin pathway. *J. Alzheimers Dis.* 63, 303–318. doi: 10.3233/JAD-180002

Conflict of Interest Statement: The authors declare that the research was conducted in the absence of any commercial or financial relationships that could be construed as a potential conflict of interest.

frontiers in Neuroscience

ORIGINAL RESEARCH
published: 10 January 2019
doi: 10.3389/fnins.2018.00956

Targeting Polyamine Oxidase to Prevent Excitotoxicity-Induced Retinal Neurodegeneration

Prahalathan Pichavaram[1,2], *Chithra Devi Palani*[1,3,4], *Chintan Patel*[1,3], *Zhimin Xu*[1,3], *Esraa Shosha*[1,3], *Abdelrahman Y. Fouda*[1,3], *Ruth B. Caldwell*[1,3,5] and *Subhadra Priya Narayanan*[1,2,3,4,5]*

[1] Vision Discovery Institute, Augusta University, Augusta, GA, United States, [2] College of Allied Health Sciences, Augusta University, Augusta, GA, United States, [3] Vascular Biology Center, Augusta University, Augusta, GA, United States, [4] Clinical and Experimental Therapeutics, College of Pharmacy, University of Georgia, Augusta, GA, United States, [5] VA Medical Center, Augusta, GA, United States

Dysfunction of retinal neurons is a major cause of vision impairment in blinding diseases that affect children and adults worldwide. Cellular damage resulting from polyamine catabolism has been demonstrated to be a major player in many neurodegenerative conditions. We have previously shown that inhibition of polyamine oxidase (PAO) using MDL 72527 significantly reduced retinal neurodegeneration and cell death signaling pathways in hyperoxia-mediated retinopathy. In the present study, we investigated the impact of PAO inhibition in limiting retinal neurodegeneration in a model of NMDA (*N-Methyl-D-aspartate*)-induced excitotoxicity. Adult mice (8–10 weeks old) were given intravitreal injections (20 nmoles) of NMDA or NMLA (*N-Methyl-L-aspartate*, control). Intraperitoneal injection of MDL 72527 (40 mg/kg body weight/day) or vehicle (normal saline) was given 24 h before NMDA or NMLA treatment and continued until the animals were sacrificed (varied from 1 to 7 days). Analyses of retinal ganglion cell (RGC) layer cell survival was performed on retinal flatmounts. Retinal cryostat sections were prepared for immunostaining, TUNEL assay and retinal thickness measurements. Fresh frozen retinal samples were used for Western blotting analysis. A marked decrease in the neuronal survival in the RGC layer was observed in NMDA treated retinas compared to their NMLA treated controls, as studied by NeuN immunostaining of retinal flatmounts. Treatment with MDL 72527 significantly improved survival of NeuN positive cells in the NMDA treated retinas. Excitotoxicity induced neurodegeneration was also demonstrated by reduced levels of synaptophysin and degeneration of inner retinal neurons in NMDA treated retinas compared to controls. TUNEL labeling studies showed increased cell death in the NMDA treated retinas. However, treatment with MDL 72527 markedly reduced these changes. Analysis of signaling pathways during excitotoxic injury revealed the downregulation of pro-survival signaling molecules p-ERK and p-Akt, and the upregulation of a pro-apoptotic molecule BID, which were normalized with PAO inhibition. Our data demonstrate that inhibition of polyamine oxidase blocks NMDA-induced retinal neurodegeneration and promotes cell survival, thus offering a new therapeutic target for retinal neurodegenerative disease conditions.

Keywords: retina, neurodegeneration, excitotoxicity, polyamine oxidase, MDL 72527

OPEN ACCESS

Edited by:
Wenbo Zhang,
The University of Texas Medical Branch at Galveston, United States

Reviewed by:
Nigel Cooper,
University of Louisville, United States
Rebecca M. Sappington,
Vanderbilt University Medical Center, United States
Manas R. Biswal,
University of South Florida, United States

***Correspondence:**
Subhadra Priya Narayanan
pnarayanan@augusta.edu

Specialty section:
This article was submitted to Neurodegeneration, a section of the journal Frontiers in Neuroscience

Received: *29 June 2018*
Accepted: *30 November 2018*
Published: *10 January 2019*

Citation:
Pichavaram P, Palani CD, Patel C, Xu Z, Shosha E, Fouda AY, Caldwell RB and Narayanan SP (2019) Targeting Polyamine Oxidase to Prevent Excitotoxicity-Induced Retinal Neurodegeneration. Front. Neurosci. 12:956. doi: 10.3389/fnins.2018.00956

INTRODUCTION

Neuronal injury in the retina is considered as a major cause of vision impairment in blinding diseases such as glaucoma (Vidal-Sanz et al., 2015; Nucci et al., 2016) and diabetic retinopathy (Yu et al., 2008; Jindal, 2015; Araszkiewicz and Zozulinska-Ziolkiewicz, 2016). Neurons in the ganglion cell layer and inner nuclear layer are affected by these pathologies. Glutamate excitotoxicity is considered as one of the mechanisms of neurodegeneration in the central nervous system, including the retina (Fahrenthold et al., 2018; Sone et al., 2018). NMDA (N-Methyl-D-Aspartate) mediated neuronal damage is a well-established model for studying mechanisms of retinal neuroprotection (Laabich and Cooper, 2000; Pernet et al., 2007; Takeda et al., 2007). It is characterized by the excessive synaptic release of glutamate, which in turn activates post-synaptic glutamate receptors and mediates excitotoxic cell death. The NMDA receptor (NMDAR) subtypes play a major role in this process, mainly by increasing intracellular calcium (Ca^{2+}). Activation of NMDAR has been shown to promote neuronal death in the retina (Shen et al., 2006; Chintala et al., 2015).

Polyamines (spermine, spermidine, and putrescine) are involved in various cellular functions, such as cell growth and proliferation (Casero and Pegg, 2009; Weiger and Hermann, 2014). However, dysregulation of polyamine catabolism is associated with various neurodegenerative disease states. Altered levels of polyamines have been implicated in neurological disease conditions such as Alzheimer's disease (Morrison and Kish, 1995; Yatin et al., 2001; Inoue et al., 2013) Parkinson's disease (Gomes-Trolin et al., 2002; Lewandowski et al., 2010; Paik et al., 2010) traumatic brain injury (Zahedi et al., 2010) and in the pathogenesis of ischemic brain damage (Ivanova et al., 2002; Takano et al., 2005; Wood et al., 2006). Even though these results suggest that polyamines play an important role in neurodegeneration, the mechanisms whereby they participate in neuronal death have yet to be elucidated.

Polyamine metabolism is finely regulated by the concerted actions of various enzymes (Casero and Pegg, 2009; Hussain et al., 2017). Spermine Oxidase (SMO), Spermine Spermidine Acetyl Transferase (SSAT), and Acetyl Polyamine Oxidase (APAO) are major enzymes regulating the backward oxidation of the polyamines-spermine, spermidine, and putrescine. Activation of polyamine oxidases (PAOs) including SMO and APAO generates toxic aldehydes and hydrogen peroxide (H_2O_2) as byproducts and leads to damage of DNA, RNA, proteins, and lipids (Seiler, 2000; Amendola et al., 2005; Casero and Pegg, 2009). PAOs are the key enzymes in polyamine catabolism, playing an essential role in maintaining polyamine homeostasis (Seiler, 2004; Cervelli et al., 2012). Increasing evidence shows the involvement of PAOs in neurodegenerative diseases (Cervelli et al., 2012; Capone et al., 2013).

MDL 72527 (N,N'-Bis(2,3-butadienyl)-1,4-butanediamine dihydrochloride) is an irreversible competitive inhibitor of the polyamine oxidases (Dogan et al., 1999b; Seiler et al., 2002; Cervelli et al., 2013b). Studies in a rat model of cerebral ischemia have shown that treatment with MDL 72527 significantly reduced brain edema, ischemic injury volume, and polyamine levels (Dogan et al., 1999b). These results are consistent with studies on brain injury models, in which MDL 72527 treatment improved neuronal survival (Dogan et al., 1999a; Liu et al., 2001). Furthermore, blockade of polyamine oxidation using MDL 72527 was found to be protective against edema and necrotic cavitation after traumatic brain injury (Dogan et al., 1999a).

Studies from our laboratory are the first to demonstrate the role of polyamine metabolism in retinal neurodegeneration (Narayanan et al., 2014). Using the mouse model of oxygen-induced retinopathy (OIR), we showed that hyperoxia-induced neuronal degeneration is associated with significant increases in PAO along with altered levels of polyamines, suggesting a significant role for polyamine oxidase in the neuronal injury (Narayanan et al., 2014). Further analysis showed for the first time that treatment with MDL 72527 limits the hyperoxia-induced oxidative stress and reduces retinal neurodegeneration, confirming the role of PAO in neurotoxicity (Narayanan et al., 2014). The role of polyamines and polyamine oxidases in excitotoxicity-induced neuronal damage in the retina is not well-studied. In the present study, utilizing the well-established NMDA model of retinal neuronal injury, we investigated whether treatment with the PAO inhibitor, MDL 72527 reduces excitotoxicity-induced neurodegeneration and its potential as a therapeutic target for retinal neurodegenerative diseases.

MATERIALS AND METHODS

Animals

All procedures with animals were performed by the ARVO Statement for the Use of Animals in Ophthalmic and Vision Research and were approved by the institutional animal care and use committee (Animal Welfare Assurance no. A3307–01) adhered to the Public Health Service Policy on Humane Care and Use of Laboratory Animals (revised July 2017). These studies were conducted using wild-type male C57BL6J mice (8–10 weeks, Jackson Laboratories, Bar Harbor, ME) and all efforts were made to minimize suffering during experimental procedures performed.

Intravitreal Treatment of NMDA

Retinal excitotoxicity was induced using NMDA (N-Methyl-D-Aspartate, Sigma) according to the published methods with minor modifications (Tsutsumi et al., 2016; Ishimaru et al., 2017). Briefly, mice were anesthetized with ketamine/xylazine (73 mg/kg ketamine hydrochloride and 7.3 mg/kg xylaxine hydrochloride, i.p., intraperitoneally), pupils were dilated with 1% tropicamide (Akorn, Lake Forest, IL, United States), and topical anesthesia (1 drop of proparacaine hydrochloride, Akorn) was applied to the cornea. Intravitreal injection of NMDA (20 nmoles/eye, 1 μl, dissolved in saline) was performed in the right eye using a WPI microsyringe. The needle was kept for additional 30 s and pulled out slowly, and antibiotic ointment was applied. For the control group, NMLA (N-Methyl L Aspartate, 20 nmoles/left eye) was used.

MDL Treatment

Treatment with PAO inhibitor was performed as described previously (Narayanan et al., 2011; Patel et al., 2016). Briefly, intraperitoneal injection of MDL 72527 (40 mg/kg body weight/day) or vehicle (normal saline) was given 24 h before NMDA or NMLA treatment and continued until the animals were sacrificed (varied from 1 to 7 days).

Immunofluorescence Staining

Immunostaining of retinal cryostat sections were performed as described previously. (Patel et al., 2016; Shosha et al., 2016) Eyes were enucleated, fixed in 4% paraformaldehyde for overnight at 4°C, washed in PBS, and cryoprotected in 30% sucrose. Cryostat sections (10 um) were obtained and mounted on glass slides. The sections were permeabilized in 0.05% Triton X-100 for 10 min and blocked in 10% normal goat serum containing 1% BSA for 1 h at room temperature. Followed by blocking, the sections were incubated with primary antibodies [SMO, Synaptophysin, Protein kinase Cα (PKCα), choline acetyl transferase (ChAT), Calbindin and Glial fibillary acidic protein (GFAP)] overnight at 4°C. Next day, they were washed and further incubated with Fluorescein-conjugated secondary antibodies (Life Technologies, Grand Island, NY, United States) for 1 h at room temperature. Finally, they were washed in PBS and covered with mounting medium and DAPI (Vectashield Vector Laboratories, Burlingame, CA, United States). Images of the stained section were obtained using a Zeiss (Thornwood, NY, United States) Axioplan Imager microscope and Zeiss Axiovision 4.8.2 software.

Retinal Thickness Measurement

Frozen retinal sections from mice treated with NMDA or NMLA, with saline or MDL treatment were used to study the retinal thickness and analyzed as described previously. (Narayanan et al., 2011; Yokota et al., 2011) Retinal cross-sections (10 um) with optic nerve attachment were prepared and the morphology was observed using H and E staining. A minimum of four sections at 20 um apart from each other were used per animal. ImageJ software was used to determine the total retinal or inner nuclear layer (INL) thickness.

RGC Loss Analysis

Immunostaining on retinal flatmounts was performed as we have described previously (Shosha et al., 2016) in our study. Briefly, eyes were enucleated, fixed in 4% paraformaldehyde overnight at 4°C, washed in PBS, and the retinas were isolated. Retinas were cut toward the optic disc to get a flower shape. The retinal tissue was permeabilized (10% Triton X-100 for 20 min), blocked (10% normal goat serum containing 1% BSA and 0.1% Triton X-100 for 1 h at room temperature), and were incubated in primary antibody (NeuN, Neuronal Nuclei) for 2 h at 37°C. Retinas were washed and incubated in respective secondary antibody overnight at 4°C. Lastly, the retinas were washed in PBS and mounted with mounting medium (Vectashield Vector Laboratories, Burlingame, CA, United States). Retinal flat mounts images were obtained using a confocal microscope (Zeiss LSM 510 META, Thornwood, NY, United States). Quantification of NeuN positive cells in the GCL layer was performed using NIH Image J software as described in the previous report from our laboratory (Yokota et al., 2011). Images were taken from each quadrant of the flat mounted retina at the midperiphery (defined as halfway between the optic nerve head and the outer periphery). This was performed using a 20X objective by counting the number of the consecutive non-overlapping fields from the optic nerve to edge. Five serial images (1 μm apart) of NeuN positive GCL were taken from each region and merged to get projection image for quantification.

TUNEL Assay

Retinal cryosections were used to study the apoptotic cells by using the TUNEL (Terminal deoxynucleotidyl transferase dUTP nick end labeling) assay, according to the manufacturer's protocol (Fluorescein Insitu Cell death detection kit, Millipore, Billerica, MA, United States). TUNEL positive cells were quantified as previously described (Narayanan et al., 2014). TUNEL based detection of apoptotic cells were performed in retinal cryostat sections (formalin fixed) and counterstained with DAPI. Staining without the TdT enzyme was used as negative control. Quantification of TUNEL-positive cells in retinal cryosections from optic disc to periphery was performed manually using a fluorescent microscope (Zeiss Axioplan 2, Thornwood, NY, United States). The number was multiplied by two to represent total number of TUNEL positive cells per retinal section. A minimum of three sections (20 μm apart) per animal were used.

Western Blotting

Retinal tissue was homogenized in RIPA buffer (Millipore, Billerica, MA, United States) containing protease inhibitor (Complete Mini) and phosphatase inhibitors (phosSTOP, Roche Applied Science, Indianapolis, IN, United States). Protein concentration was measured using the bicinchoninic acid kit (Pierce, Thermo Scientific) according to manufacturer's instructions. Protein samples (15–20 ug) per lane were separated on SDS-PAGE and electrophoretically transferred to nitrocellulose membrane (Millipore, Billerica, MA, United States), blocked in 5% dry milk in 1X Tris-buffered saline with 0.5% Tween-20 (TBST). Membranes were incubated in primary antibodies overnight at 4°C with phospho Akt, total Akt, phospho ERK1/2, total ERK1/2, Bcl-xL, BID, (Cell Signaling Technology, Danvers, MA, United States) diluted in 2% BSA, or beta-Actin (Sigma). Further, the membranes were washed with TBST and incubated with anti-rabbit or anti-mouse HRP-conjugated secondary antibodies (GE-Healthcare, Piscataway, NJ, United States), washed (TBST) and detected using enhanced chemiluminescence system (GE-Healthcare, Piscataway, NJ, United States). The band intensities were quantified by densitometry using ImageJ software and normalized to loading controls.

Statistical Analysis

GraphPad Prism 7 (GraphPad Software Inc., La Jolla, CA, United States) was used for statistical analysis. Results were presented as mean ± SD. Statistical analysis was performed using one-way or two-way ANOVA followed by Tukey test for multiple

comparisons. In case of single comparison, the Student's *t*-test was applied. $P \leq 0.05$ was considered statistically significant.

RESULTS

Increased Expression of SMO During Retinal Excitotoxicity

Our previous studies have shown increased SMO levels in the OIR retina (Narayanan et al., 2014). **Figure 1** demonstrates the expression and localization of SMO in the retina, in response to the effects of NMDA induced excitotoxicity. Immunofluorescence studies showed the elevated SMO (also called PAO in this study) expression levels in the INL and OPL of NMDA retinas, while the expression was very minimal in NMLA treated controls (**Figures 1A,B**). Increased expression in SMO was evident in retinal lysates at 24 h and 48 h following NMDA treatment (**Figure 1C**). Quantitation using Image J analysis shows significantly increased ($p < 0.05$) levels of SMO in NMDA retinas compared to respective NMLA controls at both time points analyzed (**Figure 1D**). These studies suggest the involvement of SMO in excitotoxicity induced retinal neuronal damage.

Survival of Retinal Ganglion Cells in Response to MDL Treatment

Loss of RGCs is a major feature of retinal excitotoxicity (Tsutsumi et al., 2016; Ishimaru et al., 2017). In the present study, NMDA-induced RGC loss was studied (7 days post-NMDA treatment) using retinal flatmount analysis. **Figures 2A–D** shows representative confocal images of retinal flatmounts immunostained using NeuN antibody. A marked reduction in the number of NeuN positive cells in the GCL was observed in NMDA retinas compared to their NMLA controls. However, treatment with MDL, the PAO inactivator significantly reduced the excitotoxicity-induced RGC loss. **Figure 2E** demonstrates the quantitation of the number of NeuN positive cells (RGC layer) in the retinal flatmounts of vehicle or MDL treated NMDA retinas compared to their NMLA retinas. Around 50% reduction in the number of NeuN positive cells (GCL layer) was evident in NMDA retinas compared to NMLA controls ($p < 0.01$). Treatment with MDL significantly increased the number of surviving neurons (70%) in NMDA retinas and significantly increased GCL neuronal survival compared to vehicle-treated NMDA retinas. MDL treatment did not alter RGC survival in the NMLA- treated retinas.

PAO Inhibition Reduced the Excitotoxicity-Induced Degeneration of Inner Retinal Neurons

Studies have shown that, in addition to RGCs, other retinal neurons are also impacted by NMDA-induced neurotoxicity (Chintala et al., 2015; Kuehn et al., 2017). In our present study, utilizing samples at 5 days post-injury, we investigated whether treatment with MDL improved the survival of neurons in the INL in response to NMDA treatment. **Figure 3** demonstrates representative confocal images from retinal sections immunostained using ChAT (**Figures 3A–D**, the marker for amacrine cells), PKCα **Figures 3E–H**, the marker for rod bipolar cells), or Calbindin (**Figures 3I–L**, the marker for horizontal cells). Qualitative analysis showed a trend toward reduction in amacrine cells were observed in NMDA-retinal sections, while treatment with MDL reduced this change. Excitotoxicity induced degeneration of bipolar cells is evident in NMDA retinas (vehicle treated), shown by reduced expression level of the marker, and by the presence of shortened and degenerating dendrites. These alterations were improved in NMDA retinas response to MDL treatment. Calbindin immunostaining showed loss of horizontal cells (in the OPL) in NMDA retinas compared to NMLA controls, while MDL treatment improved the survival of calbindin-positive cells.

Further studies on synaptophysin, a presynaptic marker showed a marked reduction in its level in the NMDA retinas (5 days post-injury), while MDL treatment demonstrated a significant improvement (**Figure 4**). Confocal images (**Figures 4A–D**) show reduced expression of synaptophysin in the plexiform layers of NMDA retinas. However, MDL treatment upregulated the synaptophysin levels. Western blot analysis (**Figures 4E,F**) further confirm these results. Synaptophysin levels were significantly downregulated in NMDA retinas compared to NMLA controls ($p < 0.05$), while MDL treatment resulted in a significant preservation of synaptophysin ($p < 0.05$) levels in NMDA retinas, in comparison with vehicle treated group. These results suggest that PAO inhibition improved the synaptic contacts and reduced the retinal neurodegeneration induced by excitotoxicity.

Excitotoxicity Induced Retinal Thinning Is Reduced in Response to PAO Inhibition

Thinning of retinal layers is another characteristic of retinal degeneration (Honjo et al., 2000; Wang et al., 2014; Jindal et al., 2017). In the current study, we investigated whether MDL treatment has an impact on the excitotoxicity induced retinal thinning. **Figures 5A–D** shows representative images from H and E stained retinal sections from NMDA (7 days post-injury, vehicle or MDL treated) and NMLA (vehicle or MDL treated) controls. Excitotoxicity-induced neuronal damage was evident in the sections from NMDA retinas (7 days post-injury) as seen by degeneration of retinal layers. Loss of cells in the GCL, and a significant reduction in the thickness of total retina ($p < 0.05$) and the INL ($p < 0.05$) thickness were observed in the NMDA (vehicle treated) retinas compared to respective NMLA controls. Treatment with MDL, the PAO inhibitor significantly ($p < 0.05$) protected against the reduction of retinal thickness in the NMDA retinas. **Figures 5E,F** demonstrates the quantitation of total retinal thickness and INL thickness. The significantly reduced thickness of retina and INL were evident in NMDA retinas compared to the respective NMLA controls. In both cases, a significant increase in the thickness was observed in response to MDL treatment, demonstrating the neuroprotection offered by PAO inhibition.

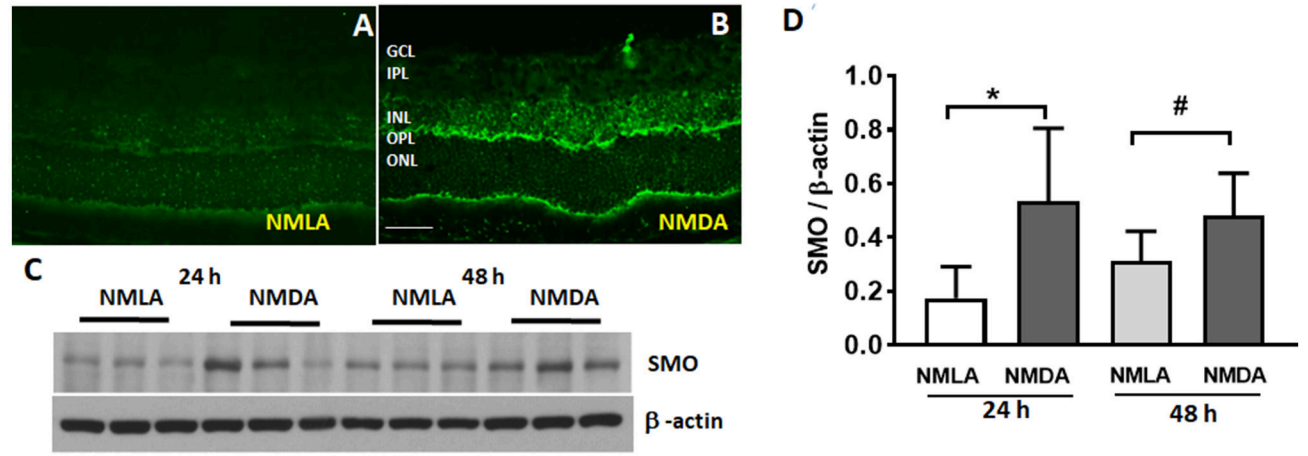

FIGURE 1 | Expression of SMO is increased in response to excitotoxicity. **(A,B)** Immunofluorescence images showing the localization and elevated expression of SMO in the NMDA retinas, 24 h following the injury. **(C)** Western blot studies showing increased SMO levels in NMDA retinas (24 h and 48 h post injury) compared to respective NMLA controls. **(D)** Quantitative analysis show significantly increased ($p < 0.05$) levels of SMO in NMDA retinas relative to respective controls. Data presented as Mean ± SD. $^{*}P < 0.01$; $^{\#}P < 0.05$, $N = 3$–6. Scale bar 50 μm. GCL, ganglion cell layer; INL, inner nuclear layer; IPL, inner plexiform layer; OPL, outer plexiform layer; ONL, outer nuclear layer.

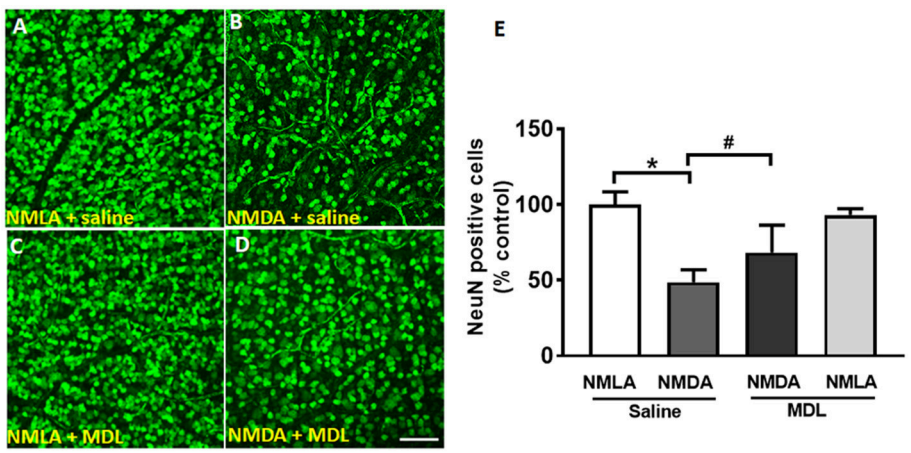

FIGURE 2 | Treatment with MDL reduced excitotoxicity-induced loss of GCL neurons. **(A–D)** Representative confocal images showing NeuN immunolabeling on retinal flat mounts (7 days post-injury) of control (NMLA) or excitotoxic (NMDA) retinas from mice treated with vehicle or MDL. **(E)** Quantitative analysis demonstrating significant loss of NeuN-positive cells in response to excitotoxicity, while MDL treatment improved the survival. Results are presented as a percentage of WT NMLA controls. Data are presented as Mean ± SD. $^{*}P < 0.01$, $^{\#}P < 0.05$. $N = 4$–6. Scale bar 100 μm.

Reduced Glial Activation in Response to MDL Treatment

Activation of glial cells (studied by GFAP upregulation) in the CNS occurs in response to neuronal injury (Hu et al., 2016). GFAP is typically expressed by astrocytes, and under conditions of retinal stress/injury, Müller cells show elevated GFAP levels. In the present study, glial activation was studied using GFAP immunolabelling of retinal cryostat sections (5 days post injury). Qualitative studies show upregulated levels of GFAP expression in NMDA retinas in comparison with their NMLA controls, while MDL treatment reduced the excitotoxicity mediated glial activation (**Figure 6**). Our data clearly show the upregulation of GFAP in Muller cells in response to excitotoxicity, as evidenced by increased levels in GCL, IPL, and INL. These changes were abrogated by MDL treatment. These results suggest that inhibition of PAO pathway limited the retinal glial activation in the NMDA-mediated neuronal injury.

MDL Treatment Reduced the Excitotoxicity-Induced Retinal Cell Death and Cell Death Signaling in the Retina

NMDA induced neurotoxicity leads to retinal cell death. In our study, we analyzed the cell death using TUNEL assay on retinal sections (3 days post injury). As shown in **Figures 7A–D**,

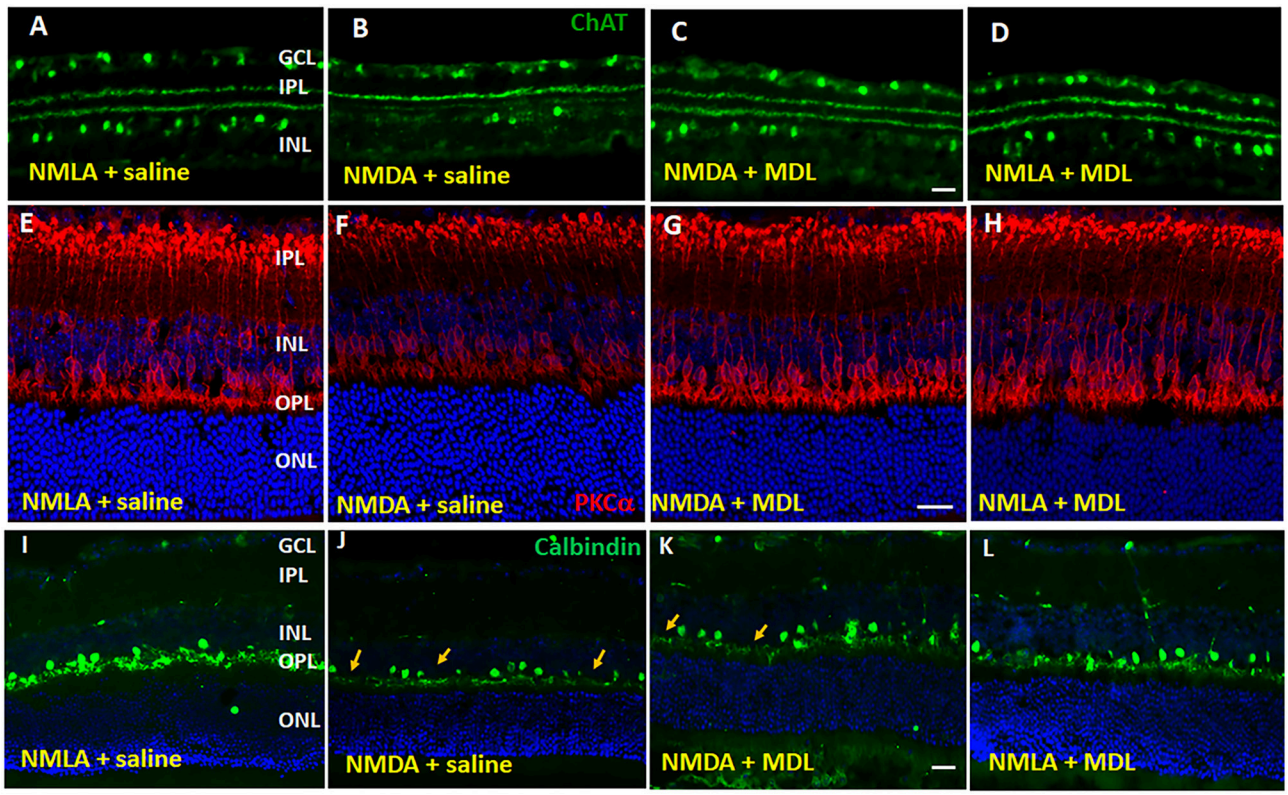

FIGURE 3 | Excitotoxicity-induced neurodegeneration in the inner retina is decreased by PAO inhibition. **(A–D)** Representative confocal images of retinal sections immunolabelled by ChAT, a marker of amacrine cells show reduced number of ChAT positive cells in GCL and INL of NMDA retinas. **(E–H)** Confocal images of retinal sections immunostained by PKCα, a marker for rod bipolar cells, showing the degenerating cells with shorter and distorted dendrites in the NMDA retina. **(I–L)** Calbindin immunolabelling shows the loss of horizontal cells along the OPL of NMDA retinas. Arrows indicate areas of cell loss. Scale bar 50 μm. GCL, ganglion cell layer; INL, inner nuclear layer; IPL, inner plexiform layer; OPL, outer plexiform layer; ONL, outer nuclear layer. $N = 4–6$, and representative images are presented.

many TUNEL positive cells were present in GCL and INL of NMDA-treated retinas. Inhibition of PAO using MDL treatment significantly reduced the number of TUNEL positive cells. NMLA treatment did not induce any cell death in the retinas studied. Quantitation of the number of TUNEL positive cells in excitotoxic retinas demonstrated a significant decrease in response to MDL treatment (**Figure 7E**). A significant increase ($p < 0.01$) in the total number of TUNEL positive cells was observed in vehicle-treated NMDA retinas compared to the respective NMLA controls. Treatment with MDL, significantly reduced ($p < 0.01$) the number of TUNEL positive cells in the NMDA retinal sections, in comparison with vehicle treated groups.

Further studies on the signaling pathways (48 h post-injury) showed downregulation of the survival signals including p-Akt and p-ERK and Bcl-xL in NMDA retinas, while these levels are normalized in response to MDL treatment (**Figure 8A**). Quantitation of the signaling studies is presented in **Figures 8B–E**. While there was a tendency toward reduction in the level of p-ERK2 in NMDA retinal samples (compared to NMLA controls), treatment with MDL significantly upregulated p-ERK2 levels in excitotoxic retinas ($p < 0.05$). There was a significant reduction ($p < 0.01$) in the level of p-Akt in NMDA retinas, while MDL treatment increased the level of Akt phosphorylation ($p < 0.05$). A reduction in the expression of total Akt was also evident in NMDA samples hence beta-actin was used to normalize p-Akt levels. A trend in the downregulation of Bcl-xL expression, another survival molecule was observed in retinas treated with NMDA, while the pattern was reversed in response to MDL treatment. However, these changes were not statistically significant. The marked increase in the level of BID, an apoptotic marker in NMDA retinas were significantly reduced ($p < 0.05$) in response to MDL treatment. These studies demonstrate the treatment with MDL, the PAO inactivator significantly reduce excitotoxicity induced retinal cell death and cell death signaling.

DISCUSSION

The present study provides the first specific evidence for the impact of MDL 72527, the PAO inhibitor in limiting excitotoxicity-induced neurodegeneration in the retina. Retinal excitotoxicity is recognized as a mechanism of neuronal

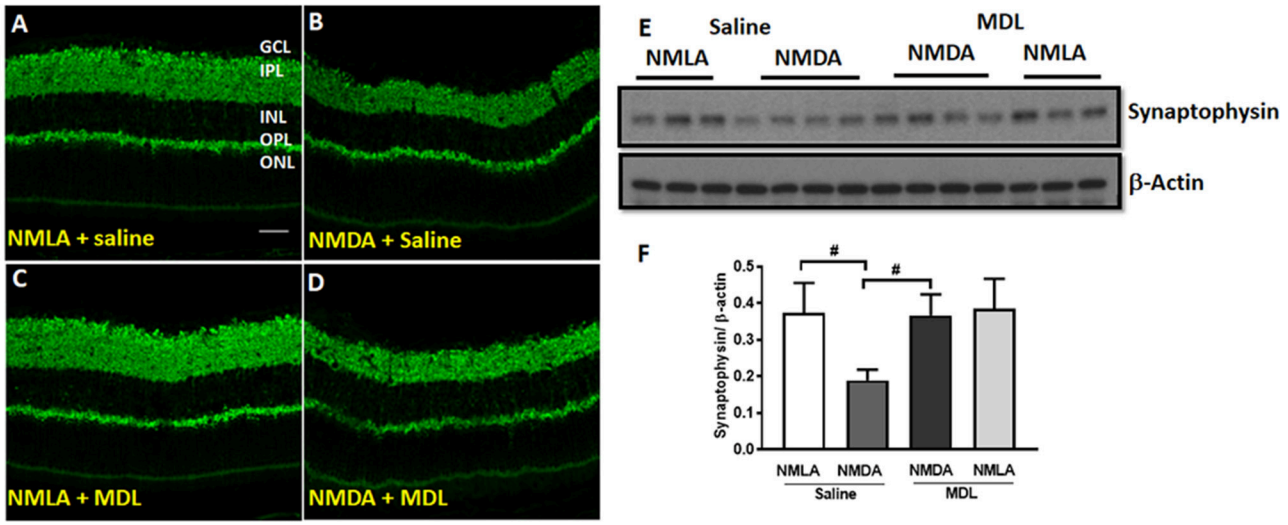

FIGURE 4 | PAO inhibition improved synaptic contacts in NMDA-treated retinas. **(A–D)** Immunofluorescence staining using synaptophysin (a pre-synaptic marker) antibody on retinal sections (5 days post-injury) demonstrating reduced synaptic contacts in NMDA retinas, while MDL treatment increased synaptophysin levels. **(E,F)** Western blot analysis and quantitation showing synaptophysin expression levels in retinal samples. A significant reduction was observed in NMDA-retinal samples, while MDL treatment significantly improved the expression of synaptophysin. Data presented as Mean ± SD. $^{\#}P < 0.05$. $N = 3$–4. GCL, ganglion cell layer; IPL, inner plexiform layer; INL, inner nuclear layer; OPL, outer plexiform layer; ONL, outer nuclear layer. Scale bar 50 μm.

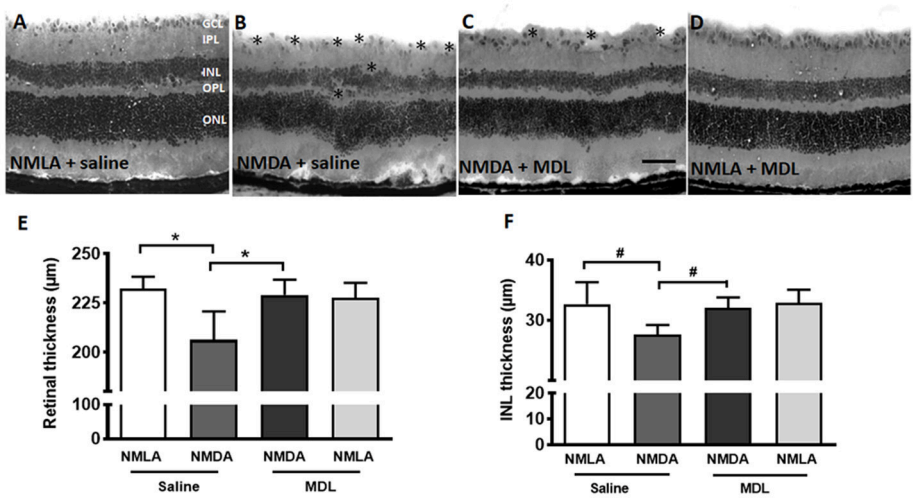

FIGURE 5 | MDL treatment preserved the retinal morphology and thickness. **(A–D)** Representative images of hematoxylin and eosin (H and E) stained retinal sections from NMDA-retinas showing reduced retinal thickness and loss of the cells in the GCL and INL (*areas of distortion/missing cells) at 7 days following the injury. This effect of excitotoxicity is markedly reduced in WT mice treated with MDL. **(E,F)** Quantitative analysis showing thickness of retina and INL using retinal sections. A significant reduction of total retinal and INL thickness was observed in the WT NMDA retinas compared to their controls, which was improved in response to MDL treatment. Data presented as Mean ± SD. $^{*}P < 0.01$, $^{\#}P < 0.05$. $N = 4$–6. GCL, ganglion cell layer; IPL, inner plexiform layer; INL, inner nuclear layer; OPL, outer plexiform layer; ONL, outer nuclear layer. Scale bar 100 μm.

death and dysfunction, and neuronal degeneration during NMDA has been studied previously by several groups (Wang et al., 2014; Ishimaru et al., 2017). However, the molecular mechanisms mediating the process are still not well-understood. Using the mouse OIR model, we have previously shown that polyamine oxidation is increased during hyperoxia-induced retinal degeneration and that treatment with MDL 72527 significantly reduced the retinal cell death in Narayanan et al. (2014) and Patel et al. (2016). In the present study, we are demonstrating neuroprotective effect of MDL 72527 on retinal degeneration in NMDA-induced excitotoxicity. To the best of our knowledge, this is the first report investigating the impact of PAO inhibition in excitotoxicity-induced neurodegeneration in the retina.

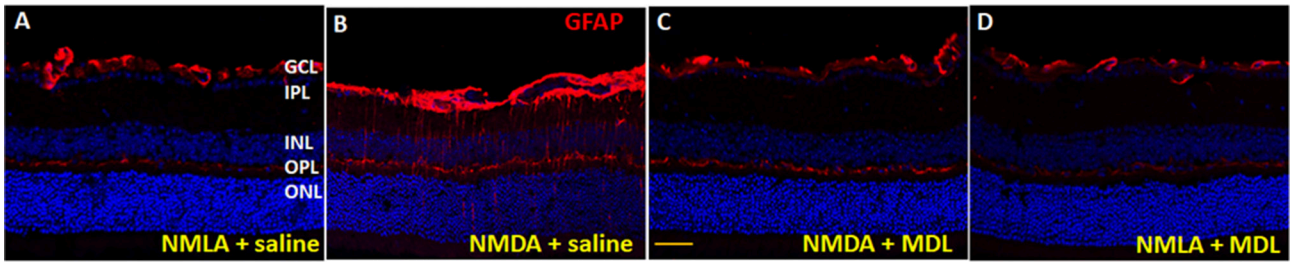

FIGURE 6 | Reduced glial activation in the MDL treated-NMDA retinas. **(A–D)** Immunofluorescence staining of retinal sections (5 days post-injury) using GFAP antibody, demonstrating activation of glial cells in the WT NMDA retina. MDL treatment markedly reduced this effect. $N = 4–6$, and representative images are presented. GCL, ganglion cell layer; IPL, inner plexiform layer; INL, inner nuclear layer; OPL, outer plexiform layer; ONL, outer nuclear layer. Scale bar 100 μm.

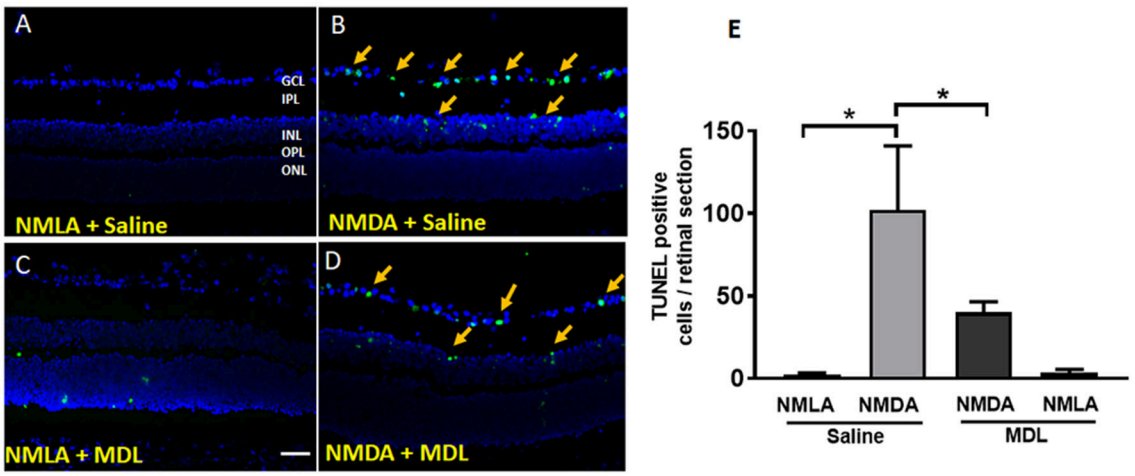

FIGURE 7 | PAO inhibition reduced excitotoxicity-induced cell death. **(A–D)** Representative images showing TUNEL labeling in retinal cryostat sections 3 days following NMDA treatment. The number of cells with fragmented DNA are increased in the WT NMDA retina. PAO inhibition using MDL treatment decreased the number of TUNEL-positive cells in NMDA retinas. Arrows indicate the presence of TUNEL positive cells. **(E)** Quantitation of TUNEL positive cells showing significantly elevated cell death in NMDA retinas, while MDL treatment reduced excitotoxicity-induced retinal cell death. Data presented as Mean ± SD. *$P < 0.01$. GCL, ganglion cell layer; IPL, inner plexiform layer; INL, inner nuclear layer; OPL, outer plexiform layer; ONL, outer nuclear layer. Scale bar 100 μm.

MDL 72527 is an irreversible competitive inhibitor of SMO and APAO, commonly known as the polyamine oxidases (Dogan et al., 1999b; Cervelli et al., 2013b). Increased expression or activity of PAO and altered levels of polyamines have been reported in CNS models of neuronal injury (Dogan et al., 1999a; Zahedi et al., 2010; Cervelli et al., 2013a). Studies in a rat model of cerebral ischemia have shown that inhibition of polyamine oxidases using MDL 72527 significantly reduced brain edema, ischemic injury volume, and polyamine levels (Dogan et al., 1999b). Furthermore, blockade of the polyamine oxidation using MDL 72527 was found to be neuroprotective against edema and necrotic cavitation after traumatic brain injury (Dogan et al., 1999a). Our present studies demonstrating increased SMO expression in the inner retina following the retinal damage, is consistent with the earlier studies showing elevated SMO levels in the OIR retina (Narayanan et al., 2014). Elevated SMO/APAO levels indicate increased polyamine oxidation and the resulting oxidative stress (Seiler, 2000).

Loss of ganglion cells is a major feature of excitotoxic injury to the retina. Consistent with other studies (Laabich and Cooper, 2000; Zhao et al., 2016; Ishimaru et al., 2017), we have demonstrated a significant loss of GCL layer neurons following the NMDA treatment. Similar to our previous report on the neuroprotective effect of PAO inhibition in the OIR model (Narayanan et al., 2014), the present studies show that treatment with MDL significantly reduced NMDA-induced neuronal death in the GCL. These results demonstrate the potential neuroprotective effect of MDL 72527 in limiting retinal neuronal injury. There is increasing evidence that in addition to RGC loss, degeneration of other inner retinal neurons, such as bipolar cells and amacrine cells as well as thinning of the INL are observed by NMDA induced retinal damage (Honjo et al., 2000; Kido et al., 2001; Kuehn et al., 2017). In the present study, we observed degeneration of amacrine, bipolar, and horizontal cells in response to NMDA treatment. Furthermore, a significant reduction in the expression of synaptophysin, a pre-synaptic marker was also evident in NMDA-treated retinas.

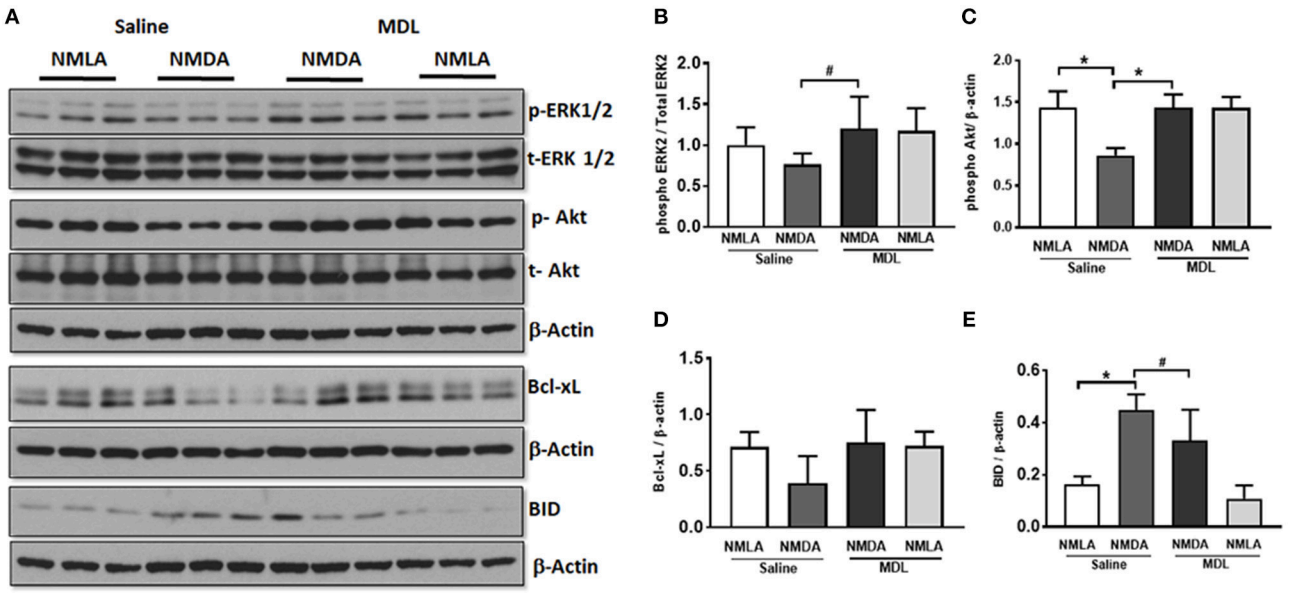

FIGURE 8 | MDL treatment upregulated survival signaling in NMDA retina. **(A)** Analysis of signaling pathways in retinal lysates (48 h post-injury) from control and NMDA retinas treated with vehicle or MDL. **(B–E)** Quantitation of Western blots showing downregulation of the survival pathways along with the upregulation of apoptotic molecules. Treatment with MDL prevented these changes in the NMDA retinas. Data presented as Mean ± SD. $^{*}P < 0.01$, $^{\#}P < 0.05$. $N = 4$–6.

PAO inhibition resulted in an upregulation of synaptophysin and improved survival of bipolar and horizontal cells in the NMDA-treated retinas. Thinning of the retina and retinal layers is another characteristic of neurodegenerative diseases of the eye (Luan et al., 2006; Gupta et al., 2016; Akaiwa et al., 2017; Ortiz et al., 2018). In the current study, a significant thinning of the total retina and INL was evident in the excitotoxic retinas, while treatment with MDL significantly prevented this degeneration, further confirming the neuroprotective effect of PAO inhibition.

Glial activation is considered as an indicator of injury to the retina during disease or stress conditions including ischemia/reperfusion (Yokota et al., 2011; Shosha et al., 2016; Renner et al., 2017), oxygen-induced retinopathy (Narayanan et al., 2011), diabetes (Fernandez-Bueno et al., 2017; Chaurasia et al., 2018) and neurotoxicity by NMDA (Casson et al., 2004; Sakamoto et al., 2017). Although a direct relationship between macroglial activation and ganglion cell death is not well defined, it can be said that Muller cell activation is a feature of retinal neurodegenerative diseases. Increased immunoreactivity for GFAP has widely used as a marker for glial activation. Our data clearly show the upregulation of GFAP in Muller cells in response to excitotoxicity, while MDL treatment abrogated this effect. The present study is the first to demonstrate that the MDL treatment decreases activation of GFAP in the glia during excitotoxicity, suggesting that inhibiting PAO reduces glial damage and limit injury of the inner retinal neurons.

In the present study, TUNEL-positive cells are located in the GCL and INL and clearly increased 3 days following excitotoxic injury, implying the release of factors to activate cell death. Further, our results demonstrate that MDL treatment significantly reduced the number of TUNEL positive cells, indicating that activation of PAO has an important role in the neuronal death process induced by excitotoxicity. A potential link between PAO activity and neuronal death has been described, which showed that inhibiting PAO function with is protective against neurodegeneration in eye disorders. Multiple pathways have been suggested to mediate excitotoxicity induced retinal neuronal death (Fan et al., 2007; Seki and Lipton, 2008; Sakamoto et al., 2016; Fahrenthold et al., 2018). In the present study, we observed downregulation of the survival pathways, Akt and ERK signaling, and upregulation of BID, an apoptotic molecule in the excitotoxic retinas. These changes were prevented in response to PAO inhibition.

Several mechanisms have been proposed responsible for NMDA-induced retinal neuronal death including inflammation and oxidative damage. The downstream mechanisms of PAO mediated excitotoxicity clearly involve oxidative stress. Oxidation of polyamines has been shown to lead to the generation of H_2O_2 and the reactive aldehydes (Seiler, 2004). We have previously shown that MDL treatment reduced H_2O_2 mediated oxidative damage in the OIR retina (Narayanan et al., 2014; Patel et al., 2016). Overproduction of H_2O_2, a mediator of oxidative stress has also been linked to excitotoxic injury in a transgenic mouse model overexpressing SMO in neonatal cortex (Cervelli et al., 2013a). However, the present study has not addressed whether polyamine oxidation causes excitotoxicity-induced cell death via ROS formation in the retina. An earlier study showed that polyamines regulate NMDA induced excitotoxic retinal neuronal death in rats (Pernet et al., 2007). The investigators found that inhibition of polyamine synthesis using DFMO (difluoromethylornithine) was neuroprotective, while administration of putrescine or

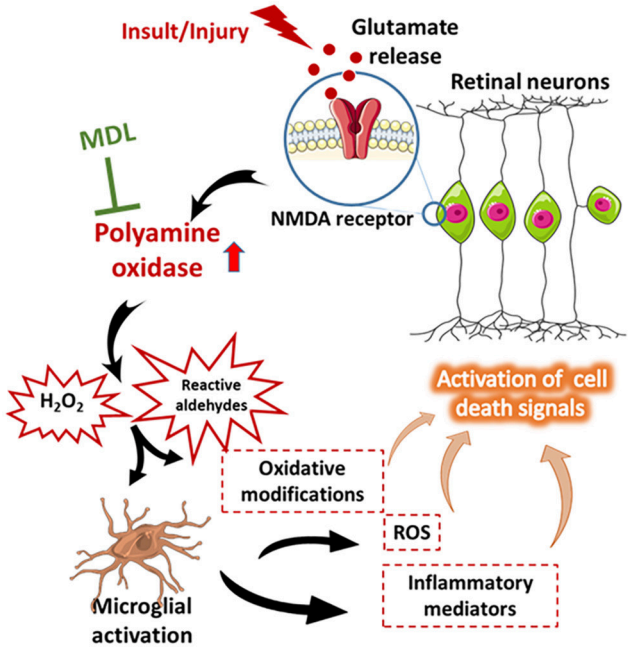

FIGURE 9 | Proposed molecular network of excitotoxicity. A diagrammatic representation of the proposed molecular mechanism of excitotoxicity-induced retinal neuronal death. This figure was prepared using Servier Medical Art (https://smart.servier.com/).

spermine potentiated NMDA-induced RGC death. However, the specific mechanisms of this excitotoxic neuronal death have not been investigated. We believe that oxidative stress could be one of the potential mediators of polyamine oxidase activity- induced retinal neuronal death.

Increasing evidence suggests that microglia, the resident immune cells of the central nervous system are activated in neurological diseases and initiate neuron damage, amplify ongoing neurotoxicity, and drive chronic neuronal loss over time (Block et al., 2007). When over activated, microglia can produce significant and highly detrimental neurotoxic effects by the excess production of array of cytotoxic factors such as superoxide (Colton and Gilbert, 1987; Kaneko et al., 2012; Zhang et al., 2012), nitric oxide (Moss and Bates, 2001; Ribeiro et al., 2013), and tumor necrosis factor-α (Yang et al., 2013; Borrajo et al., 2014; Chen et al., 2014). Reactive microglia have been demonstrated to be present in retinal samples from patients and/or disease models of diabetic retinopathy, glaucoma, ischemia reperfusion injury, and retinopathy of prematurity. Our previous study had shown that OIR-induced microglial activation and generation of inflammatory mediators are significantly reduced in response to PAO inhibition (Patel et al., 2016). Effect of MDL treatment on microglial activation and its impact on excitotoxicity-induced neuronal death will be investigated in our future studies. A proposed molecular mechanism for excitotoxicity-induced retinal neuronal death is presented in **Figure 9**.

In conclusion, our studies report for the first time the specific impact of inhibiting polyamine oxidation, using MDL 72527 treatment, in limiting excitotoxicity-induced neuronal damage in the retina. We have demonstrated a crucial role for the polyamine oxidase pathway as one of the major mechanisms associated with neuronal injury in the excitotoxic retina. Considering the need for new therapies for patients suffering from vision problems associated with retinal neurodegeneration, such as diabetic retinopathy or glaucoma, our findings are highly relevant from a clinical perspective. Our data suggest that inhibition of polyamine oxidase signaling can be considered as a therapeutic target to limit neuronal dysfunction in neurodegenerative diseases of the eye.

AUTHOR CONTRIBUTIONS

PP, CDP, and CP implemented experiments, analyzed the data, assembled the figures, and edited the manuscript. ZX generated the *in vivo* experimental model and helped with analyzing data. ES performed cell death studies and revised manuscript. AF helped analyzing experimental data and revising manuscript. RC contributed toward designing experiments and revising manuscript. SN provided experimental design and planning the entire study, and provided guidance with writing, editing, and revising the manuscript.

FUNDING

This work was supported by grants from The National Institute of Health [R01EY028569 (SN) and R01-507 EY11766 (RC)], the Department of Veterans Affairs, Veterans Health Administration (RC), Office of Research and Development, Biomedical Laboratory Research and Development (BX001233). RC is the recipient of a Research Career Scientist Award from the Department of Veterans Affairs. The contents do not represent the views of the Department of Veterans Affairs or the United States Government. The funders had no role in study design, data collection, and analysis, decision to publish, or preparation of the manuscript.

ACKNOWLEDGMENTS

We are thankful to Ms. Tahira Lemtalsi and Dr. Fang Liu for the technical assistance.

REFERENCES

Akaiwa, K., Namekata, K., Azuchi, Y., Guo, X., Kimura, A., Harada, C., et al. (2017). Edaravone suppresses retinal ganglion cell death in a mouse model of normal tension glaucoma. *Cell Death Dis.* 8:e2934. doi: 10.1038/cddis.2017.341

Amendola, R., Bellini, A., Cervelli, M., Degan, P., Marcocci, L., Martini, F., et al. (2005). Direct oxidative DNA damage, apoptosis and radio sensitivity by spermine oxidase activities in mouse neuroblastoma cells. *Biochim. Biophys. Acta* 1755, 15–24. doi: 10.1016/j.bbcan.2005.02.002

Araszkiewicz, A., and Zozulinska-Ziolkiewicz, D. (2016). Retinal neurodegeneration in the course of diabetes-pathogenesis and clinical perspective. *Curr. Neuropharmacol.* 14, 805–809. doi: 10.2174/1570159X14666160225154536

Block, M. L., Zecca, L., and Hong, J. S. (2007). Microglia-mediated neurotoxicity: uncovering the molecular mechanisms. *Nat. Rev. Neurosci.* 8, 57–69. doi: 10.1038/nrn2038

Borrajo, A., Rodriguez-Perez, A. I., Diaz-Ruiz, C., Guerra, M. J., and Labandeira-Garcia, J. L. (2014). Microglial TNF-alpha mediates enhancement of dopaminergic degeneration by brain angiotensin. *Glia* 62, 145–157. doi: 10.1002/glia.22595

Capone, C., Cervelli, M., Angelucci, E., Colasanti, M., Macone, A., Mariottini, P., et al. (2013). A role for spermine oxidase as a mediator of reactive oxygen species production in HIV-Tat-induced neuronal toxicity. *Free Radic. Biol. Med.* 63, 99–107. doi: 10.1016/j.freeradbiomed.2013.05.007

Casero, R. A., and Pegg, A. E. (2009). Polyamine catabolism and disease. *Biochem. J.* 421, 323–338. doi: 10.1042/BJ20090598

Casson, R. J., Chidlow, G., Wood, J. P., Vidal-Sanz, M., and Osborne, N. N. (2004). The effect of retinal ganglion cell injury on light-induced photoreceptor degeneration. *Invest. Ophthalmol. Vis. Sci.* 45, 685–693. doi: 10.1167/iovs.03-0674

Cervelli, M., Amendola, R., Polticelli, F., and Mariottini, P. (2012). Spermine oxidase: ten years after. *Amino Acids* 42, 441–450. doi: 10.1007/s00726-011-1014-z

Cervelli, M., Bellavia, G., D'Amelio, M., Cavallucci, V., Moreno, S., Berger, J., et al. (2013a). A new transgenic mouse model for studying the neurotoxicity of spermine oxidase dosage in the response to excitotoxic injury. *PLoS ONE* 8:e64810. doi: 10.1371/journal.pone.0064810

Cervelli, M., Polticelli, F., Fiorucci, L., Angelucci, E., Federico, R., and Mariottini, P. (2013b). Inhibition of acetylpolyamine and spermine oxidases by the polyamine analogue chlorhexidine. *J. Enzyme Inhib. Med. Chem.* 28, 463–467. doi: 10.3109/14756366.2011.650691

Chaurasia, S. S., Lim, R. R., Parikh, B. H., Wey, Y. S., Tun, B. B., Wong, T. Y., et al. (2018). The NLRP3 inflammasome may contribute to pathologic neovascularization in the advanced stages of diabetic retinopathy. *Sci. Rep.* 8:2847. doi: 10.1038/s41598-018-21198-z

Chen, C. C., Lin, J. T., Cheng, Y. F., Kuo, C. Y., Huang, C. F., Kao, S. H., et al. (2014). Amelioration of LPS-induced inflammation response in microglia by AMPK activation. *Biomed Res. Int.* 2014:692061. doi: 10.1155/2014/692061

Chintala, S., Cheng, M., and Zhang, X. (2015). Decreased expression of DREAM promotes the degeneration of retinal neurons. *PLoS ONE* 10:e0127776. doi: 10.1371/journal.pone.0127776

Colton, C. A., and Gilbert, D. L. (1987). Production of superoxide anions by a CNS macrophage, the microglia. *FEBS Lett.* 223, 284–288. doi: 10.1016/0014-5793(87)80305-8

Dogan, A., Rao, A. M., Baskaya, M. K., Hatcher, J., Temiz, C., Rao, V. L., et al. (1999a). Contribution of polyamine oxidase to brain injury after trauma. *J. Neurosurg.* 90, 1078–1082. doi: 10.3171/jns.1999.90.6.1078

Dogan, A., Rao, A. M., Hatcher, J., Rao, V. L., Baskaya, M. K., and Dempsey, R. J. (1999b). Effects of MDL 72527, a specific inhibitor of polyamine oxidase, on brain edema, ischemic injury volume, and tissue polyamine levels in rats after temporary middle cerebral artery occlusion. *J. Neurochem.* 72, 765–770. doi: 10.1046/j.1471-4159.1999.0720765.x

Fahrenthold, B. K., Fernandes, K. A., and Libby, R. T. (2018). Assessment of intrinsic and extrinsic signaling pathway in excitotoxic retinal ganglion cell death. *Sci. Rep.* 8:4641. doi: 10.1038/s41598-018-22848-y

Fan, W., Li, X., and Cooper, N. G. (2007). CaMKIIalphaB mediates a survival response in retinal ganglion cells subjected to a glutamate stimulus. *Invest. Ophthalmol. Vis. Sci.* 48, 3854–3863. doi: 10.1167/iovs.06-1382

Fernandez-Bueno, I., Jones, R., Soriano-Romani, L., Lopez-Garcia, A., Galvin, O., Cheetham, S., et al. (2017). Histologic characterization of retina neuroglia modifications in diabetic zucker diabetic fatty rats. *Invest. Ophthalmol. Vis. Sci.* 58, 4925–4933. doi: 10.1167/iovs.17-21742

Gomes-Trolin, C., Nygren, I., Aquilonius, S. M., and Askmark, H. (2002). Increased red blood cell polyamines in ALS and Parkinson's disease. *Exp. Neurol.* 177, 515–520. doi: 10.1006/exnr.2002.7952

Gupta, V. K., Chitranshi, N., Gupta, V. B., Golzan, M., Dheer, Y., Wall, R. V., et al. (2016). Amyloid beta accumulation and inner retinal degenerative changes in Alzheimer's disease transgenic mouse. *Neurosci. Lett.* 623, 52–56. doi: 10.1016/j.neulet.2016.04.059

Honjo, M., Tanihara, H., Kido, N., Inatani, M., Okazaki, K., and Honda, Y. (2000). Expression of ciliary neurotrophic factor activated by retinal Muller cells in eyes with NMDA- and kainic acid-induced neuronal death. *Invest. Ophthalmol. Vis. Sci.* 41, 552–560.

Hu, X., Yuan, Y., Wang, D., and Su, Z. (2016). Heterogeneous astrocytes: active players in CNS. *Brain Res. Bull.* 125, 1–18. doi: 10.1016/j.brainresbull.2016.03.017

Hussain, T., Tan, B., Ren, W., Rahu, N., Dad, R., Kalhoro, D. H., et al. (2017). Polyamines: therapeutic perspectives in oxidative stress and inflammatory diseases. *Amino Acids* 49, 1457–1468. doi: 10.1007/s00726-017-2447-9

Inoue, K., Tsutsui, H., Akatsu, H., Hashizume, Y., Matsukawa, N., Yamamoto, T., et al. (2013). Metabolic profiling of Alzheimer's disease brains. *Sci. Rep.* 3:2364. doi: 10.1038/srep02364

Ishimaru, Y., Sumino, A., Kajioka, D., Shibagaki, F., Yamamuro, A., Yoshioka, Y., et al. (2017). Apelin protects against NMDA-induced retinal neuronal death via an APJ receptor by activating Akt and ERK1/2, and suppressing TNF-alpha expression in mice. *J. Pharmacol. Sci.* 133, 34–41. doi: 10.1016/j.jphs.2016.12.002

Ivanova, S., Batliwalla, F., Mocco, J., Kiss, S., Huang, J., Mack, W., et al. (2002). Neuroprotection in cerebral ischemia by neutralization of 3-aminopropanal. *Proc. Natl. Acad. Sci. U.S.A.* 99, 5579–5584. doi: 10.1073/pnas.082609299

Jindal, N., Banik, A., Prabhakar, S., Vaiphie, K., and Anand, A. (2017). Alteration of neurotrophic factors after transplantation of bone marrow derived lin-ve stem cell in NMDA-induced mouse model of retinal degeneration. *J. Cell. Biochem.* 118, 1699–1711. doi: 10.1002/jcb.25827

Jindal, V. (2015). Neurodegeneration as a primary change and role of neuroprotection in diabetic retinopathy. *Mol. Neurobiol.* 51, 878–884. doi: 10.1007/s12035-014-8732-7

Kaneko, Y. S., Ota, A., Nakashima, A., Mori, K., Nagatsu, I., and Nagatsu, T. (2012). Regulation of oxidative stress in long-lived lipopolysaccharide-activated microglia. *Clin. Exp. Pharmacol. Physiol.* 39, 599–607. doi: 10.1111/j.1440-1681.2012.05716.x

Kido, N., Inatani, M., Honjo, M., Yoneda, S., Hara, H., Miyawaki, N., et al. (2001). Dual effects of interleukin-1beta on N-methyl-D-aspartate-induced retinal neuronal death in rat eyes. *Brain Res.* 910, 153–162. doi: 10.1016/S0006-8993(01)02706-8

Kuehn, S., Rodust, C., Stute, G., Grotegut, P., Meissner, W., Reinehr, S., et al. (2017). Concentration-dependent inner retina layer damage and optic nerve degeneration in a nmda model. *J. Mol. Neurosci.* 63, 283–299. doi: 10.1007/s12031-017-0978-x

Laabich, A., and Cooper, N. G. (2000). Neuroprotective effect of AIP on N-methyl-D-aspartate-induced cell death in retinal neurons. *Brain Res. Mol. Brain Res.* 85, 32–40. doi: 10.1016/S0169-328X(00)00226-6

Lewandowski, N. M., Ju, S., Verbitsky, M., Ross, B., Geddie, M. L., Rockenstein, E., et al. (2010). Polyamine pathway contributes to the pathogenesis of Parkinson disease. *Proc. Natl. Acad. Sci. U.S.A.* 107, 16970–16975. doi: 10.1073/pnas.1011751107

Liu, W., Liu, R., Schreiber, S. S., and Baudry, M. (2001). Role of polyamine metabolism in kainic acid excitotoxicity in organotypic hippocampal slice cultures. *J. Neurochem.* 79, 976–984. doi: 10.1046/j.1471-4159.2001.00650.x

Luan, H., Roberts, R., Sniegowski, M., Goebel, D. J., and Berkowitz, B. A. (2006). Retinal thickness and subnormal retinal oxygenation response in experimental diabetic retinopathy. *Invest. Ophthalmol. Vis. Sci.* 47, 320–328. doi: 10.1167/iovs.05-0272

Morrison, L. D., and Kish, S. J. (1995). Brain polyamine levels are altered in Alzheimer's disease. *Neurosci. Lett.* 197, 5–8. doi: 10.1016/0304-3940(95)11881-V

Moss, D. W., and Bates, T. E. (2001). Activation of murine microglial cell lines by lipopolysaccharide and interferon-gamma causes NO-mediated decreases in mitochondrial and cellular function. *Eur. J. Neurosci.* 13, 529–538. doi: 10.1046/j.1460-9568.2001.01418.x

Narayanan, S. P., Suwanpradid, J., Saul, A., Xu, Z., Still, A., Caldwell, R. W., et al. (2011). Arginase 2 deletion reduces neuro-glial injury and improves retinal function in a model of retinopathy of prematurity. *PLoS ONE* 6:e22460. doi: 10.1371/journal.pone.0022460

Narayanan, S. P., Xu, Z., Putluri, N., Sreekumar, A., Lemtalsi, T., Caldwell, R. W., et al. (2014). Arginase 2 deficiency reduces hyperoxia-mediated retinal neurodegeneration through the regulation of polyamine metabolism. *Cell Death Dis.* 5:e1075. doi: 10.1038/cddis.2014.23

Nucci, C., Russo, R., Martucci, A., Giannini, C., Garaci, F., Floris, R., et al. (2016). New strategies for neuroprotection in glaucoma, a disease that affects the central nervous system. *Eur. J. Pharmacol.* 787, 119–126. doi: 10.1016/j.ejphar.2016.04.030

Ortiz, G., Lopez, E. S., Salica, J. P., Potilinski, C., Fernandez Acquier, M., Chuluyan, E., et al. (2018). Alpha-1-antitrypsin ameliorates inflammation and neurodegeneration in the diabetic mouse retina. *Exp. Eye Res.* 174, 29–39. doi: 10.1016/j.exer.2018.05.013

Paik, M. J., Ahn, Y. H., Lee, P. H., Kang, H., Park, C. B., Choi, S., et al. (2010). Polyamine patterns in the cerebrospinal fluid of patients with Parkinson's disease and multiple system atrophy. *Clin. Chim. Acta* 411, 1532–1535. doi: 10.1016/j.cca.2010.05.034

Patel, C., Xu, Z., Shosha, E., Xing, J., Lucas, R., Caldwell, R. W., et al. (2016). Treatment with polyamine oxidase inhibitor reduces microglial activation and limits vascular injury in ischemic retinopathy. *Biochim. Biophys. Acta* 1862, 1628–1639. doi: 10.1016/j.bbadis.2016.05.020

Pernet, V., Bourgeois, P., and Di Polo, A. (2007). A role for polyamines in retinal ganglion cell excitotoxic death. *J. Neurochem.* 103, 1481–1490. doi: 10.1111/j.1471-4159.2007.04843.x

Renner, M., Stute, G., Alzureiqi, M., Reinhard, J., Wiemann, S., Schmid, H., et al. (2017). Optic nerve degeneration after retinal ischemia/reperfusion in a rodent model. *Front. Cell. Neurosci.* 11:e254. doi: 10.3389/fncel.2017.00254

Ribeiro, B. M., do Carmo, M. R., Freire, R. S., Rocha, N. F., Borella, V. C., de Menezes, A. T., et al. (2013). Evidences for a progressive microglial activation and increase in iNOS expression in rats submitted to a neurodevelopmental model of schizophrenia: reversal by clozapine. *Schizophr. Res.* 151, 12–19. doi: 10.1016/j.schres.2013.10.040

Sakamoto, K., Murakami, Y., Sawada, S., Ushikubo, H., Mori, A., Nakahara, T., et al. (2016). Apelin-36 is protective against N-methyl-D-aspartic-acid-induced retinal ganglion cell death in the mice. *Eur. J. Pharmacol.* 791, 213–220. doi: 10.1016/j.ejphar.2016.08.036

Sakamoto, K., Okuwaki, T., Ushikubo, H., Mori, A., Nakahara, T., and Ishii, K. (2017). Activation inhibitors of nuclear factor kappa B protect neurons against the NMDA-induced damage in the rat retina. *J. Pharmacol. Sci.* 135, 72–80. doi: 10.1016/j.jphs.2017.09.031

Seiler, N. (2000). Oxidation of polyamines and brain injury. *Neurochem. Res.* 25, 471–490. doi: 10.1023/A:1007508008731

Seiler, N. (2004). Catabolism of polyamines. *Amino Acids* 26, 217–233. doi: 10.1007/s00726-004-0070-z

Seiler, N., Duranton, B., and Raul, F. (2002). The polyamine oxidase inactivator MDL 72527. *Prog. Drug. Res.* 59, 1–40.

Seki, M., and Lipton, S. A. (2008). Targeting excitotoxic/free radical signaling pathways for therapeutic intervention in glaucoma. *Prog. Brain Res.* 173, 495–510. doi: 10.1016/S0079-6123(08)01134-5

Shen, Y., Liu, X. L., and Yang, X. L. (2006). N-methyl-D-aspartate receptors in the retina. *Mol. Neurobiol.* 34, 163–179. doi: 10.1385/MN:34:3:163

Shosha, E., Xu, Z., Yokota, H., Saul, A., Rojas, M., Caldwell, R. W., et al. (2016). Arginase 2 promotes neurovascular degeneration during ischemia/reperfusion injury. *Cell Death Dis.* 7:e2483. doi: 10.1038/cddis.2016.295

Sone, K., Mori, A., Sakamoto, K., and Nakahara, T. (2018). GYY4137, an Extended-release hydrogen sulfide donor, reduces NMDA-induced neuronal injury in the murine retina. *Biol. Pharm. Bull.* 41, 657–660. doi: 10.1248/bpb.b17-01032

Takano, K., Ogura, M., Nakamura, Y., and Yoneda, Y. (2005). Neuronal and glial responses to polyamines in the ischemic brain. *Curr. Neurovasc. Res.* 2, 213–223. doi: 10.2174/156720205436835

Takeda, H., Kitaoka, Y., Hayashi, Y., Kumai, T., Munemasa, Y., Fujino, H., et al. (2007). Calcium/calmodulin-dependent protein kinase II regulates the phosphorylation of CREB in NMDA-induced retinal neurotoxicity. *Brain Res.* 1184, 306–315. doi: 10.1016/j.brainres.2007.09.055

Tsutsumi, T., Iwao, K., Hayashi, H., Kirihara, T., Kawaji, T., Inoue, T., et al. (2016). Potential neuroprotective effects of an LSD1 inhibitor in retinal ganglion cells via p38 MAPK activity. *Invest. Ophthalmol. Vis. Sci.* 57, 6461–6473. doi: 10.1167/iovs.16-19494

Vidal-Sanz, M., Valiente-Soriano, F. J., Ortin-Martinez, A., Nadal-Nicolas, F. M., Jimenez-Lopez, M., Salinas-Navarro, M., et al. (2015). Retinal neurodegeneration in experimental glaucoma. *Prog. Brain Res.* 220, 1–35. doi: 10.1016/bs.pbr.2015.04.008

Wang, Y., Wang, Y., Yang, Q., Guo, L., Yin, Y., Fan, N., et al. (2014). Neuroprotective effects of C3 exoenzyme in excitotoxic retinopathy. *Exp. Eye Res.* 125, 128–134. doi: 10.1016/j.exer.2014.05.018

Weiger, T. M., and Hermann, A. (2014). Cell proliferation, potassium channels, polyamines and their interactions: a mini review. *Amino Acids* 46, 681–688. doi: 10.1007/s00726-013-1536-7

Wood, P. L., Khan, M. A., Moskal, J. R., Todd, K. G., Tanay, V. A., and Baker, G. (2006). Aldehyde load in ischemia-reperfusion brain injury: neuroprotection by neutralization of reactive aldehydes with phenelzine. *Brain Res.* 1122, 184–190. doi: 10.1016/j.brainres.2006.09.003

Yang, Y. M., Shang, D. S., Zhao, W. D., Fang, W. G., and Chen, Y. H. (2013). Microglial TNF-alpha-dependent elevation of MHC class I expression on brain endothelium induced by amyloid-beta promotes T cell transendothelial migration. *Neurochem. Res.* 38, 2295–2304. doi: 10.1007/s11064-013-1138-5

Yatin, S. M., Yatin, M., Varadarajan, S., Ain, K. B., and Butterfield, D. A. (2001). Role of spermine in amyloid beta-peptide-associated free radical-induced neurotoxicity. *J. Neurosci. Res.* 63, 395–401. doi: 10.1002/1097-4547(20010301)63:5<395::AID-JNR1034>3.0.CO;2-Q

Yokota, H., Narayanan, S. P., Zhang, W., Liu, H., Rojas, M., Xu, Z., et al. (2011). Neuroprotection from retinal ischemia/reperfusion injury by NOX2 NADPH oxidase deletion. *Invest. Ophthalmol. Vis. Sci.* 52, 8123–8131. doi: 10.1167/iovs.11-8318

Yu, X., Xu, Z., Mi, M., Xu, H., Zhu, J., Wei, N., et al. (2008). Dietary taurine supplementation ameliorates diabetic retinopathy via anti-excitotoxicity of glutamate in streptozotocin-induced Sprague-Dawley rats. *Neurochem. Res.* 33, 500–507. doi: 10.1007/s11064-007-9465-z

Zahedi, K., Huttinger, F., Morrison, R., Murray-Stewart, T., Casero, R. A., and Strauss, K. I. (2010). Polyamine catabolism is enhanced after traumatic brain injury. *J. Neurotrauma* 27, 515–525. doi: 10.1089/neu.2009.1097

Zhang, G., He, J. L., Xie, X. Y., and Yu, C. (2012). LPS-induced iNOS expression in N9 microglial cells is suppressed by geniposide via ERK, p38 and nuclear factor-kappaB signaling pathways. *Int. J. Mol. Med.* 30, 561–568. doi: 10.3892/ijmm.2012.1030

Zhao, J., Mysona, B. A., Qureshi, A., Kim, L., Fields, T., Gonsalvez, G. B., et al. (2016). (+)-Pentazocine reduces NMDA-induced murine retinal ganglion cell death through a sigmaR1-dependent mechanism. *Invest. Ophthalmol. Vis. Sci.* 57, 453–461. doi: 10.1167/iovs.15-18565

Conflict of Interest Statement: The authors declare that the research was conducted in the absence of any commercial or financial relationships that could be construed as a potential conflict of interest.

frontiers in Neurology

PERSPECTIVE
published: 06 February 2019
doi: 10.3389/fneur.2019.00028

microRNA-34a (miRNA-34a) Mediated Down-Regulation of the Post-synaptic Cytoskeletal Element SHANK3 in Sporadic Alzheimer's Disease (AD)

Yuhai Zhao[1,2], *Vivian R. Jaber*[1], *Ayrian LeBeauf*[1], *Nathan M. Sharfman*[1] and *Walter J. Lukiw*[1,3,4]*

[1] LSU Neuroscience Center, Louisiana State University Health Sciences Center New Orleans, New Orleans, LA, United States, [2] Department of Anatomy and Cell Biology, Louisiana State University Health Sciences Center, New Orleans, LA, United States, [3] Department of Ophthalmology, Louisiana State University Health Sciences Center New Orleans, New Orleans, LA, United States, [4] Department of Neurology, Louisiana State University Health Sciences Center New Orleans, New Orleans, LA, United States

Integrating a combination of bioinformatics, microRNA microfluidic arrays, ELISA analysis, LED Northern, and transfection-luciferase reporter assay data using human neuronal-glial (HNG) cells in primary culture we have discovered a set of up-regulated microRNAs (miRNAs) linked to a small family of down-regulated messenger RNAs (mRNAs) within the superior temporal lobe neocortex (Brodmann A22) of sporadic Alzheimer's disease (AD) brain. At the level of mRNA abundance, the expression of a significant number of human brain genes found to be down-regulated in sporadic AD neocortex appears to be due to the increased abundance of a several brain-abundant inducible miRNAs. These up-regulated miRNAs—including, prominently, miRNA-34a—have complimentary RNA sequences in the 3′ untranslated-region (3′-UTR) of their target-mRNAs that results in the pathological down-regulation in the expression of important brain genes. An up-regulated microRNA-34a, already implicated in age-related inflammatory-neurodegeneration–appears to down-regulate key mRNA targets involved in synaptogenesis and synaptic-structure, distinguishing neuronal deficits associated with AD neuropathology. One significantly down-regulated post-synaptic element in AD is the proline-rich SH3 and multiple-ankyrin-repeat domain SHANK3 protein. Bioinformatics, microRNA array analysis and SHANK3-mRNA-3′UTR luciferase-reporter assay confirmed the importance of miRNA-34a in the regulation of SHANK3 expression in HNG cells. This paper reports on recent studies of a miRNA-34a-up-regulation coupled to SHANK3 mRNA down-regulation in sporadic AD superior-temporal lobe compared to age-matched controls. These findings further support our hypothesis of an altered miRNA-mRNA coupled signaling network in AD, much of which is supported, and here reviewed, by recently reported experimental-findings in the scientific literature.

Keywords: Alzheimer's disease (AD), miRNA-34a, neurotransmission, post-synaptic density proteins, SHANK3 protein, superior temporal lobe neocortex (Brodmann A22), synaptic structure in disease, synaptic transmission

OPEN ACCESS

Edited by:
Patrice E. Fort, University of Michigan, United States

Reviewed by:
Cláudia Guimas Almeida, New University of Lisbon, Portugal
Xuping Li, Houston Methodist Research Institute, United States

***Correspondence:**
Walter J. Lukiw
wlukiw@lsuhsc.edu

Specialty section:
This article was submitted to Neurodegeneration, a section of the journal Frontiers in Neurology

Received: *05 September 2018*
Accepted: *10 January 2019*
Published: *06 February 2019*

Citation:
Zhao Y, Jaber VR, LeBeauf A, Sharfman NM and Lukiw WJ (2019) microRNA-34a (miRNA-34a) Mediated Down-Regulation of the Post-synaptic Cytoskeletal Element SHANK3 in Sporadic Alzheimer's Disease (AD). Front. Neurol. 10:28. doi: 10.3389/fneur.2019.00028

OVERVIEW

Alzheimer's disease (AD) is a complex, insidious, and ultimately lethal neurodegenerative disorder characterized by the appearance of pro-inflammatory lesions known as senile plaques and neurofibrillary tangles and a progressive disruption of the synaptic architecture of the brain. Synaptic loss and synapto-axonal pathology in AD is thought to be the strongest correlation to, and the basis for, the loss of sensory, intellectual, and cognitive function in AD patients (1–5). Indeed the most recent studies employing stepwise regression analysis has revealed that the major correlate of cognitive deficiency in AD is synaptic loss in the prefrontal cortex, and this contributes strongly to the association between global psychometric assessment and neuronal network collapse (4–7).

Because inter-neuronal signaling in the human central nervous system (CNS) is achieved through a complex network of presynaptic and postsynaptic elements essential in the conveyance of both electrical and neurochemical information, we have focused our investigations on the structural and functional integrity of key pre- and post-synaptic components in the superior temporal lobe neocortex (Brodmann A22), an anatomical region targeted by the AD process. One recently characterized core element essential for the efficient operation of this complex inter-neuronal signaling network is the relatively abundant ∼185 kDa proline-rich cytoskeletal scaffolding and post-synaptic density (PSD) protein known as SHANK3 (SH3-and multiple ankyrin repeat domains 3; encoded at human chr 22q13.33) (8, 8–13). Interestingly, disruption in the abundance of the postsynaptic SHANK3 cytoskeletal anchoring protein has been associated with neurological disorders including autism spectrum disorder (ASD), bipolar disorder (BD), Phelan-McDermid syndrome (PMS; 22q13.3 deletion syndrome), intellectual disability, schizophrenia (SZ), and sporadic AD (9, 10, 14). In this "*Perspectives*" article, we review and comment on recent advances in SHANK3 research as it pertains to age-related neurodegeneration using AD as an important example wherever possible. We also include some original data that provides evidence indicating that SHANK3 is under post-transcriptional control by an inducible NF-kB-regulated microRNA-34a in the temporal lobe neocortex, and adds to the growing list of pathological genetic mechanisms and cardiovascular and neurological disease-relevant messenger RNAs (mRNAs) targeted by the CNS-abundant miRNA-34a [see below;(15–18)].

SHANK3 DOWN-REGULATION AND SYNAPTIC SIGNALING DEFICITS

The SH3 and multiple ankyrin (ANK)-repeat domain-proteins SHANK1, SHANK2, and SHANK3 (also known as the ProSAP family, SHANK postsynaptic density proteins, the proline-rich synapse-associated family of proteins; also known as PROSAP2, PSAP2, SCZD15, SPANK-2) encode a small family of related postsynaptic scaffolding proteins that are highly abundant at glutamatergic synapses in the human CNS (8, 12). SHANK proteins are essential to post-synaptic structure and function in connecting, linking, networking and anchoring neurotransmitter receptors, ion channels, and other integral membrane proteins to the actin cytoskeleton and in the normal "homeostatic" operation of G-protein-coupled signaling pathways. Research evidence indicates that the massive SHANK3 protein (at ∼185 kDa) forms an extensive post-synaptic cytoskeletal scaffolding network (involving the linkage of multiple SHANK3 proteins at the PSD) to which the smaller PSD-95 (at ∼95kDa) protein is tethered usually via the SAPAP protein (∼100 kDa); interestingly both SHANK3 and PSD-95 proteins, highly interactive components of the PSD complex, are reduced in abundance in the temporal lobe of AD-affected brain (13, 19, 20). SHANK3 post-synaptic scaffolding proteins thereby play essential roles in synapse formation and organization, synaptic cell adhesion, dendritic spine maturation and synaptic vesicle release (4, 11, 13, 21, 22). All SHANK species are abundantly expressed in the human CNS but exhibit different anatomical, developmental, and spatial patterns of expression; SHANK3 appears to have preferential expression in the human neocortex and hippocampus. Indeed, like all SHANK proteins, SHANK3 contains multiple domains for extensive protein-protein interaction including ankyrin (ANK) repeats—hence a deficit in these central and major cytoskeletal components, key players for both synapse formation and the modulation of synaptic transmission and synaptic plasticity, may be responsible for major synaptic aberrations and loss of the capability for inter-neuronal communication, with ensuing cognitive impairment, as has been observed in multiple neurological disorders (9, 10, 12) (**Figures 1A–E**). As for mentioned, these disorders include several seemingly unrelated human neurological syndromes such as sporadic AD, ASD, BD, PMS, and SZ (8, 9, 21). Indeed, synaptic dysfunction and abnormal behaviors in transgenic murine models are apparent in mice lacking adequate SHANK3; in the CNS of the transgenic AD (TgAD) 5x familial AD murine model engineered to overexpress the 42 amino acid amyloid-beta (Aβ42) peptide, SHANK3 was also found to be significantly downregulated but the pathological mechanisms remain unclear (9, 10, 12, 21, 25–27). Interestingly, the extra-neural levels of Aβ peptide oligomers have been shown to strongly correlate with the severity of cognitive impairment (using the Blessed information-memory-concentration score and mini-mental state examination, MMSE) and with the loss of synaptic markers such as SHANK3 that results in the disruption of synaptic function (5, 28). It has been known for some time that the application of known pro-inflammatory stressors, such as the Aβ42 peptide and neurotoxic metal sulfates (such as aluminum sulfate) to human neuronal-glial (HNG) cells in primary culture also results in a significant decrease in the expression of SHANK3 (9, 10, 12). Collectively these data indicate that deficits in SHANK3-expression may be one common denominator linking a wide-range of human neurodegenerative disorders that exhibit a progressive synaptic disorganization temporally associated with progressive, developmental, and/or age-related intellectual disability combined with sensory and cognitive decline.

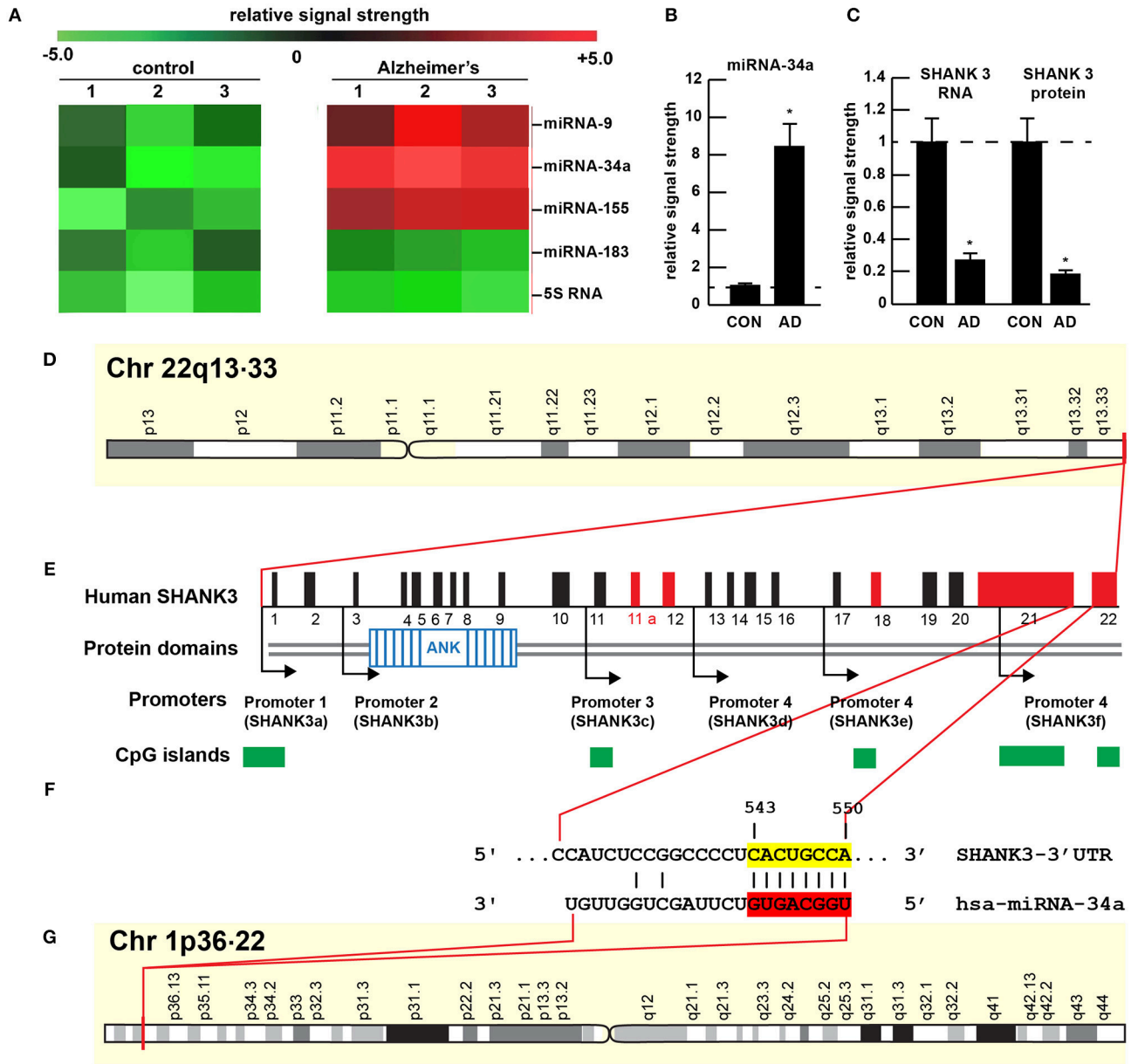

FIGURE 1 | Gene products on human chromosomes 1 and 22 interactively contribute to SHANK3 expression in CNS tissues. **(A)** Results of miRNA microfluidic array analysis; miRNA-34a is significantly up-regulated in the sporadic AD temporal lobe compared to miRNA-183 and 5S RNA control sncRNA markers; the numbers 1–3 indicates 3 separate control and age-matched AD cases; all female; control mean age 72.1 ± 6.6 years; AD mean age 73.8 ± 8.2 years; $N = 3$ control and 3 AD: all post mortem intervals <3 h; **(B)** quantitation of miRNA-34a levels in bar graph format; **(C)** quantitation of SHANK3 mRNA (using Northern analysis) and SHANK3 protein (using ELISA) in the superior temporal lobe of control and AD as previously described (9, 23); $N = 3$; $^*p < 0.001$ (ANOVA). **(D–G)** highly schematicized depiction of the human SHANK3 gene organization at chr 22q13.33 and the human miRNA-34a gene organization at chr 1p36.22; with a P_{CT} (probability of conserved targeting) or Friedman score of 83 [(24); that has been calculated for all highly conserved miRNA families]; this hsa-miRNA-34a-SHANK3-3′-UTR recognition/interaction is highly favorable and almost certain to occur in the cytoplasm/nucleoplasm of CNS cells; **(E)** has been modified from (25); the homo sapien (hsa) microRNA-34a (hsa-miRNA-34a) is encoded from the distal end of human chromosome 1p (at chr 1p36.22) and generates a 22 nt mature miRNA-34a species; hence the expression of at least two genes, one cytoskeletal and structural (SHANK3) and one regulatory (miRNA-34a) on human chromosomes 1p and 22q is required for regulating the expression of SHANK3.

miRNA-34a

The 22 nucleotide (nt) miRNA-34a (**Figures 1F**, **2**) encoded in humans as a single copy gene at chr1p36.22 has about ∼1,200 predicted human mRNA targets using standard bioinformatics analysis (miRBase; EMBL-EBI; www.genecards.org/cgi-bin/carddisp.pl?gene=MIR34A; accessed 17 January 2019); major bioinformatics- and experimentally-verified miRNA-34a-mRNA targets include those encoding TREM2, a transmembrane glycoprotein of microglial cells that plays a role in amyloid

sensing and removal (29). miRNA-34a has also been implicated in epithelial cell proliferation, in endothelial cell-mediated inflammation, in T-cell activation and in the regulation of the innate-immune system, in the down-regulation of the apoptosis regulator/suppressor Bcl-2, in both cardiovascular and neurovascular disease mechanisms involving epithelial and endothelial cell linings, and in the down-regulation of expression of specific synaptic cytoskeletal elements including SHANK3 [this publication (8, 9, 15–18)]. Recent data have further indicated that as an NF-kB-inducible microRNA, miRNA-34a appears to play analogous roles in AD, age-related macular degeneration (AMD), autism and in transgenic murine models of AD or AMD (TgAD, TgAMD) (18, 29–31). For example, miRNA-34a up-regulation in a double transgenic mouse model (APPswe/PSDeltaE9) of AD has been shown to inhibit the translation of the anti-apoptosis regulating protein Bcl-2 resulting in a progressive and pro-inflammatory neurodegeneration, and excessive miRNA-34a has a significant inhibitory effect on retinal pigment epithelial cell proliferation and migration (17, 30–32). More recently, miRNA-34a has been shown to regulate the calcium- and calmodulin-dependent serine/threonine protein phosphatase heterodimer calcineurin 1 to modulate endothelial inflammation and T-cell activation in the innate-immune system (33). We have observed a significant increase in miRNA-34a abundance in AD temporal lobe neocortex averaging a remarkable 8.1-fold increase over control in 6 AD brain tissue samples over control coupled to SHANK3 deficits, at both the SHANK3 mRNA level (to 0.27-fold of controls) and at the SHANK3 protein level (to 0.18-fold of controls) within the same neocortical tissue sample (**Figures 1A–C**). Taken together the results suggest that increases in miRNA-34a linked to SHANK3 decreases orchestrate a complex pathological program involving pro-inflammatory degeneration, endothelial and epithelial cell deficits, pro-apoptotic signaling and synaptic insufficiency in the aging human cardiovascular, neurovascular, and neurological systems.

miRNA-34a INTERACTIONS WITH THE SHANK3 mRNA 3′-UTR

The ∼7,413 nt human SHANK3 mRNA [major species SHANK3a; GenBank: AB569469.1; https://www.ncbi.nlm.nih.gov/nuccore/AB569469.1;https://www.genecards.org/cgi-bin/carddisp.pl?gene=SHANK3][1] encoded at the distal arm of human chromosome 22q (chr 22q13.33) and spliced together from a 22 exon gene includes multiple anykyrin (ANK) repeat domains and a 1986 nt 3′-UTR with multiple binding sites for miRNA-34a (from position 543–550 and 549–556 of the 22 nt miRNA-34a; **Figures 1D–G**). Interestingly these miRNA-34a binding sites have been previously shown to be immediately flanked downstream by a single miRNA-146a binding site (23); miRNA-146a is a pro-inflammatory microRNA also linked to AD neuropathology and pro-inflammatory neurodegeneration (34, 35). Hence the SHANK3 mRNA-3′UTR provides a classic example of multiple miRNAs—and in this case multiple pro-inflammatory miRNAs (miRNA-34a and miRNA-146a)–targeting the same mRNA 3′-UTR; these miRNA-mRNA recognition features for SHANK3 are shared by *Homo sapiens*, chimpanzee and Rhesus monkey (http://www.targetscan.org/cgi-bin/targetscan/vert71/viewgene.cgi? members =miR-34-5p/449-5p&show cnc =0&shownc=0&subset=1; accessed 17 January 2019) (23). Different SHANK3 gene deletions, duplications, and point mutations are also associated with ASD, intellectual disability, SZ, BD, and attention deficit hyperactivity disorder (ADHD) and these different genetic alterations may contribute to the pathophysiological and phenotypic diversity of neurological disorders related to SHANK3 gene mutations (14, 22, 36). Interestingly, multiple promoters for the human SHANK3 gene, often immediately associated with CpG islands, encode multiple SHANK3 species including SHANK3a, SHANK3b; SHANK3c, SHANK3d, SHANK3e, and SHANK3f (see **Figure 1E**); the significance of these 5 SHANK3 mRNA subspecies, all smaller than the full length SHANK3a mRNA, is not well understood but they may be involved in neuronal and synaptic development in different anatomical regions of the CNS (10, 14, 26, 37)

UNANSWERED QUESTIONS

While a considerable amount of scientific evidence suggests that miRNA-34a (and miRNA-146a) are involved in progressive and ultimately lethal degenerative pathologies in human neurological, cardiovascular and neurovascular disease, at this point in time we cannot exclude the pathological participation of other miRNA species, other small non-coding RNAs (sncRNAs) or other pathological factors in the regulation of SHANK3 expression (23). There are currently ∼2,654 known human miRNAs (http://mirbase.org/help/FAQs.shtml) but only about 30-35 miRNAs appear to be abundant in the human brain neocortex, hippocampus and retina (15, 23, 38). It will be interesting to see if miRNA-34a and miRNA-146a compete to control SHANK3-3′UTR binding and hence, ultimately SHANK3 expression and the status of the synaptic signaling network in health and in the SHANK3-mediated neuronal network collapse as typified in AD. The significance (if any) of adjacent and overlapping miRNA binding sites in the same 3′UTR is not well understood; it may be a built-in redundancy in the intrinsic miRNA-mRNA signaling system encoded on at least 2 chromosomes to ensure, for example, miRNA-34a-SHANK3 mRNA regulatory control. Very recently it has been established that the gastrointestinal (GI) tract microbiome may provide a long list of pro-inflammatory genetic mediators that are capable of transiting the aging GI tract and blood-brain barriers to upregulate a select number of pro-inflammatory miRNAs that have strong potential to induce neurological disease via the targeting of genes involved in the cytoskeleton, in the synapse, in the transit of signaling molecules across endothelial cell barriers and in the innate-immune response (5, 28, 34, 35, 39–44).

[1]SHANK3 gene expression data:https://www.genecards.org/cgi-bin/carddisp.,pl?gene=SHANK3 (2018)

A

SHANK3 3'-UTR (SHANK3 is also known as **DEL22q13.3, PROSAP2, PSAP2, SCZD15, SPANK-2**); Target Gene Accession: NM_001080420.1; SHANK3 3'-UTR (1986 nt); http://www.genecopoeia.com/product/search/detail.php?prt=16&cid=&key=HmiT021187; GeneCopia product ID: HmiT021187; last accessed 4 September 2018.

5′-GCCCCACCCCCACTCCCGCCCCGGCCGTGCCCTGCCGGCAGGGCCCCCCACCCCCACCCCGGGCCGCGGGCTCGGCCTGCCCCTTACGACGGCGCCCGGGCCAGGAATGTTGCATGA
ATCGTCCTGTTTGCTGTTGCTCGGAGACTCGCCCTGTACATTGCTTAGTGCCCTCACCGGCCGCCCAGCCCACCCAGCGCACAGTCAGGAAGGGCGTGGACCAGGGAGGCTGGGGCGGGA
GGTGCCGGGGGTGGGGTGCCCTAGCGTGACCACCTCCTTCGCAGCTCCTGGTGGCCATTCTCCCAGAGGGGGAACCTAGTCCAGCATGCGAGGTCAGGACCCGCCTTGGTGACTCGGGGG
GAGGGGGGAGACATTGGGATTCTCGATGGGGGCCAAGGAGCCCCCCTGTTTTGCATATTTTAATCCACTCTATATTTGGAACGAGAAAAGGAACAAATATCTCTGTCCGTAATAGTTTCC
TCTCCCCTCCCTTCTACTTCCACTGGTCCCACTGCAGCTGCCCAGTCTTCCATCTCCGGCCCCTCACTGCCACTGCCACCCCACAACGGGGCAGGGGACGCTCCAGCTGGTCTGGGGTTG
GCCAGGGCCCTAGTGGCCCGCCCTGGGGCCCCAGCTCGGCCCCTCGCCTCGCTGAGCTCTAGTGTGCCCCACCGACCCTTCAGGTGCTGCTCGTGGTGGGAGGGGCGGCAGGCCGCGGGT
CCTGCTGTGCACCCGCGGGACCAGCCGGCCTGGGAGACCATCGGCCGGGGGGGATGAGGGCAGGGCCCTGCCGCTCCACCGCAGCCATCTTCCTCACAGGGTCTCTCCCCAAGGAGGGGG
CTAGCTTGGTCCCCATGCTCTTGGGCAACTACAGCAGAGAAGCCTCCCTGCCTTGGACCCCAAAGTCTCCTGTCCTGCCCTTTATGTGTGTGGGTGAAACTGGGTGCGTCTGAGCACGTG
GGAGCCGTGTGTGTGCCTGATTACTGAGTGGCCACCAGGGGCCGCTCTGGACTAGCGCGGGGCCGTGGAGGCGTGCACCGTGTGCATGCGTGGGGTGTACCTGTGAGAGCACCCTGTCTC
CTCTTCCAAAGAAAGTCAGAGGCCATCCTGCACCCTGGGTCCAGCTGTTTGCCCAGCCTGTCCTTCCAGAGCCTCACCCAGCCTGAGCGGGGTTCCCTGGTGAATCCCTGCTGCTTGGGG
AGGCCCCAAGGGCCCCTTGGAGGCAGCGCCCCCACCTTGGGCTTCTGAGGGCATCATAGGGGGACCCCTAGAGTCAGTTCACCACAGGCCCTGGGGAGAGTCAAAGACCCCCGAGGGTGC
CCAGCCCCCCACACTGTGACTCCTCACACTCAGCGATGACCTGTGGGGTGGGGGGCCCTGGGACGTTTTTAAACCTAGGGTTTGGAGTCTGGACTAAGCTCCATCCACGTCACTCACAAG
TTTCTGTTTATATTTCTAGCTTTTTTTAATAAAATAAAAAAAAAAAGAAAACAGAAGTTTTCACAACCCAGGGGCCTGGCACGCCGGTCTGTGCCTGCCCGCCCCGCCCTGGCCCACCGG
CCCCACTCCCTGGGCACAGAGTCACACCCACTCATCCTTCCGCCAACAGTCCAGGTCACACAGCAGCAGTCACTGTAACAGACTGCCACATACACACTCGGTCTCACACTCACCTGTGGG
TTTTGGTTCCGTTCAATTTGGGTTTTTAACTTTACAGGGTCAGTTCCGCTTCACCTCCTTTTGTATGGAGTTCCATCCGGGGGGTTTCACCCCCTGCTCCAGTCCTGAGGCCTCCTGACC
CTGACGTTGTGATACGCCCCACAGAGATCTATGTTTCTTATATTATTATTATTGATAATAATTATTATAATATTATTATGTAATAAATTTATAAGAAATGAAG-3′

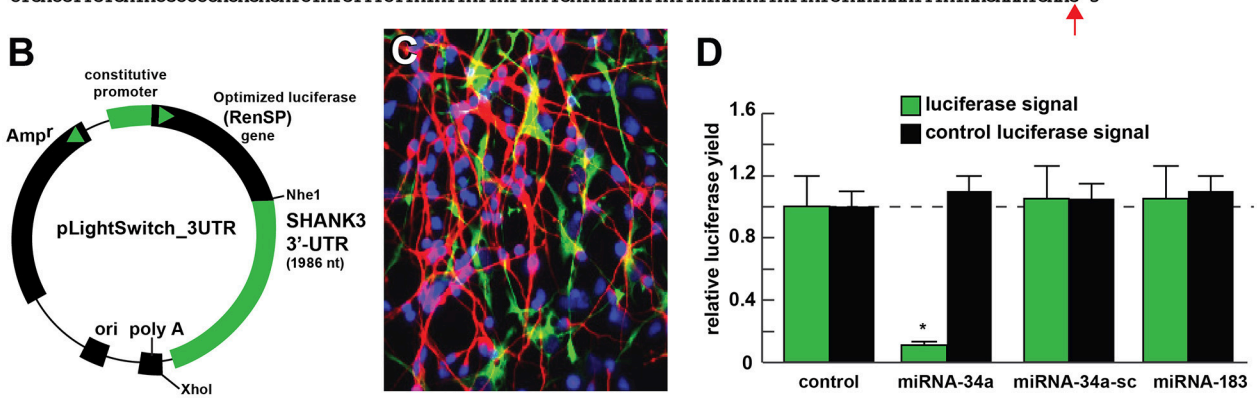

FIGURE 2 | Luciferase reporter vector-based studies of miRNA-34a and SHANK3 expression - Functional validation of a miRNA-34a-SHANK3–3′UTR interaction. **(A)** partial ribonucleotide sequence of the 1986 nt SHANK3-mRNA-3′-UTR is shown in the 5′-3′ direction; the 22 nucleotide (nt) miRNA-34a-SHANK3-3′UTR complementarity-interaction region is indicated by a black underline and the 8 nt SHANK3-mRNA-3′-UTR seed sequence is overlaid in yellow; a single vertical red arrow indicates the 5′ end of a poly A+ tail in the SHANK3 mRNA; the SHANK3 mRNA sequence derived from NM_018965; **(B)** SHANK3-mRNA-3′UTR expression vector luciferase reporter assay (pLightSwitch-3′UTR; Cat#S801178; Switchgear Genomics, Palo Alto CA); in this vector, the entire 1986 nucleotide SHANK3 3′UTR was ligated into the unique Nhe1-Xho1site; not drawn to scale; **(C)** HNG cells, 2 weeks in primary culture; neurons (red stain; $\lambda_{max} = 690$ nm), DAPI (blue nuclear stain; $\lambda_{max} = 470$ nm) and glial fibrillary associated protein (GFAP; glial-specific green stain; $\lambda_{max} = 520$ nm); the HNG cell culture is about 60% confluent and at 2 weeks of culture contains 70% neurons and 30% astroglia; human neurons do not culture well in the absence of glia; neurons also show both extensive arborization and display electrical activity (unpublished; Lonza); 40X magnification; HNG cells were transfected with the SHANK3-mRNA-3′UTR expression vector luciferase reporter were treated exogenously with a stabilized miRNA-34a, a scrambled control miRNA-34a (miRNA-34a-sc) or control miRNA-183; see references and text for further details; **(D)** compared to control, HNG cells transfected with a scrambled (sc) control pLightSwitch-3'UTR vector, the SHANK3-mRNA-3′UTR vector exhibited decreased luciferase signal to a mean of 0.16-fold of controls in the presence of miRNA-34a; this same vector exhibited no change in the presence of the control miRNA-34a-sc or miRNA-183; for each experiment (using different batches of HNG cells) a control luciferase signal was generated and included separate controls with each analysis; in addition a control vector β-actin-3′UTR showed no significant effects on the relative luciferase signal yield after treatment with either miRNA-183 or miRNA-34a (data not shown); a dashed horizontal line set to 1.0 is included for ease of comparison; $N = 6$; $^*p < 0.001$ (ANOVA). The results suggest a physiologically relevant miRNA-34a-SHANK3-mRNA-3′UTR interaction and a miRNA-34a-mediated down-regulation of SHANK3 expression in HNG cells. This pathogenic interaction may be related to the down-regulation of other immune, inflammatory, and synaptic system genes by up-regulated miRNAs in the CNS resulting in an impairment in trans-synaptic signaling and synaptic cytoarchitecture.

CONCLUSIONS

There is a remarkable amount of pathological damage in the sporadic AD brain, including the progressive and simultaneous appearance of senile plaques and neurofibrillary tangles, neuronal atrophy, the appearance of inflammatory markers and extensive synaptic disruption. Indeed a significant number of studies have indicated both a progressive and overwhelming deficit in synaptic cytoarchitecture and synaptogenesis occurs in the AD-affected brain. Our studies indicate that deficits in the SHANK3 cytoskeletal post-synaptic protein, with resulting disruption in synaptic structure and function may be mediated at least in part by inducible NF-kB regulated pro-inflammatory microRNAs such as miRNA-34a. Lastly, AD is an extremely heterogeneous disease with multiple and often strongly inter-linked pathological deficits. For example Aβ42 peptide abundance, inflammatory degeneration, loss of SHANK3 and synaptic disruption all occur concurrently, especially in the moderate-to-latter stages of AD. It would be interesting to see if Aβ42 peptide levels, miRNA-34a-mediated SHANK3 abundance

and synaptic deficits could be managed early during the course of the disease for therapeutic benefit. These data continue to indicate that increases in specific miRNAs coupled to deficits in SHANK3-expression may be one common denominator linking a wide-range of human neurological disorders that exhibit a progressive or developmental synaptic disorganization that is temporally associated with both intellectual disability and progressive cognitive decline.

ETHICS STATEMENT

All human brain tissue acquisition and handling procedures involving postmortem human tissues were carried out in strict accordance with the ethics review board policies at donor institutions. The work in this investigative study was approved by the Institutional Biosafety Committee/Institutional Review Board (IBC/IRB) at the LSU Health Sciences Center, New Orleans LA 70112 USA.

AUTHOR CONTRIBUTIONS

YZ, VJ, AL, NS, and WL: collected, analyzed, and summarized the current SHANK3 literature. YZ, VJ, AL, and NS: performed the experiments and data extraction. WL: wrote the article.

ACKNOWLEDGMENTS

The work in this article was presented in part at the Vavilov Institute of General Genetics Autumn 2017 Seminar Series (Институт общей генетики имени Вавилова Осень 2017 Семинар серии) in Moscow, Russia, October 2017, at the Society for Neuroscience (SFN) Annual Meeting, Washington, DC, USA, November 2017 and an update will be presented at the SFN 2018 meeting in San Diego CA, USA. Sincere thanks are extended to Drs. L. Carver, L. Cong, F. Culicchia, C. Eicken, K. Navel, A. I. Pogue, W. Poon, and the late Drs. J. M. Hill, P. N. Alexandrov, D. R. C. McLachlan and T. P. A. Kruck for helpful discussions in this research area, for short postmortem interval (PMI) human brain and retinal tissues or extracts, for initial bioinformatics and data interpretation, and to D. Guillot for expert technical assistance and medical artwork. We would like to further thank the following brain and tissue banks for access to high quality post-mortem tissues and valuable analytical advice: the Eunice Kennedy Shriver National Institute of Child Health and Human Development (NICHD), and the National Institute of Neurological Disorders and Stroke (NINDS), Bethesda MD USA; the Netherlands Brain Research Institute, Amsterdam, Netherlands; the New York State Institute for Basic Research, Staten Island NY, USA; the Oregon Health Sciences University, Portland OR, USA; the Southern Eye Bank, Metairie LA, USA; the University of California, Irvine CA, USA; the University of Kentucky Alzheimer's disease Brain Bank, Lexington KY, USA; the University of Maryland Brain and Tissue Bank, Baltimore MD, USA; the University of Massachusetts, Worcester MA, USA; University of Pennsylvania School of Medicine, Philadelphia PA, USA, the University of Toronto Brain Bank, Toronto ON, Canada and the many neuropathologists, physicians, and researchers in the US, Canada and Europe who have provided high quality, short PMI human brain tissue fractions for scientific analysis. Research on microRNAs, pro-inflammatory and pathogenic signaling in the Lukiw laboratory involving the microbiome, the innate-immune response, amyloidogenesis, synaptogenesis, and neuroinflammation in AD, prion, and in other neurological diseases was supported through an unrestricted grant to the LSU Eye Center from Research to Prevent Blindness (RPB); the Louisiana Biotechnology Research Network (LBRN) and NIH grants NEI EY006311, NIA AG18031, and NIA AG038834 (WL). The content of this manuscript is solely the responsibility of the authors and does not necessarily represent the official views of the National Institute on Aging, the National Center for Research Resources, or the National Institutes of Health.

REFERENCES

1. Masliah E, Mallory M, Hansen L, DeTeresa R, Terry RD. Quantitative synaptic alterations in the human neocortex during normal aging. *Neurology* (1993) 43:192–7.
2. Scheff SW, Price DA. Alzheimer's disease-related alterations in synaptic density: neocortex and hippocampus. *J Alzheimers Dis.* (2006) 9(3 Suppl): 101–15.
3. Grabrucker AM, Schmeisser MJ, Schoen M, Boeckers TM. Postsynaptic ProSAP/Shank scaffolds in the cross-hair of synaptopathies. *Trends Cell Biol.* (2010) 21:594–603. doi: 10.1016/j.tcb.2011.07.003
4. Lashley T, Schott JM, Weston P, Murray CE, Wellington H, Keshavan A, et al. Molecular biomarkers of Alzheimer's disease: progress and prospects. *Dis Model Mech.* (2018) 11:dmm031781. doi: 10.1242/dmm.031781
5. Rajendran L, Paolicelli RC. Microglia-mediated synapse loss in Alzheimer's disease. *J Neurosci.* (2018) 38:2911–9. doi: 10.1523/JNEUROSCI.1136-17.2017
6. Bisht K, Sharma K, Tremblay MÈ. Chronic stress as a risk factor for Alzheimer's disease: roles of microglia-mediated synaptic remodeling, inflammation, and oxidative stress. *Neurobiol Stress* (2018) 9:9–21. doi: 10.1016/j.ynstr.2018.05.003
7. Frere S, Slutsky I. Alzheimer's disease: from firing instability to homeostasis network collapse. *Neuron* (2018) 97:32–58.doi: 10.1016/j.neuron.2017.11.028.
8. Sheng M, Kim E. The Shank family of scaffold proteins. *J Cell Sci.* (2000) 113(Pt 11): 1851–6.
9. Alexandrov PN, Zhao Y, JaberV, Cong L, Lukiw WJ. Deficits in the proline-rich synapse-associated SHANK3 protein in multiple neuropsychiatric disorders. *Front Neurol.* (2017) 8:670. doi: 10.3389/fneur.2017.00670
10. Monteiro P, Feng G. SHANK proteins: roles at the synapse and in autism spectrum disorder. *Nat Rev Neurosci.* (2017) 18:147–57. doi: 10.1038/nrn.2016.183
11. Kanani F, Study D, Balasubramanian M. SHANK3 variant as a cause of non-syndromal autism. *Clin Dysmorphol.* (2018) 27:113–5. doi: 10.1097/MCD.0000000000000232
12. Marcello E, Di Luca M, Gardoni F. Synapse-to-nucleus communication: from developmental disorders to Alzheimer's disease. *Curr Opin Neurobiol.* (2018) 48:160–6. doi: 10.1016/j.conb.2017.12.017
13. Zhao D, Meng J, Zhao Y, Huo Y, Liu Y, Zheng N, et al. RPS23RG1 Is required for synaptic integrity and rescues Alzheimer's disease-associated cognitive deficits. *Biol Psychiatry* (2018). doi: 10.1016/j.biopsych.2018.08.009. [Epub ahead of print].

14. Amal H, Barak B, Bhat V, Gong G, Joughin BA, Wishnok JS, et al. Shank3 mutation in a mouse model of autism leads to changes in the S-nitroso-proteome and affects key proteins involved in vesicle release and synaptic function. *Mol Psychiatry* (2018). doi: 10.1038/s41380-018-0113-6. [Epub ahead of print]
15. Clement C, Hill JM, Dua P, Culicchia F, Lukiw WJ. Analysis of RNA from Alzheimer's disease post-mortem brain tissues. *Mol Neurobiol.* (2016) 53:1322–8. doi: 10.1007/s12035-015-9105-6
16. Fries GR, Carvalho AF, Quevedo J. The miRNome of bipolar disorder. *J Affect Disord.* (2018) 233:110–6. doi: 10.1016/j.jad.2017.09.025
17. Qipshidze Kelm N, Piell KM, Wang E, Cole MP. MicroRNAs as predictive biomarkers for myocardial injury in aged mice following myocardial infarction. *J Cell Physiol.* (2018) 233:5214–21. doi: 10.1002/jcp.26283
18. Wang B, Li D, Kovalchuk I, Apel IJ, Chinnaiyan AM, Wóycicki RK, et al. miRNA-34a directly targets tRNA(i) (Met) precursors and affects cellular proliferation, cell cycle, and apoptosis. *Proc Natl Acad Sci USA*. (2018) 115:7392–7. doi: 10.1073/pnas.1703029115
19. Savioz A, Leuba G, Vallet PG. A framework to understand the variations of PSD-95 expression in brain aging and in Alzheimer's disease. *Ageing Res Rev.* (2014) 18:86–94. doi: 10.1016/j.arr.2014.09.004
20. Kim DH, Lim H, Lee D, Choi SJ, Oh W, Yang YS, et al. Thrombospondin-1 secreted by human umbilical cord blood-derived mesenchymal stem cells rescues neurons from synaptic dysfunction in Alzheimer's disease model. *Sci Rep.* (2018) 8:354. doi: 10.1038/s41598-017-18542-0
21. Chen J, Yu S, Fu Y, Li X. Synaptic proteins and receptors defects in autism spectrum disorders. *Front Cell Neurosci.* (2014) 8:276. doi: 10.3389/fncel.2014.00276
22. Lee Y, Kang H, Lee B, Zhang Y, Kim Y, Kim S, et al. Integrative analysis of brain region-specific Shank3 interactomes for understanding the heterogeneity of neuronal pathophysiology related to SHANK3 mutations. *Front Mol Neurosci.* (2017) 10:110. doi: 10.3389/fnmol.2017.00110
23. Jaber V, Zhao YJ, Lukiw WJ. Alterations in micro RNA-messenger RNA (miRNA-mRNA) coupled signaling networks in sporadic Alzheimer's disease (AD) hippocampal CA1. *J Alzheimers Dis Parkinsonism*. (2017) 7:312. doi: 10.4172/2161-0460.1000312
24. Friedman RC, Farh KK, Burge CB, Bartel DP. Most mammalian mRNAs are conserved targets of microRNAs. *Genome Res.* (2009) 19:92–105. doi: 10.1101/gr.082701.108
25. Jiang YH, Ehlers MD. Modeling autism by SHANK gene mutations in mice. *Neuron* (2013) 78:8–27. doi: 10.1016/j.neuron.2013.03.016
26. Zhu L, Wang X, Li XL, Towers A, Cao X, Wang P, et al. Epigenetic dysregulation of SHANK3 in brain tissues from individuals with autism spectrum disorders. *Hum Mol Genet*. (2014) 23:1563–78. doi: 10.1093/hmg/ddt547
27. Choi SY, Pang K, Kim JY, Ryu JR, Kang H, Liu Z, et al. Post-transcriptional regulation of SHANK3 expression by microRNAs related to multiple neuropsychiatric disorders. *Mol Brain* (2015) 8:74. doi: 10.1186/s13041-015-0165-3
28. Pham E, Crews L, Ubhi K, Hansen L, Adame A, Cartier A, et al. Progressive accumulation of amyloid-beta oligomers in Alzheimer's disease and in amyloid precursor protein transgenic mice is accompanied by selective alterations in synaptic scaffold proteins. *FEBS J.* (2010) 277:3051–67. doi: 10.1111/j.1742-4658.2010.07719.x
29. Bhattacharjee S, Zhao Y, Dua P, Rogaev EI, Lukiw WJ. microRNA-34a-mediated down-regulation of the microglial-enriched triggering receptor and phagocytosis-sensor TREM2 in age-related macular degeneration. *PLoS ONE* (2016) 11:e0150211. doi: 10.1371/journal.pone.0150211
30. Wang X, Liu P, Zhu H, Xu Y, Ma C, Dai X, et al. miR-34a, a microRNA up-regulated in a double transgenic mouse model of Alzheimer's disease, inhibits bcl2 translation. *Brain Res Bull.* (2009) 80:268–73. doi: 10.1016/j.brainresbull.2009.08.006
31. Pogue AI, Lukiw WJ. Up-regulated pro-inflammatory microRNAs (miRNAs) in Alzheimer's disease (AD) and age-related macular degeneration (AMD). *Cell Mol Neurobiol.* (2018) 38:1021–31. doi: 10.1007/s10571-017-0572-3
32. Hartl M, Grunwald Kadow IC. New roles for "old" microRNAs in nervous system function and disease. *Front Mol Neurosci.* (2013) 6:51. doi: 10.3389/fnmol.2013.00051
33. Yuan HY, Zhou CB, Chen JM, Liu XB, Wen SS, Xu G, et al. MicroRNA-34a targets regulator of calcineurin 1 to modulate endothelial inflammation after fetal cardiac bypass in goat placenta. *Placenta* (2017) 51:49–56. doi: 10.1016/j.placenta.2017.01.128
34. Zhao Y, Lukiw WJ. *Bacteroidetes* neurotoxins and inflammatory neurodegeneration. *Mol Neurobiol.* (2018) 55:9100–107. doi: 10.1007/s12035-018-1015-y.
35. Zhao Y, Lukiw WJ. Microbiome-mediated upregulation of microRNA-146a in sporadic Alzheimer's disease. *Front Neurol.* (2018) 9:145. doi: 10.3389/fneur.2018.00145
36. Reim D, Distler U, Halbedl S, Verpelli C, Sala C, Bockmann J, et al. Proteomic analysis of post-synaptic density fractions from SHANK3 mutant mice reveals brain region specific changes relevant to autism spectrum disorder. *Front Mol Neurosci.* (2017) 10:26. doi: 10.3389/fnmol.2017.00026
37. Guilmatre A, Huguet G, Delorme R, Bourgeron T. The emerging role of SHANK genes in neuropsychiatric disorders. *Dev Neurobiol.* (2014) 74:113–22.doi: 10.1002/dneu.22128
38. Zhao Y, Cong L, Lukiw WJ. Plant and animal microRNAs (miRNAs) and their potential for inter-kingdom communication. *Cell Mol Neurobiol.* (2018) 38:133–40. doi: 10.1007/s10571-017-0547-4
39. Sweeney MD, Sagare AP, Zlokovic BV. Blood-brain barrier breakdown in Alzheimer disease and other neurodegenerative disorders. *Nat Rev Neurol.* (2018) 14:133–50. doi: 10.1038/nrneurol.2017.188
40. Tabouy L, Getselter D, Ziv O, Karpuj M, Tabouy T, Lukic I, et al. Dysbiosis of microbiome and probiotic treatment in a genetic model of autism spectrum disorders. *Brain Behav Immun*. (2018) 73:310–319 doi: 10.1016/j.bbi.2018.05.015
41. Wang X, Xu Q, Bey AL, Lee Y, Jiang YH. Transcriptional and functional complexity of SHANK3 provides a molecular framework to understand the phenotypic heterogeneity of SHANK3 causing autism and Shank3 mutant mice. *Mol Autism*. (2014) 5:30. doi: 10.1186/2040-2392-5-30
42. de Sena Cortabitarte A, Degenhardt F, Strohmaier J, Lang M, Weiss B, Roeth R, et al. Investigation of SHANK3 in schizophrenia. *Am J Med Genet B Neuropsychiatr Genet.* (2017) 174:390–8. doi: 10.1002/ajmg.b.32528
43. Wang X, McCoy PA, Rodriguiz RM, Pan Y, Je HS, Roberts AC, et al. Synaptic dysfunction and abnormal behaviors in mice lacking major isoforms of SHANK3. *Hum Mol Genet.* (2011) 20:3093–108.doi: 10.1093/hmg/ddr212
44. Lim LP, Glasner ME, Yekta S, Burge CB, Bartel DP. Vertebrate microRNA genes. *Science* (2003) 299:1540. doi: 10.1126/science.1080372

Conflict of Interest Statement: The authors declare that the research was conducted in the absence of any commercial or financial relationships that could be construed as a potential conflict of interest.

frontiers in Neuroscience

ORIGINAL RESEARCH
published: 19 March 2019
doi: 10.3389/fnins.2019.00217

Myelin Damage in Diffuse Axonal Injury

Jiao Mu[1], Meiyu Li[1], Tingting Wang[1], Xiujuan Li[1], Meiling Bai[1], Guohui Zhang[1] and Jiming Kong[1,2]**

[1] Department of Forensic Medicine, Hebei North University, Zhangjiakou, China, [2] Department of Human Anatomy and Cell Science, College of Medicine, University of Manitoba, Winnipeg, MB, Canada

Diffuse axonal injury (DAI) is characterized by delayed axonal disconnection. Although the effect of DAI on axonal pathology has been well documented, there is limited information regarding the role of myelin in the pathogenesis of DAI. We used a modified Marmarou method to create a moderate DAI model in adult rat and examined the corpus callosum and brain stem for myelin pathology and dynamic glial responses to DAI. During the first week following DAI, Luxol Fast Blue staining and western blot analysis for MBP showed significant loss of myelin in the corpus callosum and the brain stem. Increased apoptosis of mature oligodendrocyte, as depicted by its marker CC-1, was observed. Conversely, there was an increased number of Olig2-positive cells accompanied by hypertrophic microglia/macrophage and mild reactive astrocytes. Electron microscopy revealed degenerating axons in the corpus callosum and marked myelin abnormalities in the brain stem in the early stage of DAI. Brain stem regions exhibited myelin intrusions or external protrusions with widespread delamination and myelin collapse, leading to degeneration of accompanying axons. Our results show distinct pathologic processes involving axon and myelin between the corpus callosum and the brain stem in DAI. Oligodendrocyte selective vulnerability and subsequent demyelination may contribute to axonal degeneration in the brain stem. Defining the cause of ongoing oligodendrocyte death and promoting myelin regeneration may provide important targets for therapeutic interventions of DAI.

Keywords: diffuse axonal injury, demyelination, oligodendrocyte, axon-myelin unite, corpus callosum, brain stem

OPEN ACCESS

Edited by:
Nan-Jie Xu,
Shanghai Jiao Tong University, China

Reviewed by:
Susanna Amadio,
Fondazione Santa Lucia (IRCCS), Italy
Sudheendra N. R. Rao,
National Centre for Biological Sciences, India

****Correspondence:***
Guohui Zhang
m18931315882_1@163.com
Jiming Kong
jiming.kong@umanitoba.ca

Specialty section:
This article was submitted to Neurodegeneration, a section of the journal Frontiers in Neuroscience

Received: *08 November 2018*
Accepted: *26 February 2019*
Published: *19 March 2019*

Citation:
Mu J, Li M, Wang T, Li X, Bai M, Zhang G and Kong J (2019) Myelin Damage in Diffuse Axonal Injury. Front. Neurosci. 13:217. doi: 10.3389/fnins.2019.00217

INTRODUCTION

Diffuse axonal injury (DAI) is one of the most common and important pathologic features of traumatic brain injury (TBI), which affects millions of people worldwide (Ma et al., 2016). DAI is caused by energy transmitted to the brain via rapid head rotation or deceleration/acceleration, leading to multifocal injury of white matter tracts (Adams et al., 1989; Mu et al., 2015). Development of pathological changes in axons following DAI has been well documented including delayed axotomy caused by both initial mechanical force and complex secondary cascade (Vargas and Barres, 2007; Johnson et al., 2013; Jang and Kwon, 2016). There is, however, limited information regarding the role of myelin and oligodendrocyte in DAI.

In the central nervous system, myelin is a cholesterol-rich extension of oligodendrocyte plasma membrane, which is important for axonal maintenance and function (Aggarwal, 2011). Oligodendrocytes, as the primary cells responsible for generating and maintaining the myelin

sheath, are highly vulnerable to various stimuli, including excitotoxicity, oxidative stress, and inflammation (Bradl and Lassmann, 2010). As all the aforementioned stimuli are features of secondary cascade in DAI, it is expected that DAI has an influence on oligodendrocytes and further cause myelin loss consequently.

Indeed, the mixed and intertwined nature of axon and myelin pathology is apparent in DAI. It is understood traditionally that myelin collapse is secondary to axon degeneration (Armstrong et al., 2015). However, in a recent study, Maxwell (Maxwell, 2013) found that in stretch-injury to optic nerve fibers, myelin dislocations occur within 1–2 h after injury and damage to the myelin sheath and oligodendrocytes of the optic nerve fibers may facilitate the continuance of axonal loss. This prompted us to test a hypothesis that myelin damage plays an important role in pathophysiological processes in DAI. Here we report dynamics of demyelination and selective vulnerability of oligodendrocytes in DAI. Our results suggest a complex interplay between axonal damage, oligodendrocyte death and myelin loss in moderate DAI.

MATERIALS AND METHODS

Animals and DAI

All procedures involving animals were approved and monitored by the Animal Care Committee of Hebei North University. Adult male Sprague-Dawley rats (weighting 220–280 g) were included in our study. All rats were housed at five animals per cage on a 12 h light/dark cycle with free access to food and water.

A moderate DAI model was induced by a modified Marmarou method (Zhang et al., 2015). Animals were anesthetized with 5% isoflurane. The scalp of the anesthetized rat was shaved, a midline incision was performed, and the periosteum covering the vertex was exposed. A steel disk of 10 mm in diameter and 3 mm in thickness was fixed at the center of the vertex. Subsequently, rats were prostrated and fixed onto a sponge bed. Injury was delivered by dropping a 450 g weight freely onto the coin from a height of 1 m. Then, the rat was immediately removed, and the scalp was sutured after gently removing the steel disk from the skull. In the control group, rats (n = 11) underwent the same surgical procedure without impact. Five survival time-points were established post DAI, with animals euthanized at 1, 2, 3, 5, and 7 days following injury (n = 11 in each DAI group).

Immunohistochemistry, Immunofluorescence, and Histopathology

Once anesthetized, rats (n = 3 in each group) were perfused transcardially with 200 mL 0.01 M phosphate buffered saline (PBS) followed by 200 mL 4% paraformaldehyde. Brains were further post-fixed by immersion overnight and then to undertake dehydration, vitrification and embedding. The paraffin-embedded tissues were cut using microtome to provide 5-nm-thick tissue sections for immunohistochemistry, immunofluorescence, and histopathology.

Immunohistochemistry

After deparaffinization and rehydration of the brain sections, antigen retrieval was performed with 0.1 M sodium citrate at 100°C for 10 min. Following incubation with 3% hydrogen peroxide for 15 min, the sections were incubated with goat serum to reduce non-specific reaction for 15 min. Then, the sections were incubated with the primary antibody (detailed information in **Table 1**): olig2 (1:500) or Iba1 (1:2000) at 4°C overnight. The negative control specimens underwent the same procedures, but primary antibodies were replaced by PBS. Following washing with 0.01 M PBS, biotinylated goat anti-rabbit secondary antibody and S-A/HRP reagent were applied subsequently at 37°C for 20 min, respectively. The positive reaction was visualized with DAB, and the section was then dehydrated in graded alcohols, cleared in xylene and covered.

Immunofluorescence

After deparaffinization, rehydration and antigen retrieval, the brain sections were blocked in goat serum for 30 min at 22°C. Then, the sections were incubated with the primary antibody (detailed information in **Table 1**) – GFAP (1:200) or CC-1 (1:100) at 4°C overnight. The negative control specimens underwent the same procedures, but primary antibodies were replaced by PBS. This was followed by a 2-h incubation at 37°C with secondary antibodies conjugated with either CY3 (1:1000, A0521, Beyotime, Shanghai, China) or FITC (1:1000, bs-0295G-FITC, Bioss, Beijing, China). Sections were then washed three times in PBS and then incubated with DAPI (C1005, Beyotime, Shanghai, China) for 1 min before being coverslipped with a mounting medium.

Histopathology

Luxol fast blue (LFB) staining was used to evaluate changes in the structural integrity of myelin. Following deparaffinization and rehydration, slices were placed into an LFB staining solution for 2–4 h at 60°C and then cooled to ambient temperature. Excessive staining was removed by distilled water rinses for 1 min each. The section was dehydrated in graded alcohols, cleared in xylene, and covered.

An Olympus BX-51 fluorescent microscope (Olympus America, Center Valley, PA, United States) connected to a

TABLE 1 | Overview of primary antibodies.

Antibody	Species	Target	Product number and supplier
MBP	Anti-rabbit	Myelin	ab40390, Abcam, Cambridge, United Kingdom
Olig2	Anti-rabbit	Mature OLs and OPCs	13999-1-AP, Proteintech, Rosemont, IL, United States
CC-1	Anti-mouse	Mature OLs	ab16794, Abcam, Cambridge, United Kingdom
Iba1	Anti-rabbit	Microglia/ macrophages	ab178847, Abcam, Cambridge, United Kingdom
GFAP	Anti-rabbit	Astrocytes	16825-1-AP, Proteintech, Rosemont, IL, United States

OLs, oligodendrocytes; OPCs, oligodendrocyte precursor cells.

computer by a color CCD camera was used to obtain and edit images. The analysis software (Olympus) was used to acquire images at different magnifications. For GFAP, CC-1, and DAPI examination, the excitation spectra were 495, 550, and 340 nm, respectively, and the emission spectra were 519, 570, and 488 nm, respectively. Cell counting was conducted on nine randomly chosen fields for each sample and measured using Image-Pro Plus software (version 5.1; Media Cybernetics, Inc., Silver Spring, MD, United States).

CC-1/TUNEL Co-labeling

Cell apoptosis was assessed by TUNEL staining using a cell death detection kit (Roche, Indianapolis, IN, United States). Following deparaffinization and rehydration, the brain sections were processed for TUNEL staining according to the manufacturer's instruction. For negative control, the sections were incubated with label solution (without terminal transferase) instead of TUNEL reaction mixture. For positive control, the sections were incubated with DNase I recombinant for 10 min at 25°C to induce DNA strand breaks prior to labeling procedures. The same slides were further used for immunofluorescence with a primary antibody to CC-1 ratio of 1:100.

Western Blot Assessment

Once anesthetized, rats (n = 5 in each group) were perfused through the heart with 200 mL saline solution. The homogenates

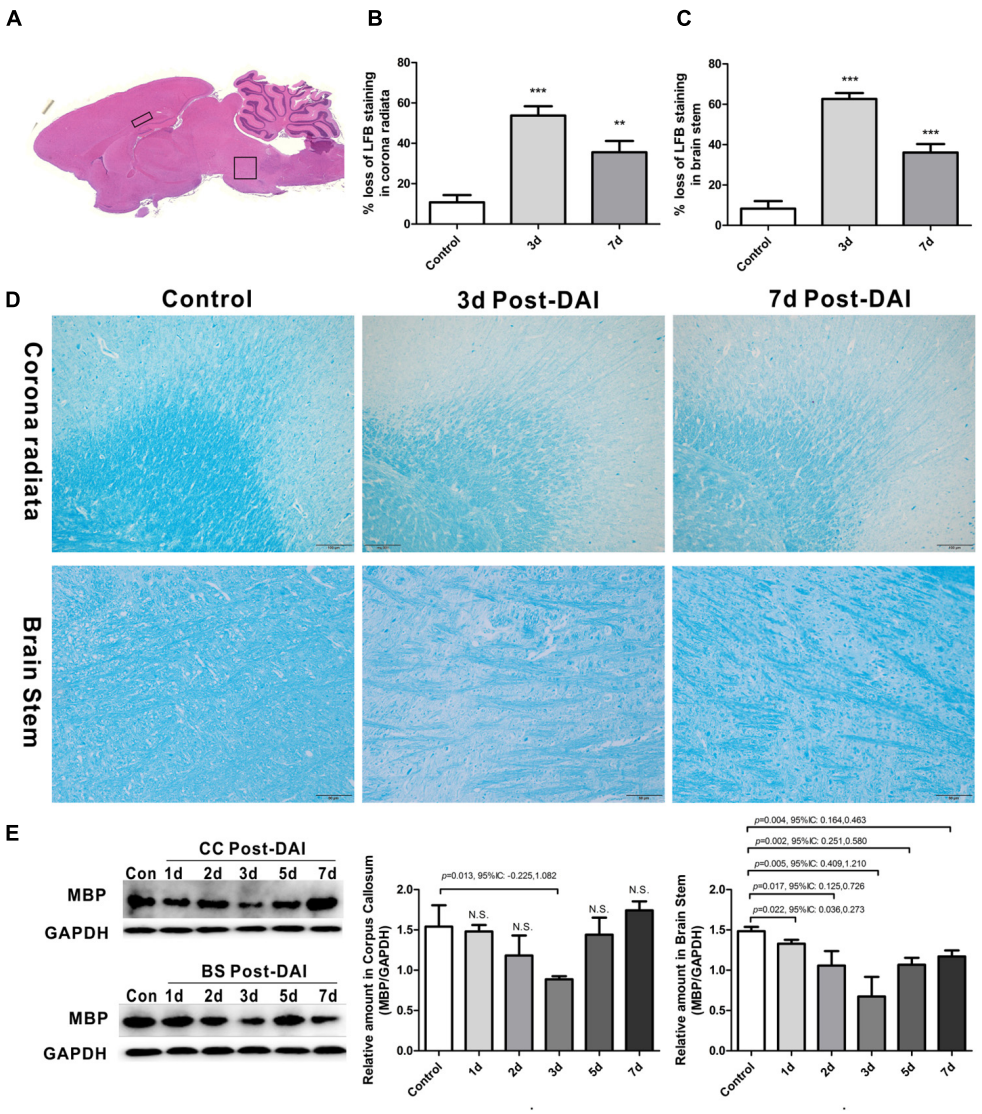

FIGURE 1 | Brain overview and myelin loss in DAI (diffuse axonal injury). **(A)** An overview of brain morphology determined on H&E-stained. Squares show ROIs focused on the CC and brain stem evaluated in the present study; **(B–D)** LFB staining at 3 and 7 days post-injury shows myelin disruption and myelin loss in the corona radiate and brain stem; **(E)** western blot analysis indicates that MBP expression was significantly decreased throughout the first week after injury in brain stem. The CC region exhibits significant decreased MBP expression at 3 days after injury. N.S. indicates no significant changes between DAI group and control group.

of the corpus callosum (CC) and brain stem were resolved on SDS PAGE and transferred to a nitrocellulose membrane using the Geni blot system (Liuyi Co., China). The membrane was blocked with 5% milk in Tris-buffered saline+tween-20 (TBST) for 2 h at room temperature and then incubated with the Anti-MBP antibody (1:2000); Anti-Olig2 antibody (1:1500); Anti-GFAP antibody (1:7000); and Anti-Iba1 antibody (1:3000) overnight at 4°C. After washing three times for 5 min each with TBST, the membrane was incubated with a corresponding secondary antibody: goat anti-rabbit (A0208, Beyotime, Shanghai, China) and goat anti-mouse (A0216, Beyotime, Shanghai, China), for 60 min at room temperature. After washing, blots were developed with a solution containing 10 ml PBS, 0.025% (v/v) H_2O_2, and 8 mg 4-chloro-1-naphthol dissolved in 2 ml of methanol. Specific immunoreactive bands were quantified by computer-assisted densitometry.

Transmission Electron Microscopy and Quantification

Once anesthetized, rats (n = 3 in each group) were perfused through the heart with 200 mL saline solution followed by 250 mL 2% paraformaldehyde and 0.5% glutaraldehyde in 0.01 M PBS. The brainstem and the CC were trimmed into blocks of 2 mm × 1 mm × 0.5 mm and conventionally fixed, rinsed, dehydrated and embedded in epoxy resin. The samples were then cut into 70-nm-thick sections, stained with uranyl acetate and bismuth subnitrate, and examined on a transmission electron microscope (JEOL, Peabody, MA, United States).

Images of brain sections through the CC and brain stem were acquired at 5,000× magnification for measurements of g-ratio. The g-ratio was calculated for each myelinated axon by dividing the average axon diameter by the average total fiber diameter. Additional images were taken at 10,000× for illustration of pathology.

Statistical Analysis

SPSS 16.0 and Prism 5.0 (GraphPad Prism Software) were used for statistical analyses and graphing of quantitative data. Independent-samples t-test analysis of variance was performed to determine significant differences across each post-injury time point compared to the control. Slopes were calculated using linear regression. Image-Pro Plus software was used for cell counting in immunohistochemistry. P-values <0.05 were considered statistically significant.

RESULTS

The injured rats showed conscious disturbance, decortication flexion deformity of the forelimbs, rigidity of hindlimbs, and momentary respiratory depression or shallow breathing in the

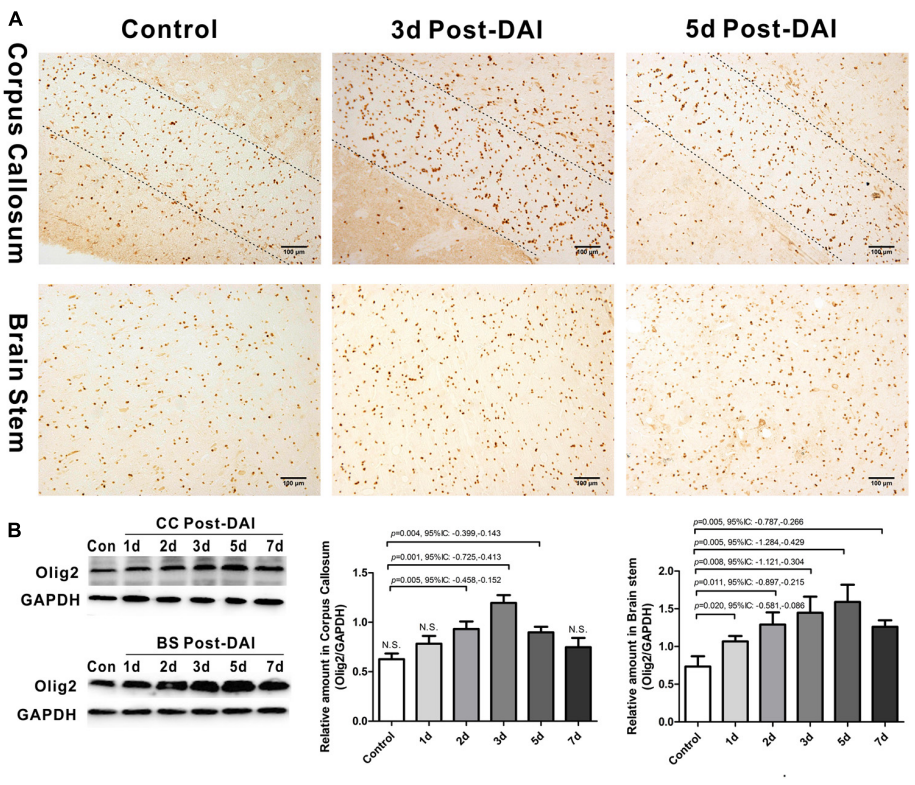

FIGURE 2 | Increased expression of Olig2-positive cells in DAI. **(A)** Immunohistochemical results show that DAI induced the increased number of Olig2-positive cells in the CC and brain stem; **(B)** western blot analysis indicates that Olig2 expression was significantly increased throughout the first week after injury in the brain stem. The CC region exhibits significant Olig2 proliferation at 2, 3, or 5 days after injury. N.S. indicates no significant changes between DAI group and control group.

DAI group after impact. The mortality was about 20%. No skull fracture, cerebral contusion or focal white matter tears were observed after closed-skull impact in adult rats. Squares show regions of interest (ROIs) focused on the CC and brain stem evaluated in the present study (**Figure 1A**).

Myelin Loss in DAI

Gross morphologic evaluations were investigated to assess myelin loss using LFB staining. Myelin was apparent as a blue substrate reaction in coronal brain sections, particularly in the corona radiata and CC. In control rats, myelin was organized in a continuous and regular pattern. After impact injury, reduced LFB staining was observed in corona radiata and brain stem. Additionally, DAI rats had a disorganized myelin stained with LFB (**Figures 1B–D**).

LFB intensity might be affected following TBI, so we examined the MBP expression by western blot to further confirm the myelin loss in DAI. In the CC, there was a significant decrease in MBP expression at day 3, which recovered to control levels by day 7 post-DAI. Compared to the control rats, the MBP expression in brain stem was significantly decreased from day 1 post-injury in the brain stem, which further decreased at day 3 post-injury and remained decreased at day 7 (**Figure 1E**). These results are consistent with LFB staining, indicating loss of myelin following DAI.

Increased Expression of Olig2-Positive Cells in DAI

Olig2 was used here as a general marker of oligodendrocyte lineage cells because Olig2 is expressed in both oligodendrocyte precursor cells and mature oligodendrocytes. In control rats, a basal level of Olig2-positive cells was observed in both the CC and the brain stem. Olig2-positive cells showed a rounded morphology with staining in the nucleus. There was an increase in Olig2-positive cell numbers in both the CC and brain stem following DAI (**Figure 2A**). We further quantified expression of Olig2 by western blot analysis. Olig2 expression was significantly increased throughout the first week after injury in the brain stem. Meanwhile, in the CC increased Olig2 expression was only observed in injured rats at day 2, 3, and 5 versus the control rat (**Figure 2B**).

Oligodendrocyte Apoptosis Following DAI

We then evaluated the number of oligodendrocyte by staining for the mature oligodendrocyte marker CC-1. CC-1 staining was

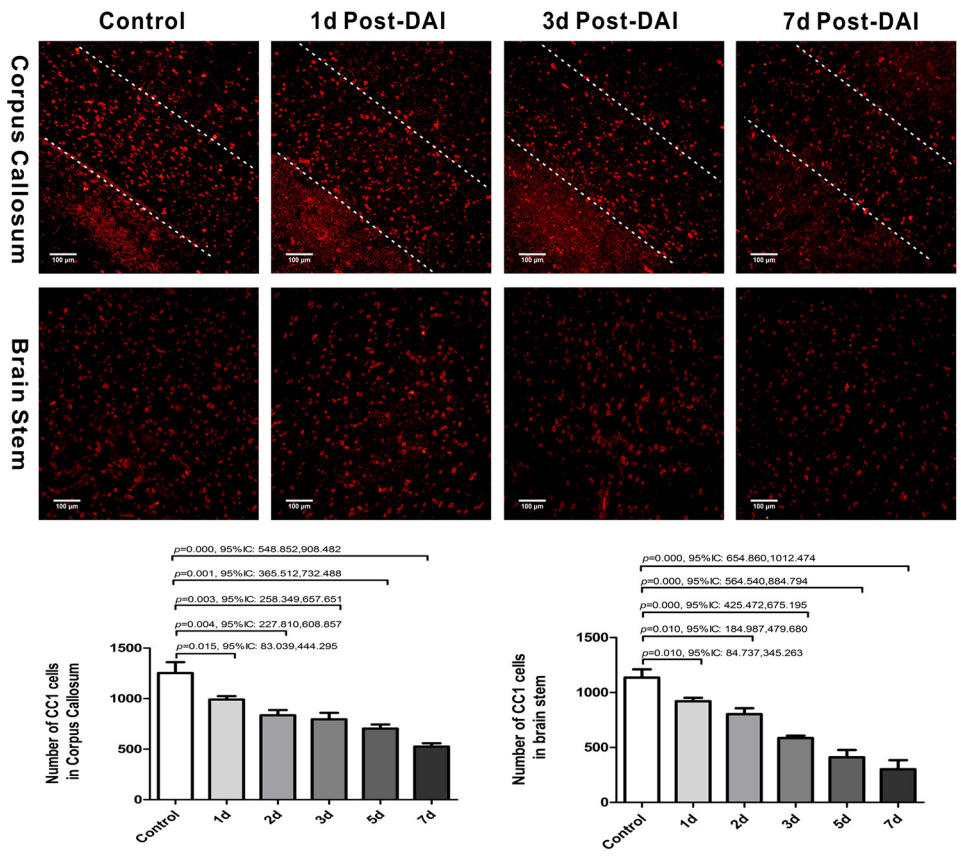

FIGURE 3 | Diffuse axonal injury results in a loss of CC-1 immunoreactivity. Immunofluorescent results showed that numbers of CC-1+ immunostained cells within the injured regions of interest were significantly decreased at each of the time points after injury.

localized to the cytoplasm and a large number of CC-1-positive cells were counted within the CC and brain stem in the control group. Numbers of CC-1 immunoreactive cells within the injured regions of interest were significantly decreased at each of the time points after injury (**Figure 3**).

We further examined oligodendrocyte apoptosis by using double immunofluorescence staining for CC-1 and TUNEL. The majority of TUNEL-labeled cells were seen within white matter tracts. In control rats, there were only rare CC-1/TUNEL co-labeled cells. Compared with the control, the number of CC-1/TUNEL-positive cells in the CC and brain stem were significantly increased at day 2 post-DAI, and it further increased with the continuous extension of injury time (**Figure 4**). The persistent increase in the number of CC-1/TUNEL co-labeled cells during myelin loss suggests that myelin loss is likely due to oligodendrocyte apoptosis in this moderate DAI model.

Activation of Microglia/Macrophage Following DAI

Iba1 immunohistochemistry was used to characterize microglia/macrophage activation after DAI. Iba1 positive cells were rarely observed in the white matter tracts of the control rats. Compared to the control, Iba1 expression with markedly increased staining intensity was evident in the CC and brain stem in DAI rats. Moreover, different hypertrophic morphology of the Iba1-immunolabeled cells was identified after injury (**Figure 5A**). Similarly, the western blot results also showed increased expression of Iba1 from days 2 to 7 after injury in the CC and brain stem (**Figure 5B**).

Mild Astrogliosis in the CC Following DAI

GFAP was used to study the expression of astrocyte. GFAP showed widespread immunoreactivity in the cortex and white matter tracts of the control rats. Following DAI, GFAP immunoreactivity showed marked staining of dense astrocyte processes within the CC (**Figure 6A**). Quantification by western blot analysis confirmed that GFAP expression is significantly increased in the CC at 3, 5, and 7 days post-DAI. However, there was no effect of DAI on GFAP expression in the brain stem (**Figure 6B**).

Ultrastructural Evidence of Axon Damage and Myelin Abnormalities After DAI

Electron microscopy of the CC and brain stem was used to investigate the ultrastructural changes of myelin and axon after DAI. In control rats, the myelin sheath was compact, with regularly organized myelin lamellae. The axolemma adhered tightly to the inner layer of myelin sheath and the axoplasmic contents such as microtubes, neurofilaments, and mitochondria were distributed regularly (**Figure 7G**).

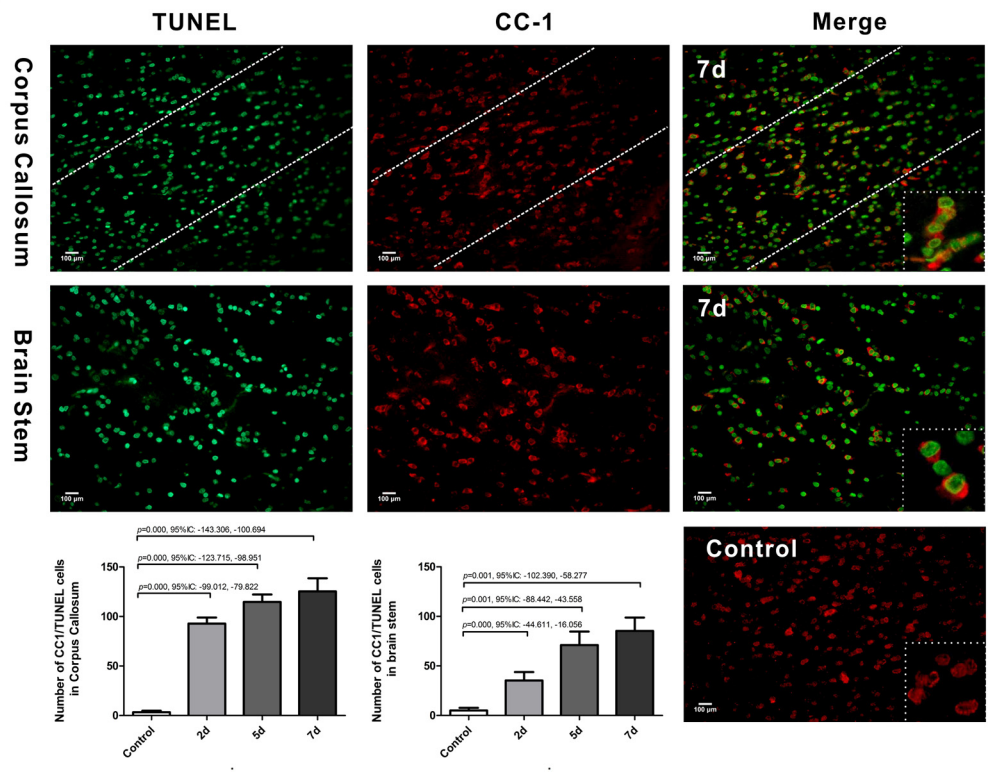

FIGURE 4 | Oligodendrocyte apoptosis in DAI. Co-labeling of the mature oligodendrocyte marker CC-1 (red) and TUNEL (green). The control showed rare CC1/TUNEL co-labeled cells. Compared with the control, DAI significantly increased the number of CC1/TUNEL-positive cells.

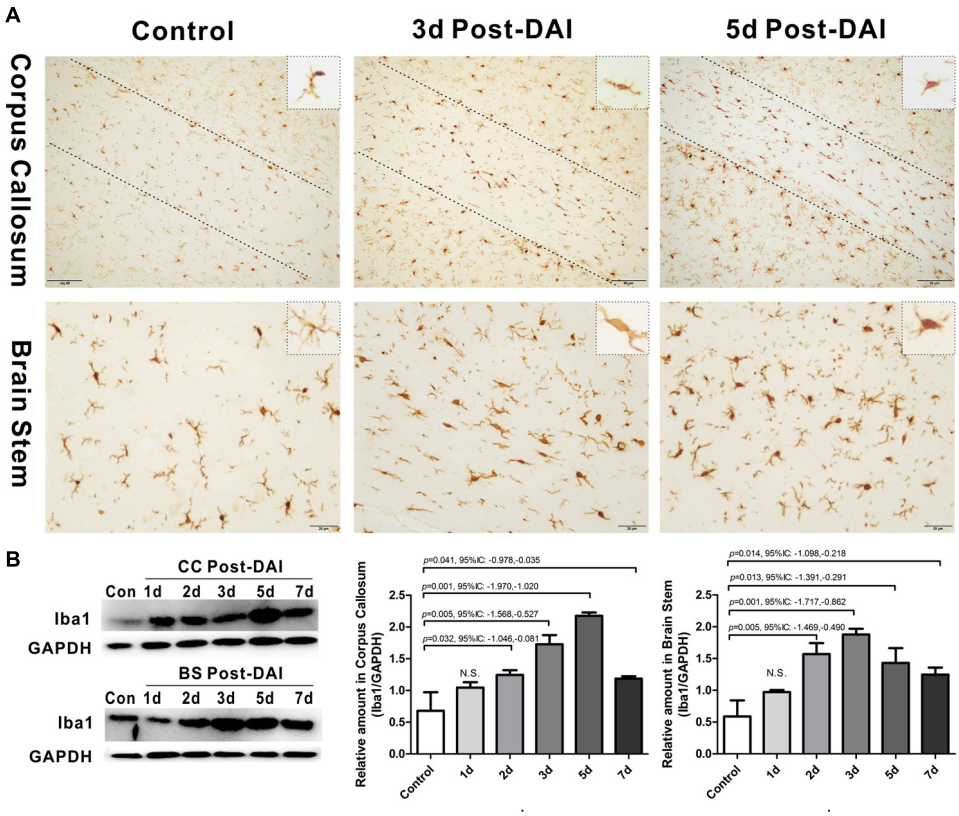

FIGURE 5 | Activation of microglia/macrophages in DAI. **(A)** Immunohistochemical results show that DAI induced an increased number of Iba1-positive cells in the CC and brain stem; **(B)** western blot analysis indicates that Iba1 expression was significantly increased from 2 to 7 days after injury in both the CC and brain stem. N.S. indicates no significant changes between DAI group and control group.

At day 3 after injury, the CC regions exhibited a focal disorganization of the myelin sheath. It is noteworthy that most axons are irregular in profile and contains reduced cytoskeleton (**Figures 7A,B**). The patches of neurofilaments indicated partial proteolysis of the axonal cytoskeleton. Moreover, a number of periaxonal spaces (pa) occur between the axon and the myelin sheath. Highly swollen mitochondria within the axoplasm contains central lacuna. Compared with the control, the g ratio relative to the axon diameter in the DAI group is increased, which may be associated with a larger caliber of swollen axons (**Figure 7M**).

Unlike CC, the brain stem regions exhibit widespread delamination of myelin lamellae at day 3 following DAI (**Figure 7D**). The myelin extended either outside (external protrusions, ep, **Figure 7J**) or inside (myelin intrusions, mi, **Figure 7E**), while the axonal cytoskeleton was generally organized and mitochondria appeared intact. In the brain stem, an increased thickness of myelin caused by disrupted myelin lamellae led to a reduction in the value of the g ratio following DAI (**Figure 7N**).

At day 7 after injury, obvious degenerating axons and abnormal myelin were observed in both the CC (**Figure 7C**) and brain stem regions (**Figure 7F**). Degenerating axons exhibited cytoskeletal dissolution (light degeneration, **Figure 7H**) or amorphous electron dense material (dark degeneration, **Figure 7I**). Meanwhile, DAI rats also showed a marked feature of myelin pathology. Most of myelin lamellae were separated diffusely and disconnected locally. Myelin sheaths often collapsed around a degenerating axon or back onto themselves if the accompanying axon was disappeared (**Figure 7K**). Moreover, excessive myelin figures were also observed (**Figure 7L**). Both the CC (**Figure 7O**) and brain stem (**Figure 7P**) showed an increased slope in the g-ratio plots at 7 days after injury.

DISCUSSION

Formerly, DAI has been classically regarded as a primarily axonal degenerative disorder and the myelin sheath collapses as the axon degenerates. However, our present study demonstrates that damage can be initiated in myelin along intact axons in the brain stem following moderate DAI. Oligodendrocyte selective vulnerability and subsequent demyelination may contribute to axonal degeneration in the brain stem.

Currently, the severity of DAI is classified based on the areas of white matter with traumatic axonal injury (TAI) (Kim et al., 2008). Both DAI and TAI refer to studies of TBIs where axonal injury is the dominant component. They are

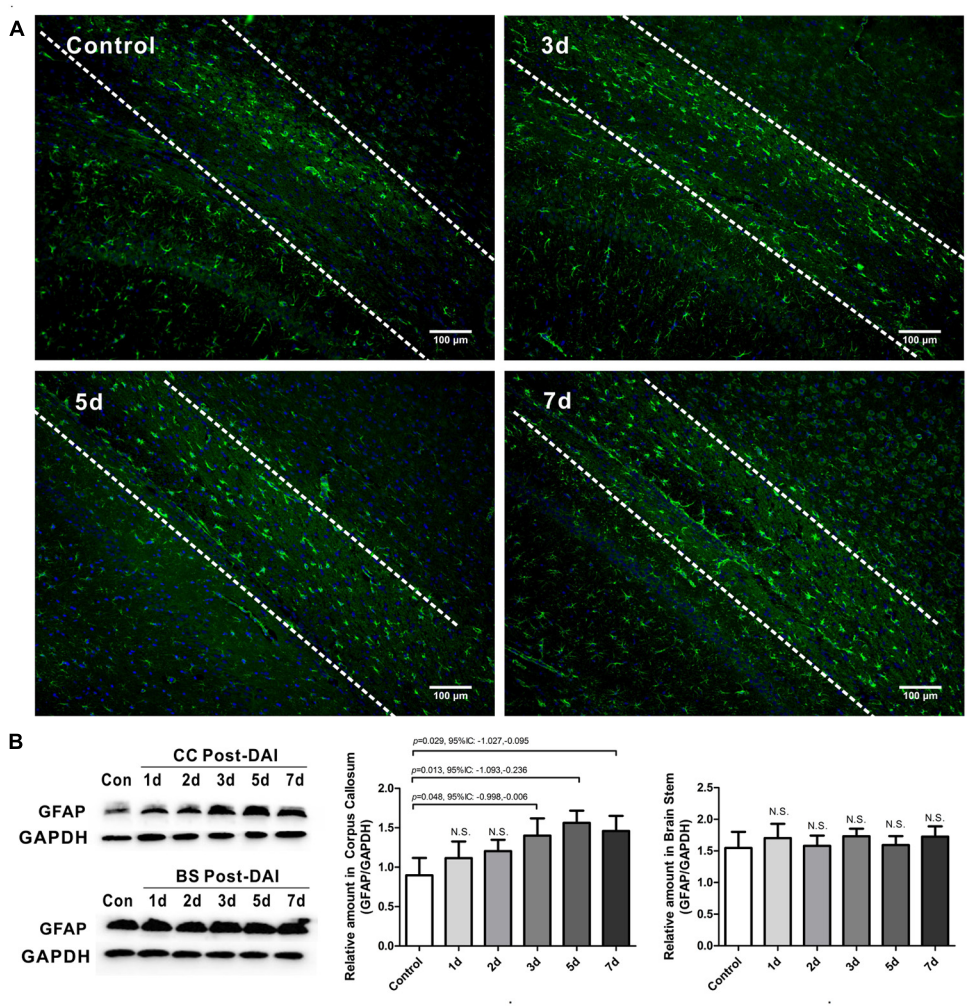

FIGURE 6 | Mild astrogliosis in the CC. **(A)** Immunofluorescence for GFAP shows reactive astrocyte is significantly increased in CC; **(B)** western blot analysis indicates that GFAP expression is significantly increased in the CC at 3, 5, and 7 days post-DAI. However, there was no effect of DAI on GFAP expression in brain stem. N.S. indicates no significant changes between DAI group and control group.

often used interchangeably, although DAI occupies the more severe end of the spectrum of diffuse trauma-induced brain injury (Geddes et al., 2010). Mild DAI involves lesions mainly in the corona radiata. Moderate DAI includes corona radiata with the addition of CC. Severe DAI involves these sites as well as the brainstem tracts. In the present study, we used a modified Marmarou method to create a moderate DAI model. Depending on different direction and intensity of mechanical force transmitted to the different brain regions, it is expected that different injured regions may exhibit separated pathological processes involving axons and myelin. Thus, both the CC and brain stem were selected to be studied.

In the present study, our results clearly demonstrated that moderate DAI leads to myelin loss, revealed by LFB staining, MBP western blot analysis and electron microscopy. Moreover, DAI induces a persistent reduction in mature oligodendrocytes, with marked increases in the numbers of apoptotic oligodendrocytes for up to 7 days post-DAI. Thus, we suggest that the delayed oligodendrocyte death may be a significant factor underlying myelin loss in DAI. Myelin allows the rapid transmission of information that is needed for normal emotional, cognitive, and behavioral function (Deoni et al., 2011; Hong et al., 2015). Consequently, oligodendrocyte loss and myelin degeneration can impair saltatory conduction and modify circuit function, which is a potential factor underlying the slow information-processing speed in patients with DAI.

Oligodendrocyte progenitor cells (OPCs), as a source of new oligodendrocytes, can be stimulated to proliferate, migrate and differentiate in response to demyelination (Zhang et al., 2001; Jankovski et al., 2010). Our present results show that the number of Olig2-positive cells was increased in the first week post-injury. In a TAI model caused by central fluid percussion injury, Flygt et al. (2017) found that the numbers of both EdU/DAPI/Olig2- and EdU/DAPI/NG2-positive cells were increased and proposed that TAI induces a transient proliferative response of residing OPCs. Moreover,

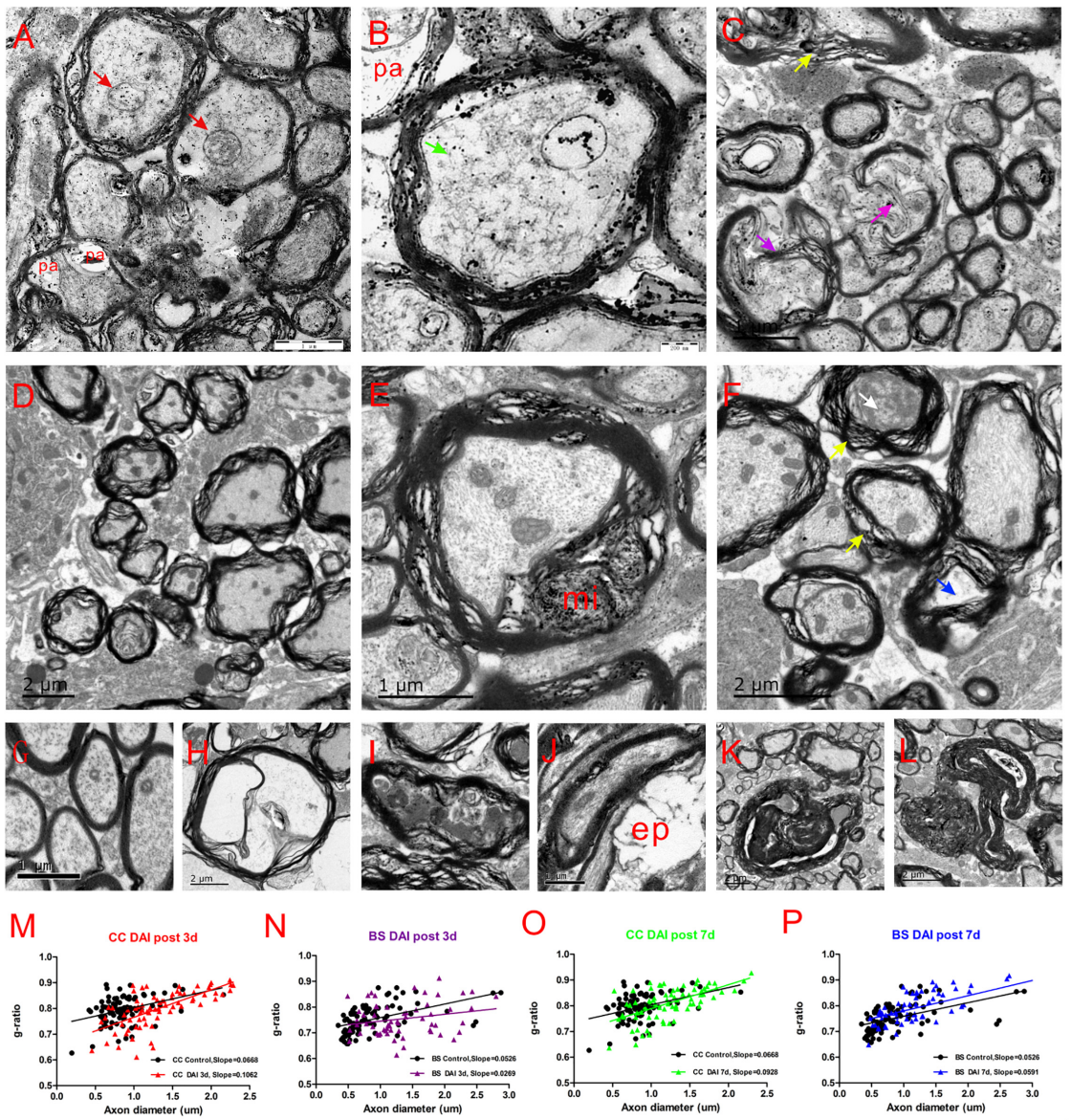

FIGURE 7 | Ultrastructural changes in the CC and brain stem after DAI. **(G)** A normal distribution of myelinated fibers in the control; **(A,B)** at 3 days after DAI, the CC exhibits reduced cytoskeleton (green arrow), highly swollen mitochondria (red arrow), and periaxonal spaces (pa); **(D)** at 3 days after DAI, the brain stem exhibits marked myelin abnormalities along viable axons. The myelin extends outside (external protrusions, ep, **J**) or inside (myelin intrusions, mi, **E**); at 7 days after DAI, both the CC **(C)** and brain stem **(F)** regions exhibit obvious degenerating axons and abnormal myelin at 7 days after DAI. There is light degeneration (**H** and blue arrow) and dark degeneration (**I** and white arrow). Typical myelin abnormalities included diffuse separation of the sheath layers (yellow arrowheads), deterioration (purple arrow), collapse of the myelin **(K)** and excessive myelin figures **(L)**; **(M–P)** the change of g-ratio (axon/fiber diameter) in the CC and brain stem.

Xu et al. (2015) transplanted OPCs into the deep sensorimotor cortex of DAI rats and found that OPCs migrate en masse along white matter tracts and differentiate extensively into ensheathing oligodendrocytes. These data suggest that proliferating OPCs may replace dead oligodendrocytes and contribute to myelin remodeling and regeneration following TAI.

The capacity for spontaneous remyelination in injured tissues can be impaired by many factors, such as inflammatory cytokine released by activated microglia and glial scars formed by astrogliosis (Gallo and Armstrong, 2008; Clarner et al., 2012). Similar to our results, Jia et al. (2012) demonstrated that DAI rats also exhibit microglial activation in the CC during the acute stage, which plays an important role in secondary pathologic changes in DAI. In our study, we found that astrogliosis is relatively mild during this first week, which is similar to Sullivan's findings in a mouse TAI model (Sullivan et al., 2013). The mild activated astrocytes can secrete a range of factors including neurotrophic factors, growth factors and cytokines that stimulate re/myelination by promoting OPC survival, proliferation and/or maturation (Kiray et al., 2016). Thus, mild astrogliosis in the

context of myelin loss plays an important role in promoting the recovery of CNS function.

The ultrastructure analysis with electron microscopy provides further evidence of pathological changes of axons and myelin post-DAI. Notably, larger myelinated nerve fibers are the primary damaged objects in the early period following DAI as the g ratio rapidly changes in larger nerve fibers. Secondly, neither axon degeneration nor myelin loss occur within a narrow time frame, but in the secondary injury stage. Lastly, different injured regions exhibit separated pathological processes involving axons and myelin.

Our ultrastructural analysis demonstrated that CC was characterized by distinct axonal pathology at day 3 post-injury. Next to the impact site, the long axonal projections that traverse CC are simulated by forces of tension, torsion and compression, and consequently cause axonemal and cytoskeletal disruption as the cell injury triggers mechanically (Montanino and Kleiven, 2018). Following the initial damage, the complex secondary insults, including calcium overload, mitochondrial dysfunction, oxidative stress, glutamate excitotoxicity, eventually cause Wallerian degeneration and irreversible axonal disconnection (Chen et al., 2002). Notably, we also found that axonal injury also leads to structural damage to the adjacent myelin membrane at 7 days post-injury. It was hypothesized that calpain leak from damaged axons may mediate detachment of MBP from myelin membranes, leading to an instability of the myelin sheath and the initiation of demyelination (Liu et al., 2010).

Unlike the CC, the brain stem, which is farther from the impact site and bears less intensity and displacement of initial mechanical force, exhibited marked myelin abnormalities along viable axons at day 3 post-injury. We speculate that oligodendrocytes with the highest metabolic rate and limited antioxidants are more sensitive to secondary insults than axons. Interestingly, myelin-oligodendrocyte disruption further destroys axonal integrity at day 7 after injury in the brain stem. In fact, demyelination has severe consequences for the axonal partner. In addition to insulating the axons by myelination, myelin-oligodendrocytes deliver critical energy substrates to the axons through the monocarboxylate transporter 1 (MCT1) (Zhou et al., 2017). So, the most immediate effect of myelin-oligodendrocyte unit damage is the loss of trophic and metabolic support for the axon. Moreover, the loss of myelin also causes an increased energy demand of axons. Following demyelination, sodium channels redistribute across the entire axonal surface, and the axon would need more energy to maintain ion gradients (Waxman et al., 2004). Finally, myelin debris, served as neurotoxic mediators, expose the axons to inflammatory cytokines (Simons et al., 2014). Thus, myelin disruption caused by delayed oligodendrocyte death may also contribute to severe axonal degeneration.

The above ultrastructure observations revealed a complex interplay between axonal degeneration and myelin damage. So, we suggest that axon-myelin should be regarded as a highly integrated structural and functional unit, rather separate entities. In addition, depending on the separate pathological processes of DAI in CC (myelin sheath degeneration subsequent to axonal transection) vs. the brain stem (axonal degeneration subsequent to myelin disruption), DAI could be further divided into a different pathological pattern. As degenerative axons are difficult to repair while remyelination is feasible, promoting myelin regeneration may be an important target for therapeutic interventions of DAI.

CONCLUSION

As a whole, the findings presented in this study highlight the need to evaluate pathological changes in both axon damage and myelin degeneration following DAI. A persistent apoptosis of mature oligodendrocytes within the CC and brain stem indicate oligodendrocyte-selective vulnerability in DAI. The axonal degeneration secondary to demyelination in the brain stem may be another pathological pattern of DAI. Defining the cause of ongoing oligodendrocyte death and promoting myelin regeneration may be important targets for therapeutic interventions of DAI.

AUTHOR CONTRIBUTIONS

JK and GZ designed the study. JM, ML, TW, XL, and MB performed the research, collected and analyzed the data. JM wrote the manuscript. All authors discussed the results and revised the manuscript.

FUNDING

This study was supported by Hebei Natural Science Foundation (Grant No. H2017405021).

REFERENCES

Adams, J. H., Doyle, D., Ford, I., Gennarelli, T. A., Graham, D. I., and McLellan, D. R. (1989). Diffuse axonal injury in head injury: definition, diagnosis and grading. *Histopathology* 15, 49–59. doi: 10.1111/j.1365-2559.1989.tb03040.x

Aggarwal, S. (2011). Central nervous system myelin: structure, synthesis and assembly. *Trends Cell Biol.* 21, 585–593. doi: 10.1016/j.tcb.2011.06.004

Armstrong, R. C., Mierzwa, A. J., Marion, C. M., and Sullivan, G. M. (2015). White matter involvement after TBI: clues to axon and myelin repair capacity. *Exp. Neurol.* 275(Pt 3), 328–333. doi: 10.1016/j.expneurol.2015.02.011

Bradl, M., and Lassmann, H. (2010). Oligodendrocytes: biology and pathology. *Acta Neuropathol.* 119, 37–53. doi: 10.1007/s00401-009-0601-5

Chen, G., Go, L., and Mao, B. (2002). [Biomechanical mechanism of diffuse axonal injury]. *Sheng Wu Yi Xue Gong Cheng Xue Za Zhi* 19, 500–5004.

Clarner, T., Diederichs, F., Berger, K., Denecke, B., Gan, L., Van der Valk, P., et al. (2012). Myelin debris regulates inflammatory responses in an experimental demyelination animal model and multiple sclerosis lesions. *Glia* 60, 1468–1480. doi: 10.1002/glia.22367

Deoni, S. C., Mercure, E., Blasi, A., Gasston, D., Thomson, A., Johnson, M., et al. (2011). Mapping infant brain myelination with magnetic resonance imaging. *J. Neurosci.* 31, 784–791. doi: 10.1523/JNEUROSCI.2106-10.2011

Flygt, J., Clausen, F., and Marklund, N. (2017). Diffuse traumatic brain injury in the mouse induces a transient proliferation of oligodendrocyte progenitor

cells in injured white matter tracts. *Restor. Neurol. Neurosci.* 35, 251–263. doi: 10.3233/RNN-160675

Gallo, D. V., and Armstrong, R. (2008). Myelin repair strategies: a cellular view. *Curr. Opin. Neurol.* 21, 278–283. doi: 10.1097/WCO.0b013e3282fd1875

Geddes, J. F., Whitwell, H. L., and Graham, D. I. (2010). Traumatic axonal injury: practical issues for diagnosis in medicolegal cases. *Neuropathol. Appl. Neurobiol.* 26, 105–116. doi: 10.1046/j.1365-2990.2000.026002105.x

Hong, S., Hu, X., Leak, R. K., Shi, Y., An, C., Suenaga, J., et al. (2015). Demyelination as a rational therapeutic target for ischemic or traumatic brain injury. *Exp. Neurol.* 272, 17–25. doi: 10.1016/j.expneurol.2015.03.017

Jang, S. H., and Kwon, H. G. (2016). Degeneration of an injured spinothalamic tract in a patient with mild traumatic brain injury. *Brain Injury* 30, 1026–1028. doi: 10.3109/02699052.2016.1146961

Jankovski, A., Garcia, C., Soriano, E., and Sotelo, C. (2010). Proliferation, migration and differentiation of neuronal progenitor cells in the adult mouse subventricular zone surgically separated from its olfactory bulb. *Eur. J. Neurosci.* 10, 3853–3868. doi: 10.1046/j.1460-9568.1998.00397.x

Jia, X., Cong, B., Wang, S., Dong, L., Ma, C., and Li, Y. (2012). Secondary damage caused by CD11b+ microglia following diffuse axonal injury in rats. *J. Trauma Acute Care Surg.* 73, 1168–1174. doi: 10.1097/TA.0b013e318246eaf4

Johnson, V. E., Stewart, W., and Smith, D. H. (2013). Axonal pathology in traumatic brain injury. *Exp. Neurol.* 246, 35–43. doi: 10.1016/j.expneurol.2012.01.013

Kim, J., Avants, B., Patel, S., Whyte, J., Coslett, B. H., Pluta, J., et al. (2008). Structural consequences of diffuse traumatic brain injury: a large deformation tensor-based morphometry study. *Neuroimage* 39, 1014–1026. doi: 10.1016/j.neuroimage.2007.10.005

Kiray, H., Lindsay, S. L., Hosseinzadeh, S., and Barnett, S. C. (2016). The multifaceted role of astrocytes in regulating myelination. *Exp. Neurol.* 283(Pt B), 541–549. doi: 10.1016/j.expneurol.2016.03.009

Liu, M. C., Akle, V., Zheng, W., Kitlen, J., O'Steen, B., Larner, S. F., et al. (2010). Extensive degradation of myelin basic protein isoforms by calpain following traumatic brain injury. *J. Neurochem.* 98, 700–712. doi: 10.1111/j.1471-4159.2006.03882.x

Ma, J., Zhang, K., Wang, Z., and Chen, G. (2016). Progress of research on diffuse axonal injury after traumatic brain injury. *Neural Plast.* 2016:9746313. doi: 10.1155/2016/9746313

Maxwell, W. L. (2013). Damage to myelin and oligodendrocytes: a role in chronic outcomes following traumatic brain injury? *Brain Sci.* 3, 1374–1394. doi: 10.3390/brainsci3031374

Montanino, A., and Kleiven, S. (2018). Utilizing a structural mechanics approach to assess the primary effects of injury loads onto the axon and its components. *Front. Neurol.* 9:643. doi: 10.3389/fneur.2018.00643

Mu, J., Song, Y., Zhang, J., Lin, W., and Dong, H. (2015). Calcium signaling is implicated in the diffuse axonal injury of brain stem. *Int. J. Clin. Exp. Pathol.* 8, 4388–4397.

Simons, M., Misgeld, T., and Kerschensteiner, M. (2014). A unified cell biological perspective on axon–myelin injury. *J. Cell Biol.* 206, 335–345. doi: 10.1083/jcb.201404154

Sullivan, G. M., Mierzwa, A. J., Kijpaisalratana, N., Tang, H., Wang, Y., Song, S. K., et al. (2013). Oligodendrocyte lineage and subventricular zone response to traumatic axonal injury in the corpus callosum. *J. Neuropathol. Exp. Neurol.* 72, 1106–1125. doi: 10.1097/NEN.0000000000000009

Vargas, M. E., and Barres, B. A. (2007). Why is wallerian degeneration in the CNS so slow? *Annu. Rev. Neurosci.* 30, 153–179. doi: 10.1146/annurev.neuro.30.051606.094354

Waxman, S. G., Craner, M. J., and Black, J. A. (2004). Na+ channel expression along axons in multiple sclerosis and its models. *Trends Pharmacol. Sci.* 25, 584–591. doi: 10.1016/j.tips.2004.09.001

Xu, L., Ryu, J., Hiel, H., Menon, A., Aggarwal, A., Rha, E., et al. (2015). Transplantation of human oligodendrocyte progenitor cells in an animal model of diffuse traumatic axonal injury: survival and differentiation. *Stem Cell Res. Ther.* 6:93. doi: 10.1186/s13287-015-0087-0

Zhang, J., Niu, F., Dong, H., Liu, L., Li, J., and Li, S. (2015). Characterization of protein alterations in damaged axons in the brainstem following traumatic brain injury using fourier transform infrared microspectroscopy: a preliminary study. *J. Forensic Sci.* 60, 759–763. doi: 10.1111/1556-4029.12743

Zhang, R. L., Zhang, Z. G., Zhang, L., and Chopp, M. (2001). Proliferation and differentiation of progenitor cells in the cortex and the subventricular zone in the adult rat after focal cerebral ischemia. *Neuroscience* 105, 33–41. doi: 10.1016/S0306-4522(01)00117-8

Zhou, P., Guan, T., Jiang, Z., Namaka, M., Huang, Q. J., and Kong, J. M. (2017). Monocarboxylate transporter 1 and the vulnerability of oligodendrocyte lineage cells to metabolic stresses. *CNS Neurosci. Ther.* 24, 126–134. doi: 10.1111/cns.12782

Conflict of Interest Statement: The authors declare that the research was conducted in the absence of any commercial or financial relationships that could be construed as a potential conflict of interest.

frontiers in Genetics

ORIGINAL RESEARCH
published: 10 July 2019
doi: 10.3389/fgene.2019.00519

Polygenic Risk Score for Alzheimer's Disease Is Associated With Ch4 Volume in Normal Subjects

Tao Wang[1†], Zhifa Han[1†], Yu Yang[2†], Rui Tian[1], Wenyang Zhou[1], Peng Ren[1], Pingping Wang[1], Jian Zong[1], Yang Hu[1] and Qinghua Jiang[1]*

[1] School of Life Sciences and Technology, Harbin Institute of Technology, Harbin, China, [2] Information Department, Jiangsu Singch Pharmaceutical Co., Ltd., Lianyungang, China

Alzheimer's disease (AD) is a common neurodegenerative disease. *APOE* is the strong genetic risk factor of AD. The existing genome-wide association studies have identified many single nucleotide polymorphisms (SNPs) with minor effects on AD risk and the polygenic risk score (PRS) is presented to combine the effect of these SNPs. On the other hand, the volumes of various brain regions in AD patients have significant changes compared to that in normal individuals. Ch4 brain region containing at least 90% cholinergic neurons is the most extensive and conspicuous in the basal forebrain. Here, we investigated the relationship between the combined effect of AD-associated SNPs and Ch4 volume using the PRS approach. Our results showed that Ch4 volume in AD patients is significantly different from that in normal control subjects (p-value $< 2.2 \times 10^{-16}$). AD PRS, is not associated with the Ch4 volume in AD patients, excluding the *APOE* region (p-value = 0.264) and including the *APOE* region (p-value = 0.213). However, AD best-fit PRS, excluding the *APOE* region, is associated with Ch4 volume in normal control subjects (p-value = 0.015). AD PRS based on 8070 SNPs could explain 3.35% variance of Ch4 volume. In addition, the p-value of AD PRS model in normal control subjects, including the *APOE* region, is 0.006. AD PRS based on 8079 SNPs could explain 4.23% variance of Ch4 volume. In conclusion, PRS based on AD-associated SNPs is significantly related to Ch4 volume in normal subjects but not in patients.

Keywords: Alzheimer's disease, single nucleotide polymorphisms, polygenic risk score, Ch4 region, *APOE*

OPEN ACCESS

Edited by:
Wenbo Zhang,
The University of Texas Medical Branch at Galveston, United States

Reviewed by:
Gang Wang,
Shanghai Jiao Tong University, China
Jianjun Chen,
Tongji University School of Medicine, China

****Correspondence:***
Qinghua Jiang
qhjiang@hit.edu.cn

† These authors have contributed equally to this work

Specialty section:
This article was submitted to Genetics of Aging, a section of the journal Frontiers in Genetics

Received: *08 September 2018*
Accepted: *13 May 2019*
Published: *10 July 2019*

Citation:
Wang T, Han Z, Yang Y, Tian R, Zhou W, Ren P, Wang P, Zong J, Hu Y and Jiang Q (2019) Polygenic Risk Score for Alzheimer's Disease Is Associated With Ch4 Volume in Normal Subjects. Front. Genet. 10:519. doi: 10.3389/fgene.2019.00519

INTRODUCTION

Alzheimer's disease (AD) is a complex and severe neurodegenerative disorder. It is characterized by progressive deterioration in cognition and behavior, which seriously affects people's daily life (Hu et al., 2017; Jiang et al., 2017; Liu et al., 2018). Genetic factors can lead to 60–80% of AD risk (Lambert et al., 2010). The *APOE* gene is the strongest genetic risk factor for late-onset AD (Corder et al., 1993). Several existing AD genome-wide association studies (GWASs) have identified many common single nucleotide polymorphisms (SNPs) with relatively small effect size (Hindorff et al., 2009; Lambert et al., 2013). The combined effect of these SNPs could make a significant contribution to AD risk. The polygenic risk score (PRS) was described to depict quantitatively the combined effect of SNPs on disease risk (International Schizophrenia Consortium, 2009). It has been reported that PRS based on disease-related SNPs was associated with disease risk and

can work as a predictor of disease risk (Escott-Price et al., 2015; Lupton et al., 2016; Escott-Price et al., 2017). In addition, several authors investigated the effect of PRS on both disease status and disease-associated phenotypes (also called endo-phenotype) (Harris et al., 2014; Marden et al., 2016; Axelrud et al., 2018). Axelrud et al. (2018) found AD PRS was an implication for memory performance and hippocampus volumes in early life. Harris et al. (2014) found there was no significant association between polygenic risk for AD and cognitive ability in non-demented older people. PRS for AD was utilized to predict memory decline in black and white Americans (Marden et al., 2016). Some studies have reported that the brain structure changes significantly in some nervous system disease compared to normal subjects by using magnetic resonance imaging (MRI) (Zhang et al., 2011; Alattas and Barkana, 2015; Mattavelli et al., 2015). In addition, brain-associated endo-phenotypes were commonly used to analyze the effect of disease-associated SNPs. Late-onset AD PRS was used to predict hippocampus function (Xiao et al., 2017). AD polygenic risk was proved to modulate precuneal volume (Li et al., 2018). Terwisscha van Scheltinga et al. (2013) found schizophrenia-associated genetic risk variants jointly modulate total brain and white matter volume by PRS approach.

Recently, a study demonstrated that basal forebrain degeneration precedes the cortical spread of AD pathology (Schmitz et al., 2016). There is the early pathological change of the nucleus basalis of meynert (NbM) in the basal forebrain (Grothe et al., 2012, 2013). Basal forebrain consists of magnocellular cholinergic cells and designated into Ch1–Ch4 according to the distribution difference of cholinergic neurons, with Ch4 corresponding to NbM (Mesulam et al., 1983). Ch4 region is the most extensive and conspicuous of Ch1–Ch4, containing more than 90% of cholinergic neurons (Mesulam et al., 1983). In fact, the Ch4 region provides the entire cortical surface with the single major source of cholinergic innervation (Mesulam et al., 1983). Ch4 region has plenty of functions, such as memory, attention, and modulation of the behavioral state (Gratwicke et al., 2013). Increasing studies have revealed that Ch4 region plays a major role in the function of memory (Butt and Hodge, 1995; Leanza et al., 1996; McGaugh, 2002). In addition, the Ch4 region and its cholinergic projections play an essential role in regulating a wide variety of attention functions (Voytko, 1996; McGaughy et al., 2002). Grothe et al. (2012) found atrophy of the cholinergic basal forebrain especially NBM (Ch4 region) in progressive AD. Previous studies have demonstrated that maximum 96% of Ch4 neuronal loss occurs in AD compared to normal control subjects (Whitehouse et al., 1981; Candy et al., 1983; Etienne et al., 1986). Volumetric MR imaging reveals that NBM (Ch4 region) significantly degenerates in AD patients compared with age-matched normal subjects (Hanyu et al., 2002). Teipel et al. (2011) discovered that the NBM (Ch4 region) cholinergic projection axons shrink in AD patients by high-resolution diffusion tensor imaging. Considering the early degeneration of Ch4 neurons in AD patients, we selected Ch4 brain region as an ideal candidate endo-phenotype to investigate the effect of AD-associated genetic risk variants.

It is well known that the *APOE* gene is significantly associated with AD risk. Therefore, in order to explore the *APOE* influence on AD PRS, PRS in this article is constructed based on AD-associated SNPs, excluding the *APOE* region and including the *APOE* region, respectively. This paper is aimed at exploring the relationship between AD PRS and Ch4 volume to answer following questions. Firstly, is there a significant difference of Ch4 volume between AD patients and normal control subjects? Secondly, is AD PRS significantly related with Ch4 volume in AD patients and normal control subjects, respectively?

MATERIALS AND METHODS

Discovery Samples

Alzheimer's disease GWAS summary data was obtained from the International Genomics of Alzheimer's Project (IGAP) (Lambert et al., 2013). IGAP is a large two-stage study based on GWAS on individuals of European ancestry. In stage 1, IGAP performed a meta-analysis on four previous-published GWAS datasets containing 17,008 AD patients and 37,154 normal controls using 7,055,881 SNPs. In stage 2, 11,632 SNPs were genotyped and tested for association in an independent population consisting of 8,572 AD patients and 11,312 normal controls (Lambert et al., 2013). The stage 1 dataset is used to identify risk variants, their *P* values and corresponding odds ratios.

Target Samples

Magnetic resonance imaging and genetic data used in this paper were available from the Alzheimer's Disease Neuroimaging Initiative (ADNI) database[1]. The ADNI was launched in 2003 as a public-private partnership, led by Principal Investigator Michael W. Weiner, MD. The primary goal of ADNI has been to test whether serial MRI, positron emission tomography (PET), other biological markers, and clinical and neuropsychological assessment can be combined to measure the progression of mild cognitive impairment (MCI) and early AD. We can obtain the SNP data and neuroimaging data of every participant at the same time in the ADNI database. In other words, both SNP and neuroimaging data are sampled from each participant in the ADNI database. We selected 108 AD patients and 182 normal control (NC) subjects according to sample diagnostic results. We removed four samples (099_S_4086, 027_S_1387, 116_S_1232, 037_S_4432) owing to their outliers of Ch4 volume. The remaining 106 AD patients (**Supplementary Table S1**) and 180 normal control subjects (**Supplementary Table S2**) were used as target samples for further analysis. All information on recruitment and diagnostic criteria could be reached on the ADNI website.

MRI Analysis

Magnetic resonance imaging data were acquired according to a standardized protocol, which included a high-quality T1-weight, magnetization prepared rapid gradient echo (MP-RAGE) sequence (Jack et al., 2008). MP-RAGE acquisition parameters

[1]www.adni-info.org

for one platform (Philips Medical Systems) are as follows: TR = 6.76 ms, TE = 3.11 ms, FA = 9°, matrix size = 256 × 256, slice thickness = 1.2 mm, number of slices = 170, voxel size x = 1.05 mm and voxel size y = 1.05 mm. Quality control of MRI data was performed at the Mayo Clinic based on centralized and standardized criteria (Jack et al., 2008).

All MRI data were transformed into NII files in the first place using MRIConvert software tool. All anatomical images were preprocessed by using the diffeomorphic anatomical registration through exponentiated lie algebra (DARTEL) in SPM12 (Ashburner, 2007). Basically, neuroimages were first segmented into the grey matter (GM), white matter (WM), cerebrospinal fluid (CSF), skull and soft tissue. Then, DARTEL was used to increase the accuracy of inter-subject alignment for generating a population template in montreal neurological institute (MNI) space. Finally, all GM neuroimages were normalized to MNI space based on the population template and smoothed with a Gaussian kernel of 8 mm, and they were subjected to modulation that depicted the tissue volumes. Voxel size for GM neuroimage was specified with 1.5 mm^3. GM, WM and CSF volumes were available from the files containing segmentation parameters. The sum of these three tissues was computed as the total intracranial volume (ICV), and the sum of GM and WM volume was computed as the total parenchymal brain volume (TBV).

ROI for Ch4 in MNI space was achieved by using the SPM Anatomy toolbox (Eickhoff et al., 2005). Zaborszky et al. (2008) presented stereotaxic probabilistic maps of the magnocellular cell groups in human basal forebrain based on 10 postmortem brains, including Ch4 region. The ROI for Ch4 was created based on Ch4 probabilistic map. Because voxel size for the Ch4 ROI is 1 mm^3, which is not consistent with smoothed and modulated GM neuroimage. It is necessary to co-register the Ch4 ROI with smoothed and modulated GM neuroimage. Co-registering Ch4 ROI and extracting ROI signals were performed utilizing DPABI software (Yan et al., 2016).

Genetic Analysis

The genetic data were available from the ADNI webpage. ADNI participants were genotyped using the Illumina Omni 2.5M SNP arrays. The genetic data consist of 2,379,855 SNPs. We extracted 2,134,825 SNPs with rs or kgp prefix, which are located in 1–22 chromosomes. We performed a series of quality control procedures on these genetic data using PLINK tool set (Purcell et al., 2007). Firstly, individuals with more than 5% missing SNPs were removed. All participants approved the filter. Then, we removed 789,861 variants owing to minor allele frequencies of less than 0.02. Thirdly, 84,891 SNPs were taken away due to more than 1% missing genotypes. Next, we removed 2,597 variants according to Hardy-Weinberg exact test at a specified significant threshold of 1×10^{-6}. Finally, in order to remove SNPs in linkage disequilibrium, 1,024,426 SNPs were pruned according to a pairwise R^2 cutoff of 0.25 and a window of 50 SNPs with shifting five SNPs at every step (Terwisscha van Scheltinga et al., 2013). In the end, 233,050 variants with rs or kgp prefix were selected. 76,312 of 233,050 variants were available in the AD summary dataset. The genomic location for *APOE* gene is chr19: 45,409,011 – 45,412,650 (GRCh37/hg19). There are 11 SNPs with a 70 kb region which surround the *APOE* gene (rs1871047, rs11879589, rs387976, rs6859, rs283814, rs157582, rs405509, rs439401, rs445925, rs3760627, rs204479). We obtained 76,301 SNPs, excluding the *APOE* gene, and 76,312 SNPs, including the *APOE* gene, for subsequent analysis.

Statistical Analysis

Individual age was computed as study date minus birth date. ICV was adjusted for age and gender. TBV, GM volume, WM volume and Ch4 volume were corrected for age, gender and ICV using linear regression in total groups. The correction method was described by Terwisscha van Scheltinga et al. (2013). Briefly, non-standard residual of volume for every participant could be obtained by linear regression. Then, the sum of non-standard residue of volume, intercept and $\sum_{i=1}^{m} beta_i \times mean_i$ was calculated as corrected volume, where m refers to the number of the covariate, $beta_i$ represents the regression coefficient of covariate i, and $mean_i$ denotes the mean of covariate i. All adjusted brain volumes are normally distributed in the total groups, AD patients and normal control subjects, respectively.

Polygenic risk score model is described by International Schizophrenia Consortium (2009). Every SNP has a corresponding P value for its association with AD. Basically, for each SNP, the variant risk score is calculated by multiplying the risk allele number (0, 1, 2) with the corresponding effect size, by the logarithm of the odds ratio. For each participant, the PRS is summed on all SNPs with P value below a threshold, P_T. PRS is calculated at a series of P value thresholds, e.g., $P_T = 0.0001$, 0.0002, . . ., 0.05, . . ., 0.1, . . .,0.5. The P value threshold, P_T, with the largest R^2 is the most predictive cutoff. We calculated the PRS using a lower bound of $P = 0$, an upper bound of $P = 0.6$ and an increment of 0.0001 by PRSice software (version 1.25) (Euesden et al., 2015). PRSice can calculate PRS at a great number of cutoffs, apply PRS and plot the results of PRS.

The first ten principal components of population structure for AD patients and normal control subjects were achieved in PLINK software using the multidimensional scaling plot option (Purcell et al., 2007). And the number of non-missing SNPs used for scoring and inbreeding coefficient for AD patients and normal control subjects were also calculated in PLINK using the het option (Purcell et al., 2007). *APOE* status is coded as 0, 1, or 2, according to the number of *APOE* ε4. We performed linear regressions using Ch4 volume as an outcome variable in AD patients and normal control subjects, respectively, and the number of non-missing SNPs, inbreeding coefficient, the first ten population structure components and *APOE* status were as covariates. R^2 was compared with a model only containing these covariates and a model containing these covariates and PRS. The difference in R^2 between the two models is used to measure variance explained by PRS. These regression analyses were performed using PRSice (Euesden et al., 2015).

Gender difference between AD patients and normal control subjects is examined by the chi-square test in SPSS (version 22; IBM). Welch t-test is applied to examine brain volume

and age difference between two groups using the R script. The p-value < 0.05 is considered statistically significant in this paper.

RESULTS

Statistical Analysis of Brain Volume

Demographic information is shown in **Table 1**. There is no significant differences in age (p-value = 0.2952) and in gender distribution (p-value = 0.1681) between AD group and normal control group. The number of participants with *APOE* ε4 in AD patients and normal control subjects is 77 and 43, respectively. In addition, it does not seem to make a difference in intracranial volume corrected for age and gender between the two groups (p-value = 0.8633). Total brain volume corrected for age, gender and intracranial volume in normal control subjects is larger than that in AD patients (p-value $< 2.2 \times 10^{-16}$). Our results indicated that both GM and WM volume adjusted for age, gender and intracranial volume in AD patients are smaller than that in normal control subjects (p-value $< 2.2 \times 10^{-16}$ and p-value = 0.0002815, respectively). In addition, Ch4 volume corrected age, gender and intracranial volume in AD patients is smaller than that in normal control subjects. Most importantly, there is a significant difference in Ch4 volume between AD patients and normal subjects (p-value $< 2.2 \times 10^{-16}$; **Figure 1**).

The AD Polygenic Risk Score Is Not Associated With Ch4 Volume in AD Patients

Alzheimer's disease PRS based on AD-associated SNPs, excluding the *APOE* region, was used to predict Ch4 volume in AD patients using linear regression. There is no significant relationship between AD PRS and Ch4 volume at the different P value cutoffs (P_T = 0.001, 0.05, 0.1, 0.2, 0.3, 0.4, 0.5), because of all p-value of PRS model (p-value = 0.674, 0.546, 0.667, 0.428, 0.638, 0.726, 0.836) > 0.05, according to the PRS bar plot (**Figure 2**). On the basis of high-resolution PRS plot (**Figure 3**), the best-fit P value threshold for the PRS model is 0.2106. However, the p-value of PRS model at the best-fit cutoff is 0.264. These high-resolution scores indicate that the results from the broad P value cutoff of **Figure 2** are not false negatives due to the small number of cutoff considered. The PRS base on AD-associated SNPs, excluding the *APOE* gene, is not related with Ch4 volume in AD patients. In addition, AD PRS, including the *APOE* gene, was utilized to predict Ch4 volume in AD patients. According to bar plot of PRS results (**Supplementary Figure S1**) and high-resolution plot (**Supplementary Figure S2**), the best-fit P value threshold for PRS model is 0.0068, and the p-value of PRS model at P_T = 0.0068 is 0.213. AD PRS, including the *APOE* gene, is also not related to Ch4 volume in AD patients. Therefore, AD PRS is not associated with Ch4 volume in AD patients. And AD PRS could not successfully measure Ch4 volume in AD patients.

The AD Polygenic Risk Score Is Significantly Associated With Ch4 Volume in Normal Control Subjects

Alzheimer's disease PRS based on AD-associated SNPs, excluding the *APOE* region, was used to predict Ch4 volume in normal control subjects. According to bar plot of PRS results (**Figure 4**), the p-value of the PRS model at P value threshold of 0.1 is 0.028. There is a significant relationship between AD PRS and Ch4 volume in normal control subjects at P value threshold of 0.1. On the basis of the high-resolution plot for PRS results (**Figure 5**), the best threshold for PRS model is 0.0944, the p-value of the PRS model is 0.015. There are 8070 SNPs (**Supplementary Table S3**) with their P value < 0.0944. AD PRS based on 8070 SNPs could explain 3.35% variance of Ch4 volume in normal control subjects. When P value threshold is more or less than the best P value threshold (P_T = 0.0944), the p-value of the PRS model will become greater than 0.015. When AD PRS contains more or fewer SNPs, the ability to account for the variance of Ch4 volume will decrease. AD PRS based on 8070 SNPs could act as a reliable measure for Ch4 volume in normal control subjects. In other words, AD PRS based on 8070 SNPs, excluding the *APOE* gene, is related to Ch4 volume in normal control subjects. Moreover, AD PRS, including the *APOE* gene, was used to predict Ch4 volume in normal control subjects. According to bar plot of PRS results (**Supplementary Figure S3**) and high-resolution plot (**Supplementary Figure S4**), the best-fit P value threshold for PRS model is 0.0944, and the p-value of PRS model at P_T = 0.0944 is 0.006. There are 8079 SNPs with their P value < 0.0944. AD PRS based on 8079 SNPs could explain 4.23% variance of Ch4

TABLE 1 | Demographic information.

	AD patients	NC subjects	Significance
Participants	106	180	ns
Gender (M/F)	59/47	85/95	p-value = 0.1681
Age in Years (SD)	77.81 (7.2507)	76.90 (6.6234)	p-value = 0.2952
Participants with APOE ε4	77	43	ns
Intracranial volume in L (SD)[a]	1.4329 (0.1027)	1.4351 (0.1102)	p-value = 0.8633
Total brain volume in L (SD)[b]	0.9051 (0.0674)	0.9963 (0.0615)	p-value $< 2.2 \times 10^{-16}$
Gray matter volume in L (SD)[b]	0.5112 (0.0651)	0.5846 (0.0455)	p-value $< 2.2 \times 10^{-16}$
White matter volume in L (SD)[b]	0.3940 (0.0411)	0.4117 (0.0354)	p-value = 0.0002815
Ch4 volume (SD)[b]	0.2430 (0.0341)	0.3097 (0.0278)	p-value $< 2.2 \times 10^{-16}$

F, female; M, male. [a]Adjusted for age and gender. [b]Adjusted for age, gender and intracranial volume.

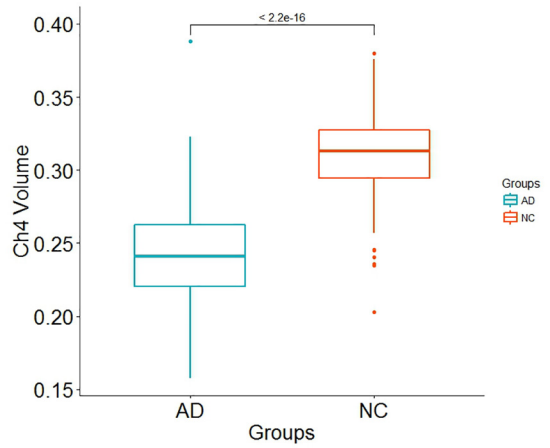

FIGURE 1 | Box plot for Ch4 volume difference between AD patients and normal control subjects.

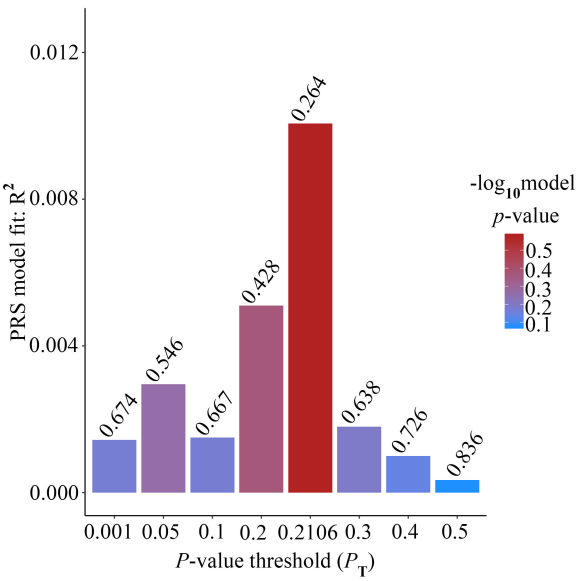

FIGURE 2 | Bar plot showing at broad *P* value thresholds for AD PRS, excluding the *APOE* region, predicting Ch4 volume in AD patients, including a bar for the best-fit PRS from the high-resolution run.

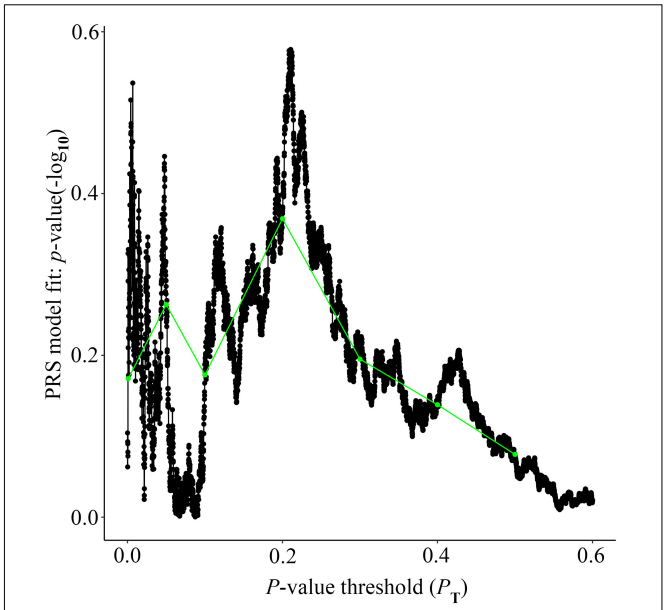

FIGURE 3 | High-resolution plot for AD PRS, excluding the *APOE* region, predicting Ch4 volume in AD patients. The thick line connects points at the broad *P* value thresholds of **Figure 2**. The best-fit PRS is at P_T of 0.2106.

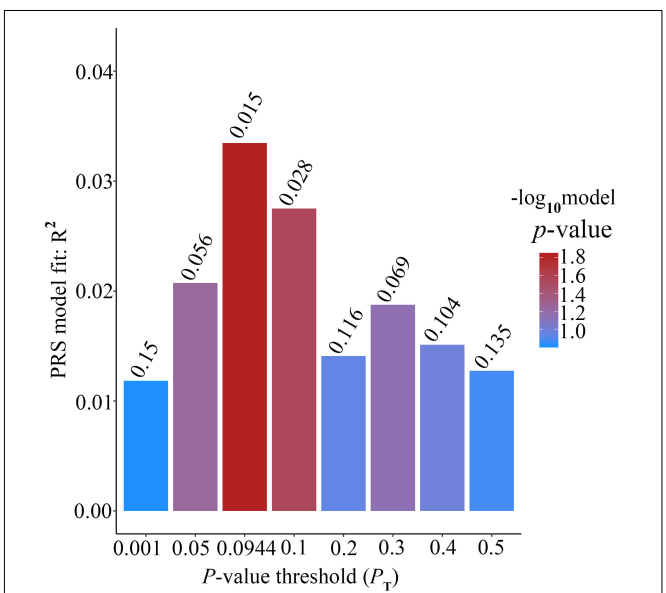

FIGURE 4 | Bar plot showing at broad *P* value thresholds for AD PRS, excluding the *APOE* region, predicting Ch4 volume in normal control subjects, including a bar for the best-fit PRS from the high-resolution run.

volume in normal control subjects. In other words, AD PRS based on 8079 SNPs, including the *APOE* gene, is significantly related to Ch4 volume in normal controls. Therefore, AD polygenic risk score is significantly associated with Ch4 volume in normal control subjects.

DISCUSSION

Alzheimer's disease is a complex and polygenic disease. Current studies have demonstrated that many genetic variations are associated with AD. These genetic variations may be beneficial to understand the mechanism of AD to some extent. On the other hand, some brain regions associated with AD atrophy in AD patients by structural MRI technology. However, the details of association between some brain regions and genetic variation is still unknown. If we know this kind of detailed association, we could further get the regulatory relationship between genetic variation and brain region, which will provide valuable insights into disease mechanism, prevention and treatment. Ch4 brain

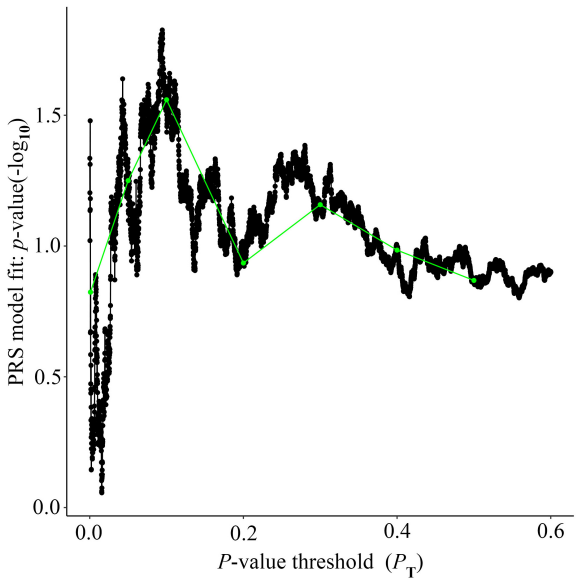

FIGURE 5 | High-resolution plot for AD PRS, excluding the *APOE* region, predicting Ch4 volume in normal control subjects. The thick line connects points at the broad *P* value thresholds of **Figure 4**. The best-fit PRS is at P_T of 0.0944.

region is associated with memory and cognition functions. Therefore, it is very important and necessary to analyze the association between genetic variation and Ch4 brain region.

The Ch4 brain region contains the largest, most hyper-chromic and polymorphic neurons in the basal forebrain, which supplies the single major source cholinergic innervation to the entire cortical surface (Mesulam et al., 1983). Ch4 volume could act as a phenotype associated with Alzheimer's disease. In this article, we investigated the relationship between the combined effect of SNPs and Ch4 volume by using PRS. Our results indicated that the Ch4 volume in AD patients is smaller than that in normal control subjects, and there is the significant difference between the two groups (p-value $< 2.2 \times 10^{-16}$), which is consistent with the previous conclusions (Grothe et al., 2012, 2013; Schmitz et al., 2016). In addition, AD PRS, excluding or including *APOE* gene, is not linked with Ch4 volume in AD patients. However, AD PRS, excluding or including *APOE* gene, is significantly associated with Ch4 volume in normal control subjects. AD PRS could work as a reliable measure for Ch4 volume in normal control subjects.

Many studies found up to 96% of Ch4 neuronal loss in AD patients (Whitehouse et al., 1981; Candy et al., 1983; Etienne et al., 1986). AD PRS, excluding or including *APOE* gene, cannot measure successfully Ch4 volume in AD patients. This may be because Ch4 brain region in AD patients have shrunk severely so that there is no difference of Ch4 volume. Therefore, AD PRS, excluding or including *APOE* gene, may not be a suitable way to measure Ch4 volume in AD patients.

Many studies investigated AD-associated variants in biomarker measurements among healthy subjects using polygenic score approach (Small et al., 2000; Reiman et al., 2004; Filippini et al., 2009; Sheline et al., 2010; Sabuncu et al., 2012; Mormino et al., 2016). Sabuncu et al. (2012) found that the polygenic risk score was correlated with AD-specific cortical thickness in clinically normal human individuals, even after controlling for *APOE* genotype and other factors. AD genetic risk score can be used to predict the thinning of hippocampus complex sub-regions in normal older subjects (Harrison et al., 2016). Elizabeth et al. discovered that higher AD PRS was associated with smaller hippocampus volume in the younger healthy group (Mormino et al., 2016). The influences of common genetic risk variants are detectable among healthy subjects and may begin in early life (Mormino et al., 2016). Furthermore, some evidence reveals that AD-specific atrophy patterns can be identified before cognitive impairment (Csernansky et al., 2005; Jagust et al., 2006). In this study, AD PRS is significantly associated with Ch4 volume in normal control individuals. Our primary analysis suggests this association could be explained by a genetic modulation of neuro-degeneration, which is consistent with the interpretation of Sabuncu et al. (2012). This result agrees that AD-associated atrophy rates accelerate before the beginning of cognitive impairment (Mori et al., 2002; Schott et al., 2010; Andrews et al., 2016). AD PRS, excluding the *APOE* gene, at best-fit *P* value threshold ($P_T = 0.0944$) is significantly associated with Ch4 volume in normal controls. The p-value of PRS model at $P_T = 0.0944$ is 0.015. AD PRS based on 8070 SNPs could explain 3.35% variance of Ch4 volume. We further obtained 5397 genes of index 8070 SNPs from the dbSNP database. There are 3163 SNPs which do not have corresponding gene. 4452 SNPs have a unique corresponding gene. The rest of 455 SNPs have more than one gene. Then, we downloaded gene expression (transcripts per million, TPM) of brain nucleus accumbens (basal ganglion) tissue from Genotype-Tissue Expression (GTEx) database. We found that TPM of 3807 genes among 5397 genes is more than 0, which is about 70.54%. TPM of 3205 genes is greater than 0.5 (59.38%) and TPM of 2959 genes is more than 1 (54.83%). We will further validate these genes using biological experiments in the following studies. Furthermore, AD PRS, including *APOE* gene, at best-fit *P* value threshold is dramatically related with Ch4 volume in normal controls (p-value = 0.006). In addition, AD PRS based on 8079 SNPs could explain 4.23% variance of Ch4 volume. AD PRS including other nine SNPs in *APOE* gene could explain more variance of Ch4 volume (rs1871047, rs387976, rs6859, rs283814, rs157582, rs405509, rs439401, rs3760627, rs204479).

In this study, we investigated the relationship between AD-associated SNPs and Ch4 volume using PRS method. The polygenic risk score combines the weak effect of every candidate SNP in an additive model (International Schizophrenia Consortium, 2009). A great number of studies explore disease-associated genetic variants in disease status and disease-associated phenotypes (Small et al., 2000; Reiman et al., 2004; Filippini et al., 2009; Sheline et al., 2010; Sabuncu et al., 2012; Harris et al., 2014; Marden et al., 2016; Mormino et al., 2016; Axelrud et al., 2018). PRS model can capture nearly all common genetic risk for AD (Escott-Price et al., 2017). In fact, PRS cannot capture rare genetic risk variants and gene-gene interactions (Sabuncu et al., 2012; Escott-Price et al., 2017). In addition, there are some genetic risk variants contributing to Ch4 volume but without effect on AD, and AD PRS cannot

capture. Lastly, some environmental factors may result in the change in brain volume, such as drugs (Navari and Dazzan, 2009; Moncrieff and Leo, 2010; Ebdrup et al., 2013). In future research, more sophisticated models considering these above factors should be constructed.

Considering that PRS based on AD-associated SNPs, excluding or including the *APOE* region, is associated with Ch4 volume in normal control subjects but not in AD patients. That is possibly because disease status severely changes the Ch4 volume to some extent (Whitehouse et al., 1981; Candy et al., 1983; Etienne et al., 1986). In conclusion, PRS based on AD-associated genetic risk variants is significantly associated with Ch4 volume in normal control subjects but not in AD patients.

Alzheimer's Disease Neuroimaging Initiative database is a very canonical dataset for AD. Many scholars all over the world make their contributions to the mechanism of AD based on mining the ADNI dataset. We find the association between AD PRS and Ch4 brain volume based on the 180 normal control subjects download from the ADNI database. We want to replicate this result in another independent dataset. Therefore, we divided 180 normal subjects into several subsets.

There are 136 ADNI 2 stage normal subjects, 29 ADNI GO stage normal subjects and 15 ADNI 1 stage normal subjects among 180 normal subjects according to the diagnose information. We utilized 136 normal subjects as a discovery dataset and 29 normal subjects as an independent dataset. The first ten principal components of population structure, the number of non-missing SNPs used for scoring and inbreeding coefficient for 136 normal subjects were obtained using PLINK. AD PRS based on AD-associated SNPs, including the *APOE* region, was used to predict Ch4 volume in 136 normal subjects. According to the PRS results (**Supplementary Figures S5**, **S6**), the best threshold for PRS model is 0.0428, the *p*-value of the PRS model is 0.001. Therefore, AD PRS is related to the Ch4 volume in 136 normal subjects. As for the independent dataset (29 normal subjects), we also obtained the first ten principal components of population structure, the number of non-missing SNPs used for scoring and inbreeding coefficient by PLINK. We used the PRSice to obtain the PRS results (**Supplementary Figures S7**, **S8**). The *p*-value of the best PRS model is 0.00011. So AD PRS is also associated with Ch4 volume in an independent dataset. In other word, the association between AD PRS and Ch4 volume can be replicated in an independent dataset.

In order to further validate the reality of this kind of association, we divided the 136 normal subjects into two equal groups. We took one group and another group as training set and test set, respectively. We utilized PLINK to obtain the first ten principal components of population structure, the number of non-missing SNPs used for scoring and inbreeding coefficient for training set and test set, respectively. The PRS results for the training set is showed as (**Supplementary Figures S9**, **S10**). The best cutoff for PRS model is 0.05 and the *p*-value of the PRS model is 0.015. According to the PRS results for the test set (**Supplementary Figures S11**, **S12**), the *p*-value of the best PRS model is 0.028.Therefore, the AD PRS is related to the Ch4 volume in training set and test set.

All in all, AD PRS is associated with the Ch4 volume in normal subjects. Our study presents several limitations. First of all, the sample size is relatively small. ADNI database provides genetic and images data of more than 800 subjects, including normal control subjects, mild cognitive impairment (MCI) subjects and AD patients. In fact, MCI subjects account for a major portion and AD patients constitute a minor percentage. We selected normal controls and AD patients according to the diagnosis information. Accordingly, we obtained the 106 AD patients and 180 normal control subjects after removing poor-quality subjects in this study. Another limitation is that AD patients were not divided into severe, moderate and mild subgroups according to disease severity. That is mainly because subgroups of AD patients cannot be achieved from the ADNI database. In the future studies, we will collect more sample size as possible as we can and categorize the sample into subgroups to explore the relationship between AD PRS and brain-associated endo-phenotypes. It is not only essential but also meaningful for academic studies.

ETHICS STATEMENT

Data used in preparation of this article were obtained from the ADNI database (adni.loni.usc.edu). Summary results data were obtained from the International Genomics of Alzheimer's Project (IGAP). Gene expression (median TPM) in multiple human tissues were downloaded from Genotype-Tissue Expression (GTEx) database.

AUTHOR CONTRIBUTIONS

QJ and YH designed the experiments. WZ and PR downloaded the MRI data from ADNI database. TW, ZH, and YY performed the experiments. All authors contributed to writing, and approved the final manuscript.

FUNDING

This work was supported by the National Natural Science Foundation of China (61822108 and 61571152), the National Science and Technology Major Project (2016YFC1202302), and the Natural Science Foundation of Heilongjiang Province (F2015006).

ACKNOWLEDGMENTS

We thank the International Genomics of Alzheimer's Project (IGAP) for providing summary results data for these analyses. The investigators within IGAP contributed to the design and implementation of IGAP and/or provided data but did not participate in analysis or writing of this report. IGAP was made possible by the generous participation of the control subjects, the patients, and their families. The i-Select chips was funded by the French National Foundation on Alzheimer's disease and related disorders. EADI was supported by the LABEX (laboratory of excellence program investment for the future) DISTALZ grant, Inserm, Institut Pasteur de Lille, Université de Lille 2, and the Lille University Hospital. GERAD was supported by the Medical

Research Council (Grant No. 503480), Alzheimer's Research United Kingdom (Grant No. 503176), the Wellcome Trust (Grant No. 082604/2/07/Z), and German Federal Ministry of Education and Research (BMBF): Competence Network Dementia (CND) Grant No. 01GI0102, 01GI0711, 01GI0420. CHARGE was partly supported by the NIH/NIA grant R01 AG033193 and the NIA AG081220 and AGES contract N01-AG-12100, the NHLBI grant R01 HL105756, the Icelandic Heart Association, and the Erasmus Medical Center and Erasmus University. ADGC was supported by the NIH/NIA grants: U01 AG032984, U24 AG021886, U01 AG016976, and the Alzheimer's Association grant ADGC-10-196728.

Data used in preparation of this article were obtained from the ADNI database (adni.loni.usc.edu). As such, the investigators within the ADNI contributed to the design and implementation of ADNI and/or provided data but did not participate in analysis or writing of this report. A complete listing of ADNI investigators can be found at: http://adni.loni.usc.edu/wp-content/uploads/how_to_apply/ADNI_Acknowledgement_List.pdf. Data collection and sharing for this project was funded by the ADNI (National Institutes of Health Grant U01 AG024904) and DOD ADNI (Department of Defense award number W81XWH-12-2-0012). ADNI is funded by the National Institute on Aging, the National Institute of Biomedical Imaging and Bioengineering, and through generous contributions from the following: AbbVie, Alzheimer's Association; Alzheimer's Drug Discovery Foundation; Araclon Biotech; BioClinica, Inc.; Biogen; Bristol-Myers Squibb Company; CereSpir, Inc.; Cogstate; Eisai Inc.; Elan Pharmaceuticals, Inc.; Eli Lilly and Company; EuroImmun; F. Hoffmann-La Roche Ltd., and its affiliated company Genentech, Inc.; Fujirebio; GE Healthcare; IXICO Ltd.; Janssen Alzheimer Immunotherapy Research and Development, LLC.; Johnson and Johnson Pharmaceutical Research & Development, LLC.; Lumosity; Lundbeck; Merck & Co., Inc.; Meso Scale Diagnostics, LLC.; NeuroRx Research; Neurotrack Technologies; Novartis Pharmaceuticals Corporation; Pfizer Inc.; Piramal Imaging; Servier; Takeda Pharmaceutical Company; and Transition Therapeutics. The Canadian Institutes of Health Research is providing funds to support ADNI clinical sites in Canada. Private sector contributions are facilitated by the Foundation for the National Institutes of Health (www.fnih.org). The grantee organization is the Northern California Institute for Research and Education, and the study is coordinated by the Alzheimer's Therapeutic Research Institute at the University of Southern California. ADNI data are disseminated by the Laboratory for Neuro Imaging at the University of Southern California. We sincerely thank the Alzheimer's Disease Neuroimaging Initiative for providing the imaging and genomic data.

SUPPLEMENTARY MATERIAL

The Supplementary Material for this article can be found online at: https://www.frontiersin.org/articles/10.3389/fgene.2019.00519/full#supplementary-material

FIGURE S1 | Bar plot showing at broad *P* value thresholds for AD PRS, including the *APOE* region, predicting Ch4 volume in AD patients, including a bar for the best-fit PRS from the high-resolution run.

FIGURE S2 | High-resolution plot for AD PRS, including the *APOE* region, predicting Ch4 volume in AD patients. The thick line connects points at the broad *P* value thresholds of **Supplementary Figure S1**. The best-fit PRS is at P_T of 0.0068.

FIGURE S3 | Bar plot showing at broad *P* value thresholds for AD PRS, including the *APOE* region, predicting Ch4 volume in normal control subjects, including a bar for the best-fit PRS from the high-resolution run.

FIGURE S4 | High-resolution plot for AD PRS, including the *APOE* region, predicting Ch4 volume in normal control subjects. The thick line connects points at the broad *P* value thresholds of **Supplementary Figure S3**. The best-fit PRS is at P_T of 0.0944.

FIGURE S5 | Bar plot showing at broad *P* value thresholds for AD PRS, including the APOE region, predicting Ch4 volume in 136 normal subjects, including a bar for the best-fit PRS from the high-resolution run.

FIGURE S6 | High-resolution plot for AD PRS, including the APOE region, predicting Ch4 volume in 136 normal subjects. The thick line connects points at the broad *P* value thresholds of **Supplementary Figure S5**.

FIGURE S7 | Bar plot showing at broad *P* value thresholds for AD PRS, including the APOE region, predicting Ch4 volume in 29 normal subjects, including a bar for the best-fit PRS from the high-resolution run.

FIGURE S8 | High-resolution plot for AD PRS, including the APOE region, predicting Ch4 volume in 29 normal subjects. The thick line connects points at the broad *P* value thresholds of **Supplementary Figure S7**.

FIGURE S9 | Bar plot showing at broad *P* value thresholds for AD PRS, including the APOE region, predicting Ch4 volume in training set, including a bar for the best-fit PRS from the high-resolution run.

FIGURE S10 | High-resolution plot for AD PRS, including the APOE region, predicting Ch4 volume in training set. The thick line connects points at the broad *P* value thresholds of **Supplementary Figure S9**.

FIGURE S11 | Bar plot showing at broad *P* value thresholds for AD PRS, including the APOE region, predicting Ch4 volume in test set, including a bar for the best-fit PRS from the high-resolution run.

FIGURE S12 | High-resolution plot for AD PRS, including the APOE region, predicting Ch4 volume in test set. The thick line connects points at the broad *P* value thresholds of **Supplementary Figure S11**.

TABLE S1 | The neuroimage ID of 106 AD patients.

TABLE S2 | The neuroimage ID of 180 NC subjects.

TABLE S3 | 8070 SNPs with *P* value below 0.0944.

REFERENCES

Alattas, R., and Barkana, B. D. (2015). "A comparative study of brain volume changes in Alzheimer's disease using MRI scans," in *Proceedings of the 2015 IEEE Long Island Systems, Applications and Technology Conference*, (Farmingdale: IEEE).

Andrews, K. A., Frost, C., Modat, M., Cardoso, M. J., and Aibl Rowe, C. C. (2016). Acceleration of hippocampal atrophy rates in asymptomatic amyloidosis. *Neurobiol. Aging* 39, 99–107. doi: 10.1016/j.neurobiolaging.2015.10.013

Ashburner, J. (2007). A fast diffeomorphic image registration algorithm. *Neuroimage* 38, 95–113. doi: 10.1016/j.neuroimage.2007.07.007

Axelrud, L. K., Santoro, M. L., Pine, D. S., Talarico, F., Gadelha, A., Manfro, G. G., et al. (2018). Polygenic risk score for alzheimer's disease: implications for memory performance and hippocampal volumes in early life. *Am. J. Psychiatry* 175, 555–563. doi: 10.1176/appi.ajp.2017.17050529

Butt, A. E., and Hodge, G. K. (1995). Acquisition, retention, and extinction of operant discriminations in rats with nucleus basalis magnocellularis lesions. *Behav. Neurosci.* 109, 699–713. doi: 10.1037/0735-7044.109.4.699

Candy, J. M., Perry, R. H., Perry, E. K., Irving, D., Blessed, G., Fairbairn, A. F., et al. (1983). Pathological changes in the nucleus of Meynert in Alzheimer's and Parkinson's diseases. *J. Neurol. Sci.* 59, 277–289.

Corder, E. H., Saunders, A. M., Strittmatter, W. J., Schmechel, D. E., Gaskell, P. C., Small, G. W., et al. (1993). Gene dose of apolipoprotein E type 4 allele and the risk of Alzheimer's disease in late onset families. *Science* 261, 921–923. doi: 10.1126/science.8346443

Csernansky, J. G., Wang, L., Swank, J., Miller, J. P., Gado, M., McKeel, D., et al. (2005). Preclinical detection of Alzheimer's disease: hippocampal shape and volume predict dementia onset in the elderly. *Neuroimage* 25, 783–792. doi: 10.1016/j.neuroimage.2004.12.036

Ebdrup, B. H., Norbak, H., Borgwardt, S., and Glenthoj, B. (2013). volumetric changes in the basal ganglia after antipsychotic monotherapy: a systematic review. *Curr. Med. Chem.* 20, 438–447. doi: 10.2174/0929867311320030015

Eickhoff, S. B., Stephan, K. E., Mohlberg, H., Grefkes, C., Fink, G. R., Amunts, K., et al. (2005). A new SPM toolbox for combining probabilistic cytoarchitectonic maps and functional imaging data. *Neuroimage* 25, 1325–1335. doi: 10.1016/j.neuroimage.2004.12.034

Escott-Price, V., Shoai, M., Pither, R., Williams, J., and Hardy, J. (2017). Polygenic score prediction captures nearly all common genetic risk for Alzheimer's disease. *Neurobiol. Aging* 49:214 e 21, e211. doi: 10.1016/j.neurobiolaging.2016.07.018

Escott-Price, V., Sims, R., Bannister, C., Harold, D., Vronskaya, M., Majounie, E., et al. (2015). Common polygenic variation enhances risk prediction for Alzheimer's disease. *Brain* 138(Pt 12), 3673–3684. doi: 10.1093/brain/awv268

Etienne, P., Robitaille, Y., Wood, P., Gauthier, S., Nair, N. P., and Quirion, R. (1986). Nucleus basalis neuronal loss, neuritic plaques and choline acetyltransferase activity in advanced Alzheimer's disease. *Neuroscience* 19, 1279–1291. doi: 10.1016/0306-4522(86)90142-9

Euesden, J., Lewis, C. M., and O'Reilly, P. F. (2015). PRSice: polygenic Risk Score software. *Bioinformatics* 31, 1466–1468. doi: 10.1093/bioinformatics/btu848

Filippini, N., MacIntosh, B. J., Hough, M. G., Goodwin, G. M., Frisoni, G. B., Smith, S. M., et al. (2009). Distinct patterns of brain activity in young carriers of the APOE-epsilon4 allele. *Proc. Natl. Acad. Sci. U.S.A.* 106, 7209–7214. doi: 10.1073/pnas.0811879106

Gratwicke, J., Kahan, J., Zrinzo, L., Hariz, M., Limousin, P., Foltynie, T., et al. (2013). The nucleus basalis of Meynert: a new target for deep brain stimulation in dementia? *Neurosci. Biobehav. Rev.* 37(10 Pt 2), 2676–2688. doi: 10.1016/j.neubiorev.2013.09.003

Grothe, M., Heinsen, H., and Teipel, S. (2013). Longitudinal measures of cholinergic forebrain atrophy in the transition from healthy aging to Alzheimer's disease. *Neurobiol. Aging* 34, 1210–1220. doi: 10.1016/j.neurobiolaging.2012.10.018

Grothe, M., Heinsen, H., and Teipel, S. J. (2012). Atrophy of the cholinergic Basal forebrain over the adult age range and in early stages of Alzheimer's disease. *Biol. Psychiatry* 71, 805–813. doi: 10.1016/j.biopsych.2011.06.019

Hanyu, H., Asano, T., Sakurai, H., Tanaka, Y., Takasaki, M., and Abe, K. (2002). MR analysis of the substantia innominata in normal aging. Alzheimer disease, and other types of dementia. *AJNR Am. J. Neuroradiol.* 23, 27–32.

Harris, S. E., Davies, G., Luciano, M., Payton, A., Fox, H. C., Haggarty, P., et al. (2014). Polygenic risk for Alzheimer's disease is not associated with cognitive ability or cognitive aging in non-demented older people. *J. Alzheimers Dis.* 39, 565–574. doi: 10.3233/JAD-131058

Harrison, T. M., Mahmood, Z., Lau, E. P., Karacozoff, A. M., Burggren, A. C., Small, G. W., et al. (2016). An alzheimer's disease genetic risk score predicts longitudinal thinning of hippocampal complex subregions in healthy older adults. *eNeuro* 3, ENEURO.98-16.2016. doi: 10.1523/ENEURO.0098-16.2016

Hindorff, L. A., Sethupathy, P., Junkins, H. A., Ramos, E. M., Mehta, J. P., Collins, F. S., et al. (2009). Potential etiologic and functional implications of genome-wide association loci for human diseases and traits. *Proc. Natl. Acad. Sci. U.S.A.* 106, 9362–9367. doi: 10.1073/pnas.0903103106

Hu, Y., Zheng, L. K., Cheng, L., Zhang, Y., Bai, W. Y., Zhou, W. Y., et al. (2017). GAB2 rs2373115 variant contributes to Alzheimer's disease risk specifically in European population. *J. Neurol. Sci.* 375, 18–22. doi: 10.1016/j.jns.2017.01.030

International Schizophrenia Consortium, Purcell, S. M., Wray, N. R., Stone, J. L., Visscher, P. M., O'Donovan, M. C., et al. (2009). Common polygenic variation contributes to risk of schizophrenia and bipolar disorder. *Nature* 460, 748–752. doi: 10.1038/nature08185

Jack, C. R., Jr., Bernstein, M. A., Fox, N. C., Thompson, P., and Alexander, G. (2008). The Alzheimer's Disease Neuroimaging Initiative (ADNI): MRI methods. *J. Magn. Reson. Imaging* 27, 685–691. doi: 10.1002/jmri.21049

Jagust, W., Gitcho, A., Sun, F., Kuczynski, B., Mungas, D., and Haan, M. (2006). Brain imaging evidence of preclinical Alzheimer's disease in normal aging. *Ann. Neurol.* 59, 673–681. doi: 10.1002/ana.20799

Jiang, Q. H., Jin, S. L., Jiang, Y. S., Liao, M. Z., Feng, R. N., Zhang, L. C., et al. (2017). Alzheimer's disease variants with the genome-wide significance are significantly enriched in immune pathways and active in immune cells. *Mol. Neurobiol.* 54, 594–600. doi: 10.1007/s12035-015-9670-9678

Lambert, J. C., Grenier-Boley, B., Chouraki, V., Heath, S., Zelenika, D., Fievet, N., et al. (2010). Implication of the immune system in Alzheimer's Disease: evidence from genome-wide pathway analysis. *J. Alzheimers Dis.* 20, 1107–1118. doi: 10.3233/Jad-2010-100018

Lambert, J. C., Ibrahim-Verbaas, C. A., Harold, D., Naj, A. C., Sims, R., Bellenguez, C., et al. (2013). Meta-analysis of 74,046 individuals identifies 11 new susceptibility loci for Alzheimer's disease. *Nat. Genet.* 45, 1452–U1206. doi: 10.1038/ng.2802

Leanza, G., Muir, J., Nilsson, O. G., Wiley, R. G., Dunnett, S. B., and Bjorklund, A. (1996). Selective immunolesioning of the basal forebrain cholinergic system disrupts short-term memory in rats. *Eur. J. Neurosci.* 8, 1535–1544. doi: 10.1111/j.1460-9568.1996.tb01616.x

Li, J., Zhang, X., Li, A., Liu, S., Qin, W., Yu, C., et al. (2018). Polygenic risk for Alzheimer's disease influences precuneal volume in two independent general populations. *Neurobiol. Aging* 64, 116–122. doi: 10.1016/j.neurobiolaging.2017.12.022

Liu, G., Zhang, Y., Wang, L. C., Xu, J. Y., Chen, X. Y., Bao, Y. J., et al. (2018). Alzheimer's disease rs11767557 variant regulates EPHA1 gene expression specifically in human whole blood. *J. Alzheimers Dis.* 61, 1077–1088. doi: 10.3233/Jad-170468

Lupton, M. K., Strike, L., Hansell, N. K., Wen, W., Mather, K. A., Armstrong, N. J., et al. (2016). The effect of increased genetic risk for Alzheimer's disease on hippocampal and amygdala volume. *Neurobiol. Aging* 40, 68–77. doi: 10.1016/j.neurobiolaging.2015.12.023

Marden, J. R., Mayeda, E. R., Walter, S., Vivot, A., Tchetgen Tchetgen, E. J., Kawachi, I., et al. (2016). Using an alzheimer disease polygenic risk score to predict memory decline in black and white americans Over 14 years of follow-up. *Alzheimer Dis. Assoc. Disord.* 30, 195–202. doi: 10.1097/WAD.0000000000000137

Mattavelli, D., Agosta, F., Weiler, M., Canu, E., Copetti, M., Magnani, G., et al. (2015). Following the spreading of brain structural changes in Alzheimer's disease: a longitudinal, multimodal MRI study. *Eur. J. Neurol.* 22, 124–124. doi: 10.3233/JAD-150196

McGaugh, J. L. (2002). Memory consolidation and the amygdala: a systems perspective. *Trends Neurosci.* 25:456. doi: 10.1016/s0166-2236(02)02211-7

McGaughy, J., Dalley, J. W., Morrison, C. H., Everitt, B. J., and Robbins, T. W. (2002). Selective behavioral and neurochemical effects of cholinergic lesions produced by intrabasalis infusions of 192 IgG-saporin on attentional performance in a five-choice serial reaction time task. *J. Neurosci.* 22, 1905–1913. doi: 10.1523/jneurosci.22-05-01905.2002

Mesulam, M. M., Mufson, E. J., Levey, A. I., and Wainer, B. H. (1983). Cholinergic innervation of cortex by the basal forebrain: cytochemistry and cortical connections of the septal area, diagonal band nuclei, nucleus basalis (substantia innominata), and hypothalamus in the rhesus monkey. *J. Comp. Neurol.* 214, 170–197. doi: 10.1002/cne.902140206

Moncrieff, J., and Leo, J. (2010). A systematic review of the effects of antipsychotic drugs on brain volume. *Psychol. Med.* 40, 1409–1422. doi: 10.1017/S0033291709992297

Mori, E., Lee, K., Yasuda, M., Hashimoto, M., Kazui, H., Hirono, N., et al. (2002). Accelerated hippocampal atrophy in Alzheimer's disease with apolipoprotein E epsilon4 allele. *Ann. Neurol.* 51, 209–214. doi: 10.1002/ana.10093

Mormino, E. C., Sperling, R. A., Holmes, A. J., Buckner, R. L., De Jager, P. L., Smoller, J. W., et al. (2016). Polygenic risk of Alzheimer disease is associated with early- and late-life processes. *Neurology* 87, 481–488. doi: 10.1212/WNL.0000000000002922

Navari, S., and Dazzan, P. (2009). Do antipsychotic drugs affect brain structure? A systematic and critical review of MRI findings. *Psychol. Med.* 39, 1763–1777. doi: 10.1017/S0033291709005315

Purcell, S., Neale, B., Todd-Brown, K., Thomas, L., Ferreira, M. A., Bender, D., et al. (2007). PLINK: a tool set for whole-genome association and population-based linkage analyses. *Am. J. Hum. Genet.* 81, 559–575. doi: 10.1086/519795

Reiman, E. M., Chen, K., Alexander, G. E., Caselli, R. J., Bandy, D., Osborne, D., et al. (2004). Functional brain abnormalities in young adults at genetic risk for late-onset Alzheimer's dementia. *Proc. Natl. Acad. Sci. U.S.A.* 101, 284–289. doi: 10.1073/pnas.2635903100

Sabuncu, M. R., Buckner, R. L., Smoller, J. W., Lee, P. H., Fischl, B., Sperling, R. A., et al. (2012). The association between a polygenic Alzheimer score and cortical thickness in clinically normal subjects. *Cereb. Cortex* 22, 2653–2661. doi: 10.1093/cercor/bhr348

Schmitz, T. W., Nathan Spreng, R., and Alzheimer's Disease Neuroimaging Initiative (2016). Basal forebrain degeneration precedes and predicts the cortical spread of Alzheimer's pathology. *Nat. Commun.* 7:13249. doi: 10.1038/ncomms13249

Schott, J. M., Bartlett, J. W., Fox, N. C., Barnes, J., and Alzheimer's Disease Neuroimaging Initiative (2010). Increased brain atrophy rates in cognitively normal older adults with low cerebrospinal fluid Abeta1-42. *Ann. Neurol.* 68, 825–834. doi: 10.1002/ana.22315

Sheline, Y. I., Morris, J. C., Snyder, A. Z., Price, J. L., Yan, Z., D'Angelo, G., et al. (2010). APOE4 allele disrupts resting state fMRI connectivity in the absence of amyloid plaques or decreased CSF Abeta42. *J. Neurosci.* 30, 17035–17040. doi: 10.1523/JNEUROSCI.3987-10.2010

Small, G. W., Ercoli, L. M., Silverman, D. H., Huang, S. C., Komo, S., Bookheimer, S. Y., et al. (2000). Cerebral metabolic and cognitive decline in persons at genetic risk for Alzheimer's disease. *Proc. Natl. Acad. Sci. U.S.A.* 97, 6037–6042. doi: 10.1073/pnas.090106797

Teipel, S. J., Meindl, T., Grinberg, L., Grothe, M., Cantero, J. L., Reiser, M. F., et al. (2011). The cholinergic system in mild cognitive impairment and Alzheimer's disease: an in vivo MRI and DTI study. *Hum. Brain Mapp.* 32, 1349–1362. doi: 10.1002/hbm.21111

Terwisscha van Scheltinga, A. F., Bakker, S. C., van Haren, N. E., Derks, E. M., Buizer-Voskamp, J. E., Boos, H. B., et al. (2013). Genetic schizophrenia risk variants jointly modulate total brain and white matter volume. *Biol. Psychiatry* 73, 525–531. doi: 10.1016/j.biopsych.2012.08.017

Voytko, M. L. (1996). Cognitive functions of the basal forebrain cholinergic system in monkeys: memory or attention? *Behav. Brain Res.* 75, 13–25. doi: 10.1016/0166-4328(95)00143-3

Whitehouse, P. J., Price, D. L., Clark, A. W., Coyle, J. T., and DeLong, M. R. (1981). Alzheimer disease: evidence for selective loss of cholinergic neurons in the nucleus basalis. *Ann. Neurol.* 10, 122–126. doi: 10.1002/ana.410100203

Xiao, E., Chen, Q., Goldman, A. L., Tan, H. Y., Healy, K., Zoltick, B., et al. (2017). Late-onset alzheimer's disease polygenic risk profile score predicts hippocampal function. *Biol. Psychiatry Cogn. Neurosci. Neuroimaging* 2, 673–679. doi: 10.1016/j.bpsc.2017.08.004

Yan, C. G., Wang, X. D., Zuo, X. N., and Zang, Y. F. (2016). DPABI: data processing & analysis for (Resting-State) brain imaging. *Neuroinformatics* 14, 339–351. doi: 10.1007/s12021-016-9299-9294

Zaborszky, L., Hoemke, L., Mohlberg, H., Schleicher, A., Amunts, K., and Zilles, K. (2008). Stereotaxic probabilistic maps of the magnocellular cell groups in human basal forebrain. *Neuroimage* 42, 1127–1141. doi: 10.1016/j.neuroimage.2008.05.055

Zhang, N. N. N., Song, X. W., Zhang, Y. T., Chen, W., D'Arcy, R. C. N., Darvesh, S., et al. (2011). An MRI brain atrophy and lesion index to assess the progression of structural changes in alzheimer's disease. mild cognitive impairment, and normal aging: a follow-up study. *J. Alzheimers Dis.* 26, 359–367. doi: 10.3233/Jad-2011-2048

Conflict of Interest Statement: YY employed by company Jiangsu Singch Pharmaceutical Co., Ltd.

The remaining authors declare that the research was conducted in the absence of any commercial or financial relationships that could be construed as a potential conflict of interest.

Advantages of publishing in Frontiers

OPEN ACCESS
Articles are free to read for greatest visibility and readership

FAST PUBLICATION
Around 90 days from submission to decision

HIGH QUALITY PEER-REVIEW
Rigorous, collaborative, and constructive peer-review

TRANSPARENT PEER-REVIEW
Editors and reviewers acknowledged by name on published articles

Frontiers
Avenue du Tribunal-Fédéral 34
1005 Lausanne | Switzerland

Visit us: www.frontiersin.org
Contact us: info@frontiersin.org | +41 21 510 17 00

REPRODUCIBILITY OF RESEARCH
Support open data and methods to enhance research reproducibility

DIGITAL PUBLISHING
Articles designed for optimal readership across devices

FOLLOW US
@frontiersin

IMPACT METRICS
Advanced article metrics track visibility across digital media

EXTENSIVE PROMOTION
Marketing and promotion of impactful research

LOOP RESEARCH NETWORK
Our network increases your article's readership